

City Research Online

City St George's, University of London

Citation: Gill, S. (1975). A study of the viscoelastic & thermal behaviour of the perforated end slabs for prestressed concrete pressure vessel cylinders. (Unpublished Doctoral thesis, The City University)

This is the accepted version of the paper.

This version of the publication may differ from the final published version. To cite this item please consult the publisher's version.

Permanent repository link: https://openaccess.city.ac.uk/id/eprint/38099/

Copyright and Reuse: Copyright and Moral Rights remain with the author(s) and/or copyright holders. Copies of full items can be used for personal research or study, educational, or not-for-profit purposes without prior permission or charge, unless otherwise indicated, provided that the authors, title and full bibliographic details are credited, a hyperlink and/or URL is given for the original metadata page and the content is not changed in any way. For full details of reuse please refer to City Research Online policy.

City Research Online: http://openaccess.city.ac.uk/ publications@citystgeorges.ac.uk

A Study of the Viscoelastic and Thermal Behaviour of the Perforated End Slabs for Prestressed Concrete Pressure Vessel Cylinders.

A thesis submitted for the degree of

Doctor of Philosophy

The City University, London

by

S. Gill, B.Sc. Tech., C. Eng., M.I.C.E., M.I. Mech. E.

Department of Civil Engineering

The City University

London

1975

SYNOPSIS

This thesis is the result of a continuing study into the analysis and design of prestressed concrete pressure vessels since 1958, (2), (3), (72), (111),(114), (116).*

Programmes of research and development on these vessels have been undertaken** both in industry and in university laboratories. The investigation described herein, concerning the end slabs of prestressed concrete cylinders has continued since 1966.

The work presented in this thesis can be summarized under five main headings.

One section of the text describes in detail the objectives, equipment and techniques of the experimental investigations.

In a further section, the literature is summarized dealing with the changes which occur with loading, time and temperature in the relevant concrete elastic constants. Changes in some of these constants have been the subject of part of the experimental work undertaken, and this is also reported.

Another section reviews and assesses the existing literature concerning the effects of loading, time and temperature on the creep and shrinkage characteristics of concrete. Experimental creep and shrinkage data obtained from tests on the concrete under review, are also presented elsewhere in the thesis.

In addition, a study is made of existing methods of elastic and time-dependent analysis, comparing and contrasting their usefulness, particularly in relation to the analytical objectives of the present investigation.

*(figures in parentheses refer throughout to the numbers in the bibliography)

**(by the author)

Finally, the most important section of work in this thesis presents a viscoelastic method of analysis, which incorporates the influence of time-dependent effects, for the end slabs to the prestressed concrete pressure vessel cylinder. The method is used to predict the total strains which occur in the end slabs under long-term external loading and temperature, and the correlation between these predictions and the measured strains during two series of model observations, is assessed.

Background to the present investigation

Concentration on the details of concrete vessels, rather than on the vessels as a whole, has led to a realization that for further advances to be made in safety, realism and economy in practical design proposals, more information was required about the material properties, more particularly about their changes with time, temperature and loading.

This information has been sought for those parts of the vessel about which least was known, whose geometry was most complicated and redundant, and upon whose long-term integrity, the vessel depended for its safe operation.

This investigation has concerned itself with the end slabs of the vessel cylinders. These slabs are perforated to permit fuel loading by the charging machine. The perforations are lined with steel liners, they are arranged in a regular lattice over the central zone of the end cap, and they are surrounded by a solid concrete annulus which spans onto the supporting cylindrical walls.

The slab is subjected to elevated temperatures and is hotter

at the centre than at the periphery of the zone. The temperature gradient across the slab accordingly varies along the diameter but is reduced in magnitude by an extensive cooling system which operates on the inner face of the slab and around the charge tube liners.

The circumferential prestressing forces applied at the rim of the slab place the concrete into precompression and it was about the retention or loss of this prestress that the United Kingdom Atomic Energy Authority were mainly concerned when the work described in this thesis was commissioned. Any cracking that might result in the experimental work undertaken, due to a loss of prestress should be predictable by the analysis proposed.

There are many variables, however, affecting a true computation of strain and stress. Moreover, the concrete constants - thermal conductivity, coefficient of thermal expansion, Young's Modulus, tensile strength and ultimate strain - which condition the flow of heat and the accommodation of strains, tend to vary with time, temperature and stress level.

However, in this experimental work, most, but not all of them, have been evaluated, under varying conditions, on control specimens.

As a consequence of these considerations, the main data required from the investigations are as follows:

1) the total strains and separately the elastic, thermal, creep and shrinkage strains in the perforated zone under temperature and external load,

2) the internal distribution of load at the boundary between the perforated zone and the outer unperforated region.

3) the internal distribution of load between the stand pipe perforations and the concrete within the perforated zone.

4) the notional material properties for an equivalent, homogeneous but hypothetical material which could replace the perforated zone and behave as the perforated zone under operating conditions.

5) a knowledge of the effect of (a) the varying elastic stiffnesses between the perforated zone and the outer zone and (b) the modifying action of creep and shrinkage on the magnitude of the applied prestress; loss of prestress could lead to cracking of the end slab as tensions develop on unloading.

6) in addition, methods of analysis are required in order to be able to forecast strains under service loading and temperature which would take into account time-dependent and thermal effects.

If this information could be assembled it was felt that future analyses might be made without recourse to model building. Specific creep curves would need to be plotted and shrinkage data obtained for the particular concrete to be used but the advantages might include

the possibility of being able to conclude an analysis for a given geometry, loading and temperature without the need for model verification.

It is considered that these aims have been achieved, that the information listed above has been obtained, and that the particular viscoelastic method of analysis proposed is practicable for a considerable range of geometries and loadings.

ACKNOWLEDGEMENTS

The author wishes to express his indebtedness to the United Kingdom Atomic Energy Authority for financing the work described in this thesis.

The author is also grateful for the advice and encouragement given by Professor P.O.Wolf, B.Sc.(Eng.), A.K.C., C.Eng.,F.I.C.E.,F.I.W.E.,F.A.S.C.E.,F.R.Met.S.,M.I.A.H.R., M.A.G.U., Professor J.E.Gibson, D.Sc.,Ph.D.,C.Eng.,F.I.C.E., M.I.Struct.E.,M.I.A.S.S., Dr. N.P.Roberts, Ph.D.,B.Sc.(Eng), C.Eng.,F.I.C.E., and by Mr P.Burhouse, M.A.,D.I.C.,C.Eng., M.I.C.E.

Sincere thanks are due to [redacted], Ph.D., D.I.C., B.Sc. for his extensive help and interest at all stages of this thesis.

The author also wishes to express his gratitude to the laboratory staff of the Department of Civil Engineering of The City University, London, in particular to M[redacted].

I N D E X

		Page No.
Title Page		
Synopsis		1
Acknowledgements		6
Index		7
List of Illustrations		11
List of Plates		14
Notation		15
Section I	Introduction	19
Section II	The Objectives of the Investigation	28
Section III	The Models	34
Section IV	The Testing Programme	38
Section V	Details of Equipment	42

1. The Specimens
2. The Concrete Mix
3. Steel Moulds and Cruciform Jig
4. The Loading Rigs
5. The Pressure Circuit
6. The Heating Circuit
7. Temperature Measurement
8. Electrical Resistance Strain Gauge Circuits
9. Demec Gauges
10. Crack-Detection Circuits.

Section VI	Experimental Procedures	83

A. The Loading and observation procedures in the Test Programme

1. Load Cycling at Ambient Temperature
2. Load at Ambient Temperature
3. Loading at 80°C
4. Load Cycling at 80°C
5. Loading at Ambient Temperature again
6. Unloading : Cracking
7. Load Cycling after unloading : Creep Recovery.

Page No

B. The Test Equipment and the reliability of Testing Techniques

1. The Loading Rigs
2. The Rubber Bags
3. The Pressure Circuit
4. The Heating Circuit
5. The Temperature Measurement Circuit
6. The Electrical Resistance Strain Gauge Circuit
7. The Crack-Detection Circuits
8. The Strain-Measuring Instruments
9. The Steel Moulds and Jig

C. The Sealing of the Specimens

Section VII — The Variation of Concrete Constants with Age and Temperature — 111

1. Compressive Strength of Concrete
2. Tensile Strength
3. Poisson's Ratio
4. Modulus of Elasticity
5. Coefficient of Thermal Expansion
6. Thermal Conductivity of Concrete

Section VIII — The Nature of Creep and Shrinkage Review of Literature — 123

A. Creep

1. The Mechanisms of Creep
2. Creep Curves; Specific Creep; Creep Coefficient
3. The Effect of Stress
4. Creep under sustained Compression
5. The Effects of Temperature
6. Other Factors affecting Creep
   a) b) c) The Effect of Water
   d) Concrete Maturity
   e) Surface/Volume Ratio & the Effect of Size
   f) The Effect of the Cement

Page No.

g) h) i) The Effect of Aggregates

7. Creep Recovery

8. The Effect of Concrete Creep on Reinforcement

B. Shrinkage

I. Theories of Shrinkage

2. Shrinkage Gradients

3. Temperature and Hygrothermal Shrinkage

4. Practical Effects of Shrinkage on Concrete

5. Summary of Factors affecting Shrinkage

6. Curing and Storage Conditions

7. The Effect of Aggregate-Cement Ratio and Aggregate Grading

8. Shrinkage in Reinforced and Prestressed Concrete Members

9. The Separation of the Strain Components

Section IX Analytical Methods 146

A. Elastic Methods of Analysis

I. General Approach to Analysis

2. Review of Analytical Methods

3. Analysis of Large Sections of the Vessel: Thin Plates and Cylinders

4. Finite Differences

5. Dynamic Relaxation

6. Finite Element Method

7. Existing Elastic Methods of Analysis for Perforated Slabs

i) Sheffield's Theory

ii) Slot's Method

iii) Harrop and Abdul-Wahab

Page No.

iv) Kinkead

v) Bailey and Hicks

vi) Bailey and Fidler

vii) Horvay

B. Analysis of Time-Dependent Strains

I. The Reduced Modulus Method

2. The Effective Modulus Method

3. The Rate of Creep Method

4. The Method of Superposition

5. The Strain Hardening Method

6. The Relaxation Method

7. The Steady State Method

8. Complementary Power Theory

9. Viscoelasticity

Section X. The Theoretical Analysis 217

I. Introduction

2. General Considerations

3. The Finite Element Solution

4. Matrix Formulation

5. The Viscoelastic Analogue

6. The Time-Dependent Solution

7. Thermoelastic Considerations

8. Creep Considerations

9. Shrinkage Considerations

IO. The Computer Programme

Section XI. Presentation of Observed Results 277

Section XII. Interpretation of Results 329

Section XIII. Correlation of Predicted and Observed Results 338

Section XIV. Conclusions and Recommendations 379

Section XV. Appendices 387

Section XVI. Bibliography 438

LIST OF ILLUSTRATIONS

Fig. 1. The first French P.C.P.V.

Fig. 2. The first British P.C.P.V.

Fig. 3. The Wylfa Head Reactor

Fig. 4. The Dungeness B. Vessel

Fig. 5. The French Bugey 1 Vessel

Fig. 6. The Five Concrete Test Specimens

Fig. 7. Series 1. Test Programme

Fig. 8. Series 2. Test Programme

Fig. 9. Models 1/2 and 7/8 (solid)
Typical Arrangement of Demec Gauge Points

Fig.10. Models 3/4 and 5/6
Typical Arrangement of Standpipes
(Model 9/10 arrangement identical)

Fig.11. Model 9/10 composite
Typical Arrangement of Demec Gauge Points in the Annulus.

Fig.12. Layout of thermocouples in the Solid Specimens
(Models 1/2 and 7/8)

Fig.13. Layout of thermocouples in the 36" diameter Composite Specimen.

Fig.14. Standpipe and hexagonal fixing details

Fig.15. A Vertical Section through 36" diameter specimen loading rig.

Fig.16. Detail of 36" diameter rig.

Fig.17. Layout of Rigs and Frames

Fig.18. Layout of Pressure Circuit and Test Specimens.

Fig.19. Karlit Heating Shield showing arrangement of Isopad Heating Tapes.

Fig.20. Thermocouple Circuit

Fig.21. E.R.S.G. Layout (Perforated Specimens).

Fig.22 E.R.S.G Layout (Solid Specimen).

Fig.23 E.R.S.G Circuit.

Fig.24 Crack Detection Circuit.

Fig.25 Check on the uniformity of radial pressure.

Fig.26 Series 1. Chronology of Events.

Fig.27 Series 2. Chronology of Events.

Fig.28 Demec Point and Thermocouple Positions for Sides 1 and 2.

Fig.29 Demec Point, Thermocouple and Standpipe Diameter Point Positions for Sides 3 and 4.

Fig.30 Demec Point, Thermocouple and Standpipe Diameter Point Positions for Sides 5 and 6.

Fig.31 Demec Point and Thermocouple Positions for Sides 7 and 8.

Fig.32 Demec Point Positions for Sides 9 and 10.

Fig.33 Thermocouple and Standpipe Diameter Point Positions for Sides 9 and 10.

Fig.34 Thermocouple Calibration Graph.

Fig.35 Relationship between curing temperature, crushing strength and age in Portland Cement Concrete.

Fig.36 Creep of Concrete under Load.

Fig.37 Elastic Strain, Shrinkage and Creep.

Fig.38 Influence of ambient relative humidity on concrete creep.

Fig.39 Elastic Methods of Analysis.

Fig.40 Cumulative Creep Strains. Rate of Creep.
Cumulative Creep Strains. Strain Hardening.

Fig.41 Creep and Recovery.

Fig.42 Maxwell Model and Response. Kelvin Model and Response.
Three-element Model and Response.

Fig.43 Burgers and other models.

Fig.44 Rim Compression Components at Boundary Nodal Points.

Fig.44a The Element Stiffness Matrix.

Fig.45 Typical Triangular Element.

Fig.46 Structural Idealization for Model 1/2.

Fig.47 Structural Idealization for Model 3/4.

Fig.48 Structural Idealization for Model 9/10.

Fig.49 Proposed Rheological Model.

Fig.50 Three-parameter Solids and Maxwell Model in series.

Figs 51, 51a, 52, 52a et seq. represent the experimental results and the corresponding theoretical results. They are presented with their captions in Sections XI and XIII.

LIST OF PLATES

Plate 1. General Layout of Test Specimens.

Plate 2. Layout Showing Sides 1/2, 3/4, 5/6, 7/8, and Air-Hydro Pump.

Plate 3. Model 3/4 with Heat Shield removed.

Plate 4. Models 5/6 and 7/8 with Heat Shield removed.

Plate 5. Model 9/10 with Heat Shield removed.

Plate 6. Insulation Shielding and Thermocouple Leads for Models 3/4 and 9/10.

Plate 7. Steel Moulds for Models 1/2, 3/4, and 9/10.

Plate 8. E.R.S.G. wiring during final unloading phase.

Plate 9. Surface Cracking on Model 5/6 on removal of heat.

Plate 10. Crack Pattern. Sides 9/10. Series 1 and 2.

NOTATION

Symbols other than those listed in this notation have been used in the text. Such symbols have been used only once and have been defined in the thesis in the context of their presentation.

In general, where already-established material has been presented the notation used has followed that of the original sources. This has led to duplication since some symbols of this kind do not necessarily correspond to those employed for the same entity in the remaining sections of this work.

For other reasons also, a few symbols represent more than one quantity, the particular use being defined locally in the text.

Conversely, one quantity has been signified by more than one symbol in different sections in the thesis. Again local definition has avoided confusion.

English Symbols

A, Δ	=	area of element
A_h	=	area of hole
A_p	=	area of plate
A_s	=	area of liner
a	=	radius
A/C	=	aggregate/cement ratio by weight
C_1, C_2, C_3, C_4	=	deformation coefficients
c	=	specific creep
$c_{K\infty}$	=	ultimate Kelvin specific creep
D	=	hole diameter
D_c	=	creep compliance
D_s	=	stress relaxation compliance
d	=	displacement ; depth ; thickness ; diameter
E	=	elastic modulus ; spring stiffness
E'	=	effective elastic modulus

E_c = concrete secant elastic modulus

E_s = steel elastic modulus

E_k = Kelvin spring stiffness

E_m = Maxwell spring stiffness

e = Naperian base

F, f = force

F_{cs} = creep load vector

F_d = dashpot force

F_s = spring force

F_{ss} = shrinkage load vector

f_{cu}, u = concrete cube crushing strength, 28 days

K = structure stiffness matrix

K, K_2, K_3 = constants governing rate of Kelvin creep

k = element stiffness matrix

l = length, span

n = number of holes

P, p = pressure ; force

p_1, p_i = externally-applied distributed load

p_2 = distributed load at periphery of perforated zone

R = resultant load vector ; hole radius

r = radius

r, θ = polar co-ordinates

S' = induced stresses (Kinkead)

T_n = thickness of liner (Kinkead)

T = temperature ; absolute temperature

t = time ; element thickness

U_x, U_y = displacements in Cartesian co-ordinates

U_r, U_θ = displacements in polar co-ordinates

u, v = nodal displacement components

V = volume

W = plate width

W/C = water/cement ratio by weight

x, y = Cartesian co-ordinates

y/y_d = ratio of outer boundary co-ordinate to the plate size

---

Greek Symbols

α = coefficient of linear thermal expansion

α, κ = age at loading

$\Delta(t)$ = Heaviside step function

δ_{ij} = Kronecker delta

γ = fluidity at zero time

ε = strain

ε_r = recovery strain

ε_c = creep strain

ε_{el} = elastic strain

ε_s = shrinkage strain

ε_{in} = instantaneous elastic strain

$\varepsilon_{th}, \varepsilon_t$ = thermal strain

ε_v = strain due to a combination of drying shrinkage, hygrothermal movements, and physico-chemical changes

ν = Poisson's ratio

ν_c = creep Poisson's ratio

ν_s = Poisson's ratio for steel

σ = stress

σ_i = threshold stress

σ_{el} = elastic stress

σ_o = immediate stress

σ_r, σ_θ = stress components in polar co-ordinates

λ = reciprocal of retardation time

τ_{ret} = retardation time

η = viscous coefficient of viscoelastic element

$\phi(T)$ = temperature function

SECTION I

INTRODUCTION

The concept of the prestressed concrete vessel as a pressure container for a nuclear reactor, has passed through several stages of development in the last decade and a half.

In the first application of concrete vessels for this purpose in France, the former steel vessel and its concrete bio-shield were merely replaced by a single cylindrical prestressed concrete envelope which excluded the associated steam-raising units (1). See Fig.1.

The next application, developed in Britain, provided a cylindrical prestressed concrete container which included the steam-raising units and the cooling gas circuits, (Fig. 2).

A further development at Wylfa Head housed the complete nuclear, steam-raising and cooling complex within a spherical vessel, a design which sought the advantages of membrane stressing and minimum concrete volume, at the expense unfortunately, of simplicity in layout and construction. (Fig. 3).

The most recent designs have again employed the cylinder, giving more consideration to the fact that a reactor core is itself cylindrical. Moreover, the desirable orthogonal arrangement of prestressing cables in the longitudinal and circumferential directions is most conveniently provided about a cylinder, and, in general, the layout, analysis and construction of prestressed concrete pressure vessel cylinders have proved to be acceptably practicable. Development and research have continued in phase with current design and construction. See Figs 4 and 5.

As a result, the design of P.C.P.V.s has shown increasing sophistication in recent years. The more advanced the designs have become, the more concerned have the designers been, in terms of

safety (2), (70), (71) and serviceability, with the effects of secondary stresses, with cracking, with thermal phenomena and, in particular, with time-dependent behaviour resulting from creep and shrinkage in the concrete.

Cracking, for example, can be either harmful or advantageous in P.C.P.V.s depending on its location and on its severity. That is to say, in some positions, deep cracks, perhaps symptomatic of poor layout and detailing, may become stress-raisers, widening under the resulting stress concentrations and giving rise at best to reinforcement exposure and possible deterioration and at worst to local or general failure of the vessel.

Under other circumstances and in less critical positions, evenly-distributed micro-cracking may be considered to be one way in which over-stress may be dissipated and re-distributed.

Similarly, time-dependent strains such as those resulting from creep may either cause concern with regard to pre-stress loss in critical sections, or they may be helpful deformations, redistributing locked-in stresses and assisting the concrete to take up a least-stressed condition. The concrete is slowly but incompletely relieved of stress. The degree to which creep can operate, whether harmfully or advantageously, varies with concrete age and with age at loading since for this type of deformation, the rate of strain decreases significantly with time.

Temperatures and temperature gradients have the effect of

(a) increasing the volume of vessel concrete

(b) causing direct and bending stresses in constrained sections

(c) reducing the strength of the concrete

(d) accelerating the rate of shrinkage strain

(e) enhancing the rate of creep strain.

Accordingly, it is clear that thermal loading of the vessel has both a direct and an indirect effect on the behaviour of the vessel concrete. At one and the same time, elevated temperature may increase the imposed stress within the concrete and yet act upon the creep and shrinkage rates in a way which permits a greater relief of stress. Thus again, we have a conflicting pattern of behaviour.

One thing is clear. The concrete, under the influence of changing stress, temperature and age alters its nature and properties. As a consequence, the refinements which have been and are now being developed affecting the analyses and designs of vessels, must take into account a wide range of changing material constants and design parameters.

These difficulties have been intensified by the highly redundant nature of the P.C.P.V. structure. Most analyses, in the past, have depended for their verification on results of tests on whole models of the structure (3) and on the ability of investigators to record strains, temperatures and loadings in situations and under conditions which could only be assumed to correspond to those applying in practice.

This state of affairs has been acceptable hitherto since it has led to the substantiation of whole-vessel analyses and this aspect of progress has now been well-founded and documented.

As designs developed, and as experience matured, it became clear, however, that if further significant advances were to be made, more detailed information was necessary about the behaviour of certain critical parts of the vessels, for example, the end slabs to the cylinders, so that design calculations might become more realistic,

so that greater safety might be achieved and so that the materials of construction might be utilized and operated under the most favourable and economic conditions.

It was with these aims in mind that the United Kingdom Atomic Energy Authority decided in 1966 to commission the work described in this thesis.

Attention was focused on the perforated end slabs of the pressure vessels in order to ascertain to what extent creep and shrinkage within the concrete ligaments were affecting the effective prestress within the perforated zone. This prestress is applied externally at the periphery of the end slabs and concern was felt at the possibility of serious losses occurring in the ligaments as a consequence of time-dependent deformations. Different stiffnesses in the perforated zone and the solid outer annulus would also affect the stresses at the interface.

To this end, it was hoped that a reasonable correlation could be established between experimental observations of total strains in the ligaments and the values of these strains forecast by a suitably-developed theory.

These total strains comprise the algebraic sums of the elastic, thermal, creep and shrinkage strains developing as a result of the temperature and mechanical loading.

SECTION II

THE OBJECTIVES OF THE INVESTIGATION

It has previously been explained that the designers of P.C.P.Vs have, for some time, been turning their attention from the study of whole vessels towards an examination of those critical parts of the vessels about whose detailed behaviour under load least was known and upon whose satisfactory operating performance the integrity of the vessels depends.

The overall performance of the complete vessel has been extensively investigated by the testing of models and by elastic analyses of the finite difference, finite element and dynamic relaxation type. Designs have been carried out both in the elastic range and at the ultimate load stage.

To do this, simplifying assumptions have had to be made about the geometry of the vessels, about stress distributions, about the way in which the various elements of the vessels mutually interacted, about the operating temperatures and mechanical loadings and about the material properties.

In design work hitherto the effects of secondary stresses have not been taken into account in any realistic way, the designers proceeding intuitively on the assumption that relief of localized stresses has been occurring due to micro-cracking and creep.

These assumptions have probably been well-founded but, even so, many factors are at work which have not always been fully considered. These factors comprise inter alia,

(a) the high level of structural redundancy in the vessels,

(b) the effect of cold-worked reinforcement liberally provided in some designs to prevent local structural cracking.

(c) the stiffening effect of local insertions such as the lugged steel liner on the inside face of the vessel, the reinforcement provided by the extensive secondary cooling system pipework near the inside face of the concrete wall and roof, and pipe penetrations and other insertions,

(d) the long-term effect of irradiation,

(e) the effect of unlocated and unknown hot spot temperatures in the concrete in the event of insulation or cooling failure,

(f) the changing behaviour of the concrete at the stages of construction, commissioning and operation,

(g) the considerable degree of three-dimensional restraint provided by the neighbouring concrete mass when any particular section is under review.

Many of these factors have an important influence on local stresses, but may cause only unimportant alterations to the general stress pattern. For example, if the forces acting in the elastic range, on a section of concrete are modified locally by one of the above items, although these modifications of loading may produce considerable changes in local stress, they may have a negligible effect on the stresses at a greater distance from the load source. This is not only due to time-dependent phenomena, but also by virtue of Saint-Venant's principle.

The present investigation has concentrated on very few of the above factors, and has limited itself to one important vessel section. The part of the vessel with which this thesis is concerned is the end slab or charging face slab of the vessel.

The charging face roof slab is undoubtedly one of the most

critical parts of the P.C.P.V. Not only is it perforated with a regular pattern of charging holes over its central portion, but it is also subject to temperature gradients across its thickness which diminish in magnitude along a radius from the centre.

The holes are lined with steel tubes or standpipes as they are called, and both the hotter inside face of the slab and the periphery of the holes through the slab are cooled by an extensive cooling system. The concrete ligaments between holes are reduced in dimension by the inclusion of annular lobes round the steel tube liners in order to provide this cooling. There is thus little room, in this position, to insert either prestressing ducts or cold-worked reinforcement and the slabs are commonly prestressed only by circumferential cables placed around their periphery.

It is not surprising therefore that one of the major pre-occupations of designers has been with the possibility of a "plug" of the slab being punched upwards under the influence of the bending forces and shears caused by the internal gas pressure.

Loss of prestress at the interface between the perforated zone and the outer solid annulus of concrete in the slab or within the ligaments would accentuate the danger of a "plug" of concrete being punched out.

Several factors might influence the prestress pattern in the slab. Relaxation of steel stress by creep in the concrete is an obvious cause for concern. The magnitude of stress at the interface of the perforated zone and the solid concrete would also be affected by the relative stiffnesses of the two zones. The stiffnesses are a function of the slab geometry, in particular the hole diameter,

the pitch of holes and the liner thickness. Moreover at all levels of loading, temperature and age, the concrete constants affecting structural behaviour are changing.

One of the more important subsidiary investigations in this present study has been to evaluate most of these constants, under the required varying conditions, on control specimens, for the particular concrete mix used. Certain other constants, for example, Young's Modulus, have been measured on the actual models themselves.

As a consequence of these considerations, the objectives of this investigation may be listed as follows:

i) to measure or calculate the strains in the perforated zone and outside it, for the end slabs to P.C.P.V.; these strains would be (a) the total strains and (b) the separate elastic, thermal, creep and shrinkage strains which together make up the total strains in the composite specimen when subjected to external load and temperature; enough specimens were cast to enable the above strain components to be quantified separately.

ii) to assess by measurement and calculation as a result of experimental observations, the internal distribution of load at the boundary between the perforated zone and the outer unperforated zone.

iii) to arrive at by measurement and calculation the internal distribution of load between the standpipe liners and the concrete in the ligaments within the perforated zone.

iv) to assess the notional material properties for an equivalent, homogeneous, but hypothetical material which could replace the perforated zone and behave as the

perforated zone under operating conditions, i.e. a notional material having an elastic response equivalent to that of the perforated region.

v) to evaluate on the models or on other control specimens those concrete parameters affecting the response with time of the material to stress and temperature, e.g. compressive strength, tensile strength, Young's Modulus, the coefficient of thermal expansion, the specific creep and the shrinkage.

vi) to gain an understanding (a) of the effect of varying the relative elastic stiffness between the perforated zone and the outer zone; two series of models were tested each series having a different standpipe thickness in those models which were perforated and (b) of the modifying action of creep and shrinkage on the magnitude of the effective prestress within the slab; loss of prestress could lead to cracking of the end slab as tensions develop on unloading.

vii) to develop a method of analysis for the composite slab which would successfully predict its response under externally applied loading and uniform temperature and which would therefore take into account time-dependent and thermal effects.

The following text starts by describing the models, equipment and experimental procedures and later presents the experimental results. A literature survey is made relating to the elastic constants of concrete and its creep and shrinkage properties.

Finally existing elastic and time-dependent methods of analysis are reviewed, a viscoelastic method is presented, observed and predicted results correlated and conclusions drawn.

SECTION III

THE MODELS

The geometry of the models tested is shown in Fig. 6. They were not constructed to any particular reduced scale nor were they precisely related to any particular prototype. They were representative, however, in a general sense, of the arrangement of the top slabs of reactor vessels, in which the penetrations are lined with steel tubes and form a rectangular or triangular lattice over the central zone of the end cap charging face. Similarly, outside the perforated zone, a solid annulus of concrete was arranged as in typical full-scale structures.

The actual dimensions of the models were such as to allow significant measurable strains to be developed over the gauge lengths and under the imposed loadings chosen for the tests. The thickness of the models was sufficient to prevent curvature under the radial compression. Strain readings on each of the faces of the models, in corresponding positions, were observed and averaged, and this also circumvented inaccuracies due to any in-plane curvature of the slabs.

All the important interfaces, discontinuities and stress-concentrating ligaments were introduced in approximately the correct geometrical ratios, and the materials used correspond to those likely to be utilized in practice.

Although absolute symmetry was not provided in the layout of the twelve standpipe tube penetrations, the area covered by the group of perforations was large enough to achieve symmetry within the central part of the perforated zone, and thus to permit repeat readings in the appropriate corresponding ligaments in each face.

Two series each of five specimens.

Model 7-8

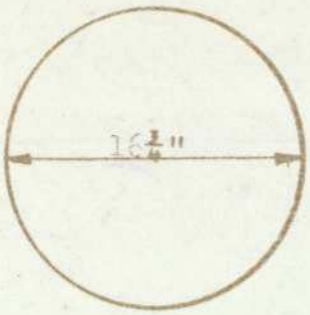
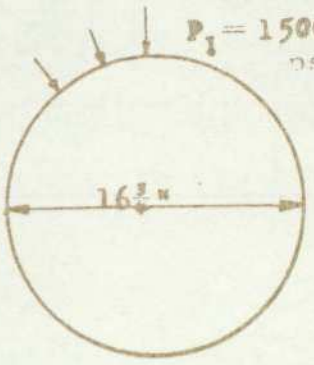


Fig. (a)

Model 1-2

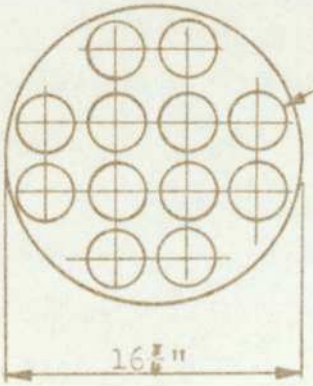


Creep & Shrinkage Specimen

Fig. (b)

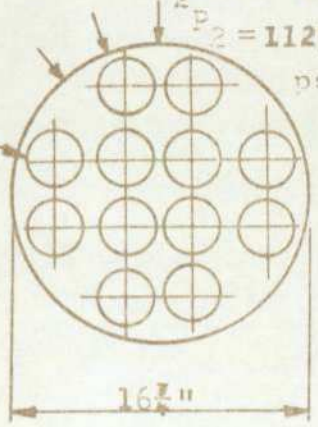
Shrinkage Specimen

Model 5-6



Shrinkage Specimen

Fig. (c)

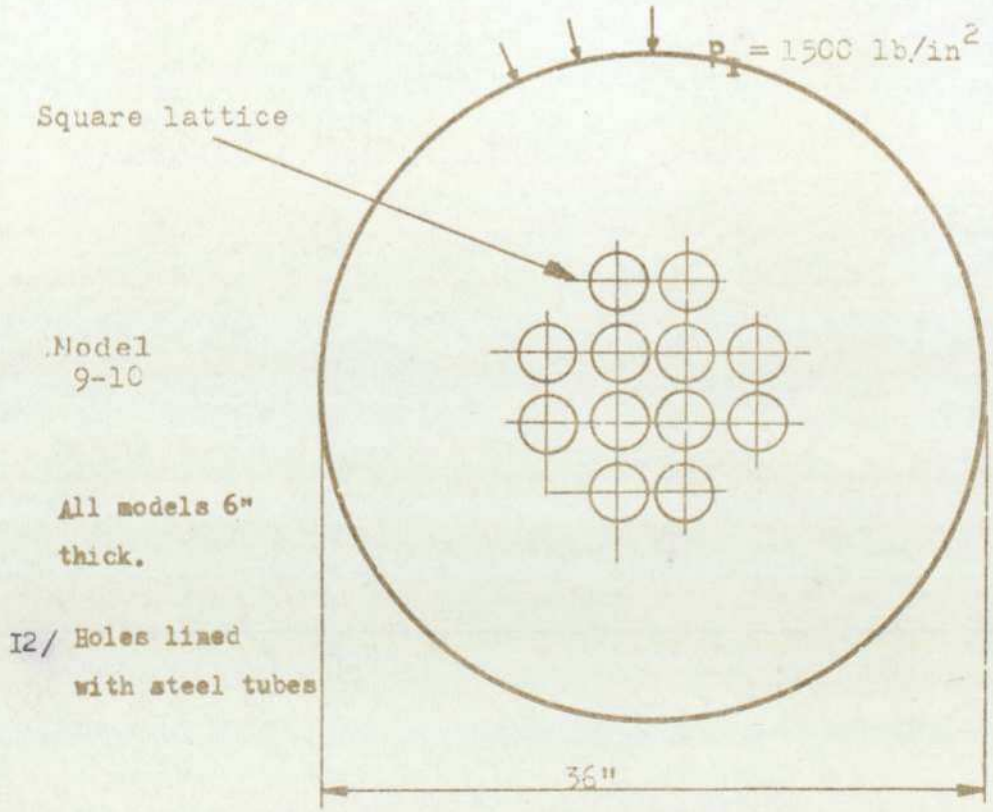


Model 3-4

Liner Tubes.
Series I. I/16" tn.
Series 2. 1/4" tn.

Creep & Shrinkage Specimen

Fig. (d)



Model 9-10

All models 6" thick.

12/ Holes lined with steel tubes

Fig. (e)

FIG. 6.

Since one of the main objectives of this investigation was to devise a general method of analysis for end slabs rather than to check, for one particular prototype geometry, the suitability of an already existing analytical procedure, some freedom of choice existed for the slab arrangement. It is considered, therefore, that the geometry tested was sufficiently representative of the general form of end slabs likely to be adopted in practice.

Two series of model slabs were tested each series consisting of five specimens. The only difference between the two series lay in the wall thickness of the standpipe tube liners.

Of the five slabs in a series only one, larger in size than the others, contained both the perforated central zone and the solid outer annulus. The other four were, in effect, control slabs, in so far as they were intended to permit the numerical breakdown of the total strain observed in the large specimen into its separate components of elastic, thermal, creep and shrinkage strains.

These four slabs were identical in dimensions to the perforated zone of the large slab. Two of them were of solid concrete and two of them were perforated in exactly the pattern of the perforated zone of the large slab.

Of the two solid slabs, one was allowed only to shrink whilst the other was radially compressed and thus exhibited both shrinkage and creep. It was thus possible to separate the creep and shrinkage strains in the concrete assuming that the two slabs had shrunk equally. Similarly, of the two small perforated slabs, one was allowed to shrink and the other under loading gave shrinkage and creep strains. Again the creep and shrinkage strains could be

separated, this time giving information about the perforated concrete only. Note also that the difference between readings before and immediately after loading gave values of elastic strain directly for the solid and perforated concrete.

On applying an elevated temperature (80°C) to the two pairs of small slabs, the magnitudes of thermal creep and shrinkage could be separately evaluated for the solid and perforated concrete.

The four small control slabs thus provided all the data required in the subsequent interpretation and evaluation of the main results obtained from the large specimen, (referred to subsequently as the composite specimen slab).

As will be seen from the testing programme, mechanical and thermal loading, applied and removed over a period of time, revealed the required components of strain at various ages of the concrete specimens.

SECTION IV

THE TESTING PROGRAMME

A graphical indication of the sequence of the testing programmes is shown in Figs.7 and 8.

Since the testing programmes allowed for the simultaneous rim loading of the large composite specimen, and one solid, and one perforated small specimen, and also allowed for the unloaded shrinkage of the other small solid and perforated specimens, it became possible to obtain the values of all the separate strain-causing effects i.e. the elastic, the creep and the shrinkage effects of all the specimens.

In addition, at the heating stage of the programme, the thermal expansions caused by the uniform temperature of 80°C which was applied to all five specimens in a series, could be measured experimentally.

Thus it was possible, by simple subtraction to obtain the necessary creep data for all specimens. These creep data were plotted in the form of specific creep curves. Specific creep data thus became available, in fact, for both solid and perforated concrete areas, for ambient and elevated temperature and at any age of the concrete.

Load cycling was carried out, at the start of the programme and at each change of loading regime, including temperature changes. Thus the various concrete parameters required in the subsequent calculations, became available.

Control tests on specimens, other than the main five were carried out to give data on tensile strengths, crushing strengths,E values, and the coefficient of thermal expansion.

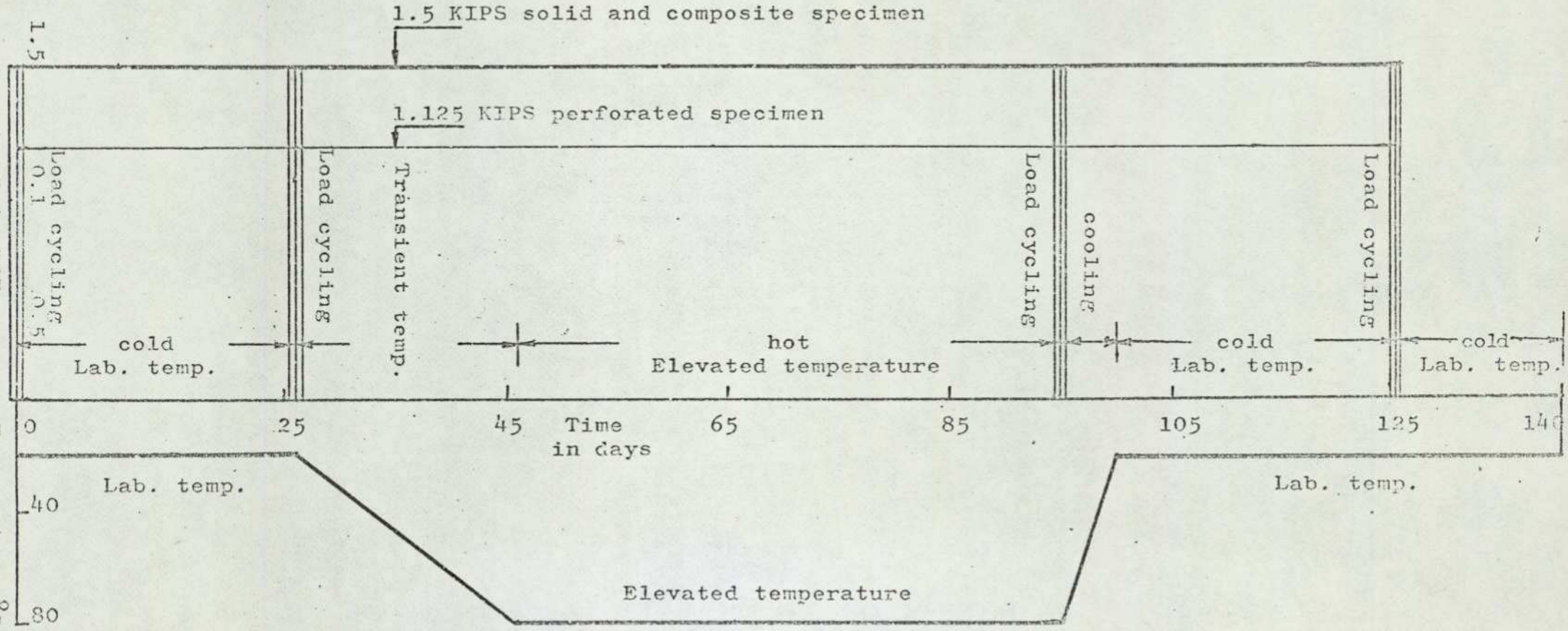


FIG. 7. SERIES 1 TEST PROGRAMME

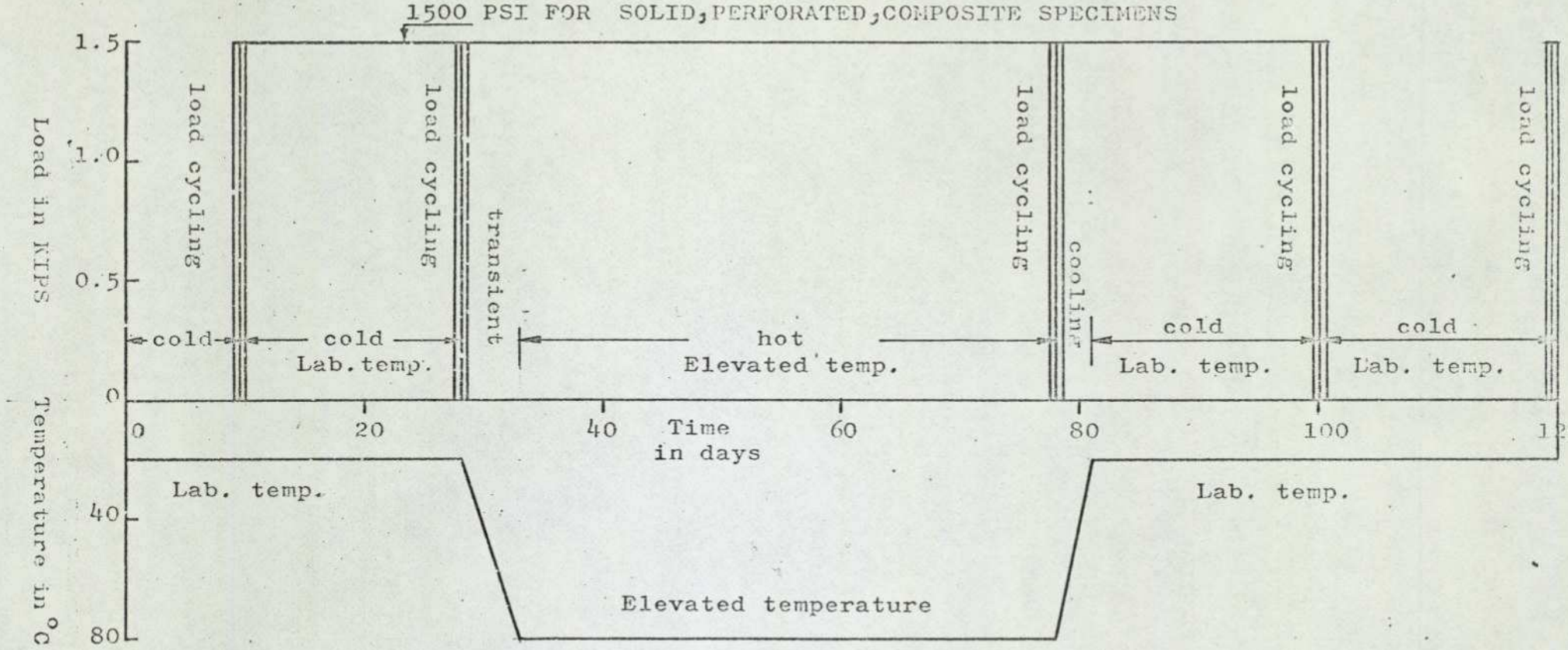


FIG. 8. SERIES 2 TEST PROGRAMME

The sequences of loading and heating in the tests were intended to represent, in a general sense, the procedures followed in initially prestressing, commissioning and operating an actual reactor vessel.

The initial ambient rim loading corresponds to the stage of construction at which the peripheral prestress is applied to the slab before the reactor has become critical. The thermal loading phase of the test occupies the longest individual period in the middle of the programme and is equivalent to the commissioning or operational condition when the end cap is both hot and prestressed.

When the heat is removed from the specimens, simulation of reactor shut down is achieved under the operating condition in which prestress is still acting as the slab cools down.

Each loading phase of the test programme was arranged to be of such a length and the frequency of readings was chosen, so that recognisable trends, under stress and temperature were achieved and recorded in the specimens. Thus the concrete had sufficient time to exhibit adequately the behaviour resulting from each loading condition. The number and frequency of readings was such that clear trends were displayed in the plotted curves even though an observational error or variation might be present in any one reading.

SECTION V

DETAILS OF EQUIPMENT

1. The Specimens

Two series of concrete slab specimens were cast, each series consisting of five specimens.

The only difference between the two series lay in the thickness of the steel liners to the standpipe holes. The three perforated specimens in series 1 had $\frac{1}{16}$" (1.570 mm) liner tubes whilst the three in series 2 had $\frac{1}{4}$" (6.35 mm) thick liner tubes.

The five specimens comprising a series were as follows:

1 composite 36" ($\triangleq$ .915 mm) diameter, 6" (152 mm) thick concrete bi-axial creep and shrinkage specimen having a perforated central zone and an annular unperforated outer zone: Sides 9/10.

1 solid $16\frac{3}{4}$" (425 mm) diameter, 6" (152 mm) thick concrete shrinkage specimen: Sides 7/8

1 solid $16\frac{3}{4}$" (425 mm) diameter, 6" (152 mm) thick concrete bi-axial creep and shrinkage specimen: Sides 1/2

1 perforated $16\frac{3}{4}$" (425 mm) diameter, 6" (152 mm) thick concrete shrinkage specimen: Sides 5/6

1 perforated $16\frac{3}{4}$" (425 mm) diameter, 6" (152 mm) thick concrete bi-axial creep and shrinkage specimen: Sides 3/4.

All specimens contained cross members of hexagonal section, $\frac{1}{4}$" (6.35 mm) across the flats and tapped and threaded in each end. These members were cast into the concrete normal to the plane circular faces and were 6" (152 mm) long. 1" (25.4 mm) long hexagonal brass studs were subsequently screwed into the two ends of the cross members.

The brass studs thus projected clear from the concrete face and their ends were indented with Demec centering holes.

The patterns of standpipe tubes and Demec gauge points were as shown in Figs. 9, 10 and 11.

The brass studs were arranged to form 2" (50.8 mm) and 11.438" (290.5 mm) Demec gauge lengths as shown. These large gauge lengths represented three standpipe pitches.

Before concreting, a series of thermo-couples were positioned in the ligaments and elsewhere according to the arrangements shown in Figs. 12 and 13.

In the case of the specimens containing standpipes, the thermo-couples were introduced down the standpipe tubes and entered the concrete ligaments via mid-depth holes in the tube walls. In the solid specimens, the thermo-couples were merely pushed directly into the stiffening concrete at the required positions.

Nine thermo-couples were cast into each of the $16\frac{3}{4}$" (425 mm) specimens in an arrangement of three sets of three spaced across the diameter. Of each set of three one thermo-couple was at mid-slab and the other two were arranged each 1" (25.4 mm) from opposing concrete faces.

Twenty one thermo-couples were placed in the 36" ($\simeq$ 915 mm) diameter specimen in an arrangement of seven sets of three. Three of these sets were in positions corresponding to those in the $16\frac{3}{4}$" (425 mm) slabs. The other four sets were arranged with one set in each quadrant in the outer unperforated region.

Two steel thermostat tubes were also cast into each specimen near the ends of a diameter to take thermostat probes.

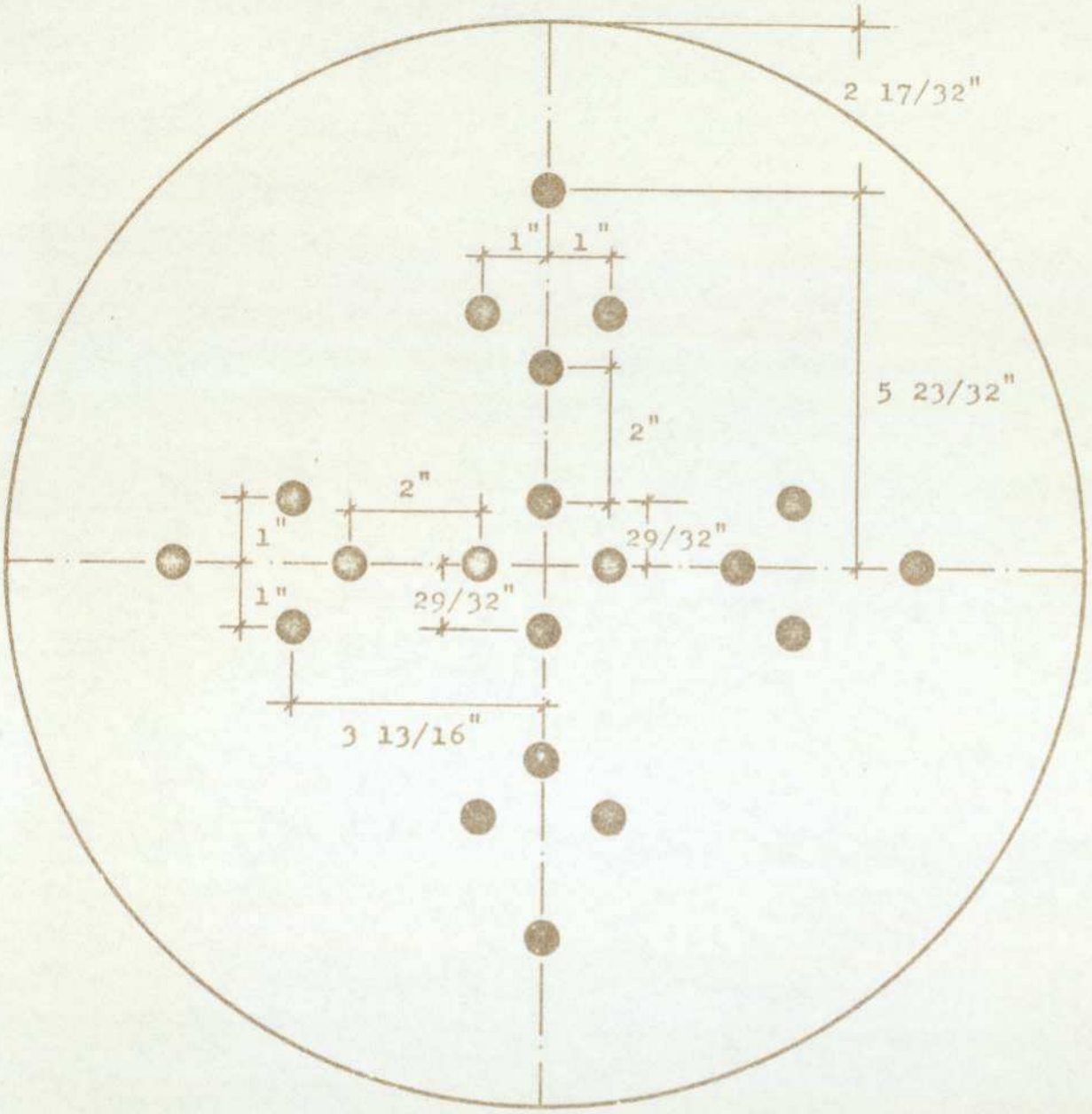


FIG. 9. MODELS 1/2 AND 7/8(SOLID)
TYPICAL ARRANGEMENT OF DEMEC GAUGE POINTS

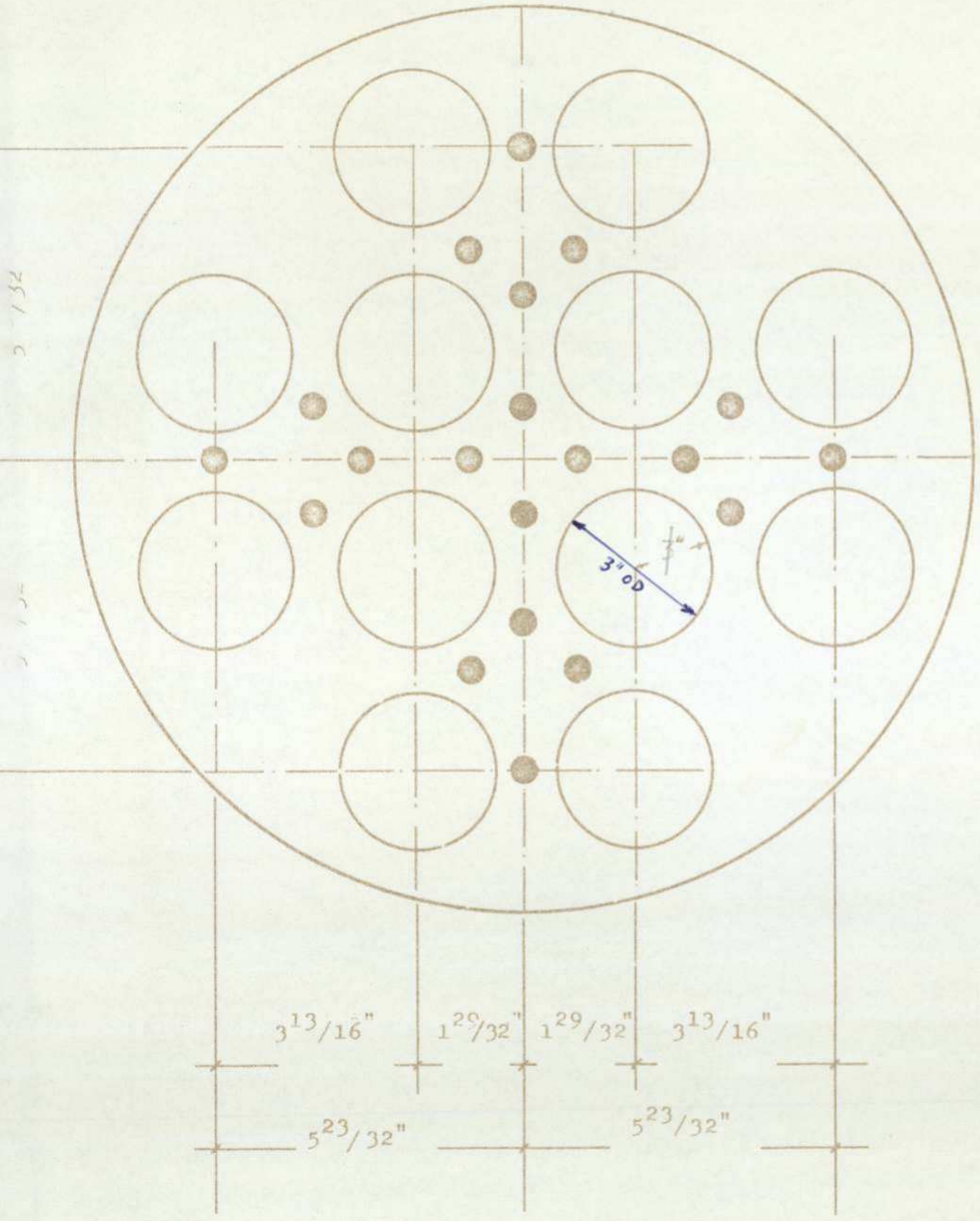


FIG. 10. MODELS 3/4 AND 5/6
TYPICAL ARRANGEMENT OF STANDPIPES
(MODEL 9/10 ARRANGEMENT IDENTICAL)
IN THE CENTRE.

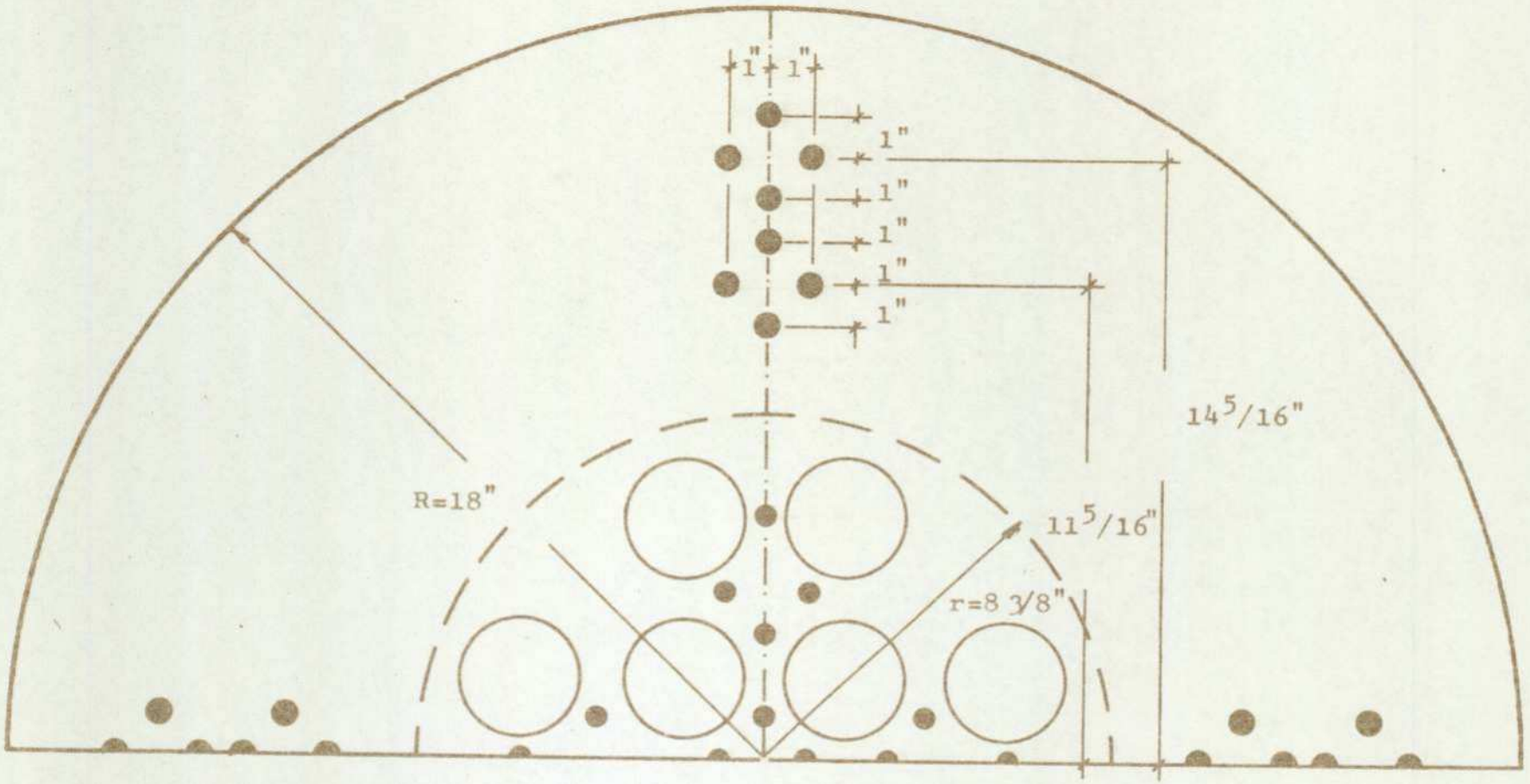
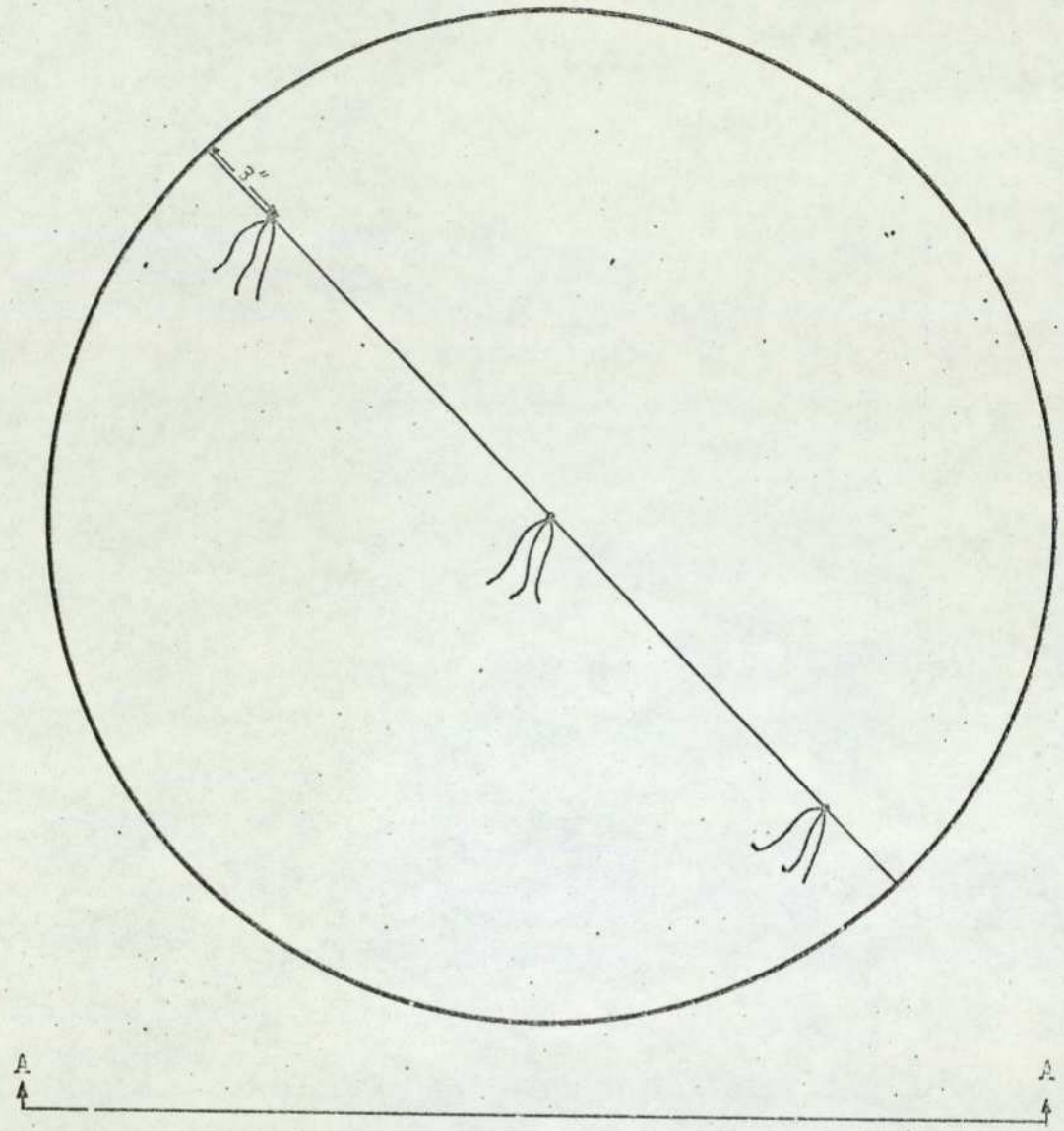


FIG. 11 MODEL 9/10 COMPOSITE
TYPICAL ARRANGEMENT OF DEMEC GAUGE POINTS IN THE ANNULUS

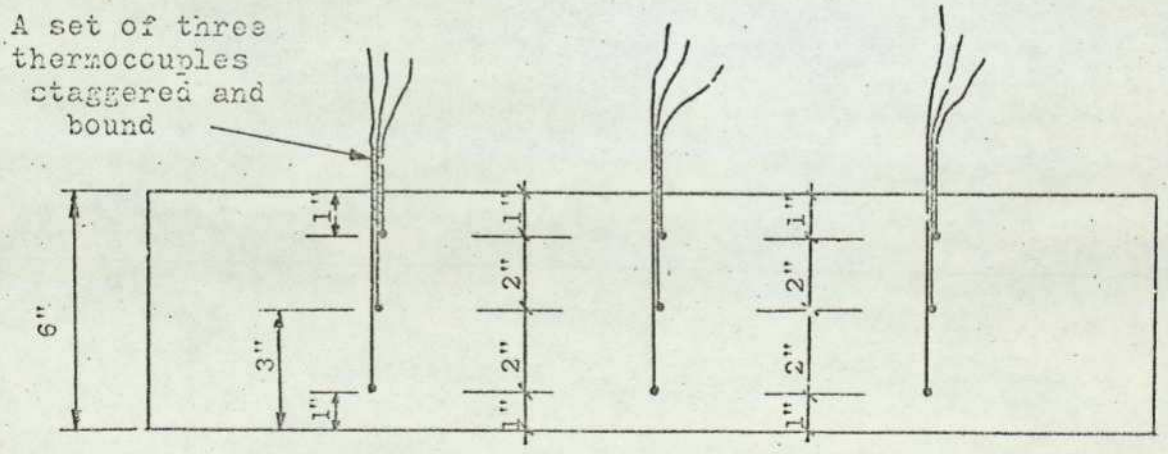
LAYOUT OF THERMOCOUPLES IN THE SOLID SPECIMENS

(MODELS 1/2 AND 7/8)

Nine thermocouples in three sets of three



PLAN

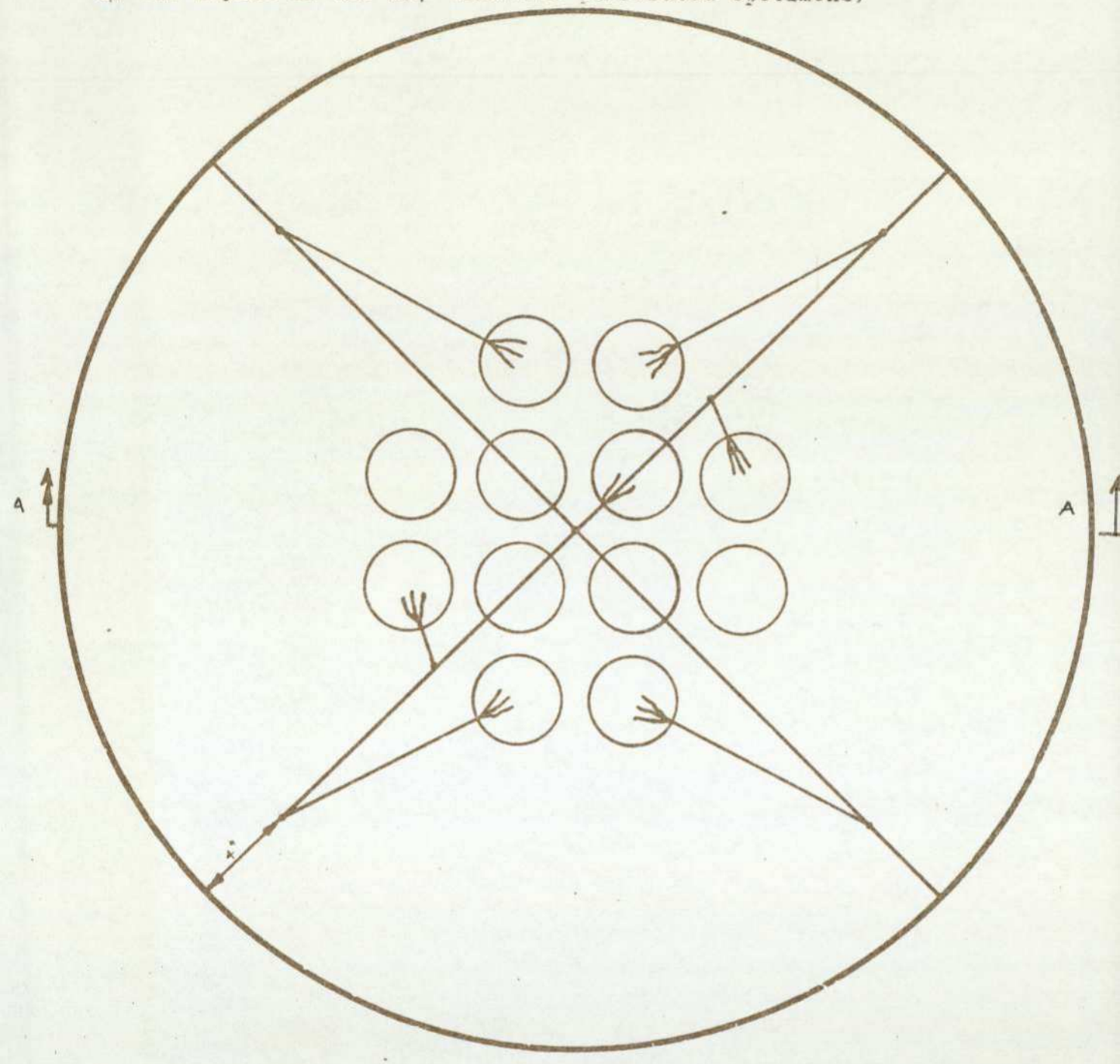


VIEW ON A-A

FIG. 12

LAYOUT OF THE THERMOCOUPLES IN THE 36" DIAMETER COMPOSITE SPECIMEN

(The layout of the thermocouples in the perforated zone is typical of the layout in the 16½" diameter perforated specimens)



Twenty-one thermocouples in seven sets of three

PLAN

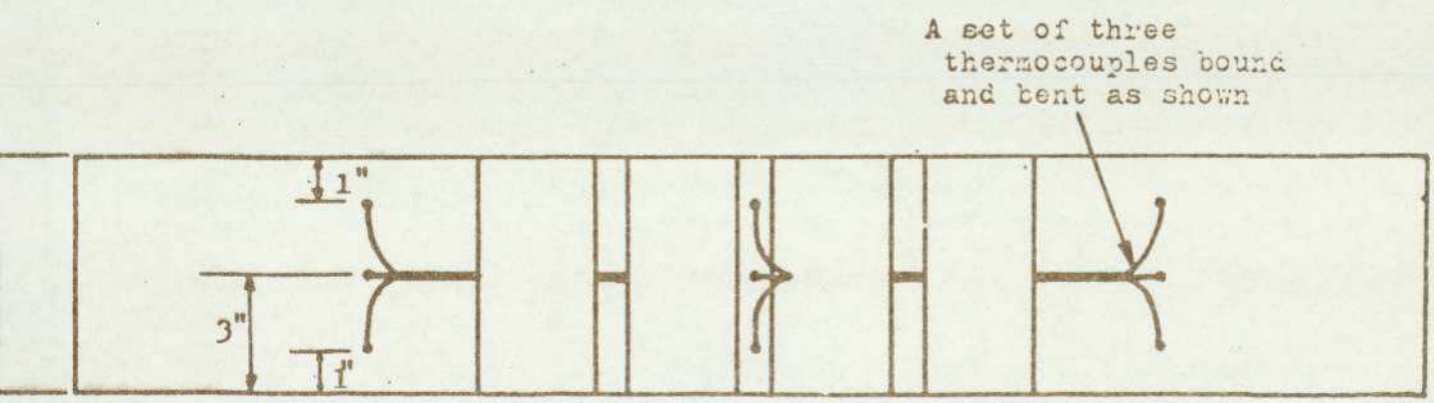


FIG. 13 -- VIEW ON A-A

The concrete specimens were each painted on their rim surfaces with three coats of thixotropic paint after curing to inhibit shrinkage and water loss in the radial direction.

2. The Concrete Mix

A concrete was required having a strength of the order of 6000 p.s.i. (40 N/mm^2) at 28 days. A workability corresponding to a slump of approximately 3" (75 mm) was considered appropriate. This would be suitable for vibrational methods of compaction and would provide good mobility.

The creep, shrinkage and thermal properties of the proposed concrete were of interest and should be those of normal concretes in use in pressure vessel construction.

Thames Valley gravel was available locally and was representative of typical economic aggregates.

The mix design was carried out on the basis of the paper by Erntroy and Shacklock (117) and Road Note No. 4. The cement, supplied by the Cement Marketing Company Limited, from their Kent works, was limited in the mix, since it was considered appropriate to prevent excessively high creep and shrinkage rates. The aggregate/cement ratio was kept above 3.0.

The sand content of the mix was kept to the order of 25% to 30% by weight of the total aggregate.

The maximum size of aggregate was $\frac{3}{8}$" (9.5 mm) and was designed to facilitate the flow of fresh concrete into the forms and between the ligaments. To achieve good workability, a larger size would have been preferable.

The grading of the aggregates which were classified as irregular, was as follows:

	Percentage Passing						
	$\frac{3}{8}$"	$\frac{3}{16}$"	No7	No14	No25	No52	No100
			B. S. Sieves				
$\frac{3}{8}$" - $\frac{3}{16}$" Thames Valley gravel	99	2	0	0	0	0	0
Sand* $\frac{3}{16}$" - B.S.Sieve 100	100	100	91	75	54	13	2

* Zone 2 sand B.S. 882 : 1954

Trial mixes were made of the following proportions:

Trial Mix	Agg/cement ratio by wt	Sand %:wt	Vol.fraction Coarse Agg,%	Water/cement ratio	
				Total	Effective
C1	4.0	25	49	0.55	0.48
C2	3.75	30	44	0.564	0.50

The workability and strength of these mixes were as follows:

Trial Mix	Slump ins	Compacting factor	Cube strength (p.s.i.)		
			7 days	14 days	28 days
C1	3"	0.980	5480, 5400 } 5440	6130, 6500 } 6315	7250, 7300 } 7275
C2	3.5"	0.955	4760, 4560 } 4660	5550, 5580 } 5565	6650, 6720 } 6685

Dummy specimens were cast from these two mixes and subsequently they were broken and examined.

As a result of the workability, strength and casting tests and as a result of the visual examination mix C2 was chosen.

The volume of concrete in the five specimens was such that the 150 litre Eirich counter flow pan mixer was required to mix three

batches each of approximately 3 cubic feet (0.085 m^3) to cast all the specimens at one time.

The coarse aggregate, sand and cement were added to the mixer simultaneously followed by the metered water. Mixing continued for 10 minutes.

The quantities of materials used for each batch were, by weight:

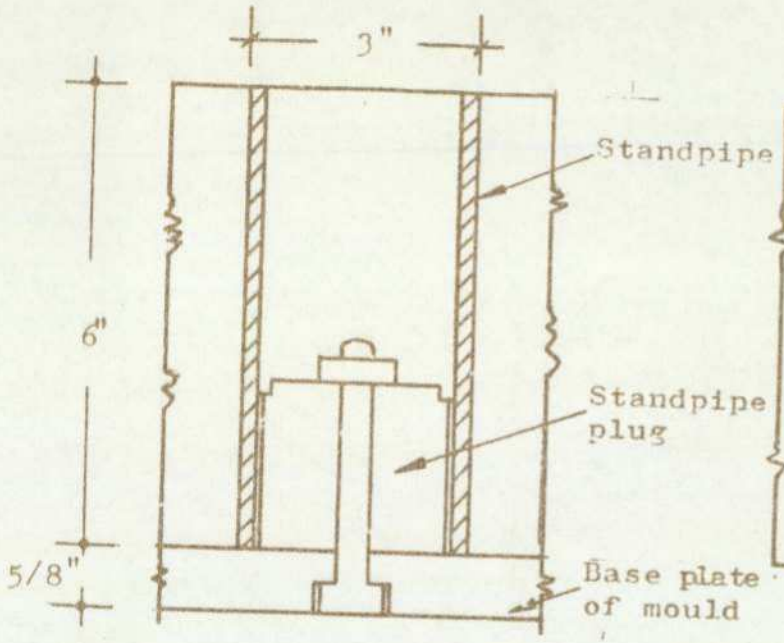
Sand $\frac{3}{16}$" to No. 25 sieve	31.5 Kgs
Sand No.25 to No. 100 sieve	13.5 Kgs
Coarse Aggregate $\frac{3}{8}$" - $\frac{3}{16}$"	105.0 Kgs
Cement	40.0 Kgs
Water	22.5 Kgs

3. Steel Moulds and Cruciform Jig

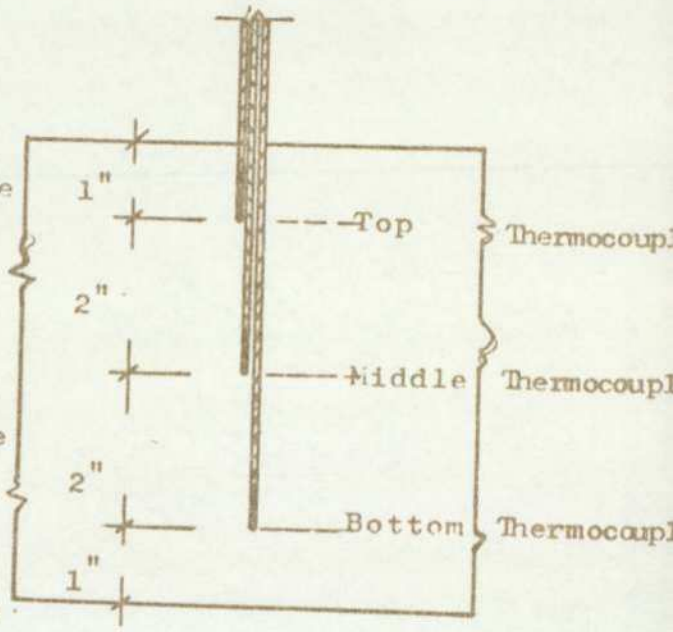
Each mould for the concrete specimens consisted of a machined steel baseplate and semi-circular steel side walls. The walls were bolted together and then bolted down to the baseplate. Four $16\frac{3}{4}$" (425 mm) diameter moulds, and one 36" ($\simeq$ 915 mm) diameter mould were used to cast the five specimens in each series.

The steel standpipe liners for the perforated slabs were located and rigidly fixed to the baseplate at the bottom only, by a tight push-fit over male steel plugs, recessed and secured to the baseplate by countersunk bolts. Twelve standpipes were provided for each of the three perforated slabs. Fixing details are shown in Fig. 14.

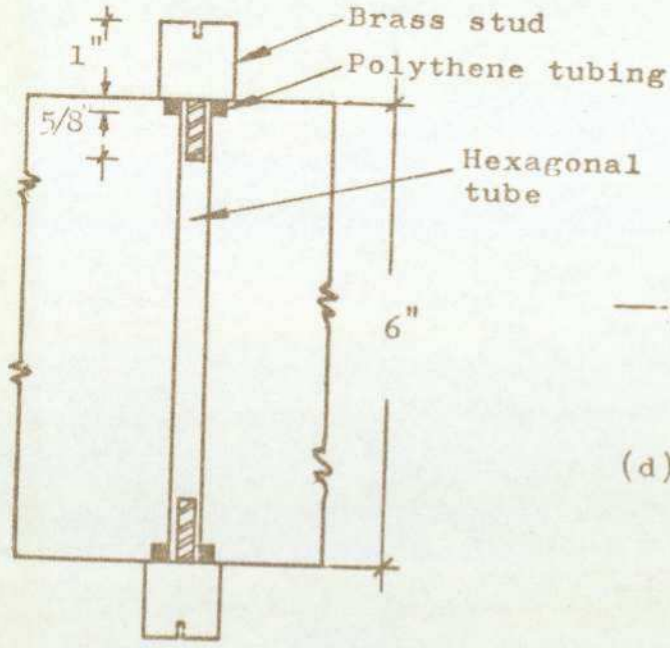
In addition, for all specimens, end-threaded hexagonal bars were bolted to the baseplate. These hexagonals were required to



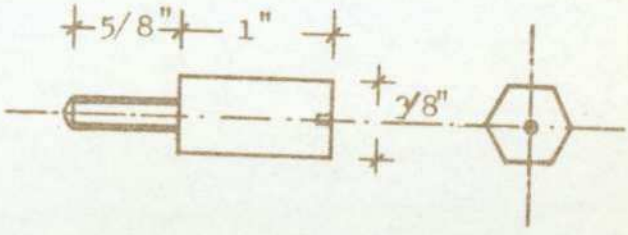
(a) Section through specimen showing standpipe in position.



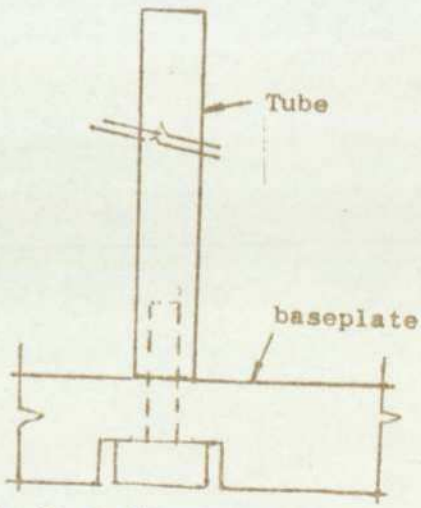
(b) Section through specimen showing positions of thermocouples.



(c) Section through specimen showing arrangement of brass stud and hexagonal bar



(d) Demec gauge brass stud



(e) End threaded tube bolted on the base plate.

FIG. 14.

take the brass studs which were subsequently screwed on to them to provide the Demec reading points. The brass studs were indented in their ends with Demec centering holes.

To ensure accuracy in positioning the Demec points, a cruciform jig was fabricated in the form of a steel template. Conical steel spigots were screwed through the arms of the jig in positions which corresponded with the Demec gauge points.

The jig was used initially for drilling the fixing points of the hexagonals in the baseplate and subsequently for correcting and locating the tops of the hexagonals before and during concreting. The jig could be clamped in a fixed position on top of the steel mould.

4. The Loading Rigs

The layout of a section of a radial loading rig is shown in Figs.15&16 The rig arrangement is also shown in Plate 1 and Fig. 17.

The upper part of the rig consisted of a vertical circular loading arrangement which was removable from its supporting stand.

This upper section consisted essentially of a vertical steel retaining hoop between which and the installed circular concrete specimen within, was confined a stiff neoprene rubber water bag. The bag had an air vent connection at its top, and a water inlet at the bottom, both accessible through the hoop thickness.

As the water bag was inflated from the pressure circuit, it was constrained between the hoop and the specimen, thus applying a radial compression to the concrete.

A VERTICAL SECTION THROUGH 36" DIAMETER SPECIMEN LOADING RIG

(Model 9/10)

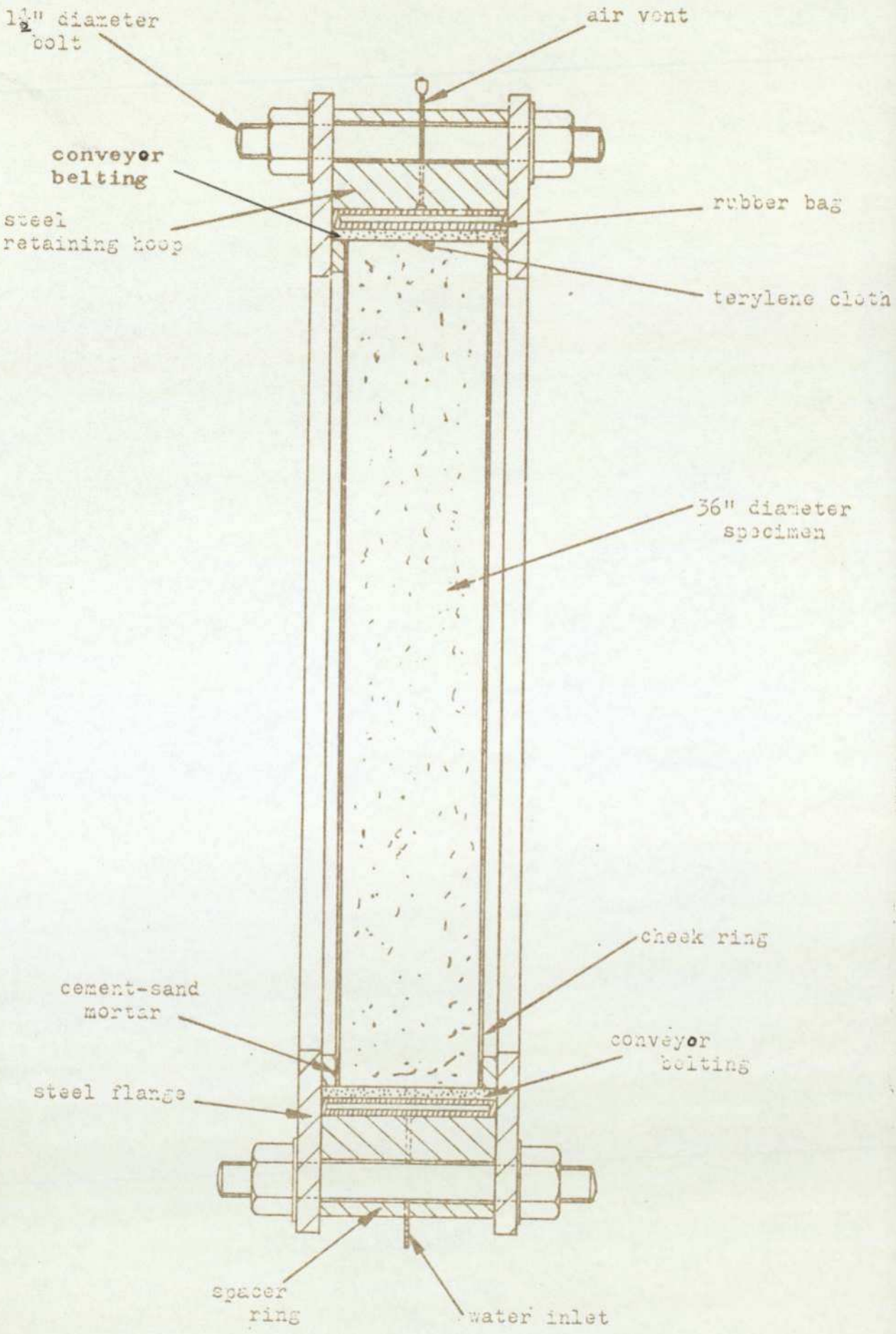
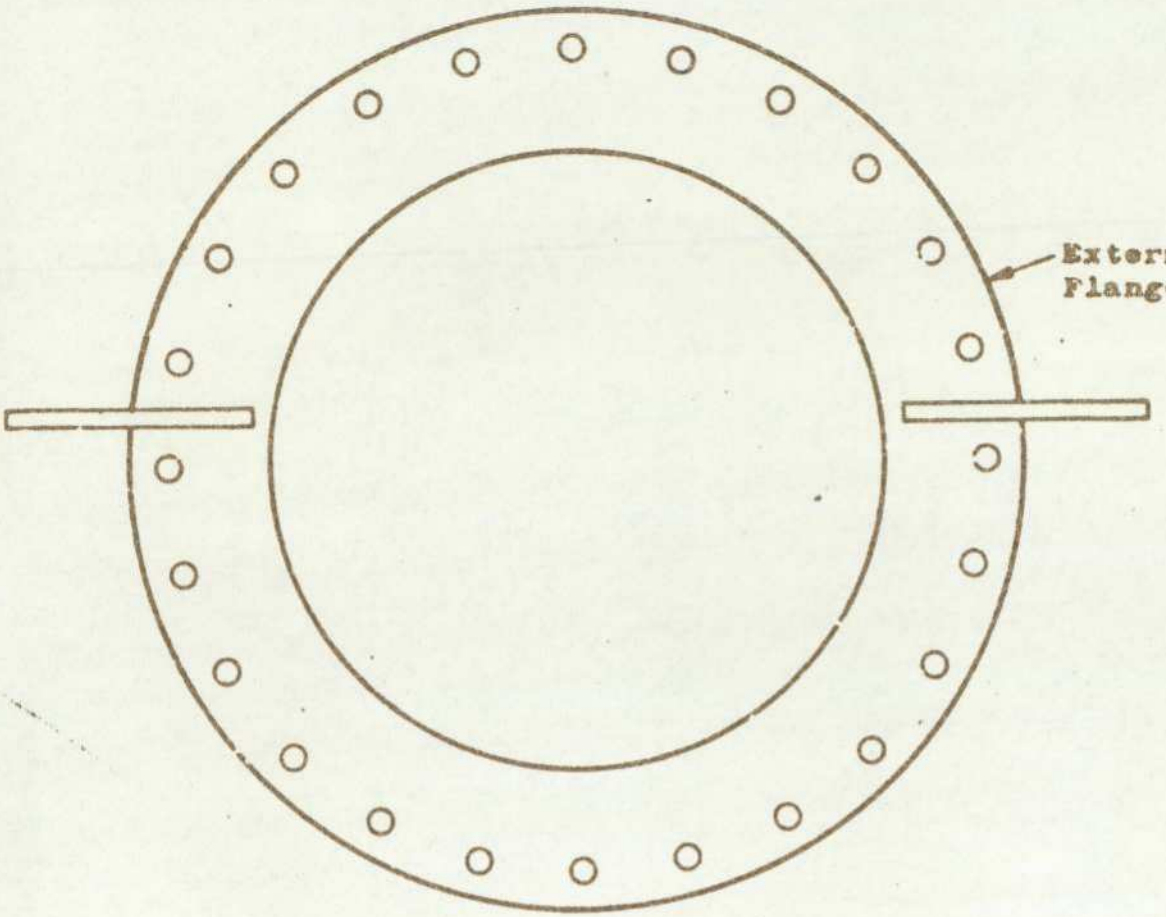
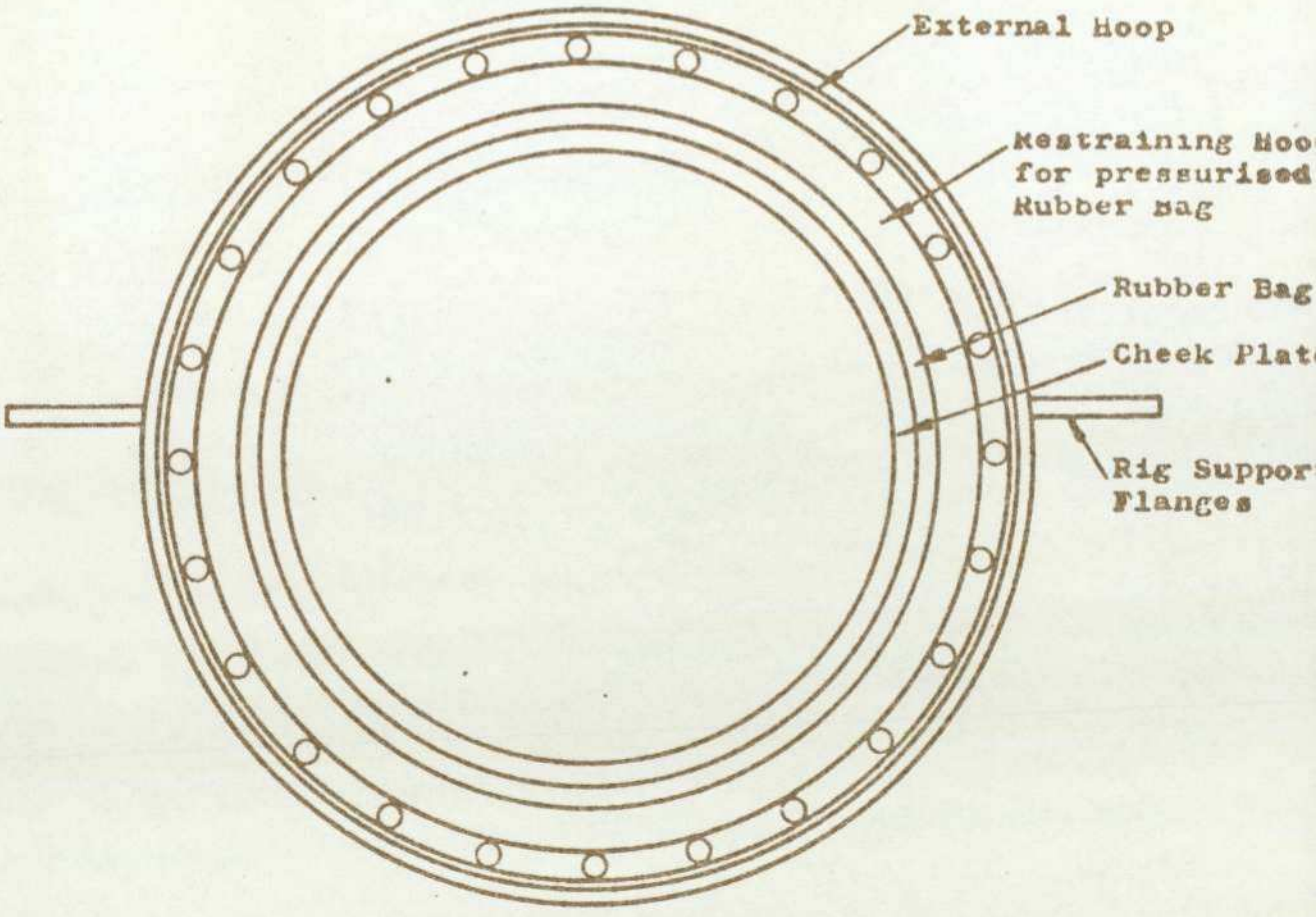


FIG. 15.



(a) VIEW WITH FLANGE PLATE IN POSITION



(b) VIEW WITH FLANGE PLATE REMOVED

FIG. 16. DETAIL OF 36" DIAMETER RIG

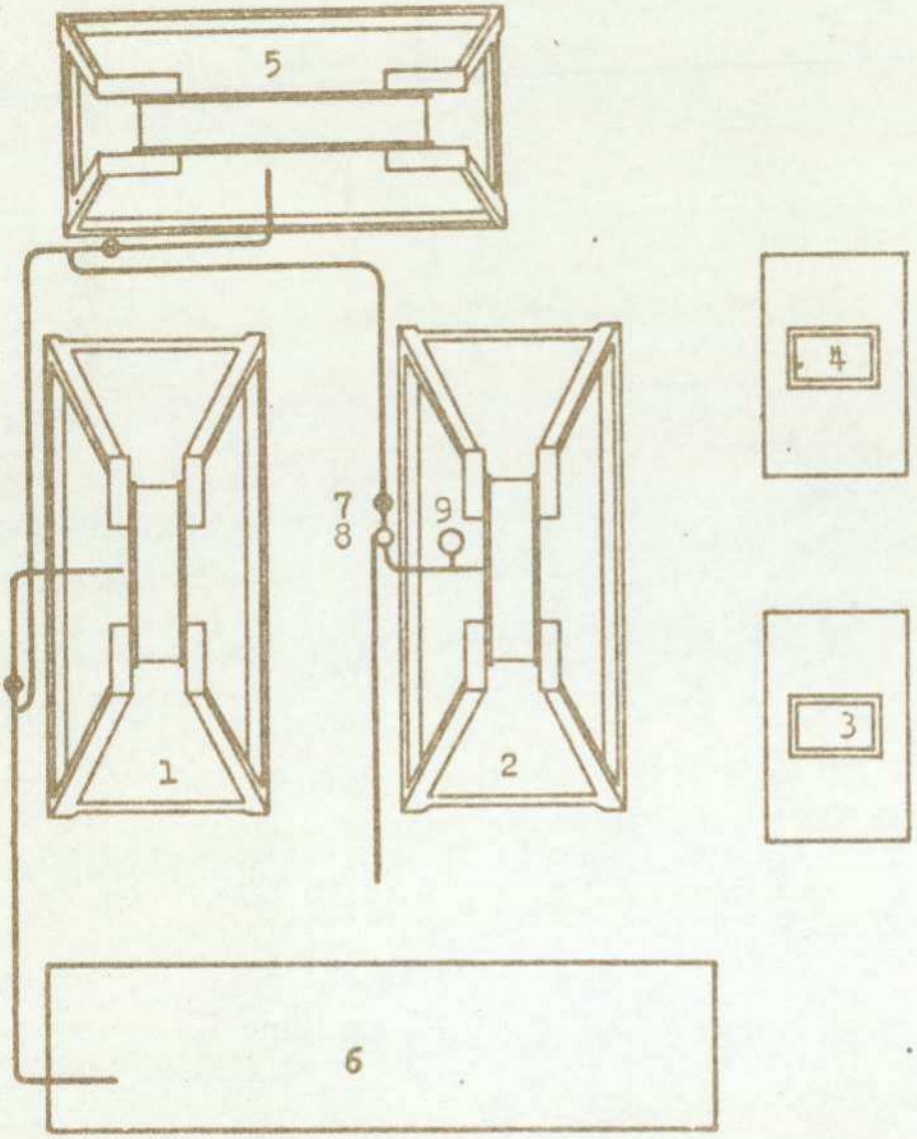


FIG. 17 LAYOUT OF RIGS AND FRAMES

1. Rig for 16 3/4" diameter solid specimen
2. Rig for 16 3/4" diameter perforated specimen
3. Saddle for 16 3/4" diameter perforated specimen
4. Saddle for 16 3/4" diameter solid specimen
5. Rig for 36" diameter composite specimen
6. Table assembly
7. Pressure relief valve
8. Pressure reducing valve
9. Pressure gauge

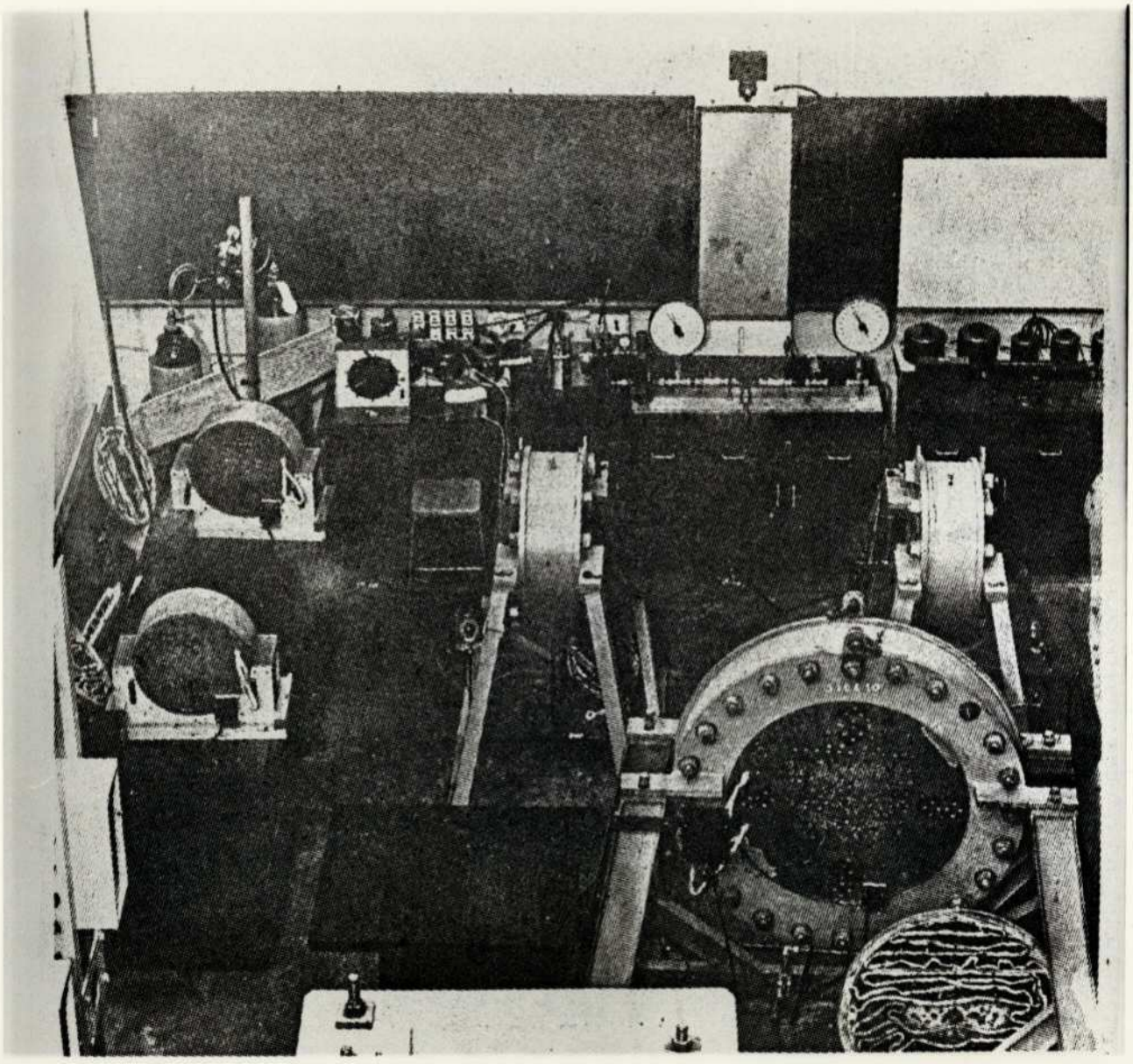


PLATE 1. General Layout of Test Specimens.

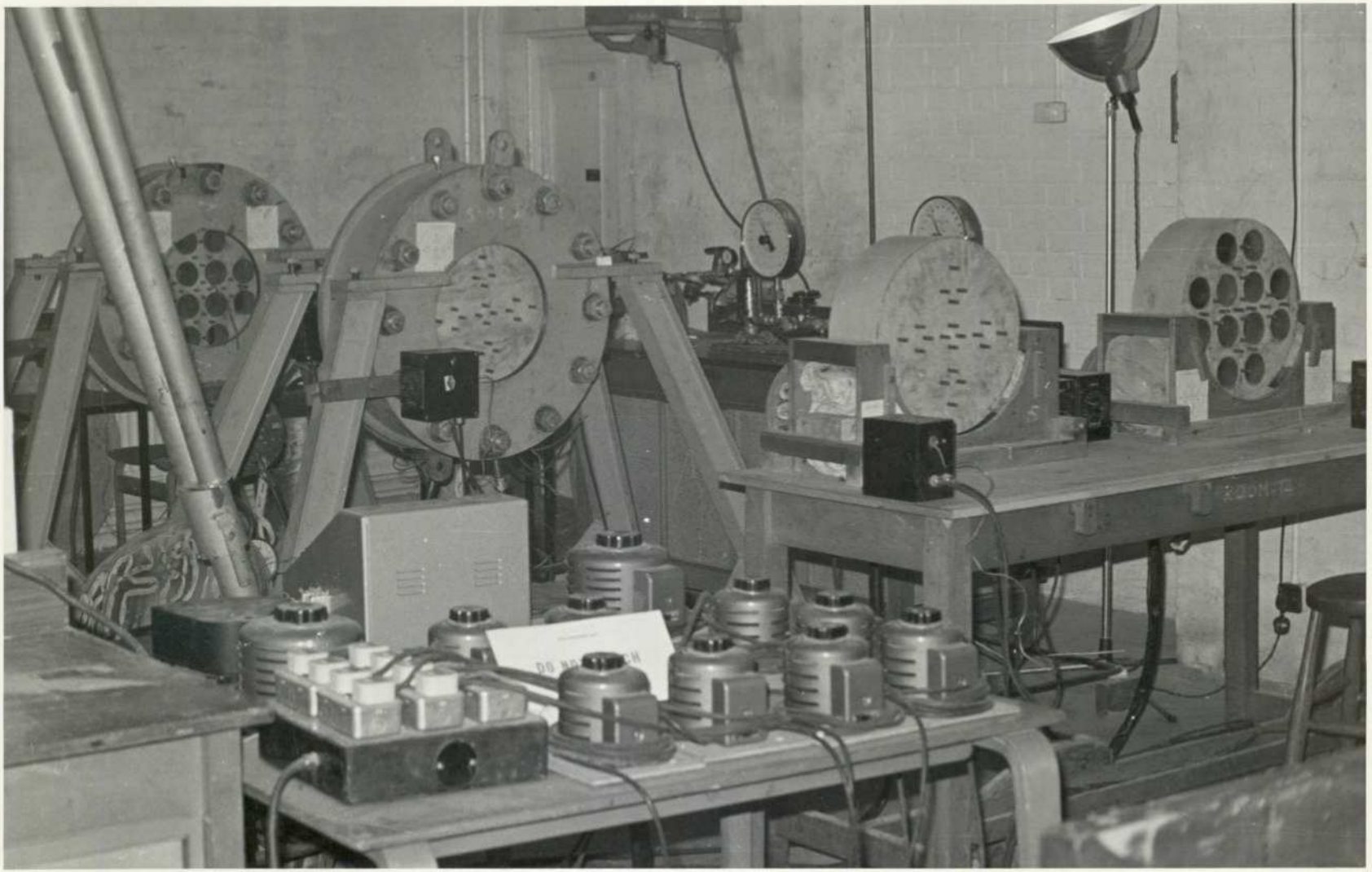


PLATE 2. Layout Showing Sides 1/2, 3/4, 5/6, 7/8 and Air-Hydro Pump.

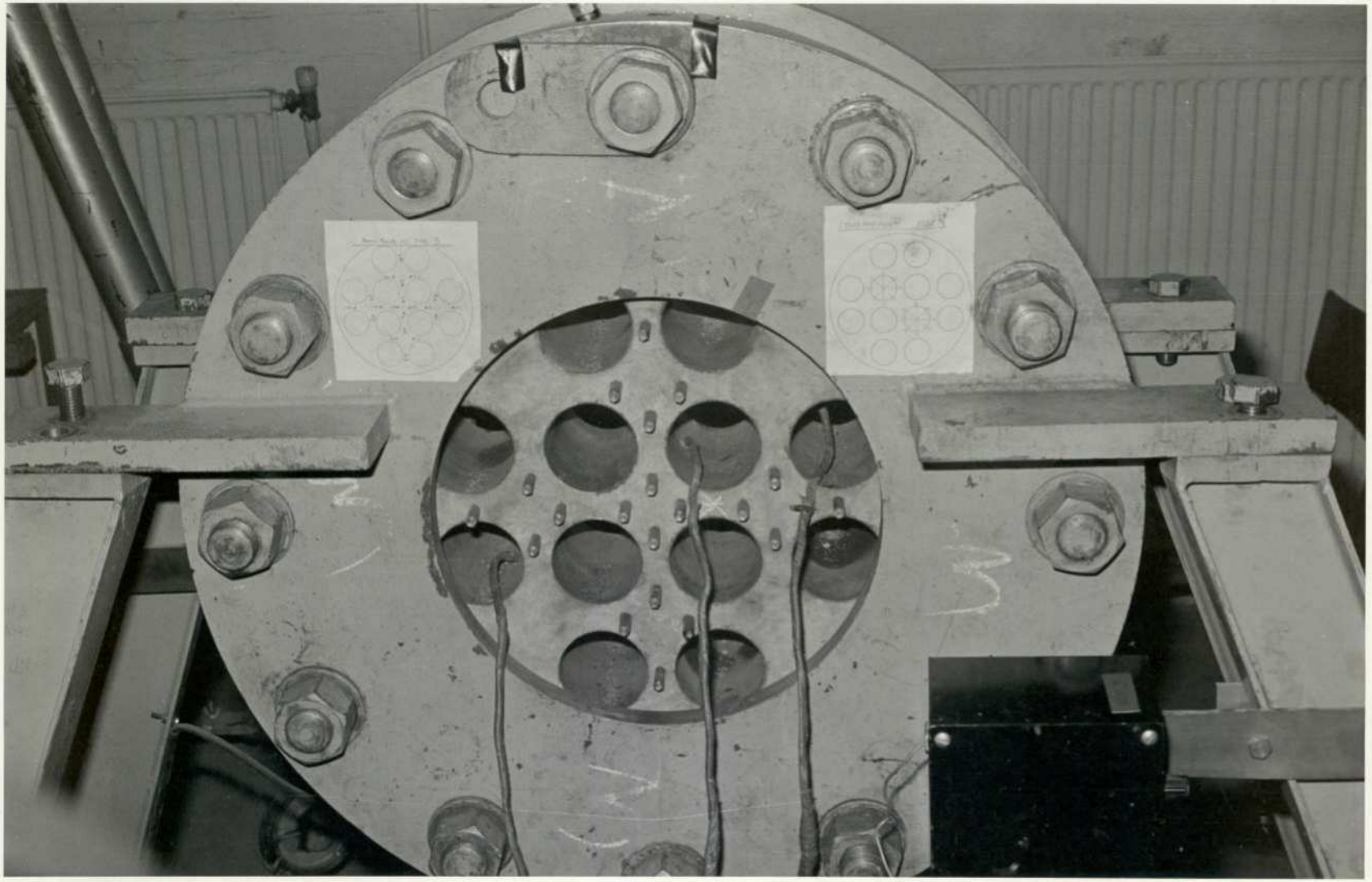


PLATE 3. Model 3/4 with heat shield removed.

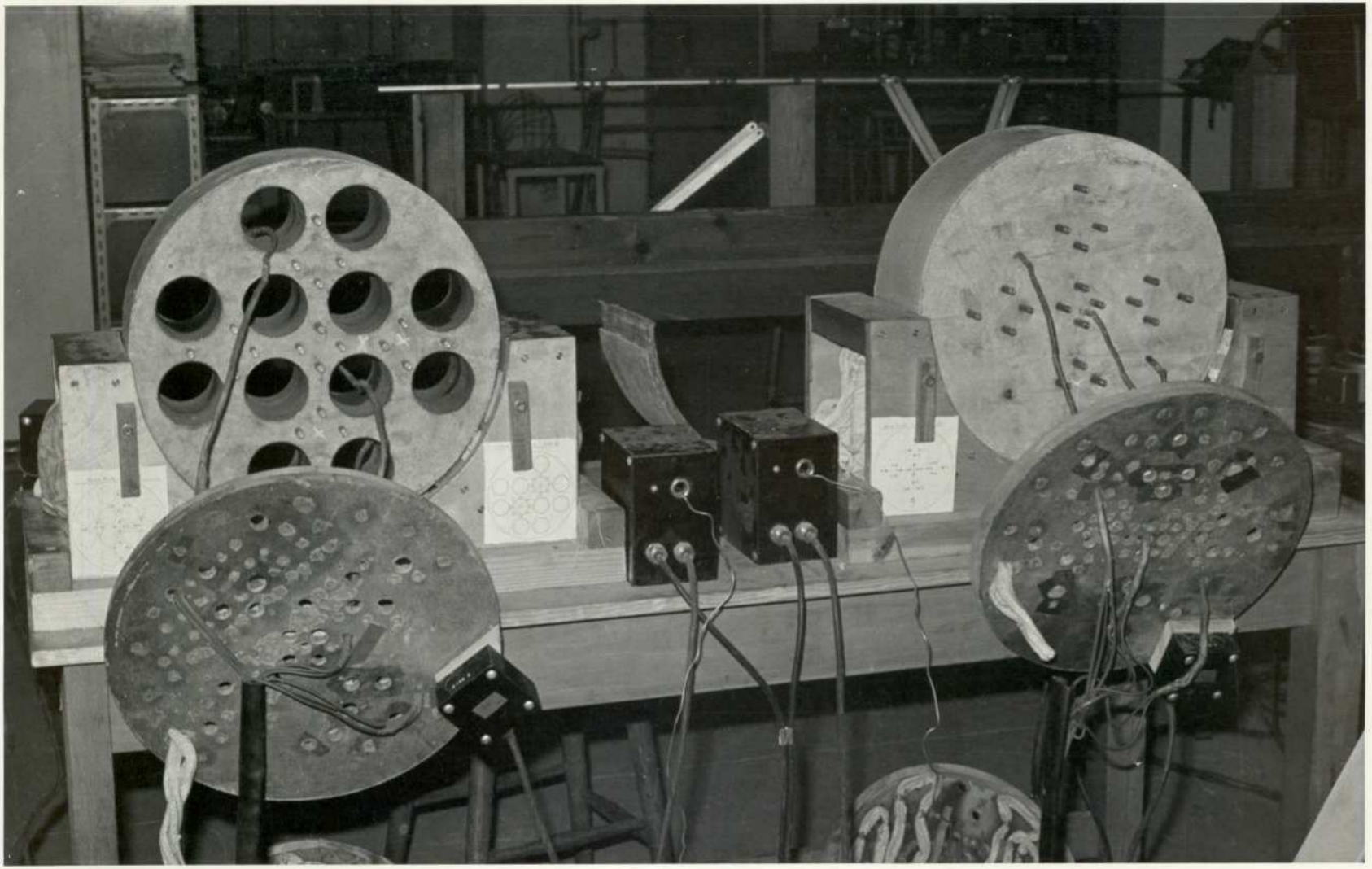


PLATE 4. Models 5/6 and 7/8 with heat shield removed.

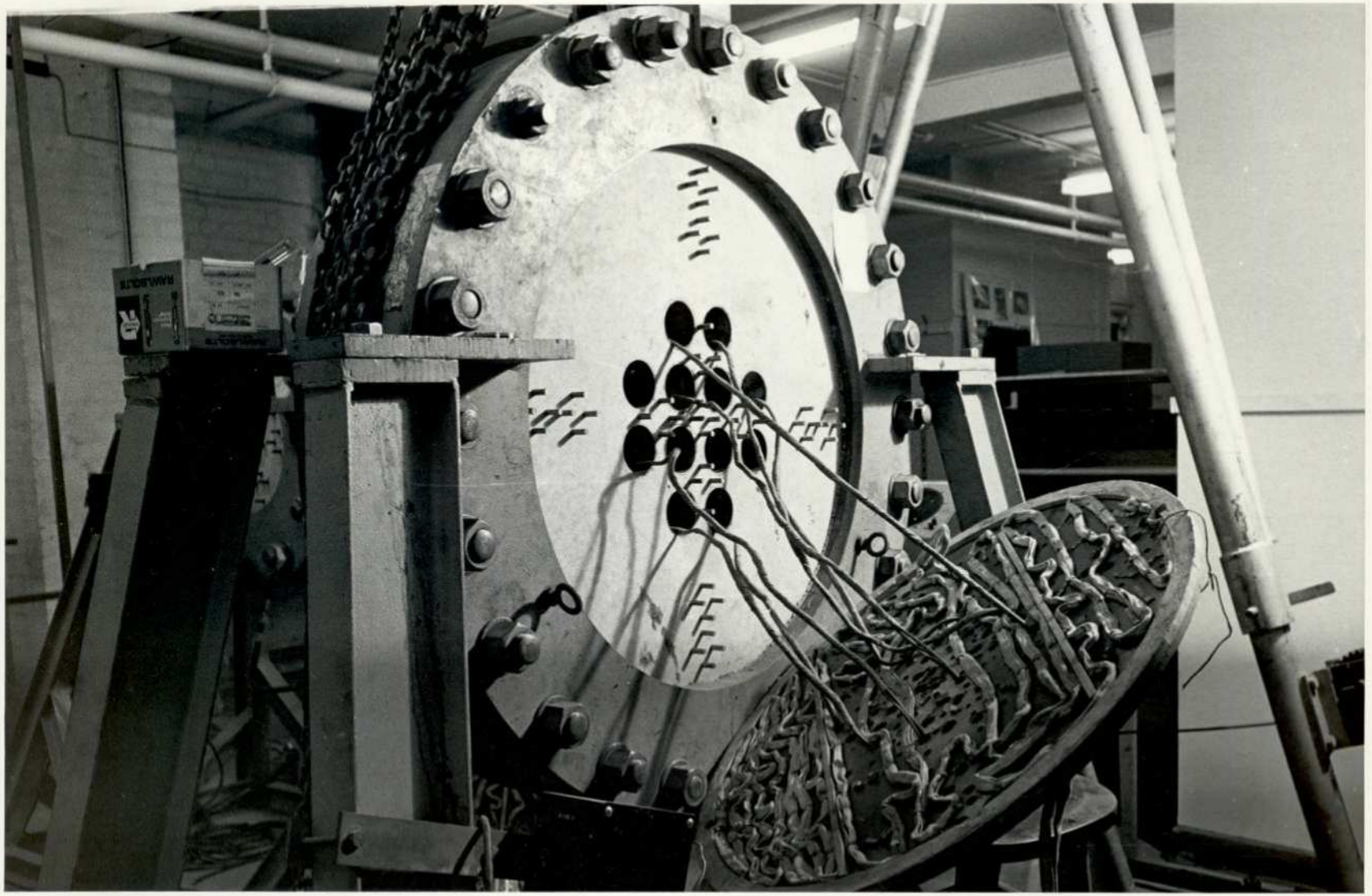
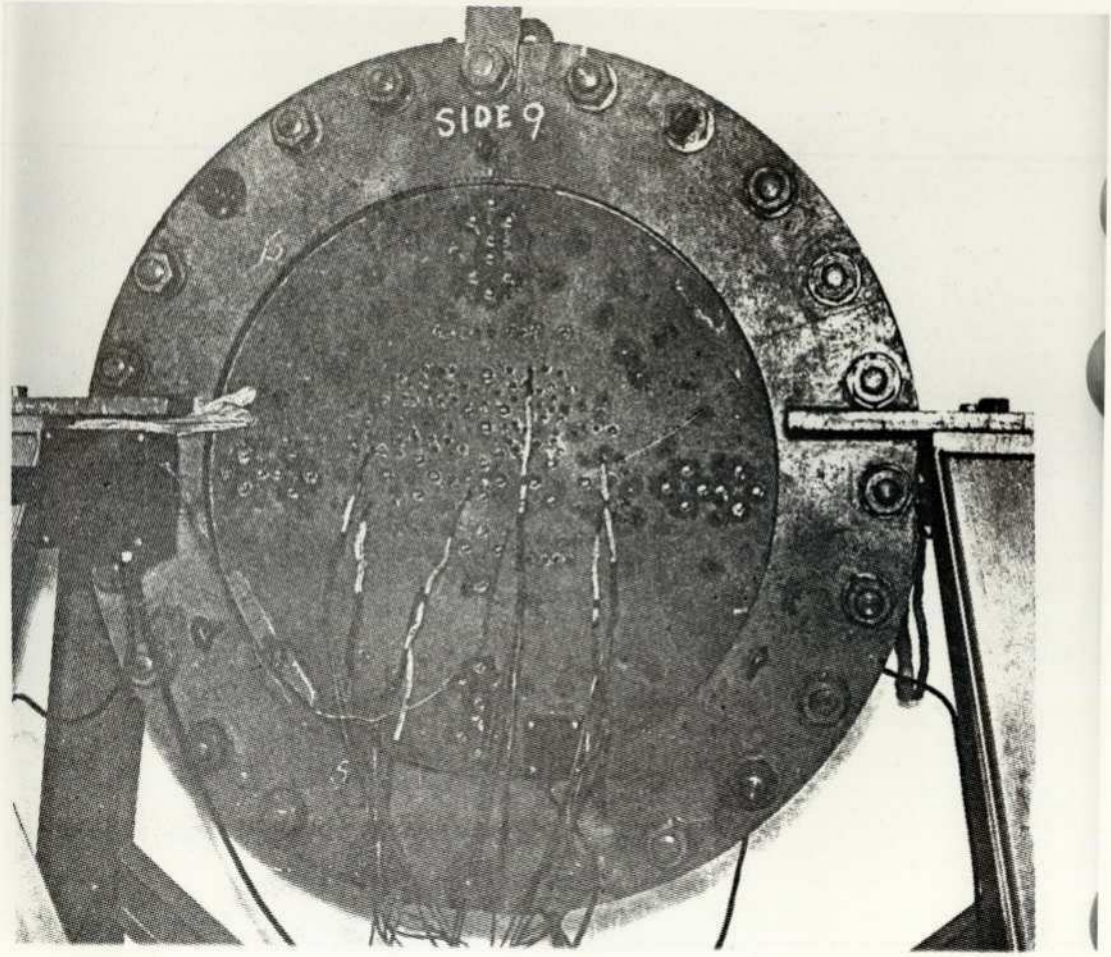


PLATE 5. Model 9/10 with heat shield removed.



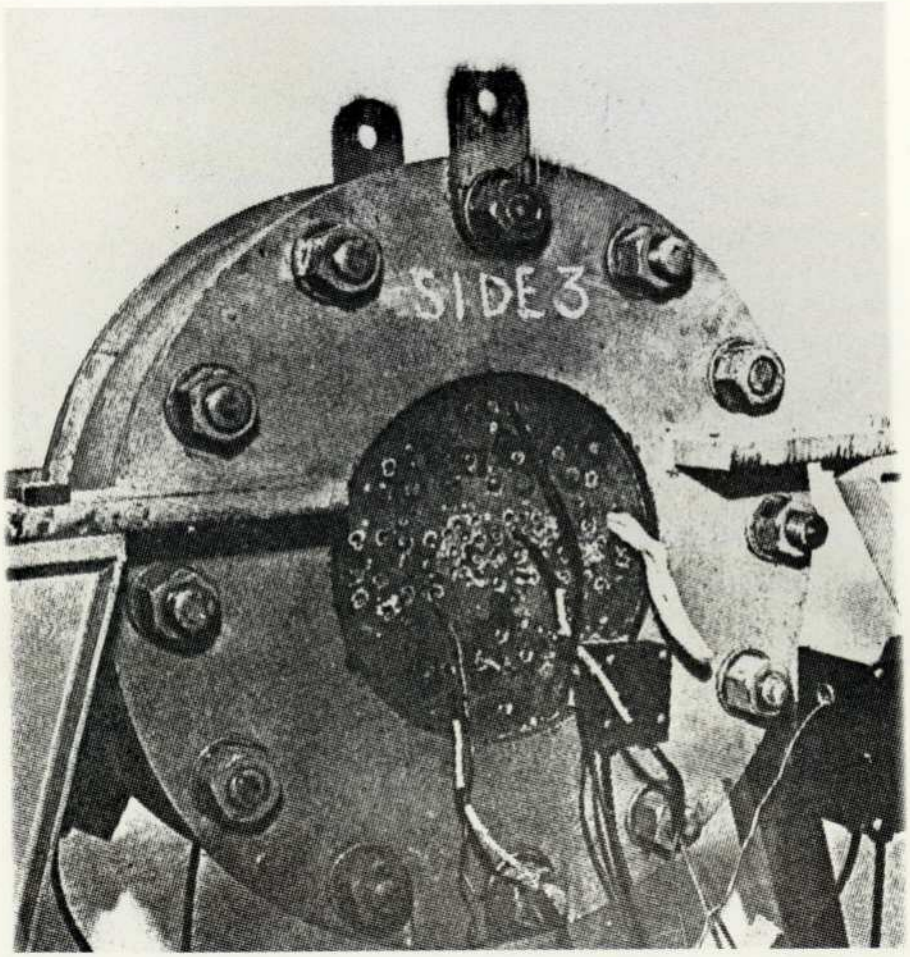


PLATE 6. Insulation Shielding and Thermocouple leads for Models 3/4 and 9/10.

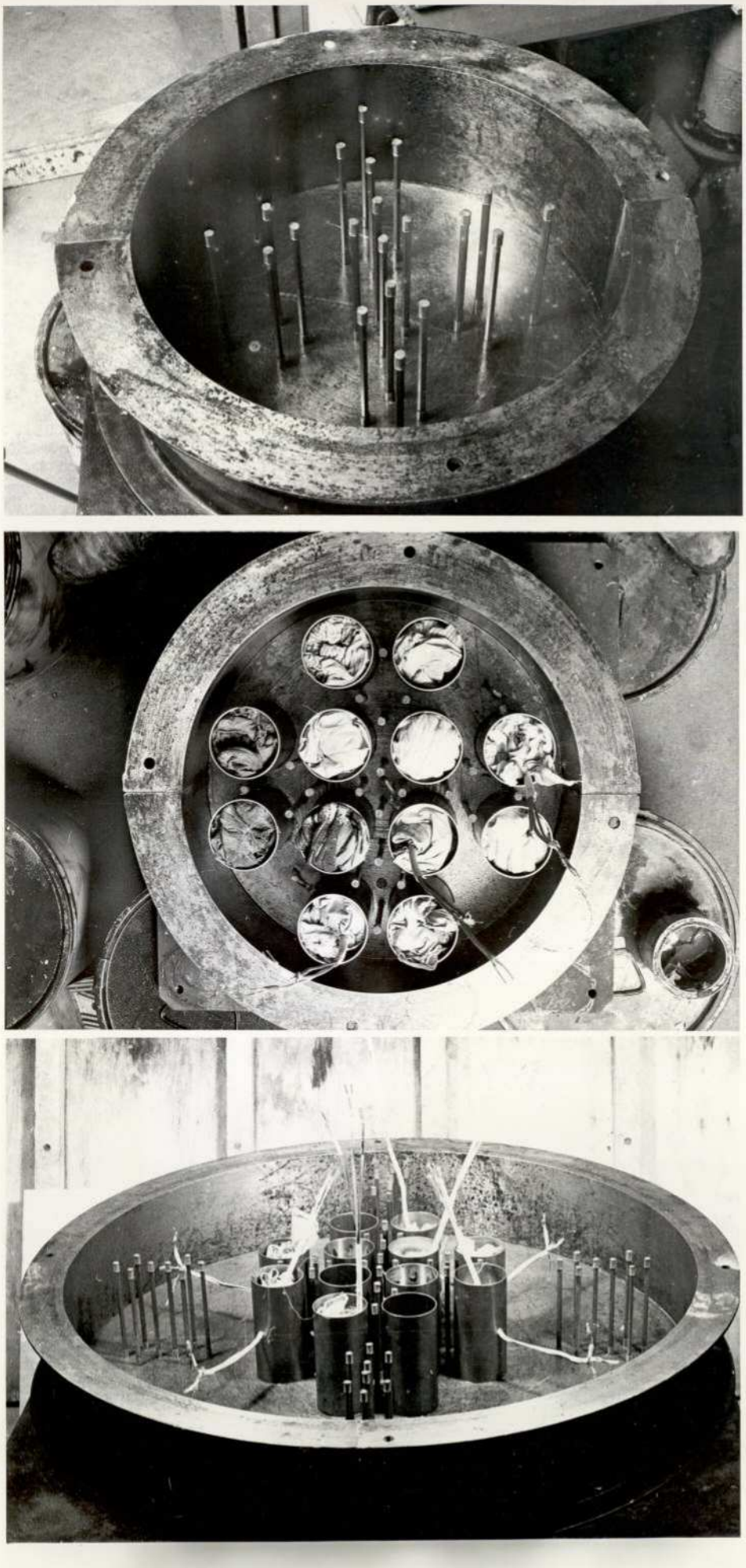
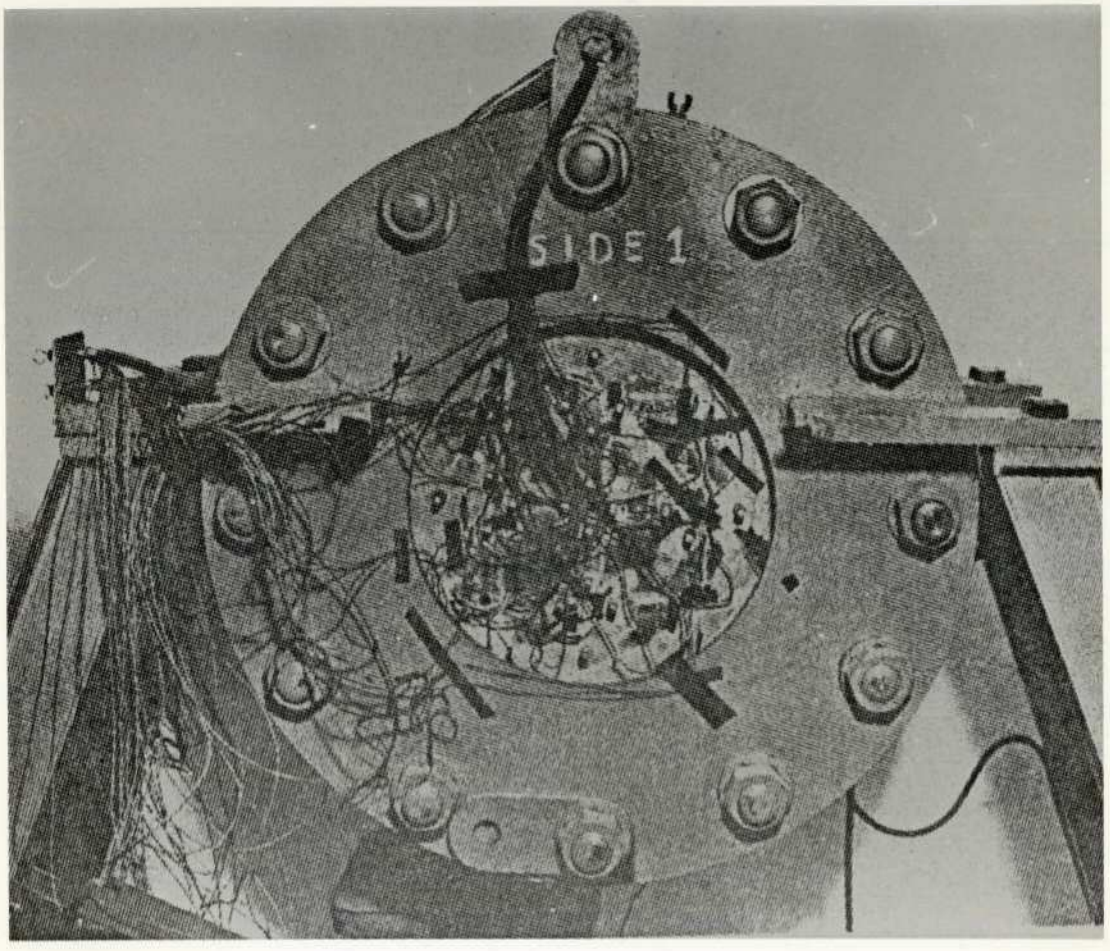


PLATE 7. Steel Moulds for Models 1/2, 3/4 and 9/10.



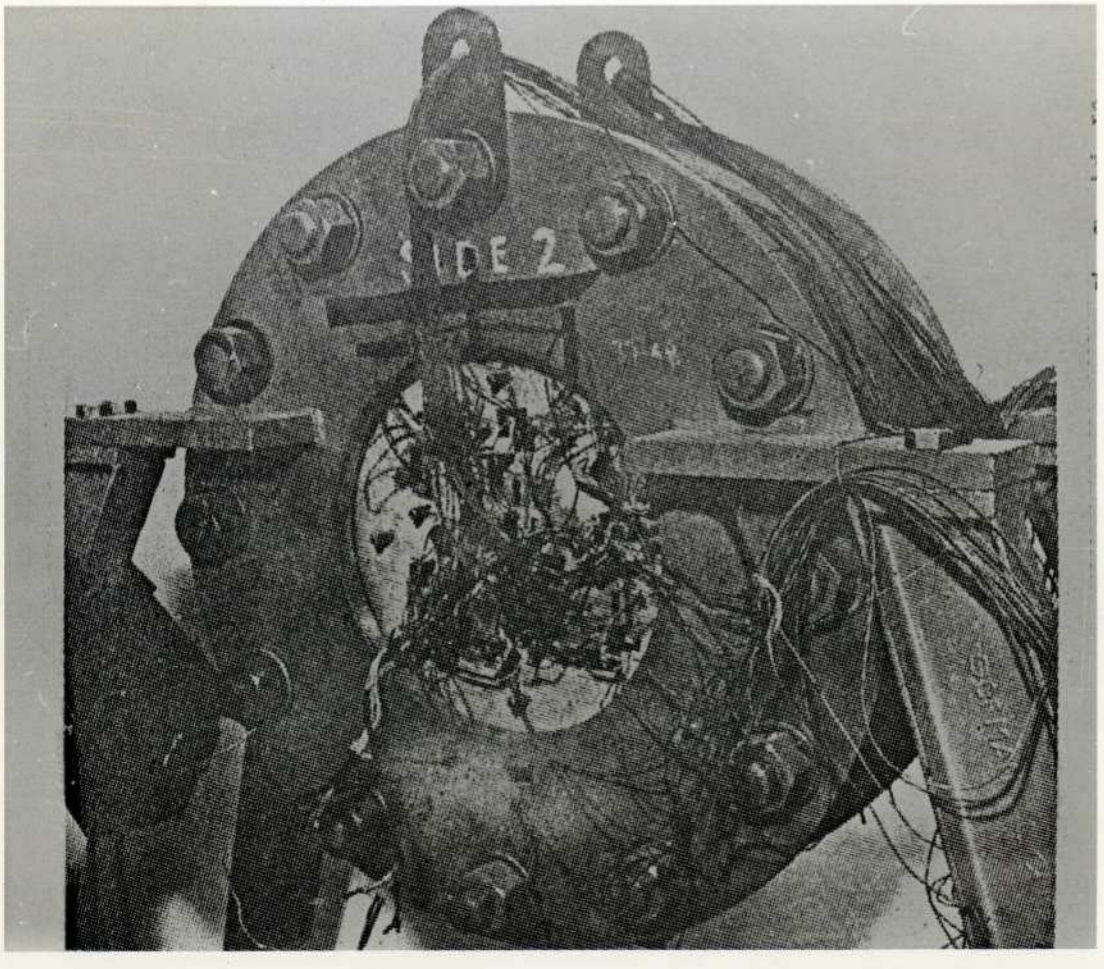


PLATE 8. E.R.S.G. Wiring during final unloading phase.

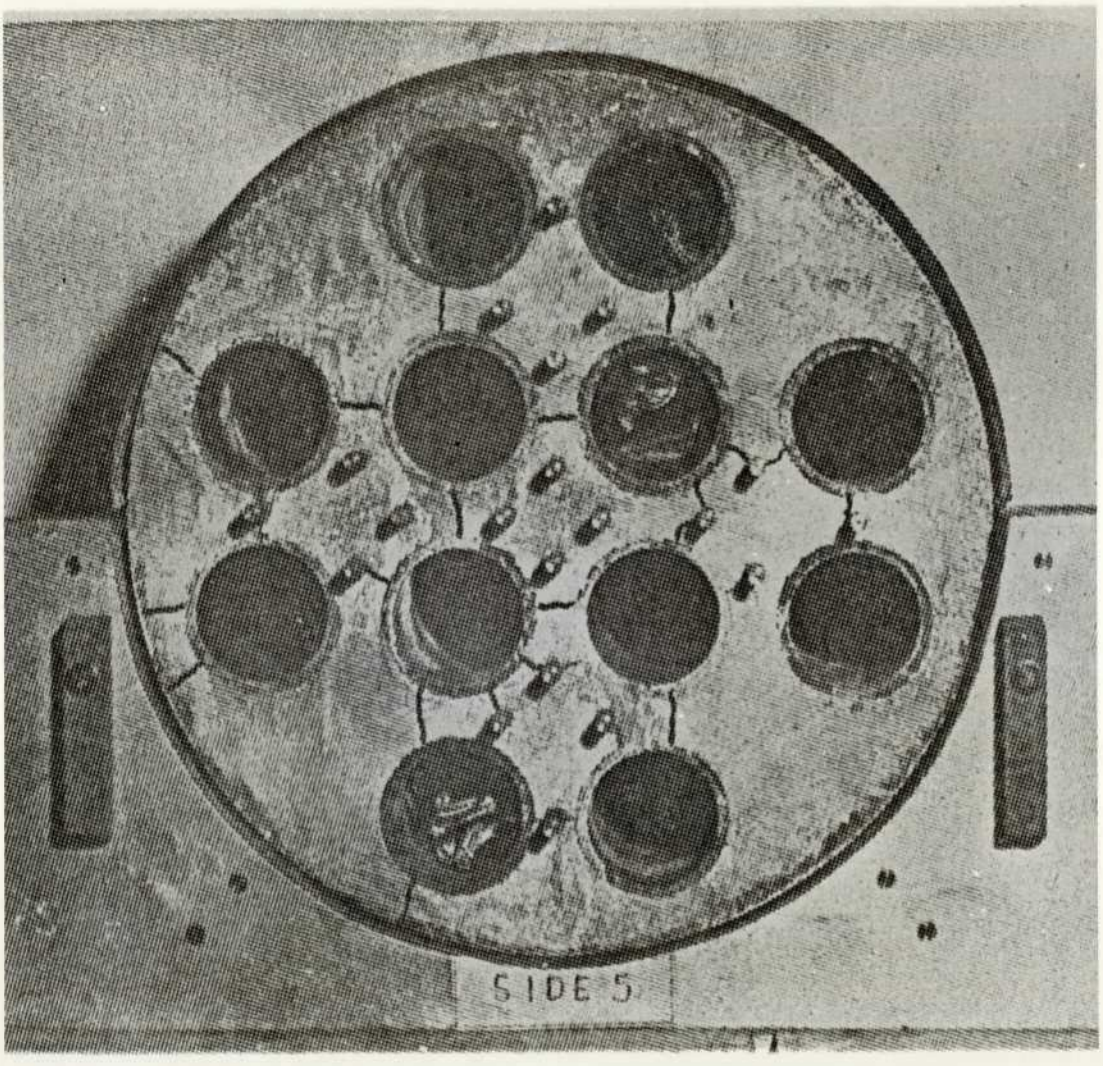


PLATE 9. Surface Cracking on Model 5/6 on removal of heat.

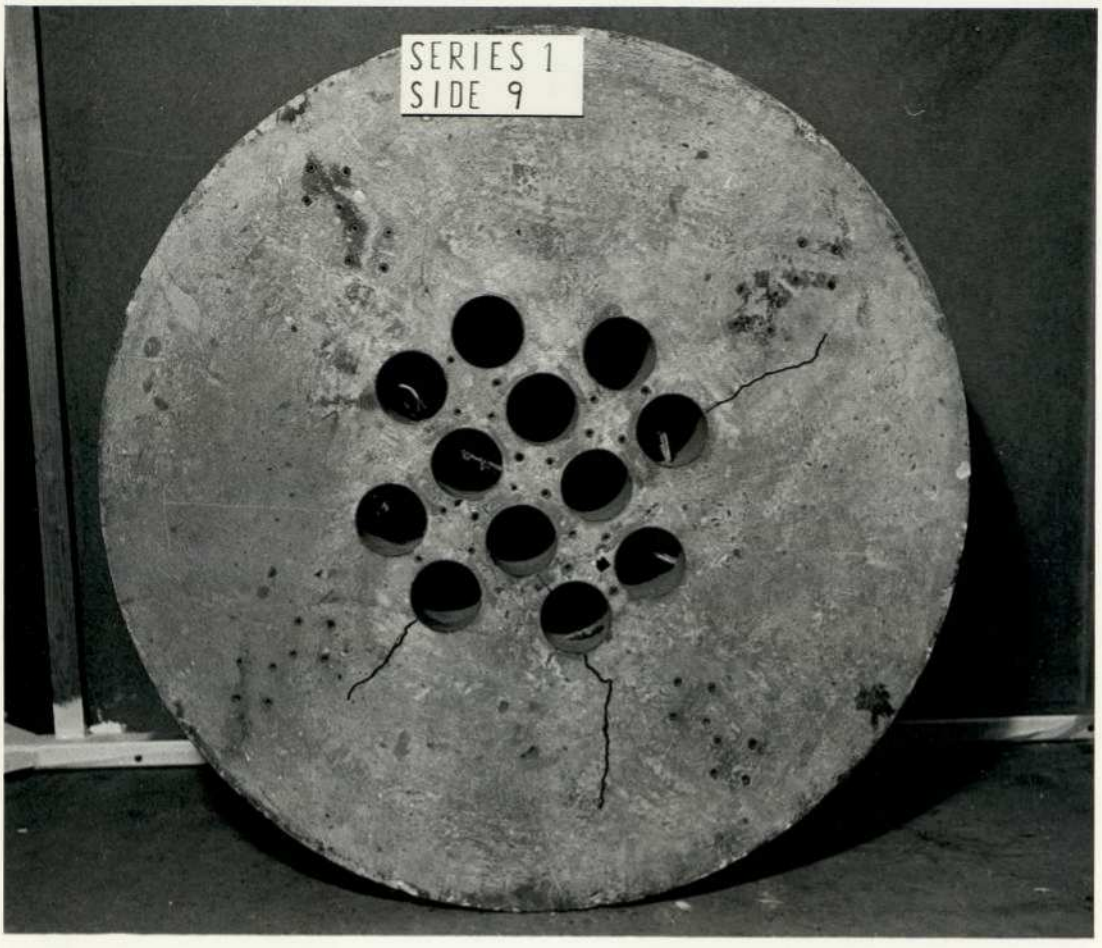
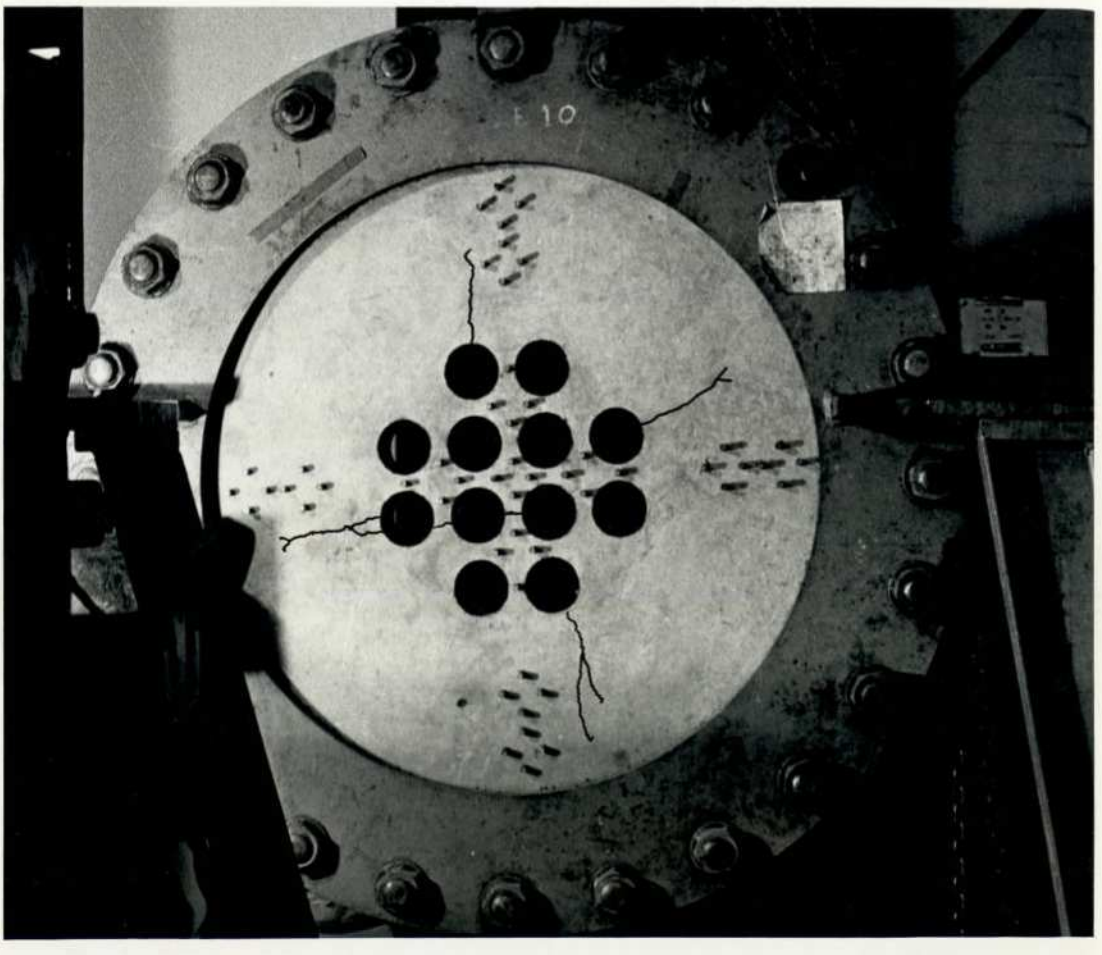


Plate 10. Crack Pattern. Series 1. Side 9.
Series 2. Side 10.



The hoop, which for the 36" ($\simeq$ 915 mm) specimen, was $38\frac{1}{2}$" I.D. x $42\frac{3}{4}$" O.D. x $7\frac{1}{2}$" wide x $2\frac{1}{8}$" thick, (980 mm x 1085 mm x 190 mm x 54 mm), was forged from a single steel piece. The steel faces were machined.

Between the concrete specimen and the rubber bag was positioned a $7\frac{1}{2}$" wide x $\frac{1}{4}$" thick (190 mm x 6.3 mm) section of tough conveyor belting designed to protect the rubber bag from friction effects and from the effects of the 80°C temperature to which the specimens were subjected.

Steel shims were used to mask the joining edges of the belting and a heavy terylene cloth was also inserted to prevent damage to unprotected surfaces. French chalk was applied to the various interfaces to reduce friction during installation and operation.

The side reaction from the edge of the rubber bag was taken by two machined mild steel flanges, one on each side of the bag. The flanges took the form, for the 36" ($\simeq$ 915 mm) specimen, of rings 33" I.D. x $48\frac{1}{2}$" O.D. x $\frac{15}{16}$" thick, (840 mm x 1232 mm x 22.5 mm), arranged in a vertical plane. The two flanges one on each side of a rig were held $7\frac{1}{2}$" (190 mm) apart, and the side thrust taken by 24/$1\frac{1}{2}$" (38 mm) H.T. bolts (for the big composite specimen) tightened with a torque spanner. These bolts were spaced on a pitch circle immediately outside the position of the hoop.

To keep the flanges in equilibrium by balancing the bolt thrust, a machined steel spacer ring was arranged outside the bolt pitch circle. The spacer ring was $46\frac{1}{4}$" I.D. x $47\frac{1}{4}$" O.D. x $7\frac{1}{2}$" wide (1175 mm x 1200 mm x 190 mm) for the big composite specimen.

For the two small loading rigs, the flange ring dimensions were $13\frac{3}{4}$" I.D. x $29\frac{1}{2}$" O.D. x $\frac{15}{16}$" thick (349.3 mm x 749.3 mm x 22.5 mm) and for the hoop the dimensions were $18\frac{3}{4}$" I.D. x 23" O.D. x $7\frac{1}{2}$" wide x $2\frac{1}{8}$" thick (476.3 mm x 584 mm x 190 mm x 54 mm).

12/$1\frac{1}{2}$" (38 mm) bolts were provided to secure the flanges for each small rig.

Since the space between the inner faces of the two M.S. flanges was $7\frac{1}{2}$" (190 mm), and the concrete specimen was only 6" (153 mm) wide, two machined steel cheek rings were required, one on each side of the specimen, to take up some of this gap and to help restrain the specimen in a vertical position. The cheek rings were bedded onto the concrete specimen with a cement and sand mortar. This was done during the installation of the specimen in the ring, an operation which was performed with the removable section of the rig lying on its side on the laboratory floor. The gap ($\frac{1}{8}$") (3.2 mm) on each side of the specimen, filled by the mortar bed, was intended to provide a tolerance for manufacture and installation.

The whole of the rig described was arranged for testing with the specimen supported in a vertical plane. Brackets were welded to the outsides of the steel flanges at positions which permitted a four point support onto a robust M.S. angle framework. The circular section of rig could thus be bolted to the framework, and could be manoeuvred on and off by overhead crane for installation or removal of the specimens.

5. The Pressure Circuit

This circuit is shown diagramatically in Fig. 18 and several components including the air-hydro pump are shown in Plate 2.

The pressure was developed by an air-hydro pump which was actuated on the inlet side by compressed air from an adjacent compressor. A water supply was led to the pump by gravity feed from an overhead tank, the water-level of which was maintained from the mains supply.

The working pressure was transmitted on the outlet side of the pump to the specimens through a $\frac{3}{4}$" (19 mm) O.D. water pipeline.

An air filter and a water filter governed the quality of the flows to the inlets to the pump. A pressure reducing valve and a pressure relief valve were provided at the air inlet, the former bringing down the pressure of the air from the compressor to the required order of magnitude for the pump, and the latter being set to ensure that the test pressure in the loading rigs should not exceed the determined value of 1500 p.s.i. (10342 kN/m^2). An air pressure gauge on the inlet side of the pump indicated the pressure at this position.

A water bleed-off point on the outlet side of the pump, incorporating a needle stop valve provided means of reducing pressure in the circuit, during commissioning and subsequently during operation.

It was considered advisable to provide a further pressure control valve in the outlet pipe just before the main service pressure gauge. This valve was preset at a few pounds pressure above 1500 p.s.i. (10342 kN/m^2).

LAYOUT OF PRESSURE CIRCUIT AND TEST SPECIMENS

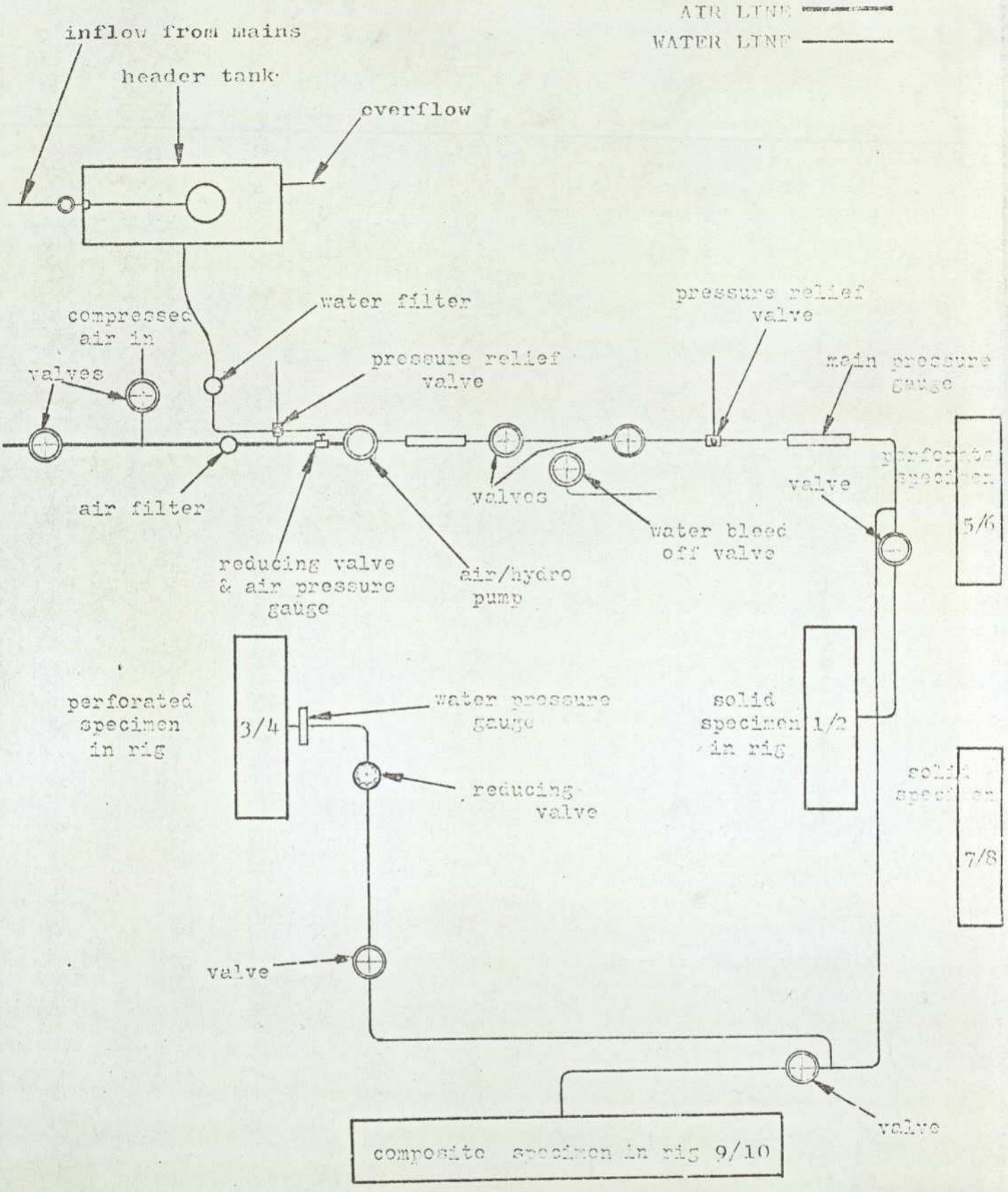


FIG. 18.

After the main service pressure gauge, the water circuit served the three pressure-loading rigs via three pipelines in parallel each of which was separately valved to permit loading of any one or all of the rigs.

6. The Heating Circuit

Heat was applied to the ten faces of the five specimens in each series, by means of Isopad heating tapes protected with an outer cover of glass cloth. Each face was heated by an independent circuit. Details are shown in Fig. 19.

The tapes were fixed not to the concrete but to the inner faces of circular shields $\frac{1}{2}$" ($\triangleq$ 12 mm) thick made of Karlit insulation boarding. The diameter of the shields was such as to provide a close fit inside the mild steel cheek rings of the loading rigs. For the unloaded slabs the shields were clamped to the concrete faces.

A wooden rim around the periphery of the inside face of the insulation shields, held off the central part of the shield, with its heating tapes, from contact with the concrete surface. Hot spots on the concrete were thus avoided.

The tapes were fixed horizontally in rows on the shield at centres which increased from the bottom to the top of the shield. This arrangement favoured a uniform temperature distribution since the circulation by convection of hot air enclosed between the shield and concrete would otherwise have raised the concrete temperature unduly at the top of the slab.

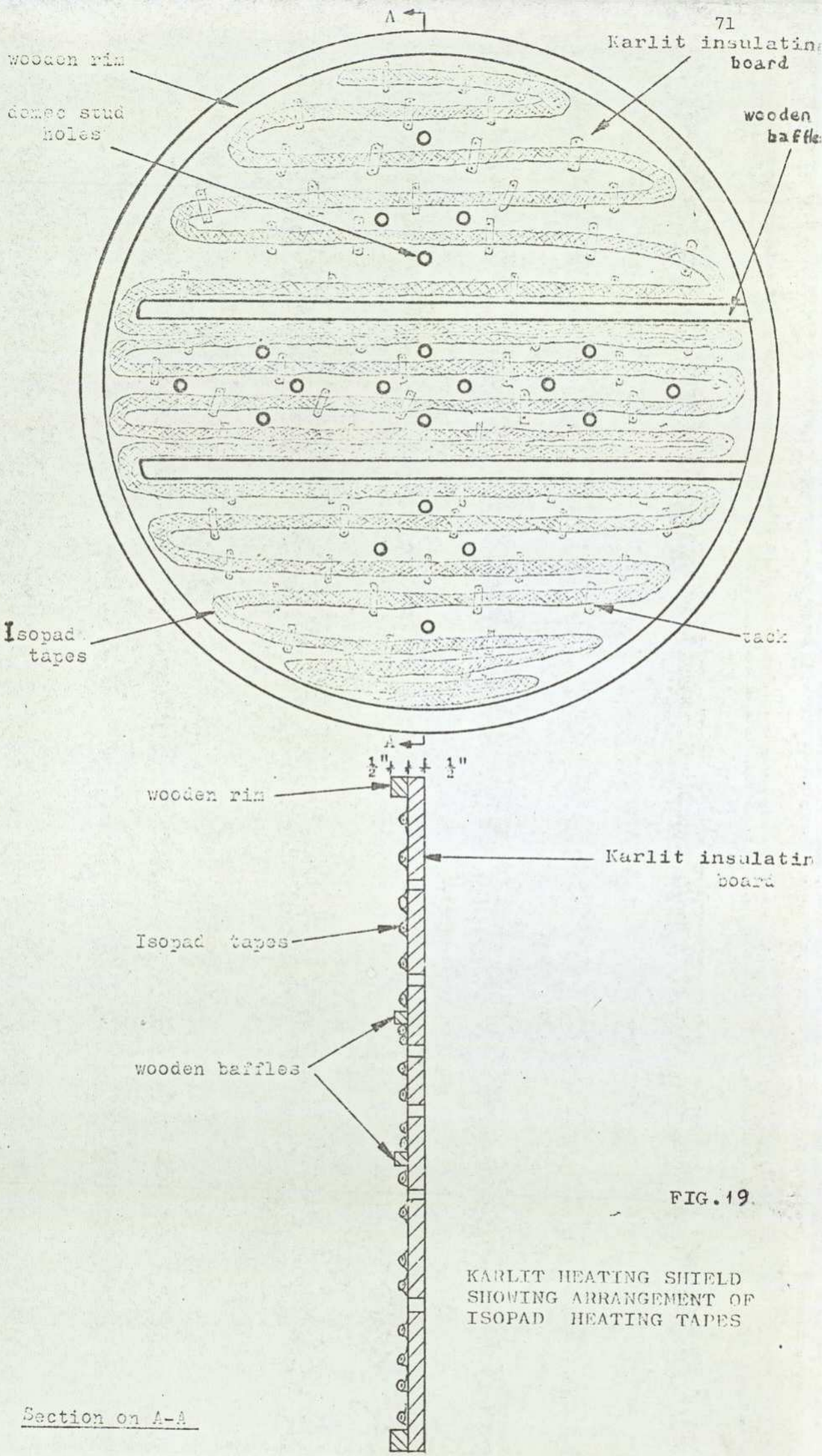


FIG. 19.

KARLIT HEATING SHIELD SHOWING ARRANGEMENT OF ISOPAD HEATING TAPES

In addition, two wooden battens were provided across the shield horizontally with the object of evening out the temperature distribution, by restricting air convection to local sections of the inner shield face.

Holes were bored in the insulation shields at positions corresponding to the arrangement of the projecting brass Demec studs. The holes had to be generously large to permit the shield to be pushed fully home without the danger of touching or deflecting the studs.

The length of studs and the thickness of the shield were approximately the same. Thus Demec gauge readings could be taken with the heating on without removing the shields.

In addition a pattern of ventilating holes was drilled to encourage a local differential cooling of hotter areas in the concrete, as these revealed themselves during testing when the thermo-couples were scanned by means of the switchbox.

The heating tapes were of the I.T.A. type, those for the large 36" ($\triangleq$ 915 mm) specimen being of 750 watts capacity, and those for the smaller specimens of 260 watts capacity.

These tapes led from the insulation shield to TM 500 thermo-regulators (thermostats) suitable for the limits 30°C - 200°C but set to function over an operating control range of 5°C. One regulator was provided for each face circuit. These regulators were each supplied from a variac variable transformer of up to 270 volt capacity.

The control probe of each thermo-regulator was initially inserted into the specimens through the cast-in thermostat tube.

The thermo-regulators monitored the temperature of the specimens and cut out the heaters at the top of the temperature range.

The intention was, in fact, to use the thermostats as upper limit controls to prevent temperature surges in the concrete due to malfunction of the transformers.

In the event, however, the on-off temperature response of the equipment led to undesirable and relatively slow fluctuations and militated against a close control of temperature near 80°C.

Consequently the probes were withdrawn from the specimens. It proved possible to maintain a reasonably steady temperature by fine adjustment of the variacs alone.

7. Temperature Measurement

The thermo-couples installed in all the specimens were made from chromel/alumel wire 19 s.w.g. (1.016 mm), type IC Insuglas. The insulation of this wire is limited to use below 150°C.

The wires were spot-welded at their junction and were then dipped in P.S. adhesive. This formed a waterproof, quick-setting and heat-resistant coating over the junction. 19" (≏480 mm) long sections of thermo-couples were cast in at temperature measurement positions in all the slabs. This dimension permitted sufficient free wire outside the concrete, however remote the thermo-couple position, to make satisfactory connections to the compensating cables.

The thermo-couple wires were of the single strand twinned type, each wire being insulated and the two insulated wires being themselves enclosed by further insulation.

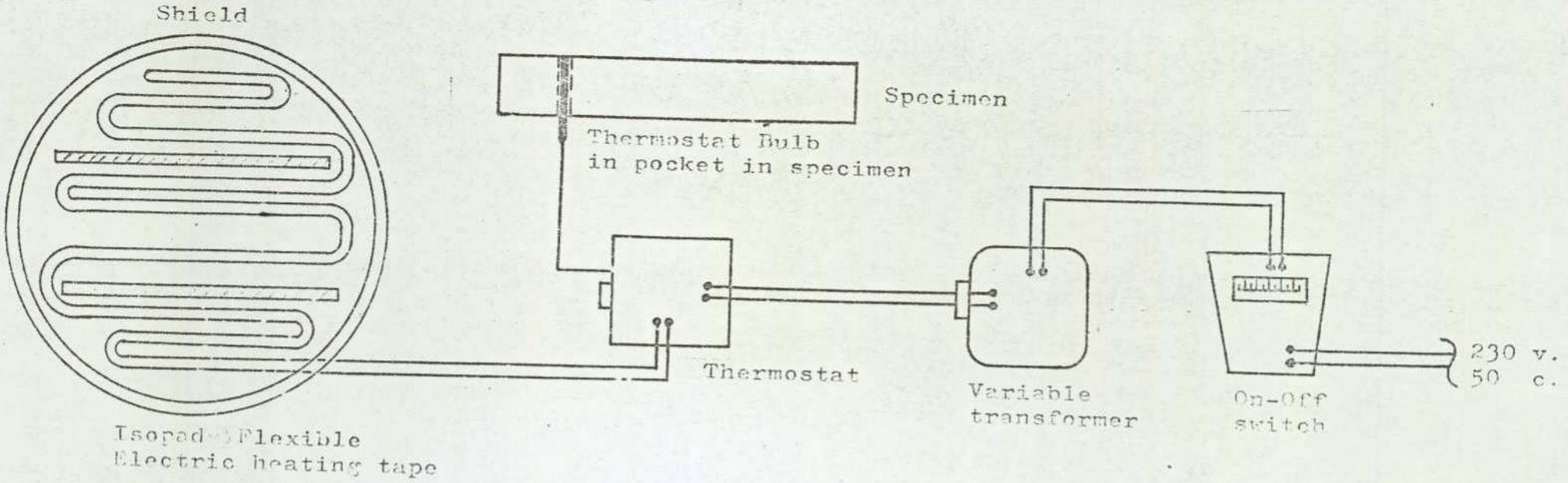
The flexible lead compensating cables which were joined to the thermo-couples, were multi-strand wires paired in an insulating cover.

To make the connection between the thermo-couple and the compensating cable, each of the four wire ends were bared, and the two appropriate pairs of ends tightly twisted together and soldered. Each connection was then wrapped in insulating tape. The two joints thus formed were arranged in close proximity along the wires so that the temperatures of the two connections would not differ.

The lengthsof all cable leads were identical and thus the cables were of equal resistance. They were connected to 25-way Amphenol plugs.

The 57 thermo-couples involved were distributed between four such Amphenol plugs, the plugs being connected to a multi-way switchbox.

The switchbox was itself connected to a Pye Scalamp thermo-couple meter reading directly in degrees Centigrade. The Scalamp and thermo-couple circuit needed calibration against fixed point temperatures, and the Scalamp reading scale was adjusted accordingly. Details are shown in Fig. 20.



HEATING CIRCUIT

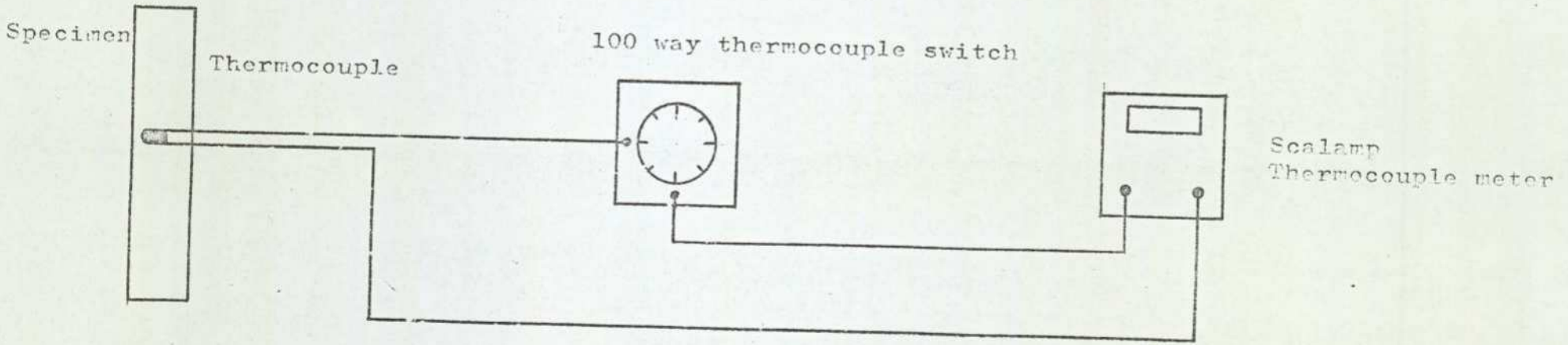


FIG. 20. THERMOCOUPLE CIRCUIT (temperature measurement circuit)

8. Electrical Resistance Strain Gauge Circuits

The strain gauges were used only during the short term elastic unloading tests at the end of each of the two test series.

Because of the generally recognised problems of long-term drift and instability with electrical resistance strain gauges, it was not considered practicable to attempt to record creep and shrinkage strains by this means over the several months that each test lasted.

The gauges used were $\frac{1}{2}$" ($\triangleq$12 mm) Budd E.R. S.G.s of the foil type specified by the Budd numbers C6 - 181B. They had a gauge factor of 2.08 $\pm$ $\frac{1}{2}$% and a resistance of 120 $\pm$ 0.2 ohms.

There were 8 E.R.S.Gs on each face of each pressurized specimen, making 48 in all in each test series. For the perforated $16\frac{3}{4}$" (425 mm) specimen and the 36" ($\triangleq$ 915 mm) specimen, the gauges were fixed along the ligament lengths. For the pressurized solid $16\frac{3}{4}$" (425 mm) specimen, the gauges were fixed in exactly identical positions. Figs. 21&22 illustrate the positioning of the gauges, and Fig. 23 shows the circuit layout.

Before fixing the gauges on the specimens, the concrete surface was first smoothed and cleaned with acetone. The adhesive used was a Japanese PS polyester resin containing a filler. The filler helped to make an intimate contact with the concrete by penetrating the surface. The PS adhesive is quick-setting and temperature proof.

The concrete surface was primed by smearing with a thin layer of PS adhesive. This was wiped off whilst wet so that the concrete was again exposed but the pores filled. After drying and smoothing a second layer of PS was applied and the gauge pressed on to the

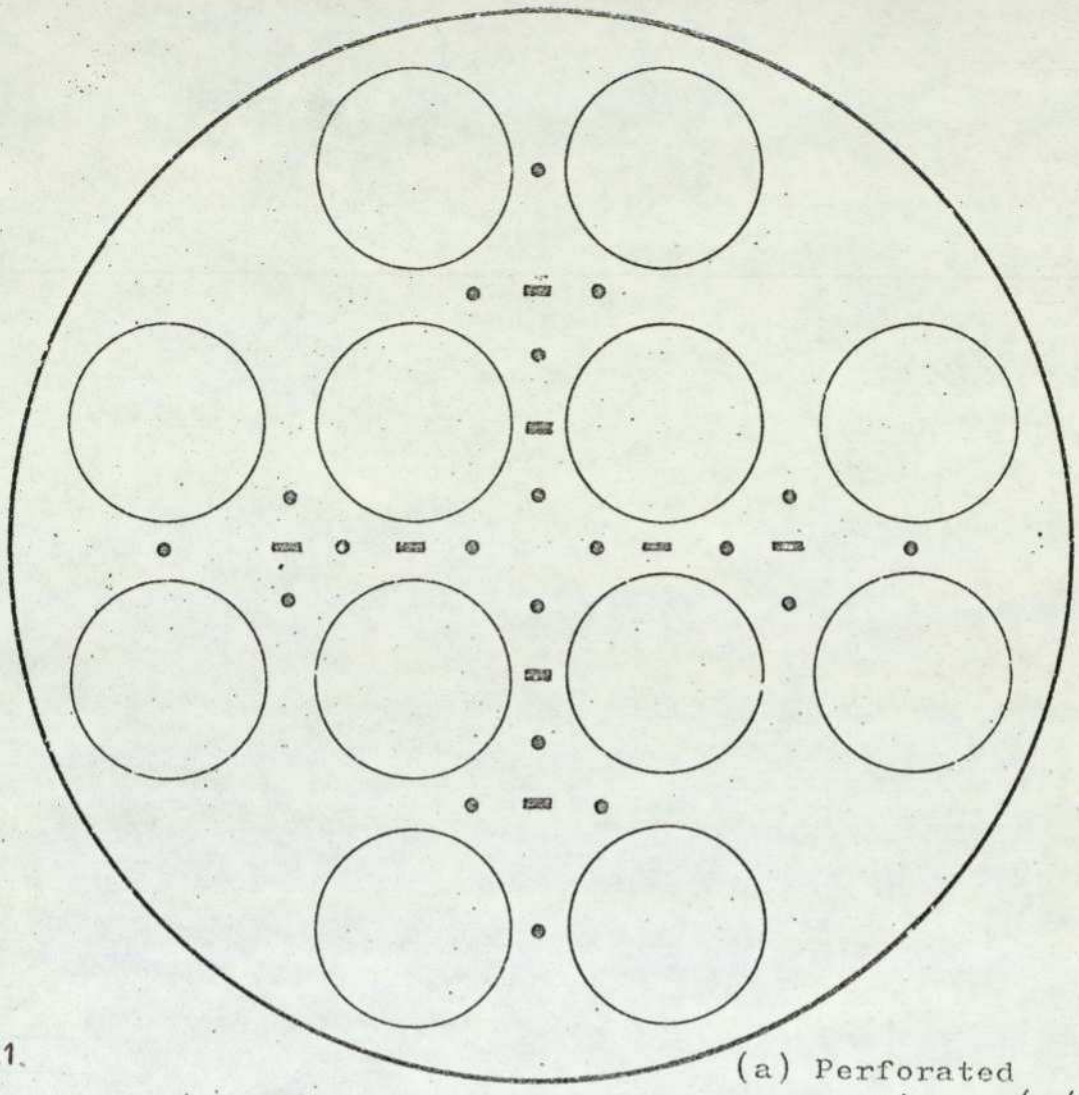


FIG. 21. (a) Perforated specimens (3/4) and (9/10)

ERSG

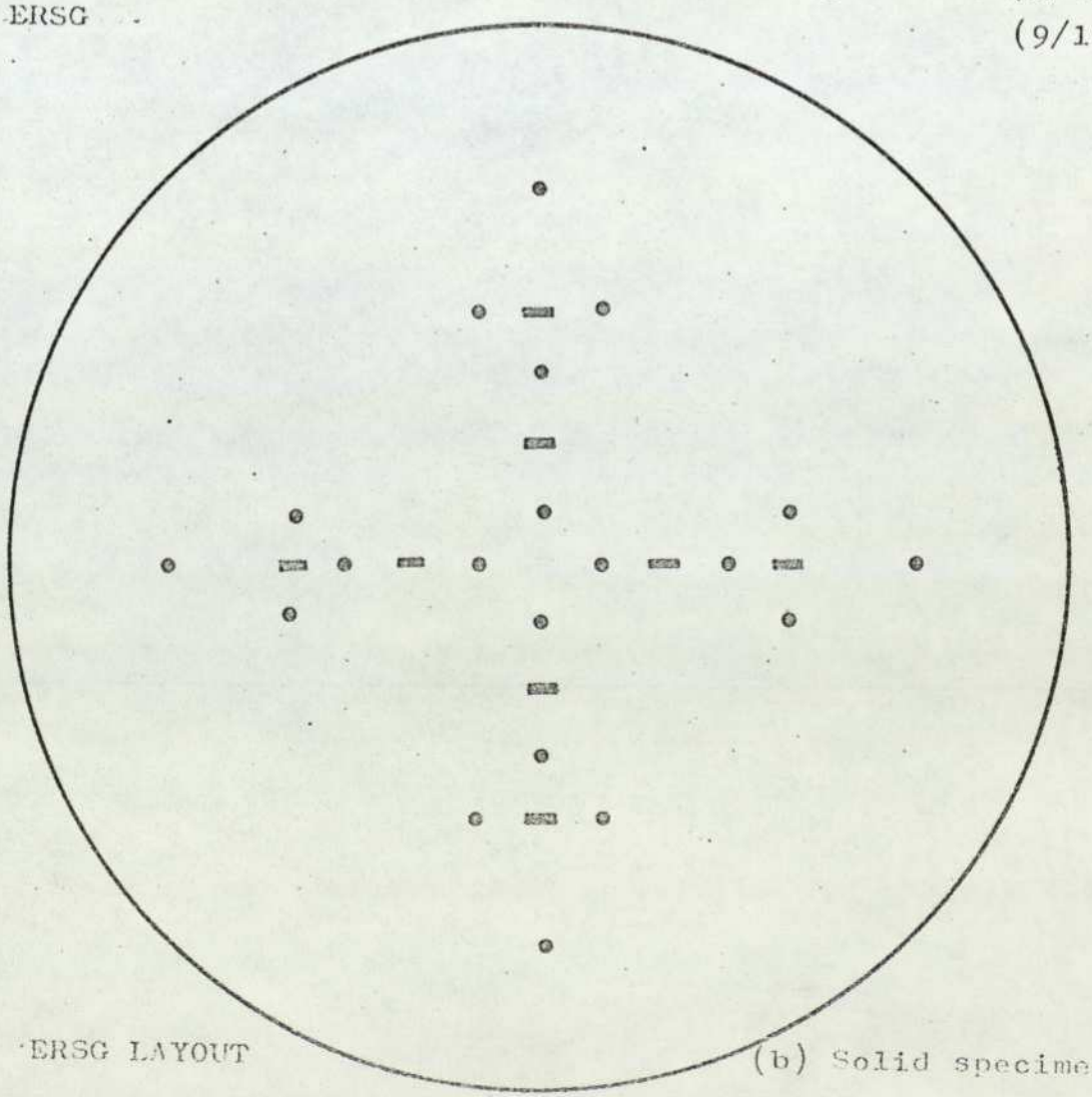


FIG. 22. ERSG LAYOUT (b) Solid specimen ($\frac{1}{1}$)

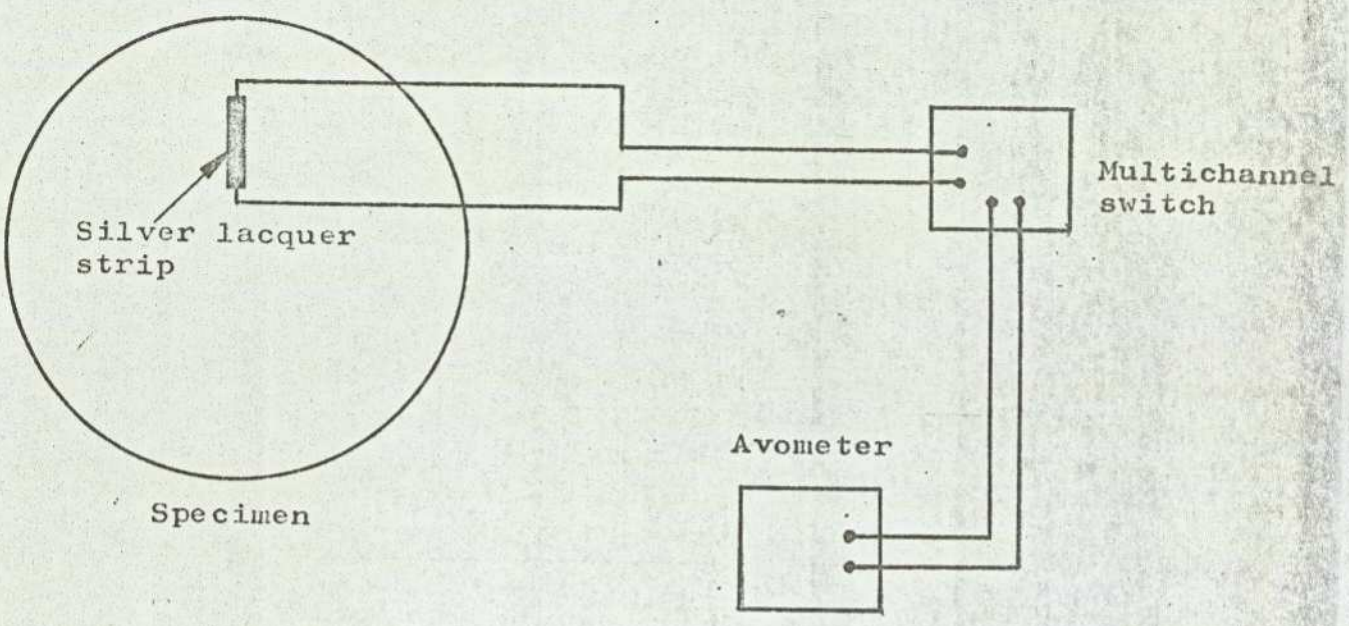


FIG.24. CRACK DETECTION CIRCUIT

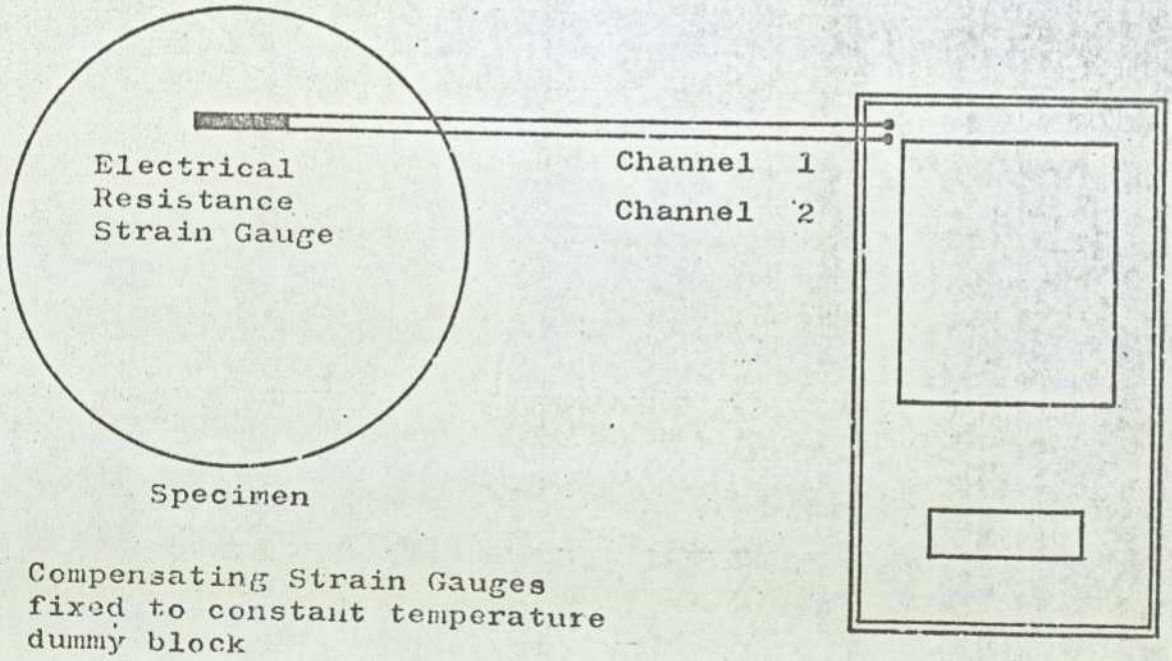


FIG.23. ELECTRICAL RESISTANCE STRAIN GAUGE CIRCUIT

concrete surface so that it was firmly in contact. At the time of pressing on, the gauge was covered and secured with a pressure-sensitive tape to permit final drying and hardening of the adhesive without the danger of the gauge peeling off.

The lead connections to each E.R.S.G. were made by soldering. The leads, which ran from the gauges to the Solartron Data Logger, were 14/0.0076" (0.193 mm) multi-strand wires and were PVC covered. The connections to the Solartron were made through standard Amphenol plugs.

The Solartron had separate sockets for the active gauges and for the dummy gauges. The resistances of all leads for the active and dummy gauges were made the same. The Solartron layout incorporated half the Wheatstone Bridge, the power supply, and amplifier. The gauge channels were scanned through a commutator switchbox. The amplifier output led to a digital voltmeter, all channels being automatically scanned, and the output reading given directly in microstrain as explained hereafter. The data were presented in the form of in-line printed figures on continuous output paper.

To obtain direct microstrain readings from the Solartron, it was necessary to calibrate it, assuming a gauge factor k of 2, by means of a standard microstrain calibration box. Thus the output readings gave the value of $\frac{1}{k} \frac{\Delta R}{R}$ directly. This is the strain required, from the relationship $\frac{\Delta L}{L} = \frac{1}{k} \frac{\Delta R}{R}$. To correct the readings to allow for the fact that the gauge factor was, in practice, 2.08, the Solartron reading was multiplied by $\frac{2.0}{2.08}$.

9. Demec Gauges

Two types of Demec gauge were used throughout the experiments. Most strain readings were taken with a standard 2" (50.8 mm) gauge. This instrument was read by means of a dial gauge, one division of which was equivalent to 25.3 microstrain. Thus the gauge factor used for converting reading differences into strain was 2.53×10^{-5}.

The other Demec gauge used, operated over a gauge length of 11.438" (290.5 mm). This dimension was specially required to take readings over a distance equal to three standpipe pitches. Demec points were provided on the ends of 1" (25.4 mm) long hexagonal brass studs positioned in two pairs at right angles to each other across each slab, each Demec point in a pair being three standpipe pitches from its neighbour. A standard 12" (304.8 mm) Demec gauge was specially drilled and provided with a registering point to suit the dimension of 11.438" (290.5 mm). One division on the dial gauge of this instrument was equivalent to 6.99 microstrain. Thus the gauge factor used in converting reading differences to strains was 6.99×10^{-6}.

These types of gauge were developed and are calibrated by the Cement and Concrete Association and are manufactured under license by W. H. Mayes & Son.

The diameters of the standpipes were measured with a modified Mercer bore gauge. The modification took the form of shortening the length of the standard gauge and substituting conical spigots for the normal ends, in a manner which, keeping the leverage ratios the same, thereby left the gauge factor unchanged.

Two bores were measured in each perforated specimen. The bores were measured over four diameters each 45° apart around the circumference. Both ends of each standpipe were read to obtain average readings.

10. Crack-Detection Circuits

These circuits were devised for use during the unloading phase towards the end of the testing programme. They were set up, therefore, only when they were required at this late stage.

Cracking was anticipated at a low magnitude of loading and the intention was to identify the load level marking the onset of cracks in any of the expected locations. The concrete ligaments were the points of greatest interest.

Accordingly crack-detecting strips of conducting paint were applied at each ligament.

The conducting paint, Dag dispersion 962, contained silver in alcohol and was applied to the ligaments in strips in such a way that the connecting cable ends were fixed. This conducting paint has satisfactory properties of conduction, adhesion and brittleness.

The connecting cables from the strips lead to a multi-way switchbox which could scan each strip. The aim was to identify breaks in any circuit, due to cracking, at each load decrement.

Two methods of detecting circuit failure were tried. The first method used a bulb with a 9-volt battery. The bulb gave an indication of cracking by flickering and failing. It was necessary to ensure equal resistances in each circuit in order to make the light intensity of the bulb visually comparable on scanning. Even so the method proved too insensitive and indeterminate.

The second method involved the use of an Avometer and battery in conjunction with the switchbox. The pointer registered infinite resistance on the meter scale when a crack was encountered. Fig. 24 shows the circuit arrangement.

SECTION VI

EXPERIMENTAL PROCEDURES

A. The loading and observation procedures in the test programme

A diagrammatic representation of the testing programme is shown in Fig. 7. Readings of ambient temperature and relative humidity were taken at the start of the test and on each subsequent occasion when readings were being observed. After sealing the rims of all specimens with thixotropic paint, datum strain readings were taken on 2" (50.8 mm) Demec and 11.438" (290.5 mm) Demec gauge lengths and stand pipe diameters. These datum readings were taken at ambient temperatures. See also Figs. 26 and 27.

1. Load Cycling at Ambient Temperature

At the start of each test series, the specimens to be loaded were cycled in the loading rigs, at ambient temperature, over their loading range three times. In the case of the large 36" (914 mm) composite specimen this gave the elastic response of the perforated and solid zones together. For the small $16\frac{3}{4}$" (425 mm) solid specimen it gave the elastic modulus of the actual concrete and for the small $16\frac{3}{4}$" (425 mm) perforated specimen it gave the effective modulus of the perforated zone.

The other two small specimens were unloaded and were allowed to shrink only, resting upon wooden saddles under the same ambient conditions as the loaded specimens.

2. Loading at Ambient Temperature

The three specimens which were required to give creep and shrinkage strains were then loaded to their maximum constant compressive loads, which were 1500 p.s.i. (10342 kN/m^2) for the large composite specimen and for the small solid specimen, and 1125 p.s.i.

(7756 kN/m^2) (for series 1 only where the tube wall thickness was $\frac{1}{16}$" (1.59 mm)) for the small perforated specimen. For the second series with wall thickness of $\frac{1}{4}$" (6.35 mm), the maximum load for the small perforated specimen was 1500 p.s.i. (10342 kN/m^2). Readings of strain were taken with the 2" (50.8 mm) Demec gauge and the 11.438" (290.5 mm) Demec gauge at approximately every third day for a three week period. Readings were also taken, on the same occasions, in the two stand pipe tubes selected for each perforated specimen, across four diameters, with the Mercer bore gauge.

Again for the first series, the constant load on the small perforated specimen was 1125 p.s.i. (7756 kN/m^2) and for the second series 1500 p.s.i. (10342 kN/m^2).

Shrinkage readings were also taken on the two unloaded specimens on the same days and over the same three week period.

3. Loading at 80°C.

The heating tapes on the inner faces of the insulation shields were then activated and the temperature of all the specimens was raised over a period of a few days to 80°C. The temperatures during the transient period were measured with the thermo-couples and recorded.

Strains of all specimens were measured and stand pipe diameters taken for a further period of six weeks, with the temperature maintained at 80°C. The accelerated rates of shrinkage and of creep and shrinkage together were recorded under the same constant pressure on the loaded specimens as before, every two or three days.

4. Load Cycling at 80°C.

Immediately before removing the heat, the loaded specimens were cycled down and up several times over a range of pressure which was not allowed to fall below 800 p.s.i. (5515 kN/m^2) to avoid cracking any of the specimens.

This process obtained, at 80°C, the respective elastic responses, and elastic moduli, real and effective, as had been obtained at ambient temperature.

5. Loading at Ambient Temperature again.

The heat was turned off and the insulation shields were removed. During the ensuing cooling, the transient temperatures were recorded.

After a further restricted load cycling at ambient temperature, a further three weeks' regime of strain and diameter readings was pursued. The shrinkage and the creep and shrinkage strains were observed for all specimens, with the loaded specimens still under pressure.

6. Unloading : Cracking.

The pressure was then reduced slowly in decrements.

During this phase the elastic unloading strains were measured with electrical resistance strain gauges, which were installed on the concrete ligaments of all loaded specimens; the loads were gradually reduced whilst the onset of cracking was sought in the ligaments. The E.R.S.G. readings were recorded on the Solartron Data Logger.

In addition, the conducting paint crack-detection equipment had also been affixed to the ligaments in positions which coincided

as near as possible with the electrical resistance strain gauges.

It proved difficult to detect the cracks which finally appeared at very low levels of loads. Four methods were used:

1) visual inspection with a magnifying glass under a powerful light
2) identification of sudden reading changes or null readings on the Data Logger
3) breakage of the crack-detection circuits
4) examination for large Demec reading differences.

The crack-detection circuits worked through scanning, by means of a switchbox, all the ligament positions at each load decrement. A crack caused a break in the circuit which was indicated by a zero reading on the attached Avometer. This method of crack-detection proved insensitive and it is possible that the installations of E.R.S.Gs. and conducting strips interfered with each other physically, if not electrically. The strips certainly prevented an easy, visual crack identification.

7. Load cycling after unloading; Creep Recovery.

The final elastic responses were obtained for both cracked and uncracked specimens by a further load cycling at this stage.

After a final unloading, strain measurements were continued during the period of creep recovery until a steady state was reached.

B. The Test Equipment and the reliability of Testing Techniques

The test equipment consisted of

1. three radial loading rigs containing rubber water bags (1 rig for the 36" (914 mm) specimen and 2 rigs for the $16\frac{3}{4}$" (425 mm) specimens)
2. the rubber water bags themselves
3. the pressure circuit
4. the heating circuits
5. the temperature measurement circuits
6. the electrical resistance strain gauge circuits
7. the crack-detection circuits
8. the strain measuring instruments
9. the steel moulds and jig.

1. The Loading Rigs

On the whole, the loading rigs performed their function in a satisfactory manner.

The solid steel hoop which sustained the outward thrust through the rubber bag under pressure, was forged and machined from a solid piece of steel. The side thrust was taken by machined steel flange rings which were bolted across the width outside the steel hoop by high tensile steel bolts set to a given torque with a torque spanner.

The flanges under the tightening effect of the bolts were kept at the correct fixed distance apart by the outermost spacer ring.

This meant that the water inlet to the bags and the air outlet, which were respectively at the bottom and top of the rig on opposite ends of a diameter, passed through holes in the spacer ring and hoop in order to connect to the rubber bag inside.

The space remaining, at the inner radii of the flanges, between them and the specimen was occupied by two identical cheek rings, one on each side of the specimen. The $\frac{1}{8}$" (3.1 mm) gap remaining on each side between the cheek ring and the specimen was filled at the time of installation of the specimen with a fairly dry-mix cement mortar.

Between the rubber bag and the specimen a layer of thick insulation conveyor belting and thick terylene cloth were introduced. Their purpose was twofold. They protected the rubber bag both mechanically and thermally from the effects respectively of physical contact and temperature from the specimen.

The whole rig was supported in a vertical plane in a robust structural steelwork support to which it could be bolted through lugs on the outer flanges.

To dismantle the rig and remove the specimen, the upper circular section of the rig could be lifted off the support by overhead crane. It could then be rested horizontally on the floor of the laboratory while the nuts were unscrewed and removed. The upper flange ring could then be lifted off, and the exposed cheek ring with it. The specimen was then accessible for removal.

For installation it was found necessary to use steel shims to mask the meeting edges of the insulating belting. This prevented damage to the rubber bags. To assist the sliding of the specimen horizontally downwards into the tight space provided for it within the belting, French chalk was applied to the surfaces. If the specimen was not lowered in the correct plane, it proved very difficult to manoeuvre it down into place.

Another difficulty lay in the positioning of all the bolts down the corresponding holes in the two flange rings. The rig had to be kept off the floor on chocks in a truly horizontal plane to achieve this. The bolts had to be tightened in two stages; once on the floor before the cement mortar packing had finally hardened and a second time, to the required torque, when the rig had been erected in its vertical position on its stand.

2. The Rubber Bags

The bags were made of neoprene rubber and were formed into a rectangular cross-section consisting of four sections of rubber joined at the four corners. The bags had, in effect, a double wall thickness, containing an inner tube within the outer section. The outer dimensions of the bag were such as to fill exactly the rectangular space left for it in the rig.

Leaks were experienced from time to time and repairs were carried out by Dunlops Limited at their Manchester works. In one phase of the experiments fully extruded rubber bags were tried with little success.

The bags, had to be made to accurate dimensions if they were to be successful. Although the bags were only required to transmit the maximum pressure to the surfaces with which they were in contact and were not expected to withstand this pressure, they nevertheless were presented with a difficult duty to perform, particularly when the maximum pressure was associated with elevated temperature. Points of weakness occurred at the corners and at the points of insertion of the inlet and outlet. Load cycling probably represented the greatest test on the bags when they were expected to inflate and deflate alternately as the pressure was raised and lowered.

When the bags were being commissioned it took about twenty minutes for the air-hydro pump to fill the total volume of pipework and the three bags with water. The air outlets were left open and permitted to flow freely until all air had been ejected and all the bags were full of water. The outlets were then sealed. After this point in time, the subsequent pressure rise to the maximum was accomplished by very few strokes of the pump.

A pressure relief valve was provided on the top of the outlet valve of each bag to prevent overload of the bags in the event of failure of the main pressure control valve in the water pressure circuit.

A difficulty was encountered with the threaded brass spindles of the inlets to the bags. They had to be over 4" (101.6 mm) long to pass through the thickness of hoop and outer spacing ring. Due to their structural weakness, it proved a delicate operation to make strong watertight connections at these positions to the main water circuit. Too great a force in tightening the unions usually resulted in a shearing of the soft brass. Steel spindle inlets were not available after enquiries to suppliers.

A check was made on the uniformity of rim loading in the case of the large composite specimen. It was felt to be necessary to check that the bag was applying, in practice, a uniformly distributed load over the rim surface of the specimen.

Electrical resistance strain gauge readings were taken on each side steel cheek ring during a short load cycling test.

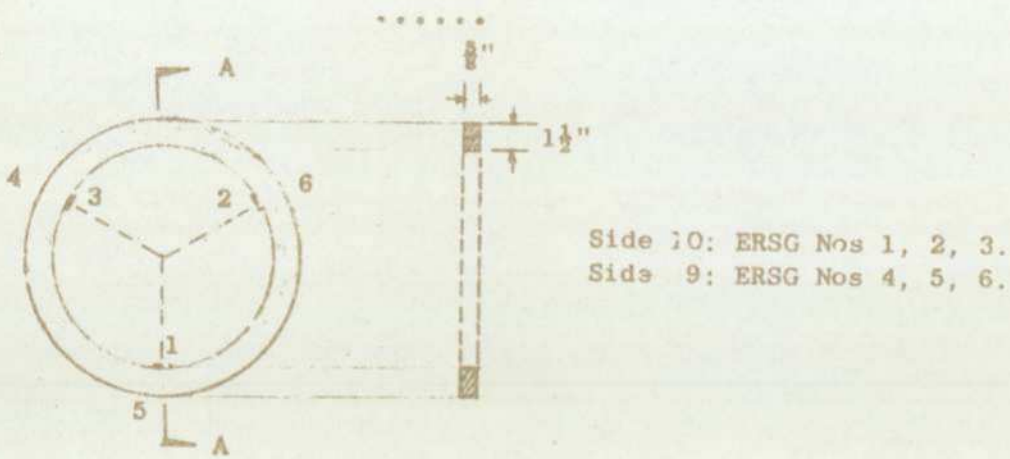
The strain readings resulting from this test indicated that this fear was groundless. See Fig. 25.

CHECK ON THE UNIFORMITY OF RADIAL PRESSURE:

SIDE NO:	ERSG. NO:	READING:	PRESSURE IN psi:	STRAINS:
10	1	1432.0)	zero.	
	2	1607.0 (		
	3	1518.6)		
9	4	1587.0 (		
	5	1585.0)		
	6	1506.2 (		
10	1	1366.0)	1500.	660
	2	1551.0 (		560
	3	1462.0)		566
9	4	1505.0 (		820
	5	1527.0)		580
	6	1459.0 (		472

Strain = Difference of reading x $\frac{2.00}{2.08}$ (in microstrains).

Note: The ERSG., paired on cpposite sides:-
1 & 5, 2 & 6, 3 & 4.



Ring Elevation and Section

FIG. 25.

SERIES 1 - CHRONOLOGY OF EVENTS

Days from start of test	Date	Operation
	20. 6.1967	Casting of Specimens
0	24.11.1967	Load cycling
1	25.11.1967	Readings. Loaded at lab. temp.
4	28.11.1967	
6	30.11.1967	
11	5.12.1967	
19	13.12.1967	
25	19.12.1967	
26	20.12.1967	Heat applied-transient period
46	9. 1.1968	
47	10. 1.1968	Readings. Loaded elevated temp.
49	12. 1.1968	
54	17. 1.1968	
55	18. 1.1968	
59	22. 1.1968	
60	23. 1.1968	
61	24. 1.1968	
62	25. 1.1968	
66	29. 1.1968	
67	30. 1.1968	
68	31. 1.1968	
69	1. 2.1968	
73	5. 2.1968	
74	6. 2.1968	
76	8. 2.1968	
80	12. 2.1968	
82	14. 2.1968	
83	15. 2.1968	
88	20. 2.1968	
90	22. 2.1968	
94	26. 2.1968	
97	29. 2.1968	Load cycling - H O T
98	1. 3.1968	Heat switched off-cooling period
101	4. 3.1968	
101	4. 3.1968	
102	5. 3.1968	Readings. Loaded lab. temp.
108	11. 3.1968	
109	12. 3.1968	
110	13. 3.1968	
111	14. 3.1968	
116	19. 3.1968	
117	20. 3.1968	
118	21. 3.1968	
122	25. 3.1968	
123	26. 3.1968	

FIG. 26.

(Continued - SERIES 1)

Day from start of test	Date	Operation
129	1. 4.1968	Readings. Unloaded lab. temp.
130	2. 4.1968	
136	8. 4.1968	
137	9. 4.1968	
139	11. 4.1968	
144	16. 4.1968	
145	17. 4.1968	
146	18. 4.1968	
150	22. 4.1968	
151	23. 4.1968	
153	25. 4.1968	
154	26. 4.1968	E N D

FIG. 26.

SERIES 2 - CHRONOLOGY OF EVENTS

Days from start of test	Date	Operation
	6.3.1968	Casting of Specimens
1	1.5.1968	
2	2.5.1968	Readings.
3	3.5.1968	Unloaded lab. temp.
6	6.5.1968	
8	8.5.1968	
9	9.5.1968	Load cycling
10	10.5.1968	
13	13.5.1968	
15	15.5.1968	
17	17.5.1968	Readings.
20	20.5.1968	
22	22.5.1968	Loaded lab. temp.
24	24.5.1968	
27	27.5.1968	
28	28.5.1968	
29	29.5.1968	
31	31.5.1968	Heat applied - transient period
32	1.5.1968	
36	5.6.1968	
38	7.6.1968	
41	10.6.1968	
44	13.6.1968	
48	17.6.1968	Readings.
51	20.6.1968	
56	25.6.1968	Loaded elevated temp.
58	27.6.1968	
62	1.7.1968	
65	4.7.1968	
70	9.7.1968	
73	12.7.1968	
76	15.7.1968	
78	17.7.1968	Load cycling - H O T
79	18.7.1968	Heat switched off-cooling period
81	20.7.1968	
84	23.7.1968	
86	25.7.1968	Readings.
90	29.7.1968	
92	31.7.1968	Loaded lab. temp.
94	2.8.1968	
96	4.8.1968	
98	6.8.1968	
100	8.8.1968	Load cycling - unloading stage
104	12.8.1968	
108	16.8.1968	
111	19.8.1968	Readings.
114	22.8.1968	Unloaded lab. temp.
118	26.8.1968	
119	27.8.1968	
120	28.8.1968	E N D

FIG. 27

3. The Pressure Circuit

This circuit contained the valves, gauges, air-hydro pump and pipework necessary to circulate the water at the required pressure to the three loading rigs.

An air supply at about 80 p.s.i. (550 kN/m^2) was provided to the top of the pump and a water supply to a position below the piston. Leakage of water at the piston and the lower gland of the pump caused considerable difficulty, and several times the pump had to be stripped and cleaned and new glands provided.

Leaks also occurred at various valves and gauges as well as from the pump and the accuracy and control of the steady pressure conditions were from time to time affected. This led to the air-hydro pump cutting in to maintain pressure at a frequency and over periods of time not anticipated when the circuit was designed. Infrequently the pump stuck and failed to cut in early enough. The maximum range of variation, however, did not lead to errors greater than about 10% of the maximum pressure.

For the test series which required the small perforated specimen to be tested at a pressure no higher than 1125 p.s.i. (7756 kN/m^2), a pressure reducing valve was introduced into the pipeline to this specimen. The valve proved very insensitive to changes in pressure and to attempts to adjust it manually. This led to delays in taking readings, but not to inaccuracy in the pressure registered.

After experience had been obtained in the operation of the pressure circuit and its valves, it was possible to adjust the pressure in the loading rigs and hold it acceptably accurately for

the necessary periods, for reading and load cycling. For the long test periods when no pressure variations were called for, the system maintained the required pressure values to a good accuracy, very few adjustments being necessary, the pump fulfilling its function by maintaining the gauge readings by cutting in from time to time.

4. The Heating Circuit

Practice heating runs on dummy specimens were carried out before the start of the experiments, and it was found possible to maintain a steady temperature.

However, during the tests themselves, some inequality of temperature control was encountered. There was little difficulty in maintaining the constant temperature for the shrinkage specimens but the loaded specimens showed considerable variations, within a specimen, and between specimens. This was because the boundary cooling conditions were different along the rims of the loaded and unloaded specimens.

The loaded specimens were next to the water-filled rubber bags (except for the insulation belting) and were naturally cooled to a greater extent than the shrinkage specimens. The shrinkage specimens were insulated around their rims with conveyor belting and other insulating materials.

To equilibrate the heating of a specimen to achieve as even a distribution of temperature as possible, the following techniques were used:

i) the heating tapes were wound on to the inside face of the insulation heat shields at closer centres at the bottom than at the top

ii) wooden baffles were affixed horizontally across the insides of the shields to prevent the convection of hot air to the top of the specimens

iii) holes were bored through the shields in clusters over hot spots as they revealed themselves from the thermo-couple readings, to facilitate cooling by ventilation

iv) sheets of aluminium foil were spread over the faces of the concrete specimens being carefully threaded over the brass hexagonals, in an attempt to distribute the temperature evenly over the concrete by conduction.

Difficulty was experienced with the operation of the thermostats which controlled the heating circuits, Each face of each specimen had a separate heating circuit connected to a separate variac transformer. Inserted into the concrete, one on each side of a specimen were thermostat probes intended to limit the concrete heat input so that a narrow range of temperature variation was experienced.

However, the thermostats seemed in general too insensitive to maintain the constant temperature of 80°C, and the on-off temperature range of the thermostats too great for close control.

In later work it was found possible to maintain a much steadier level of temperature, merely by the fine adjustment of the variacs alone.

To prevent the heating tapes on the inner faces of the insulation shields from touching the concrete, it was found necessary

to keep back the shields a fixed distance and to wedge it in this position during the interim periods between readings. Hotspots on the concrete faces were thus avoided. At the time of taking readings, however, it was necessary to push the shield fully home over the brass hexagons in order to be able to position the Demec gauges freely over the Demec studs without touching the shield.

The thickness of the shields and the capacity of heating tapes were arrived at after calculating the requirements of heat flow, and after taking into account heat losses and the thermal capacity of the concrete specimens.

The inside faces of the wooden shields were painted with three coats of a fire retardant paint to offset the danger of catching fire. This precaution proved to be necessary and some shields were found after the series of tests to be charred.

Heat losses occurred, leading to a fall in the outer thermo-couple temperatures of from 2°C to 4°C, every time the heating shields had to be removed, to take diametral strain readings across the standpipe tube penetration liners, with the Mercer bore gauge. This loss occurred over a period of a few minutes, first on one face, then on the other of a specimen, as readings were taken, usually every 48 hours.

5. The Temperature Measurement Circuit

The technical details of the thermo-junctions and wires used for thermo-couple temperature measurement have been given.

No difficulty was experienced at the time of concrete casting in positioning those thermo-couples which occurred in the perforated specimens since entry and fixing in accurate positions could be arranged utilizing the support of the standpipes themselves.

The solid specimens, however, presented some difficulties since there were no items to be cast in these specimens to which the thermo-couples could be attached. They were, in the event, merely pushed into the concrete surface to a marked depth at a stage when the concrete had taken a slight stiffness.

The thermo-couples were inserted in clusters of three, with the wires staggered and fastened together, the upper and lower ones being positioned one inch from each concrete face and the centre thermo-couple lying in the centre of the slab.

The runs of both the thermo-couples themselves and the compensating cables to which they were soldered were of identical lengths so that the resistances were equal in all cases. The necessary cold junction was incorporated in the galvonometer instrument.

A calibration test was carried out on the thermo-couples and the Scalamp galvonometer by reference to the readings of a spare thermo-couple and compensating cable of a length identical to the working circuits. This spare thermo-couple was placed in melting ice and the output connected to the galvonometer which was adjusted to read zero.

A mercury thermometer and the spare thermo-couple were then placed in boiling water and calibration readings taken and subsequently plotted, of the temperatures displayed by the galvonometer and the thermometer as cooling occurred. See Fig. 34.

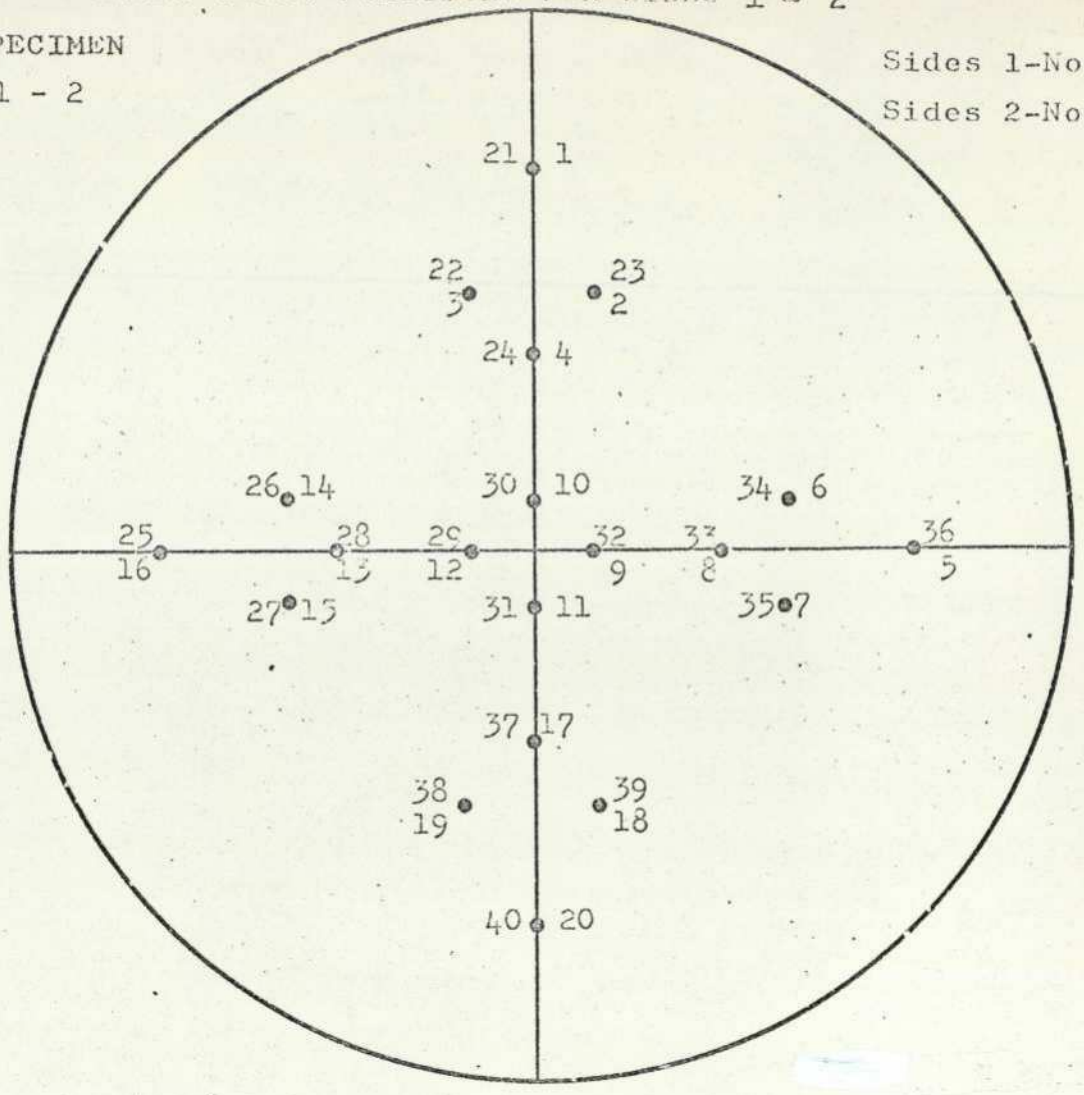
During the test, the temperatures of the thermo-couples could be manually scanned by means of a multi-way switchbox to which the compensating cables were connected by Amphenol plugs.

The thermo-couple, demec point and standpipe diameter measuring positions are shown in Figs. 28, 29, 30, 31, 32 and 33.

DEMEC POINT POSITIONS FOR SIDES 1 & 2

SPECIMEN
1 - 2

Sides 1-Nos.1-20
Sides 2-Nos.21-40



THERMOCOUPLE POSITIONS VIEWED FROM SIDE 2(TOP)

SPECIMEN
1-2

t - top
m - middle
b - bottom

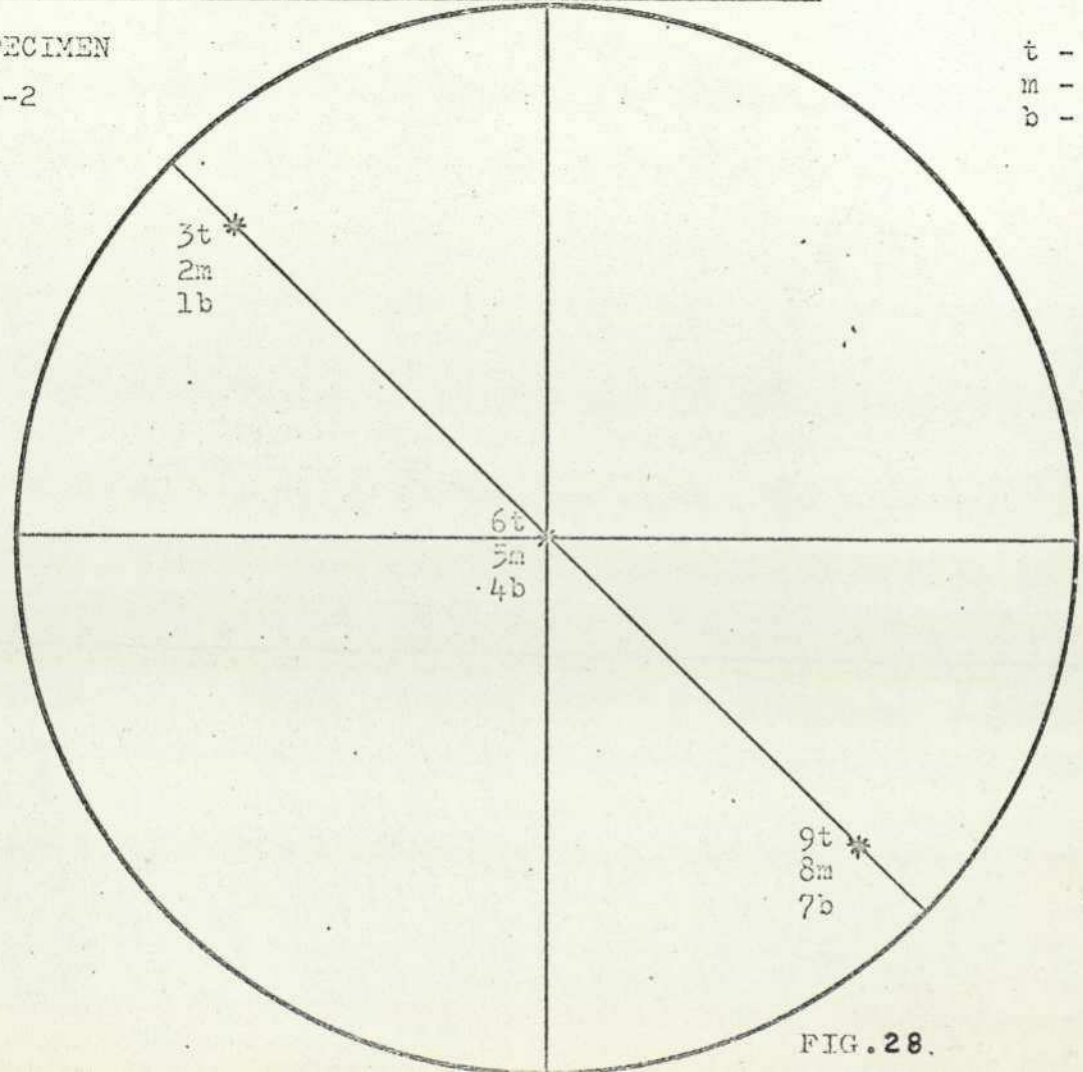
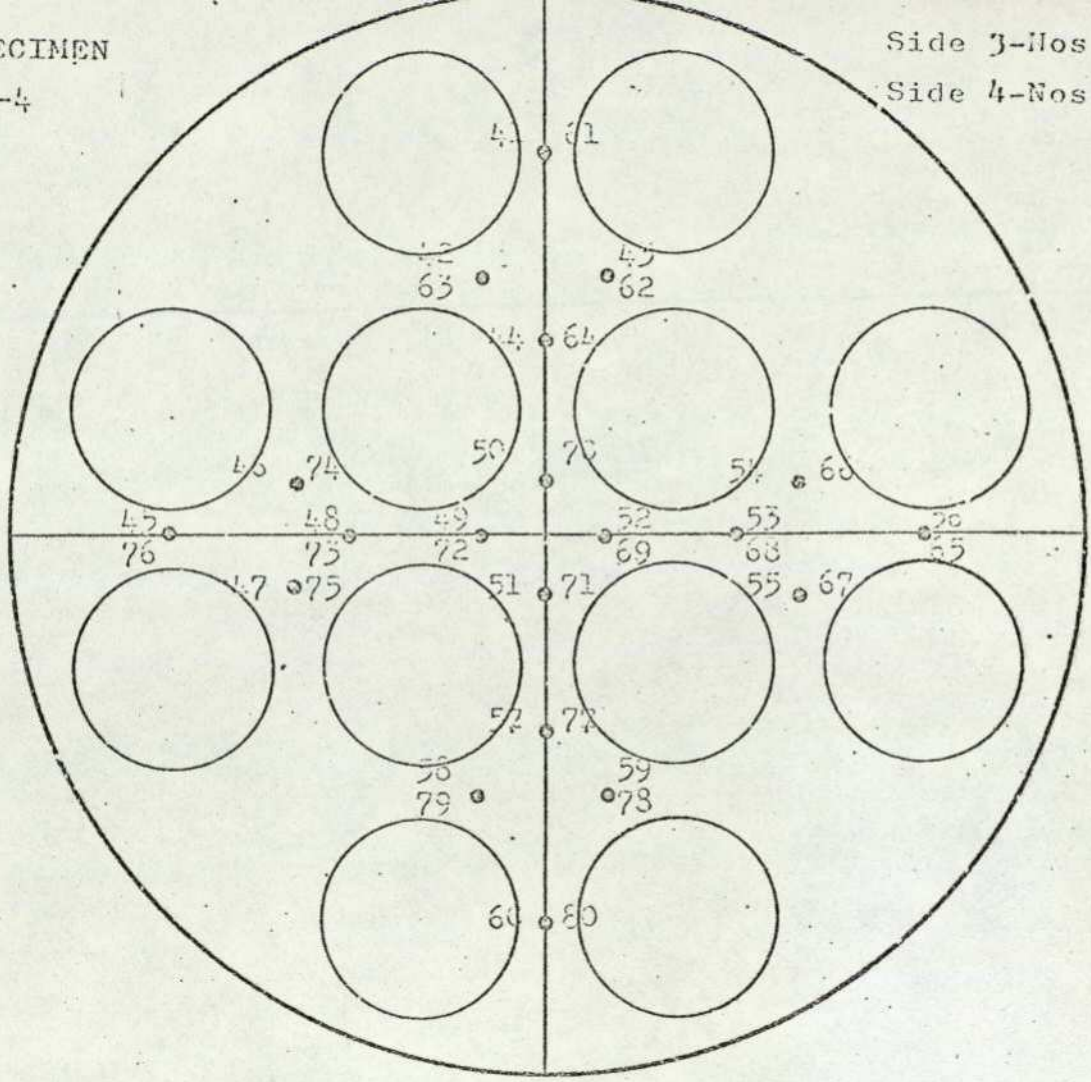


FIG.28.

SPECIMEN
3-4

Side 3-Nos. 41-60
Side 4-Nos. 61-80



THERMOCOUPLE POSITIONS VIEWED FROM SIDE 3(TOP) & STANDPIPE POINTS

SPECIMEN
3-4.

t - top
m - middle
b - bottom

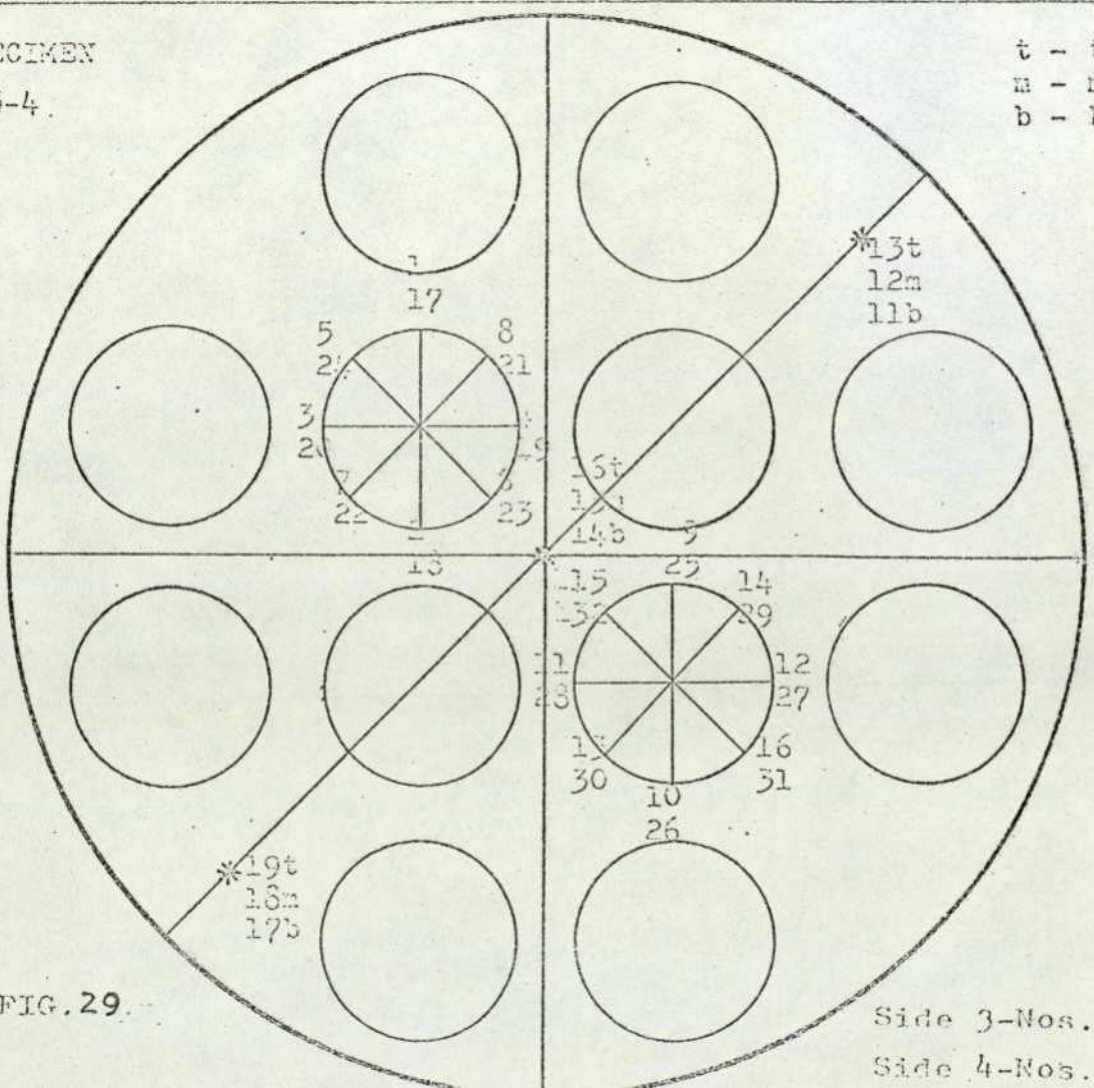


FIG. 29.

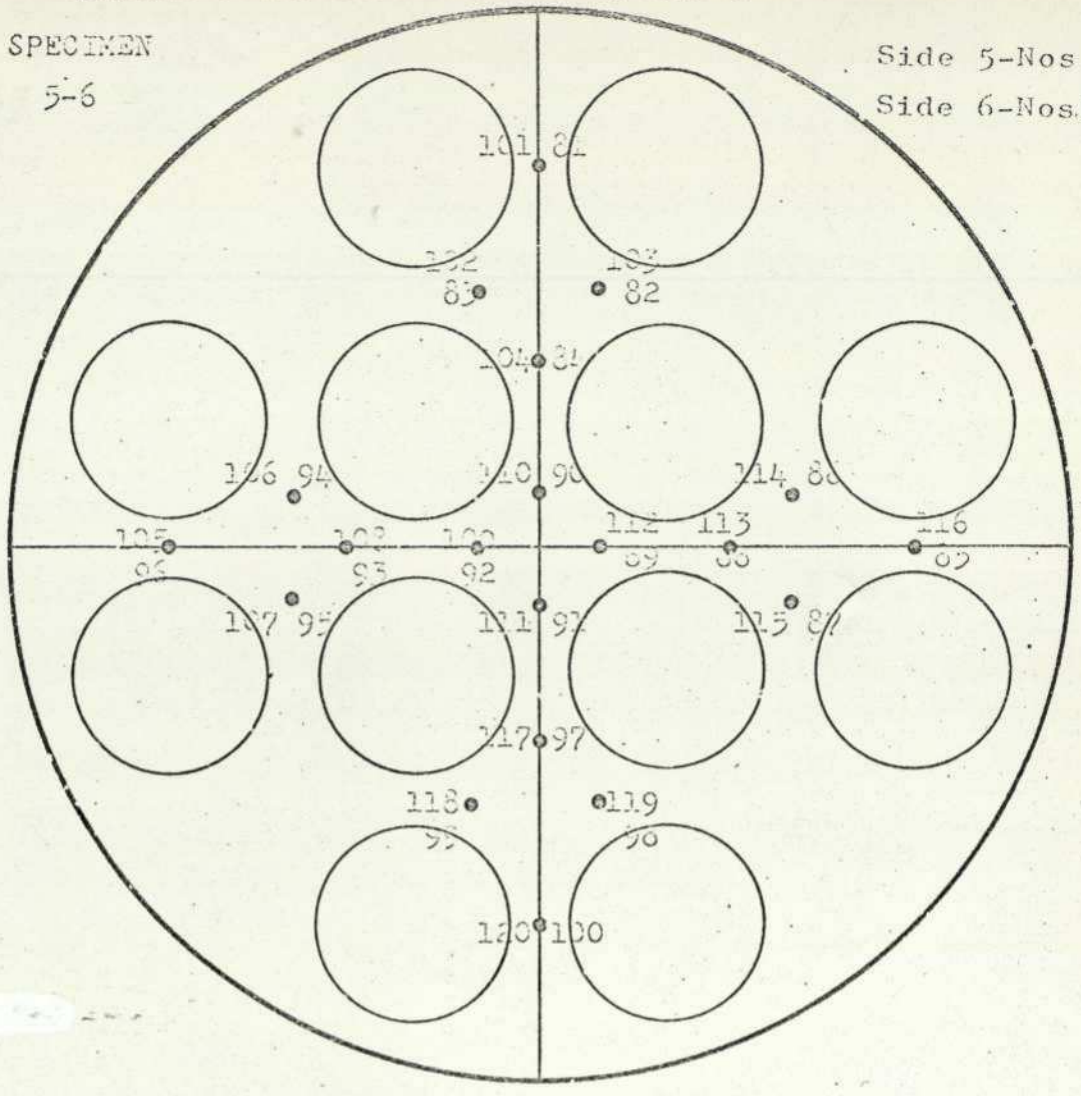
Side 3-Nos. 1-16.
Side 4-Nos. 17-32

SPECIMEN

5-6

Side 5-Nos.81-100

Side 6-Nos.101-120



THERMOCOUPLE POSITIONS VIEWED FROM SIDE 6(TOP) & STANDPIPE POINTS

SPECIMEN

5-6

t - top
m - middle
b - bottom

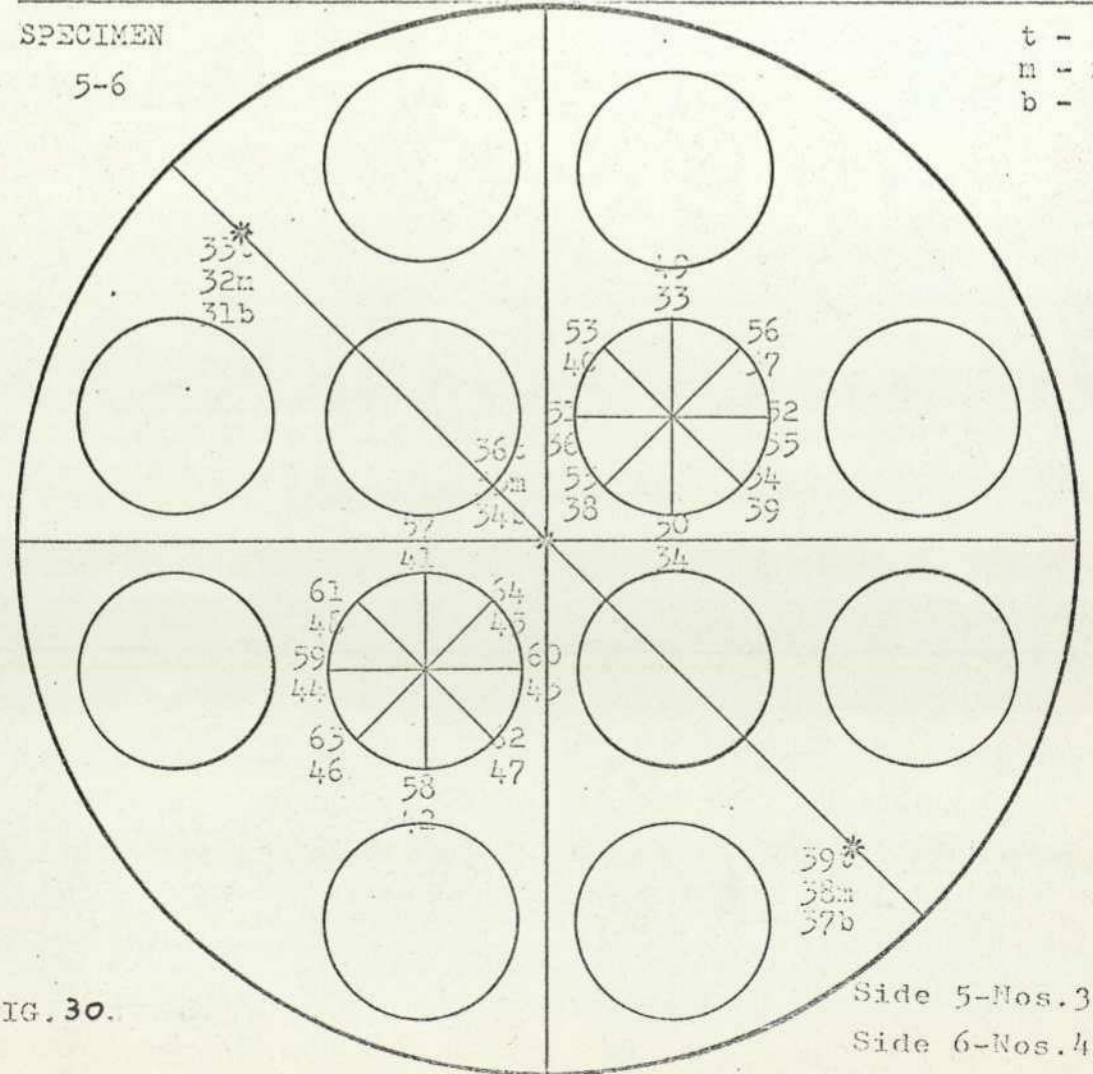


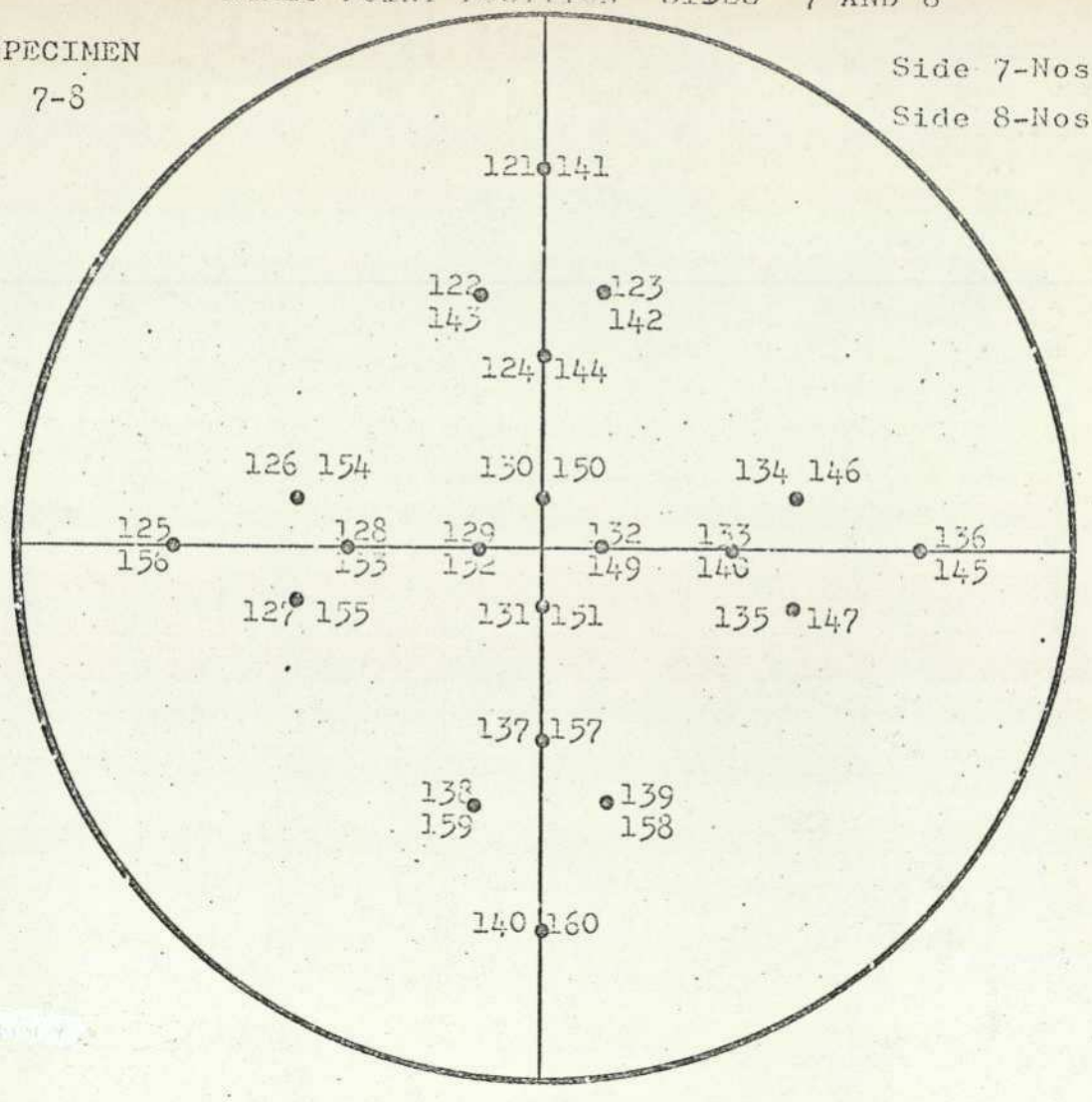
FIG. 30.

Side 5-Nos.33-48.

Side 6-Nos.49-64

SPECIMEN
7-8

Side 7-Nos. 121-140
Side 8-Nos. 141-160



THERMOCOUPLE POSITIONS VIEWED FROM SIDE 7(TOP)

SPECIMEN
7-8

t - top
m - middle
b - bottom

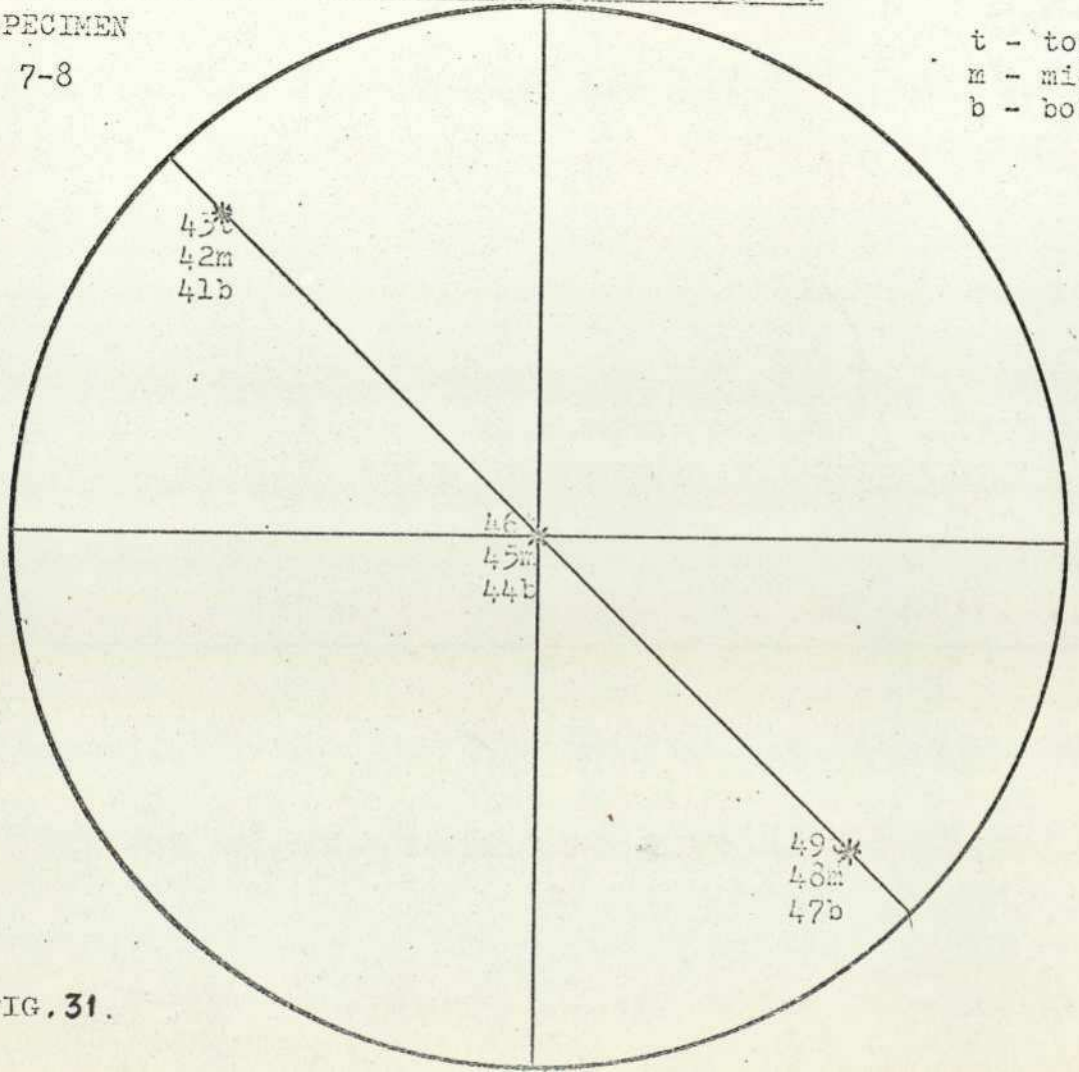


FIG. 31.

DEMEC POINT POSITIONS FOR SIDES 9 & 10

SPECIMEN

9-10

Side 9-Nos. 161-212

Side 10-Nos. 213-264

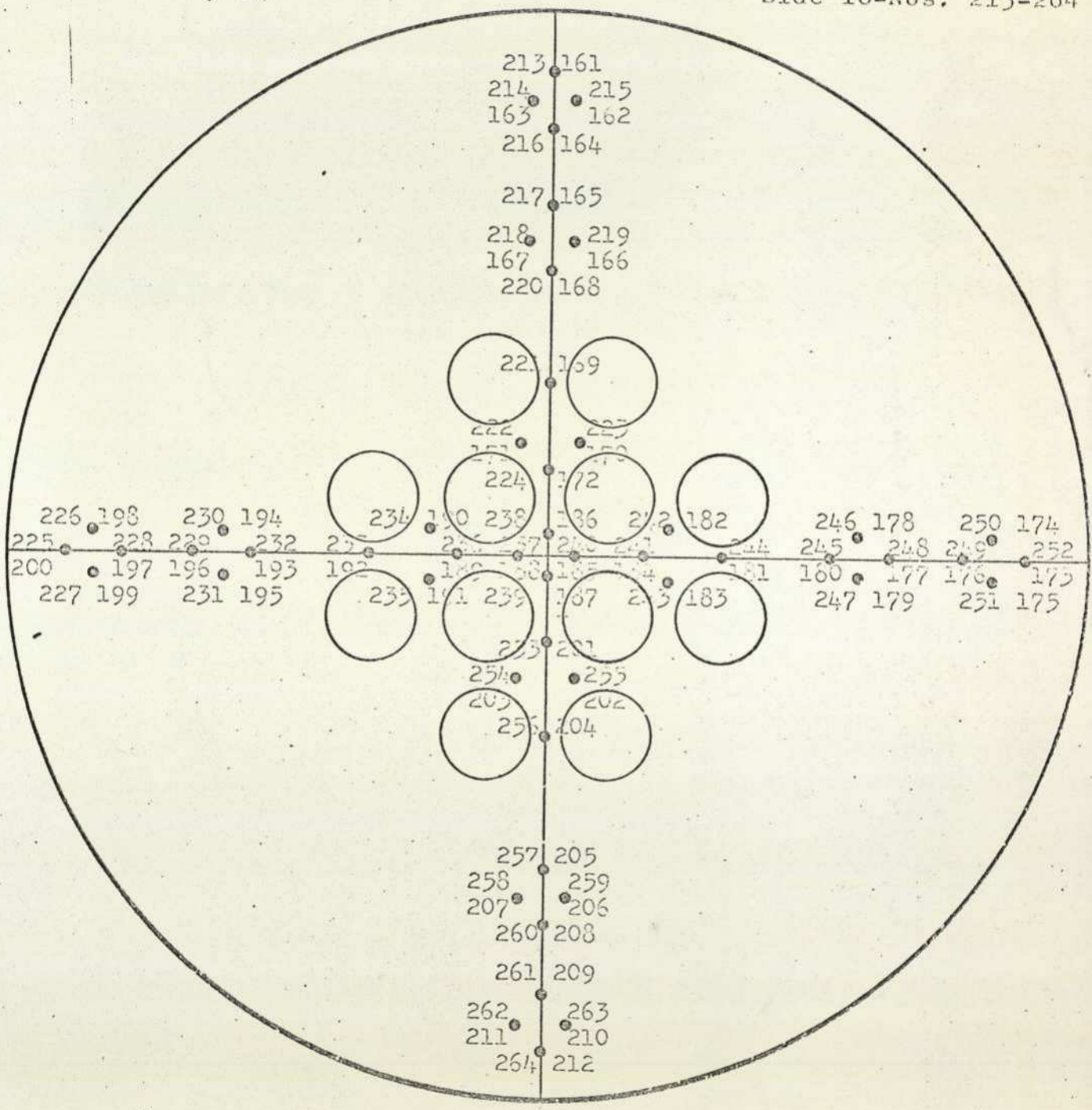


FIG. 32.

THERMOCOUPLE POSITIONS VIEWED FROM SIDE 9 & STANDPIPE POINTS

SPECIMEN
9-10

Side 9-Nos.65-80
Side 10-Nos.81-96

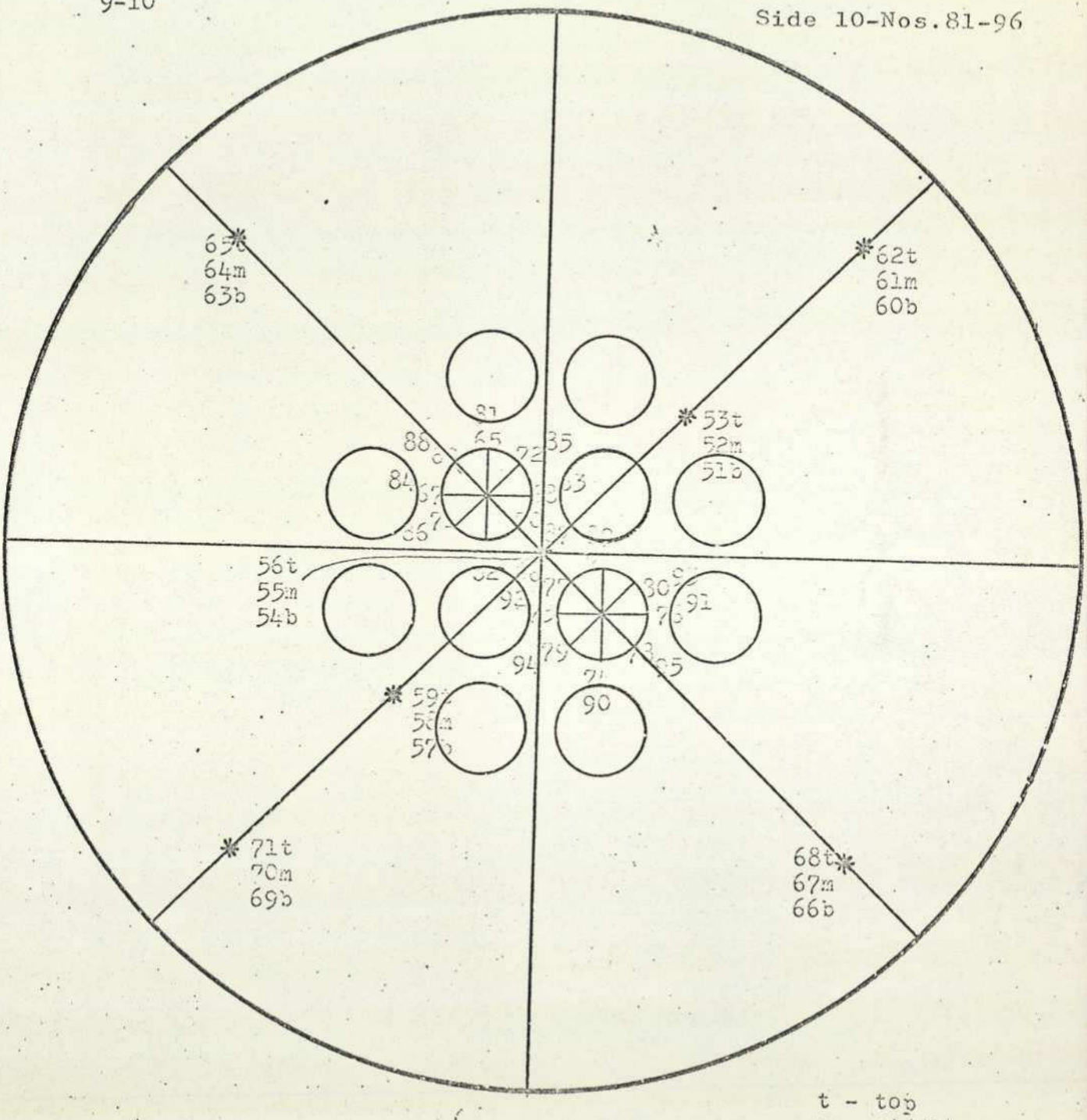


FIG. 33

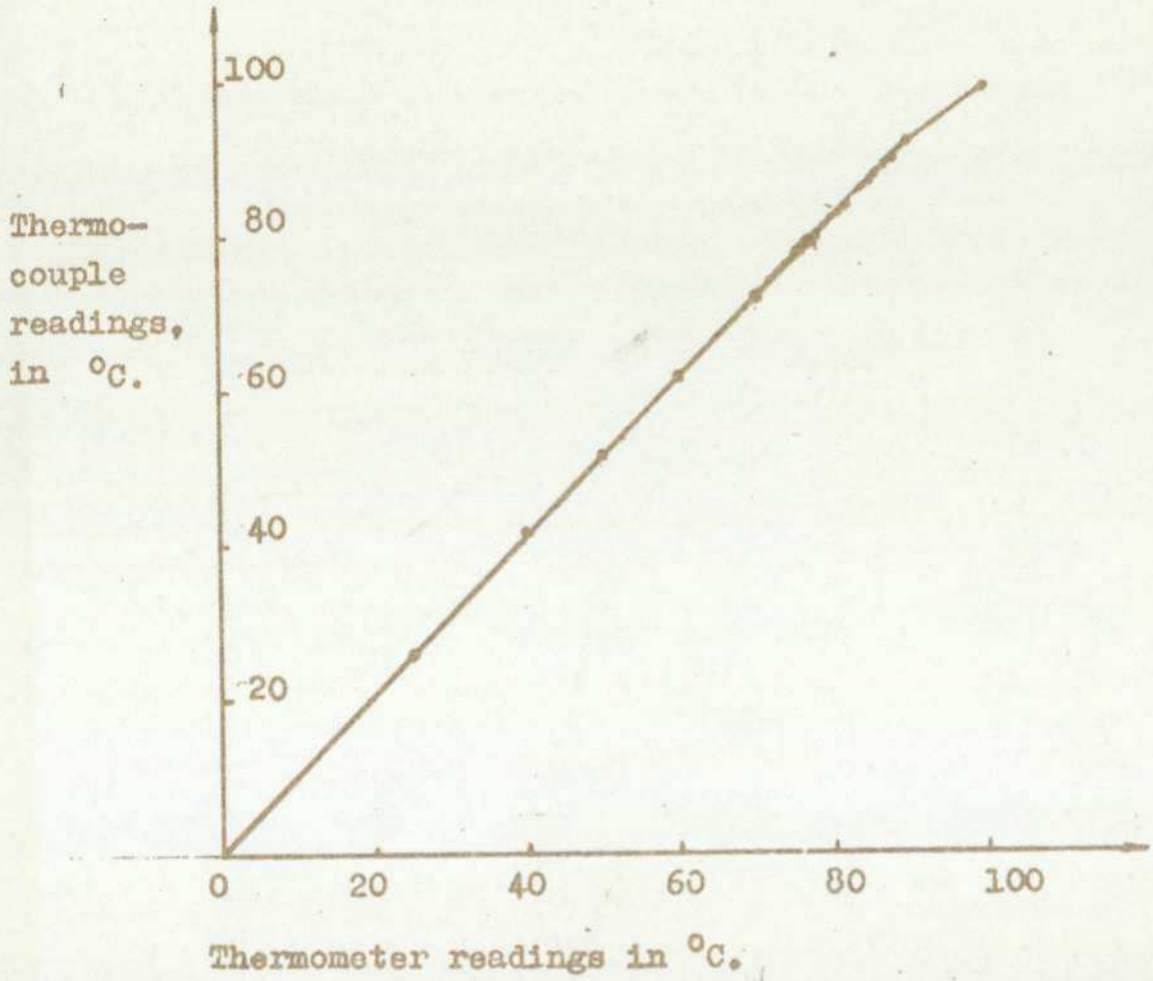


FIG. 34. Thermocouple calibration graph.

Thermocouple calibration
for series 1 & 2.

6. The Electrical Resistance Strain Gauge Circuit

The special techniques employed in fixing the strain gauges have been previously described in detail. Two points are of interest. The pores of the concrete were filled with the adhesive filler so that the gauges when fixed were in intimate contact with the surface along their lengths. The other point is that at the time of pressing on the gauges, they were held with pressure-sensitive tape to permit hardening of the fixative without the gauges peeling off.

The details of the circuitry have already been described.

7. The Crack-detection Circuits

These cannot be claimed to have been a success. It is possible that the strips of conducting paintapplied in the ligaments were too thick to allow the paint to exhibit its brittleness adequately when concrete cracking took place. The use of small bulbs to indicate circuit breaks was too insensitive a technique for this purpose and Avometer readings were taken instead.

Cracking was finally discovered by large changes in E.R.S.G. readings or by visual inspection rather than by the crack-detection circuits. In any case the concentration of fixed E.R.S.G.s and conducting paint strips on the ligaments together with the mass of electrical leads from the connections, was so great that visual inspection was hampered and the method was subject to random circuit breaking and the consequent misleading signals.

8. The Strain-measuring Instruments

The technique of obtaining accurate readings from Demec gauges can only be developed by practice and experience. Differences in readings can occur due to differences in individual pressures and temperaments. Meaningful readings can be obtained by the application of uniform procedures over a period of time.

It was discovered that readings taken with the large Demec gauge, 11.428" (290.5 mm), were more uniform and consistent than those taken with the 2" (50.8 mm) gauge. The large gauge was physically easier to mount and read, and the percentage accuracy was generally greater than for the small gauge.

It is also possible that the heat of the hand over long periods of reading caused expansion errors in the main bar of the instruments although this possibility was not investigated.

The Mercer bore gauge was an instrument of low sensitivity in spite of the considerable modifications made both to the instrument and to the measuring technique and arrangements within the standpipe bore. Although expected trends were apparent in the diametral readings obtained, the validity of any one reading was frequently in question.

In the infancy of the experiments, it was discovered that too great a length of brass hexagonal stud projecting from the concrete face led, under pressure from the Demec gauges when they were being applied to the Demec points, to a lateral deflection which made nonsense of any attempt to read the instruments. It is recommended that studs of these dimensions should not project any more than 1" from the concrete face.

9. The Steel Moulds and Jig

The moulds for the concrete specimens consisted of machined steel baseplates and semi-circular steel side walls. The walls were bolted together, and then bolted down to the baseplates. This formed a robust arrangement capable of withstanding the placement, the compaction and the vibration of the concrete during casting of the specimens.

The 6" (152.4 mm) long by 3" (76.2 mm) O.D. standpipe liners for the perforated specimens were located and rigidly fixed to the baseplate, at the bottom only, by a tight push fit over male steel plugs recessed and secured to the baseplate by countersunk bolts.

Countersunk fixing bolts were used to secure the bottom ends of the hexagonal bars which were arranged to lie across the specimen thickness to take the brass studs subsequently. The strains experienced by the Demec points were thus generated across the thickness of the specimen and not merely surface effects. This expedient led to the desired strains being recorded and a firm fixing being achieved for Demec points on both sides of the specimens.

Two further points are of interest with regard to these cross bars. They were made hexagonal to prevent rotation in the concrete when, subsequently the brass studs were being screwed into their ends and secondly their ends were encased in $\frac{3}{8}$" (9.5 mm) long soft plastic tubular sleeves. The softness of the plastic material was intended to eliminate stresses on the bars due to surface effects.

To ensure accuracy of positioning of the hexagonal bars and thus of the Demec points, a cruciform jig was made up in the form of a steel template through which a series of conical steel spigots

were threaded. When the cruciform jig was bolted into position over the top of the mould the conical spigots registered in precise positions over the fixed bars. The jig was used for drilling the baseplate. It was also used as a check for hexagonal bar positioning before and during concreting and was removable.

C. The Sealing of the Specimens

As soon as the specimens were removed from curing conditions it was necessary to seal their outer rim surfaces.

The point of this was to simulate as near as practicable the condition of the end slab in an actual reactor vessel which, because of its continuity and contact with the cylindrical walls, is unable to lose moisture in this direction. Shrinkage could only be allowed from each flat face therefore and after drying, the rims were painted with three coats of Peridite thixotropic paint, viz a primer, a sealer and a finishing coat.

Not only had time to be allowed for the concrete surface to dry out before applying the first coat, but periods of time were required for the same purpose between coats. Several days of shrinkage were consequently lost after curing before the initial datum readings could be taken.

Nothing could be done about this, since painting, stud fixing and Demec reading could not be allowed to continue concurrently. This difficulty, however, cannot be considered critical.

SECTION VII

THE VARIATION OF CONCRETE CONSTANTS WITH AGE AND TEMPERATURE

Concrete is a most adaptable building material, combining to a marked degree the virtues of economy, ease of construction, and versatility in many different applications.

It can be used in varied shapes, in large masses, and in thin reinforced sections; in the prestressed concrete vessel application it functions in the twin roles of biological shield and pressure container. When too much is demanded of it, in places of local overstress, it modifies its nature and adapts its response to the conditions by flowing plastically, by micro-cracking and by deforming visco-elastically so that a new regime of stress equilibrium and geometrical compatibility is established without major breakdown of the structure.

Computer-aided numerical solutions of the finite element type, employed in the analyses of concrete structures, even for complex continua, have now eliminated the need for short-cut approximations, since the many arithmetical computations involved can now be economically and swiftly resolved.

Nevertheless, since the adaptability of concrete depends in large measure on its ability to modify its behaviour according to the demands made upon it, proposed analyses however sophisticated, must still take into account the changes in those material constants which condition the flow of stress, the conduction of heat and the accommodation of strain.

In the finite element approach, for example, displacement functions can be chosen which uniquely define the state of strain within an element in terms of nodal displacements. Since these

strains, taking into account the properties of the material, will define the stress state at the boundaries of, and within the element at any moment, even in assessing the elastic response of the material, it is necessary to know the value of the changing concrete constants at that moment.

Accordingly, it is essential to be aware of the effects, on the behaviour of the material, of ageingand temperature, two factors influencing the long-term loading and operation of a prestressed concrete pressure vessel.

1. Compressive Strength of Concrete

This property increases with age according to well-established laws. See Fig. 35. This is due, in the main to continued hardening of the concrete as the cement hydration continues.

Some remote particles of cement may only meet with the necessary moisture for hydration after considerable time has elapsed and further time may be required for the innermost parts of some cement grains to be hydrated.

It is thus clear that the rate of development of compressive strength and, to some extent, the ultimate magnitude of compressive strength depend to a considerable degree on the relative humidity of curing conditions and the subsequent hardening conditions. For moist-cured concrete, the increase in strength with age, may be arrested by a sudden withdrawal of moisture especially at an early age, (28).

When the time under load is considered, Fulton (44) finally

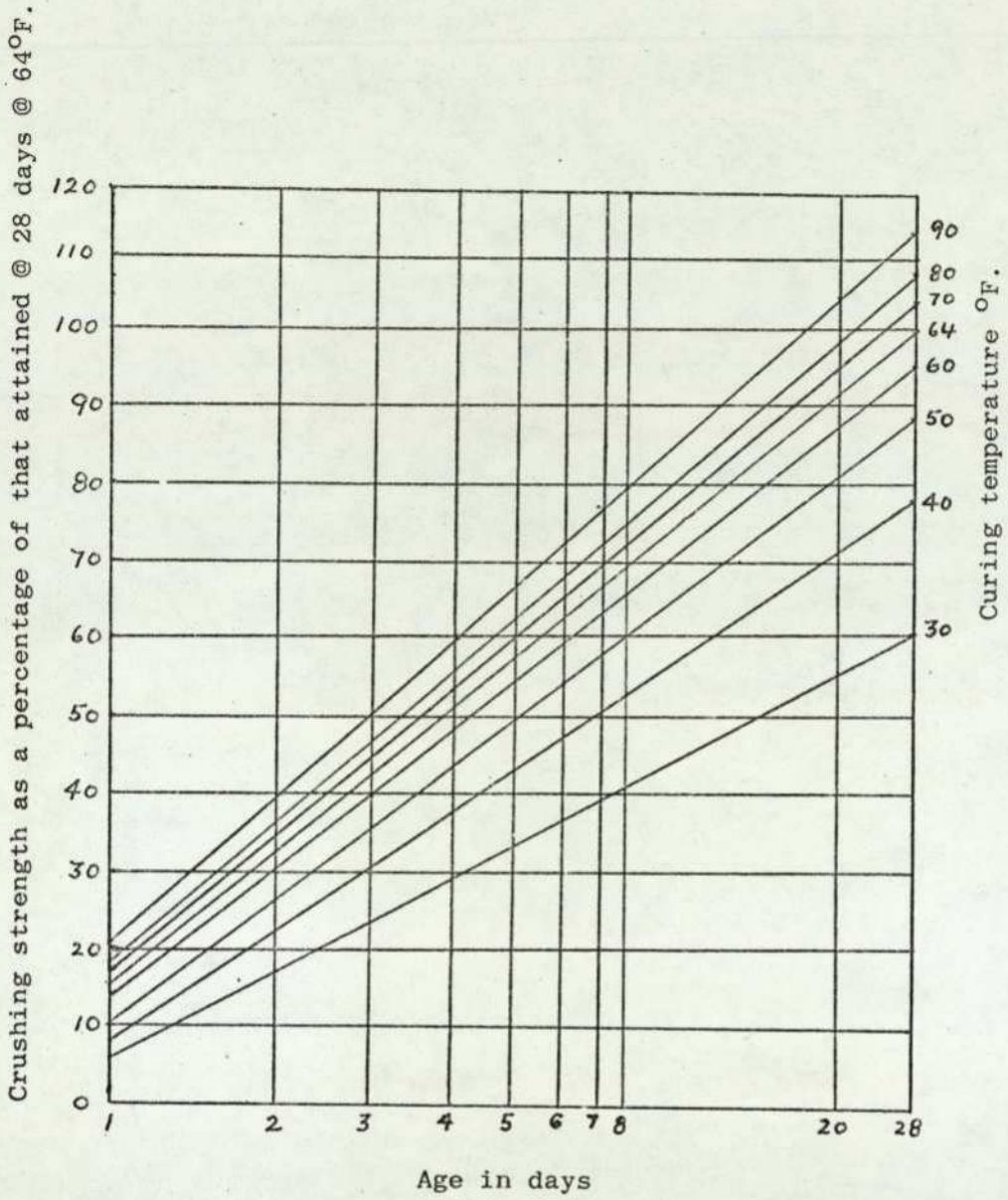


Fig.35. Relationship between curing temperature, crushing strength and age in Portland cement concrete

concludes that under long-term loading, concrete specimen failure occurs at stresses below the ultimate as determined by the normal test procedure.

It has been well-established that for almost all cements, the hydration reaction is accelerated when heat is applied to a concrete during setting and in the early days of the hardening process. Conversely, some cements will not set in concrete mixtures at ambient temperatures at or near freezing point. The assistance given to the very early hardening process by the application of elevated temperature is short-lived, because moisture is driven off rapidly and the further normal stage of hardening due to continuing hydration is prohibited. The gain in early compressive strength levels off rapidly as a result. Over a period, a loss in strength is experienced by the concrete under these conditions, (44), (50).

Again, for mature concretes which have experienced normal setting, curing and hardening conditions, the subsequent application of elevated temperature drives off the moisture and compressive strength is lost (36).

Murdoch (49) has also indicated the relationship between curing temperature, compressive strength and age for Portland cement concretes. See Fig. 35.

Saemann and Washa (42) state that a loss in compressive strength of about 10% occurs in concrete at a temperature of about 90°C to 100°C.

2. Tensile Strength

The tensile strength of concrete bears a relationship to the compressive strength, being of the order of $\frac{1}{10}$th to $\frac{1}{12}$th of the compressive strength. The tensile strength increases with age.

It is not common practice to measure the tensile strength of concrete by conducting pulling tests on specimens. This is mainly due to the effect on the results, caused by the influence of the gripping devices in the testing machines.

In the so-called Brazilian test, cylinders are compressed in a horizontal position so that they split in two along the longitudinal axis. This is considered to give a measure of the splitting strength of the cylinder and thus indirectly, the tensile strength of the concrete.

Beam tests may be carried out which can indicate the bending tensile strength of the concrete. The strength in flexure of concrete (42) depending closely on the tensile strength, decreases under elevated temperatures rather more rapidly than does the compressive strength.

The degree to which the cement paste can bond together the fine and coarse aggregates in a concrete, is the main factor in determining the tensile strength. The ratio of tensile strength to compressive strength at ambient temperatures is influenced (28) by the properties of the fine aggregate, the shape, texture, and grading of the coarse aggregate, the compaction technique, the curing conditions and the age of the concrete.

The relatively low tensile strength of concrete, resulting in part from its brittleness, determines the stress level at which

cracking can be expected, and in forecasting the cracking behaviour of a structure in prestressed concrete a knowledge of the magnitude of the tensile strength is essential.

3. Poisson's Ratio

Poisson's Ratio has a range of values for concretes from about 0.08 to 0.21. Values frequently taken in calculations are of the order of 0.11 to 0.18. The ratio varies in magnitude with the factors which affect the other concrete properties. The values given above apply only at low levels of stress, since as the stress increases the volumetric strain sustained by the concrete begins to owe much of its magnitude to the spread of micro-cracks which affect the apparent Poisson's Ratio.

The "Poisson's Ratio effect" is responsible for an effective increase in stiffness in slabs where the transverse strain accompanying the longitudinal stress causes an additional restraint on bending. The stiffness in a unit width of the slab is represented by the term $\frac{Ed^3}{12(1-\nu^2)}$ rather than, as for a laterally unrestrained beam, $\frac{Ed^3}{12}$, where d is the thickness and ν the Poisson's Ratio of the material.

Poisson's Ratio may be quoted in three forms:

(a) the ratio between the elastic lateral and longitudinal deformations on loading,

(b) the ratio, after sustained loading, between the lateral and longitudinal deformations due to creep alone

(c) the ratio of the total lateral deformations to the total longitudinal deformations, taking both the elastic and creep strains together; this is known as the effective Poisson's Ratio.

There is a tendency for Poisson's Ratio to increase with time under continued uniaxial loading. Davis and Troxell (51) concluded that the creep Poisson's Ratio increased with age, but became sensibly constant after 500 days of sustained loading. Similarly Kordina (48) found that the effective Poisson's Ratio increased under long-term loading by between 25% and 33%.

L'Hermite (52), Duke (53) and Hannant (54) concluded separately that the elastic and creep Poisson's Ratios are similar in magnitude. Hannant's work extended to temperatures up to 95°C. He investigated the strain behaviour of concrete for varying stresses and sustained loading.

Modulus of Elasticity

It has been well-established that Hooke's Law applies only to concrete at low levels of stress and that as the stress increases or is sustained even at low levels, inelastic strains occur which make the stress-strain relationship non-linear.

Above the low level of stress up to which linearity obtains, there will therefore occur a reduction in the magnitude of the modulus of elasticity.

Several moduli may thus be recognised. The tangent modulus of elasticity is obtained from the gradient of that initial instantaneous section of the stress-strain curve where linearity and Hooke's Law apply. This value of the elastic modulus represents a temporary even unrealistic condition, and although it is frequently used in practical design calculations, it can give rise to misleading assessments of structural strength.

At higher levels of stress, the stress-strain relationship will be showing a marked curvature, and the secant modulus of elasticity can be determined at any point along this curving line by dividing the stress by the total strain in the usual way. Clearly a secant modulus will be lower in value than the corresponding tangent modulus.

The normal practice in conducting a loading test on a concrete specimen, is to apply the load at a rate of about 2000 p.s.i. (13,800kN/m^2) per minute and to consider the initial deformation on loading to be the elastic strain and the subsequent increase of strain with time to be the creep.

If the load is maintained for a period or increased, the strain will continue to increase for a very small rise in stress, or even without a rise in stress, and it is common practice to consider an effective modulus of elasticity after such a period which will take into account a realistic amount of creep. Such a modulus would represent more nearly the state of affairs for an installed concrete structure under a constant load over a long period of time.

Effective modulus calculations relating to the models in the present series of tests have been given in the Appendices to this thesis. The use, however, of a single value of modulus in such calculations, must lead to errors in time, as the nature of the concrete and its real modulus continue to change.

Ultrasonic methods of testing concrete measure the velocity of impulses in the material or the natural frequency of vibration in long prismatic members.

The time for the test is very short and the velocity of the impulses very great, so that the effect of creep can be ignored. The dynamic modulus of elasticity so obtained, after adjustment, is found to be close in magnitude to the tangent modulus.

The value of elastic moduli in concrete depends upon the stiffness of the cement matrix, on the nature and grading of the aggregates, and on the degree of compaction of the mixture. It is also related to those other properties and placement techniques which lead to good concrete of high strength. The air content and free water content in a concrete will influence its rheological behaviour and play a part in determining the magnitude of its modulus of elasticity and other elastic constants. Most of the factors

which ensure high compressive strength, affect the elastic stiffness of the concrete and thus ensure high moduli of elasticity.

The European Committee for Concrete (55), has suggested that the secant modulus may be related to the 28 day cube strength, u by the empirical relationship:

$$E_c = 71000\sqrt{u}$$

where E_c is the secant modulus for instantaneous or rapidly-changing loads.

Hansen (37) supports, with a theoretical and experimental investigation, the view that there is a considerable degree of correlation between elastic modulus and concrete strength.

Neville (28) points out, however, that at later ages, the modulus increases more rapidly than the concrete strength.

When the effect of elevated temperature is considered, greater strains are noted for a given loading on a concrete specimen than for the same loading at ambient temperature. Greater creep occurs at higher temperature and this partly explains the greater strains, but a reduction in the modulus of elasticity is considered to be responsible for the remainder of the strain increase.

This view is supported by Philleo (56), who found that the dynamic modulus decreased with an increase in temperature. He observed a reduction of this modulus by 11% to 14% as the test temperature was increased from ambient to 90°C.

These findings are confirmed by Saemann and Washa (42) who state that their experiments showed a reduction in the modulus of elasticity of between 10% and 25% as the test temperature was raised to 100°C.

Hansen (37) states that if E is the elastic modulus, T is the absolute temperature and A and B are empirical constants, a relationship exists of the form

$$E = A - BT.$$

The values of A and B may be fixed from experimental data.

The effect of moisture loss and temperature on the modulus of elasticity was investigated by England (45). After 80 days of loading at 1000 p.s.i. (6900 kN/m^2), covering a temperature range from 20°C to 140°C, both sealed and unsealed specimens, on unloading, showed a reduction in the value of modulus of elasticity of 20% to 25%.

The reduction in the modulus of elasticity due to elevated temperature, appears to occur immediately after the application of heat. Further changes under continued heating appear negligible.

5. Coefficient of Thermal Expansion

It is desirable to limit the extent to which concrete expands when heated, so far as this is practicable. A low value for the coefficient of thermal expansion of concrete ameliorates to some degree the problem of secondary thermal stresses.

Work carried out by Bonnell and Harper (57) has shown that the expansion coefficient of the aggregate used has a direct effect on the expansion coefficient of the resulting concrete. Gravel aggregate concrete exhibits the greatest expansion whilst limestone concretes show the least expansion.

The effect of age on unsealed concrete is to decrease the value of the expansion coefficient with time.

An increase in relative humidity also causes a decrease in the coefficient.

For a considerable increase in the temperature of concrete, the coefficient of thermal expansion is unaffected. Above about 800°F, however, there is an increase in the value of the coefficient.

Browne (39) concluded that as concrete dries out from saturation, the coefficient of thermal expansion increases to a maximum at 70% relative humidity and subsequently, at lower humidities, decreases slowly. If sealed specimens are allowed to age at ambient temperature, no significant changes in the coefficient are discernible (39). This would indicate that changes in coefficient with age, observed by other investigators, are related more to moisture changes than to the ageing process.

6. Thermal Conductivity of Concrete

This property of concrete is very closely related to the free water content and also varies as the density.

Particularly in concrete structures of the nuclear reactor vessel type, it is not practicable to prohibit moisture movement. The thermal conductivity is likely to vary from member to member and from point to point within the structure, nor is it easy to carry out conductivity tests with any degree of reliability on the full-scale structure. The conditions of laboratory experiments, moreover, are likely to be basically different from full-scale operational conditions.

The tests carried out by the United States Bureau of Reclamation on the Boulder Dam and other projects have given conductivity values which are amongst the most useful data available.

Two other concrete properties affecting temperature distributions throughout a concrete member are the specific heat and the thermal diffusivity.

Diffusivity is related closely to the type of aggregate and is obtained from the thermal conductivity of concrete by calculation; it is also related to the heat capacity of the concrete per unit volume.

Klein (40) states that the diffusivity of adiabatically-cured concrete is found to decrease by about 20% as the temperature rises by 55^{o}C. The diffusivity decreases with age.

A method for predicting the temperature distributions throughout a concrete mass has been indicated by Ross (58), which takes into account the heat of cement hydration, the thermal properties of the concrete, the method of construction and the ambient conditions.

SECTION VIII

THE NATURE OF CREEP AND SHRINKAGE

A. CREEP

Creep in concrete reveals itself as a dimensional change in the material under the influence of sustained mechanical loading (4), (5), (6), (7), (8), (11). Quite small loads will cause the concrete to deform. Even the self-weight of a concrete member is sufficient to initiate creep.

The phenomenon of creep occurs at elevated as well as at ambient temperatures. Elevated temperatures, in fact, increase the rate of creep.

Creep causes, in a loaded member, a stress redistribution, during the transient period before steady state stress conditions are reached after several months. In some circumstances, stress redistribution can be beneficial, for example in the relief of locked-in stress, but in others disadvantageous, as in the relaxation of steel prestress.

Concrete is a material of such variability that elastic and creep data obtained from observations on a concrete structure under particular loadings and circumstances can be considered characteristic only of that concrete and those circumstances.

There is a general inter-relationship between concrete strength and creep (28), (29) ; the stronger the concrete, the smaller the creep.

It has long been established that creep strain is time-dependent, and the total amount of creep at any time, increases at a decreasing rate.

Creep is more a property of the cement paste than of the aggregates, although crystalline mineralogical creep deformations contribute to the total dimensional changes involved.

1. THE MECHANISMS OF CREEP

To explain the creep behaviour of concrete, the most favoured theory (9) supposes that the deformation process occurs as a result of a combination of (a) seepage and (b) viscous flow.

In justifying the theory of seepage it has been claimed that creep is due to the movement or expulsion of gel water from within the gel pores. The water, under the influence of loading, migrates from the most heavily stressed regions through the pores and capillaries in the concrete.

The viscous flow theory sees the water as a lubricant which permits sliding, relative to one another, of the crystalline surfaces in the cementitious compounds under the shear forces set up by the load. The deformation is seen as a viscous or plastic flow in the cement paste which thus transfers the load into the interlocked mass of aggregate particles.

2. CREEP CURVES; SPECIFIC CREEP; CREEP COEFFICIENT

Representative curves of creep strain plotted against time are shown in Fig. 36 . A concrete specimen subjected to uniaxial compression manifests an immediate elastic deformation. If the load is sustained, additional strains due to creep occur, the rate of which decreases with time in the manner shown. On removing the load there is an immediate elastic recovery followed by a recovery of creep strain the rate of which rapidly decreases with time. A residual strain is left greater in magnitude than the initial elastic strain. It must be realized that during the period of such a test, other important concrete constants will have been changing. Young's Modulus for instance will have been increasing as the concrete

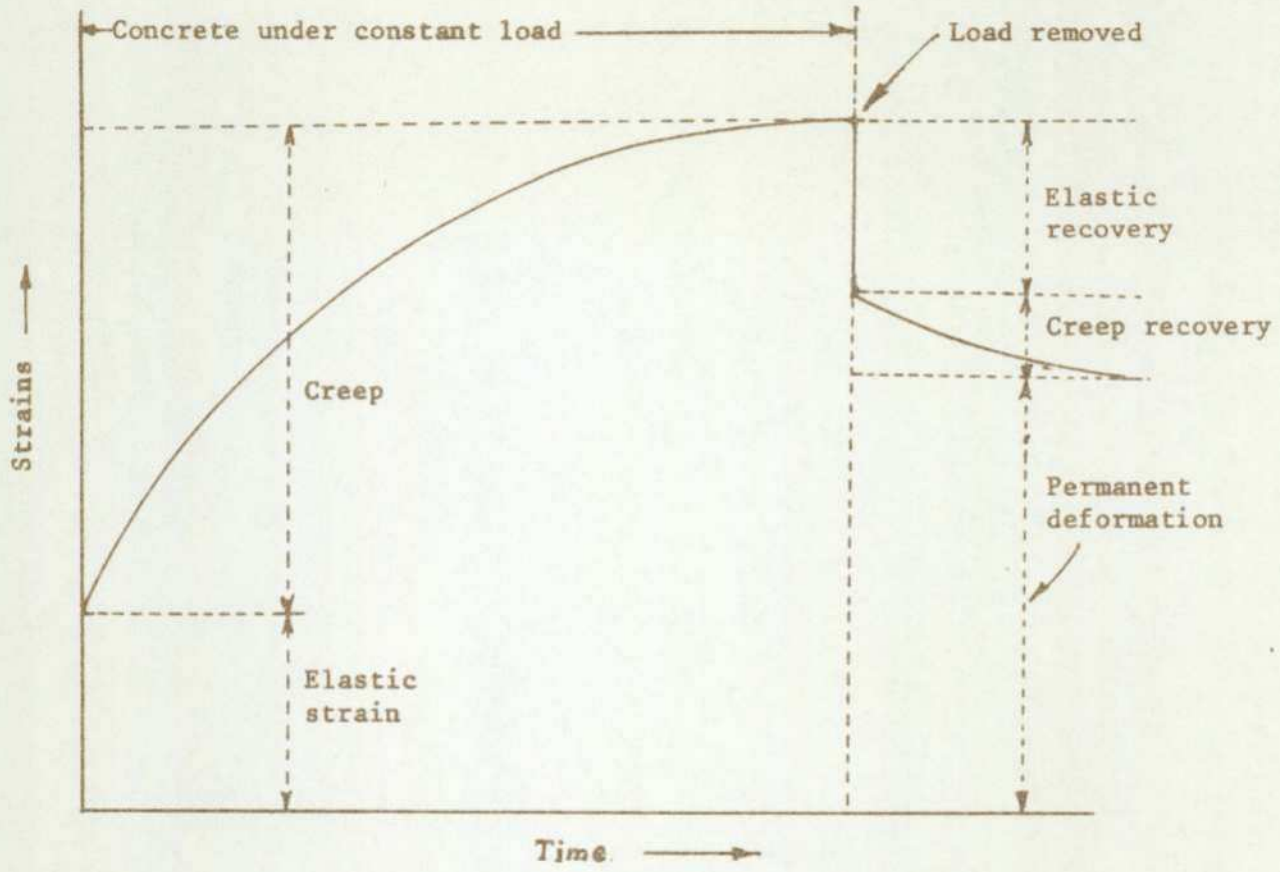


Fig. 36. Creep of concrete under load

strength increases with time and thus the material will show increased resistance to effects such as creep and load changes, towards the end of the test.

At relatively low levels of stress, creep is roughly proportional to stress and it has been found convenient to introduce the concept of specific creep or creep strain per unit stress. This is a useful comparative indicator of creep effects, since references to the magnitude of creep strain without an indication of the stress causing it, are without much value.

In addition, the term creep coefficient is used to denote the ratio of the ultimate long-term creep strain to the instantaneous elastic strain under a given load.

It is common practice to express creep data obtained from control tests on concrete specimens by plotting specific creep curves against time rather than simple creep strains.

3. THE EFFECT OF STRESS

It is not possible to measure separately on the same specimen the creep strains and the shrinkage strains which occur during a test.

If three identical specimens are cast from one batch of concrete, however, one of which is permitted only to shrink and the other two are loaded at different ages to cause creep strains, it is possible to observe several interesting effects. Figure 37 shows the diagrams of shrinkage and creep which result, if the two loads are equal.

The shrinkage specimen exhibits the curve free from discontinuities which is characteristic of drying shrinkage.

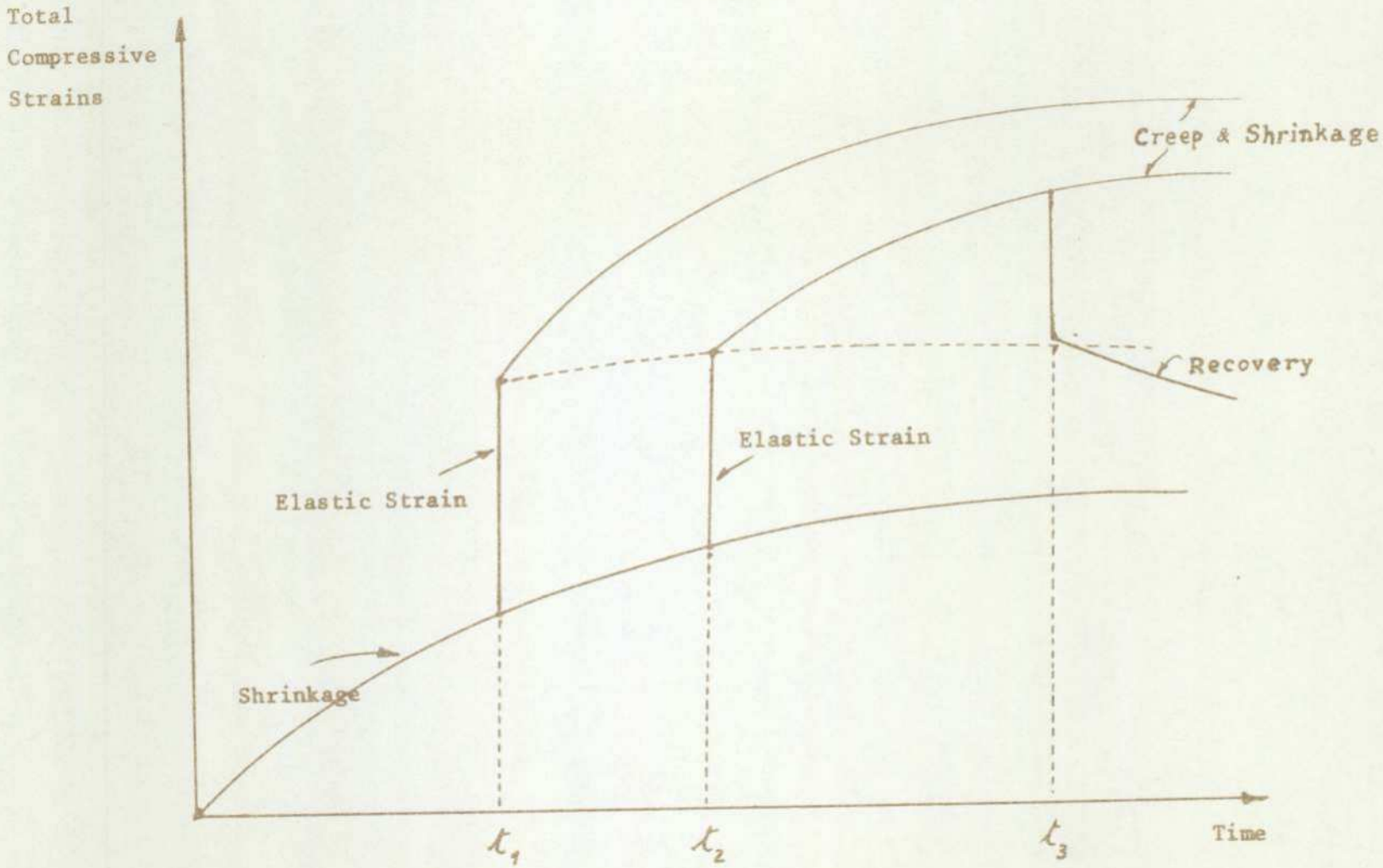


Fig. 37. Elastic Strain, Shrinkage and Creep

If the second specimen is loaded at time t_1 there will be an immediate elastic strain followed by a creep strain at a rate decreasing with time, superimposed on the base of the shrinkage which has occurred in the second specimen up to time t_1.

Similarly if the third specimen is loaded at time t_2, the immediate elastic strain is smaller than that occurring on loading the second specimen, and the subsequent creep strains plotted against time will follow a curve lower than that for the second specimen. The ultimate total creep in the third specimen will be lower than that for the second specimen. Increasing the age at loading therefore decreases the amount of creep available, (10), (11),(12),(13).

The reasons for this are clear. The increase in the degree of hydration of the cement paste in the third specimen, during the time interval $t_2 - t_1$, is sufficient to increase the strength of the concrete, to increase its Young's Modulus, to increase its elastic stiffness and thus to reduce the elastic strain and subsequent creep strain when it is finally loaded. Moreover the increased hydration and the continued drying shrinkage have both decreased the free water content in the concrete, a factor which, under both seepage and viscous flow theories, is likely to reduce creep effects.

If the third specimen is unloaded at time t_3, there occurs an instantaneous elastic strain recovery followed by a partial creep strain recovery. The elastic strain recovery is approximately equal to the elastic strain which would have been sustained if the third specimen had been loaded for the first time at time t_3.

4. CREEP UNDER SUSTAINED COMPRESSION

The level of sustained stress is important. Creep is generally proportional to the applied stress upto approximately one half of the ultimate strength of the concrete (14), (15), (16).

At stresses above three quarters of the ultimate strength of the concrete, proportionality certainly does not apply. Plastic behaviour independent of time, and extensive micro-cracking is likely to occur.

These general conclusions about the creep behaviour of concrete under compression appear to be valid also under tension (17), torsion (18), and multi-dimensional stress (18), (19).

5. THE EFFECTS OF TEMPERATURE

At elevated temperatures, not only do the compressive and tensile strengths of the concrete reduce, but the creep rate under a given load, increases on first raising the temperature (20), (30), (31), (32).

The thermal total strain curves relating to the present work and presented with the results, reveal this increased rate of creep. This increased rate of "hot" creep occurred after the specimens had been creeping under the same load, for several weeks at ambient temperatures. On cooling, a lower rate of creep was again assumed.

When time-dependent strains are occurring in concrete loaded for an extended period, a fairly steady condition of internal stress exists. Only very small and slow stress changes occur as creep continues, provided the load and temperatures are constant (21). Changes in load will cause an internal stress change. In other words, a transient regime will have been created in which the change of strain will give rise to a consequential redistribution of stress.

A change in temperature will have a similar effect. Application or

removal of heat will initiate an immediate internal stress re-distribution which will also cause a deviation from the original steady stress pattern.

Slowly a new steady state regime of stress will be re-established under the new conditions of load or temperature.

The effect of temperature on the creep rates of concrete is essentially a problem of the change in creep rates in the cement paste.

6. OTHER FACTORS AFFECTING CREEP

Creep is also affected by the following additional factors (22)

(a) the water-cement ratio (27)

(b) the conditions of curing

(c) the ambient relative humidity

(d) the maturity of the concrete at the time of loading

(e) the surface-volume ratio of the concrete member (23),(24)

(f) the type and fineness of the cement (25),(26)

(g) the nature of the aggregate

(h) the aggregate grading

(i) the aggregate-cement ratio.

(a),(b),(c) THE EFFECT OF WATER

Since both the seepage and viscous flow theories of creep consider the effect of water to be paramount, it is reasonable to expect that the water-cement ratio (27), the conditions of curing, and the ambient humidity will have an influence on the rate and degree of creep. See Fig. 38. Creep varies as the W/C ratio.

Colloidal seepage is governed by water content and, in addition, the degree of hydration, influenced by the amount of water present

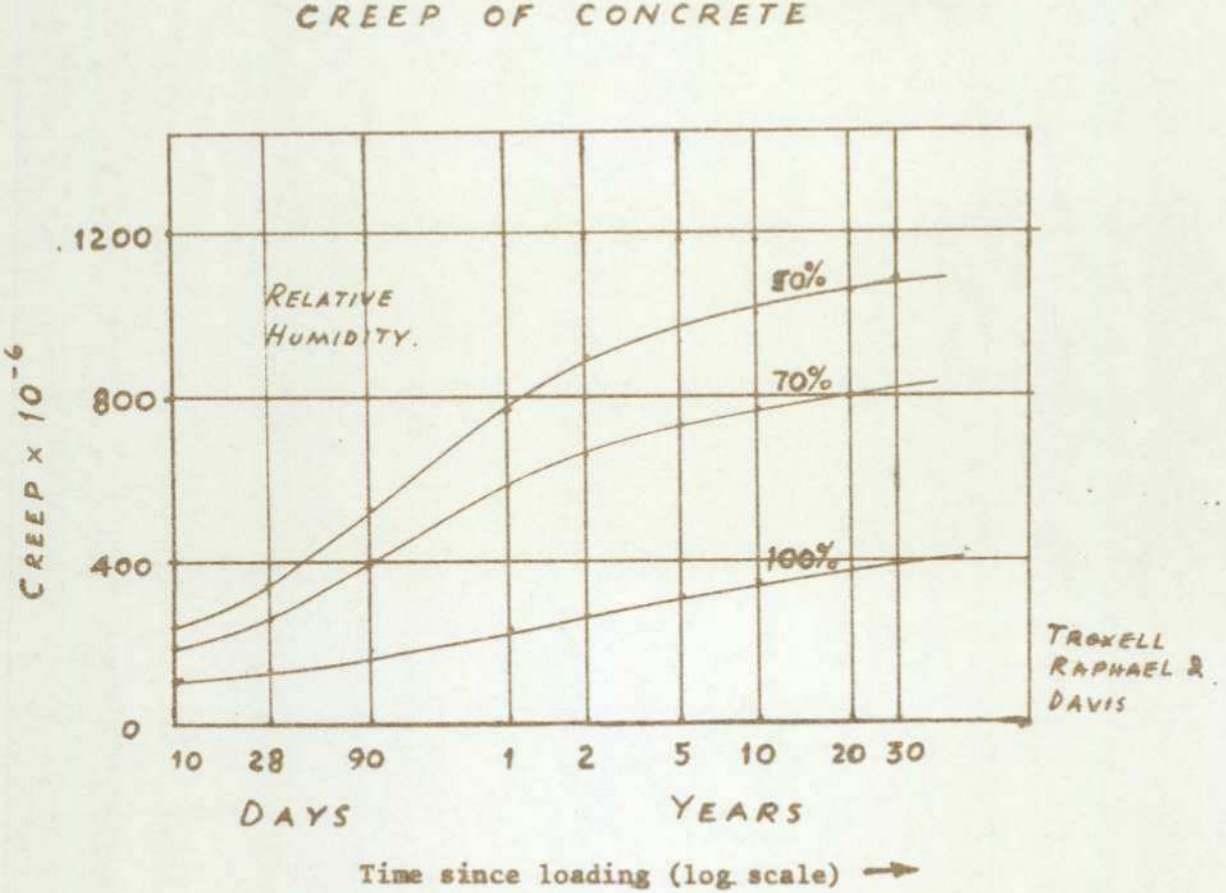


Fig.38. Influence of ambient relative humidity on concrete creep

or available, directly affects the strength of the concrete and its creep. The greater the degree of hydration and hardening, the less creep will be permitted. Furthermore, free moisture adjacent to or within the concrete will result in swollen concrete more susceptible to creep, for example, than dry-cured concrete.

(d) CONCRETE MATURITY

The strength of concrete is a function of the degree of hydration and so is proportional to age. Creep can be said to vary roughly inversely as the strength of concrete and the ultimate total creep decreases with increase in hydration.

Thus the total creep and the rate of creep reduce with an increase of the age at first loading (10),(11).

Creep effects can be reduced in concrete framework structures by (a) delaying the time of striking of the supporting formwork and (b) by delaying, as long as practicable, the application of live loading.

At great ages, the creep rate is small and is practically independent of age of loading.

(e) SURFACE-VOLUME RATIO AND THE EFFECT OF SIZE

Ross found that creep is a function of the surface-volume ratio (23).

It is certainly true that as the length of capillary channel increases, the frictional resistance to seepage increases.

Tests by Hansen and Mattock (18) confirm that creep decreases with increase in specimen dimensions but expulsion of water from the outer gels is unaffected. For very large members the creep approaches the values obtained from similar sealed specimens.

(f) THE EFFECT OF THE CEMENT

Davis has shown that creep is proportional both to the cement content and to the W/C ratio (25).

Creep (and shrinkage) are, in fact, properties of the cement paste rather than of the aggregate. Since finer cements hydrate more quickly than other types, high strengths are obtained relatively quickly although ultimate strengths may not be greatly affected. It cannot be concluded, however, that the finer the cement the lower the creep rate exhibited. The findings of Bennett and Loat (131) are briefly reported in a summary of factors affecting creep at the end of this section.

Neville (14) has shown that mixes having the same paste content develop the same proportion of their long-term creep after any given time.

Creep increases with cements in the order aluminous, rapid-hardening Portland, ordinary Portland, blast furnace Portland cement.

(g),(h),(i) THE EFFECT OF AGGREGATES

Aggregates also have an effect on the degree of concrete creep. Efficient grading of aggregates increases the compressive strength of a concrete and thus reduces creep. Crystalline creep in the mineral aggregates varies with the different types, and porosity of the stone has a strong influence on the seepage of water and thus on the creep of a concrete.

Sandstone aggregates tend to exhibit greater mineralogical creep when used in concrete than do limestone aggregates.

The amount of creep decreases with increase in maximum size of aggregate. If the concrete is well-compacted and the stone well-graded, a strong interlocking framework is formed which tends to resist creep deformations well.

7. CREEP RECOVERY

On unloading a concrete specimen there occurs an immediate elastic unloading of strain which is slowly followed by a recovery of the creep strain (38) extensive at first but reducing after a short period of time. A residual, irrecoverable creep strain will remain.

8. THE EFFECT OF CONCRETE CREEP ON REINFORCEMENT

One result of creep under sustained loading is to permit the concrete slowly to transfer its load to the reinforcement steel. A lowering of the effective value of Young's Modulus is associated with this transfer.

One point concerning the disadvantageous effect of creep in prestressed concrete has already been mentioned. The general result in a prestressed member is a loss of prestress as the creep deformations in the concrete relax the tensioned steel.

Various mathematical expressions proposed by investigators to represent creep-time laws are listed in the Appendices. Sections IX and X deal specifically, under the discussion on viscoelasticity, with the treatment of particular creep laws in the development of the analysis.

B. SHRINKAGE

Shrinkage can be considered to be a time-dependent deformation in the concrete which occurs due to the movement of gel water from within the gel pores. The evaporative effect of the drying out of the concrete is sufficient to cause these shrinkage strains. See Fig.37.

In other words, stress is not involved in this process although shrinkage due to drying out and creep due to stress occur in the same concrete member. Since moisture seepage takes place in the cases of both shrinkage and creep, it is not possible to observe the two phenomena separately in the same specimen.

The type of cement has an influence on the shrinkage of the resulting concrete,(33). Carlson claims that shrinkage increases in the sequence ordinary Portland cement, low heat cement, Portland pozzolana cement.

The fineness of cements has been commented on by Davis, Carlson, Troxell and Kelley (34) in connection with the construction of the Hoover Dam. Finer cements showed a slight increase in shrinkage.

As would be expected, experiments linking shrinkage and water-cement ratio indicate a direct proportional relationship (33).

Both the type of aggregate (35) and its maximum size (122) affect shrinkage. Shrinkage decreases as the maximum size of aggregate increases.

Shrinkage rate decreases with time and shrinkage strain-time curves take a very similar form to creep-time curves. Wet curing of concrete specimens can be expected to delay the process of drying shrinkage. If the onset of shrinkage can be held back, the concrete will have an opportunity to increase its tensile strength with time,

Thus, as would be expected, a high relative humidity considerably inhibits drying shrinkage.

1. THEORIES OF SHRINKAGE

Shrinkage, however, is now generally assumed to be made up of two parts

(a) the drying shrinkage due to the evaporative loss of the free water

(b) the chemical shrinkage resulting from the cement hydration.

The cement and water at mixing occupy a larger physical volume than do the products of chemical reaction after hydration. Although drying shrinkage is the predominant component of the total, both components influence construction techniques to a considerable extent and not only in the curing procedures.

It is common practice to cast concrete road slabs and sections of concrete walls, for example, in bays, frequently alternately, so that some part of the shrinkage can occur without cracking and so that contraction joints may be constructed to deal with the remainder and so prevent uncontrolled cracks.

The chemical, or plastic shrinkage naturally increases with cement content and can result in a shrinkage of the order of 0.6% of the original volume during the first few hours after mixing, (118). Concrete forms are usually filled 3 or 4 mm proud to offset this form of shrinkage which manifests itself as a settlement of the top surface of the concrete as it sets.

2. SHRINKAGE GRADIENTS

Drying shrinkage in large concrete members, exhibits itself to a greater degree on the surface and adds to thermal contraction

stresses in producing cracking.

As shrinkage continues, a balance in internal vapour pressure is eventually struck at a level dictated by the ambient temperature and humidity. The volumetric change which occurs is a function of distance into the concrete mass and of time. This suggests that there may exist a shrinkage gradient into the concrete, and some large concrete members may never actually dry out in their centres. The differential shrinkage resulting from this gradient causes internal stresses which may be relieved by creep. The surface-volume ratio of the concrete may influence the shrinkage to the extent that members may alter their shape as well as their size.

The standard British test specimen of B.S. 1881, which is 76 mm x 76 mm x 254 mm in size takes at least six months to dry out from saturation to moisture equilibrium under controlled conditions of 20^{o}C and 65% relative humidity, (122). The drying out process causing the shrinkage proceeds probably by a combination of capillary seepage, diffusion and water vapour migration as a result of small pressure differentials.

3. TEMPERATURE AND HYGROTHERMAL SHRINKAGE

As would be expected elevated temperature increases the rate of drying shrinkage but the chemical or plastic creep, occurring immediately after hydration, cannot be affected.

Hygrothermal shrinkage is defined as the additional volume change which takes place when normal drying shrinkage at ambient temperature is increased by higher imposed temperatures. The change in temperature causes an imbalance in pressure between the water in the gel and the water in the adjacent voids and capillaries encouraging a transfer to restore equilibrium.

Work carried out by England and Ross (31) on unsealed specimens of reinforced concrete maintained at various constant temperatures has shown that the shrinkage at 100°C after 60 days may be as much as four times greater than that at 20°C after 60 days.

As the water capable of being driven off by the increased temperature decreases so the shrinkage rate falls off quite rapidly.

Work carried out by Hannah (36) on concrete beams and slabs has indicated a high degree of differential shrinkage across such members due to the application of a temperature gradient through the concrete. The shrinkage was of such a high order that the deformations expected due to the temperature gradient were reversed.

4. PRACTICAL EFFECTS OF SHRINKAGE ON CONCRETE

The setting of the pressure vessel concrete is attended by the release of heat of hydration, which causes thermal expansions in the material as it hardens. This process occurs without introducing significant internal stresses initially, due to the relatively large degree of plastic flow or creep. Tensile contraction stresses of opposing sense are subsequently imposed on the concrete when, several days after setting, the rate of cooling becomes greater

than the rate of generation of hydration heat.

These contraction stresses add arithmetically to the shrinkage stresses which are now beginning to develop through loss of moisture.

Although during construction and the subsequent period before operation, creep is still acting to relieve locked-in stresses, the degree to which it is able to do so decreases with time.

Surface cracking due to drying shrinkage relieves these effects in the outer concrete layers, but the internal stresses are only slowly and incompletely relieved by creep during the period before the shield is commissioned.

The European Committee for Concrete has published a set of graphs to facilitate the forecasting of shrinkage. These graphs are intended to permit the choice of a concrete of suitable mix proportions to give a comparative approach to the problem of reducing shrinkage in a given application.

As a result, joints can be fixed in position and frequency. Since shrinkage strains in concrete of the order of 400×10^{-6} are not uncommon, it is frequent practice to provide expansion or contraction joints to suit this value, which represents a shrinkage of about $\frac{1}{4}$" (6mm) in 50 feet (15 metres). In addition, "shrinkage" steel may be provided to give the concrete assistance in tension. The internal restraint of the reinforcement is usually sufficient to reduce visible cracks in the concrete.

5. SUMMARY OF FACTORS AFFECTING SHRINKAGE

Troxell, Raphael and Davis (22) state that the factors affecting shrinkage include

(a) the aggregate-cement ratio (122) (high values reduce shrinkage)

(b) the water-cement ratio (33) (proportional to shrinkage)

(c) the conditions of curing (43) (see below)

(d) the ambient relative humidity (high values inhibit shrinkage)

(e) the type of cement (33), (34) (finer cements increase shrinkage)

(f) the aggregate grading (35), (122).

6. CURING AND STORAGE CONDITIONS

Saemann, Warren and Washa (43) have reported on the effect of curing on shrinkage cracking in concrete blocks. The duration of curing has a small effect on the shrinkage. Very wet curing conditions may even swell a concrete member and this swelling should be deducted from the total movement if the net shrinkage is desired.

Conversely, the magnitude of shrinkage strains is higher under low ambient humidity conditions.

Although, if the temperature of storage is high, the shrinkage will be proportional to it, the shrinkage rate under maintained high temperature will fall off later quite rapidly as the free water continues to be driven off.

7. THE EFFECT OF AGGREGATE-CEMENT RATIO AND AGGREGATE GRADING

Since the aggregate particles and the cement matrix have different elastic moduli, localized stresses are likely to occur at the aggregate-matrix interface and cracking may result. The distribution of aggregate within the matrix and the maximum size of aggregate are likely to be influential on shrinkage behaviour.

Carlson (33) and Mamillan (123) showed in fact that the influence on shrinkage of aggregate particles finer than about 7mm

was small. Carlson attributes the shrinkage decrease which is observed in concretes with particles larger than 7 mm, to internal cracking.

Mears (122), however, states that for constant mix proportions, at a water-cement ratio of 0.47, and aggregate-cement ratio in the range 2.38 to 4.0, aggregate grading and size have no systematic effect on drying shrinkage or shrinkage rate. This applies to drying at 30% and 65% relative humidity and 20°C.

Mears also states that over the small range examined, drying shrinkage is inversely related to aggregate-cement ratio. He also suggests that the drying shrinkage of concrete could often be found more rapidly by testing small mortar specimens of the same water-cement and aggregate-cement ratios as the concrete.

8. SHRINKAGE IN REINFORCED AND PRESTRESSED CONCRETE MEMBERS

An unpublished communication by Smolira (119) suggests a method of evaluating the steel and concrete stresses due to shrinkage in a reinforced concrete beam. The procedure is based upon the fact that the reinforcement, bonded to the concrete, prevents the latter shrinking to its full potential value.

The communication also shows how the effect of shrinkage on statically indeterminate structures can be evaluated based on the angular deformations at the supports.

A method of calculating shrinkage stresses in composite pre-stressed beams in which the shrinkage of in situ concrete may induce effects in the precast concrete, is given by Evans and Bennett (120).

9. THE SEPARATION OF THE STRAIN COMPONENTS

The total strains occurring in the concrete end slabs consist of the elastic, the creep, the shrinkage and the thermal strains, and the value of the strains measured experimentally must be the algebraic sum of these components.

The elastic strain can be observed directly after loading the specimens as can the thermal strains immediately after heat application. The thermal strains can, in any case, be arrived at by calculation knowing the coefficient of linear thermal expansion of the concrete. The shrinkage strains can be plotted against time, as a result of continuous observations on unloaded specimens which are allowed only to shrink. This implies, as has already been explained, having sufficient control models of the end slabs, to achieve these objectives.

Thus each of the components of strain can be separately evaluated for use in the subsequent calculations as required.

There is an interrelationship between creep and shrinkage since they are both greatly influenced by the ambient relative humidity. There is also some evidence to indicate that shrinkage strains in causing stresses, may increase creep strains, and consequently the simple isolation of creep by subtracting the other components of strain, including shrinkage, from the total, may lead to small errors.

However most analytical work on this problem in the past has assumed that creep is independent of shrinkage, that loading neither increases nor decreases shrinkage and that shrinkage, either uniform or non-uniform, does not increase the stress.

Summary.

Variables affecting creep

1) Constituents	Influence
a) Cement ; Type, Fineness, Paste. b) Aggregates ; Strength, Size, Grading, Texture c) Water ; W/C ratio, Workability	Greater fineness in a cement leads to more rapid hardening and to greater strength. To compare fineness therefore, tests were made (131) on cements of different fineness when they had reached the same strength. For cements of three different finenesses, it was found that creep after 1000 days was approximately the same in all cases, but very early creep was higher the finer the cement. Creep varies as the cement content. Those properties of aggregates which lead to high strength in concrete i.e high strength and good grading, lead to reduced creep. Creep varies as W/C ratio. Creep varies inversely as A/C ratio. Creep varies as workability.
2) Mixing and Placement.	Good compaction ensures satisfactory strength which varies inversely as creep.
3) Curing. a) Duration b) Temperature c) Humidity	Adequate humidity and duration of curing is essential for good concrete. Temperature during

Variables affecting creep	Influence
	curing increases strength gain. These three factors therefore produce concrete of high strength and thereby reduce creep.
4) Age at Loading	Creep is inversely proportional to age at loading.
5) Stress.	Creep varies as stress upto about half the ultimate strength.
a) Type	
b) Magnitude	Creep occurs under sustained loading and the rate reduces with time.
c) Duration	
6) Concrete Strength.	Creep is inversely proportional to concrete strength.
7) Ambient Relative Humidity.	Creep varies inversely as ambient humidity during service.
8) Ambient Temperature.	Creep varies as ambient temperature during service.
9) Shrinkage.	Both shrinkage and creep are affected by moisture loss from the concrete; it would appear that there should be a mutual interaction; it is usually assumed in analysis that they occur independently.
10) Shape and Size of Specimen.	These affect concrete creep in the same way as they affect moisture loss.
11) Effect of Reinforcement.	Creep and shrinkage help the concrete to pass on its stress to the steel.

Summary.

Variables affecting shrinkage	Influence
1) Constituents	
a) Cement	Finer-ground cements tend to increase shrinkage.
b) Aggregates	High values of A/C ratio reduce shrinkage.
c) Water	Mears (122) claims that aggregate grading and size have no systematic effect on drying shrinkage or shrinkage rates. Shrinkage varies as the W/C ratio. Magnitude of shrinkage is greater under low ambient humidity. If temperature of storage is high the shrinkage is proportional to it but the shrinkage rate falls off rapidly as free water is driven off.
2) Strength	High strength and particularly high tensile strength tends to restrict shrinkage strains.
3) Shape and Size of Specimen	These affect concrete shrinkage in the same way as they affect moisture loss.
4) Temperature	Shrinkage increases with the temperature. The shrinkage law for Series 1 concrete at 80°C corresponded to the expression $s = 0.9894 \times 10^{-3} (1 - e^{-0.7794 \times 10^{-2}.t})$

SECTION IX

ANALYTICAL METHODS

A. ELASTIC METHODS OF ANALYSIS

1. General approach to Analysis.

The prestressed concrete pressure vessel is essentially a simple symmetrical structure whatever its overall shape. The conceptual simplicity is lost, however, and the geometry made complex by the need for discontinuities such as steps, penetrations, ribs, and anchor blocks in the walls and end slabs of the vessels.

It becomes necessary, therefore, to simplify the problem of analysis and this may be done in one of three ways : first by reducing the number of dimensional variables, secondly by reducing the complexity of the problem by breaking it down into several simpler problems requiring the solution of simpler functions of lower continuity, and thirdly by breaking down the vessel into its constituent parts, large or small, and thus reducing the physical continuity of the structure, (69).

The number of dimensional variables can be reduced, for example, by turning a three-dimensional analysis into a two or one-dimensional analysis, by adopting a thin shell approach instead of the more appropriate thick shell approach, and accepting and assessing the consequent disadvantages. However, such steps are rarely necessary, in view of the recent advances in analysis and the versatility of the digital computer.

Alternatively, devising or assuming axial symmetry for a thick shell similarly reduces the dimensional variables.

Again, by breaking down a vessel into its constituent parts, either into large units such as the end caps and walls, or into

small pieces such as rings, finite elements, or even further into nodal systems, the continuity of the structure may be reduced.

Whatever analytical method is adopted, it must be versatile enough to allow for variations in temperature along and across the vessel members, it must also be capable of permitting the use of an effective Young's Modulus varying with time and position, and it must also take into account varying applied forces such as prestressing, gas pressure, dead load and frictional effects ,(75).

So far, the analysis of whole vessels has been under discussion and some of the methods described in what follows are also appropriate only for the full vessels. However, at the end of this section on general analytical methods, a summary is made of existing elastic analyses of the perforated end cap itself.

2. Review of Analytical Methods

Whatever devices are used in tackling these problems, for a viable analytical determination to be achieved of the stress and strain ,a solution must be obtained of the equations of elasticity, which is able to satisfy the boundary conditions of external load and temperature and of displacement. These equations of elasticity comprise groups of expressions governing the material properties, the geometrical compatibilities, and the equilibrium of force components in the structure.

Once the structural concept or idealization has been decided upon, appropriate analytical methods may be chosen. Of the two main divisions of structural analyses - the numerical and the analytical - the numerical method is much the more versatile, and this is particularly true for complex structures.

Again, of the numerical methods of analysis, two groups can be recognised. The first group provides direct numerical solutions of the appropriate governing differential equations in terms of the displacements or stresses. Finite difference techniques, dynamic relaxation and numerical integration are included in this group.

The second group, based upon the structural idealization of finite elements of the structure, most frequently utilizes matrix formulations. Either displacement (stiffness) methods or force (flexibility) methods may be used. See Fig. 39.

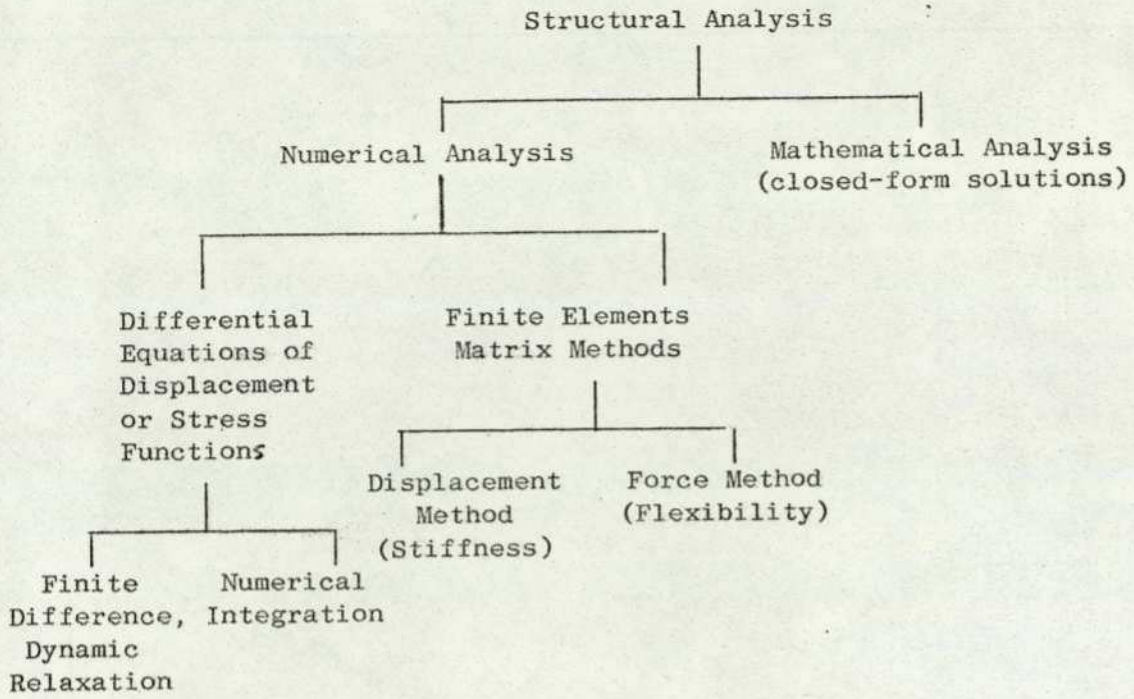
3. Analysis of Large Sections of the Vessel : Thin Plates and Cylinders

The method of analysis based on breaking down the vessel into large sections is rarely used in modern practice.

One form of this method is the thin shell approximation. The adequacy of thin shell elastic analyses has, with reservations, been demonstrated for radius-thickness ratios as low as 6 to 1, by experiments on vessels of particular configurations (3). When a cylinder is considered for which radius-thickness ratios lie below 4 to 1 thin shell analysis is really invalid. In other words, this ratio when greater than about 6 to 1 ensures that little variation of stress occurs across the wall.

Thermal stress calculations are difficult to include and the only real usefulness of thin vessel approximations for the P.C.P.V. is in obtaining a first estimate of vessel size in the early stages of design.

The method of analysis which splits up the vessel into plates (end caps) and ring (cylinder) suffers from the same objections.



Elastic Methods of Analysis

1. Analysis of Large Sections of Vessel.

   used when radius/thickness ratio $>$ 6:1

   (a) Ring and Plate Approximations

   (b) Thin Shell Approximations

2. Finite Differences

3. Dynamic Relaxation

4. Finite Elements

5. Elastic Analyses for Perforated Slabs(see text).

Fig. 39.

The process consists of setting up in matrix form, the equations of equilibrium and compatibility at the meeting interfaces of large parts of the vessels such as the cylindrical walls, the end slabs and any ring beams, real or assumed.

Inversion of the matrix and solution by computer gives the required displacements and stresses.

The method only considers the elastic response, in general, for the main members of the vessel at their interfaces. It is necessary in practice to carry out further elastic calculations at several points along the walls and slabs.

At discontinuities such as steps, penetrations and corners, the method fails to provide a solution to the stress concentrations.

Although, thin shell analyses and other methods of this type are considered unsuitable for modern P.C.P.V. it is possible that these approaches would be useful for the solution of thin containment structures or vessels where low containment pressures may need to be resisted by membrane-type barriers forming part of the reactor service building outside the main pressure vessel.

4. Finite Differences

This is one of the techniques of numerical analysis which permits the solution of the differential equations representing the displacement or stress function, (73), (74).

The elastic continuum under consideration is set out with a mesh network formed by sets of lines at preset intervals related to the chosen co-ordinate system. The intersection points of the mesh are known as the nodal points.

The nodal values of the assumed displacement or stress function and the first and second order derivatives are arrived at from the

nodal point values of the function adjacent to the points under consideration.

The nodal values of the function are substituted into the governing differential equations of elasticity and the resulting set of simultaneous equations is solved by computer for the displacements and stresses.

5. Dynamic Relaxation

Dynamic relaxation is an iterative numerical technique of stress analysis and can be adapted for use in one, two or three-dimensional cases. The method can be used to solve the finite difference formulations of the equations of elasticity with the aid of the digital computer.

Otter (64) has described the procedure in detail in its application to the cylindrical pressure vessel and has also defined its relationship to other relaxation methods, (67).

Dynamic relaxation is essentially a step-by-step integration of critically-damped vibrations applied to a structure. The problem of a stress wave moving through a material is considered. The stress oscillations converge to a static steady state solution when a suitable damping mode is applied. The damping term is chosen to give a critically-damped oscillation and thus ensures rapid convergence to a static condition in a short number of iterations.

If a suitable finite difference mesh is chosen, the boundary conditions may be accommodated. The system can be used on all forms of continuous structures and involves the solution of the dynamic equations applying to elastic isotropic materials. The derivation of these equations requires the separate consideration of both the motion of an element of the body under internal and

external forces, and the elastic relationship between the stresses and deformations in the element during such motion.

Difficulty is experienced in applying this method to the end slabs of reactors because of the complex geometry of the standpipe penetrations.

Dynamic relaxation is merely another method of solving sets of simultaneous equations. Where finite difference equations are being utilized, the task remains for every structural problem of setting up the equations involved, of representing the boundary conditions, and of converting these equations into finite difference formulations. Dynamic relaxation methods help the computer to speed up numerical operations after this stage.

6. Finite Element Method

This method mobilizes the advantages of matrix formulation in structural analysis, (76), (77), (78).

A mathematical model is conceived which idealizes the entire structure in the form of discrete or finite units which, being connected together at the nodes with pinjoints can be combined in a manner which represents the total structure.

The units or finite elements into which the whole structure is sub-divided, may be bar or beam elements, (for structural units or frameworks), or they may be triangular, rectangular, or quadrilateral plate elements, (for continua), or solid tetrahedrons, (for three-dimensional analysis).

The finite elements replacing the actual continuous structure have elastic, inertial and geometric properties expressible in matrix form. The relationships between the elements are governed by the classical equations of elasticity. The equilibrium, the

compatibility and the material properties of the elements, together with the external load vectors operating, can be formulated and combined in matrix form and solved for the displacements and hence the stresses of the whole continuous structural system.

Thus the elastic data of each individual element are assessed in matrix form and the static elastic response of the complete structural system emerges as the required solution, when the finite elements are assembled to form the full structure.

As the size of the finite elements is diminished and as the resulting mesh is reduced, the solution of the displacement behaviour of the idealized model converges to that of the continuum it simulates.

The digital computer is essential to the deployment of matrix techniques to their best advantage. The computer not only solves the many basic simultaneous equations of elasticity involved, but is also employed in all the processes of input data preparation and output presentation and in the manipulation and inversion of the matrices.

The advantages of matrix formulation as used with the finite element method, need no emphasis. Not only is the use of matrix algebra a most useful structural shorthand to save time and space in writing out the equations in full, but it represents a systematic and convenient procedure for compiling and presenting the required input data to the computer for subsequent solution.

Using the matrix displacement (stiffness) method for a continuum, the steps in a finite element formulation, for the case of two-dimensional stress analysis, might take the following general form:

i) The structure is divided up into the chosen shape and type of elements and the basic data compiled; the elements' material and geometric characteristics are considered (these affect the stiffness); the elements and the nodal points are positioned in relation to two major orthogonal axes of symmetry.

ii) The local co-ordinates (x, y) are determined.

iii) The element stiffness matrix $[k]$ for each element is then calculated in local co-ordinates, utilizing the elastic and geometrical properties of the element.

iv) The direction cosines for each element are determined; (inapplicable for the geometry of the models in the present investigation).

v) The element stiffness matrices are calculated in the global co-ordinates of the major datum axes.

vi) From the element stiffness matrices, the total structure stiffness matrix $[K]$ may be computed; each element adjacent to a nodal point will contribute to the total structure stiffness matrix.

vii) The rigid-body degrees of freedom are eliminated to obtain the reduced structure stiffness matrix.

viii) The pressure distribution is converted into concentrated nodal forces; the element thermal forces are calculated and added to obtain the structure thermal forces; the consequent combined resultant loading vector $[R]$ from mechanical and thermal loads is calculated.

ix) The structure stiffness matrix is inverted and $[d]$, the nodal displacements may be obtained from the relationship:

$$[d] = [K]^{-1} \cdot [R]$$ where $[R]$ is the resultant external load vector matrix.

x) The stresses and strains in the structure may be obtained from the nodal displacements for each element.

7. Existing Elastic Methods of Analysis for Perforated Slabs

(i) Sheffield's Theory

Several computations have been made by Sheffield (88) in the field of circular perforated slabs of the pressure vessel end cap type.

He considered the stress distributions in a circular plate with applied external in-plane pressures. The plate contained penetrations of a circular form, the penetrations having their centres on a regular square lattice. The holes were all of equal size. Holes unreinforced and also reinforced with liners were examined.

His first computation gave the stress distribution in an approximate form taking into account general hole size, spacing and uniform boundary conditions.

The governing stress equations for this problem, since we are dealing with a plane uniform plate, are written in terms of a single scalar function U which satisfies the expression:

$$\nabla^2(\nabla^2 U) = 0$$

Where $\nabla^2 = \frac{\partial^2}{\partial x^2} + \frac{\partial^2}{\partial y^2}$ using Cartesian co-ordinates.

The stresses are given by

$$\sigma_x = \frac{\partial^2 U}{\partial y^2}$$

$$\sigma_y = \frac{\partial^2 U}{\partial x^2}$$

$$\tau_{xy} = -\frac{\partial^2 U}{\partial x \, \partial y}$$

The solution to the original stress equation is obtained in the form:

$$U(\underline{r}) = -\left[\frac{p - n P \mu}{1 - n\mu}\right]\left[\frac{\underline{r}\cdot\underline{r}}{2} - \frac{a^2(p-P)}{p - n P\mu}\sum_{i=1}^{n} \log |\underline{r} - \underline{r}_i|\right]$$

where p is the externally-applied pressure

$\underline{r}$ is the polar co-ordinate of any point (r, θ) in the system

$\underline{r}_i$ is the co-ordinate of the centre of the ith hole

a is the radius of the ith hole

n is the number of holes

P is the internal pressure at the hole boundaries (equal for all holes)

$$\mu = \left(\frac{a_j}{a_0}\right)^2$$

where a_j is the radius of the jth hole and a_0 is the plate radius.

In the event of all n holes being of the same radius a

$a_1 = a_2 \ldots\ldots = a_j = a_n = a$ and $\mu_1 = \mu_2 \ldots\ldots = \mu_j = \mu_n = \mu = \frac{a^2}{a_0^2}$

This is referred to by Sheffield as the zeroth order solution.

Two cases are of interest:

i) that in which P = 0 i.e. the unreinforced hole case, and

ii) that in which p = P i.e. the case in which the liner thickness is such that the end cap perforated zone has a stiffness and response as if it were a solid central zone without apertures.

In case i), the expression for $U(\underline{r})$ becomes

$$U(\underline{r}) = -\frac{-p}{1 - n\mu}\left[\frac{\underline{r}\cdot\underline{r}}{2} - a^2\sum_{i=1}^{n} \log |\underline{r} - \underline{r}_i|\right]$$

and in case 2)

$$U(\underline{r}) = -\frac{p r^2}{2}$$

which is the solution for a uniform plate without apertures.

Sheffield's results for his zeroth order solution are tabulated in his paper and it is found that the outer boundary condition is well satisfied on the zero order model, but that the inner boundary conditions are not so well satisfied. This is particularly true of cases where the hole radii are not small compared with their separation i.e. their pitch or their ligament width.

Sheffield accordingly continued to develop a further more accurate solution, which he refers to as an Nth order solution.

The problem was formulated and the general equations were established in terms of complex functions in the manner of Sokolnikoff (90) and Muskhelishvili (91), and the equations were solved by a method of successive approximations.

The Nth order solution is presented in the form of additional correction terms to be applied to the zeroth order solution in respect of the $(\sigma_x + \sigma_y)$ and $(\sigma_x - \sigma_y)$ and τ_{xy} stresses.

Effective Modulus of Elasticity.

A further and most important application of Sheffield's work is in respect of the theoretical determination of an effective Young's Modulus for the perforated zone of the end cap.

If we define an effective Young's Modulus (E_e) as the value of the elastic modulus for a solid hypothetical zone of the same dimensions and having the same elastic responses to load as the perforated zone with its lined penetrations, Sheffield's expression

for the ratio $\frac{Ee}{Ec}$ where E_c is the Young's Modulus for the concrete, gives a method of arriving at Ee.

According to Forbe's (89) amendment to Sheffield's expression,

$$\frac{Ee}{Ec} = \left[\frac{1 - \nu_c}{\frac{1 + \Omega(1-2G)}{1 - \Omega} - \nu_c} \right]$$

where $$G = \frac{2}{1-\Omega} \Big/ \left\{ \frac{1 + \Omega}{1 - \Omega} + \nu_c + \left[\frac{2Ah - As}{As} - \nu_s \right] \frac{Ec}{Es} \right\}$$

$$\Omega = \frac{\text{Area of holes}}{\text{Area of plate}} = \frac{nAh}{Ap}$$

As = Cross-sectional area of the liner

Ah = Cross-sectional area of one hole

Ap = Area of plate

Ec = Young's Modulus for the concrete

Es = Young's Modulus for the steel liner

Ee = Effective Modulus for the perforated zone

ν_c = Poisson's Ratio for the concrete

ν_s = Poisson's Ratio for the steel.

It should be noted that the ν_c in the numerator in the expression for $\frac{Ee}{Ec}$ should strictly be ν_e the "effective" Poisson's Ratio for the perforated zone. The difference between the two ratios will be small.

Although Sheffield gives no direct means of evaluating ν_e, the following relationship is of assistance in this respect:

$$\frac{Ee}{1 - \nu_e} = K \frac{Ec}{1 - \nu_c}$$

where K = the effective stiffness of the perforated zone.

K can be obtained, in practice, without the need to know ν_e by substituting for $\frac{E_e}{1-\nu_e}$ from the expression

$$\frac{E_e}{E_c} = \frac{1-\nu_e}{\frac{1+\Omega(1-2G)}{1-\Omega} - \nu_c}$$

obtained as a result of taking $\nu_c = \nu_e$.

As Sheffield's expressions stand, of course, they take no direct account of time-dependent effects such as creep, nor of elevated temperature, applying only to elastic loading and ambient conditions.

The subsequent comparison made in this thesis, however, of the experimental and calculated values of $\frac{E_e}{E_c}$ show close agreement at ambient and at 80°C and after several weeks' ageing.

(ii) Slot's Method for Square Plates with Pressurized Central Circular Holes

Slot (80) has reported accurate elastic solutions for perforated square plates subjected to internal pressure for $\frac{\text{hole diameter}}{\text{plate width}}$ ratios of 0.5, 0.6, 0.7, 0.8, 0.85, and 0.90.

The solutions satisfy the internal and external boundary conditions, the former accurately and the latter approximately.

Plane stress and plane strain conditions are considered, and the solution for external pressure is obtained from the internal pressure solution by superposition.

The stresses and displacements for the plane stress and plane strain cases are:

Plane Stress

Inner Boundary

$$\frac{\sigma_r}{p} = \frac{\sigma_\theta}{p} = -1$$

$$\frac{E\,U_r}{p\,R} = -(1-\nu)$$

$$U_\theta = 0$$

Outer Boundary

$$\frac{\sigma_x}{p} = \frac{\sigma_y}{p} = -1$$

$$\frac{E\,U_x}{p\,R} = -(1-\nu)\left(\frac{W}{D}\right)$$

$$\frac{E\,U_y}{p\,R} = -(1-\nu)\left(\frac{W}{D}\right)\left(\frac{y}{y_0}\right)$$

Plane Strain

Inner Boundary

$$\frac{\sigma_r}{p} = \frac{\sigma_\theta}{p} = -1$$

$$\frac{\sigma_z}{p} = -2\nu$$

$$\frac{E\,U_r}{p\,R} = -(1+\nu)(1-2\nu)$$

$$U_\theta = 0$$

Outer Boundary

$$\frac{\sigma_x}{p} = \frac{\sigma_y}{p} = -1$$

$$\frac{\sigma_z}{p} = -2\nu$$

$$\frac{E\,U_x}{p\,R} = -(1+\nu)(1-2\nu)\left(\frac{W}{D}\right)$$

$$\frac{E\,U_y}{p\,R} = -(1+\nu)(1-2\nu)\left(\frac{W}{D}\right)\left(\frac{y}{y_0}\right)$$

where σ_r, σ_θ are stress components in polar co-ordinates

$\sigma_x, \sigma_y, \sigma_z$ are stress components in cartesian co-ordinates

p is the pressure loading vector

ν is Poisson's ratio

E is Young's Modulus

U_r, U_θ are displacements in polar co-ordinates

U_x, U_y are displacements in cartesian co-ordinates

W is the width across the square plate

R and D are the radius and diameter of the hole

$\frac{y}{y_D}$ is the ratio of outer boundary co-ordinate to the plate dimension.

(iii) Harrop and Abdul-Wahab: Rigidity of Perforated Plates With Reinforced Holes

The authors of the above paper (87) present a simplified method of analysis for perforated plates with reinforced and unreinforced holes on a triangular grid. In-plane loading and peripheral bending moments are applied to the plate. The solution is presented in their paper in the form of typical curves for the effective rigidity related to a wide range of modular ratios, liner thickness and ligament efficiency.

This case is very similar to the one under study in this thesis and although the work is presented in general form, it applies particularly to the effect of liner reinforcement on the rigidity of perforated zones for end caps for P.C.P.V.

The approach is that of the thick cylinder analogy and for fully bonded hole liners, the system is considered to be in the form of two concentric cylinders.

For unstiffened holes the ratio $\frac{Ee}{E}$ is given by

$$\frac{1 - \nu e}{\frac{(1 + \frac{b^2}{a^2})}{(1 - \frac{b^2}{a^2})} - \nu}$$

where E_e = equivalent Young's Modulus for the perforated plate.

E = Young's Modulus for the plate material

ν_e = equivalent Poisson's ratio for the perforated plate

ν = Poisson's ratio for the plate material

a = outer radius of the "elemental thick-walled cylinder"

b = inner radius of the "elemental thick-walled cylinder".

A corresponding expression is obtained for the lined (bonded) hole case by considering the compatibility of radial deformations at the interface of the two "cylinders" and also at the outer boundary of the "outer elemental thick-walled cylinder", as follows:

$$\frac{E_1}{E_{er}} = \frac{E_1}{E_e} - R$$

where R = "reinforcement factor " (not to be confused with that of Bailey and Fidler).

$$= \frac{4\left(\frac{b^2}{a^2}\right)}{(1-\nu_e)\,(1-\frac{b^2}{a^2})^2\left[\frac{1+(\frac{b^2}{a^2})}{1-(\frac{b^2}{a^2})} + \nu_1 + \frac{1}{m}\left\{\frac{1+(\frac{c^2}{b^2})}{1-(\frac{c^2}{b^2})} - \nu_2\right\}\right]}$$

$$\frac{E_1}{E_{er}} = \frac{\frac{1+(\frac{b^2}{a^2})}{1-(\frac{b^2}{a^2})} - \nu_1}{1-\nu_e} - R$$

where E_1 = Young's Modulus of the plate material : "outer cylinder".

ν_1 = Poisson's ratio of the plate material :"outer cylinder"

ν_2 = Poisson's ratio of the liner material

a = outer radius of "outer cylinder"

b = inner radius of "outer cylinder" (=outer radius of "inner cylinder")

c = inner radius of "inner cylinder" i.e. the liner.

m = modular ratio, $\frac{E_2}{E_1}$

E_2 = Young's Modulus of liner material

E_{er} = equivalent Young's Modulus for the equivalent solid cylinder comprising liner and "outer cylinder".

The above expressions do not include the effect of peripheral bending and so correspond to the case under consideration in this thesis. However, the plate is assumed to be perforated over its whole area and has no outer solid annulus. Moreover, the analysis cannot be rigorous as it is based on the simplifying assumption intrinsic in the thick-cylinder analogy.

In a final section of the paper, bending is considered and further expressions are presented to allow for this, relating E_1 to E_{er}.

iv) Kinkead : Round Holes in Reactor Vessels

Kinkead's approach (81) is to consider the stress concentrations which occur around openings in plates subjected to uni-axial, bi-axial or uniform plane stress.

Where the openings are close enough together the overlapping of the stress concentrations causes peak values to occur in the ligaments.

Kinkead provides an approximate solution by carrying out both a stress and a strain analysis in the case of reinforced holes.

An empirical model is assumed of a series of annular discs in tangential edge contact, with an outer radius ρ and an inner radius R.

This arrangement is assumed analogous to a row of circular reinforced openings spaced equidistantly across an infinite plate on a line normal to the direction of a stress field S.

Stress Analysis

If σ_r is the stress in the slab in a direction radial to the hole centre, r is the radial distance from the hole centre and ρ is the half pitch of the slab openings, then

$$\sigma_r = \tfrac{1}{2} S \quad \text{at} \quad r = \rho \qquad \text{(the outer boundary).}$$

Also, for equality of circumferential strain at the junction between the liner and the slab

$$\frac{\sigma_1}{E_s} = \frac{1}{E_c} \left(\sigma_{\theta i} - \gamma \sigma_{ri} \right)$$

where σ_1 = liner circumferential stress

E_s = modulus of elasticity for the liner material

E_c = modulus of elasticity for the slab concrete

σ_θ = stress in slab in a direction circumferential to the hole centre

γ = Poisson's ratio for the slab concrete.

For equilibrium of radial forces at the junction of liner and slab

$$\sigma_{ri} = \sigma_1 \frac{T_n}{R}$$

where T_n = thickness of liner

R = inner radius of opening.

Also for equilibrium of shearing forces at the junction

$$\tau_{r\theta i} R . d\theta = - T_n \, d\sigma_1$$

From these stress equations, the ensuing stress components may be established:

$$\sigma_r = \frac{C_o}{r^2} + 2C_1 - (C_2 + \frac{C_3}{r^4} + \frac{2C_4}{r^2}) \cos 2\theta$$

$$\sigma_\theta = -\frac{C_o}{r^2} + 2C_1 + (C_2 + 2C_5 r^2 + \frac{C_3}{r^4}) \cos 2\theta$$

$$\tau_{r\theta} = (C_2 + C_5 r^2 - \frac{C_3}{r^4} - \frac{C_4}{r^2}) \sin 2\theta$$

where C_o C_1 C_2 C_3 C_4 C_5 are constants for which Kinkead gives the values.

To make the empirical model operate, further induced stresses S^1 must be applied to the outer boundary in a direction transverse to the applied stress. These induced stresses ensure strain compatibility by keeping the discs in contact under load.

Strain Analysis

The uniform plane stress deflections give

$$u_\rho = \frac{1}{E_c} \left[-\frac{C_o}{\rho} (1 + \nu) + 2C_1 \rho (1 - \nu) \right]$$

The pure shear deflections from $\theta = 0$ to $\theta = 90^o$ give

$$u_{\rho 90} = -\frac{1}{E_c} \left[-C_2 (1 + \nu) \rho + \frac{C_3}{3} \rho^3 (1 + \nu) + \frac{2C_4}{\rho} - \frac{2}{3} C_5 \nu \rho^3 \right]$$

and $v_{\rho 90} = -u_{\rho 90}$

where u is the radial component of displacement and v is the circumferential component. For the condition of zero displacement at $r = \rho$ and $\theta = 90^o$

$$U_{T\rho S} - \frac{\nu S \rho}{E_c} \equiv V_{T\rho S'}$$

from this, the ratio $\frac{S^1}{S}$ may be obtained.

$U_{r\rho s}$ = total radial deflection at the outer boundary over 90° arc arising from both uniform plane stress and shear stress systems comprising an applied unidirectional stress.

$V_{r\rho s'}$ = corresponding circumferential displacement comprising an induced unidirectional stress.

The peak stresses in the ligaments resulting from Kinkead's analysis are considered to be conservative.

v) Bailey and Hicks : Behaviour of Perforated Plates Under Plane Stress

End-loaded rectangular plates (84) were analysed under two conditions of loading,

(a) unequal biaxial extensions

(b) uniform shear.

The plates were perforated with circular holes on a square and on a diagonal grid.

The work applies to an infinite plate and solutions were obtained for a range of hole pitch: hole diameter ratios from 1.2 to 3.0.

For each of the cases of a square grid of holes and a diagonal grid, the elastic relationships of stress and displacement are obtained for both the unequal biaxial strain loading and for the uniform shear loading.

The unknowns which areobtained in this first step are the effective Young's Modulus, the effective Poisson's ratio and the

effective shear modulus.

The maximum stress and hence the stress concentration factors around the holes are then obtained for the biaxial loading and also for the shear loading, again for both the rectangular and diagonal grids.

The results were plotted in the form of curves relating the effective Young's modulus, the shear modulus, the Poisson's ratio, ligament stress, the external load and the stress concentration factors.

The work of Bailey and Hicks was conceived initially in relation to steel pressure vessels for nuclear reactors.

vi) Bailey and Fidler : Stress Analysis of Perforated Plates With Reinforced Holes

This paper (85) analyses elastically the stress distributions around reinforced holes in perforated plates under biaxial external loading.

Curves are presented which illustrate the variation of the effective Young's modulus and the maximum stress concentration with pitch:diameter ratio and amount of reinforcement of the holes. Both square and triangular lattice patterns are investigated.

These curves are used to satisfy the external boundary conditions and also the boundary conditions around the hole.

vii) Horvay : Ligament Theory

Horvay has produced a paper (82), also relevant to the elastic stress analysis of perforated plates.

He investigates the inplane stress distribution and the bending in honeycombs and triangularly perforated plates of infinite size.

Because of the narrow ligaments of honeycomb -type plates he has assumed that the ligaments may be replaced by parallel-sided load-carrying members.

This grid-analogy assumption, sometimes referred to as a "ligament" theory underestimates the effective modulus for large pitch:diameter ratios.

Horvay produces curves relating effective Young's moduli and effective Poisson's ratios and the appropriate stress concentration factors.

B. ANALYSIS OF TIME-DEPENDENT STRAINS

Time, temperature, creep and shrinkage adjust the initially-assumed elastic stress state of a concrete structure when it is under uniform external loading.

The nature of the material changes, the elastic constants are modified, and creep and shrinkage strains approach asymptotic values. These effects take a considerable time to occur.

In general, compressive stresses lessen under conditions of restraint, where the concrete, flowing viscously under the load, attempts to assume its least-stressed condition. Moisture migration by seepage, and the slow equilibration of water vapour pressure along the capillaries cause the gel and interstitial configurations to modify themselves internally, resulting in the flowing, deformation and micro-cracking of the concrete.

It is clear, therefore, that the stress distribution in a structure immediately on loading, and the distribution after the concrete has been allowed to settle down to a constant response under the same steady uniform loading conditions, constitute two extremes of stress state.

These two extremes may be considered to form an upper and lower bound solution to the stress variation function under the given loading. Such loading may be taken to include both mechanical and thermal effects.

After a period of time under uniform external loading, a steady state of stress will be achieved. This period of time may be as short as six months, but the condition is certain to have been assumed after several years.

The total strain ε, in a concrete element, at any time, under a given stress and a given humidity and temperature, may be written as the following algebraic sum:

$$\varepsilon_{in} + \varepsilon_{th} + \varepsilon_{v} + \varepsilon_{c}$$

where ε_{in} = the instantaneous elastic strain due to loading

ε_{th} = the strain due to thermal expansions or contractions

ε_{v} = the strain due to drying shrinkage, hygrothermal moisture movements, and physico-chemical deformations

ε_{c} = the strain resulting from creep caused by a given stress history.

It is usually assumed in computation that these strains occur independently and can be predicted independently. One of the limitations of time-dependent analysis may lie in this assumption, although the practice commands wide assent.

Variations in stress and environmental history have an important result on the structural behaviour of the material. For example, repeated hygrothermal changes of state may lead to residual deformations.

Several methods of time-dependent analysis are able to cope with the problem of constant externally-applied stress and temperature. Under these circumstances strains may continue to increase with time while the internal stresses are sustained at a constant value.

Methods of analysis do exist, however, such as the rate of creep, the relaxation, and the strain-hardening procedures which are capable of dealing with the problem of varying applied stresses.

For full time-dependent analysis of prestressed concrete pressure vessels, it is expected that the following conditions should be dealt with:

i) changes with time or with reactor operational procedures, of mechanically-applied loadings such as the prestressing force, the internal gas coolant pressure, or frictional forces,

ii) changes of thermal loading with time,

iii) changes in the elastic constants of concrete with time,

iv) changes in specific creep rates with time, temperature, concrete age and stress level,

v) effects of shrinkage.

1. THE REDUCED MODULUS METHOD

The simplest possible approach to the problem of stress relaxation in concrete due to time-dependent effects, is merely to adopt a constant reduced value of Young's modulus, which does not vary with temperature. Where this has been done, the elastic modulus has been multiplied by a factor of 0.4 or 0.5 to obtain a reduced value.

Stresses due to both applied mechanical loading and temperature, are calculated simultaneously using the reduced modulus.

Thermal stress decay is underestimated by the reduced modulus method and after a period of time as the effective modulus departs grossly from the constant reduced modulus value, the errors in stress estimation also become gross.

Since a constant modulus is utilized across a section, over the full life of the structure, the method gives stresses at great age, identical to the early time-dependent values.

2. THE EFFECTIVE MODULUS METHOD IN CONSIDERING TIME-DEPENDENT BEHAVIOUR

This method has been described by Ross (11). The normal elastic modulus is replaced by an effective modulus at each appropriate point

of the structure. The effective modulus, E', is lower than the normal modulus and allows for both elastic and creep strains.

The relationship between the two moduli is given by

$$E' = \frac{1}{\frac{1}{E} + c}$$

where E = elastic Young's Modulus

c = specific creep, i.e. the creep strain per unit stress, after time t and at the given temperature

i.e. $\frac{\varepsilon_c}{\sigma}$

This relationship is developed by defining the effective modulus as the elastic stress divided by the sum of the elastic and creep strains.

Thus $E' = \frac{\sigma_{el}}{\varepsilon_{el} + \varepsilon_c}$

$$= \frac{\frac{\sigma_{el}}{\varepsilon_{el}}}{1 + \frac{\varepsilon_c}{\varepsilon_{el}}}$$

$$= \frac{E}{1 + \frac{\varepsilon_c}{\varepsilon_{el}} \times \frac{\sigma_{el}}{\sigma_{el}}}$$

$$= \frac{E}{1 + \frac{\varepsilon_c}{\sigma_{el}} \times E}$$

$$\therefore \quad E' = \frac{E}{1 + E.c.}$$

The effective modulus is a function of strain, stress, time and temperature although for the work described in this thesis, it is likely to remain uniform at one point in time throughout the specimens since the temperature is uniform.

The values of c used in the calculations may be obtained from the appropriate part of the specific creep, or specific thermal creep curves applicable at the time considered. They may also be calculated by dividing the total creep strain at any time by the applied stress.

The use of the effective modulus leads to the computation of fairly representative stress in the material in, for example, a prestressed member after the steel and concrete stresses have been reduced by creep. This method, however, has limitations for conditions of varying stress. The strain predicted relates only to the stress acting at a given time and the method disregards stress history.

In the course of time, the stress in the concrete declines due to transfer to the steel, and the effective modulus method accordingly underestimates the strain in the concrete.

If the externally-applied load is reduced to zero, residual strains will, in practice, remain in the concrete, but the effective modulus method incorrectly leads to the assumption of complete recovery of strain.

For uniform temperature and for sustained loading, and particularly for cases in which strains after unloading are not required, the method has the advantage of involving a single set of calculations in each case. It appears suited to the computation of approximate

strains in the intermediate regimes of the test programme described herein. Since the temperature is uniform for these parts of the test programme, the creep and shrinkage functions will also remain constant and the effective modulus method should produce acceptable results.

Effective modulus calculations are presented in the Appendices for the periphery of the perforated zone.

3. THE RATE OF CREEP METHOD

If the rate of creep obtained from a specific creep curve is denoted by dc/dt, at any time t and stress σ, the increase in creep in time dt can be written σ.dc. The specific creep curve can be obtained experimentally.

Thus the total creep strain after time t is equal to $\int_0^t \sigma . \frac{dc}{dt} . dt$ and this is the basic equation in the rate of creep method.

To solve the more general cases of time-dependent thermal creep, the concept of specific thermal creep is employed, taking account of the influence of temperature. The rate of specific thermal creep can be defined by the equation

$$\frac{d\,\varepsilon_c}{dt} = \phi(T) . \sigma . \frac{dc}{dt}$$

Here $\frac{d\,\varepsilon_c}{dt}$ is the rate of creep strain under the applied stress σ, dc/dt is the rate of specific thermal creep and $\phi(T)$ is a function of temperature. This function may be approximated to a linear function of T in the range 20°C to 100°C (31), (32).

The governing equation becomes

$$\Delta \varepsilon_c = \phi(T) . \sigma . \Delta c$$

In summation form, for small intervals of time, the total creep strain is given by

$$\varepsilon_c = \sum_{t=0}^{t=t_1} \phi(T) . \sigma . \delta c$$

The rate of creep method is based upon the assumption that, at any age of the concrete, the creep rate is independent of the age at loading.

The stress history of the concrete is taken into account in this method only insofar as all elementary increments of creep are integrated. This applies, however, to increases in creep only since, when a stress is removed, σ. dc/dt = 0 and therefore no creep recovery

is predicted. Thus the assumption that dc/dt is independent of previous stress history leads, under decreasing stress, to an overestimation of creep.

The accumulation of creep strains with time under varying stress and temperature conditions is shown in Fig. 40 . During each of the three time intervals considered, the stresses and temperatures have constant values σ_1 and T_1 , σ_2 and T_2, σ_3 and T_3. The rate of creep method indicates that a change in the values of σ and T represents a transference to another curve in the family of curves.

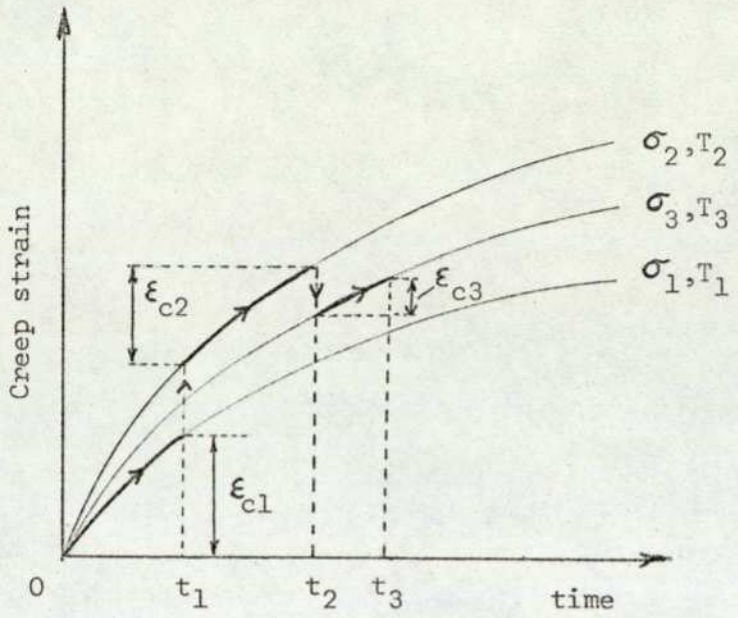
The creep strains for the first and second intervals are therefore ε_{c1} and ε_{c2}. These values are independent of previous stress history and are only influenced by the magnitudes of current stress and temperature and age since loading.

Similarly, the strain in the third interval is ε_{c3}. The total strain due to creep is the sum $\varepsilon_{c1} + \varepsilon_{c2} + \varepsilon_{c3}$.

Thus changes in stress and temperature with time are not taken account of in the rate of creep method and errors are introduced due to the theory not allowing for transient effects of this nature. For many classes of problem, however, changes in stress and temperature may not occur and thus transient conditions are notencountered.

In a step-by-step analysis, the original elastic solution based upon the finite element approach, will include thermal and external elastic effects only, and it is necessary to devise a routine for the time-dependent effects which will allow for the creep strains by modifying the values obtained from the elastic solution.

Thus the elastic solution can, in effect, be repeated, introducing merely, the modifications at each time interval, due to the creep strains and other variations, for example, changes in the elastic modulus with time. It is assumed that the stress stays constant during



Cumulative creep strains.
Rate of creep method.

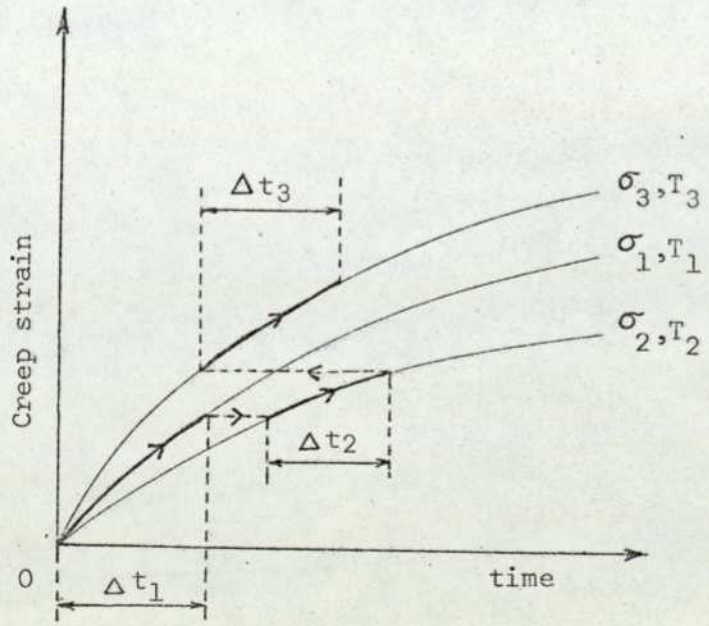


Fig. 40. Cumulative creep strains.
Strain hardening method.

any particular short time interval. Thus the creep strains that develop under these constant conditions, during the time interval, destroy the compatibility and thus modify the strain distributions applying at the start of the interval, obtained from the previous step. Compatibility is again restored at the end of each interval.

The creep strain calculation for any interval utilizes the increment for that interval on the specific thermal creep curve, which is applied uniformly throughout the structure. The specific thermal creep becomes the independent variable.

The modification of the threshold value of the preceding free strains from the previous step of the analysis, is carried out according to the equation

$$\varepsilon'_f = \varepsilon_f - \Delta\varepsilon_c$$

where ε'_f and ε_f are the threshold free strain and the modified strain respectively, and $\Delta\varepsilon_c$ is the incremental creep strain during the interval.

The rate of creep method is relatively simple to operate in practice requiring experimental data only in the form of a specific thermal creep curve and the variation in value of the elastic modulus. A knowledge of the appropriate shrinkage laws is also required if this is to be included in the analysis.

The solution at each time considered is the total creep strain at that time. No record of creep strain need be kept for subsequent time intervals. The method is thus economical in computer storage and time.

4. THE METHOD OF SUPERPOSITION

If the separate deformations, at any time, due to several separate loads applied to a concrete member are summated, the result

will equal the total deformation, at that time, due to a loading representing the sum of all the separate loads applied together.

McHenry (96) stated this principle of superposition in the following form : " the strains produced in concrete at any time t by a stress increment applied at any time t_o are independent of the effects of any stress applied either earlier or later than t_o " ; the stresses may increase or decrease. In other words, the stress increments may either be positive or negative, but stresses which approach the ultimate are excluded.

To obtain the stress-strain history of the material would involve taking experimental creep measurements from a large number of tests with varying ages at loading and any other appropriate changes in conditions. This is because the desired state of strain of the concrete at any time is a function not only of the forces acting at that time but also of the entire stress history. This is difficult to fulfil for a complex loading and temperature regime.

The complete stress-strain-time relationship required, really demands a family of experimental creep curves, preferably a creep surface having creep, age at loading, and age since loading as variables.

The concept of such a surface calls for the development of a mathematical equation with coefficients and indices evaluated to fit the experimental data. Supplying the computer with a unit surface in the form of a mathematical expression is also a convenient way of handling the principle of superposition method in analysis.

McHenry (96) has suggested the following expression

$$c = \alpha(1 - e^{-rt}) + \beta e^{-pk}(1 - e^{-mt})$$

where c = the creep strain due to unit load

k = the age at loading

t = the time after loading

α, β, r, p, m = creep constants determined from laboratory tests.

5. THE STRAIN HARDENING METHOD

Creep is dependent upon the nature and the structure of the material under load. When the material changes its shape and its structure under deformation caused by loading, it is not only creeping, it is also undergoing a strain hardening process.

When used for the computation of concrete creep, the strain hardening method takes into account strain history by considering the creep rate to be a function of the total creep strain since loading. The creep rate is given by

$$\frac{d\varepsilon_c}{dt} = f(T, \sigma, \varepsilon_c)$$

This equation is valid as it stands for a regime in which the stress and temperature are unchanged and for which creep data relating

to one age of loading are available.

Changes in stress and temperature can be, however, dealt with in this method, as if they were changes in the age at loading ie time changes.

Thus a shift in the time scale is necessary since the method is dependent on the cumulative value of creep at any stage. In Fig 40 for example, a horizontal distortion of the time scale would be necessary to accommodate changes in stress and temperature.

The method is suitable for a step-by-step procedure. The evaluation of the incremental specific thermal creep for an element, however, depends on the accumulated creep strain already generated in the element. This is a significant difference from the way increments are handled in the rate of creep method for example.

Let us suppose that at the end of an interval, the stress, temperature and total creep strain were σ_1, T_1 and ε_{c_1} respectively. It is required to obtain the effective increment in specific thermal creep c_e for the next step.

Assume that a new regime represented by σ_2 and T_2 is imposed. It is necessary to consider that the total accumulated creep strain has been developed under this regime since the beginning of loading. To be able to do this, a time shift is necessary and the concept of "effective" time must be introduced.

The effective specific thermal creep at the start of the interval becomes

$$c_e = \frac{\varepsilon_{c_1}}{\phi(T_2)\,\sigma_2}$$

For each value of c_e, there will be an effective time t_e, and this will be different for each element.

The incremental Δ_c for the next time interval Δ_t is then the diff-

erence between the values of c at times $(t_e + \Delta t)$ and t_e. The free creep strains may then be calculated for the particular stresses and temperatures of the elements, and may then be used to adjust the free strains from the preceding step. Additional adjustments will also be necessary in the stresses to re-establish geometrical compatibility and equilibrium. The process is repeated step-by-step.

The strain hardening method finds its best application for regimes of increasing stress.

England (99) states that although the method may be applied to cases of moderately declining stress, marked stress reductions with time lead to difficulties. For example, a reduction in stress corresponds to a horizontal shift to the right from a specific creep curve representing the initial stress, to a point on a second curve representing the reduced stress. Such a point may not exist if the creep curves have limiting values.

6. THE RELAXATION METHOD

Relaxation may be considered to be a decrease in stress with time under a constant deformation.

Accordingly, in this method of time-dependent analysis, it is the strains, and not the stresses which are maintained constant during each step in the analysis. England (99) has described the method in a paper in which comparisons are made with the rate of creep and the strain hardening methods.

The stresses are considered to vary according to the relaxation function

$$\sigma = \sigma_i \cdot e^{-E\phi(T)c},$$

where σ_i is the threshold stress at the start of the interval,

σ is the relaxed stress at the end of the interval, E is the Young's modulus for the concrete, $\phi(T)$ is a function of temperature, c is the specific thermal creep (99), and e, here, is the Naperian base.

This equation represents the decay law characterizing the dashpot relaxation in Maxwell's rheological model of a spring and dashpot in series.

The process of adjusting the initial stress values is, in effect, a process of restoring equilibrium at each step. Equilibrium is lost and must be restored at each step, whereas compatibility is maintained.

The restoration of equilibrium is achieved by superposing additional stresses on the relaxed stress distribution. This results in a balance with the stresses acting on the section. These additional stresses correspond to additional elastic strains, which must also conform to the compatibility conditions.

The next step in the analysis starts with the final strains and stresses obtained from the previous interval. The strains are maintained constant during the interval, but the stresses are modified according to the relaxation law, by the creep occurring in the interval.

The final stresses at the end of the interval are thus the relaxed stresses added to the additional stresses required to restore equilibrium. In contrast, the strains are the sum of the initial constant values and those strains corresponding to the stresses which restore equilibrium.

A disadvantage of the relaxation method is that it does not take into account the recovery of creep on the removal of stress.

The method is best suited to the solution of displacement-induced, rather than to load-induced problems.

7. STEADY STATE STRESS

One effect of the dissipation and redistribution of stresses due to creep in a reinforced concrete member, is for the concrete to pass on its stresses increasingly to the reinforcement. This is known to occur in reinforced beams and columns.

Tests carried out (31), (102) have shown that as a result of this redistribution the concrete stresses, which are time-dependent, tend towards limiting values within several months of loading, even though creep strain has not ceased. In general, there are no defined values of strain corresponding to the steady state stresses.

Two forms of steady state stress are recognised. One occurs where a steady state is reached even though the full creep capacity of the concrete has not been utilized. This is known as limiting steady state stress. The other, known as stable stress, is a condition which will apply if the creep capacity is not great enough to allow the limiting steady state stress to be fully achieved.

In carrying out steady state calculations, the assumption is made that sections plane before loading remain so after loading. The stresses which occur in a concrete member due to a non-uniform temperature and stress acting together, give rise to time-dependent and temperature-dependent creep which cause the redistribution of stress.

If the temperature and loading are sustained, redistribution will continue until steady state values of stress are reached even though the material's strain capacity may not have been exhausted.

The elastic stress distribution immediately consequent upon loading and the final steady state stress distribution due to creep, form upper and lower bound solutions, which represent, for the

designer, invaluable information about the long-term serviceability and safety of his structure.

The initial elastic solution will provide the instantaneous stress and strain distributions due to the temperature and external loading.

As these initial distributions change due to creep, they must at all stages of the redistribution process and at all sections of the member, satisfy the requirements of equilibrium and compatibility.

During a small time interval, for which the stresses may be assumed constant, unrestrained creep strains occur which are non-linear over the section, although proportional to the product of the linear distributions of stress and temperature.

If the criterion of geometrical compatibility is to be satisfied, i.e plane sections remain plane after loading, then the total strain distributions, i.e the sum of the elastic and creep strains must remain linear. This will call for adjustments to the strains with consequent alterations to the stress distributions, at the end of the intervals. The stress distributions also thus become non-linear.

These adjustment processes may be considered to occur at each time interval and the changes become smaller. The stresses thus tend towards the limit at the steady state when no further changes in stress occur.

The following brief treatment illustrates the method.

Specific thermal creep may be defined by

$$\frac{d\varepsilon_c}{dt} = \frac{dc}{dt} \cdot T \cdot \sigma.$$

where ε_c is the creep strain, c the specific thermal creep, T is

the temperature, σ the stress and t is the time.

The total strain is given by

$$\varepsilon = \varepsilon_c + \varepsilon_{el}$$

where ε_{el} is the elastic strain.

The linear strain distribution follows the law

$$\varepsilon = a + bx$$

$\therefore \varepsilon_c + \varepsilon_{el} = a + bx$, giving a rate of change of uni-axial strain of

$$\frac{d\varepsilon}{dt} = \frac{d\varepsilon_c}{dt} + \frac{d\varepsilon_{el}}{dt} = \frac{da}{dt} + \frac{x.db}{dt}$$

$$\therefore \frac{d\varepsilon_c}{dt} = \frac{da}{dt} + \frac{x.db}{dt} - \frac{d\varepsilon_{el}}{dt}$$

From the specific thermal creep equation above,

$$\frac{dc.T.\sigma}{dt} = \frac{da}{dt} + \frac{x.db}{dt} - \frac{d\varepsilon_{el}}{dt}$$

When stresses have reached their limiting steady state, the rate of change of elastic strain will be zero.

$$\therefore \frac{d\varepsilon_{el}}{dt} = 0$$

$$\therefore \frac{dc.T.\sigma}{dt} = \frac{da}{dt} + \frac{x.db}{dt}$$

$$\therefore T.\sigma = \frac{da/dt}{dc/dt} + \frac{x.db/dt}{dc/dt}$$

$$= A + B.x$$

Note that da/dt and db/dt represent the rates of change of centroidal strain and curvature respectively, due to creep.

The strain parameters A and B are independent of time since T and σ are also independent of time. A and B are constants for a particular cross-section.

The equation

$$T.\sigma = \frac{da/dt}{dc/dt} + \frac{x.db/dt}{dc/dt}$$

$$= A + B.x \quad \text{is analogous to}$$

the conventional elastic stress-strain relationship in which Young's modulus is represented by a reciprocal of temperature $\frac{1}{T}$

$$\text{i.e } \sigma = \frac{1}{T} (A + B.x)$$

This conceptual modulus can be modified to $\frac{1}{T - D}$

where T is the temperature and D is a constant depending on the creep characteristic of the material, (105).

This reciprocal of temperature function, however, varies throughout the member.

In practice, since creep strain is proportional to stress, for analyses of parts of the P.C.P.V, the stresses due to gas pressure and to applied prestress, may be calculated separately from those due to non-uniform temperature. The combined stress effect may then be obtained by superposition.

The differences in temperature along the P.C.P.V end slabs and cylinder walls, permit the redistribution of loading effects from the hotter areas where the creep strain is greatest, to the colder areas. This differential creep takes place rapidly. The majority of such distribution takes place in one year and the two year and twenty year cases are very similar (105).

Theoretically, the steady state for thermal effects is zero stress. However, Irving and Lewis (105) have proposed a modification to the normal steady state solution in which a residual thermal stress is included. Thermal stresses redistribute and decay swiftly with time due to relief of the initial restraints by creep. 12% of the initial hot face stress, however, is present after two years (105). Irving and Lewis have therefore suggested that the residual effect

of thermal stress may be taken account of by superposing a percentage, of this order, of the initial thermal stress on the steady state distribution.

For the two-dimensional case, the initial specific thermal creep equation given above, becomes

$$\left(\frac{d\varepsilon_c}{dt}\right)_x = \frac{dc}{dt} \cdot T\,(\sigma_x - \nu\sigma_y)$$
$$\left(\frac{d\varepsilon_c}{dt}\right)_y = \frac{dc}{dt} \cdot T\,(\sigma_y - \nu\sigma_x)$$

Finally, England (102) draws the following conclusions, inter alia, about steady state theory :

a) steady state stresses are relatively insensitive to changes in the value of Poisson's ratio for creep.

b) conventional elastic theory and steady state theory are analogous; it seems probable that steady state stress solutions may be obtained for any structure that has a calculable elastic solution; elastic stresses and steady state stresses can be computed from a single programme.

c) although the initial elastic solutions may be based on a single value of elastic modulus, it is possible to reflect the consequences of the temperature-dependence of this quantity in the subsequent analysis.

d) in the practical cases of reactor blow-down and cooling, the steady state theory provides a means for estimating the stresses and general behaviour.

8. COMPLEMENTARY POWER THEORY

Between the initial elastic stress solution at the instant

of loading a concrete structure, and the steady state solution after the lapse of several months under sustained loading, there exists a zone of transient effects.

During this transient period, stresses and strains may be changing even though the external loading may remain constant. The stresses tend to drift towards the steady state condition.

The method of solution offered by England (103) described herein, permits a direct study of the transient effects using variational principles. It is a direct method of estimating the transient stresses, particularly in heated concrete structures such as P.C.P.V, and avoids repetitive calculations which require the storage of historical strain.

If a body is acted upon by a system of external forces P and supported by a series of reactions R, the applicable conservation of energy equation may be presented in a form which relates the rate of working i.e the power of the external loads and reactions to the rate of internal work.

That is, using the dot notation $\dot{\varepsilon} = \frac{d\varepsilon}{dt}$, $\dot{u}_P = \frac{du_P}{dt}$, $\dot{u}_R = \frac{du_R}{dt}$,

then $$\int \sigma \dot{\varepsilon} \, dV = \sum (P\dot{u}_P + R\dot{u}_R)$$

Here V represents the whole volume of the body and σ and $\dot{\varepsilon}$ refer respectively to the internal stresses and strain rates resulting from the loads and reactions. The terms u_P and u_R represent respectively the applied load displacements and the reaction displacements, taken in the directions of these forces. The integration is taken over the whole body volume and the summation of the right hand side of the equation includes all the forces and reactions and their corresponding displacements.

The internal rate of working includes the rate of change of

stored energy which results from stress redistribution, and the rate at which energy is dissipated from the body.

To establish the variational principles, simultaneous small variations are given to the strain rates and stresses. During these variations the support reactions will undergo corresponding changes. Their displacement rates will remain unaltered, however.

These variational changes lead to the following equation, ignoring second order terms,

$$\int (\dot{\varepsilon}\, \delta\sigma)\, dV + \int (\sigma\, \delta\dot{\varepsilon})\, dV = P\, \delta \dot{u}_P + \dot{u}_P \delta P + \dot{u}_R \delta R$$

If the external loads are not subject to variation then $\delta P = 0$ and the equation becomes

$$\int (\dot{\varepsilon}\, \delta\sigma)\, dV - \dot{u}_R \delta R = -\left\{ \int (\sigma\, \delta\dot{\varepsilon})\, dV - P\, \delta \dot{u}_P \right\}$$

The left hand side of this equation shows the strain and displacement rates corresponding to the true stress system multiplied by the variational set of stresses.

If the equation is modified by multiplying throughout by Δt, the work rates are transformed into work quantities and by the principle of virtual work, the left hand side of the equation, so modified, vanishes.

$$\therefore \int (\dot{\varepsilon}\, \delta\sigma)\, dV - \dot{u}_R\, \delta R = 0$$

This equation is analogous to the variational principle applying in elasticity in the theory of complementary energy, except that here rates of strain and displacement replace strains and displacements. Since rate of working is defined as power, by analogy the method is referred to as the theory of complementary power.

The above equation gives the variation of the total complementary power and is defined by

$$\delta (Q_I + Q_E) = 0$$

where Q_I and Q_E are the contributions from the internal stresses and external reactions respectively.

England (103) defines the variational principle as follows:

"The total complementary power at any instant has a stationary value with respect to small variations of stress from the true equilibrium state at that instant".

The terms in the expression on the right hand side of the above equation

$$\text{i.e} \int (\sigma \, \delta \dot{\varepsilon}) \, dV - P \, \delta \dot{u}_p$$

represent the true internal stresses and the actual set of external loads P, multiplied respectively by the variational set of strain rates and surface displacement rates which constitute, themselves, a compatible system.

Thus a further application of the principle of virtual work during a time interval Δt as before, gives the second variational principle,

$$\int (\sigma \, \delta \dot{\varepsilon}) \, dV - P \, \delta \dot{u}_p = 0$$

This is analogous to the variational principle in elasticity known as the minimum of total potential. It is of interest in determining strains and displacements, but is not germane to the development of the present complementary power theory.

The strain rate law for concrete may be written in the form

$$\frac{d\varepsilon_c}{dt} = \sigma \, \phi(T) \, \frac{dc}{dt}$$

Because the curve of c, the specific thermal creep, is single-valued, it may be used as the independent variable in place of t.

Thus $$\frac{d\varepsilon_c}{dc} = \sigma \, \phi(T)$$

Including the effect of elastic strain this expression becomes

$$\frac{d\varepsilon}{dc} = \frac{1}{E} \frac{d\sigma}{dc} + \sigma \, \phi(T)$$

This is a well-known expression for representing viscoelastic behaviour and may be used in the rate of creep formulation with c

as the independent variable.

Expressions of this nature are appropriate for use with uniform temperature distributions, and in such cases, approximate to the homogeneous Maxwellian material in which $\frac{1}{\phi(T)}$ substitutes for the viscous coefficient in the Maxwellian dashpot, and c replaces t.

When $\phi(T)$ is not uniform, the concrete behaves like a non-homogeneous Maxwellian material and stress redistribution takes place.

For the bi-axial case, two equations are applicable for total strains, of the form,

$$\left(\frac{d\varepsilon}{dc}\right)_x = \frac{1}{E}\frac{d[\sigma_x - \nu\sigma_y]}{dc} + \phi(T)[\sigma_x - \nu_c\sigma_y]$$

$$\left(\frac{d\varepsilon}{dc}\right)_y = \frac{1}{E}\frac{d[\sigma_y - \nu\sigma_x]}{dc} + \phi(T)[\sigma_y - \nu_c\sigma_x]$$

where ν and ν_c are the elastic and creep Poisson's ratios respectively.

It is clear that a further analogy exists between the elastic relationship of stress and strain and the relationship between creep and temperature.

The elastic modulus may be replaced by the reciprocal of the function of temperature. The quantity $\frac{1}{\phi(T)}$ may thus be regarded as a creep modulus under direct stress conditions. The shear modulus for creep may also be represented by $\frac{1}{\phi(T)(1+\nu_c)}$.

Thermal creep problems are characterized by multiple internal redundancies, and in order to use the variational principle

$$\int(\dot{\varepsilon}\,\delta\sigma)\,dV - \dot{w}_R\,\delta R = 0$$

to the best advantage, it may be utilized as an optimization procedure in conjunction with the concrete stress-strain law described, and an appropriately chosen set of stress distributions.

The problem is to choose a set of stress distributions representing a finite number of internal stress redundancies, which when combined, correspond, to as close a degree as possible, to the true equilibrium stress distribution states.

The chosen stress distributions are subject only to the restriction that they must be in equilibrium, at any instant, with the system of external loads and reactions.

The stresses are optimized with the aid of the variational principle to obtain the best solution i.e the solution which, consistent with the chosen stress distributions, gives rise to a minimum value, with respect to stress, for the total complementary power, at any instant in time.

To ensure equilibrium of the whole system, a choice of stress distributions in equilibrium within themselves may be made, and one or more distributions which together satisfy the external boundary conditions.

If the initial elastic stress distributions and the final steady state distributions were known or could be calculated, upper and lower bound stress conditions would be revealed within which the self-equilibrating transient stress distribution patterns to be chosen, might be pitched.

England (103) suggests that a series of terms of the form

$$\sigma = \sigma_0 + a_1\sigma_1 + a_2\sigma_2 + \ldots\ldots a_n\sigma_n$$

might be postulated as a convenient choice of stress distribution. Here σ_0 represents a distribution of stress which equilibrates the external loads, and σ_1, σ_2 .... σ_n are the self-equilibrating internal redundant distributions. The multipliers a_1, a_2, etc, are determined from the optimization procedure using the variational

principle.

Using England's series of terms above, and the strain rate law for creep and elastic strains,

$$\frac{d\varepsilon}{dc} = \frac{1}{E}\frac{d\sigma}{dc} + \sigma\phi(T),$$

in conjunction with the variational principle

$$\int(\dot{\varepsilon}\,\delta\sigma)\,dV - \dot{u}_R\,\delta R = 0$$

the latter will then represent expressions for the variations of the total complementary power, with respect to each of the stresses taken in turn.

The equation

$$\delta\,(\,Q_I + Q_E\,) = 0$$

then yields a set of simultaneous linear first order differential equations for the multipliers $a_1, a_2 \ldots\ldots a_n$ by the optimization procedure. Q_I and Q_E are the respective contributions from the internal stresses and external reactions as given in the variational principle equation.

The multipliers are determined in terms of c, the specific thermal creep, and by substitution into the chosen stress distribution equation, the transient stress distributions due to creep are obtained.

England (103) reports that close matching with true solutions from other sources is possible with only a few redundant self-equilibrating stress distribution terms.

9. VISCOELASTICITY

The Rheology of Viscoelastic Materials

In contrast with those elastic materials whose strain response when subjected to stress is linearly elastic, the response of viscoelastic materials is one in which time and rate effects play a dominant role.

Simple viscoelastic behaviour is shown in Fig 41 . Assuming

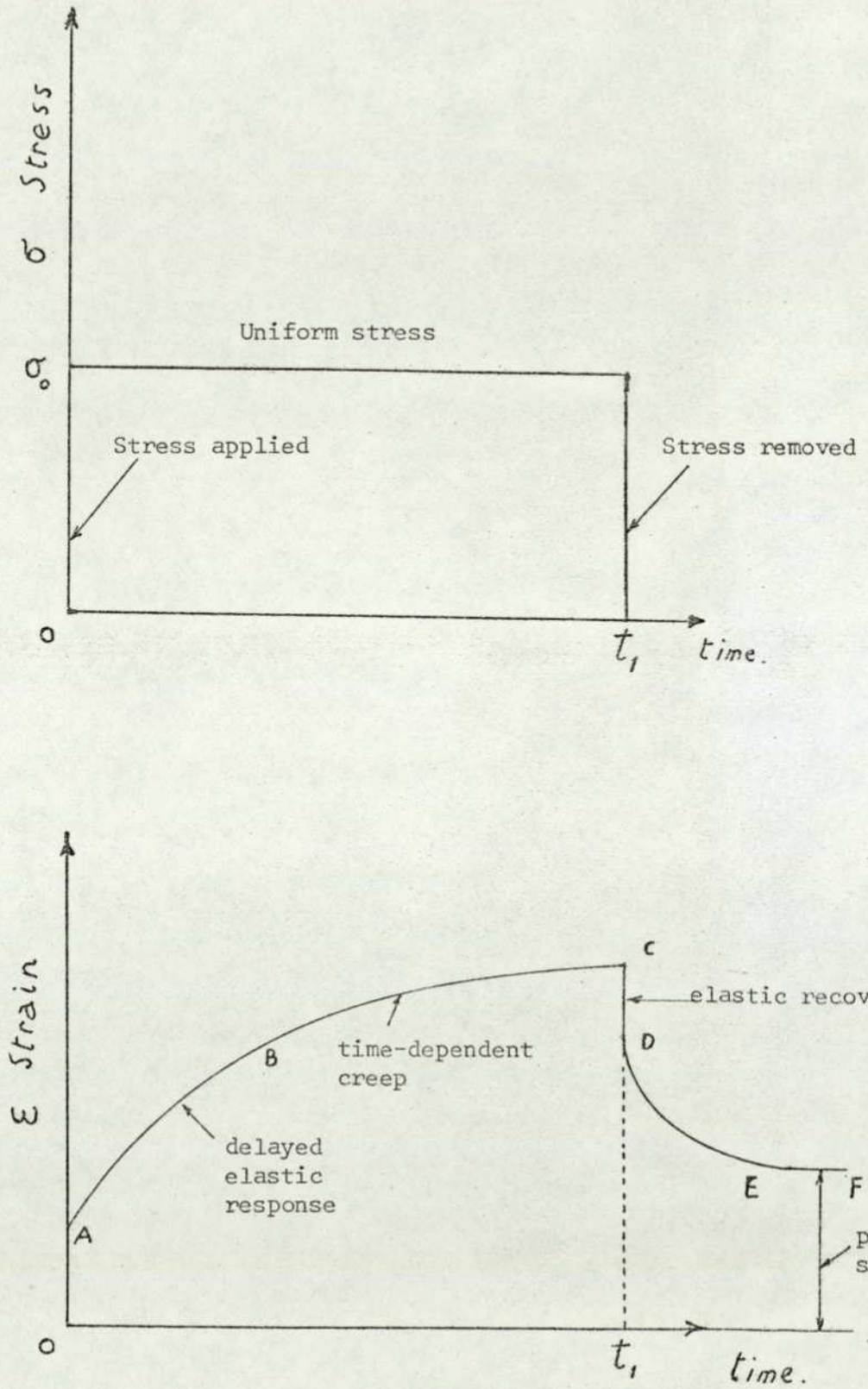


Fig. 41. Creep and Recovery.
Stress and strain variation
with time.

a uni-axial stress σ_o is applied to the specimen of viscoelastic material at zero time, ϵ represents the corresponding strain. The strain variation shows immediate elastic response OA, followed by a delayed elastic response AB and by continuous time-dependent viscous flow BC.

On unloading at time t_1 an immediate elastic recovery CD occurs followed by a delayed elastic recovery DE, leaving the permanent strain at EF associated with the viscous flow.

This kind of complex response to loading differs markedly from that of a simple elastic material for which the strain behaviour will mirror the stress variation to some scale related to the modulus of elasticity.

In time-dependent analysis, it is desirable to be able to describe the viscoelastic properties of a material so that its response to any known stress history may be assessed.

Model analogues may be devised for this purpose which represent in a general sense at least, the behaviour of such viscoelastic materials.

For the simulation of the rheology of the material under a regime of applied, sustained, and withdrawn loading, such a model must exhibit the following:

a) an immediate elastic response

b) a delayed elastic response

c) a viscous time-dependent straining related to the stress

d) an immediate elastic recovery on unloading

e) adelayed viscoelastic recovery

f) a permanent irrecoverable deformation after removal of loading

Using spring elements to represent the linear elastic behaviour of the viscoelastic material and dashpot elements containing a viscous liquid to represent the time-dependent behaviour, it is possible, by suitably combining such elements, either in series or parallel, to devise a model the overall response of which mirrors broadly the characteristics of the material and which is therefore analogous to it.

The general properties of the material, if the analogy is close enough, might then be described by reference to the stiffnesses of the springs and to the viscous coefficients of the liquids in the dashpots.

Thus both a qualitative and a quantitative simulation is sought.

The model need simulate only the observed outward behaviour and not any inner molecular mechanism of the material. The macro- and not the micro-rheology is under review. A conceptual model is all that need be envisaged. There is no necessity to fabricate an actual mechanical working system.

Rheological models do no more than represent the functions of deformation, that is the elastic and creep response functions, in an alternative form. A model may be arranged to fit experimental results, and in such a case, the experimental data are used to predict the model and its parameters. Broadly, however, the model system, its arrangement, and its deformational parameters emerge from a process of reciprocal appraisal and synthesis, as a knowledge of the experimental viscoelastic behaviour of the real material is built up.

Simple, linear viscoelasticity should be capable of representation by springs and dashpots only, combined in a suitable system.

Departures from truly viscoelastic response in a material, might require, for their simulation, the inclusion in the system of approp-

riate elements other than straightforward springs and dashpots. For example, springs working in dashpots encountering friction at the cylinder walls, have been suggested. Sorption cells, wedges, elastic claws, porous pistons and telescopic capillary tubes have all been proposed by different investigators.

As concrete does not behave in a perfectly viscoelastic manner throughout the range of stress and strain to which it is likely to be subjected, other expedients than simple springs and dashpots may well be justified for a completely general rheological model.

If however, high stress levels are excluded, concrete may be termed quasi-viscoelastic, both from a structural and from a phenomenological viewpoint.

It will be assumed, in what follows, that viscoelastic rheological models may be used to approximate the behaviour of concrete.

Creep and Relaxation

A creep modulus may be defined as $\frac{\sigma}{\varepsilon_{el} + \varepsilon_c}$, and one way of describing the viscoelastic behaviour of a material would be to express the creep modulus as a function of time. It is sometimes more convenient to express viscoelastic response in terms of the creep compliance. This is merely the reciprocal of the creep modulus and equals $\frac{\varepsilon_{el} + \varepsilon_c}{\sigma}$.

Stress relaxation is another manifestation of viscoelastic behaviour which can be investigated by an experiment in which a specimen of the material is clamped at a fixed strain whilst the stress relaxes.

In such an experiment, let us suppose that an immediate stress σ_o is developed at t_1 the instant at which strain is applied. The strain is maintained constant until time t_2 whilst the stress relaxes

with time by an amount σ_s .

If, at time t_2, the strain is instantaneously reduced to zero and the material is then reclamped, the stress will fall immediately by an amount σ_o , causing a stress in the opposite sense to be developed i.e a tensile stress is generated if the original stress was compressive, and vice-versa. This residual stress will again relax with time to leave the material finally unstressed. This is a manifestation of viscoelastic behaviour.

A stress relaxation modulus can be defined as $\frac{\sigma_o - \sigma_s}{\varepsilon}$. This can also be expressed as a function of time. Again, it is sometimes more convenient to express relaxation behaviour in terms of the stress relaxation compliance, which is the reciprocal of the stress relaxation modulus.

Creep and stress relaxation may be considered to be separate manifestations of the same phenomenon, and it should therefore be possible to predict by calculation, the response of a viscoelastic material in one of these modes of behaviour, if its response has been observed in an experiment in the other.

Rheological Models

The simplest viscoelastic relationship between stress and strain may be expressed by equations of the form

$$P\left[\sigma(t)\right] = Q\left[\varepsilon(t)\right] ,$$

where σ is a single component of stress, ε is the corresponding component of strain, t is the time, and P and Q are differential or integral rate operators.

When P and Q are low order differential rate operators, they may be utilized to express the rate of change of strain in the following simple typical viscoelastic law which is characteristic of what

is known as the Maxwell "material".

$$\frac{d\varepsilon}{dt} = \frac{1}{E}\frac{d\sigma}{dt} + \frac{\sigma}{\eta}$$

where ε is the strain, σ is the stress, E and η are the material constants relating to the spring and dashpot respectively in the Maxwell model.

Maxwell suggested a simple model comprising a spring and dashpot in series. See Fig. 42 . The spring has a stiffness E such that a tensile force F will produce an extension x given by

$$F = E.x$$

The dashpot liquid has a viscous coefficient η such that a tensile force F will cause a constant rate of extension $\frac{dx}{dt}$ which is given by

$$F = \eta . \frac{dx}{dt}$$

The full response of a Maxwell model to loading is shown in Fig. 42 .

For the Maxwell material there is no delayed elastic component of the strain variation.

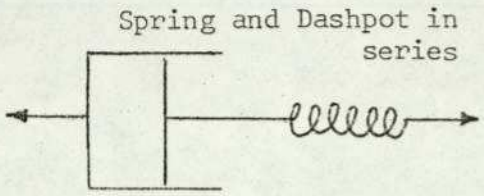
The creep strain can be deduced from

$$\frac{d\varepsilon}{dt} = \frac{1}{E}\frac{d\sigma}{dt} + \frac{\sigma}{\eta}$$

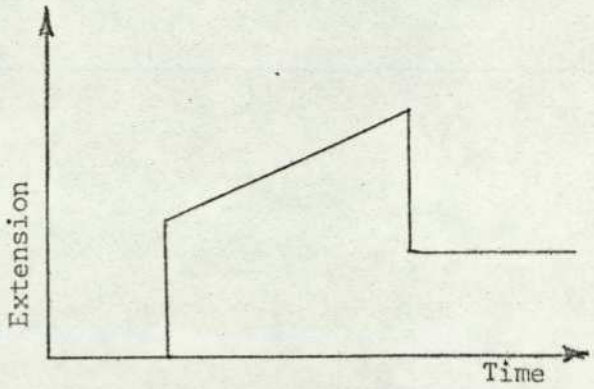
by substituting $\sigma = \sigma_o \Delta(t)$

where σ_o is the initial stress at time t_0, and $\Delta(t)$ is the Heaviside step function. The discontinuity in stress at zero time gives the initial strain response, and thereafter the constant stress σ_o gives a constant strain rate.

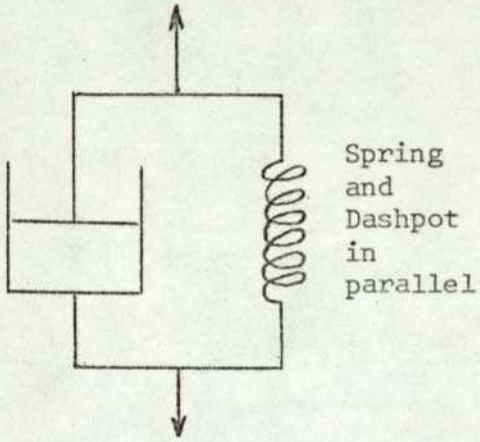
If we look at the relaxation aspect of viscoelasticity wherein stress variations are considered corresponding to instantaneously applied constant strain, we obtain a stress relaxation curve with



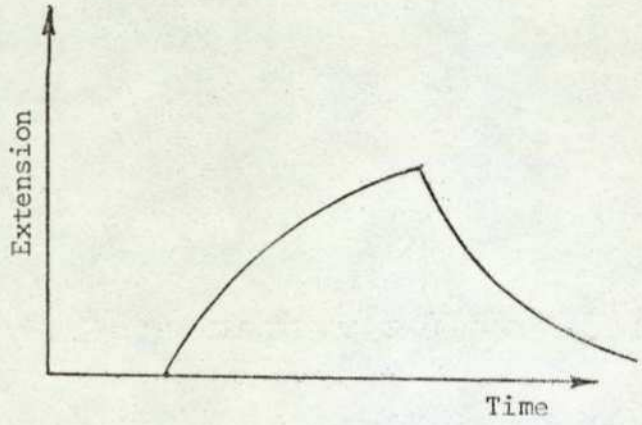
Maxwell model



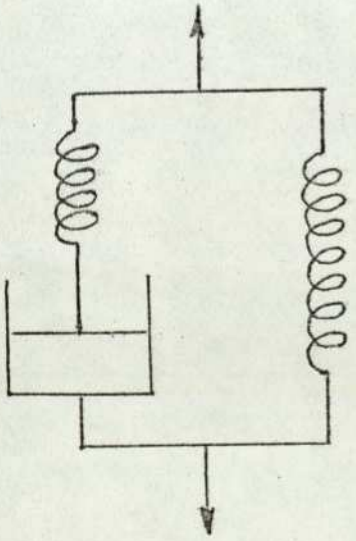
Maxwell model. Response to load.



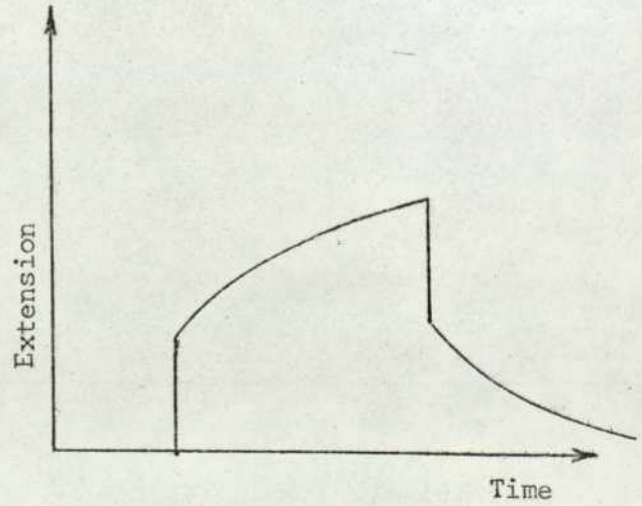
Kelvin model



Kelvin model. Response to load.



Three-element model



Three-element model. Response to load

Fig 42. Rheological models. Response to load.

the Maxwell model obtained by substituting

$$\varepsilon = \varepsilon_o \Delta(t) \quad \text{into}$$

$$\frac{d\varepsilon}{dt} = \frac{1}{E}\frac{d\sigma}{dt} + \frac{\sigma}{\eta}$$

where $\Delta(t)$ is again the Heaviside step function, and ε_o is the initial and constant strain.

The solution for stress is

$$\sigma = E\ \varepsilon_o\ e^{\frac{-t}{\tau}}\Delta(t)$$

where $\tau = \frac{\eta}{E}$ and is knownas the relaxation time.

Kelvin suggested another simple model comprising a spring and dashpot in parallel. See Fig.42 .

The spring has a stiffness E_1 such that a tensile force F_s will produce an extension x given by

$$F_s = E_1 x$$

The dashpot liquid has a viscous coefficient η_1 such that a tensile force F_d will cause a rate of extension $\frac{dx}{dt}$ which is given by

$$F_d = \eta_1 \frac{dx}{dt}$$

and $F = F_d + F_s$

When the force F is first applied, the dashpot prevents any instantaneous extension. Under the steady force, extension does, however, take place.

As the extension proceeds, its rate decreases. When the force is removed, instantaneous recovery of the spring is prevented by the dashpot. The extended spring ,however, causes a force to act upon the dashpot, the consequent movement of which represents extension recovery.

The behaviour of these two models relates imperfectly to a material like concrete. The analogues of spring extension to

elastic strain, and of dashpot extension to creep strain, are clear. The Kelvin model comes near to representing creep recovery qualitatively.

However, the Maxwell model exhibits only a constant rate of creep, and no creep recovery, whereas the Kelvin model fails to indicate elastic responses on loading and unloading and shows no permanent strain after the load is removed.

The simplest general law representing the Kelvin model takes the form

$$\sigma = E_1 \varepsilon + \eta_1 \frac{d\varepsilon}{dt}$$

The creep curve equation is obtained by substituting the stress variation $\sigma_0 \Delta(t)$ into this law and solving for ε, to give

$$\varepsilon = \frac{\sigma_0}{E_1}\left(1 - e^{-\frac{t}{\tau_1}}\right)\Delta(t)$$

where τ_1 equals $\frac{\eta_1}{E_1}$, e is the Naperian base, and $\Delta(t)$ is the Heaviside step function.

It can be seen that the strain approaches the value $\frac{\sigma_0}{E_1}$ asymptotically with a characteristic time τ_1, known here as the retardation time.

Other more complicated systems combining springs and dashpots have been considered. The three-element model, known also as the standard linear solid, utilizes a Maxwell model combined in parallel with a spring element, and it produces a response on unloading which fails to maintain a permanent deformation. The full loading response of a three-element model is shown in Fig.42 .

Another material represented by a Kelvin model in series with a dashpot exhibits delayed elasticity and viscous flow but no instantaneous elastic response to load. This is known as the three-element viscous model or the Newton-Kelvin material.

These three-element models, although they produce less restricted deformational characteristics than the simple Maxwell or Kelvin models, still fail to describe adequately the behaviour of a quasi-viscoelastic material like concrete,

The four-element material, known variously as the Burgers model or the Kelvin-Maxwell model consists of a spring, a Kelvin model and a dashpot in a series of three. This is in effect, a series combination of the Kelvin and Maxwell models. See Fig. 43 .

This material gives a qualitative deformational response under a load applied, sustained, and removed very close to that of concrete, meeting most of the desired criteria.

The linear Burgers model is, in fact, the simplest viscoelastic model which exhibits all three types of viscoelastic response - instantaneous and delayed elasticity, and viscous flow. There is a creep recovery response, together with a permanent deformation on unloading.

In order to discuss the Burgers model, it is noted that:

a) a linear dashpot provides a rate of deformation proportional to the appliedload

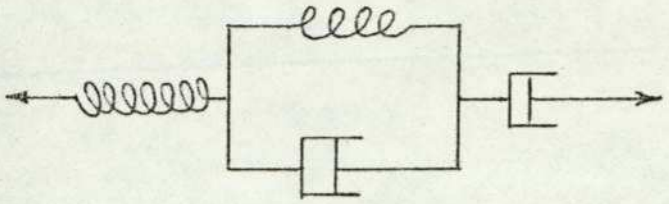
b) a linear spring provides a magnitude of deformation proportional to the applied load

c) a parallel system is characterized by equality of deformations and addition of loads

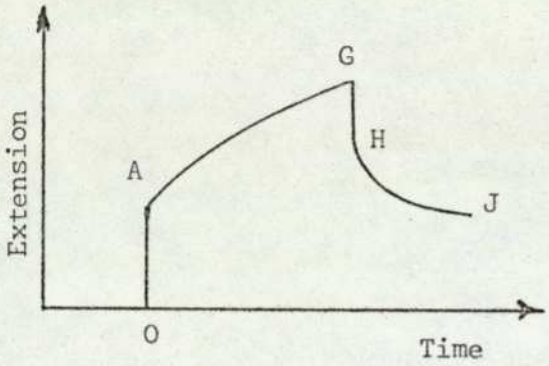
d) a series system is characterized by the addition of deformations and the equality of loads.

Suppose a four-element Burgers model to be subjected to an instantaneous load, which is sustained. The total deformation with time will be represented by curve OAG in Fig. 43 . Let the material

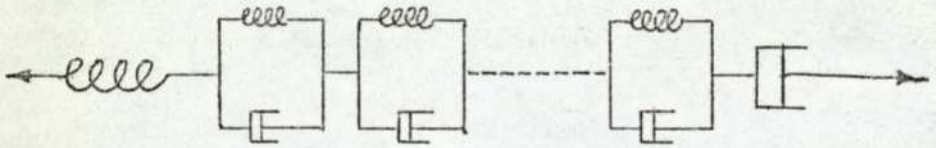
Maxwell and Kelvin elements in series.



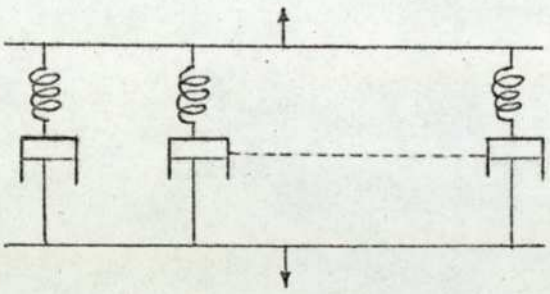
Burgers model



Response of Burgers model to load.



Generalized Kelvin Model



Generalized Maxwell Model

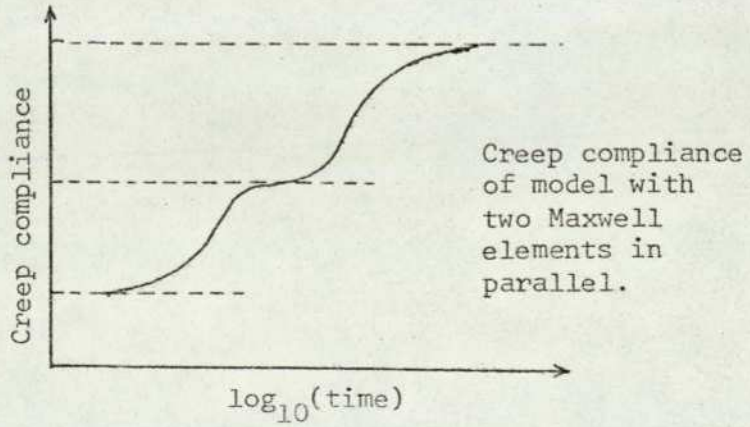


Fig. 43. Burgers and other models.

deformational parameters for the Maxwell and Kelvin springs be respectively E_m and E_k and for the viscous dashpots, η_m and η_k.

When the load is removed the recovery path traversed will be GHJ. The total deformation is the sum of the Maxwell and Kelvin elements' responses.

Thus under load F, the Maxwell spring will show an instantaneous deformation given by

$$OA = \frac{F}{E_m},$$

followed by a viscous flow proportional to time.

Thus the total deformation at time t will be given by

$$\frac{F}{E_m} + \frac{Ft}{\eta_m}$$ for the Maxwell element alone.

The Kelvin response will consist of a deformation reaching a value $\frac{F}{E_k}$, the deformation at any time being given by

$$\frac{F}{E_k}\left(1 - e^{-\frac{E_k}{\eta_k}.t}\right)$$

The total response of the Burgers model after time t, being the sum of the deformations of the Maxwell and Kelvin components in series, will be

$$\varepsilon(t) = \frac{F}{E_m} + \frac{Ft}{\eta_m} + \frac{F}{E_k}\left(1 - e^{-\frac{E_k}{\eta_k}.t}\right)$$

The creep deformation alone is

$$\varepsilon_c = \frac{Ft}{\eta_m} + \frac{F}{E_k}\left(1 - e^{-\frac{E_k}{\eta_k}.t}\right)$$

and the specific creep is given by

$$c = \frac{1}{E_k}\left(1 - e^{-\frac{E_k}{\eta_k}.t}\right) + \frac{t}{\eta_m}$$

The immediate elastic recovery GH, due to the Maxwell spring, occurs when the load is removed and is followed by an exponential delayed recovery HJ due to the Kelvin model. This tends asymptotically to reduce to the original Kelvin deformation on first loading. The magnitude of permanent deformation finally equals the deformation of the Maxwell dashpot on first loading.

Vaishnav and Kesler (125) point out, however, that a simple, linear Burgers model implies an exponential Kelvin response with a constant retardation time τ , together with an infinite Maxwell creep.

Thus, although the linear model gives a good qualitative simulation of concrete, it cannot be said to give a valid quantitative simulation.

Vaishnav and Kesler consider that the concrete material they examined corresponded to an exponential Kelvin response, but not with a constant retardation time. The Maxwell response furthermore, should indicate a limiting value of creep.

Accordingly, they suggested a time-dependent retardation for the Kelvin response and also that the Maxwell dashpot should be of the age-thickening type with an infinite viscous coefficient at infinite time. This latter suggestion was put forward on the basis that it would conform with the effects of progressive hydration of the cement paste in the gels. It could mean finite or infinite creep depending on the law governing the age-dependence of the viscous coefficient.

A power law of time-dependence of viscous behaviour, for example, leads to infinite creep, whilst an exponential law leads to finite ultimate creep, a condition tallying with experience.

For such a modified Burgers model as suggested by Vaishnav and Kesler, therefore, the Maxwell viscous coefficient would take the form

$$\eta_m = \frac{1}{\gamma} . e^{\beta t}$$

where $\frac{1}{\gamma}$ equals the viscous coefficient at zero time, and $\frac{1}{\beta}$ equals a constant governing the fluidity decay rate.

Making the assumption that the retardation time τ_k of the Kelvin element is proportional to the square root of time, the Kelvin dashpot viscous coefficient becomes according to Vaishnav and Kesler

$$\eta_k = \frac{2t^{0.5}}{p_k \cdot c_{k\infty}}$$

where p_k represents a coefficient controlling the change in retardation time and $c_{k\infty}$ is the ultimate specific Kelvin creep.

The general expression for the specific Kelvin creep will be

$$c_k = c_{k\infty}(1 - e^{-p_k \cdot t^{0.5}})$$

and the general expression for the specific Maxwell creep will be

$$c_m = \frac{\gamma}{\beta}(1 - e^{-\beta t})$$

Thus the expression for the total specific creep is the sum of those of the Kelvin and Maxwell components

$$c = c_{k\infty}(1 - e^{-p_k \cdot t^{0.5}}) + \frac{\gamma}{\beta}(1 - e^{-\beta t})$$

The generalized Kelvin model consisting of a number of Kelvin elements in series, presents some advantages in viscoelastic analysis. See Fig. 43 .

A direct generalization of the simple viscoelastic law

$P\ [\sigma(t)] = Q\ [\epsilon(t)]$ in which P and Q are rate operators, may be achieved by employing the differential rate operator form of P and Q, for which

$$P = \sum_0^p p_r D^r \quad \text{and} \quad Q = \sum_0^q q_r D^r$$

where p, p_r, q, q_r are material constants.

The total strain may be considered to be the sum of the strain contributions of each of the elements

$$\therefore \epsilon = \left(\frac{1}{E_o} + \sum_1^{n-1} \frac{1}{E_r + \eta_r D} + \frac{1}{\eta_n D}\right)\sigma$$

Such a total viscoelastic strain distribution is characteristic of a spring plus a number of Kelvin elements plus a dashpot all in

series. The spring stiffness would be E_o and the dashpot viscous coefficient would be η_n and (n-1) would be the number of intermediate Kelvin components between the spring and dashpot. D would be the differential rate operator $\frac{d}{dt}$.

To clear D from the denominators of the above equation, both sides of the equation can be multiplied by

$$\eta_n D \prod_{r=1}^{n-1} (E_r + \eta_r D)$$ to give a relation with the orders p and q of the operators P and Q both equal to n.

A Maxwell model would correspond to n=1, and a Burgers model with four elements to n=2.

The particular advantage in the generalized Kelvin model is that by selecting a retardation time $\tau_r = \frac{\eta_r}{E_r}$ different for each Kelvin element, it is possible, for constant stress conditions, to fit as closely as desired to an observed creep curve.

Each Kelvin element makes an exponentially-varying contribution. A carefully conceived and detailed model might consist of several or even of an infinite number of Kelvin elements in series, with retardation times distributed according to a chosen retardation time spectrum. This could be made to fit the apparent time-dependence of the retardation times of the Kelvin elements, detected in experiments on an analogous real material.

This suggestion offers the possibility of fitting the experimental creep curve by the sum of exponential terms and a linear term. For the four-element Burgers model, in contrast, a single exponential and linear term only is available for fitting the creep curve.

With the generalized Kelvin model, it would be possible to achieve any desired degree of closeness of fit, by increasing the number of elements. As the number of elements increased, however, higher order differential operators would be required.

The spring E_o can be considered to be a Kelvin element with zero retardation time and the dashpot η_n one with infinite retardation time, the intermediate elements providing a spectrum of increasing retardation times.

Such a generalized Kelvin series model is suited to problems in which the stress history is prescribed and it is desired to predict the strain distribution. The stress applied is common to all the Kelvin components, and the total strain is simply the sum of the individual component contributions.

Zienkiewicz et alia (108), has proposed a numerical method of viscoelastic analysis suitable for concrete and related to a generalized type of model with Kelvin elements in series, as follows.

The simple Kelvin model gives a creep stress-strain relationship for uni-axial conditions of the following form

$$\sigma = E_i \varepsilon_c + \eta_i \frac{d\varepsilon_c}{dt}$$

where ε_c the creep strain, is here separated from the instantaneous elastic strain which has been omitted.

This can be written

$$\frac{d\varepsilon_c}{dt} = \frac{1}{\eta_i}\sigma - \frac{E_i}{\eta_i}\varepsilon_c = a\sigma - b\varepsilon_c$$

Thus the creep rate can be seen to be a function of a) current stress and b) total accumulated creep strain. The latter can be kept in computer storage without a complete record of previous stress history being necessary.

For the generalized model with several Kelvin elements in series, a more complex response, better fitting concrete behaviour is obtained.

Thus

$$\frac{d\varepsilon_c}{dt} = \sum_{r=1}^{r=n} \frac{d\varepsilon_c^r}{dt} = \left(\sum_{r=1}^{r=n} a_r\right)\sigma - \sum_{r=1}^{r=n} b_r \varepsilon_c^r$$

$\left(\sum_{r=1}^{r=n} a_r\right)$ can be evaluated as a constant for the system. The term $\sum_{r=1}^{r=n} b_r \varepsilon_c^r$ gives the sum of the accumulated creep strains due to the individual elements.

Thus, in a step-by-step computer analysis, a record of creep strain ε_c^r for each Kelvin element may be kept separately. This avoids storage difficulty in assessing the rate of total creep in any time interval.

Zienkiewicz considers that, in practice, no more than two Kelvin elements should be needed to simulate concrete behaviour and a running sum of two quantities would suffice to represent previous stress history.

For short time intervals, the total elemental creep strain within each interval becomes

$$\Delta \varepsilon_c = \sum_{r=1}^{r=n} \Delta \varepsilon_c^r = \left[\sum_{r=1}^{r=n} (a_r \sigma - b_r \varepsilon_c^r)\right] \Delta t ,$$

where σ and ε_c^r are the threshold values of stress and creep strain at the start of each interval.

Integration may be used as an alternative to summation, to provide an alternative expression for evaluating creep strain. Thus, if

$$\frac{d\varepsilon_c}{dt} = a\sigma - b\varepsilon_c$$

is integrated on the assumption that σ, a_r and b_r remain constant within the interval, and $(\varepsilon_c^r)_{t+\Delta t}$ represents the r^{th} component creep strain at the end of an interval and $(\varepsilon_c^r)_t$ the value of the creep strain at the start of the interval, then on integration

$$(\varepsilon_c^r)_{t+\Delta t} = (e^{-b_r \Delta t})(\varepsilon_c^r)_t + \frac{a_r \sigma}{b_r}(1 - e^{-b_r \Delta t})$$

Thus, if a finite element solution of the elastic problem has initiated the analytical procedure, the modified threshold values of σ and ε_c^r are utilized at the start of each step. The process

then merely involves re-solving the "elastic" problem at each successive step, employing modified stress and strain values, and where appropriate, the changing elastic constants, as they are altered with ageing and temperature.

If the parameters of the various viscous elements are also age and temperature-variable, it may also be assumed that they change abruptly at the start of an interval and remain constant throughout the interval.

The above expressions relate to uni-axial conditions but it is relatively straightforward to generalize them for bi-axial stresses.

On the assumption that Poisson's ratio for creep strains in concrete is approximately the same as that for elastic strains, the equation

$$\frac{d\,\varepsilon_c}{dt} = a\sigma - b\,\varepsilon_c \qquad \text{for}$$

uni-axial conditions can be transposed to

$$a\sigma = \frac{d\,\varepsilon_c}{dt} + b\,\varepsilon_c$$

$$\therefore\ \varepsilon_c = \left(\frac{a}{\frac{d}{dt} + b}\right)\sigma$$

$$\therefore\ \varepsilon_c = \left(\frac{a}{D + b}\right)\sigma$$

where the operator $\left(\frac{a}{D + b}\right)$ replaces $\frac{1}{E}$ corresponding to an elastic relationship, D here being the simple differential operator $\frac{d}{dt}$.

For multi-axial conditions, this expression becomes

$$\{\varepsilon\}_c = \frac{1}{E}\,[A]\,\{\sigma\}$$

in which $[A]$ is an elasticity matrix dependent on Poisson's ratio, and $\{\varepsilon\}_c$ and $\{\sigma\}$ are creep strain and stress component vectors.

Using the operator form of $\frac{1}{E}$ and noting that $[A]$ is a constant matrix, the two equations above for creep strain, developed for uni-axial conditions, will generalize to

$$\Delta\{\varepsilon\}_c = \left[\sum_{r=1}^{r=n} \left(a_r [A]\{\sigma\} - b_r \{\varepsilon_c^r\} \right)\right] \Delta t$$

and

$$\{\varepsilon_c^r\}_{t+\Delta t} = e^{-b_r \Delta t} \{\varepsilon_c^r\}_t + a_r \frac{[A]\{\sigma\}}{b_r} \left(1 - e^{-b_r \Delta t} \right)$$

The corresponding model to the generalized Kelvin series model is the generalized Maxwell parallel model. This consists of a number of Maxwell components connected in parallel and which, when the number of components is infinite, is known as the Wiechert model. The relaxation times of adjacent Maxwell components are made, in the Wiechert model, to differ infinitesimally to fit a chosen spectrum.

Fig. 43 shows how the experimental curve of creep compliance against $\log_{10}(t)$ for a viscoelastic material could be approximated by curves for models containing large numbers of Maxwell elements. An infinite number would fit the experimental curve exactly.

If $E(\tau)$ is the spring stiffness of a Maxwell element having a relaxation time τ and there are an infinite number of such elements then a graph of $E(\tau)$ against (τ) could be drawn to give the distribution of relaxation times, known as a relaxation time spectrum.

It should be possible to choose a distribution function of relaxation times so that a model characterized by this function would reproduce the curve of creep compliance against log time obtained experimentally for the material.

The calculated responses of such a model could then be compared with the observed experimental behaviour of the real material under a variety of creep straining and stress relaxing conditions. This would confirm the validity of the practice of predicting viscoelastic behaviour in terms of relaxation time spectra.

The generalized Maxwell model in the Wiechert form is best suited to finding the stress associated with a prescribed strain distribution. This is because the prescribed strain variation is applied to each Maxwell element individually and the total result-

ing stress is the sum of the contributions from individual elements.

The corresponding differential operator, in this case, derived from the basic Maxwell equation

$$\frac{d\epsilon}{dt} = \frac{1}{E}\frac{d\sigma}{dt} + \frac{\sigma}{\eta}$$

is

$$\sigma = \left(\sum_{r=1}^{r=m} \frac{D}{\frac{D}{E_r} + \frac{1}{\eta_r}} \right) \epsilon$$

The denominators containing the differential operator D are removed by multiplying both sides by $\prod_{r=1}^{r=m} \left(\frac{D}{E_r} + \frac{1}{\eta_r} \right)$

Lee (109) points out that a particular pair of operators such as P and Q of the same order, can thus be represented by models in the form of either the generalized Kelvin model or the generalized Maxwell model.

The determination of the model involves dividing through by either P or Q and representing the quotient by partial fractions. Division by P gives the generalized Maxwell model and division by Q gives the generalized Kelvin model. For operators of a given order, n equals m.

Use of the Viscoelastic Deformation Functions in Numerical Methods of Time-dependent Analysis

The choice and arrangement of the viscoelastic model and its elements determine the general qualitative form of the creep law equation analogous to the behaviour of the real material.

By carrying out the sort of tests which form the substance of these investigations on various identical specimens of the material, the immediate and time-dependent strains can be separately evaluated and specific creep curves obtained.

These specific creep curves, representing the real material, will determine, through curve-fitting procedures, the numerical values of the coefficients and exponents involved.

In other words, the elastic and viscous constants of the model/material and the consequent relaxation or retardation times will have been evaluated. These are referred to here as deformation functions.

These functions may then be used to modify the initial stress distributions determined at the start of each small time interval.

At the start of the process, the initial stress distributions are those resulting from the immediate elastic analysis. Thereafter, the threshold stresses assumed at the start of each subsequent time interval, are the stresses modified successively by the creep law data.

Using the finite element method to obtain the initial elastic solution, a large number of simultaneous equations for displacements and stresses must be solved at each step.

For uniaxial conditions

$$\varepsilon_{el} = E^{-1}\sigma$$ but generally for multiaxial conditions, using the matrix convention,

$$\{\varepsilon_{el}\} = [D]^{-1}\{\sigma\}$$

where $[D]$, the elasticity matrix can be a function of temperature and age.

Assuming the various loading vectors are applied stepwise at each short time interval, the following solution process is followed:

a) The initial loading conditions at t=0, generate an elastic stress distribution $\{\sigma\}_o$. This stress distribution is assumed to remain constant during a short time interval Δt_1. The material properties are also assumed constant during the interval. The creep strains $\{\varepsilon_c\}_1$ at the end of the interval are found.

b) At the threshold of the next interval, additional forces are applied. Material properties are assumed to change abruptly. If the

loads are summed, and current values of temperature are taken, and considering $\{\epsilon_c\}_1$ as an "initial" strain imposed, the "elastic" problem is solved again resulting in a stress distribution $\{\sigma\}_1$.

c) This stress distribution $\{\sigma\}_1$ is assumed to remain constant during the next time interval Δt_2 as are the material properties, and the total creep strain at the end of the second interval is found, $\{\varepsilon_c\}_2$.

d) Step b) is repeated to give $\{\sigma\}_2$ at the start of the third interval Δt_3 and $\{\varepsilon_c\}_3$ obtained at the end of this third interval, and so the process is continued.

SECTION X

THE THEORETICAL ANALYSIS

1. INTRODUCTION

It is the purpose of this section to describe the thermoviscoelastic method of analysis chosen from those listed in the previous section, to justify this choice, to describe its assumptions and limitations, to explain its philosophical background, to detail its intermediate steps, to report the techniques by which data have been prepared and subsequently handled, and to present the numerical values of the constants employed.

Biaxial stress analysis, based upon a mathematical approach, has been successfully carried out in the past using the long-established principles of linear elasticity and structural mechanics.

The resulting differential or integral equations can be relatively easily handled when the structural geometry is straightforward and the problem remains in the linear elastic range.

For complicated profiles and discontinuous geometry, however, the formulation and solution of the governing equations are not straightforward, and although the approach has been established for over a century, closed form solutions are available for only a limited number of practical structural configurations.

The finite element method, however, provides, for a very wide range of geometries and problems, a practical numerical technique of solving for the internal stresses and displacements. The procedure depends for its success upon the structural idealization or approximation of, for example, a real continuum by means of an element network. The finer the mesh of the network, the more nearly the structural approximation simulates the continuum, and the more accurate the

resulting solution.

The system of simultaneous equations set up is linear and the method has shown itself extremely versatile in solving a wide range of indeterminate problems.

The previous section has summarized the analytical methods available for both the elastic and the time-dependent investigation of the P.C.P.V. and its elements, and of perforated continua in particular.

It is now proposed to describe in more detail the time-dependent thermoviscoelastic method chosen. Details are presented of the finite element elastic solution, and of the thermal and time-dependent considerations which together represent the particular form of the viscoelastic approach appropriate to the present problem.

Three of the five specimens in each series were loaded with an in-plane radial compression and were subjected, as were all the specimens, to a uniform temperature of 80°C. Two of these three specimens were small representing the inner zone of the end slab. Of these two, one was solid and the other perforated. The third loaded slab was the large composite model having a perforated inner zone and a solid outer annulus. The fourth and fifth slabs were shrinkage specimens only. The slab perforations were lined with steel sleeves, Series 1 and Series 2 having liners of different thicknesses.

The problem has been investigated as a bi-axial one, intensified by the additional time-dependent strains of creep and shrinkage under an elevated temperature. The method of approach to the problem has been one in which first an elastic analysis has been applied to the perforated end slabs under the mechanical and thermal loading, and secondly a time-dependent analysis has been proposed, using creep and shrinkage laws, which could be fitted into the elastic

analysis and which could permit a stepwise repetitive modification of the results of the elastic solution in the light of the observed behaviour of the material with time. This behaviour is characterized by thermal creep straining and shrinkage straining.

The chosen routine solves the "elastic" problem again and again using the time-dependent data to modify each solution.

The composite slab has been considered as a continuum discretized by an equivalent system of triangular elements interconnected at the nodal points.

By making certain assumptions about the displacements within each element, geometrical compatibility can be explicitly satisfied at the nodes. The structural network brought into being by the element idealization is highly indeterminate but may be solved by a displacement method. One of the great advantages of the finite element technique is that the resulting system of linear simultaneous equations is more suitable for solution by digital computer than the system of partial differential of integral equations which normally results from the more exact mathematical formulations.

2. GENERAL CONSIDERATIONS.

(I) Assumptions

The following assumptions have been made in the analysis:

(a) Concrete is isotropic and homogeneous.

(b) Plane sections remain plane after loading.

(c) Shrinkage strain occurring in an unloaded specimen is of the same nature and magnitude as in a loaded specimen of the same age; this assumption presupposes that shrinkage and creep in a single concrete specimen are independent of each other; uniform shrinkage was assumed for all elements of the structure.

(d) The total strain in the concrete may be considered to be compounded, where appropriate, of elastic, thermal, creep and shrinkage strains.

(e) The values of the elastic constants obtained from control tests, may be used in the analyses related to the structure proper, provided the concretes come from the same batch.

(f) The temperature function $\phi(T)$ can be taken as T the temperature itself

(g) Creep is proportional to stress upto at least the stress levels applied to the loaded specimens.

(h) Creep is proportional to temperature upto at least the temperature levels applied to the specimens.

(i) Creep and shrinkage in the elements of the steel liners were neglected.

(2) Sign Convention.

Tension loads, and the consequent displacements, stresses and strains are assumed to be positive. Conversely, compression loadings

with the corresponding displacements, stresses and strains are assumed negative.

Thermal strains due to expansions consequent upon a rise in temperature are considered positive.

Shrinkage strains are negative and, as such, are always opposite in sign to thermal expansion strains.

Creep strains may be positive or negative depending on the sign of the loading causing the creep.

(3) Treatment of External Mechanical Loads.

The treatment of the uniformly distributed rim compression is shown in Fig.44 . The distributed load p_i was imposed on the peripheral boundary nodal points by dealing with it as a series of concentrated loads R_i.

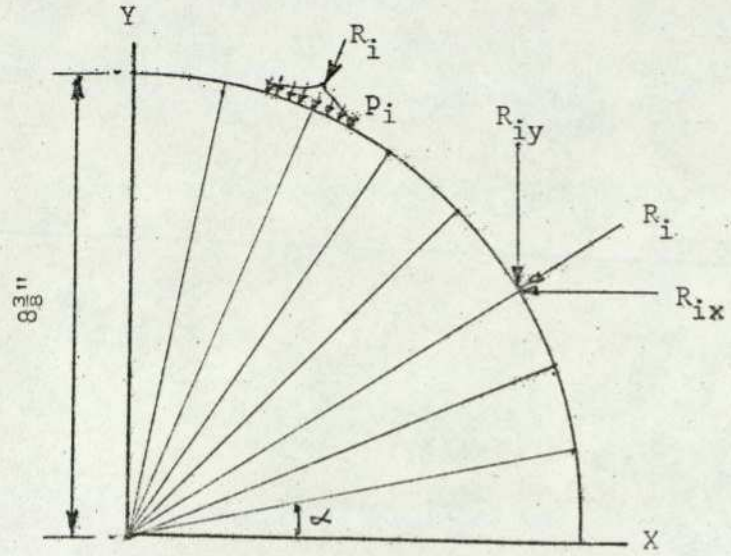
The quadrant boundaries of the loaded perforated and composite specimens were divided into nine equal parts by ten nodal points. For the loaded solid specimen eight equal arcs were formed by nine nodal points.

In order to resolve R_i in the directions x and y of the axial co-ordinate system, components $R_i\cos\alpha$ and $R_i\sin\alpha$ were calculated. These components formed the external mechanical load system.

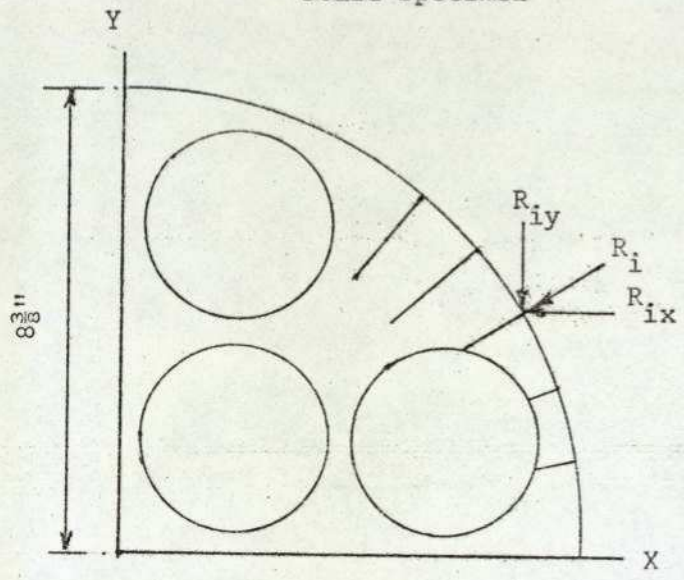
(4) Design Methods and Experimental Data Preparation for the Analysis.

To obtain the separate elastic, thermal, creep and shrinkage strains, the experimental data from the test specimens and also from the control specimens, were analysed in stages. The values of creep and shrinkage strain increments were taken from the specific creep-time and shrinkage strain-time laws respectively, obtained as a result of the present experiments.

Thus, experimental data have been used in a form suitable for feeding into the analytical programme. Accordingly, implicit in



Solid specimen



Perforated specimen.

p_i = radial u.d.l.

R_i = radial point load at nodal point.

$R_{ix} = R_i . \cos\alpha .$

$R_{iy} = R_i . \sin\alpha .$

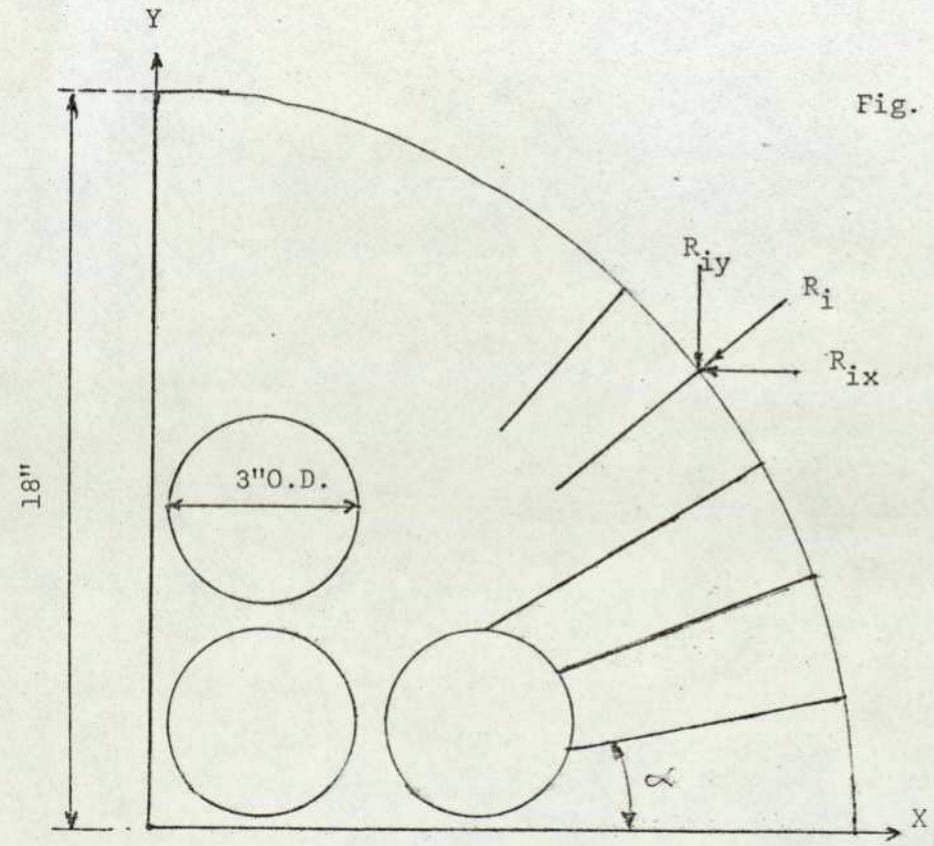


Fig. 44. Rim compression components at boundary nodal points.

the method, is the assumption that either experimental creep and shrinkage results particular to a structural concrete can be obtained by testing, or that general creep laws and shrinkage laws for similar concretes are otherwise available.

To facilitate the finite element analysis, the loaded specimens were structurally idealized into a network of elements. The mesh was close in the perforated zone and nodes were made to coincide with the gauge points used in the experimental observations. Elsewhere, in the solid annulus, for example, the mesh did not need to be so fine.

The test duration was divided into a series of time intervals corresponding to those points in time at which observed and predicted values were required for comparison. The estimated rate of change of strain also influenced the assessment of time intervals.

The analysis examined the behaviour of the specimens at the following stages:

(a) At ambient temperature, under applied loading causing elastic strains only

(b) At ambient temperature, under sustained load with creep and shrinkage effects

(c) At $80^{o}C$, under sustained load with thermal, creep and shrinkage effects

(d) At ambient temperature again, under sustained load with creep and shrinkage effects

(e) At ambient temperature, during unloading.

During regime (a), the external loads R are applied and the elastic solution is obtained for elastic displacements d_e, strains ε_e, and stresses σ_e, using the following equations

$$\{R\} = [k]\{d_e\}$$

$$\{\varepsilon_e\} = [B]\{d_e\}$$

$$\{\sigma_e\} = [D][B]\{d_e\}$$

$[B]$ and $[D]$ are defined later.

During regime (b), the creep strains and shrinkage strains were computed for the incremental creep and shrinkage occurring in a particular interval according to the following equations:

$$\begin{bmatrix} \varepsilon_{cx} \\ \varepsilon_{cy} \\ \varepsilon_{cxy} \end{bmatrix} = \phi(T)\, dc \begin{bmatrix} I & -\nu & 0 \\ -\nu & I & 0 \\ 0 & 0 & 2(I+\nu) \end{bmatrix} \begin{bmatrix} \sigma_x \\ \sigma_y \\ \sigma_{xy} \end{bmatrix}$$

and

$$\begin{bmatrix} \varepsilon_{sx} \\ \varepsilon_{sy} \\ \varepsilon_{sxy} \end{bmatrix} = \phi(T)\, ds \begin{bmatrix} I \\ I \\ 0 \end{bmatrix}$$

respectively

The stresses in the creep matrix equation above are those obtained from the elastic solution.

The creep and shrinkage strains calculated are treated as initial strains for the next time interval, and fictitious nodal forces F_c and F_s, (pseudoforces), are calculated for each element for the creep and shrinkage effects respectively.

These pseudoforces are those imagined to be acting to restore the geometrical compatibilities lost by creep and shrinkage deformations during an interval.

The sum of these nodal forces for all the elements connected to any nodal point, will give the structure load vectors F_{cs} and F_{ss}. The load vectors for creep and shrinkage must be added to the external mechanical load vector R.

Thus the operative equation becomes

$R + F_{cs} + F_{ss} = [K]\{d\}$, the solution of which gives the displacements and finally the strains and stresses.

Young's modulus for the concrete was taken in the calculations as 5.0×10^6 p.s.i. For the steel liners, a value for Young's modulus of 30.0×10^6 p,s.i was taken.

The value of the coefficient of thermal expansion for concrete used in the analysis, was obtained by averaging results from tests on control specimens. The value taken was 13.5×10^{-6} per ^{o}C. A similar value was used for the steel.

The value of Poisson's ratio for concrete was taken as 0.18 and that for steel as 0.30. These were assumed not to change with time and temperature.

The delayed strain recovery known as creep recovery which is exhibited by concrete on removal of load was recorded unsatisfactorily in the experimental observations. An attempt to analyse this phase of the tests could not be supported with adequate data, and has not therefore been considered justified.

The temperatures of the specimens were not controlled as accurately as was required during certain stages of the tests. Fluctuations occurred which are shown in the temperature and relative humidity charts for the two series. This was partly due to oversensitive thermostat operation, and was more serious for the first series.

The heating period lasted for approximately 70 days for series I and approximately 50 days for series 2, and temperature irregularities rarely lasted for more than two days at a time before correction. The impact of this on the creep and shrinkage in practical terms, may not have been so great as was feared at the time, because of the averaging-out of the effect with time.

3. THE FINITE ELEMENT SOLUTION

The finite element method was chosen for the theoretical analysis because of its versatility, because of its particular suitability for continua such as the end slabs under consideration, because of the simplicity with which time-dependent modifications could be incorporated, and because of its well-established effectiveness in conjunction with matrix formulation and computer programming. Some details concerning the technique have been given in the previous section.

Two concepts have always been entertained about the basis of finite elements. One is concerned with the physical significance of the method; the other derives from the mathematical philosophy intrinsic to it.

The physical concept is commonly expressed in the following form. Finite element analyses, in general, having commenced by the discretization and simulation of, say, a real continuum, by means of a structural fragmentation or network, proceed by making inspired assumptions about the displaced form of the basic elements.

The assumed displacement function plays a major role in determining the element stiffness matrix. This matrix governs the relationship between the nodal displacements of the elements and the fictitious set of forces acting at the nodes.

These element stiffness matrices are compounded, using considerations of equilibrium and compatibility, to form the structure stiffness matrix for the entire system.

The second view considers the finite element method to be a minimization procedure in which the unknown nodal displacements occur in the expression for the total potential energy of the system. To obtain the total potential energy, the strain energy of the

structure is required, and this is determined from the displacement function assumed for the elements.

Those nodal displacements which give rise to a minimum potential energy in the whole structural system, represent the correct finite element solution to the problem.

The compounding of the element stiffness matrices to form the structure stiffness matrix, corresponds, in this view, to the summing of the energy contributions of all the elements.

The first of these views not only emphasizes the physical significance of the procedures, it also notes that the actual computational operations follow the physical explanations. The true mathematical basis of the method, however, lies in the second philosophical viewpoint.

For the application of the finite method in the elastic solution of the model end caps, (and subsequently in the time-dependent solution), the first step is to divide the geometry of the specimens into the elements considered suitable. The shape and type of the elements chosen are those of the triangular plate, and quadrants of the model end slabs are thus examined as a network assemblage of this type of discrete element. Only the quadrant of each specimen needs to be investigated because of the symmetrical geometry.

The positions of demec gauge points determined the precise size and arrangement of the elements near the ligaments. The perforations also had a major influence. In this area also, as fine a mesh as practicable was necessary to obtain as much information about the rapidly changing strains as possible. Elsewhere, away from the centre of the slabs, the mesh was somewhat more gross.

The sizes of elements were such in relation to the overall

size of the specimen that displacement fields within the elements were assumed to vary linearly, and thus the strains and stresses within each element were assumed to be constant.

Each of the three nodal points of each element has two degrees of freedom and thus has two unknown displacements and it is as functions of these unknown displacements that the displacements within each element and subsequently the strains and stresses, can be expressed.

Nodal forces are necessary to restore geometrical compatibility to the elements by action at the nodes after each step. These forces are, in effect, fictitious but are uniquely defined by the displacements of the nodes.

These nodal forces must be made statically equivalent to the boundary loads and distributed loads acting on the structure. This is done using the principle of virtual work. The elemental nodes are subjected to virtual nodal displacements. The equations are obtained by balancing the internal work done by the stresses with the external work done by the nodal forces in their corresponding displacements. This application of the virtual work principle gives the stiffness relationship between nodal displacements and nodal forces for each element.

The equilibrium equations for the nodal points for the entire structure are obtained by superposing the stiffness relationship of all the elements in the network.

These structure equilibrium equations are solved for the nodal displacements by matrix inversion. The stresses and strains in the structure may then be obtained from the nodal displacements for the elements.

The steps in the finite element method when used also as a

medium for time-dependent analysis, may be summarized as follows:

(a) Division of the structure into a network of triangular elements; this is known as a structural idealization.

(b) Determination of the local and global co-ordinates for the nodes of the elements and for other aspects of the geometry.

(c) Evaluation of the element stiffness matrix $[k]$.

(d) Transformation from local to global co-ordinates.

(e) Determination of the structure stiffness matrix $[K]$.

(f) Introduction of the known force and displacement boundary conditions.

(g) Calculation of the resultant load vector for the structure by summation of the thermal, creep and shrinkage load vectors.

(h) Formulation of the equilibrium equations and their solution for displacements by matrix inversion.

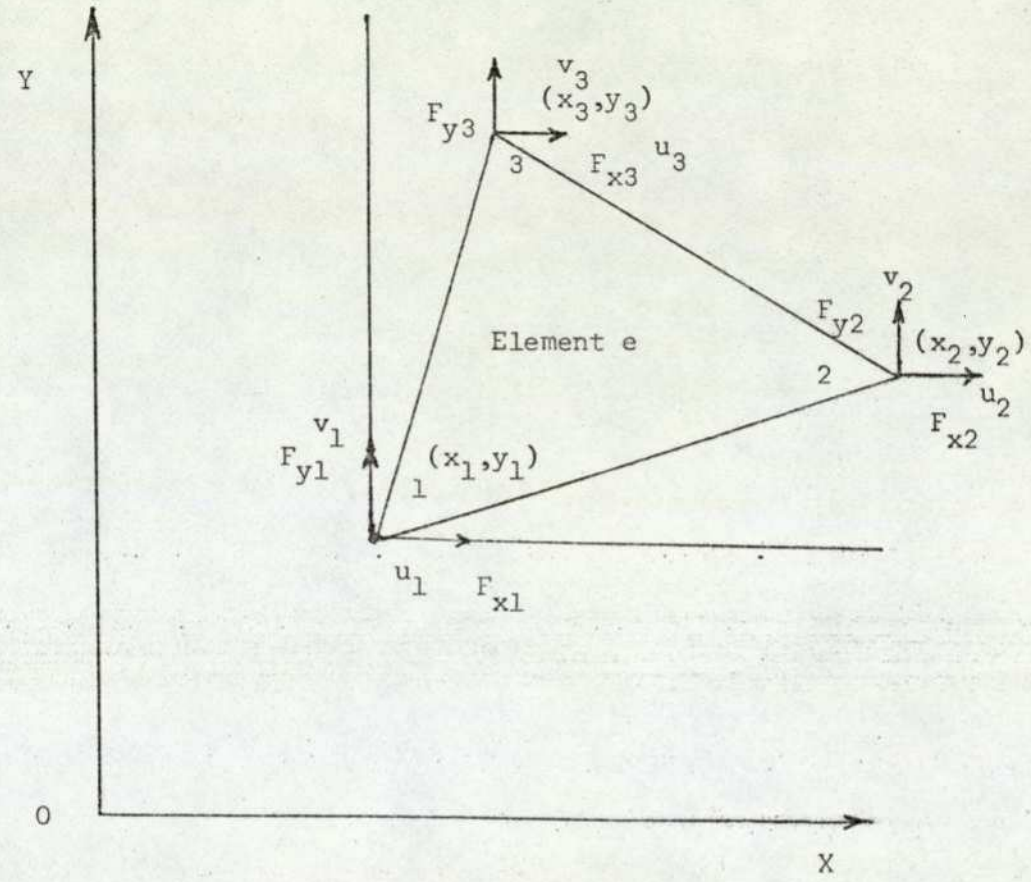
(i) Computation of element stresses and strains from the nodal displacements.

It is proposed to describe these processes in greater detail as they affect the present analysis.

(a) The triangle was chosen because it can be readily adapted in the mesh to fit the required geometry. This shape is also easy to operate and simplifies the computation for the element stiffness matrix. See fig 45 . The structural idealizations chosen are shown in Figs 46,47,48.

The nodal points were arranged to correspond not only with the demec gauge points, but also with the diametral Mercer bore gauge steel liner measuring positions.

Model I/2 had 60 nodal points and 94 elements. Model 3/4 had I46 nodal points and 22I elements. Ninety six of these were steel elements. Model 9/IO had I92 nodal points and 303 elements. Again,



$$\text{Nodal Forces} = [F] = \begin{bmatrix} F_1 \\ F_2 \\ F_3 \end{bmatrix} = \begin{bmatrix} F_{x1} \\ F_{y1} \\ F_{x2} \\ F_{y2} \\ F_{x3} \\ F_{y3} \end{bmatrix}$$

Fig. 45. Typical triangular element.
Nodal Points (1,2,3).
Nodal Co-ordinates (x,y).
Nodal Displacements (u,v).

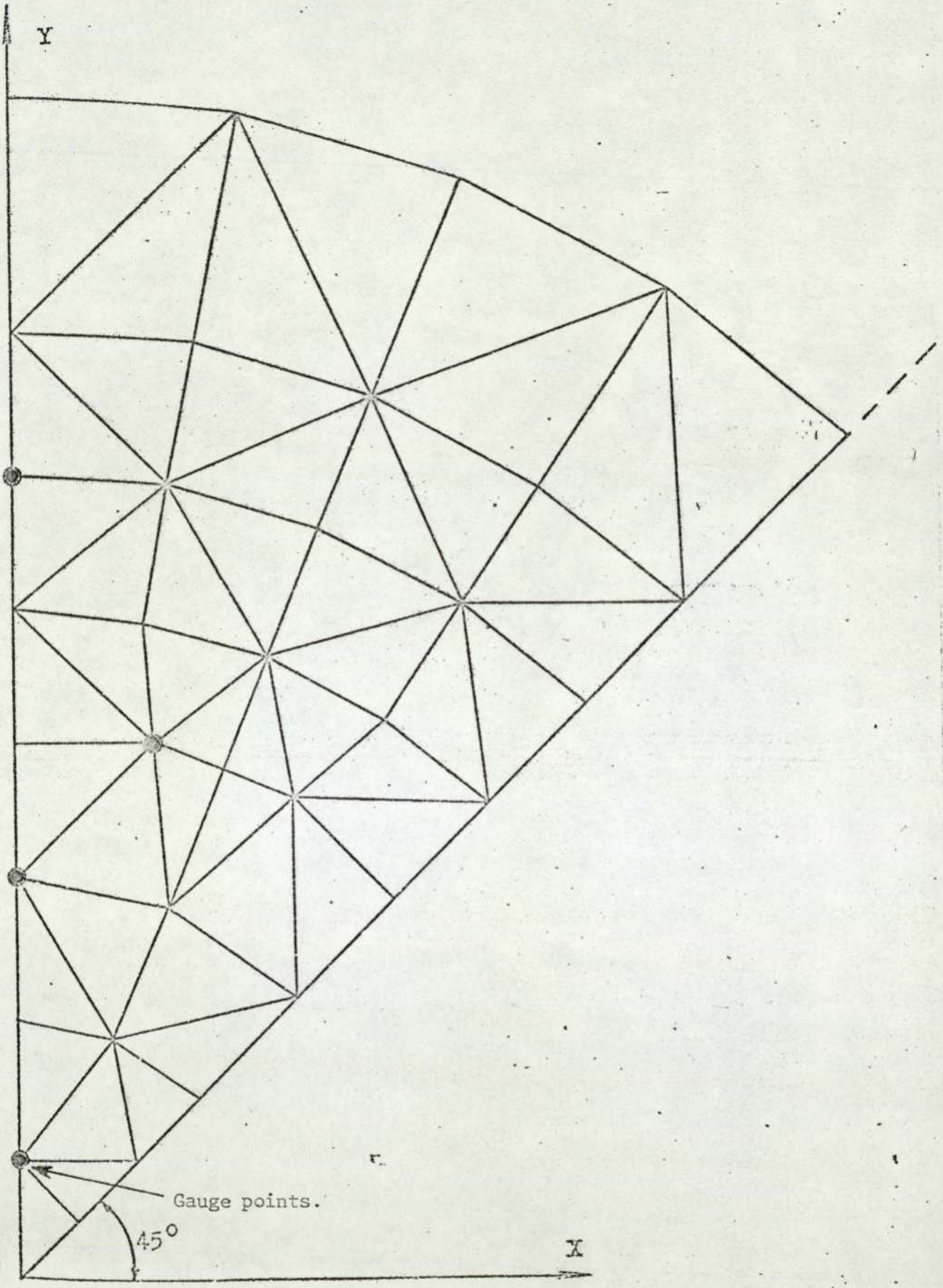


Fig. 46. Structural idealization for model 1/2.

45° sector

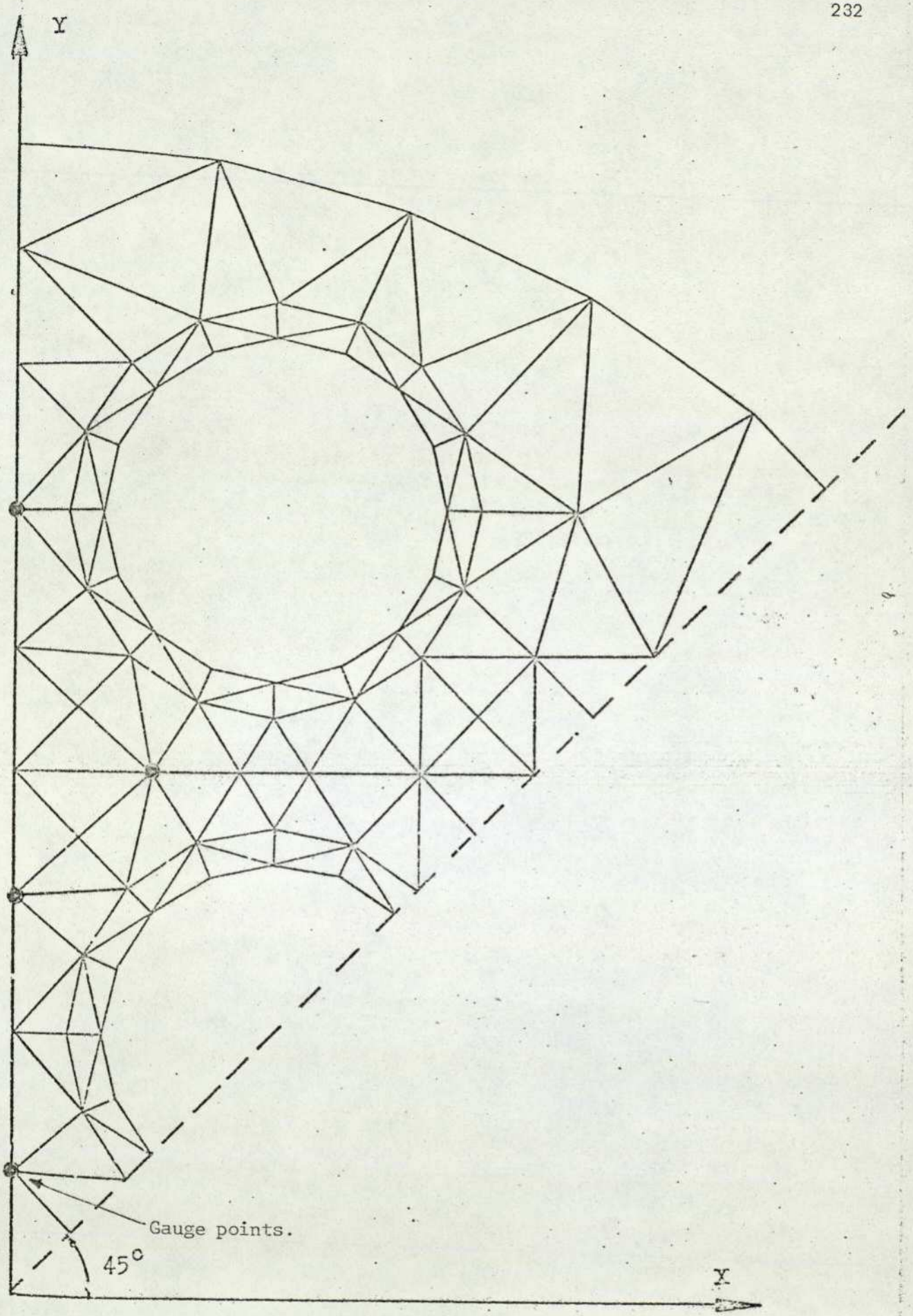


FIG. 47. STRUCTURAL IDEALIZATION
FOR THE 16 3/4" DIAMETER SPECIMEN
45° SECTOR
Series 2 (1/4" liners)
Series 1 (1/16" liners).

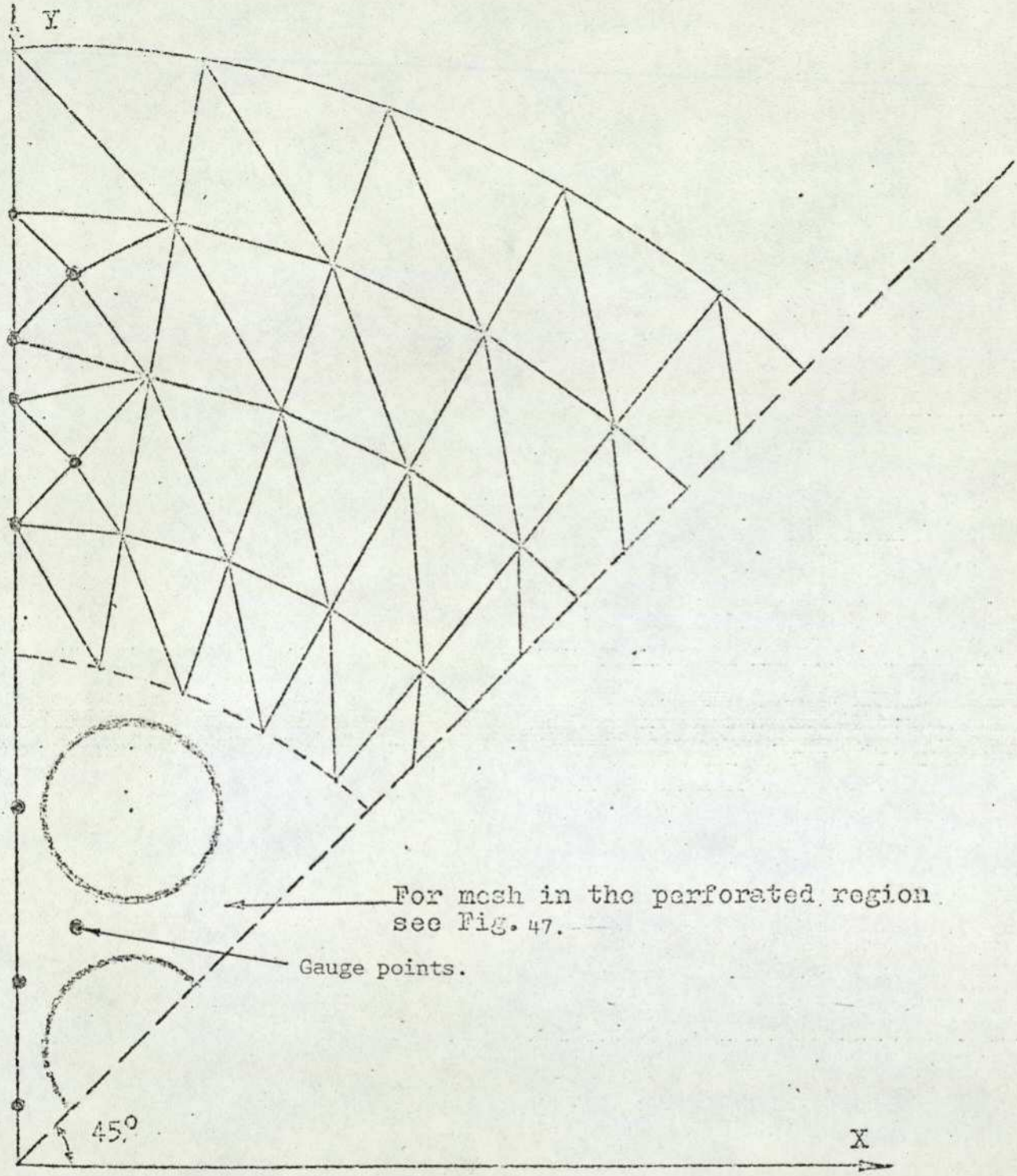


FIG. 48. Structural idealization for the 36" diameter specimen 45° sector.

ninety six elements were located in the steel sleeve liners.

Since the elements had a thickness equal to the thickness of the concrete specimens, this dimension was uniformly 6" throughout.

The uniformly distributed radial compression acting as the live external mechanical load on the rim of the specimens, was evaluated as statically equivalent point loads imposed on the boundary of the network at the nodal points. Dead loads were assumed to be negligibly small.

(b) Local and global co-ordinates were represented in the Cartesian system. Transformation from local to global systems was not necessary since the nodal points were related to the main orthogonal axes of the quadrants from the outset.

(c) The derivation of the element stiffness matrix is the most detailed and critical process in the analysis. The basic steps for the triangular finite element are as follows: (See Fig. 44a).

Step I. After the structure has been divided into elements and a suitable co-ordinate and nodal numbering system chosen, the degrees of freedom of the element are defined and hence the nodal displacement vector $\{d\}$ and the nodal force vector $\{F\}$ are established.

The stiffness matrix of the element e, (see Fig 45), is defined by the equation

$$\{F^e\} = [k^e] \{d^e\}$$

where

$$\{d^e\} = \begin{Bmatrix} d_I \\ d_2 \\ d_3 \end{Bmatrix} = \begin{Bmatrix} u_I \\ v_I \\ u_2 \\ v_2 \\ u_3 \\ v_3 \end{Bmatrix}$$

Fig 44a.

$[F] = [k][d]$ is the matrix equation relating the nodal forces $[F]$ to the nodal displacements $[d]$ in terms of the stiffness coefficients k_{ij}.

The stiffness matrix $[k]$ of the element is always a square matrix and is given by :

$$k = \begin{matrix} \\ 1 \\ 2 \\ 3 \end{matrix} \begin{bmatrix} k'11 & k'12 & k'13 \\ k'21 & k'22 & k'23 \\ k'31 & k'32 & k'33 \end{bmatrix}$$

Each element in this matrix is itself a square 2 x 2 matrix.

For example, $k'11 = \begin{bmatrix} k11 & k12 \\ k21 & k22 \end{bmatrix}$

Thus the full stiffness matrix for the element is given by :

$$k = \begin{bmatrix} k11 & k12 & k13 & k14 & k15 & k16 \\ k21 & k22 & . & . & . & . \\ k31 & . & . & . & . & . \\ k41 & . & . & . & . & . \\ k51 & . & . & . & . & . \\ k61 & . & . & . & . & . \end{bmatrix}$$

$[F] = [k][d]$ fully expanded therefore becomes :

$$\begin{bmatrix} F1 \\ F2 \\ F3 \\ F4 \\ F5 \\ F6 \end{bmatrix} = \begin{bmatrix} k11 & k12 & k13 & k14 & k15 & k16 \\ k21 & . & . & . & . & . \\ k31 & . & . & . & . & . \\ k41 & . & . & . & . & . \\ k51 & . & . & . & . & . \\ k61 & k62 & k63 & k64 & k65 & k66 \end{bmatrix} \begin{bmatrix} d1 \\ d2 \\ d3 \\ d4 \\ d5 \\ d6 \end{bmatrix}$$

Fig. 44a. The Element Stiffness Matrix.

$$\left\{F^e\right\} = \left\{\begin{matrix}\{F_I\}\\ \{F_2\}\\ \{F_3\}\end{matrix}\right\} = \left\{\begin{matrix}F_{xI}\\ F_{yI}\\ F_{x2}\\ F_{y2}\\ F_{x3}\\ F_{y3}\end{matrix}\right\}$$

Step 2. A displacement function is chosen $\left[f(x,y)\right]$ which defines the displacements $\left\{d(x,y)\right\}$ at any point in the element.

$$\left\{d(x,y)\right\} = \left[f(x,y)\right]\left\{\alpha\right\}$$

where $$\left\{d(x,y)\right\} = \begin{Bmatrix}u\\ v\end{Bmatrix}$$

$$\left[f(x,y)\right]\left\{\alpha\right\} = \begin{bmatrix}1 & x & y & 0 & 0 & 0\\ 0 & 0 & 0 & 1 & x & y\end{bmatrix}\left\{\begin{matrix}\alpha_1\\ \alpha_2\\ \alpha_3\\ \alpha_4\\ \alpha_5\\ \alpha_6\end{matrix}\right\}$$

$$u = \alpha_1 + \alpha_2 x + \alpha_3 y$$

and $$v = \alpha_4 + \alpha_5 x + \alpha_6 y$$

Step 3. The state of displacement is obtained at any point within the element in terms of the nodal displacements $\left\{d^e\right\}$.

$$\left\{d(x,y)\right\} = \left[f(x,y)\right]\left[A^{-1}\right]\left\{d^e\right\}$$

where for node I the element nodal displacement $\left\{d_I^e\right\}$ is given by

$$\left\{d_I^e\right\} = \left\{d(x_i,y_i)\right\} = \left[f(x_i,y_i)\right]\left\{\alpha\right\}$$

and for the element

$$\left\{d^e\right\} = \left\{\begin{matrix}\{d_I^e\}\\ \{d_2^e\}\\ \{d_3^e\}\end{matrix}\right\} = \left[\begin{matrix}[f(x_I,y_I)]\\ [f(x_2,y_2)]\\ [f(x_3,y_3)]\end{matrix}\right]\left\{\alpha\right\}$$

or $$\left\{d^e\right\} = \left[A\right]\left\{\alpha\right\}$$

and $$\left\{\alpha\right\} = \left[A^{-1}\right]\left\{d^e\right\}$$

$$\left[A\right] = \begin{bmatrix}1 & x_I & y_I & 0 & 0 & 0\\ 0 & 0 & 0 & 1 & x_I & y_I\\ 1 & x_2 & y_2 & 0 & 0 & 0\\ 0 & 0 & 0 & 1 & x_2 & y_2\\ 1 & x_3 & y_3 & 0 & 0 & 0\\ 0 & 0 & 0 & 1 & x_3 & y_3\end{bmatrix}$$

Step 4. The strains $\left\{\epsilon(x,y)\right\}$ are related at any point

in the element to the displacements $\{d(x,y)\}$ and hence to the nodal displacements $\{d^e\}$.

$$\{\varepsilon(x,y)\} = [B(x,y)]\{d^e\}$$

where
$$\{\varepsilon(x,y)\} = \begin{bmatrix} 0 & 1 & 0 & 0 & 0 & 0 \\ 0 & 0 & 0 & 0 & 0 & 1 \\ 0 & 0 & 1 & 0 & 1 & 0 \end{bmatrix} \begin{Bmatrix} \alpha_1 \\ \alpha_2 \\ \alpha_3 \\ \alpha_4 \\ \alpha_5 \\ \alpha_6 \end{Bmatrix}$$

or
$$\{\varepsilon(x,y)\} = [C]\{\alpha\}$$
$$= [C][A^{-1}]\{d^e\}$$
$$= [B]\{d^e\}$$
$$[B] = [C][A^{-1}]$$
$$= \frac{1}{2\Delta}\begin{bmatrix} y_2-y_3 & 0 & y_3-y_1 & 0 & y_1-y_2 & 0 \\ 0 & x_3-x_2 & 0 & x_1-x_3 & 0 & x_2-x_1 \\ x_3-x_2 & y_2-y_3 & x_1-x_3 & y_3-y_1 & x_2-x_1 & y_1-y_2 \end{bmatrix}$$

Step 5. The stresses $\{\sigma(x,y)\}$ in the element are related to the strains $\{\varepsilon(x,y)\}$ and hence to the nodal displacements $\{d^e\}$

$$\{\sigma(x,y)\} = [D]\{\varepsilon(x,y)\}$$
$$= [D][B(x,y)]\{d^e\}$$

For the plain stress problem

$$\{\varepsilon(x,y)\} = \begin{Bmatrix} \varepsilon_x \\ \varepsilon_y \\ \gamma_{xy} \end{Bmatrix} = \frac{1}{E}\begin{bmatrix} 1 & -\nu & 0 \\ -\nu & 1 & 0 \\ 0 & 0 & 2(1+\nu) \end{bmatrix} \begin{Bmatrix} \sigma_x \\ \sigma_y \\ \tau_{xy} \end{Bmatrix}$$

$$\{\sigma(x,y)\} = \begin{Bmatrix} \sigma_x \\ \sigma_y \\ \tau_{xy} \end{Bmatrix} = \frac{E}{1-\nu^2}\begin{bmatrix} 1 & \nu & 0 \\ \nu & 1 & 0 \\ 0 & 0 & \frac{1-\nu}{2} \end{bmatrix} \begin{Bmatrix} \varepsilon_x \\ \varepsilon_y \\ \gamma_{xy} \end{Bmatrix}$$

or
$$\{\sigma(x,y)\} = [D]\{\varepsilon(x,y)\}$$

where
$$[D] = \frac{E}{1-\nu^2}\begin{bmatrix} 1 & \nu & 0 \\ \nu & 1 & 0 \\ 0 & 0 & \frac{1-\nu}{2} \end{bmatrix}$$ = the elasticity matrix

Step 6. The element stresses $\{\sigma(x,y)\}$ are replaced by the

nodal forces $\{F^e\}$, the nodal forces are related to the element nodal displacements $\{d^e\}$ and hence the element stiffness matrix is obtained, from virtual work considerations.

$$\{F^e\} = \int [B(x,y)]^T [D] [B(x,y)] \, dx \, dy \, dz \, \{d^e\}$$

or $$\{F^e\} = \left[[B(x,y)]^T [D] [B(x,y)] \Delta t \right] \{d^e\}$$

in which $$\Delta = \frac{1}{2} \begin{vmatrix} 1 & x_1 & y_1 \\ 1 & x_2 & y_2 \\ 1 & x_3 & y_3 \end{vmatrix}$$

and t = the thickness of the element

Thus $[k^e]$, the element stiffness matrix

$$= [B(x,y)]^T [D][B(x,y)] \Delta t$$

Step 7. The element stresses are determined from the displacements

$$\{\sigma(x,y)\} = [H] \{d^e\}$$

where $$[H] = [D][B]$$

(d) Transformation from local to global co-ordinates was not necessary in the analysis, because the local and global axes were the same.

(e) The structure stiffness matrix $[K]$ was determined using a direct stiffness approach which superposed the stiffness contributions of all the elements to each nodal point of the system.

The equilibrium equation for the entire structure

$$\{R\} = [K] \{d\}$$

governs the relationship between the nodal load vectors and the nodal displacements.

(f) The boundary conditions can, at this stage, be specified ie the known forces and known displacements at the boundaries of the system can be introduced as non-zero items in the force and displacement vectors.

(g) The next stage, in which the load vectors are determined, reveals an important and essential aspect in the time-dependent treatment of the finite element method. For the thermal, creep and shrinkage strains, which cause geometrical incompatibilities, fictitious forces are considered to act and to restore the necessary compatibility. These forces can be computed from the finite element matrix equation

$$\{F\} = \int_V [B]^T [D] \Delta\varepsilon \, dV$$

The load vectors for each of these effects, which must be applied to the entire structure at the nodal points, can be obtained from these fictitious loads.

These additional load vectors are added to the externally-applied load vector to give the resultant load vector.

(h) The simultaneous equilibrium equations can now be formulated and solved for the displacements, by matrix inversion, from the relationship

$$\{d\} = \{F\}[K^{-1}]$$

(i) Finally the stress distributions may be obtained from the nodal displacements using the following relationship

$$\{\sigma(x,y)\} = [H]\{d^e\}$$

where $[H] = [D][B]$

4. MATRIX FORMULATION

The starting point in the present biaxial plane stress analysis is the set of elastic equations representing stress and strain:

$$\sigma_z = \sigma_{zx} = \sigma_{zy} = 0$$

$$\varepsilon_x = \frac{I}{E}(\sigma_x - \nu\sigma_y)$$

$$\varepsilon_y = \frac{I}{E}(\sigma_y - \nu\sigma_x)$$

$$\varepsilon_{xy} = 2\frac{(I+\nu)}{E}\sigma_{xy}$$

The strains may be written

$$\begin{bmatrix} \varepsilon_x \\ \varepsilon_y \\ \varepsilon_{xy} \end{bmatrix} = \frac{I}{E} \begin{bmatrix} I & -\nu & 0 \\ -\nu & I & 0 \\ 0 & 0 & 2(I+\nu) \end{bmatrix} \begin{bmatrix} \sigma_x \\ \sigma_y \\ \sigma_{xy} \end{bmatrix}$$

which, in matrix form, becomes

$$\{\varepsilon\} = [D]^{-I} \{\sigma\}$$

This gives equations for stresses of the form

$$\begin{bmatrix} \sigma_x \\ \sigma_y \\ \sigma_{xy} \end{bmatrix} = \frac{E}{I-\nu^2} \begin{bmatrix} I & \nu & 0 \\ \nu & I & 0 \\ 0 & 0 & \frac{I-\nu}{2} \end{bmatrix} \begin{bmatrix} \varepsilon_x \\ \varepsilon_y \\ \varepsilon_{xy} \end{bmatrix}$$

which, in matrix form, becomes

$\{\sigma\} = [D]\{\varepsilon\}$, $[D]$ being the elasticity matrix.

Nodal point I of a typical triangular element would have the co-ordinates (x_I, y_I) and displacement components, $d_I = u_I, v_I$.

The displacement functions chosen within the element were two linear polynomials of the form

$$U_{(x,y)} = \alpha_I + \alpha_2 x + \alpha_3 y$$

and $$V_{(x,y)} = \alpha_4 + \alpha_5 x + \alpha_6 y$$

where $U_{(x,y)}$ = the displacement along the x-axis of any point (x,y).

$V_{(x,y)}$ = the displacement along the y-axis of any point (x,y).

and α_I to α_6 = constants

These equations may be represented in matrix form as follows:

$$\{u\} = [M]\{\alpha\}$$

where $\{u\}$ and $\{\alpha\}$ are column vectors and $[M]$ is the displacement transformation matrix relating the two vectors.

$$\left[M\right] = \begin{bmatrix} I & x & y & 0 & 0 & 0 \\ 0 & 0 & 0 & I & x & y \end{bmatrix}$$

When evaluated at the nodal points, the nodal displacements, d, (where $d = d_I, d_2, d_3$), can be written

$$\{d\} = [A]\{\alpha\}$$

where $$\{d\} = \begin{bmatrix} u_I & v_I \\ u_2 & v_2 \\ u_3 & v_3 \end{bmatrix}$$

and $[A]$ is the matrix of the nodal co-ordinates. This equation gives $\{\alpha\}$ in terms of the nodal displacements.

$$\therefore \{\alpha\} = [A]^{-I}\{d\}$$

If this equation is now substituted back into

$\{u\} = [M]\{\alpha\}$, the element displacements can be evaluated in terms of the nodal displacements.

Thus

$$\{u\} = [M][A]^{-I}\{d\}.$$

Let $[M][A]^{-I} = [N]$

$$\therefore \{u\} = [N]\{d\}$$

The strain-displacement relationships can be written as

$$\{\varepsilon\} = [L]\{u\}$$

where $$\{\varepsilon\} = \begin{bmatrix} \varepsilon_x \\ \varepsilon_y \\ \varepsilon_{xy} \end{bmatrix}$$

and $$[L] = \begin{bmatrix} \frac{\partial}{\partial x} & 0 & 0 \\ 0 & \frac{\partial}{\partial y} & 0 \\ 0 & 0 & \frac{\partial}{\partial x} + \frac{\partial}{\partial y} \end{bmatrix}$$ where $\frac{\partial}{\partial x} = \frac{\partial(x,y)}{\partial x}$

Substituting for $\{u\}$ from $\{u\} = [N]\{d\}$,

the element strains are obtained in terms of the nodal displacements.

$$\{\varepsilon\} = [B]\{d\}$$

where $[B] = [L][N]$

The matrix $[B]$ may be determined by calculating the displacement function constants α in terms of the nodal displacements.

A linear stress-strain relationship can be expressed in the

form

$$\{\sigma\} = [D](\{\varepsilon\} - \{\varepsilon_o\})$$

$$\{\sigma\} = [D][B]\{d\} - [D]\{\varepsilon_o\}$$

where $\{\sigma\} = \begin{bmatrix} \sigma_x \\ \sigma_y \\ \sigma_{xy} \end{bmatrix}$

$\{\varepsilon_o\}$ represents the initial strains due to thermal, creep or shrinkage effects. $[D]$ is the elasticity matrix, and for the plane stress case, takes the form

$$[D] = \frac{E}{1-\nu^2}\begin{bmatrix} 0 & \nu & 0 \\ \nu & 1 & 0 \\ 0 & 0 & \frac{1-\nu}{2} \end{bmatrix}$$

The general equation

$$\{F_o\} + \{F_g\} + \{F_p\} + \{R_e\} = [k^e]\{d\}$$

represents the equilibrium condition, which, resulting from applying a virtual nodal displacement, equates the external work done by the nodal forces to the internal work done by the stresses during the displacement.

Here $[k^e] = \int_V [B]^T [D][B]\, dV$ = the element stiffness matrix

$\{F_o\} = \int_V [B]^T [D]\{\varepsilon_o\}\, dV$ = the equivalent nodal forces due to the initial strains

$\{F_g\} = \int_V [N]^T . g . dV$ = the equivalent nodal body forces

$\{F_p\} = \int_S [N]^T . p . dV$ = the equivalent nodal forces due to surface tractions

$\{R_e\}$ = the concentrated forces applied to the nodes of the element

$\{\varepsilon_o\}$ = the initial strains

g = the body forces per unit volume

p = the surface tractions

If $\{F\}$ denotes the total equivalent nodal force vector ie $\{F\} = \{F_\sigma\} + \{F_g\} + \{F_p\} + \{R_e\}$, the stiffness-displacement relationship can be written

$$\{F\} = [k^e]\{d\}$$

The final equations for all the nodes in the structural network are obtained by superposing all the element equations, and, using now the structure stiffness matrix

$$\{R\} = [K]\{d\}$$

The unknown nodal displacements d, corresponding to specific loading conditions caused by thermal strains, body forces, surface tractions and concentrated nodal forces, may be solved for by introducing the displacement boundary conditions into the equations.

The element strains may be obtained from the nodal displacements through the relationship

$$\{\varepsilon\} = [B]\{d\}$$

Similarly, the element stresses are evaluated from the equation

$$\{\sigma\} = [D][B]\{d\} - [D]\{\varepsilon_o\}$$

If the values of nodal co-ordinates are substituted into the two polynomial displacement functions assumed for the elements, then the following equations emerge

$$u_{(x,y)} = \frac{I}{2A}\left[(\alpha_I + \beta_I x + \gamma_I y)\, u_I + (\alpha_2 + \beta_2 x + \gamma_2 y)\, u_2 + (\alpha_3 + \beta_3 x + \gamma_3 y)\, u_3\right]$$

and

$$v_{(x,y)} = \frac{I}{2A}\left[(\alpha_I + \beta_I x + \gamma_I y)\, v_I + (\alpha_2 + \beta_2 x + \gamma_2 y)\, v_2 + (\alpha_3 + \beta_3 x + \gamma_3 y)\, v_3\right]$$

where

$$u_I = \alpha_I + \alpha_2 x_I + \alpha_3 y_I$$

$$u_2 = \alpha_I + \alpha_2 x_2 + \alpha_3 y_2$$

$$u_3 = \alpha_I + \alpha_2 x_3 + \alpha_3 y_3$$

and

$$\alpha_I = x_2 y_3 - x_3 y_2$$

$$\beta_I = y_2 - y_3 = y_{23}$$

$$\gamma_I = x_3 - x_2 = x_{32}$$

Thus

$$[B] = \frac{I}{2A}\begin{bmatrix} \beta_I & 0 & \beta_2 & 0 & \beta_3 & 0 \\ 0 & \gamma_I & 0 & \gamma_2 & 0 & \gamma_3 \\ \gamma_I & \beta_I & \gamma_2 & \beta_2 & \gamma_3 & \beta_3 \end{bmatrix}$$

The equation of the area A of the elemental triangle is equal to

$$A = \frac{Det}{2}\begin{vmatrix} I & x_I & y_I \\ I & x_2 & y_2 \\ I & x_3 & y_3 \end{vmatrix}$$

To summarize, the following matrix equations are basic to the elastic solution.

(a) $\{\varepsilon\} = [B]\{d\}$

(b) $\{\sigma\} = [D][B]\{d\} - [D]\{\varepsilon_o\}$

(c) $[k] = [B]^T[D][B] \cdot t \cdot A$

where t = element thickness

A = element area

(d) $\{F\} = [k^e]\{d\}$

(e) $\{R\} = [K]\{d\}$

The solution of equation (e) was carried out by matrix inversion and direct elimination.

The normal advantages of economy in computing requirements associated with matrix inversion were to some extent offset by the need for the large storage typical of matrices such as the stiffness matrix K. However, some reduction in storage was achieved, as follows.

The maximum number of elements connected to any one nodal point was fifteen and consequently the structure stiffness matrix K was sparsely populated. A diagonal matrix resulted in which the maximum number of non-zero terms in any row did not exceed fifteen.

In storing the matrix K , the non-zero terms in any given row were shifted to the extreme left, which resulted in a rectangular matrix having the numbers of rows equal to those of the original matrix but with only as many columns as there were terms in the band-width.

Thus it was possible to make a considerable reduction in the storage capacity required.

5. VISCOELASTIC ANALOGUE

If it is accepted that a mathematical analogue may be derived on the basis of a set of deformational mechanisms conceived as representing the constituents of concrete and their responses to load, three steps are necessary. First a descriptive analysis is required of the physical components and phases that make up the concrete. Secondly, a viscoelastic model corresponding to the general rheology and behaviour under load of the constituent materials, must be synthesized and assessed. Thirdly, a mathematical form must be given to the viscoelastic simulation. Alternatives have been examined for steps 2 & 3.

Step 1. Descriptive Analysis

Concrete has both fluid and solid viscoelastic properties. It consists of large and small interlocked particles of aggregate embedded in a matrix of viscous cement paste.

These statements are true not only when the concrete is fresh, but also when it sets and as it hardens, the viscous coefficients of the different phases of the paste ranging from those corresponding to an almost solid material to those of a fluid.

Air and water are also present in the discrete spaces between the solid materials. These spaces may be of capillary size or they may be voids of larger dimensions, depending upon the degree of compaction and also upon the aggregate shape and grading.

The aggregate particles themselves display both elastic and mineralogical creep behaviour.

The cement paste component of the concrete mixture is particularly viscoelastic, containing interlocked hard material consisting of hydrates and other solids. The interstices in these solid materials are also filled with air and water.

It is acknowledged that the solids of the paste comprise a

fluid gel phase, (having a highly viscous nature), as well as the solid crystalline phase.

Unhydrated cement grains will also be present in the concrete mixture even when it has hardened, part of the increase in strength with age of the concrete being due to the eventual long-term hydration of the more remote unwetted grains and of their innermost particles.

The supposition is made that, as hydration proceeds over many months, the viscous and viscoelastic responses to loading of these various components of the concrete change with time as free water is lost by chemical action, evaporation and migration and as the mass consequently becomes harder and dryer.

Step 2 a) Synthesis of Model Analogue

The elastic behaviour of the aggregates may be represented by a suitable spring of stiffness E_1 whilst the mineralogical creep may be idealized by a dashpot in series having a viscous coefficient η_1 increasing exponentially with time. This is a modified Maxwell model.

The solid phase of crystals within the paste can be represented by a spring E_2 and the fluid gel phase may be represented by a second dashpot with a viscous coefficient η_2 increasing in relation to some function of time. These elements are placed in parallel as in a Kelvin model and the joint response to load of the cement paste mechanisms is exponential.

The free air and water within the cement paste are likely to manifest only restricted movement under load in their interstitial spaces, due to their virtually total constraint. A spring of constant stiffness E_4 is proposed to reflect this behaviour.

The unhydrated cement particles, effectively case-hardened by setting hydrates, and affected peripherally by the presence of moisture, appear likely to have an elastic and a viscous response

to load of a low order. Again, a suitable spring E_3 and a third dashpot in parallel should constitute a reasonable rheological analogue. The dashpot coefficient should increase with some time function when the viscous response stiffens as drying occurs.

Finally, a spring may be used to represent the constrained water and air in the discrete voids between the aggregate particles. It is suggested that the stiffness of this spring E_5 should remain constant. This is because, even though moisture movements will occur, the response to load can be expected to remain sensibly unchanged.

It should be noted that the behaviour of the cement paste and its associated air and water, corresponding in this hypothesis to that of a Kelvin model in series with a spring element, represents what is known as a three-parameter solid.

The air and water in the aggregate voids, physically adjacent to and chemically interacting with the unhydrated cement grains, have been rheologically associated with the grains in the model. Thus, the E_3 spring and the η_3 dashpot in parallel, representing the cement grains, have been arranged in series with the spring E_5 corresponding to the air and water in the aggregate voids. This second three-parameter solid has been placed in parallel with the previous three-parameter solid envisaged, and both have been arranged in series with the Maxwell model simulating the aggregate behaviour.

Step 2b) Assessment of the Model

To judge the suitability of the full model proposed and illustrated in Fig 49, in representing concrete behaviour, it is first necessary to list the different forms such behaviour takes when the concrete is loaded and unloaded.

The degree to which the model proposals reproduce the real behaviour can then be assessed.

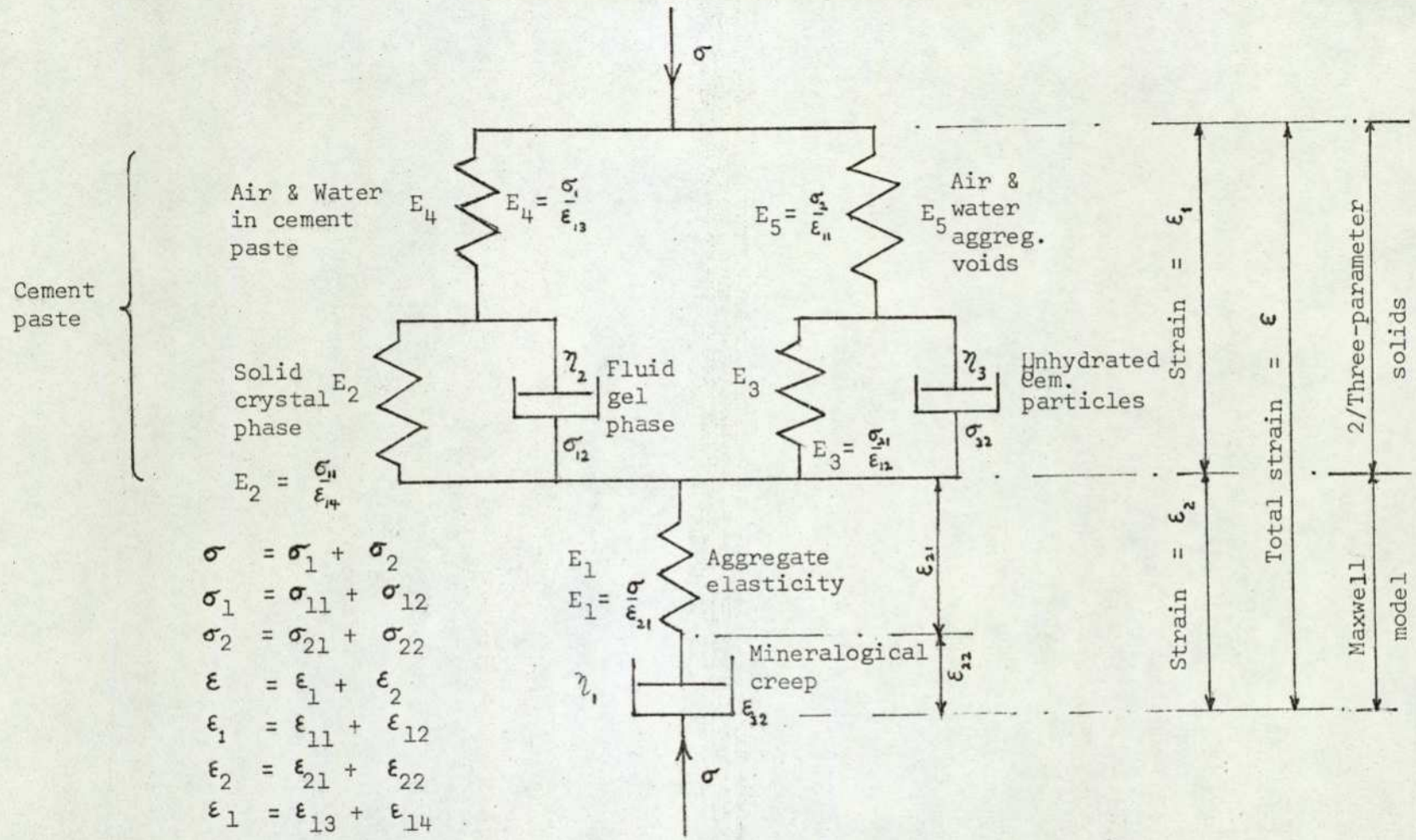


Fig. 49. Proposed Rheological Model.

The responses observed on loading concrete are those of elastic strain, delayed elastic strain and time-dependent creep strain. On unloading, there is an elastic strain recovery followed by a creep recovery and there remains an irrecoverable residual strain.

Qualitatively the model suggested satisfies these requirements. Quantitative assessment of the model system demands experimental observations from which strain-time relationships may be established in order to evaluate the deformational coefficients.

Elastic response on loading and unloading will be provided by the aggregate spring E_1. The Maxwell model simulating the aggregates will also display residual strain.

Delayed elasticity in a concrete has been explained as resulting from

a) micro-cracking at the aggregate-paste interface

and b) the nature and behaviour of the cement paste itself.

The responses of the springs and dashpots in parallel, ie in the Kelvin components E_2/η_2 and E_3/η_3, suggested for the cement paste and the unhydrated cement grains respectively, appear likely to represent adequately the appropriate delayed elasticity.

The Kelvin systems generally will display the necessary creep behaviour. Dashpots η_1, η_2, and η_3 should generate the creep recovery under the extending influences of their associated springs on unloading.

A general justification of the way in which the mechanisms representing the major constituents of the concrete have been juxtaposed must now be developed.

The fine aggregate particles interpenetrate the voids in the larger particles, the aggregate mass when compacted forming a stable, interlocked and interdependent structure.

The cement paste and the cement particles, associated with the

air and water in their voids, form a matrix recognisably discrete and rheologically independent of the aggregates, yet physically connected by adhesion to the aggregate structure.

The physical separation of the aggregate structure and the cement-based matrix justifies the series connection in their model simulation. This arrangement appears to satisfy the requirements of both the spatial independence of these two main parts of the concrete and their mutual structural interaction.

Similarly, the grouping of the cement paste and the cement particles in the parallel arrangement in the model analogue, acknowledges their physical intermingling in the matrix and recognises their simultaneous loading in time.

The model implies equal stressing and shared straining between the Maxwell model representing the aggregate structure and the cement matrix models. Conversely, for the two three-parameter solids simulating the main constituents of the matrix, equal straining and shared stressing may be inferred.

Finally, the different rheological elements of this model system, characterized by time-dependent coefficients, will reflect the way in which the deformational properties of the concrete change with age, with one important proviso. Unless the viscous coefficient of the Maxwell dashpot is required to increase exponentially with time, infinite Maxwell creep will be predicted, which is unacceptable. The consequences of this modification are described in the following section.

Step 3. Development of the Deformational Expressions for the Model

The responses to loading of the Maxwell model and the three-parameter solid, revealing changes in strain under constant stress and stress relaxations under constant strain, have been the subject

of well-established analyses, and the treatment is fully documented in standard texts on viscoelasticity viz Flugge (130), inter alia.

The general expression for strain for the Maxwell material is represented by the relationship :

$$\varepsilon = \frac{\sigma}{E} + \frac{\sigma t}{\eta}$$

where ε is the total strain at any time after loading

σ is the applied stress

E and η are the respective elastic and viscous coefficients

and t is the time since loading

The corresponding equation for strain for the three-parameter solid is represented by the exponential relationship :

$$\varepsilon = \frac{\sigma}{q_1}\left[\frac{1}{\lambda}\left(1 - e^{-\lambda t}\right) + p_1 e^{-\lambda t}\right]$$

where $q_1 = \dfrac{E_4 \eta_2}{(E_4 + E_2)}$ for the cement paste component

or $q_1 = \dfrac{E_5 \eta_3}{(E_5 + E_3)}$ for the unhydrated cement component

$$p_1 = \frac{\eta_2}{(E_4 + E_2)} \text{ or } \frac{\eta_3}{(E_5 + E_3)} \text{ respectively}$$

$$\lambda = \frac{E_2}{\eta_2} \text{ or } \frac{E_3}{\eta_3} \text{ respectively}$$

Thus

$$\varepsilon = \frac{\sigma(E_4 + E_2)}{E_4 \eta_2}\left[\frac{\eta_2}{E_2}\left(1 - e^{-\frac{E_2}{\eta_2} t}\right) + \frac{\eta_2}{(E_4 + E_2)} \cdot e^{-\frac{E_4}{\eta_2} t}\right]$$

for the cement paste

or

$$\varepsilon = \frac{\sigma(E_5 + E_3)}{E_5 \eta_3}\left[\frac{\eta_3}{E_3}\left(1 - e^{-\frac{E_3}{\eta_3} t}\right) + \frac{\eta_3}{(E_5 + E_3)} \cdot e^{-\frac{E_3}{\eta_3} \cdot t}\right]$$

for the unhydrated cement

In these expressions no allowance has been specifically made to accommodate the proposed exponential changes in the viscous coefficients. Moreover, since the two three-parameter solids are in parallel each of their total strains must be equal, and the magnitude of the strain for the full model system may therefore eventually be expressed in two alternative forms.

However, for convenience the form of the strain expression corresponding to the cement paste analogue only, has been developed further.

Accordingly, the total strain for the system becomes, including the Maxwell aggregate strain :

$$\varepsilon = \frac{\sigma (E_4 + E_2)}{E_4 \eta_2} \left[\frac{\eta_2}{E_2} \left(1 - e^{-\frac{E_2}{\eta_2} t} \right) + \frac{\eta_2}{(E_4 + E_2)} \cdot e^{-\frac{E_2}{\eta_2} t} \right] + \sigma \left(\frac{1}{E_1} + \frac{t}{\eta_1} \right)$$

Although the equation as it stands represents the total strain occurring with time for classical viscoelastic elements with constant coefficients, for the purposes of the actual prediction of strains for the computer programme, only specific creep data are required, the elastic strains being obtained directly from the initial finite element elastic solution.

If the viscous coefficient η_1 of the Maxwell element is required to increase exponentially with time, (its fluidity, the reciprocal of η_1 therefore reducing exponentially), the dashpot law becomes consistent with a finite creep value at $t = \infty$,and we may write for the creep rate :

$$\frac{dc}{dt}_{Maxwell} = \frac{1}{\eta_1} = \gamma . e^{-\beta t}$$

where c is the specific creep

$e^{-\beta t}$ is the suggested exponential law

γ is a constant denoting fluidity at zero time

and β is a constant governing the rate of decrease of fluidity.

Integrating this expression,

$$c_M = -\frac{\gamma}{\beta} e^{-\beta t} + A$$

where A is an arbitrary integration constant.

For $c = 0$ at $t = 0$, the value of A is $\frac{\gamma}{\beta}$ and

$$c_M = \frac{\gamma}{\beta} (1 - e^{-\beta t})$$

It should be noted that this expression happens also to represent the specific creep of a classical Kelvin model having an elastic spring coefficient of $\frac{\beta}{\gamma}$ and a constant dashpot retardation time of $\frac{1}{\beta}$.

In order to obtain the creep strain only of the three-parameter solid, it is necessary to subtract the elastic strain occurring in spring E_4 under the stress σ_1. This is $\frac{\sigma_1}{E_4}$.

Thus the creep strain in the three-parameter solid becomes :

$$\varepsilon_c = \frac{\sigma_1 (E_4 + E_2)}{E_4 . E_2}\left(1 - e^{-\frac{E_2}{\eta_2}t}\right) + \frac{\sigma_1}{E_4} . e^{-\frac{E_2}{\eta_2}t} - \frac{\sigma_1}{E_4}$$

and the specific creep becomes :

$$c = \frac{(E_4 + E_2)}{E_4 . E_2}\left(1 - e^{-\frac{E_2}{\eta_2}t}\right) - \frac{1}{E_4}\left(1 - e^{-\frac{E_2}{\eta_2}t}\right)$$

When t is zero, this expression correctly gives the three-parameter specific creep as zero. When t is infinite, the expression gives an ultimate specific creep of $\frac{1}{E_2}$.

We have now obtained separately the specific creep expressions for the three-parameter solid and for the Maxwell model, but since these specific creeps are caused in each case by different stresses, it is not possible to add the two expressions together, as they stand, in order to obtain the total specific creep for the system.

Instead, the total creep strain from the three-parameter solid and the Maxwell model must be obtained by summing the contributions of creep strain from each, and then dividing by σ the externally-applied stress.

The elastic strain for the three-parameter solid is $\frac{\sigma_1}{E_4}$ and that for the Maxwell model is $\frac{\sigma}{E_1}$. Thus the total creep strain is obtained by subtracting for each component the respective elastic strains from the respective total strains and adding the two resulting creep strains together.

Thus the total strain is :

$$\varepsilon_{total} = \underbrace{\frac{\sigma_1 (E_4 + E_2)}{E_4 \eta_2} \left[\frac{\eta_2}{E_2} \left(1 - e^{-\frac{E_2}{\eta_2}.t}\right) + \frac{\eta_2}{(E_4 + E_2)} . e^{-\frac{E_2}{\eta_2}.t} \right]}_{\text{Three-parameter solid}} + \underbrace{\left[\frac{\sigma}{E_1} + \frac{\sigma t}{\eta_1} \right]}_{\text{Maxwell model}}$$

$$\therefore \varepsilon_{creep} = \frac{\sigma_1 (E_4 + E_2)}{E_4 . E_2} \left(1 - e^{-\frac{E_2}{\eta_2}.t}\right) + \frac{\sigma_1}{E_4} . e^{-\frac{E_2}{\eta_2}.t} - \frac{\sigma_1}{E_4} + \left(\frac{\sigma}{E_1} + \frac{\sigma t}{\eta_1}\right) - \frac{\sigma}{E_1}$$

$$= \frac{\sigma_1}{E_2} \left(1 - e^{-\frac{E_2}{\eta_2}.t}\right) + \frac{\sigma . t}{\eta_1}$$

$$\therefore c = \frac{\sigma_1}{E_2 \sigma} \left(1 - e^{-\frac{E_2}{\eta_2} t}\right) + \frac{t}{\eta_1}$$

As previously demonstrated, $\frac{\gamma}{\beta}\left(1 - e^{-\beta t}\right)$ may be substituted for $\frac{t}{\eta_1}$ to avoid the prediction of infinite Maxwell creep, by making η_1 vary exponentially.

$$\therefore c = c_{3\text{-}P} + c_M$$

$$= \frac{\sigma_1}{E_2 \sigma} \left(1 - e^{-\frac{E_2}{\eta_2} t}\right) + \frac{\gamma}{\beta} \left(1 - e^{-\beta . t}\right)$$

However, to accord with experience, η_2 should not remain constant as in the form implied here for classical three-parameter models, and from empirical considerations the retardation time has been taken to vary as $t^{2/3}$

Thus if $\eta_2 = K . t^{3/2}$

and $\frac{E_2}{\eta_2} = \frac{1}{\tau_{ret}}$ where τ_{ret} is the retardation time

then $\frac{E_2 . t}{\eta_2} = \frac{t}{\tau_{ret}} = \frac{E_2 . t}{K . t^{3/2}} = \frac{E_2 . t^{2/3}}{K}$

Thus the final expression for total creep becomes :

$$c = c_{3\text{-}P} + c_M$$

$$\therefore \quad c = \frac{\sigma_1}{E_2 \sigma}\left(1 - e^{-\frac{E_2}{K}.t^{\frac{2}{3}}}\right) + \frac{\gamma}{\beta}\left(1 - e^{-\beta t}\right)$$

$$= C_1\left(1 - e^{-C_2.t^{\frac{2}{3}}}\right) + C_3\left(1 - e^{-C_4 t}\right)$$

where $C_1 = \frac{\sigma_1}{E_2 \sigma}$; $C_2 = \frac{E_2}{K}$; $C_3 = \frac{\gamma}{\beta}$; $C_4 = \beta$

The coefficients C_1, C_2, C_3, C_4 are evaluated by curve-fitting the experimental specific creep/time data. The ultimate specific creep will be the sum of the coefficients C_1 and C_3 i.e $\frac{\sigma_1}{E\sigma} + \frac{\gamma}{\beta}$.

It should be noted that specific creep data were required for the prediction of total strains in three separate test regimes for Series 1 and in a further three for Series 2. These test regimes were the first loaded ambient temperature period, the 80°C loaded period and finally the second loaded ambient temperature period. Three separate creep laws must therefore be established for each series, and a separate origin must be taken for each of the three regimes. The algebraic form of each of these laws will be the same, but the numerical form, when the coefficients are evaluated, will clearly not be identical.

Alternative Hypothesis

An alternative hypothesis could be sustained requiring the two three-parameter models to be placed in series with each other and also with the modified Maxwell model. See Fig 50.

This arrangement would represent the cement paste and the unhydrated cement particles as withstanding the externally-applied stress equally, but contributing different strains towards the total strains. The argument seems not unacceptable rheologically.

In this proposal, as far as creep is concerned, the two springs E_4 and E_5 may be ignored and the mathematical development is as follows :

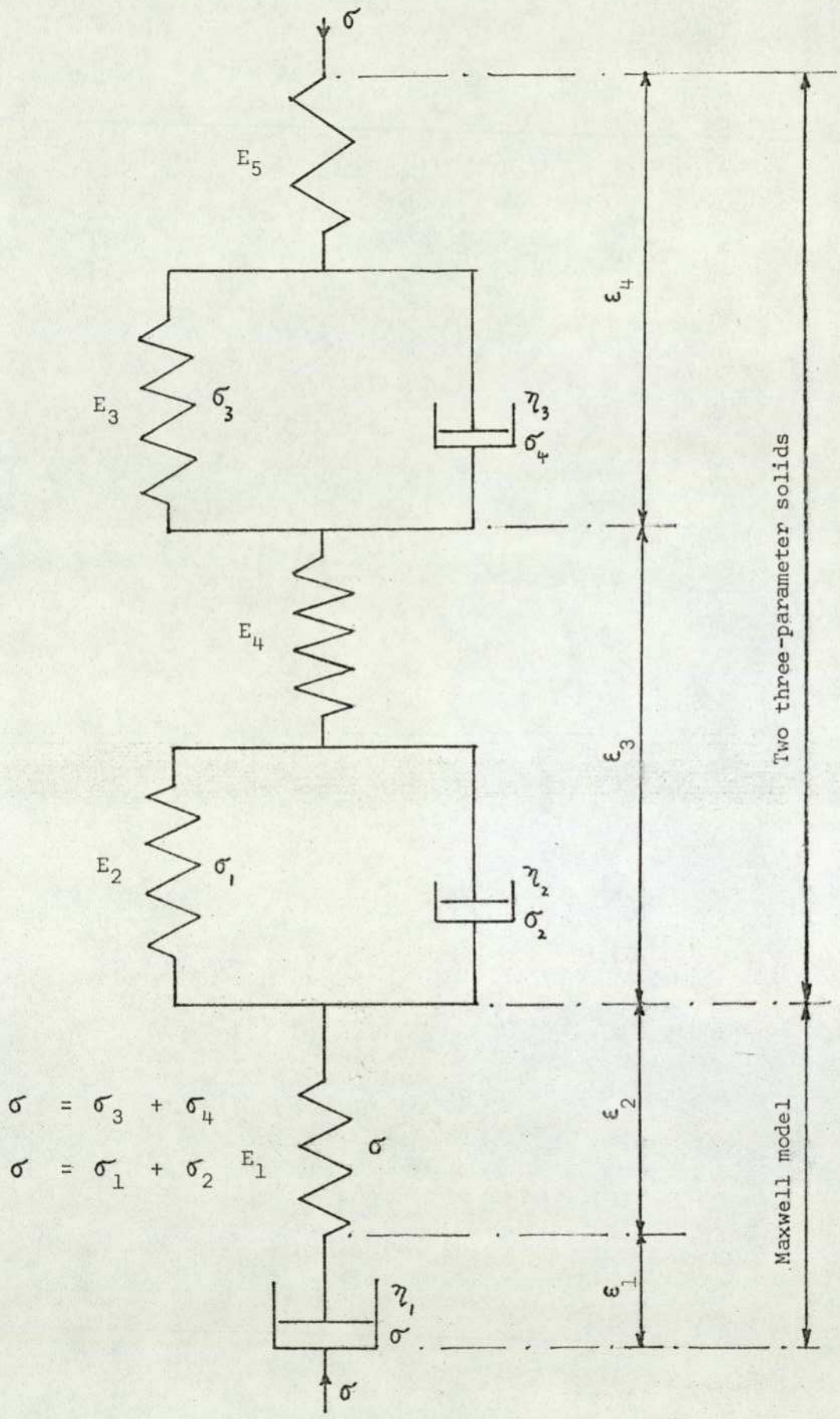


Fig 50 Three-parameter solids & Maxwell model in series.

The creep strain and the specific creep respectively for the elements E_2/η_2 are :

$$\varepsilon_c = \frac{\sigma}{E_2}\left(1 - e^{-\frac{E_2}{K_2}.t^{2/3}}\right)$$

$$\kappa = \frac{1}{E_2}\left(1 - e^{-\frac{E_2}{K_2}.t^{2/3}}\right) \qquad \eta_2 = K_2.t^{3/2}$$

The creep strain and the specific creep respectively for the elements E_3/η_3 are :

$$\varepsilon_c = \frac{\sigma}{E_3}\left(1 - e^{-\frac{E_3}{K_3}.t^{2/3}}\right)$$

$$\kappa = \frac{1}{E_3}\left(1 - e^{-\frac{E_3}{K_3}.t^{2/3}}\right) \qquad \eta_3 = K_3.t^{3/2}$$

The specific creep for the Maxwell model E_1/η_1 is :

$$\kappa = \frac{\gamma}{\beta}\left(1 - e^{-\beta t}\right)$$

Therefore , the total specific creep is given by :

$$\kappa = \frac{1}{E_2}\left(1 - e^{-\frac{E_2}{K_2}.t^{2/3}}\right) + \frac{1}{E_3}\left(1 - e^{-\frac{E_3}{K_3}.t^{2/3}}\right) + \frac{\gamma}{\beta}\left(1 - e^{-\beta t}\right)$$

This expression demands the fitting of six coefficients from the data and seems somewhat ambitious on these grounds alone.

A close simulation of the real concrete could presumably be achieved if an infinite number of 3-P solids were placed in series with each other and with the modified Maxwell model ; the coefficients of the Kelvin dashpots would be required to range over a spectrum of corresponding retardation times specified according to the data obtained from the specific creep observations.

The Evaluation of the Creep Law Coefficients.

The creep law corresponding to the viscoelastic model illustrated in Fig. 49 has been adopted.

As a result of the curve-fitting procedures the following numerical values were obtained for the creep laws appropriate to the three test regimes in each series :

Series 1 Stress in kips units

Ambient First Time

$$c = 0.1774.10^{-2}(1 - e^{-0.4519.10^{-2}.t^{2/3}}) + 0.3839.10^{-3}(1 - e^{-0.2623.10^{-2}.t})$$

Temperature 80°C

$$c = 0.4088.10^{-2}(1 - e^{-0.2555.10^{-5}.t^{2/3}}) + 0.1285.10^{-3}(1 - e^{-0.1076.t})$$

Ambient Second Time

$$c = 0.4203.10^{-3}(1 - e^{-0.1054.t^{2/3}}) + 0.9321.10^{-1}(1 - e^{-0.3492.10^{-3}.t})$$

Series 2

Ambient First Time

$$c = 0.3522.10^{-2}(1 - e^{-0.6856.10^{-6}.t^{2/3}}) + 0.1199.10^{-3}(1 - e^{-0.9384.10^{-1}.t})$$

Temperature 80°C

$$c = 0.8093.10^{-2}(1 - e^{-0.1084.10^{-4}.t^{2/3}}) + 0.5692.10^{-3}(1 - e^{-0.9766.10^{-1}.t})$$

Ambient Second Time

$$c = 0.1652.10^{-2}(1 - e^{-0.1534.10^{-4}.t^{2/3}}) + 0.1064.10^{-3}(1 - e^{-0.6471.10^{-1}.t})$$

A typical output from the curve-fitting programme is shown in the Appendices.

General Application of the Viscoelastic Analysis.

To generalize the application of these viscoelastic laws for structural analysis, it would be necessary to carry out long-term creep strain measurements against time for a variety of different concretes under different conditions.

For any particular set of circumstances the most suitable creep law with its appropriate evaluated coefficients would be chosen.

A list of concrete variables to be investigated experimentally would include :

a) Type of cement

b) Cement content

c) Type of Aggregate

d) W/C Ratio

e) Curing conditions of humidity and temperature

f) Service conditions of humidity and temperature

g) Age at loading

h) Surface/Volume ratio of member

i) Strength of concrete

Not all these variables are independent nor need so extensive a range be tested in practice.

A set of calibration curves relating the significant concrete variables with the creep law coefficients would thus be needed. This represents an immense task which has not been undertaken in the present work.

In the creep laws quoted, the effect of temperature has only been given significance to the extent that the thermal creep data obtained during the 80°C regime in each test series has influenced the numerical magnitude of the coefficients.

The immediate thermal expansion and contraction strains have been included in the analysis in the manner described under the section dealing with thermoelastic considerations.

6. THE TIME-DEPENDENT SOLUTION.

As a result of the experimental observations on the concrete models, it has been possible to plot specific creep-time curves for the different regimes of loading, loading and heating etc, to which the specimens were subjected.

The exponential nature of the law governing the rate of decay of specific creep is apparent from the form of these curves. The conception of an algebraic format for appropriate exponential equations to suit the plotted curves, is necessary, and this conception is influenced both by the observed results and by the rheological model under review.

The coefficients and exponents of the exponential equations chosen, may be readily evaluated by a simple computer programme based upon a least squares fitting procedure, employing data from the specific creep-time curves. However, the mathematical form of the equation must first be postulated before the curve-fitting programme can provide numerical answers for the constants.

The basis of the time-dependent method proposed, lies in the stepwise modification of the initial finite element elastic solution by introducing creep data obtained from the specific creep laws.

When the external mechanical loading is imposed on the end slab structure, the latter settles immediately and elastically into equilibrium and geometrical compatibility. As time passes, creep strains inevitably occur in the concrete which can be considered to cause incompatibilities.

There is little difficulty in computing these creep strains given the creep decay law. It is done by computing at any time the total specific creep by substituting into the creep law equation.

For example, for any two time values t_1 and t_2, delineating the two limits of a short time interval, the difference in the magnitudes of the evaluated creep equation at t_1 and t_2, will give the incremental specific creep for that time interval. If this is multiplied by the current stress and by $\phi(T)$, the temperature function, the incremental creep strain will be obtained.

These creep strains, in the method proposed, may be considered to correspond to and result from the fictitious forces which are assumed to be acting on the elements. These fictitious forces are those which would have to be applied to restore geometrical compatibility after the creep straining.

Moreover, these forces can be computed from the finite element matrix equation

$$\{F\} = \int_V [B]^T [D] \Delta\varepsilon_c \, dV$$

where $\{F\}$ = the fictitious forces

$[B]^T$ = the transposed $[B]$ matrix

$[D]$ = the elasticity matrix

$\Delta\varepsilon_c$ = the incremental creep strain

V = the volume of the structure

The load vectors due to creep, which must be applied to the entire structure at the nodal points, can thus be obtained from the fictitious forces. The unknown displacements can then be obtained from the relationship

$$\{F\} = [K] \{d\}$$

This computation, as described, gives the unknown displacements for the effect of creep only. The same process may also be undertaken for the displacements due to temperature and shrinkage. All three sets of values are then added to the elastic displacements to get the total displacements comparable with the observed results.

The stress distributions may finally be obtained from the nodal displacements.

7. THERMOELASTIC CONSIDERATIONS.

Structures or members of structures unrestrained at their supports or boundaries suffer no thermal stress due to elevated temperatures although they will suffer thermal strains. Restraint, however, will cause the member or structure to experience thermal stresses at the supports or boundaries.

Such thermal stresses are normally assumed to be independent of stresses due to externally-applied loading.

All stress-strain equations reflecting equilibrium or compatibility conditions must therefore include the effects of temperature.

However, a variation in temperature along or across an unrestrained member, whether externally-loaded or not, will also cause additional stresses.

The specimens tested in this investigation fall into two main categories

(a) model I/2 - uniformly heated and free to expand with no external restraints and zero temperature gradient across the slab thickness (I6¾" diameter solid specimen)

(b) models 3/4 and 9/I0 - uniformly heated but with internal restraints, and zero temperature gradient across the slab thickness (I6¾" perforated small specimen (3/4) and perforated composite specimen (36", 9/I0))

Practical difficulties prevented the achievement of a perfectly uniform temperature in the radial direction in the composite specimen, particularly in the first test series. The temperature diff-

erence was approximately $8^{o}C$ to $12^{o}C$. Thus additional thermoelastic stresses were caused. There was however, no temperature gradient through the slab thickness, and the stresses in this direction were not affected.

It has been assumed that for a material such as concrete the free thermal expansions, consequent upon a uniform temperature rise, occur independently of position and direction and without angular distortion. The coefficient of expansion α, of the concrete will also be independent of position and direction.

For an unrestrained element, thermal strains are given by

$$\varepsilon_{t_{ij}} = \delta_{ij} . \alpha . dT \quad ,$$

this equation determining normal thermal strains only, thermal shear strains being zero.

In this expression

i,j = x,y,z

dT = the rise in temperature

α = the coefficient of linear thermal expansion for concrete

δ_{ij} = the Kronecker delta for which

δ_{ij} = I when i=j, and

δ_{ij} = 0 when $i \neq j$.

An element subjected to non-uniform temperature will suffer thermal strains $\varepsilon_{t_{ij}}$ due to the temperature rise plus an elastic-type strain due to the displacement discontinuity from the non-uniform nature of the temperature distribution.

The true elastic strains developing from any externally-applied load system operating on the element, are normally lumped together with the elastic strains resulting from the non-uniform temperature. These total elastic strains will be indicated by ε_{ij}.

The total strain ε_T in a free element can therefore be represented by

$$\varepsilon_T = \varepsilon_{t_{ij}} + \varepsilon_{ij}$$

After substitution for $\varepsilon_{t_{ij}}$, this becomes

$$\varepsilon_T = \alpha \, dT \, \delta_{ij} + \varepsilon_{ij}$$

Considering the stress-strain relationships in the plane stress analysis for isotropic and homogeneous materials, we have the following equations

$$\sigma_z = \sigma_{zx} = \sigma_{zy} = 0$$

$$\varepsilon_x = \frac{I}{E}(\sigma_x - \nu \sigma_y)$$

$$\varepsilon_y = \frac{I}{E}(\sigma_y - \nu \sigma_x)$$

$$\varepsilon_{xy} = 2\frac{(I+\nu)}{E}\sigma_{xy}$$

and substituting these equations into the equation above for total strain gives the total elastic and thermal strains for the free element:

$$\varepsilon_x = \frac{I}{E}(\sigma_x - \nu \sigma_y) + \alpha \, dT \quad (\text{ie } i=j)$$

$$\varepsilon_y = \frac{I}{E}(\sigma_y - \nu \sigma_x) + \alpha \, dT \quad (\text{ie } i=j)$$

$$\varepsilon_{xy} = 2\frac{(I+\nu)}{E}\sigma_{xy} + 0 \quad (\text{ie } i \neq j)$$

Thus

$$\begin{bmatrix} \varepsilon_x \\ \varepsilon_y \\ \varepsilon_{xy} \end{bmatrix} = \frac{I}{E}\begin{bmatrix} I & -\nu & 0 \\ -\nu & I & 0 \\ 0 & 0 & 2(I+\nu) \end{bmatrix}\begin{bmatrix} \sigma_x \\ \sigma_y \\ \sigma_{xy} \end{bmatrix} + \alpha \, dT \begin{bmatrix} I \\ I \\ 0 \end{bmatrix}$$

or, $\{\varepsilon_T\} = [D]^{-I}\{\sigma\} + [DT]$

where $[DT] = \alpha \, dT \begin{bmatrix} I \\ I \\ 0 \end{bmatrix}$, the thermal strain matrix.

Similarly, the stress equations become

$$\begin{bmatrix} \sigma_x \\ \sigma_y \\ \sigma_{xy} \end{bmatrix} = \frac{E}{1-\nu^2} \begin{bmatrix} 1 & \nu & 0 \\ \nu & 1 & 0 \\ 0 & 0 & \frac{1-\nu}{2} \end{bmatrix} \begin{bmatrix} \varepsilon_x \\ \varepsilon_y \\ \varepsilon_{xy} \end{bmatrix} - \frac{E \alpha dT}{1-\nu} \begin{bmatrix} 1 \\ 1 \\ 0 \end{bmatrix}$$

or, $\{\sigma_T\} = [D]\{\varepsilon\} - \underline{DT}$

where $\underline{DT}$ is the thermal stress matrix.

It is now necessary to develop expressions for the thermal load vector for the structure. For doing this, two approaches are possible.

(a) the method of restraint in which the so-called "freezing" technique is used, and

(b) the method of direct formulation.

The second approach is the one used in this analysis. The thermoelastic effects are investigated by imposing a set of hypothetical boundary loadings and body forces at the nodal points. These forces and loads are fictitious, and are such as would result from the normal stresses which would be necessary to cause the same displacements as the actual temperature gradient. Such fictitious loads can then be treated as the thermal load vector for each element.

By adding together the contributions of all the elements to the nodes to which they are connected, the thermal load vector for the whole structure can be obtained.

The complete structure can then be analysed under the thermal load vector for the structure. It should be noted, however, that to obtain the correct stress values, the fictitious normal stresses which were considered to simulate thermal stresses, must be subtracted from the calculated stresses in the elements.

The appropriate thermoelastic equations therefore become

(a) $$\{F_{te}\} = [B]^T [D]\{\varepsilon_t^f\} \, t \, A$$

where $$\{\varepsilon_t^f\} = \alpha \, dT \begin{bmatrix} 1 \\ 1 \\ 0 \end{bmatrix} = \text{free thermal strain}$$

in a triangular element subjected to a temperature rise dT,

and t = the element thickness

A = the element area

$\{F_{te}\}$ = the nodal forces on the element.

(b) $$\{F_{ts}\} = \sum ([B]^T . [D] . \{\varepsilon_t^f\} \; t \; A)$$

where $\{F_{ts}\}$ = the load vector for the structure

(c) $$\{F_{ts}\} = [K] . \{d_t\}$$

(d) $$\therefore \{d_t\} = [K]^{-1} . \{F_{ts}\}$$ = the displacements

(e) $$\{\varepsilon_t\} = [B] . \{d_t\}$$ = the strains

(f) $$\{\sigma_t\} = [D] . (\{\varepsilon_t\} - \{\varepsilon_t^f\})$$

or $$\{\sigma_t\} = [D] . [B] . \{d_t\} - [D]\{\varepsilon_t^f\}$$

} = the stresses

8. CREEP CONSIDERATIONS.

The thermal creep strains per unit stress, observed in the tests on the loaded and uniformly-heated specimen, ie the specific thermal creep values, have been plotted on a time base, to obtain a specific thermal creep curve. The equation for this curve was numerically evaluated by curve-fitting procedures. At any time interval, therefore, values of thermal creep strain could be obtained for use in the step-by-step analysis by which the elastic solution was extended into the time-dependent range.

Thus $\varepsilon_c = \sigma . \phi(T) . c$, and the incremental creep strains so computed at the end of a particular time interval may be introduced into the analysis as initial strains.

Consider the specimen subjected to the mechanical loads and to the uniform elevated temperature. Elastic and thermal strains and stresses develop in the elements. These are given in the biaxial plane stress case by the following equations:

$$\begin{bmatrix} \varepsilon_x \\ \varepsilon_y \\ \varepsilon_{xy} \end{bmatrix} = \frac{1}{E} \begin{bmatrix} 1 & -\nu & 0 \\ -\nu & 1 & 0 \\ 0 & 0 & 2(1+\nu) \end{bmatrix} \begin{bmatrix} \sigma_x \\ \sigma_y \\ \sigma_{xy} \end{bmatrix} + \alpha\, dT \begin{bmatrix} 1 \\ 1 \\ 0 \end{bmatrix}$$

and

$$\begin{bmatrix} \sigma_x \\ \sigma_y \\ \sigma_{xy} \end{bmatrix} = \frac{E}{1-\nu^2} \begin{bmatrix} 1 & \nu & 0 \\ \nu & 1 & 0 \\ 0 & 0 & \frac{1-\nu}{2} \end{bmatrix} \begin{bmatrix} \varepsilon_x \\ \varepsilon_y \\ \varepsilon_{xy} \end{bmatrix} - \frac{E\alpha\, dT}{1-\nu} \begin{bmatrix} 1 \\ 1 \\ 0 \end{bmatrix}$$

After a short time interval, the concrete elements will creep uniformly according to the specific creep law.

Assuming the material properties, the stresses and the temperatures to remain constant during the interval, the creep strains at the end of the interval become

$$\begin{bmatrix} \varepsilon_{cx} \\ \varepsilon_{cy} \\ \varepsilon_{cxy} \end{bmatrix} = \underbrace{\phi(T)\, dc \begin{bmatrix} 1 & -\nu & 0 \\ -\nu & 1 & 0 \\ 0 & 0 & 2(1+\nu) \end{bmatrix}}_{[D\,C]} \begin{bmatrix} \sigma_x \\ \sigma_y \\ \sigma_{xy} \end{bmatrix}$$

In matrix form,

$$\{\varepsilon_c\} = [D\,C]\,\{\sigma\}$$

where $\{\varepsilon_c\}$ = the creep strain vector in the element

$\{\sigma\}$ = the stresses due to mechanical and thermal loading at the start of an interval

$[D\,C]$ = the specific thermal creep matrix, as given in the above equation.

The total strain ε_T is the sum of the elastic, thermal and creep strains,

$$\therefore \quad \varepsilon_T = \varepsilon_{el} + \varepsilon_{th} + \varepsilon_c$$

$$\begin{bmatrix} \varepsilon_{Tx} \\ \varepsilon_{Ty} \\ \varepsilon_{Txy} \end{bmatrix} = \frac{I}{E} \begin{bmatrix} I & -\nu & 0 \\ -\nu & I & 0 \\ 0 & 0 & 2(I+\nu) \end{bmatrix} \begin{bmatrix} \sigma_{elx} \\ \sigma_{ely} \\ \sigma_{elxy} \end{bmatrix} + \propto dT \begin{bmatrix} I \\ I \\ 0 \end{bmatrix} + \begin{bmatrix} D\ C \end{bmatrix} \begin{bmatrix} \sigma_x \\ \sigma_y \\ \sigma_{xy} \end{bmatrix}$$

In matrix form,

$$\{\varepsilon_T\} = [D]^{-I}\{\sigma_c\} + [D\ T] + [D\ C]\{\sigma\}$$

Thus we now have the following matrices established.

$[D]$ = the elasticity matrix

$$= \frac{E}{I-\nu^2} \begin{bmatrix} 1 & \nu & 0 \\ \nu & 1 & 0 \\ 0 & 0 & \frac{1-\nu}{2} \end{bmatrix}$$

$[D]^{-I}$ being $\frac{I}{E} \begin{bmatrix} I & -\nu & 0 \\ -\nu & I & 0 \\ 0 & 0 & 2(I+\nu) \end{bmatrix}$

$[D\ T]$ = the thermal strain matrix $= \propto dT \begin{bmatrix} I \\ I \\ 0 \end{bmatrix}$

$[D\ C]$ = the specific thermal creep matrix $= \phi\, Tdc \begin{bmatrix} I & -\nu & 0 \\ -\nu & I & 0 \\ 0 & 0 & 2(I+\nu) \end{bmatrix}$

With the stresses, the strains and the creep matrix defined for the free elements, the element and structure creep load vector may be established by the method of direct formulation as described previously for the thermoelastic effects.

The matrix equations for the creep effects thus become :

(a) Nodal forces for the element

$$\{F_{ce}\} = [B]^T . [D] . \{\varepsilon_c^f\} . t . A$$

(b) Load vector for the structure

$$\{F_{cs}\} = \sum \left([B]^T . [D] . \{\varepsilon_c^f\} . t . A \right)$$

(c) Equilibrium equations

$$\{F_{cs}\} = [K].\{d_c\}$$

(d) Displacements

$$\{d_c\} = [K]^{-1}.\{F_{cs}\}$$

(e) Strains

$$\{\varepsilon_c\} = [B].\{d_c\}$$

(f) Stresses

$$\{\sigma_c\} = [D].(\{\varepsilon_c\} - \{\varepsilon_c^f\})$$

$$\text{hence } \{\sigma_c\} = [D].[B].\{d_c\} - [D].\{\varepsilon_c^f\}$$

9. SHRINKAGE CONSIDERATIONS.

The magnitude of shrinkage strains has been shown to be affected by the ambient temperature and humidity. For structures operating at elevated temperatures such as the P.C.P.V and the structural slabs tested in these experiments, shrinkage is important enough to be treated as additional loading in the analysis.

In the case of the end slabs, the uniform temperature of 80°C simplified the problem, and it was assumed that shrinkage strain-time curves could be plotted from direct shrinkage strain measurements on the slabs. This involves the further assumption that shrinkage everywhere in the concrete was uniform.

The shrinkage analysis described here has been based upon the supposition that the shrinkage in unloaded concrete is of the same magnitude as that in loaded concrete.

The further supposition has been made that the shrinkage strains at any time may be considered as initial strains and may be introduced into the finite element analysis as known strains, in much the same way as was done for the creep and thermal strains. This was achieved by the direct formulation method, which has been fully described earlier in this section.

It should also be noted that thermal strains and shrinkage strains have been taken as having opposite signs. Thermal strain ε_t may be equated to $\alpha\, dT$ for an increase in length due to a temperature rise dT, and the shrinkage strain ε_s may be represented in the analysis in a similar way since $-\varepsilon_s$ is equivalent to $\alpha\, dT$.

Shrinkage strains ε_s in a finite element thus become

$$\varepsilon_s = \begin{bmatrix} \varepsilon_{sx} \\ \varepsilon_{sy} \\ \varepsilon_{sxy} \end{bmatrix} = \phi(T).ds \begin{bmatrix} I \\ I \\ 0 \end{bmatrix}$$

where $\phi(T).ds \begin{bmatrix} I \\ I \\ 0 \end{bmatrix}$ is the shrinkage strain matrix, $[D\ S]$

This is identical to the way thermal strains are dealt with. Note that normal shrinkage strains are assumed to operate. Shear shrinkage strains are not involved.

The total strain on an element is

$$\varepsilon_T = \varepsilon_e + \varepsilon_c + \varepsilon_t + \varepsilon_s$$ which becomes, when expanded

$$\begin{bmatrix} \varepsilon_{Tx} \\ \varepsilon_{Ty} \\ \varepsilon_{Txy} \end{bmatrix} = \frac{I}{E} \begin{bmatrix} I & -\nu & 0 \\ -\nu & I & 0 \\ 0 & 0 & 2(I+\nu) \end{bmatrix} \begin{bmatrix} \sigma_{ex} \\ \sigma_{ey} \\ \sigma_{exy} \end{bmatrix} + \alpha.dT \begin{bmatrix} I \\ I \\ 0 \end{bmatrix}$$

$$+ \phi T.dc \begin{bmatrix} I & -\nu & 0 \\ -\nu & I & 0 \\ 0 & 0 & 2(I+\nu) \end{bmatrix} \begin{bmatrix} \sigma \\ \sigma_{ey}^{ex} \\ \sigma_{exy} \end{bmatrix}$$

$$+ \phi T.ds \begin{bmatrix} I \\ I \\ 0 \end{bmatrix}$$

$$\therefore \quad \{\varepsilon_T\} = [D]^{-I}.\{\sigma_e\} + [D\ T] + [D\ C]\{\sigma_e\} + [D\ S]$$

The matrix equations for shrinkage become

(a) Nodal forces for the element

$$\left\{F_{se}\right\} = \left[B\right]^T \left[D\right] \left\{\varepsilon_s^f\right\} t\, A$$

(b) Load vector for the structure

$$\left\{F_{ss}\right\} = \sum \left[B\right]^T \left[D\right] \left\{\varepsilon_s^f\right\} t\, A$$

(c) Equilibrium equations

$$\left\{F_{ss}\right\} = \left[K\right] \left\{d_s\right\}$$

(d) Displacements

$$\left\{d_s\right\} = \left[K\right]^{-I} \left\{F_{ss}\right\}$$

(e) Strains

$$\left\{\varepsilon_s\right\} = \left[B\right] \left\{d_s\right\}$$

(f) Stresses

$$\left\{\sigma_s\right\} = \left[D\right] \left(\left\{\varepsilon_s\right\} - \left\{\varepsilon_s^f\right\}\right)$$

hence

$$\left\{\sigma_s\right\} = \left[D\right]\left[B\right]\left\{d_s\right\} - \left[D\right]\left\{\varepsilon_s^f\right\}$$

IO. THE COMPUTER PROGRAMME.

(a) Objective

The objective of the computer programme, implicit in the whole investigation, was to provide a means of predicting by calculation, the displacements, stresses and strains in a two-dimensional structural system. These predictions could then be compared with the results of the experimental observations to assess the validity of the theoretical analysis proposed.

The computer language used throughout was Fortran.

(b) Analysis

Both the elastic and time-dependent sections of the analysis have previously been described in detail.

The finite element procedure has been utilized, and two-dimensional triangular plate elements, in an appropriate network mesh, idealize the structural continuum.

The programme sets up in matrix form the various equilibrium

equations, using the direct stiffness method.

The input data contains the necessary information about the geometry of the nodal points, the elements and the quadrant. The elastic constants of the concrete and steel, the loading vectors, the support conditions and the time intervals are also provided in the input.

The programme solves the equilibrium equations for the nodal displacements by direct elimination. The elastic problem is solved repeatedly, using the thermal, creep and shrinkage data to modify the initial elastic approach in order to obtain the time-dependent solution.

Finally, the programme, having thus obtained the nodal displacements, computes the stresses and strains at the centroids of the elements and also at the nodal points.

(c) Details of Input Data

The full data comprise details of the mesh geometry , the material and plate properties, the loading and boundary conditions. The data are printed out as soon as they are read in, which simplifies the checking.

The global Cartesian co-ordinates of all the nodal points are given with respect to the main orthogonal axes of the quadrant in the form of an array which specifies each nodal point number and the corresponding co-ordinates.

Similarly, the element array specifies each element number together with each of its three nodal point numbers defined in an anti-clockwise direction.

The numbering of the elements and the nodal points affects closely the structure stiffness matrix band-width. First, the nodal points and the elements should be numbered and follow each other

consecutively. Secondly, the nodal point indices of the element must be so ordered that the elements are correctly developed. This may be achieved by ensuring that the product of the number of degrees of freedom per node and the maximum difference in numbering of adjacent nodes, is numerically equal to the band-width. Meeting this condition saves time in solution and space in storing the matrix.

The moduli of elasticity and the Poisson's ratios for the concrete and the steel, constitute material properties which are assigned and fed in as data. The elements are scanned to select the appropriate value.

Loading data are fed in at the boundary nodal points by converting the radial uniformly-distributed compression which represents the externally-applied mechanical loading into a series of statically equivalent point loads. These are applied in the form of a loading array of x and y co-ordinate load values at each node.

The coefficients of linear thermal expansion are specified for the concrete and steel together with the current time intervals. The input data on thermal properties is completed by specifying the appropriate temperature difference.

A further input data array defines the values of the creep and shrinkage functions with the required time intervals.

The quadrant boundary conditions are specified by listing the appropriate zero displacements or the known displacements at the nodal points.

Finally, the support conditions are prescribed as free or fixed. This is given for the supports in the x and y directions.

The input data cards take the following form:

Title: This contains information identifying the programme and giving the title to be printed.

Control Card: Maximum number of time intervals.

Plate Properties: Young's modulus : steel
Ditto : concrete
Poisson's ratio : steel
Ditto : concrete
Plate thickness.

Thermal Properties: Coefficient of thermal expansion : steel
Ditto : concrete

Elements, Nodal Points,	Number of elements
Loaded Nodal Points,	Number of nodal points
Support Nodal Points,	Number of loaded points
Specified Displacements	Number of support points
for Nodal Points:	Number of points with specified displacements.

Nodal Point Array:
Nodal point number
x co-ordinates
y co-ordinates

Triangular Element Array:
Number of elements
Number of node i
Number of node j
Number of node k
} anti-clockwise

Support Condition Array:
0 = x fixed: y fixed
I = x fixed: y free
2 = x free : y fixed
3 = x free : y free

Material Property Array:
I = steel element
2 = concrete element

Loading Array:
Nodal point number
Load in x
Load in y

Data Array: Time interval dt
Temperature increment dT
Value of creep function
Value of shrinkage function

(d) Output

A typical set of output results for displacements, stresses and strains is shown in the Appendices for the various time intervals.

These intervals cover the several different experimental regimes during the testing.

Tensile displacements, stresses and strains are taken to be positive. The displacements are given in inch units and the stresses in kips per square inch.

The nodal point displacements and the element stresses and strains are obtained as solutions to the equations:

$$\{R\} = [K]\{d\}$$

$$\{\sigma\} = [D](\varepsilon - \varepsilon_o)$$

$$\{\varepsilon\} = [B]\{d\}$$

SECTION XI

PRESENTATION OF OBSERVED RESULTS

A list of the graphs and curves obtained from the results, followed by the graphs themselves, is presented in this section.

From these graphs, which show total strains in some cases and shrinkage and thermal strains together in others at different ages and temperatures, it is possible to evaluate separately each of the elastic, creep, shrinkage and thermal strain components of the total strains.

For example, in each series, the shrinkage and thermal strains were available from one unloaded solid specimen (7/8), and from one unloaded perforated specimen (5/6).

The combined elastic, creep, shrinkage and thermal strains were obtained from one loaded solid specimen (1/2), and from one loaded perforated specimen (3/4). The loaded composite specimen (9/10) also provided elastic, creep, shrinkage and thermal strains for the combined perforated zone and outer solid annulus.

The elastic strains were immediately identifiable experimentally from the sudden jump in the strain graph on first loading. They were also calculable.

Similarly, the thermal strains were apparent on heating. Thus, by appropriate subtraction, it was possible to identify separately each of the effects of elastic loading, and thermal, creep and shrinkage straining, for each specimen.

The readings were taken in the manner and in the positions described in Section VI. To obtain the values of strain, the difference between any individual reading and the initial datum reading was multiplied by the Demec gauge factor.

Measurements were taken for each series,

a) of the four radial and four tangential strains on each side of each specimen over 2" gauge lengths; also two sets of readings were taken on each face over 11.438" gauge lengths (3 standpipe pitches); this was done with Demec gauges.

b) across four diameters of each of two symmetrically-disposed steel standpipes on each face of all perforated specimens, by means of a modified Mercer bore gauge.

Loadings, specimen temperatures, and ambient temperatures and relative humidities were also observed with each set of strain readings.

The eight 2" gauge length readings and the two 11.438" readings taken on each face of all small specimens, were in the ligaments, or in positions in the solid specimens, corresponding to the ligament positions. Such ligament gauge lengths were also measured on the large specimen, and in addition for this specimen, groups of four 2" gauge lengths, known as the inner and outer satellites, were measured to ascertain the strains in the outer solid annulus.

The strains plotted were averages of the corresponding strains from the two faces of each specimen. The averaging procedure tended to eliminate errors due to inaccuracies in reading, inequalities in rim loading, in-plane curvature of the slabs, and variations in temperature.

The cracking observed in model 5/6 as a result of heating and revealed on cooling, resulted from the tensile strains which are recorded in the graphs for this specimen.

SERIES 1

Fig 51 Tangential gross strains. Model 1/2.

Fig 52 Radial gross strains. Model 1/2.

Fig 53 Diametral gross strains. Model 1/2.

Fig 54 Tangential gross strains. Model 3/4.

Fig 55 Radial gross strains. Model 3/4.

Fig 56 Diametral gross strains. Model 3/4.

Fig 57 Tangential shrinkage and thermal strains. Model 5/6.

Fig 58 Radial shrinkage and thermal strains. Model 5/6.

Fig 59 Diametral shrinkage and thermal strains. Model 5/6.

Fig 60 Tangential shrinkage and thermal strains. Model 7/8.

Fig 61 Radial shrinkage and thermal strains. Model 7/8.

Fig 62 Diametral shrinkage and thermal strains. Model 7/8.

Fig 63 Tangential gross strains. Perforated zone. Model 9/10.

Fig 64 Radial gross strains. Perforated zone. Model 9/10.

Fig 65 Diametral gross strains. Perforated zone. Model 9/10.

Fig 66 Tangential gross strains. Outer satellite. Model 9/10.

Fig 67 Radial gross strains. Outer satellite. Model 9/10.

Fig 68 Tangential gross strains. Inner satellite. Model 9/10.

Fig 69 Radial gross strains. Inner satellite. Model 9/10.

SERIES 2

Fig 70 Tangential gross strains. Model 1/2.

Fig 71 Radial gross strains. Model 1/2.

Fig 72 Diametral gross strains. Model 1/2.

Fig 73 Tangential gross strains. Model 3/4.

Fig 74 Radial gross strains. Model 3/4.

Fig 75 Diametral gross strains. Model 3/4.

Fig 76 Tangential shrinkage and thermal strains. Model 5/6.

Fig 77 Radial shrinkage and thermal strains. Model 5/6.

Fig 78 Diametral shrinkage and thermal strains. Model 5/6.

Fig 79 Tangential shrinkage and thermal strains. Model 7/8.

Fig 80	Radial shrinkage and thermal strains.	Model 7/8.
Fig 81	Diametral shrinkage and thermal strains.	Model 7/8.
Fig 82	Tangential gross strains. Perforated zone.	Model 9/10.
Fig 83	Radial gross strains. Perforated zone.	Model 9/10.
Fig 84	Diametral gross strains. Perforated zone.	Model 9/10.
Fig 85	Tangential gross strains. Outer satellite.	Model 9/10.
Fig 86	Radial gross strains. Outer satellite.	Model 9/10.
Fig 87	Tangential gross strains. Inner satellite.	Model 9/10.
Fig 88	Radial gross strains. Inner satellite.	Model 9/10.
SERIES 1		
Fig 89	Temperature and relative humidity.	Model 1/2.
Fig 90	Temperature and relative humidity.	Model 3/4.
Fig 91	Temperature and relative humidity.	Model 5/6.
Fig 92	Temperature and relative humidity.	Model 7/8.
Fig 93	Temperature and relative humidity.	Model 9/10.
SERIES 2		
Fig 94	Temperature and relative humidity.	Model 1/2.
Fig 95	Temperature and relative humidity.	Model 3/4.
Fig 96	Temperature and relative humidity.	Model 5/6.
Fig 97	Temperature and relative humidity.	Model 7/8.
Fig 98	Temperature and relative humidity.	Model 9/10.
SERIES 2		
Fig 99	Standpipe diametral strains at positions 1/2, 3/4, 9/10, 11/12.	Model 3/4.
Fig 100	Standpipe diametral strains at positions 5/6, 13/14.	Model 3/4.
Fig 101	Standpipe diametral strains at positions 7/8, 15/16.	Model 3/4.

Fig 102	Standpipe diametral strains at positions 33/34, 35/36, 41/42, 43/44.	Model 5/6.
Fig 103	Standpipe diametral strains at positions 37/38, 45/46.	Model 5/6.
Fig 104	Standpipe diametral strains at positions 39/40, 47/48.	Model 5/6.
Fig 105	Standpipe diametral strains at positions 65/66, 67/68, 73/74, 75/76.	Model 9/10.
Fig 106	Standpipe diametral strains at positions 69/70, 77/78.	Model 9/10.
Fig 107	Standpipe diametral strains at positions 71/72, 79/80.	Model 9/10.
Fig 108	Series 1. Specific creep curve.	
Fig 109	Series 2. Specific creep curve.	

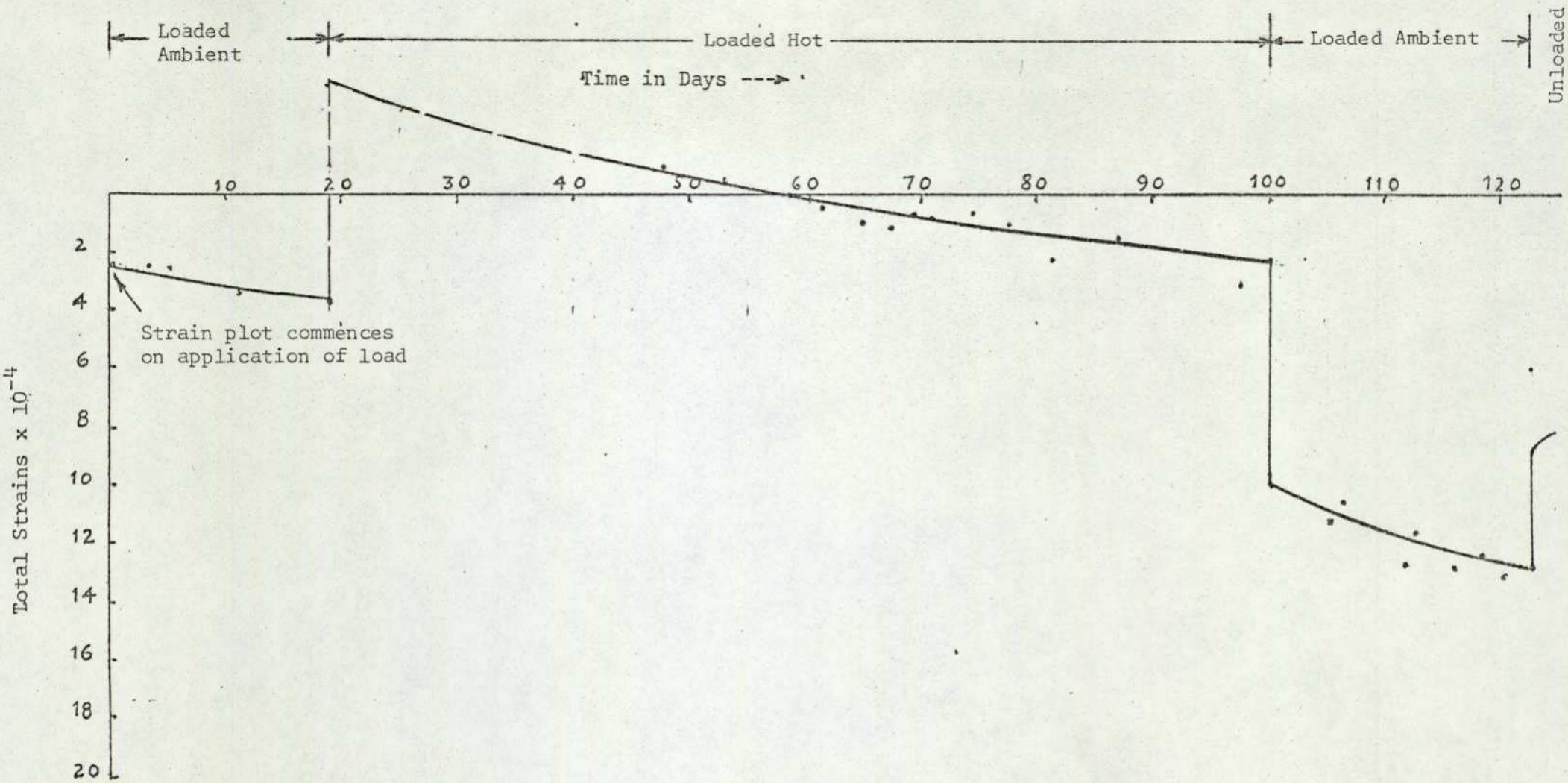


FIG 51 SERIES 1 SIDES 1/2 SOLID 1

TANGENTIAL TOTAL STRAINS 2"

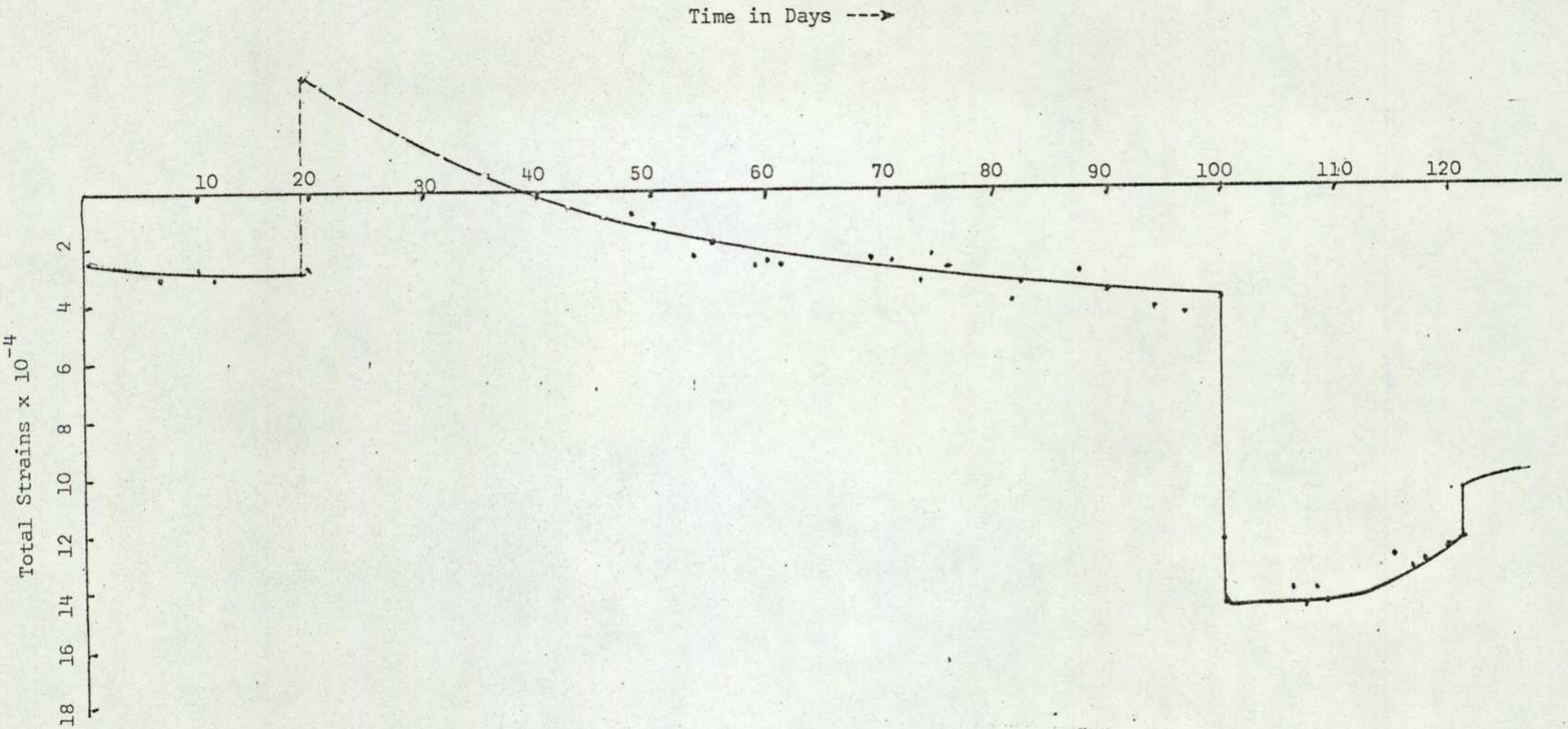


FIG 52 SERIES 1 SIDES 1/2 SOLID 1
RADIAL TOTAL STRAINS 2" G.L.

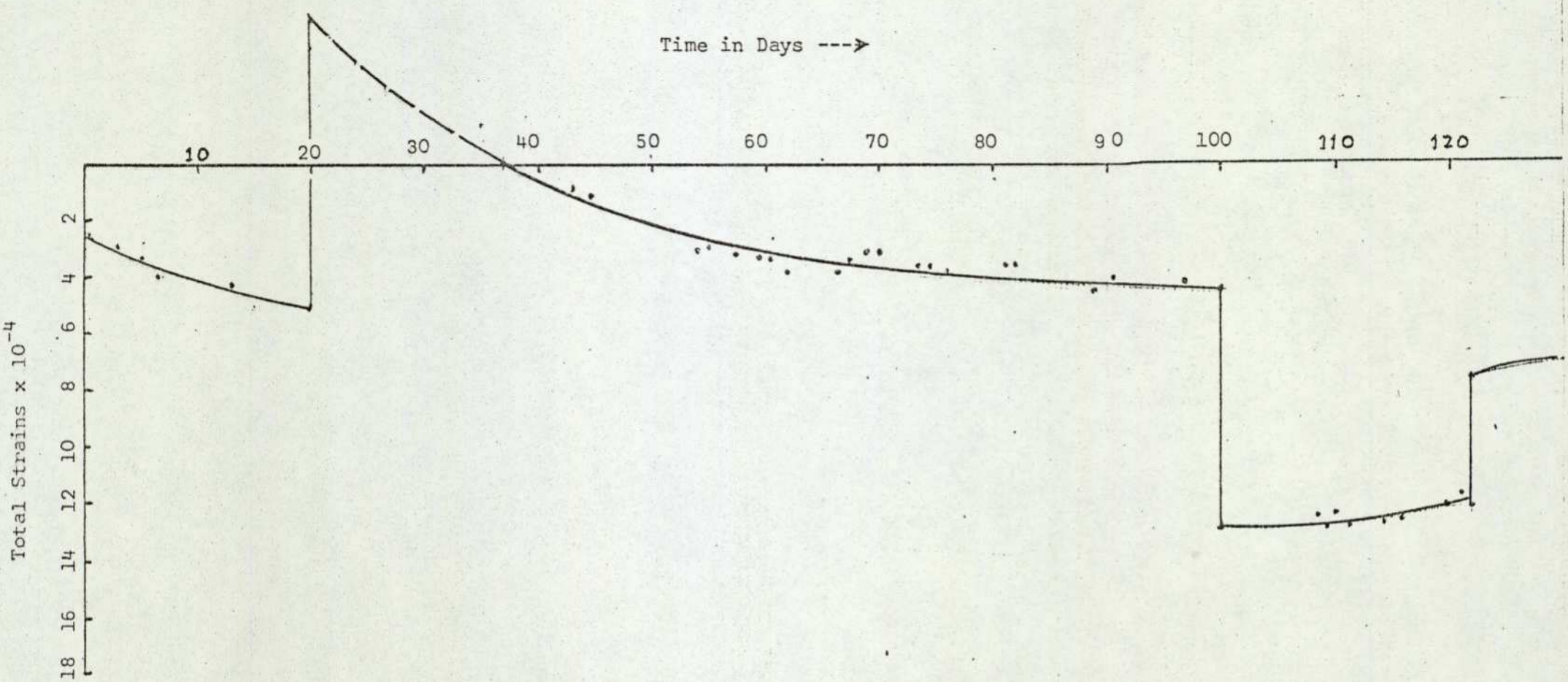


FIG 53 SERIES 1 SIDES 1/2 SOLID 1
THREE PITCH TOTAL STRAINS

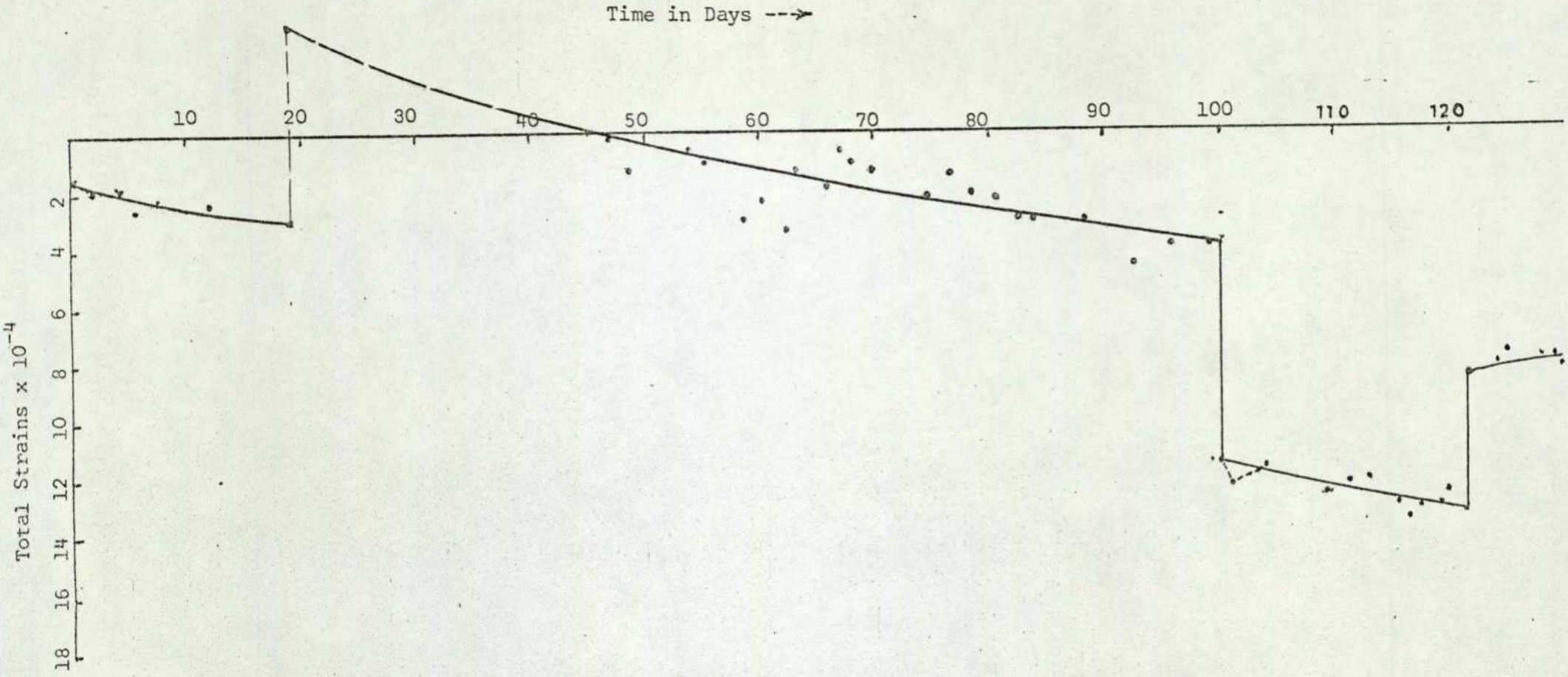


FIG 54 SERIES 1 SIDES 3/4 PERFO 1

TANGENTIAL TOTAL STRAINS 2" G.L.

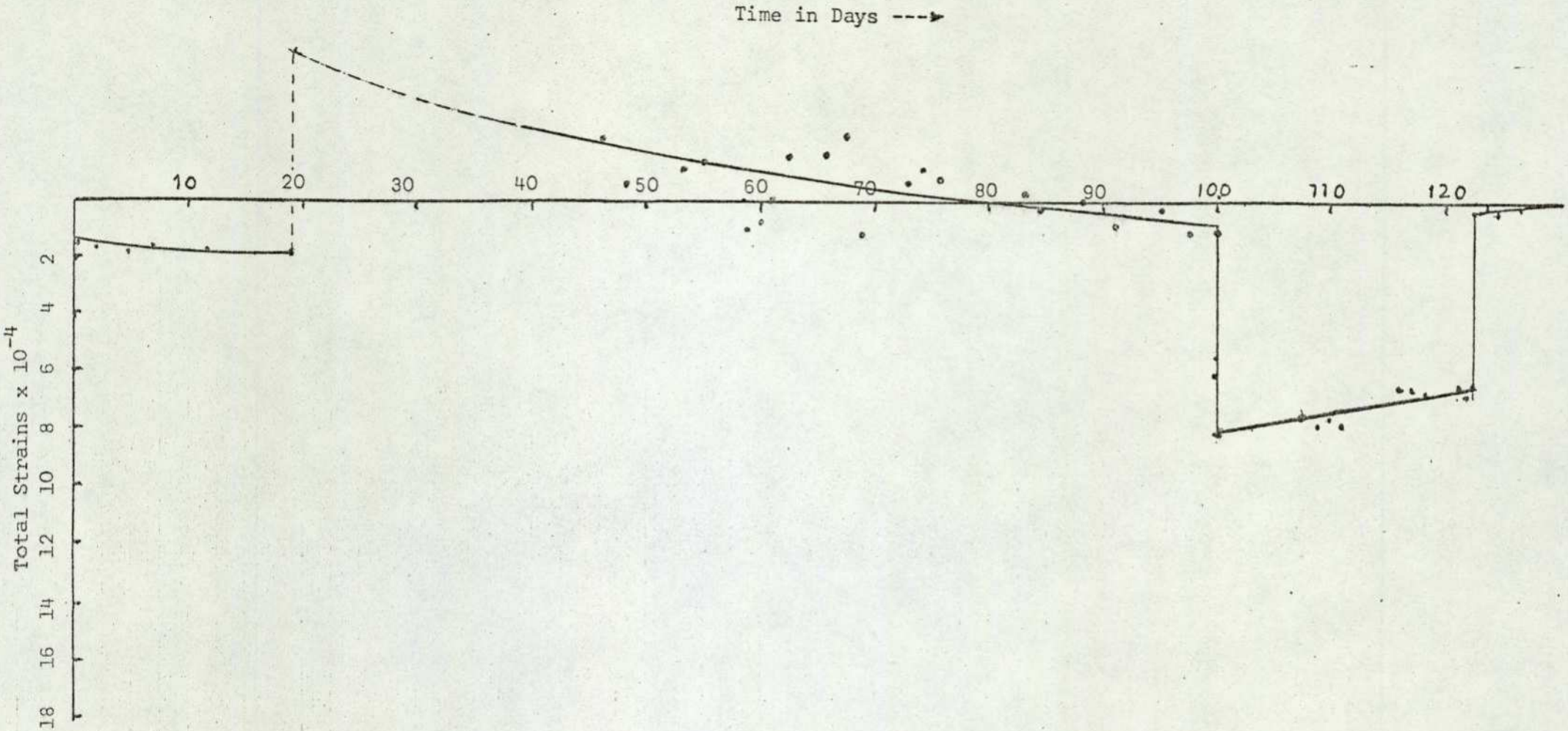


FIG 55 SERIES 1 SIDES 3/4 PERFO 1

RADIAL TOTAL STRAINS 2" G.L.

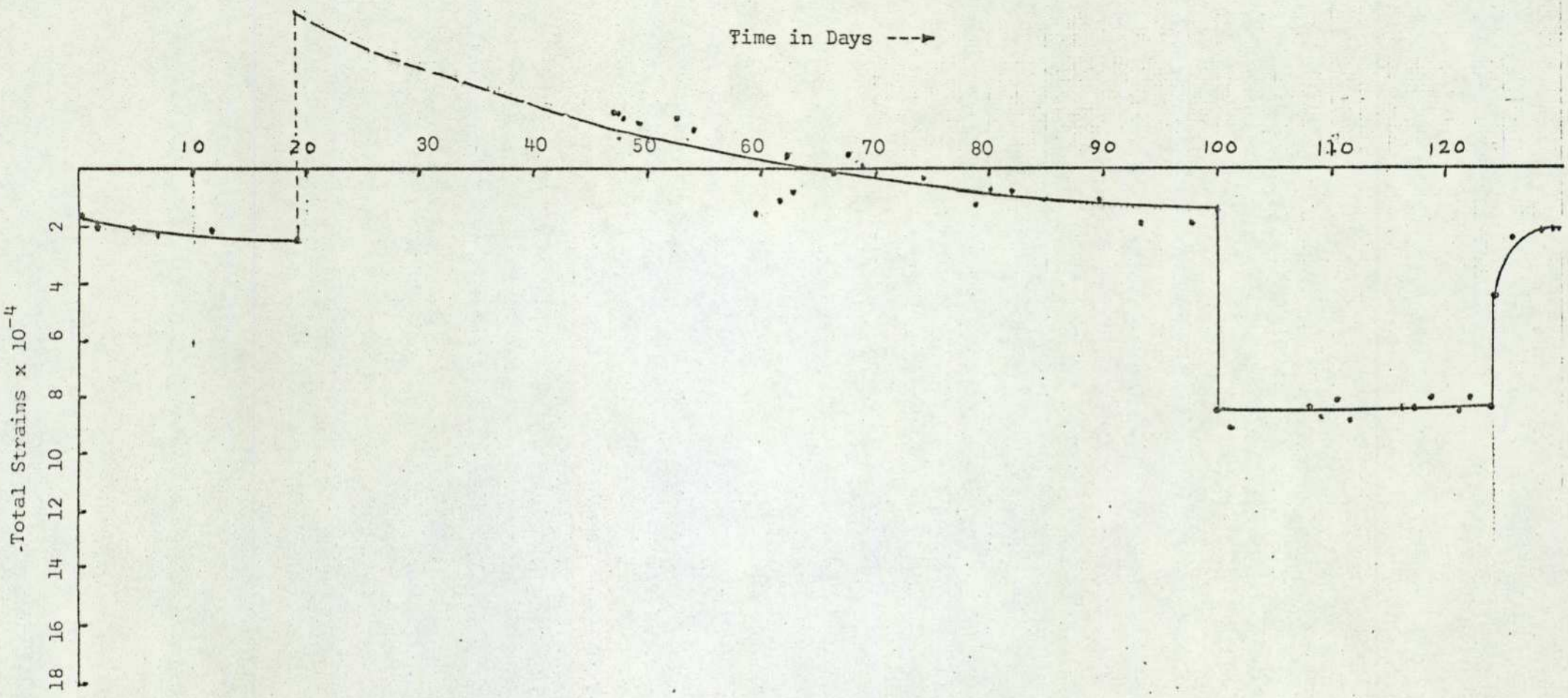


FIG 56 SERIES 1 SIDES 3/4 PERFO 1
THREE PITCH TOTAL STRAINS

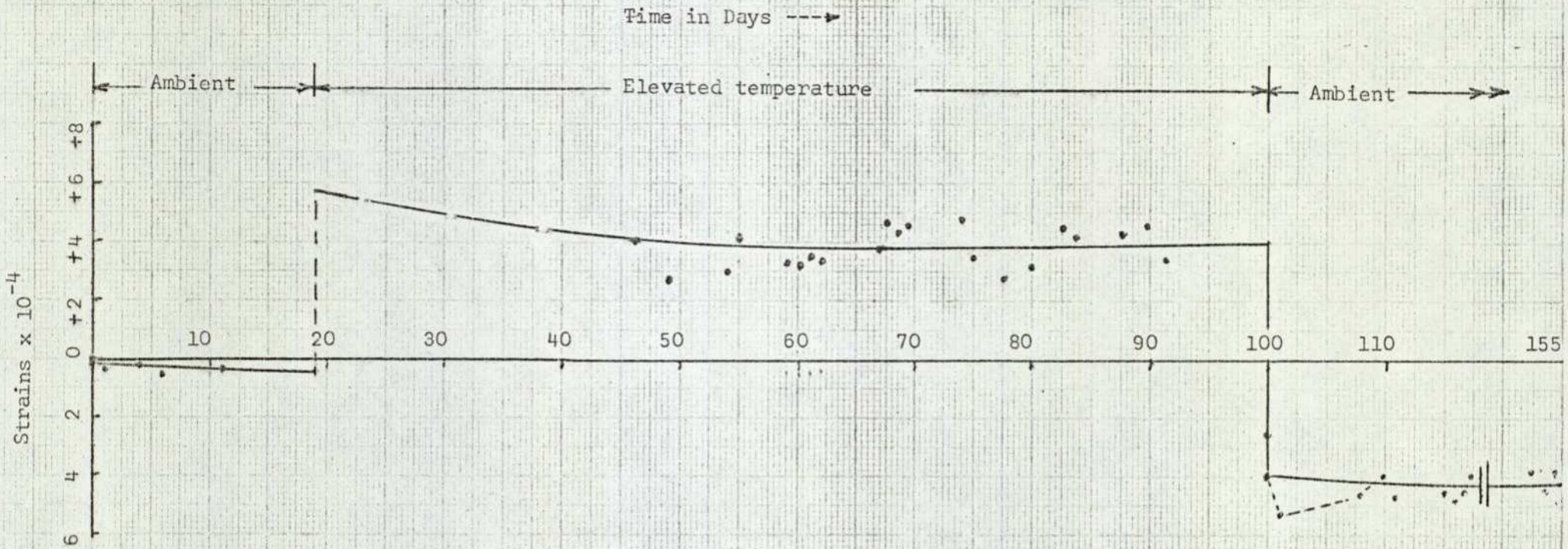


FIG 57 SERIES 1 SIDES 5/6
TANGENTIAL SHRINKAGE STRAINS 2" G.L.

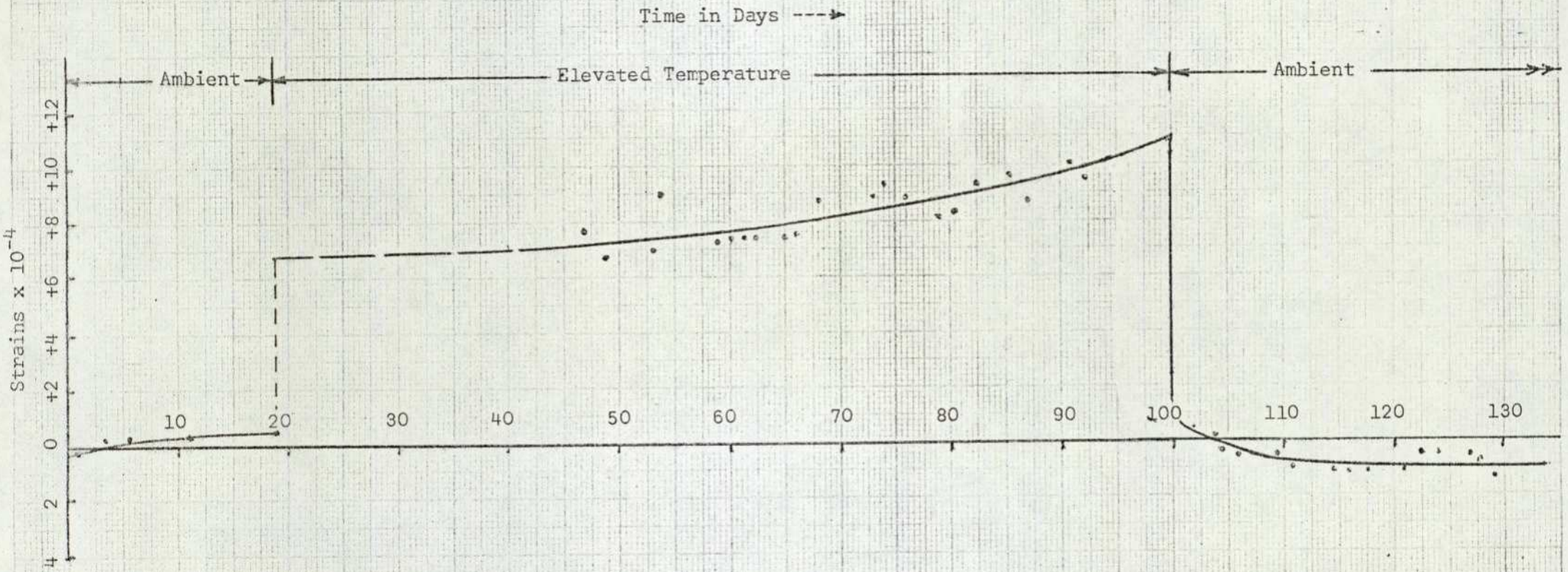


FIG 58 SERIES 1 SIDES 5/6

RADIAL SHRINKAGE STRAINS 2" G.L.

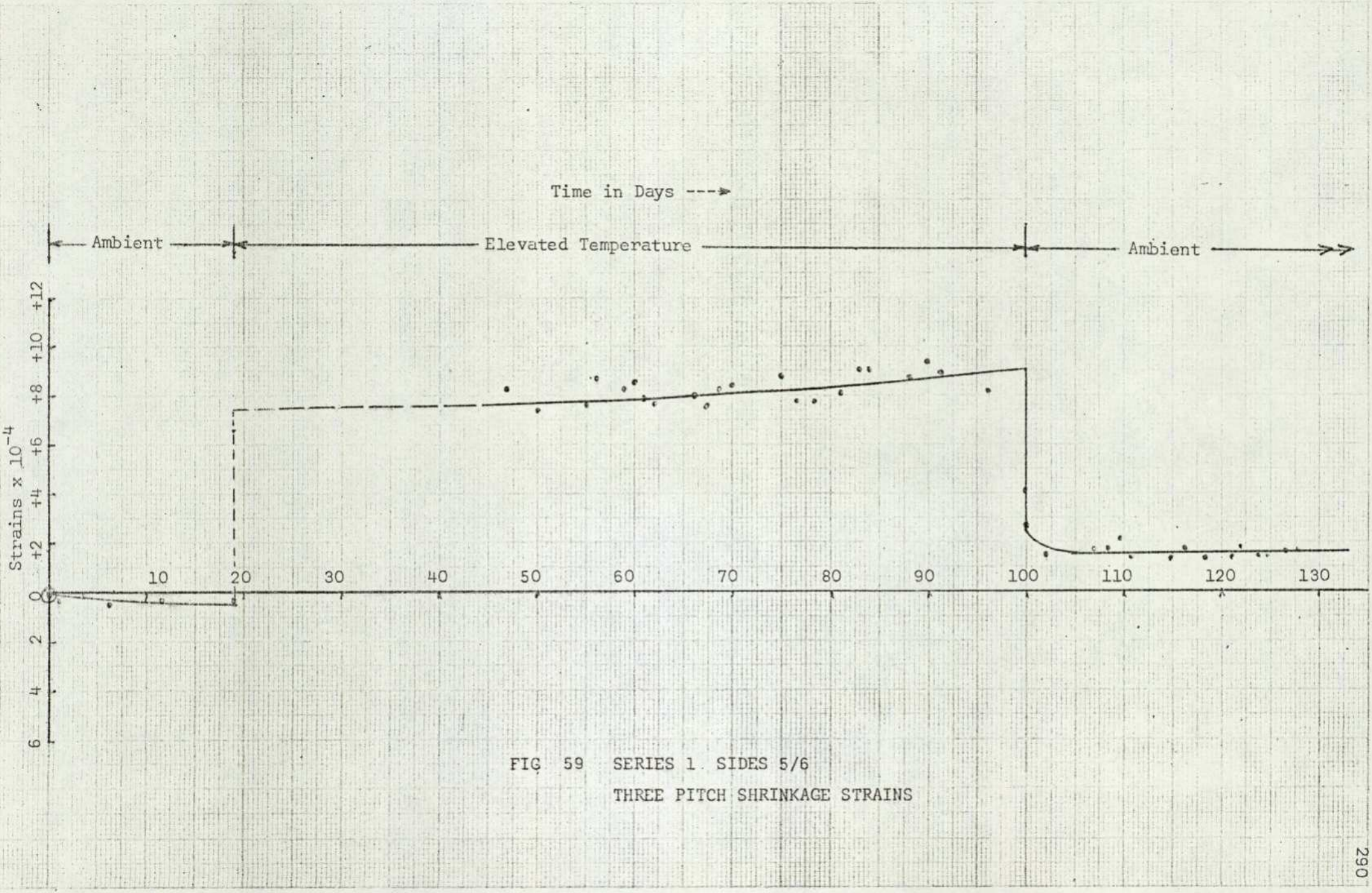


FIG 59 SERIES 1 SIDES 5/6
THREE PITCH SHRINKAGE STRAINS

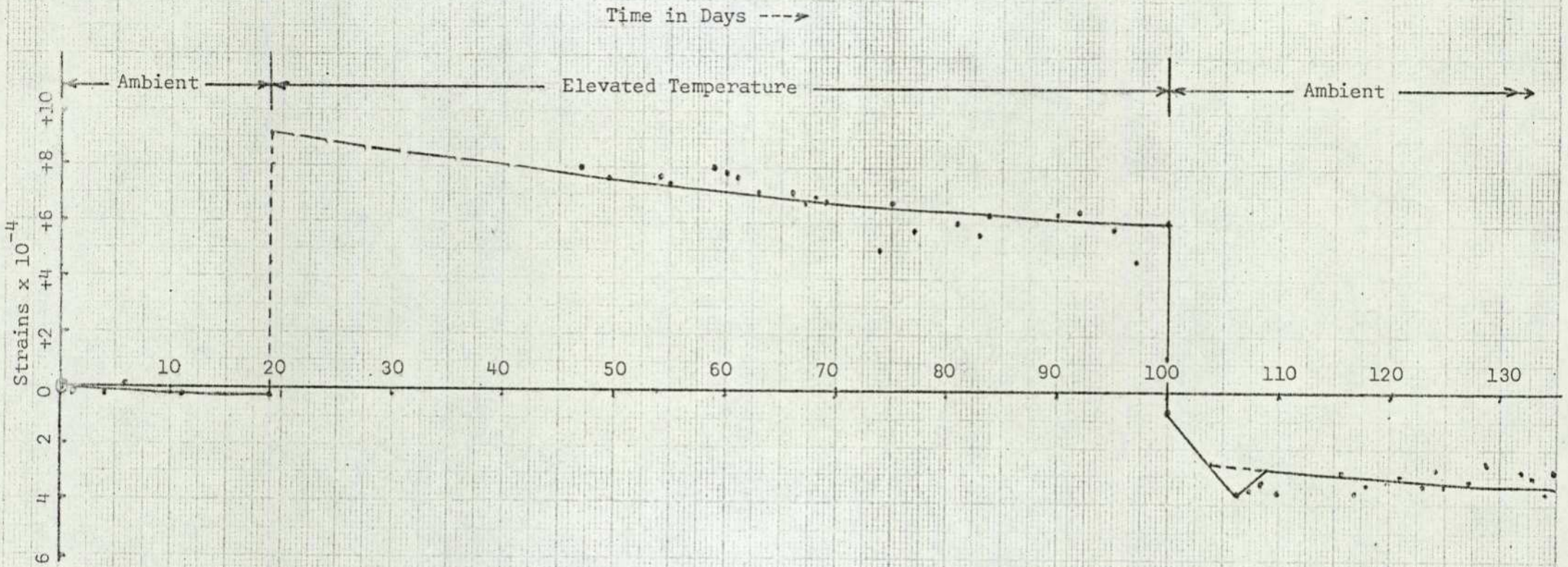


FIG 60 SERIES 1 SIDES 7/8

TANGENTIAL SHRINKAGE STRAINS

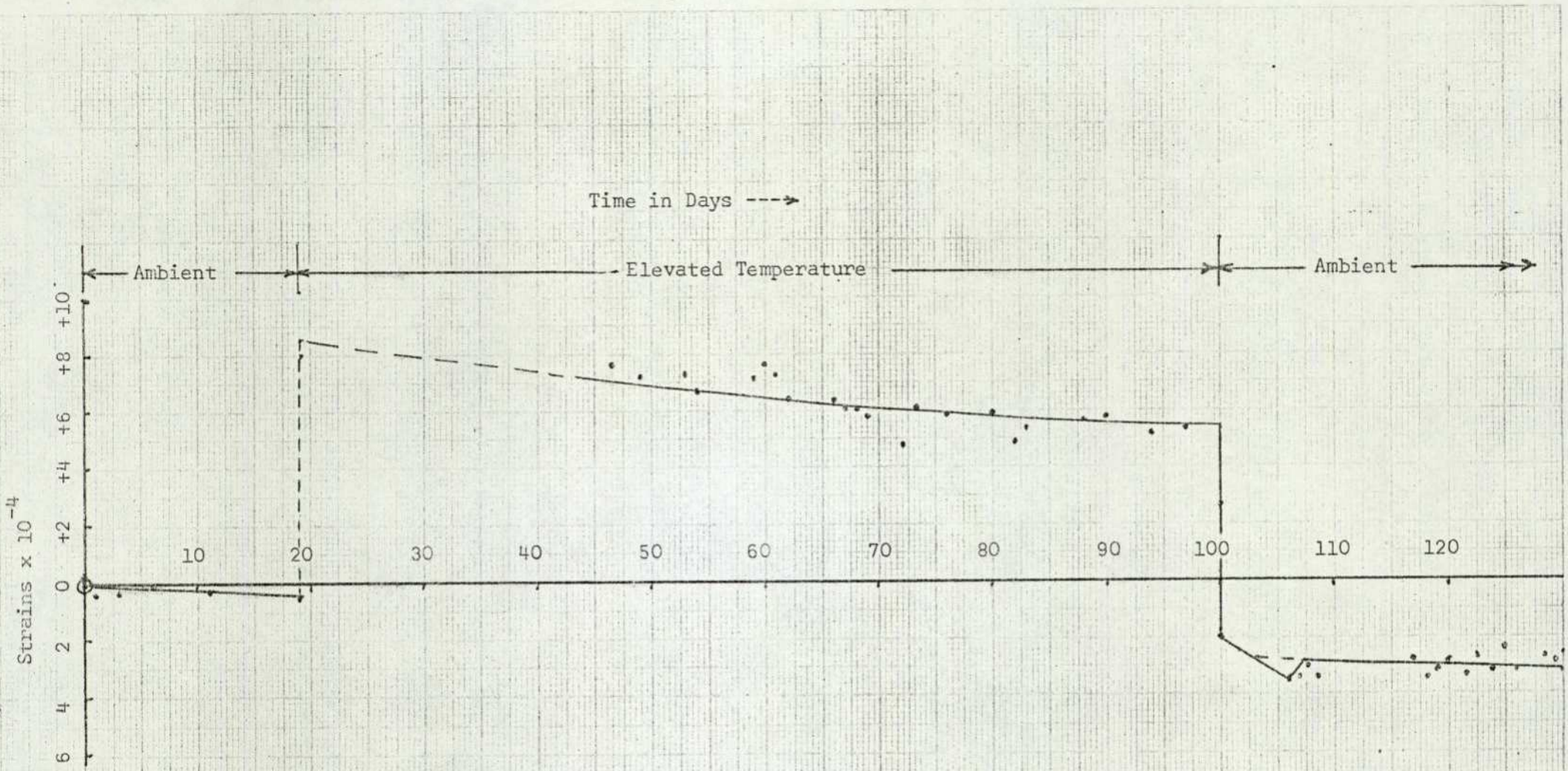


FIG 61 SERIES 1 SIDES 7/8
RADIAL SHRINKAGE STRAINS

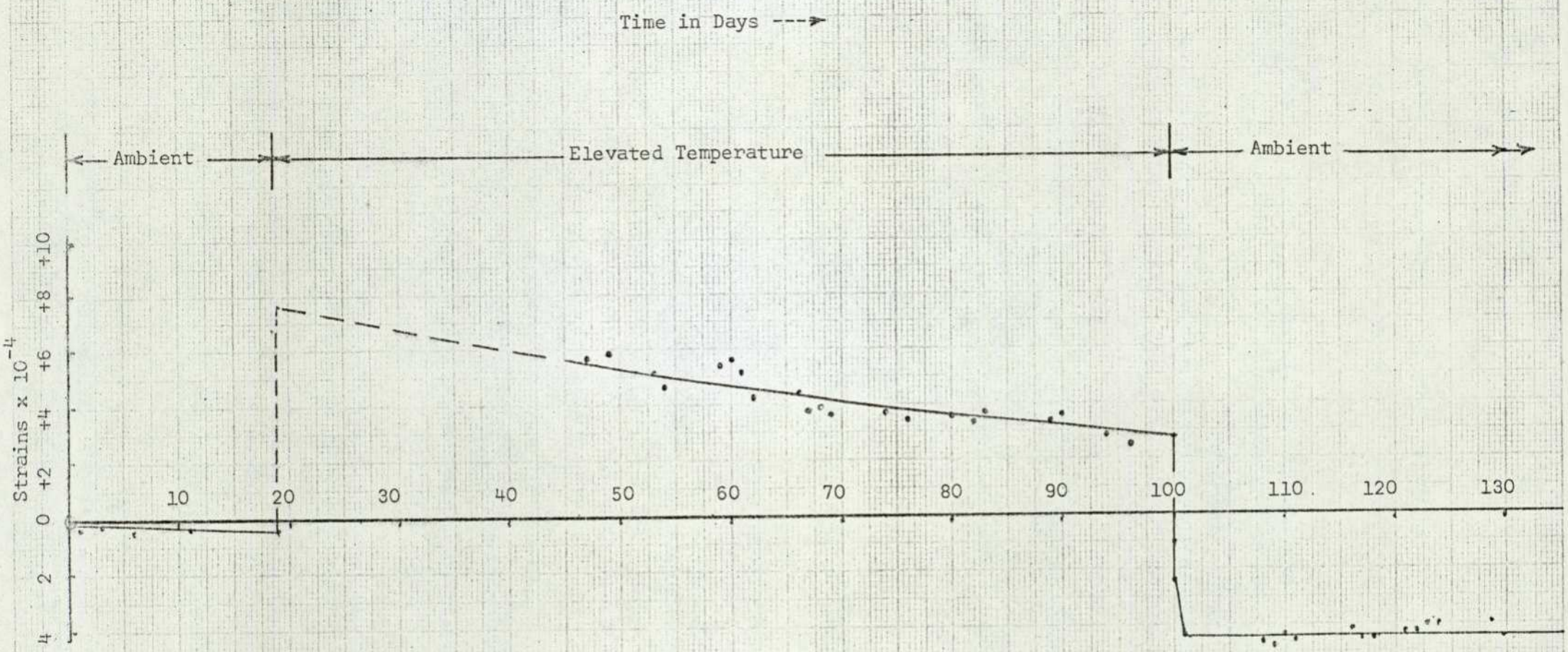


FIG 62 SERIES 1 SIDES 7/8
THREE PITCH SHRINKAGE STRAINS

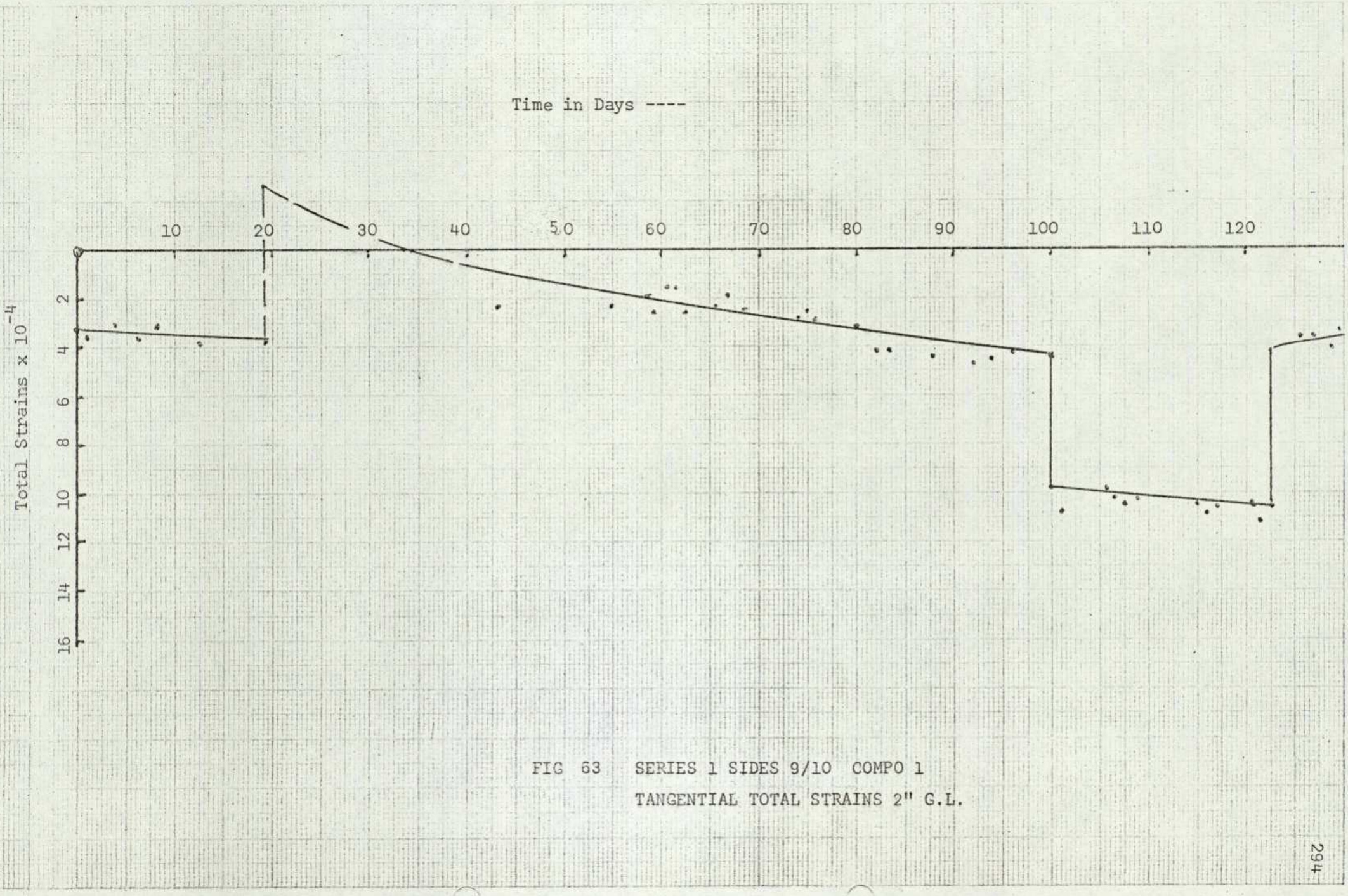


FIG 63 SERIES 1 SIDES 9/10 COMPO 1
TANGENTIAL TOTAL STRAINS 2" G.L.

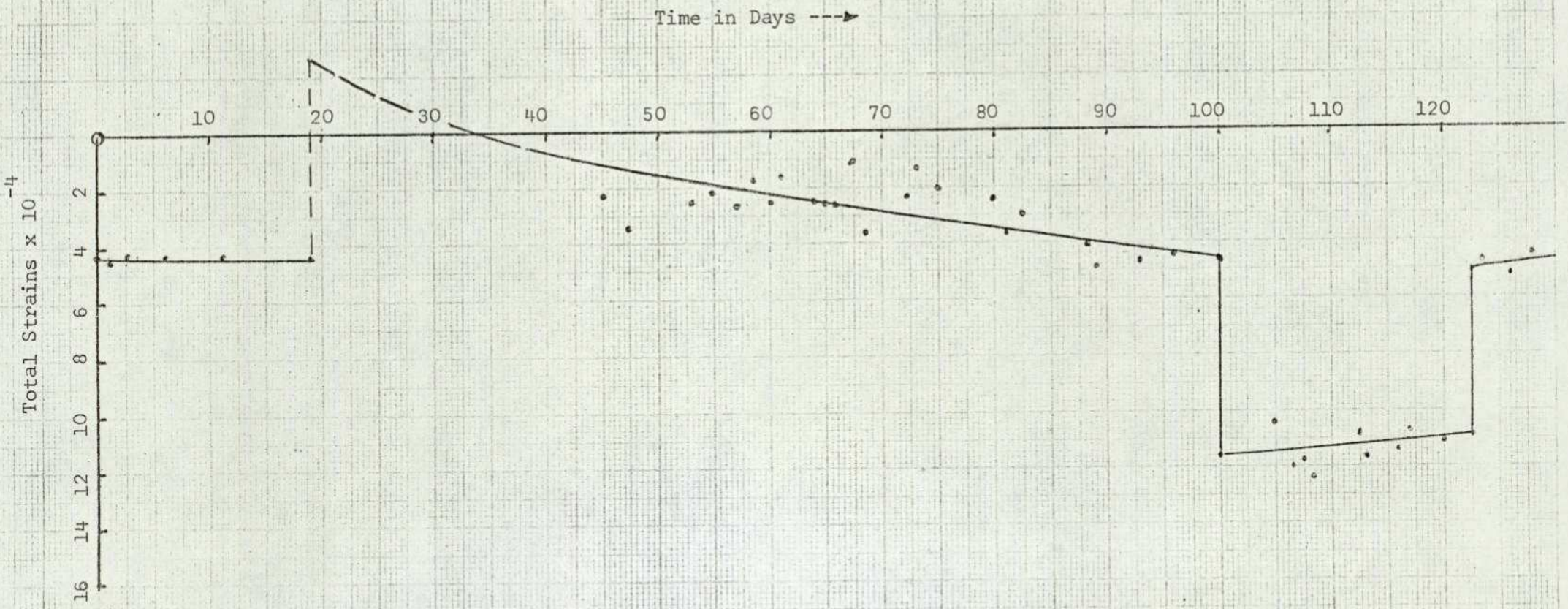


FIG 64 SERIES 1 SIDES 9/10 COMPO 1
RADIAL TOTAL STRAINS 2" G.L.

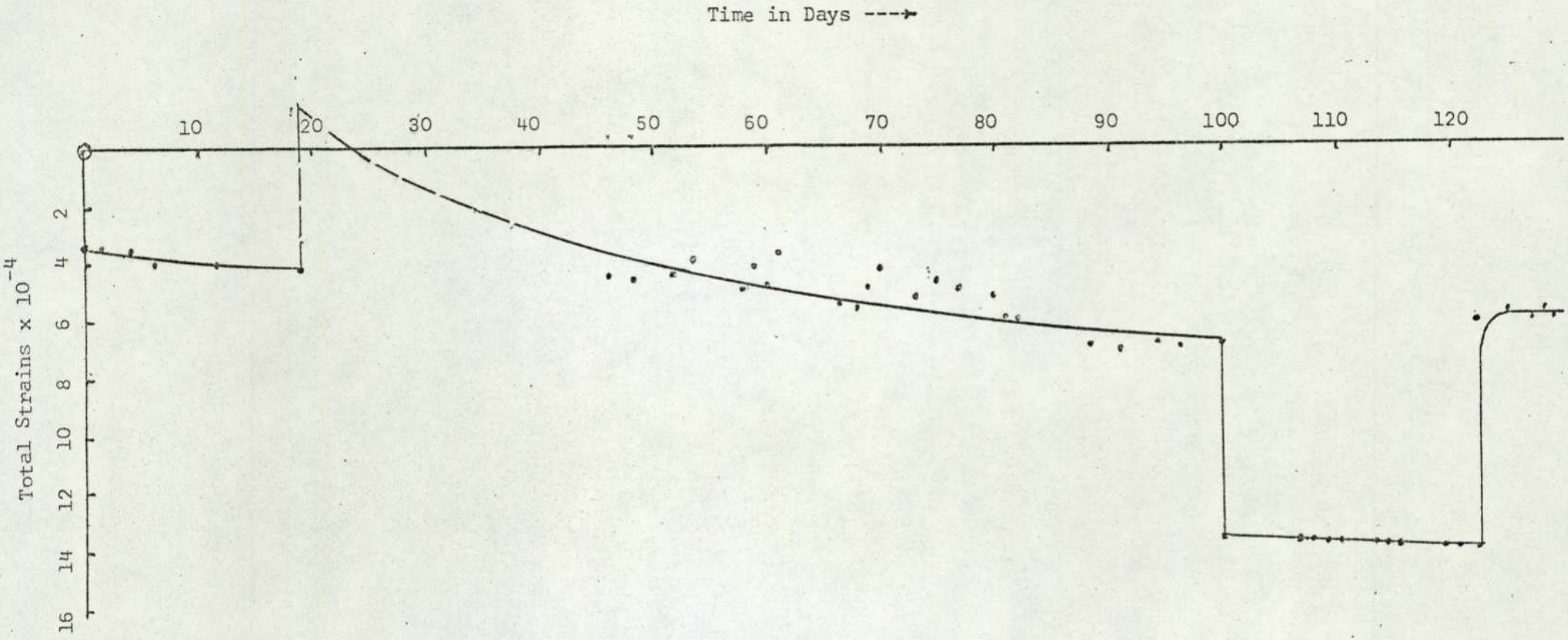


FIG 65 SERIES 1 SIDES 9/10 COMPO 1
THREE PITCH TOTAL STRAINS

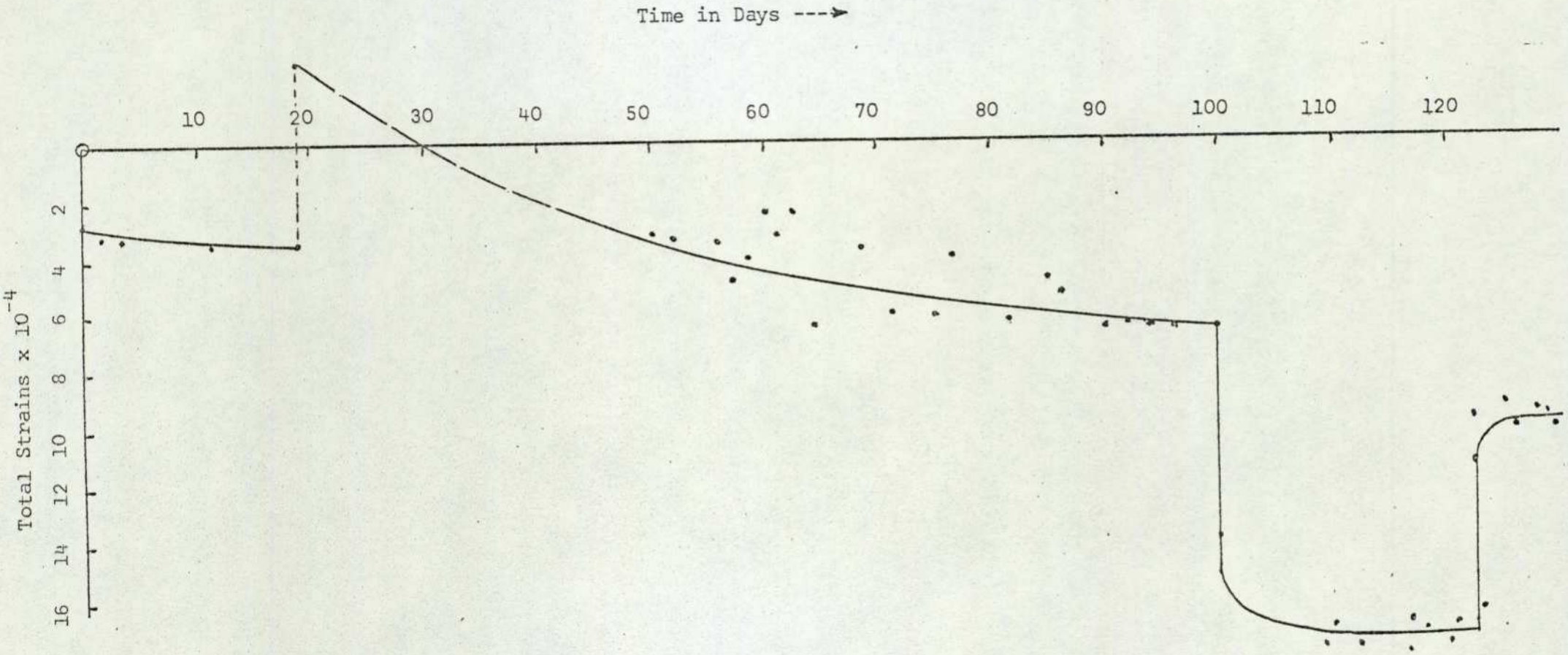


FIG 66 SERIES 1 SIDES 9/10 COMPO 1

OUTER SATELLITE TANGENTIAL STRAINS 2" G.L.

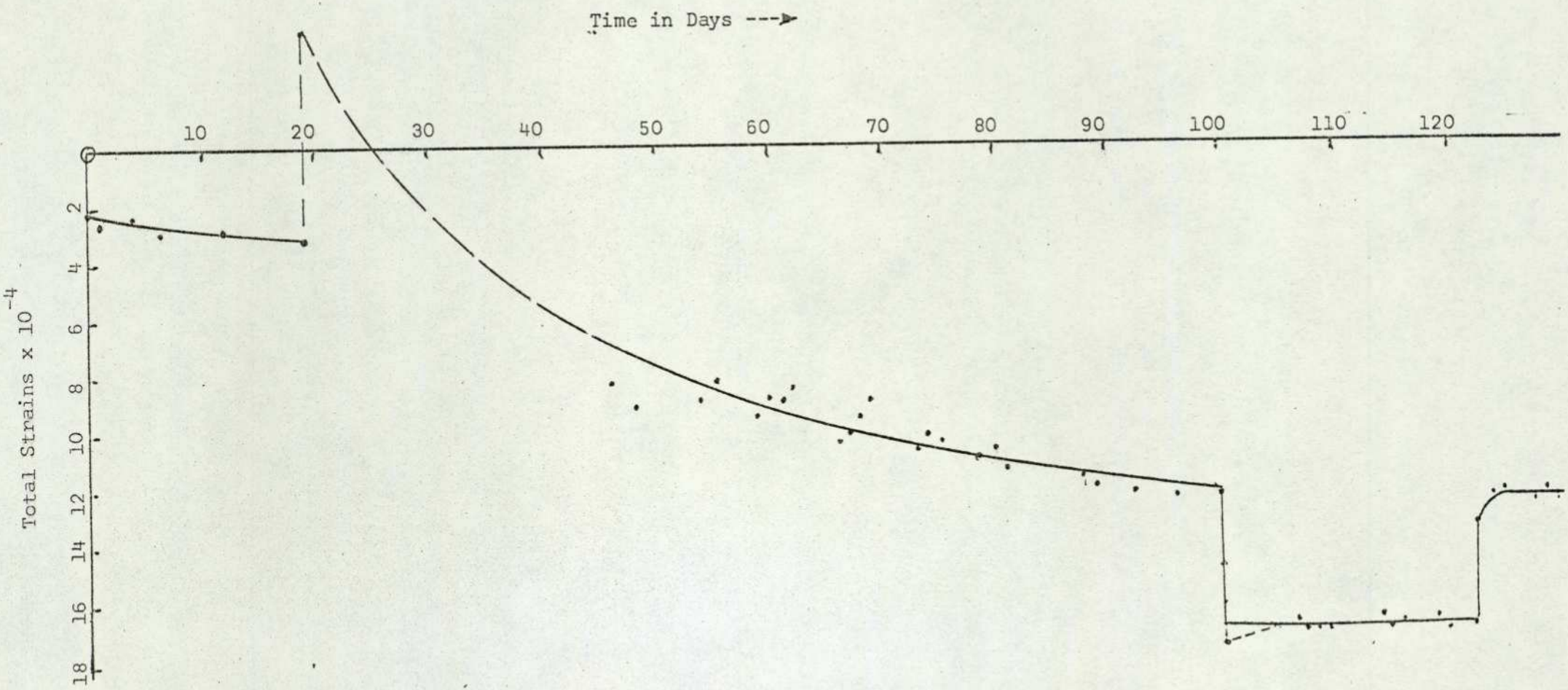


FIG 67 SERIES 1 SIDES 9/10 COMPO 1

OUTER SATELLITE RADIAL STRAINS 2" G.L.

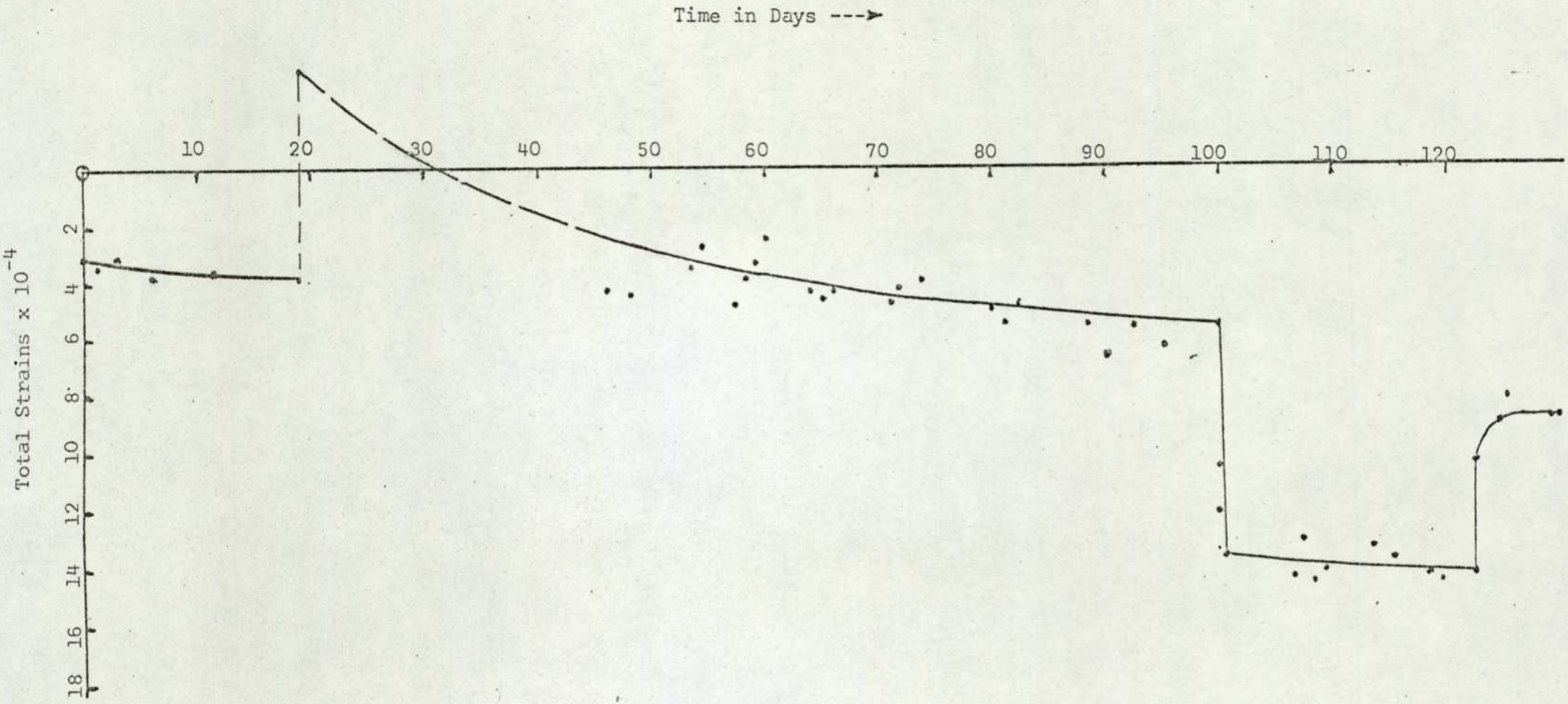


FIG 68 SERIES 1 SIDES 9/10 COMPO 1

INNER SATELLITE TANGENTIAL STRAINS 2" G.L.

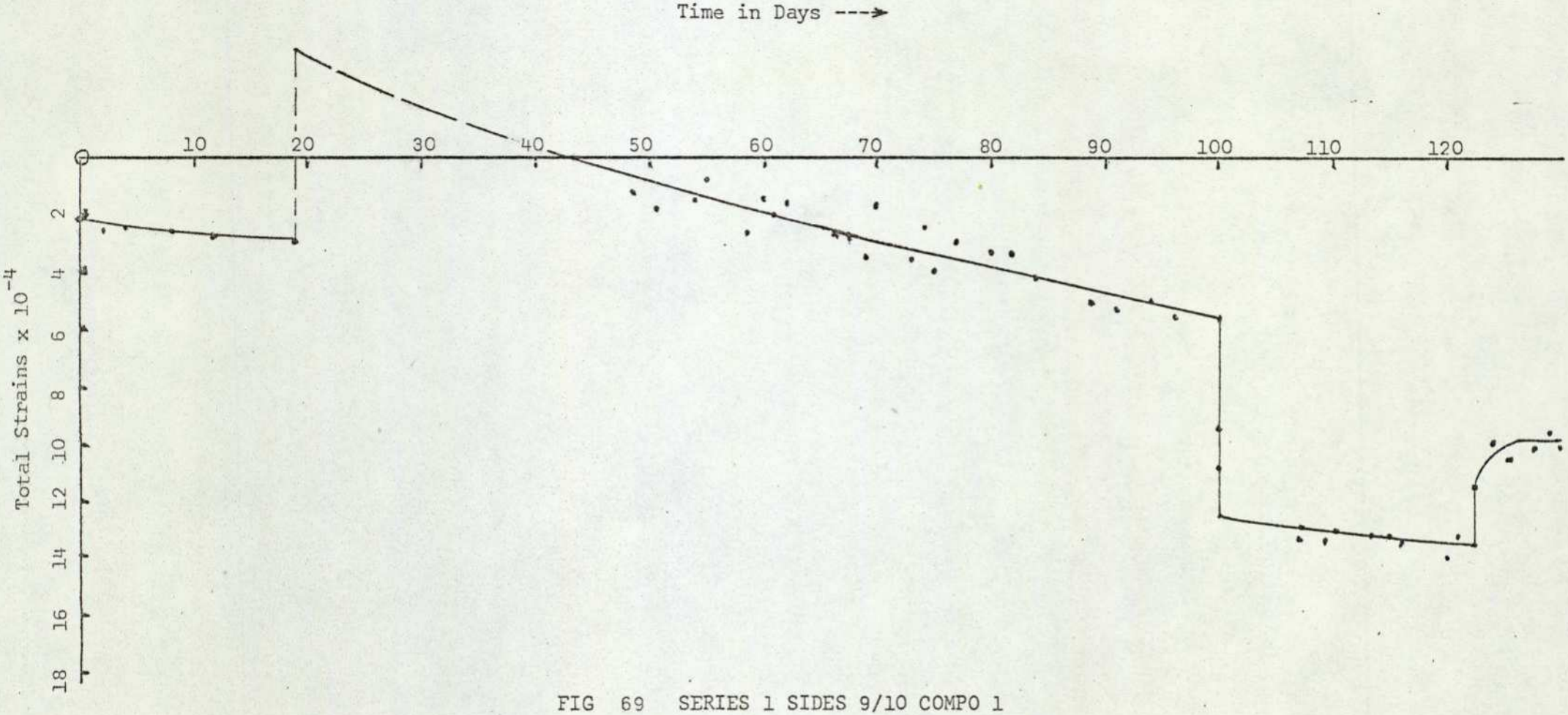


FIG 69 SERIES 1 SIDES 9/10 COMPO 1

INNER SATELLITE RADIAL STRAINS 2" G.L.

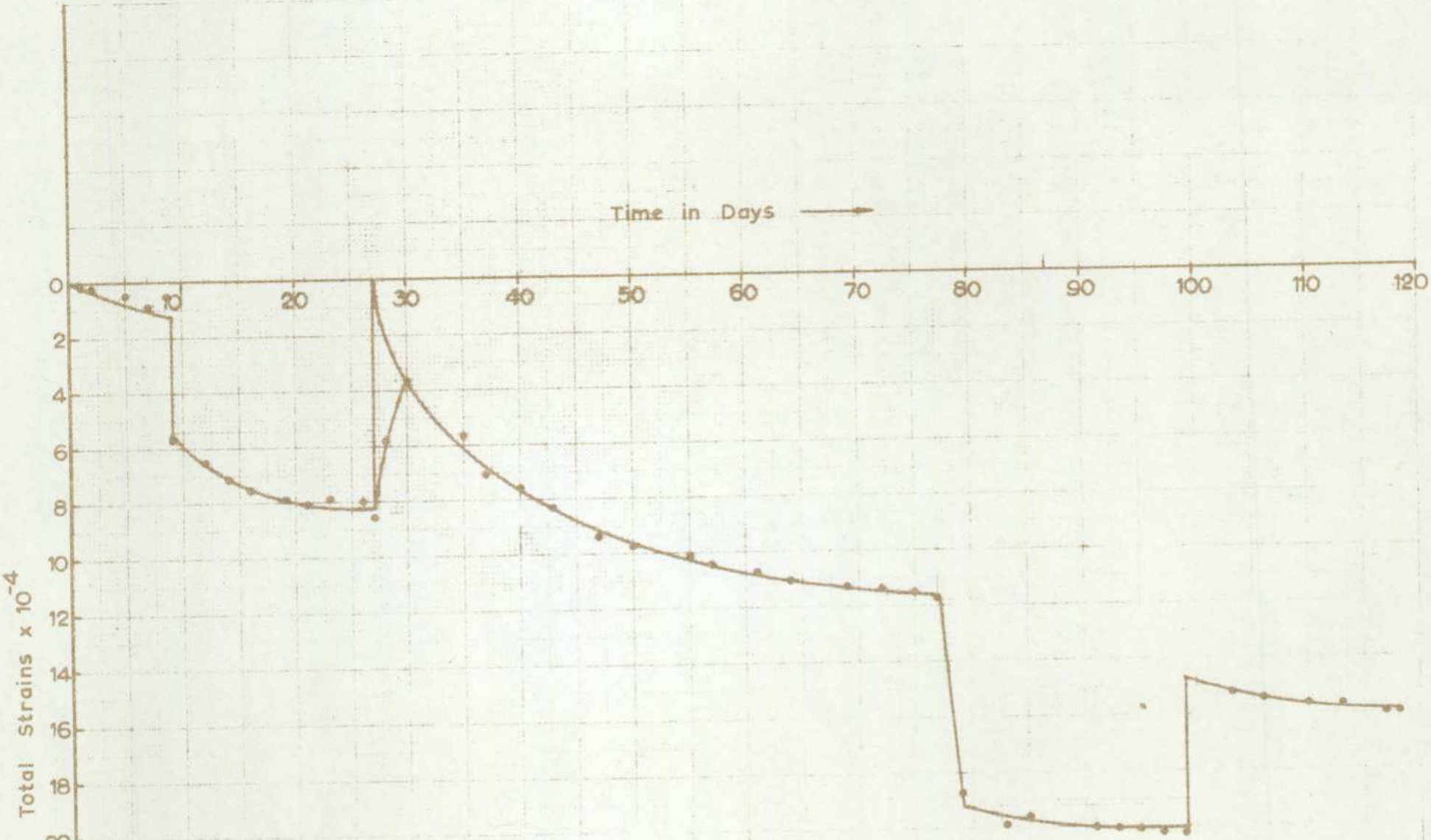


FIG 70 SERIES 2. SIDES I/2.

TANGENTIAL TOTAL STRAINS.

2" G.L.

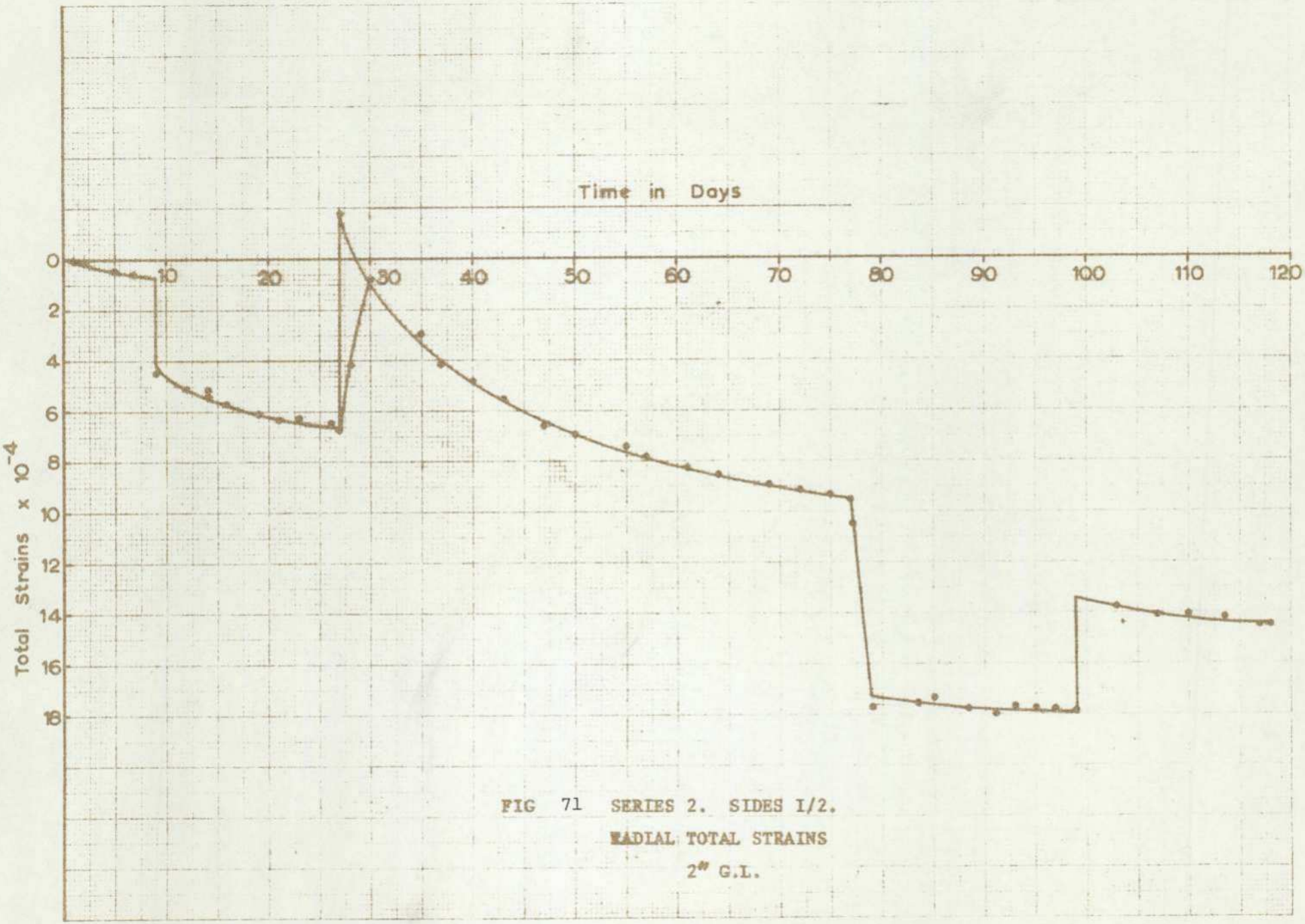


FIG 71 SERIES 2. SIDES I/2.
RADIAL TOTAL STRAINS
2" G.L.

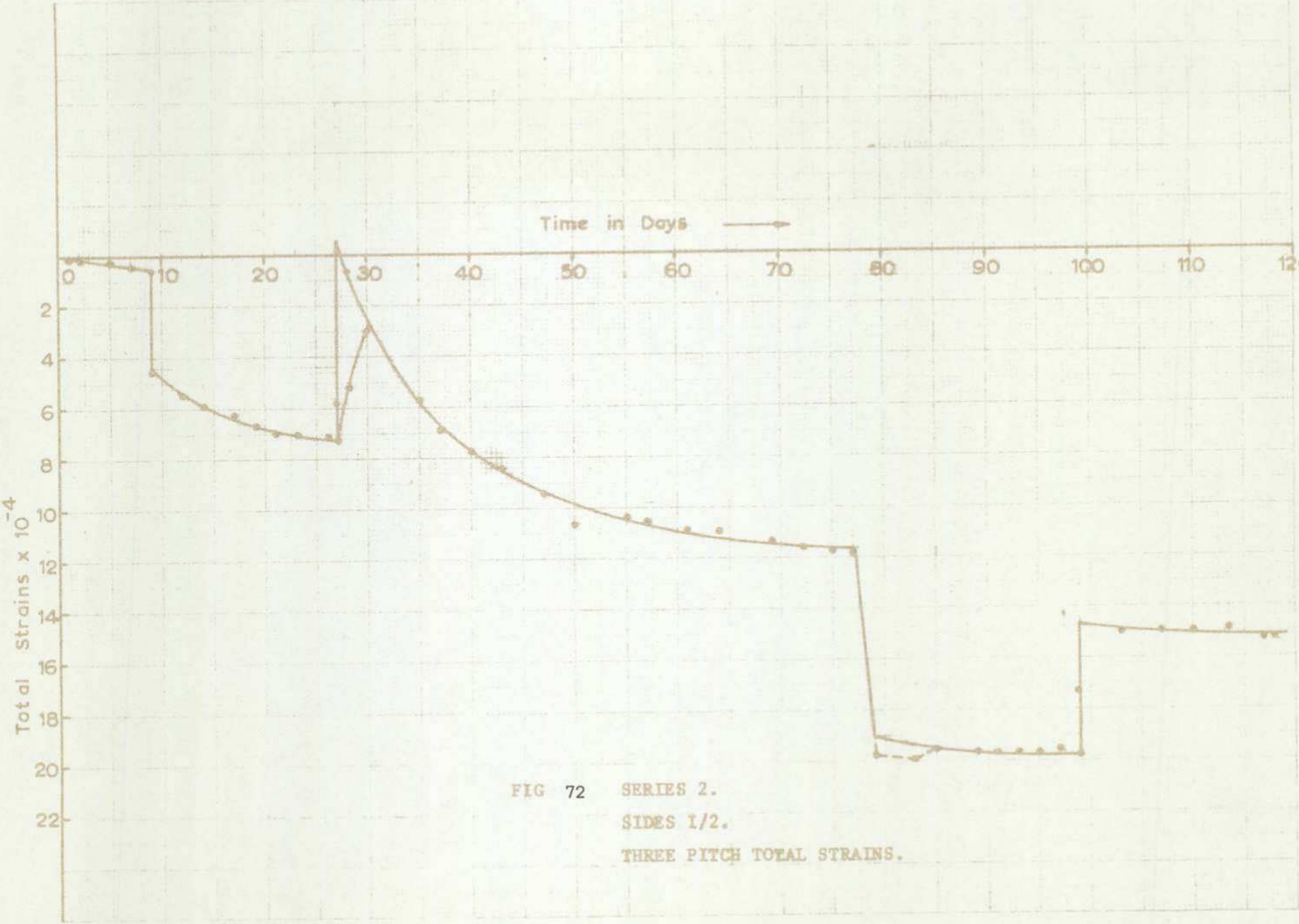


FIG 72 SERIES 2.
SIDES 1/2.
THREE PITCH TOTAL STRAINS.

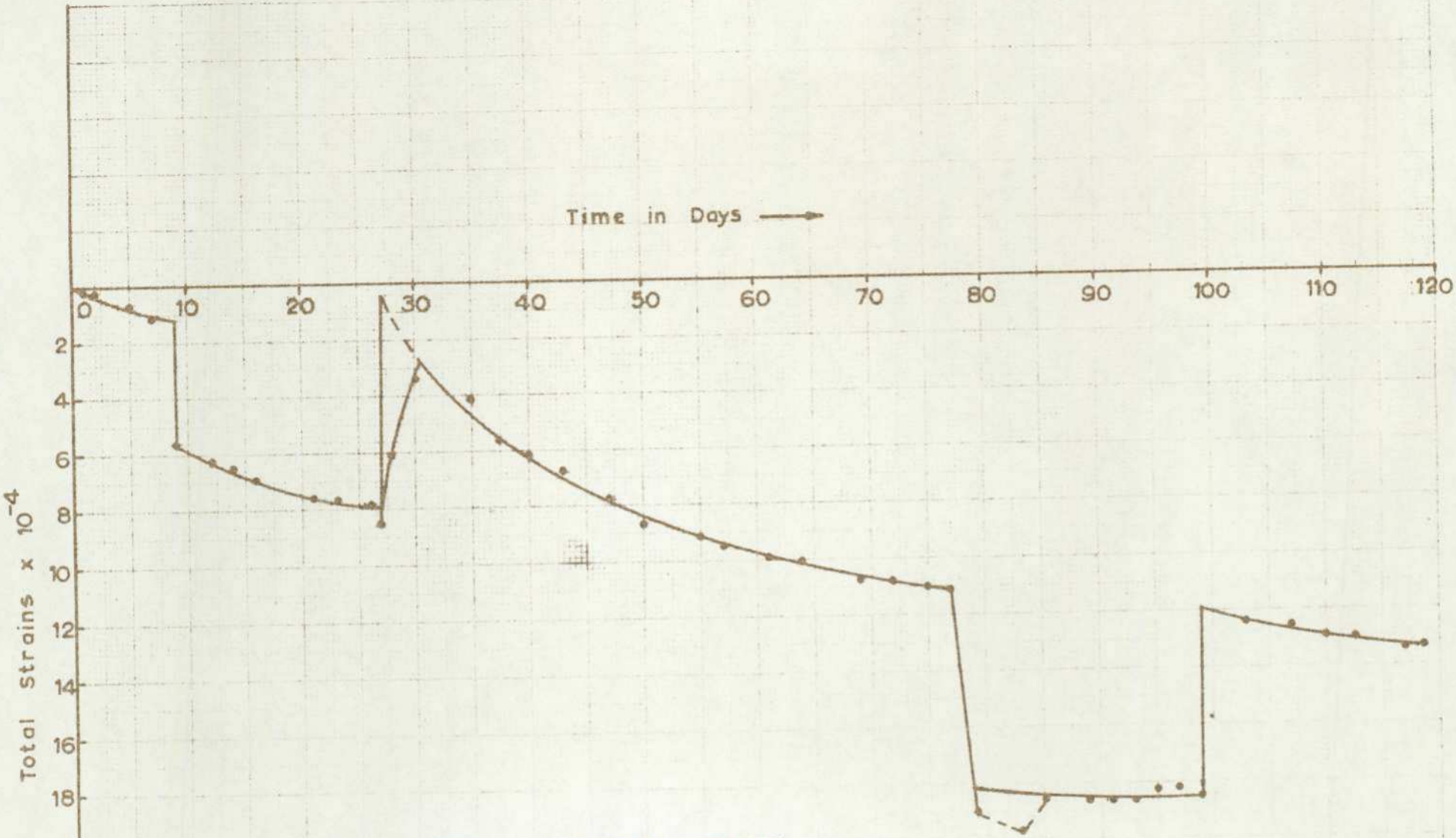


FIG 73 SERIES 2. SIDES 3/4.
TANGENTIAL TOTAL STRAINS. 2" G.L.

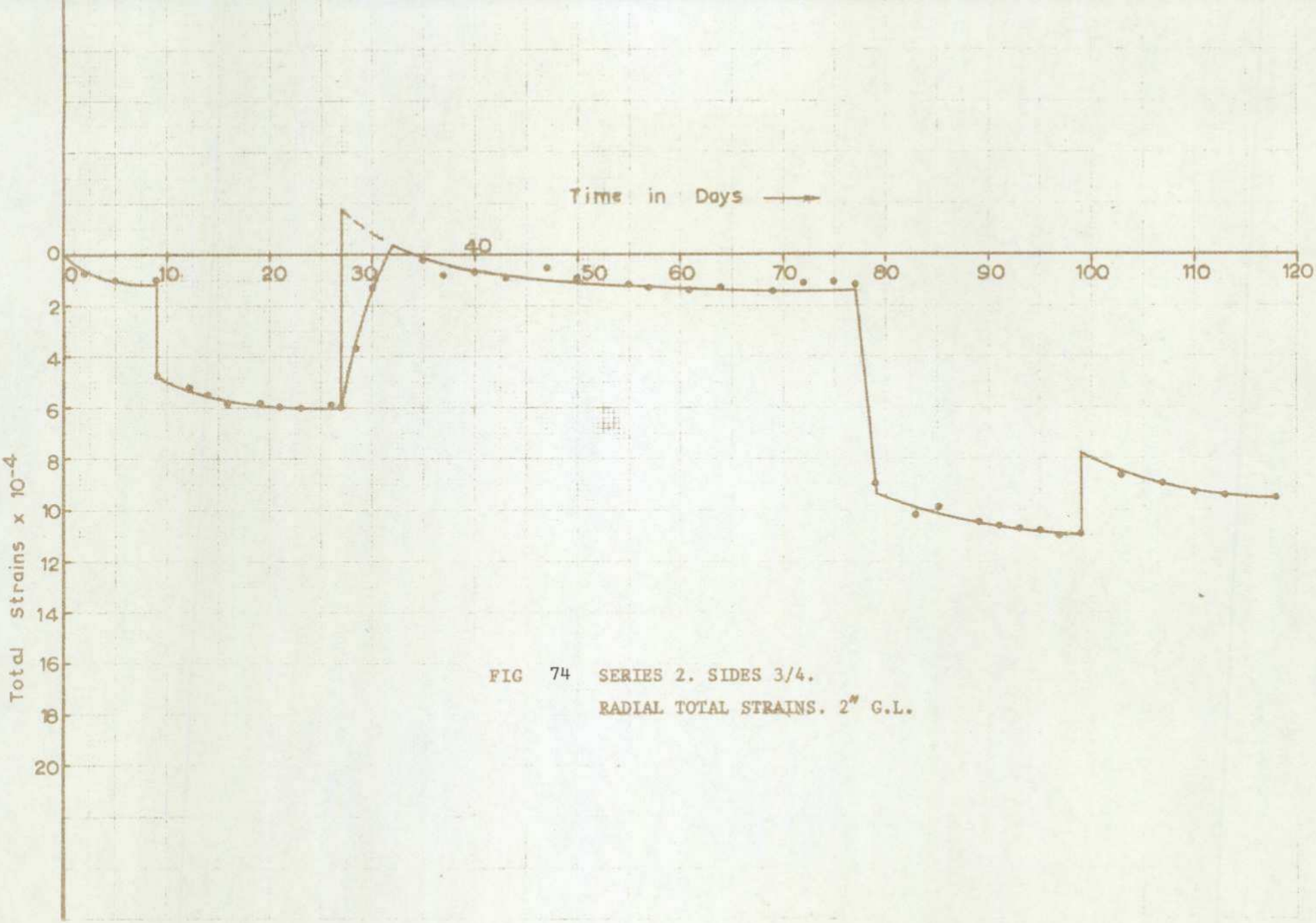


FIG 74 SERIES 2. SIDES 3/4.
RADIAL TOTAL STRAINS. 2" G.L.

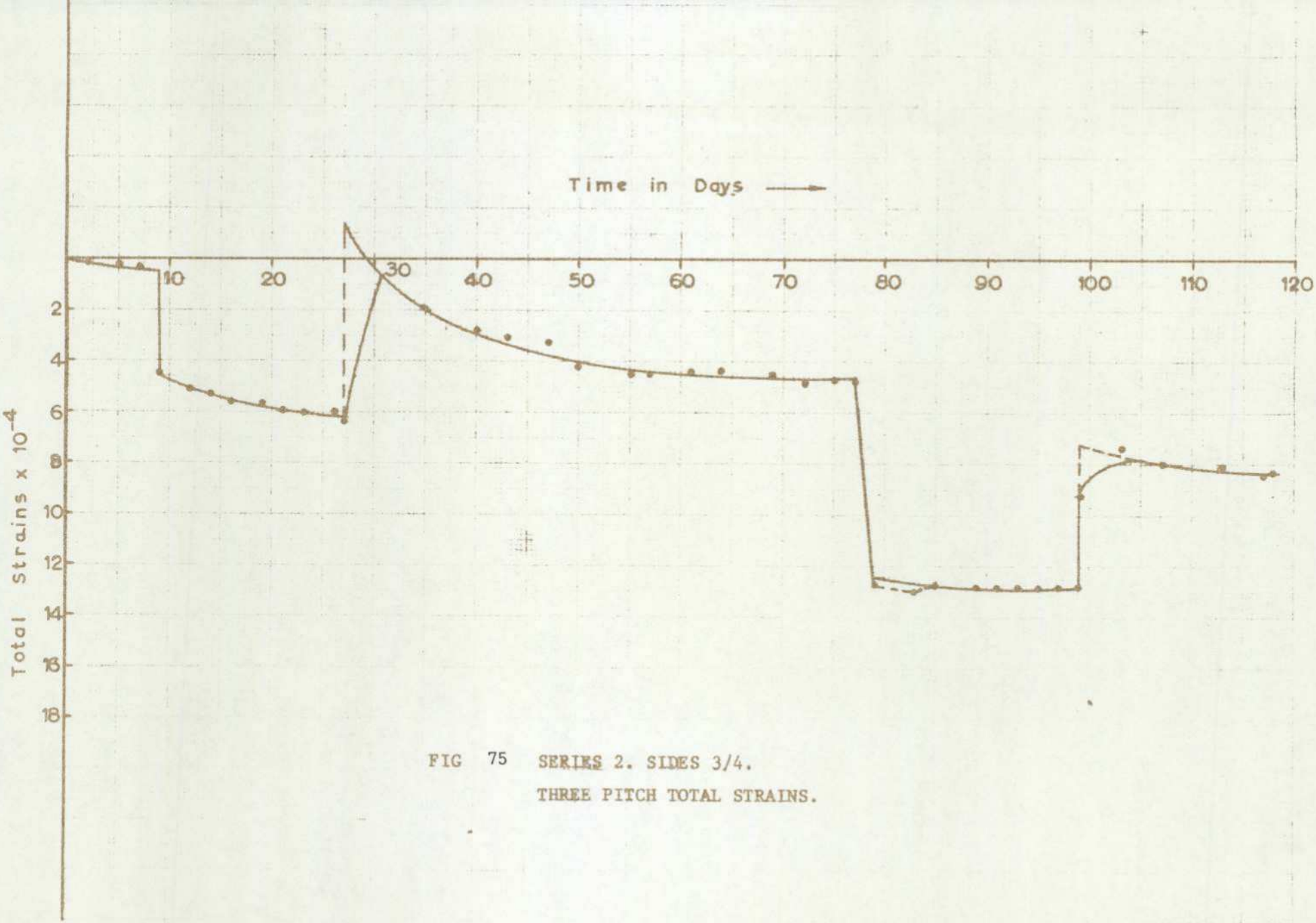


FIG 75 SERIES 2. SIDES 3/4.
THREE PITCH TOTAL STRAINS.

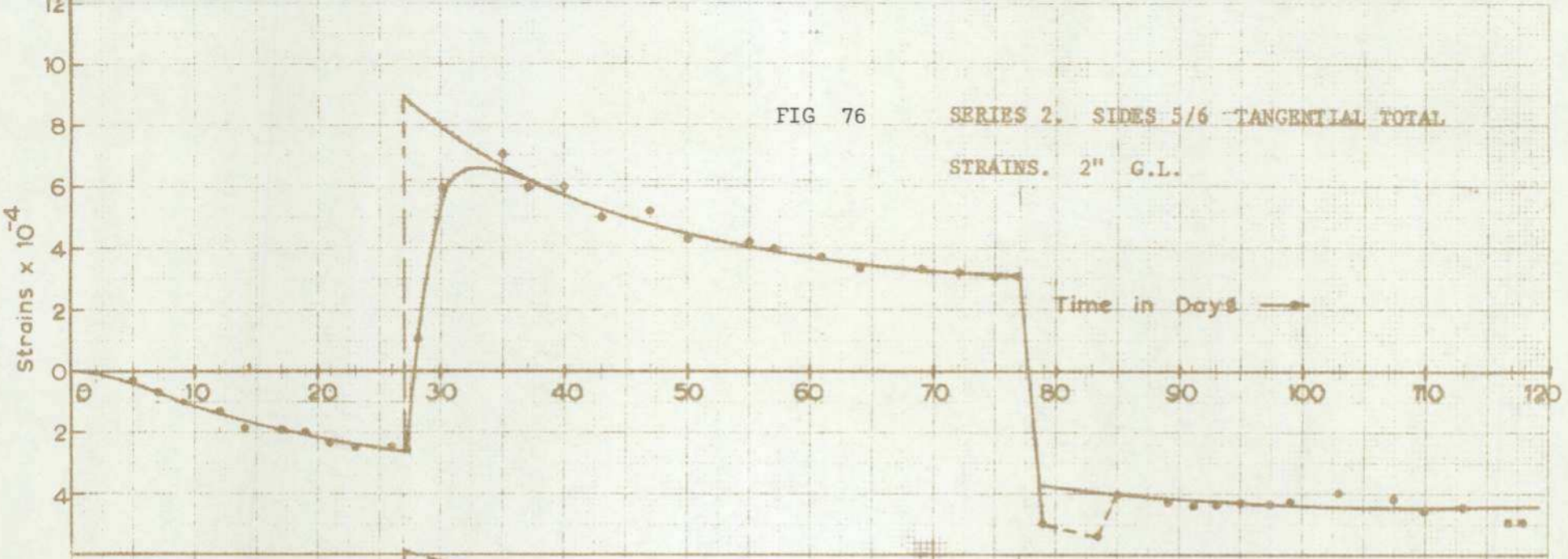


FIG 76 SERIES 2. SIDES 5/6 TANGENTIAL TOTAL STRAINS. 2" G.L.

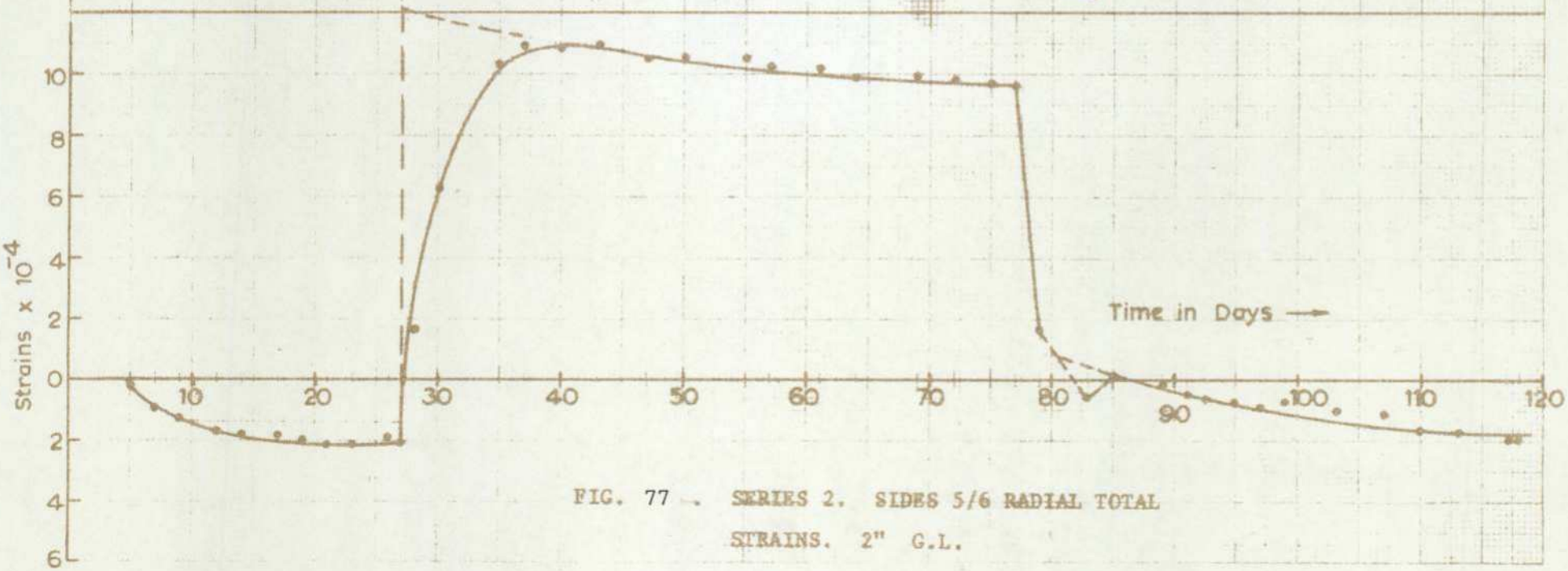


FIG. 77 . SERIES 2. SIDES 5/6 RADIAL TOTAL STRAINS. 2" G.L.

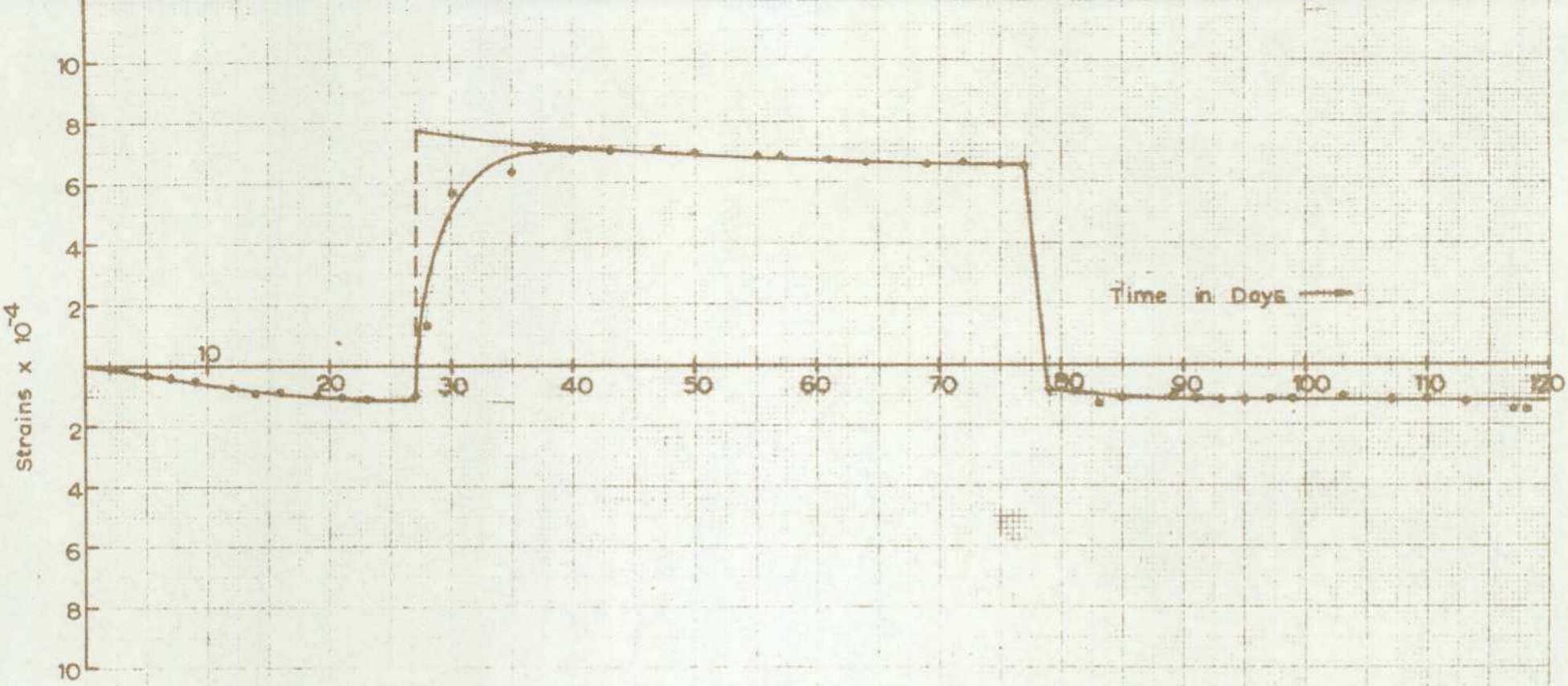


FIG 78 . SERIES 2. SIDES 5/6.
THREE PITCH TOTAL STRAINS.

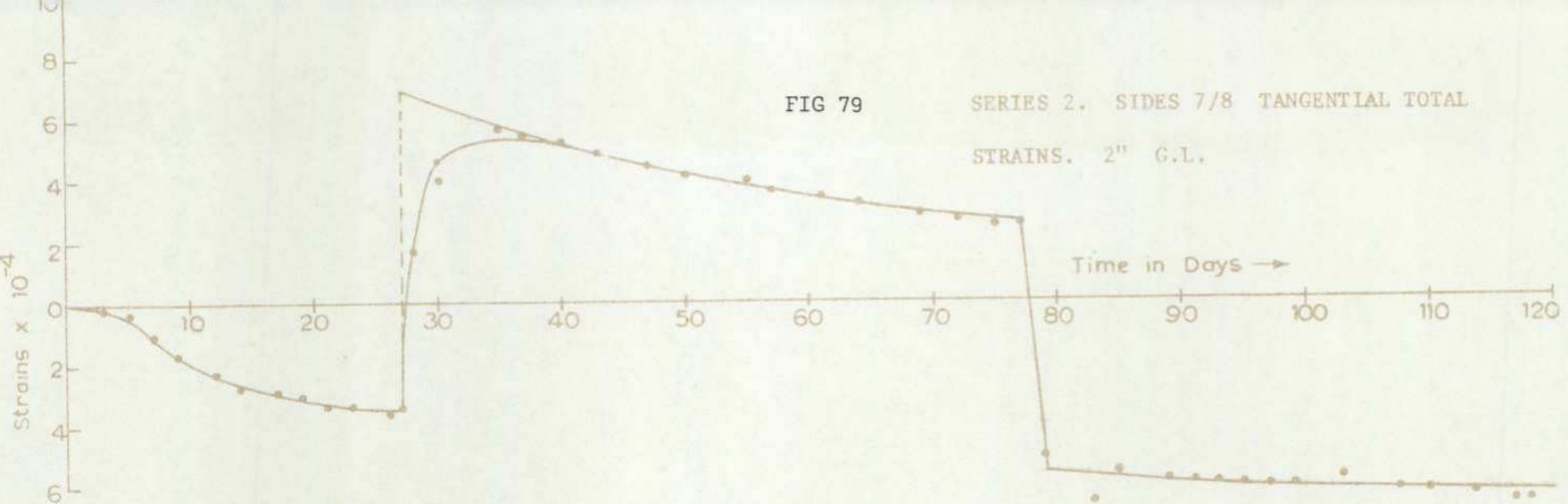


FIG 79 SERIES 2. SIDES 7/8 TANGENTIAL TOTAL STRAINS. 2" G.L.

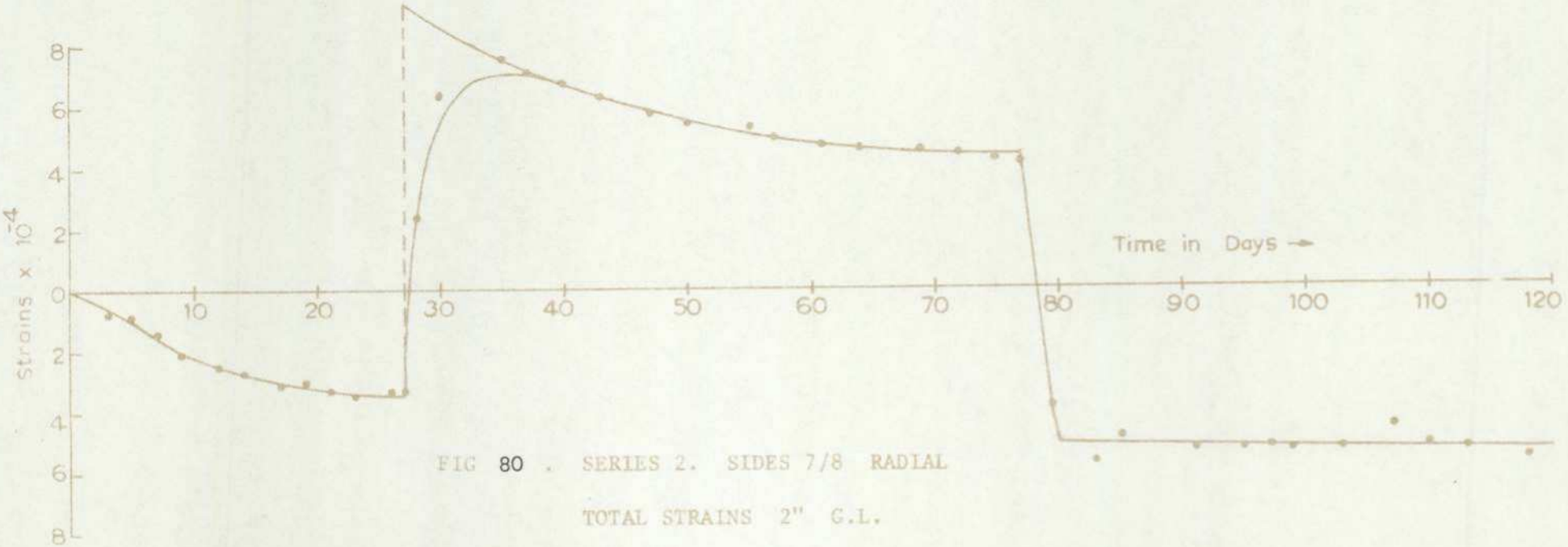


FIG 80 . SERIES 2. SIDES 7/8 RADIAL TOTAL STRAINS 2" G.L.

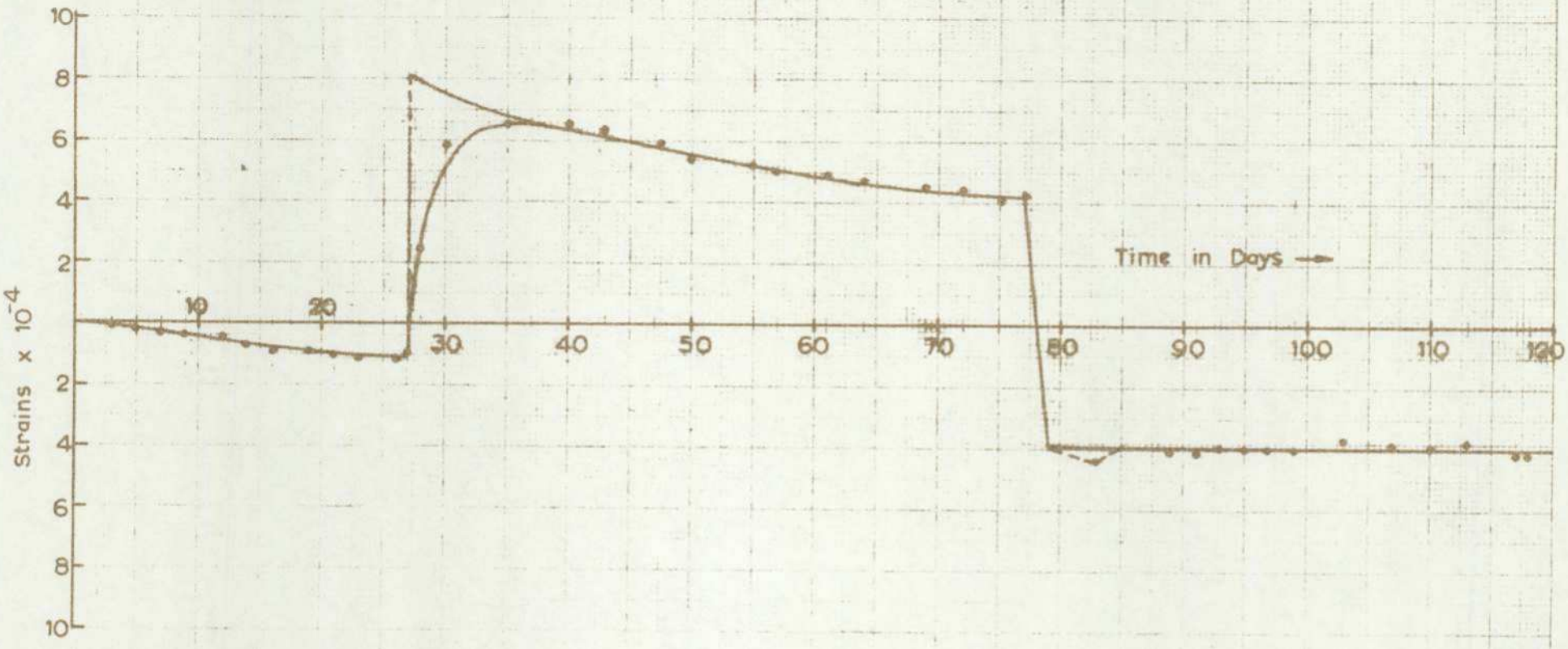


FIG 81 . SERIES 2. SIDES 7/8
THREE PITCH TOTAL STRAINS.

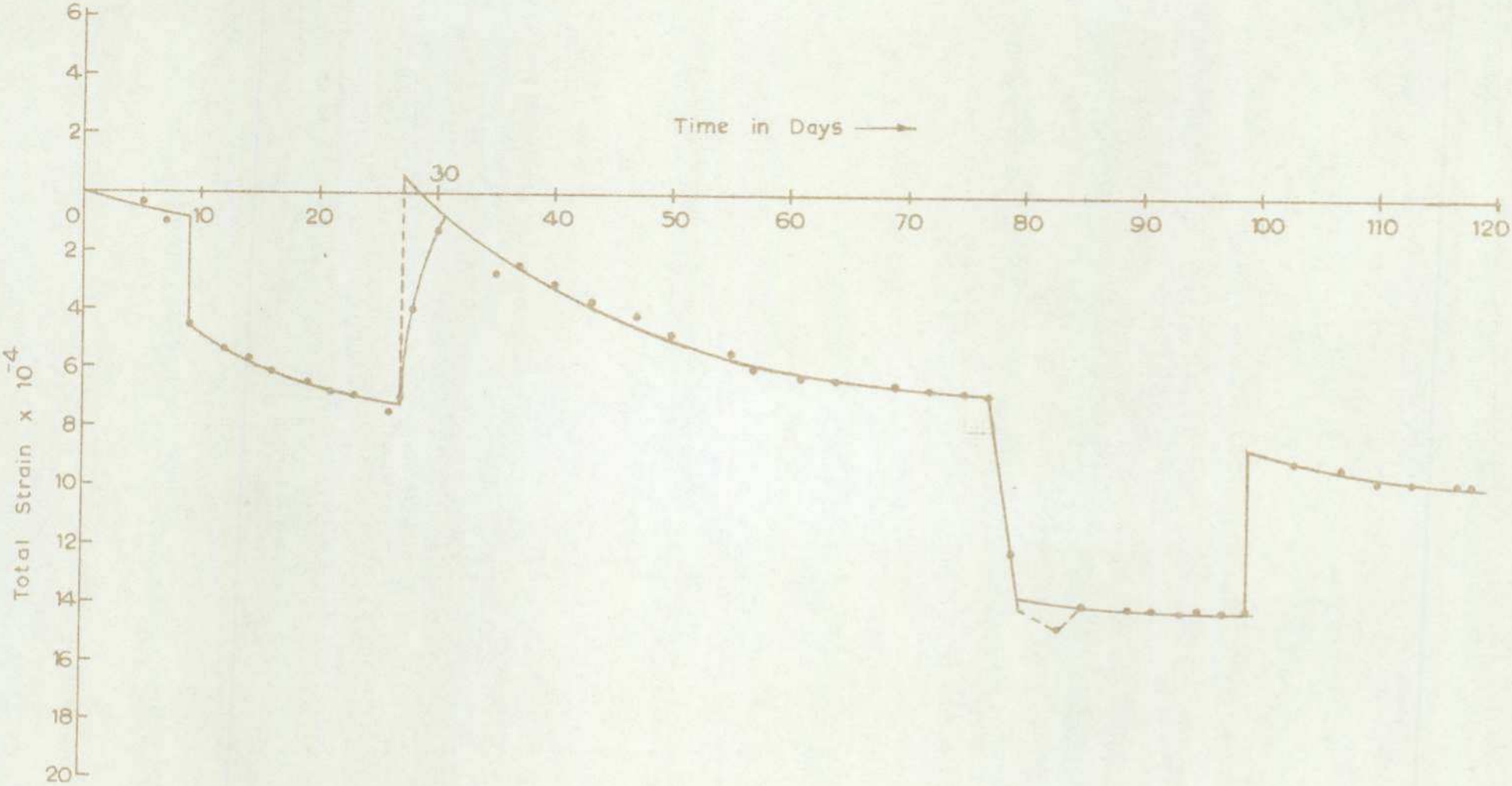


FIG 82 . SERIES 2. SIDES 9/10

TANGENTIAL TOTAL STRAINS 2" G.L.

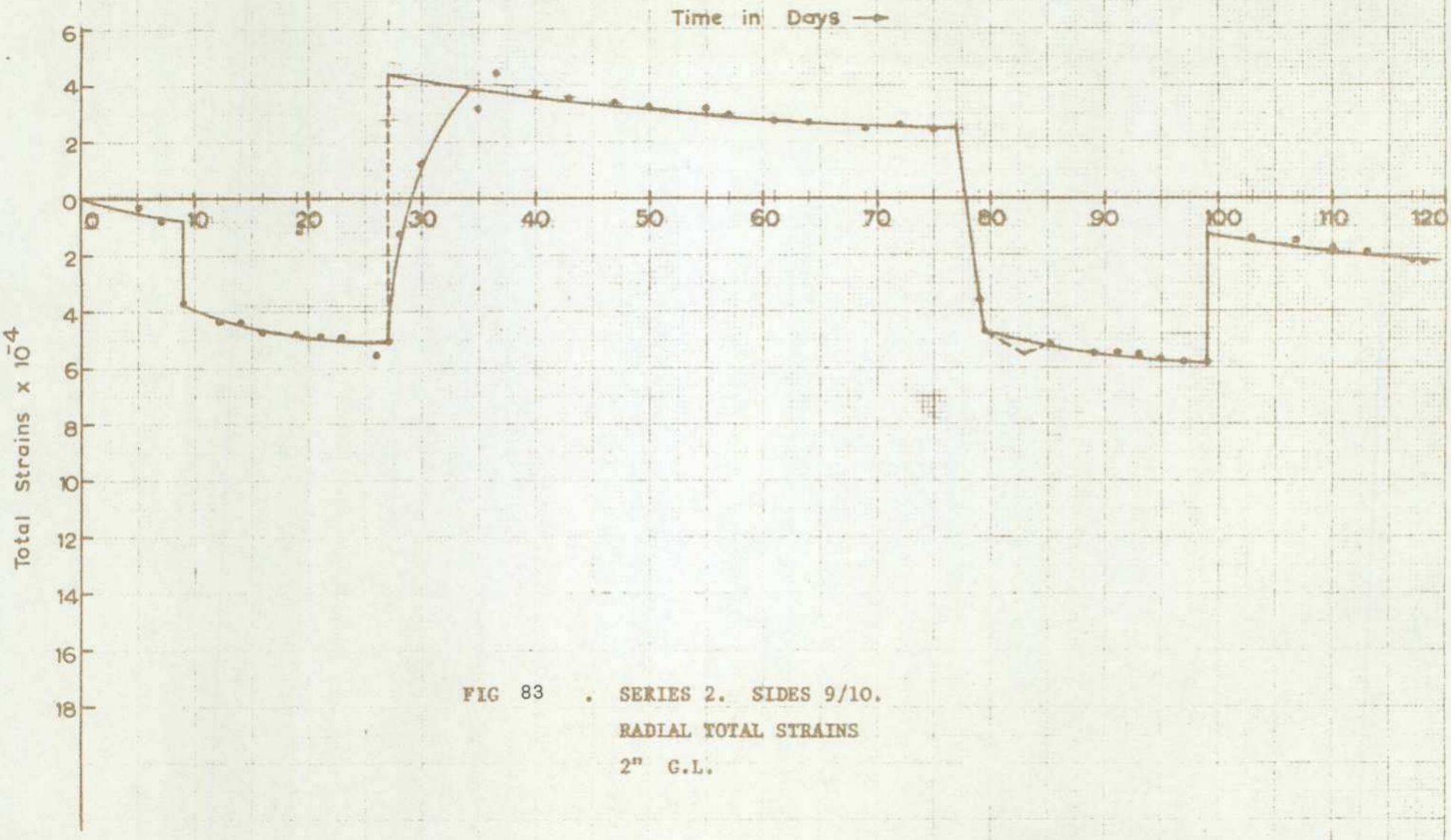


FIG 83 . SERIES 2. SIDES 9/10.
RADIAL TOTAL STRAINS
2" G.L.

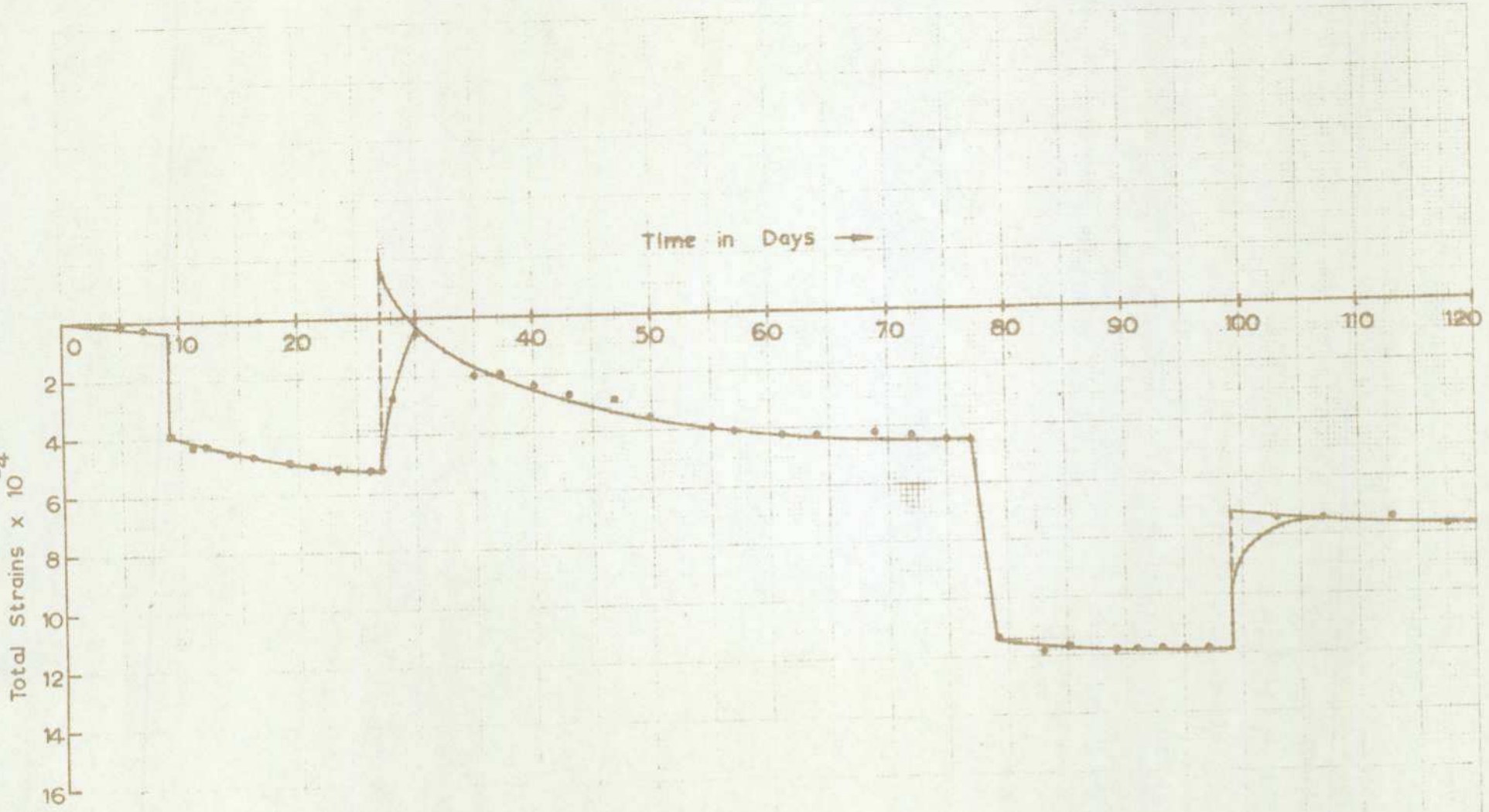


FIG 84 . SERIES 2. SIDES 9/10. THREE PITCH TOTAL STRAINS.

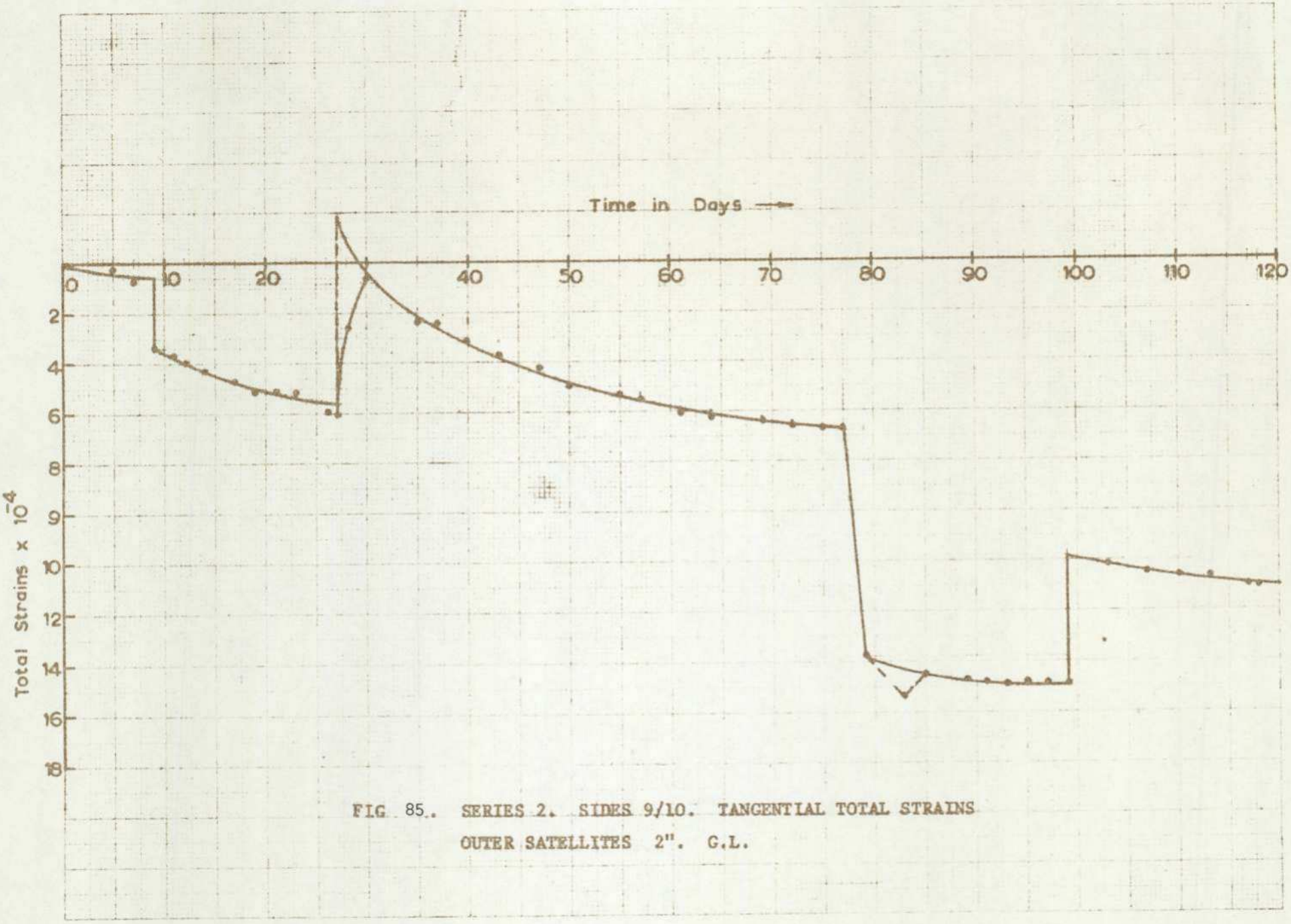


FIG 85. SERIES 2. SIDES 9/10. TANGENTIAL TOTAL STRAINS
OUTER SATELLITES 2". G.L.

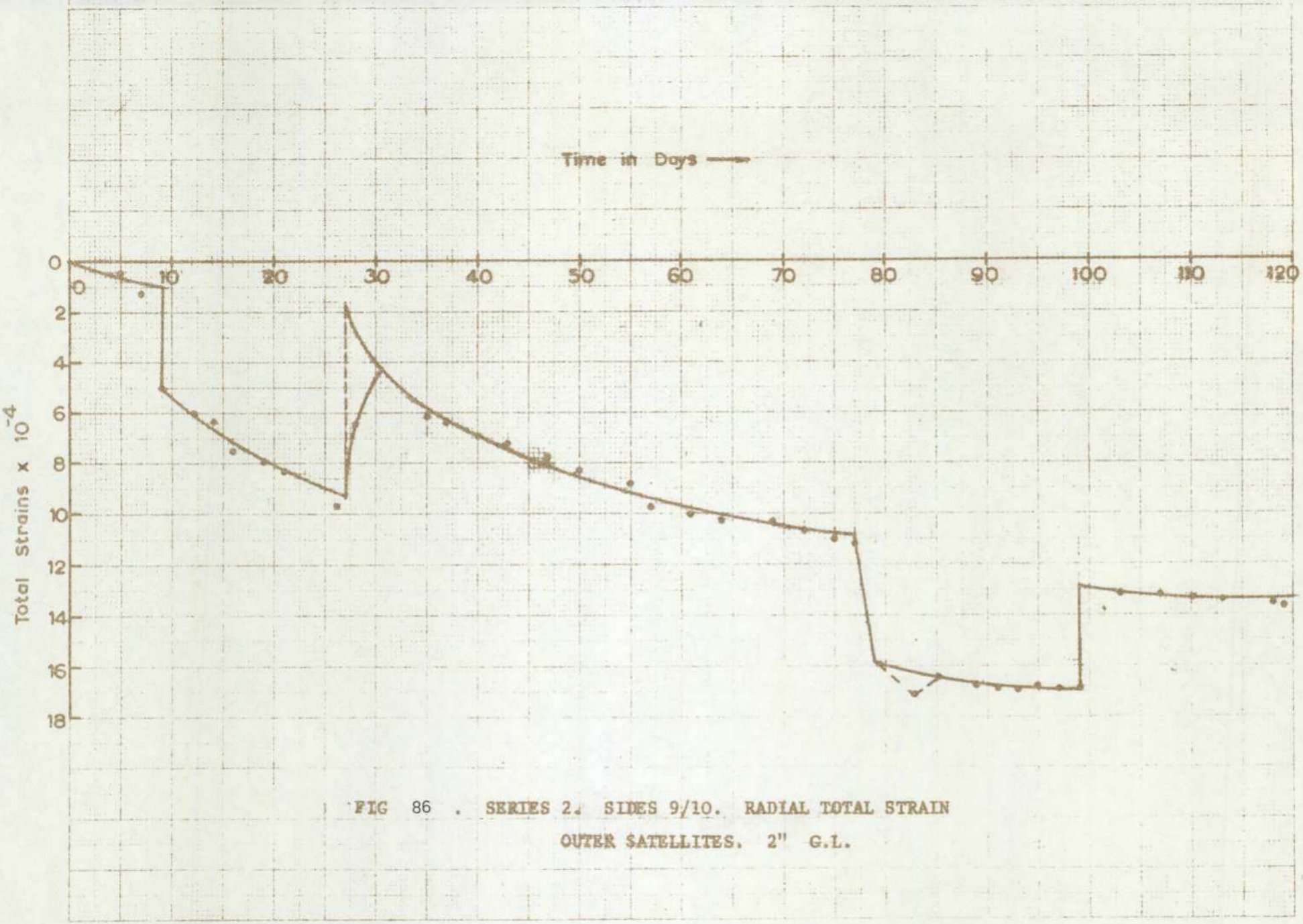


FIG 86 . SERIES 2. SIDES 9/10. RADIAL TOTAL STRAIN
OUTER SATELLITES. 2" G.L.

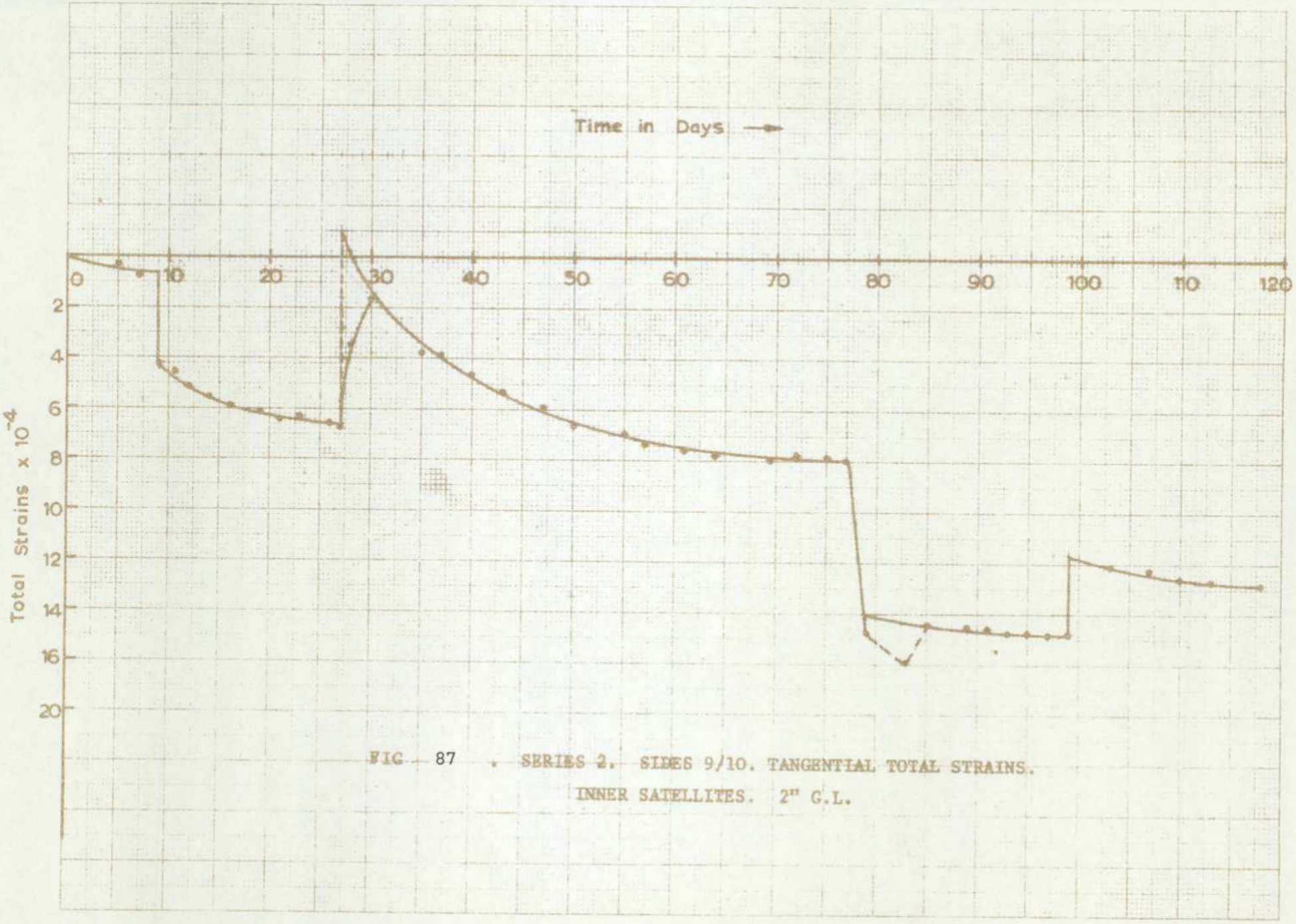


FIG. 87 . SERIES 2. SIDES 9/10. TANGENTIAL TOTAL STRAINS.
INNER SATELLITES. 2" G.L.

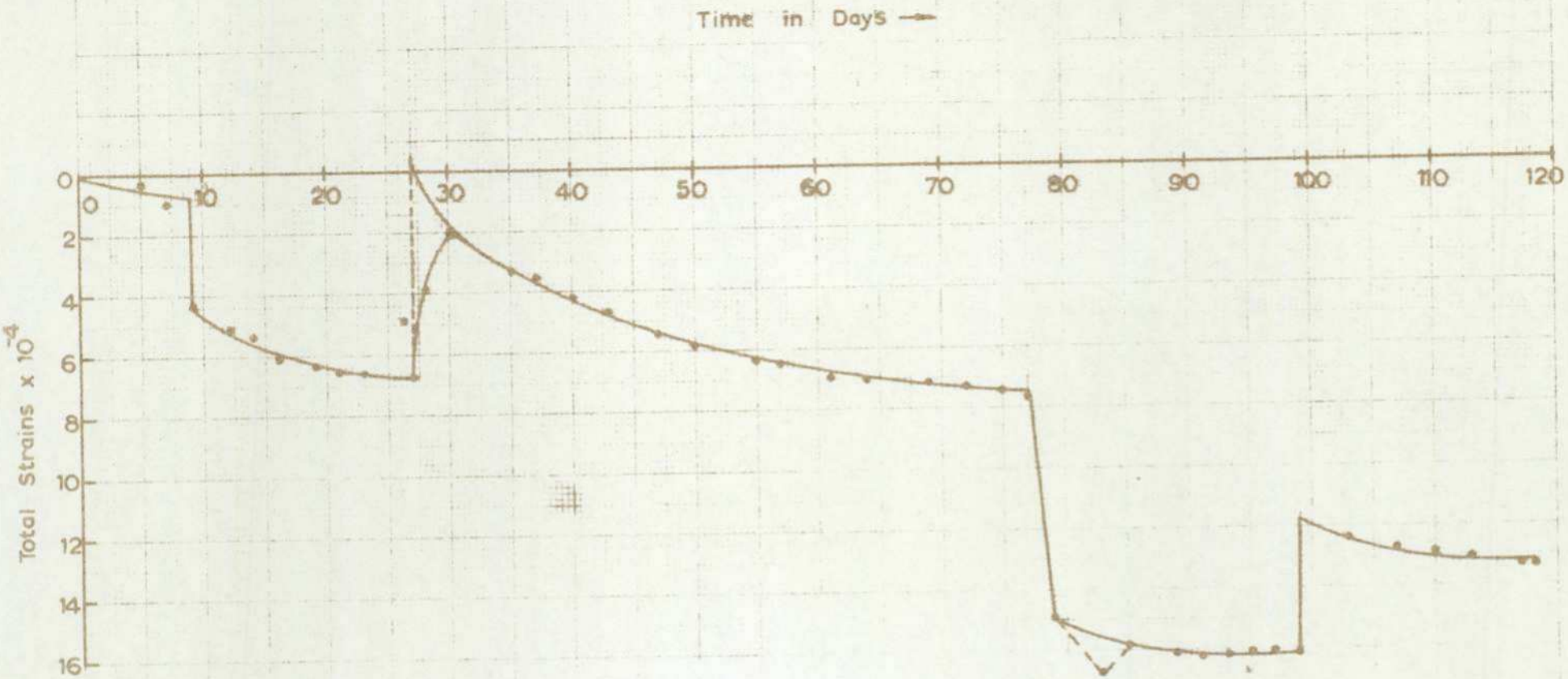


FIG 88 . SERIES 2. SIDES 9/10. RADIAL TOTAL STRAINS.
INNER SATELLITES. 2". G.L.

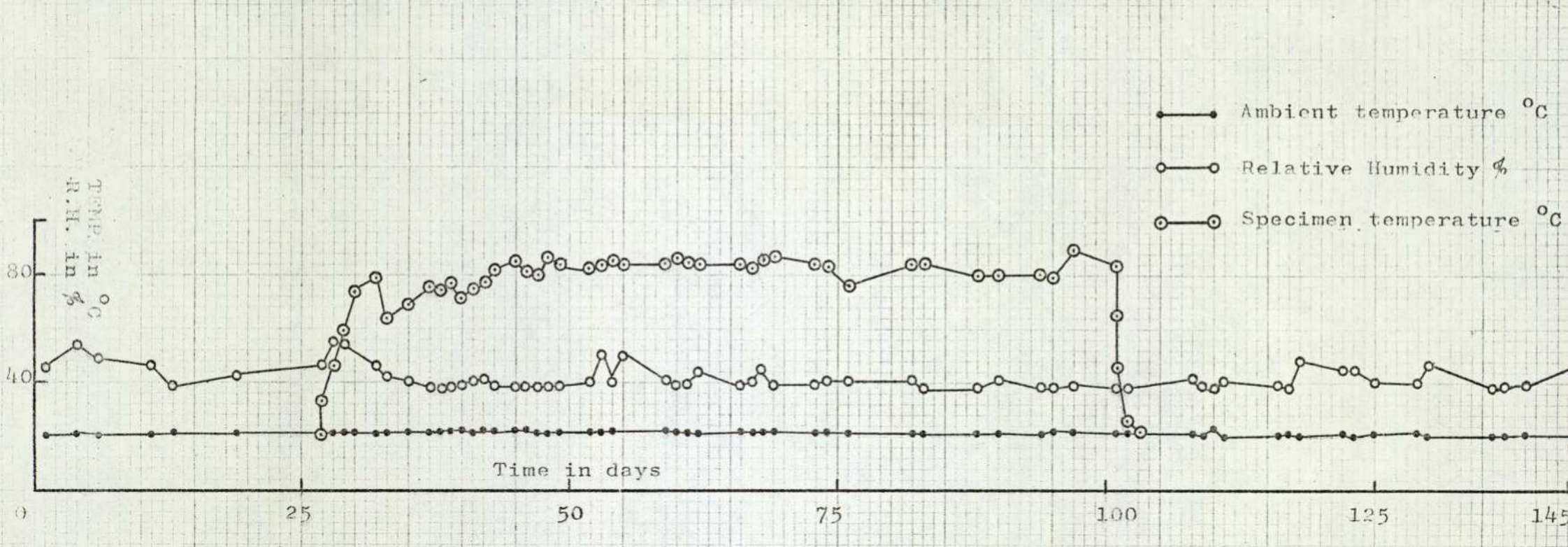


FIG. 89 SERIES 1
MODEL 1/2 TEMPERATURE AND RELATIVE HUMIDITY

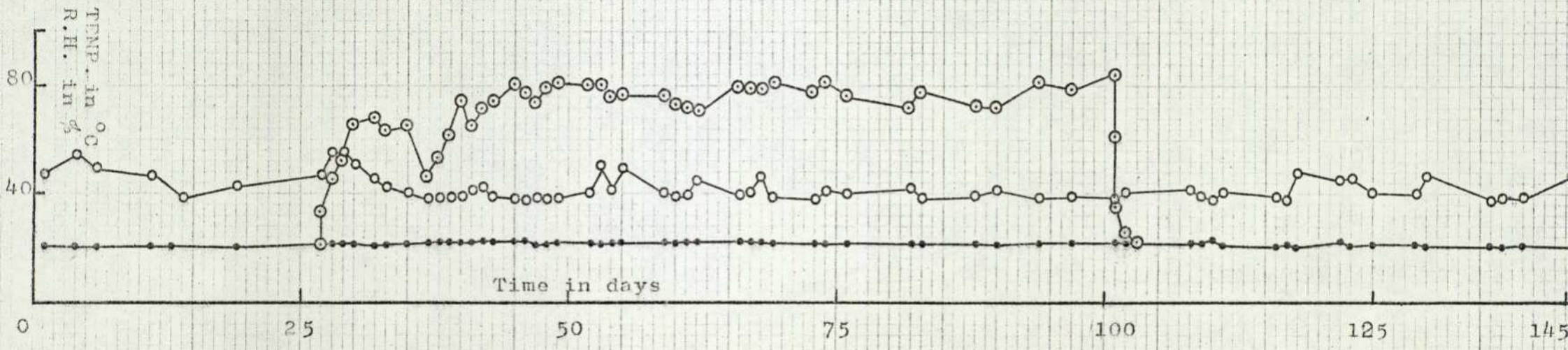


FIG. 90 SERIES 1
MODEL 3/4, TEMPERATURE AND RELATIVE HUMIDITY

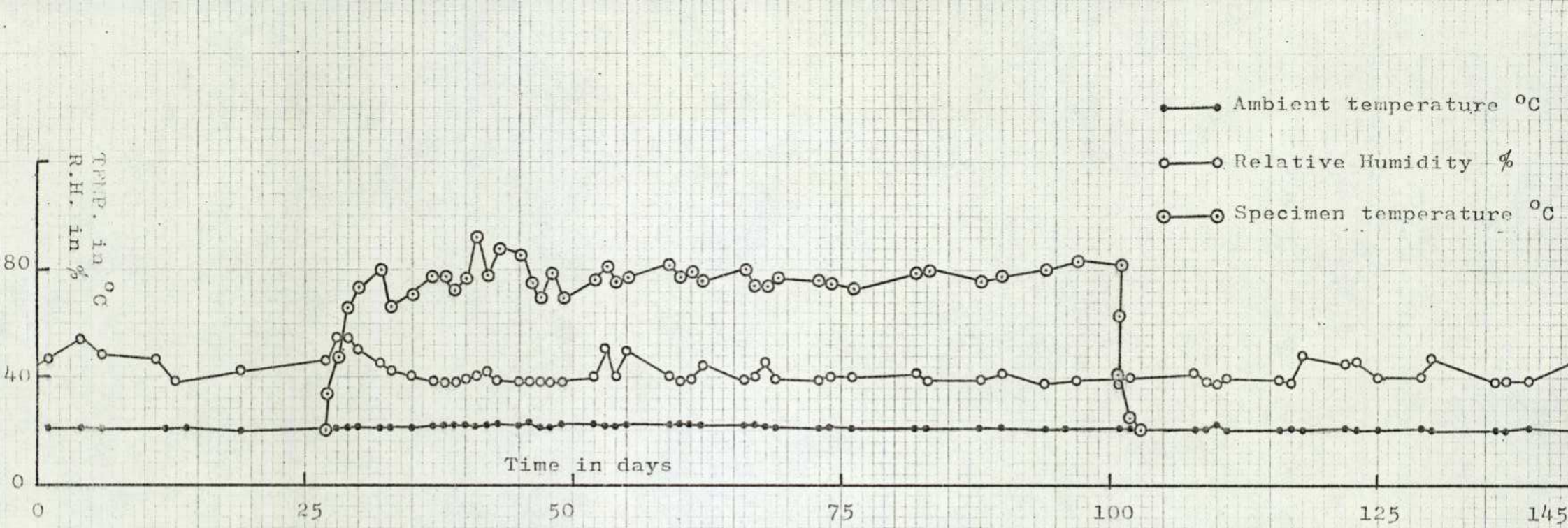


FIG. 91 SERIES 1
MODEL 5/6, TEMPERATURE AND RELATIVE HUMIDITY

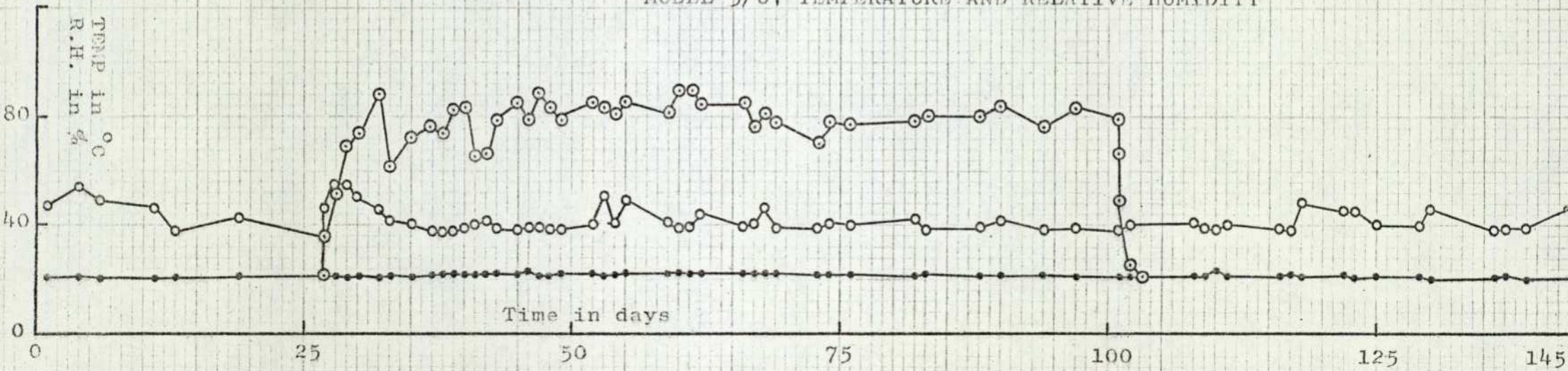


FIG. 92 SERIES 1
MODEL 7/8, TEMPERATURE AND RELATIVE HUMIDITY

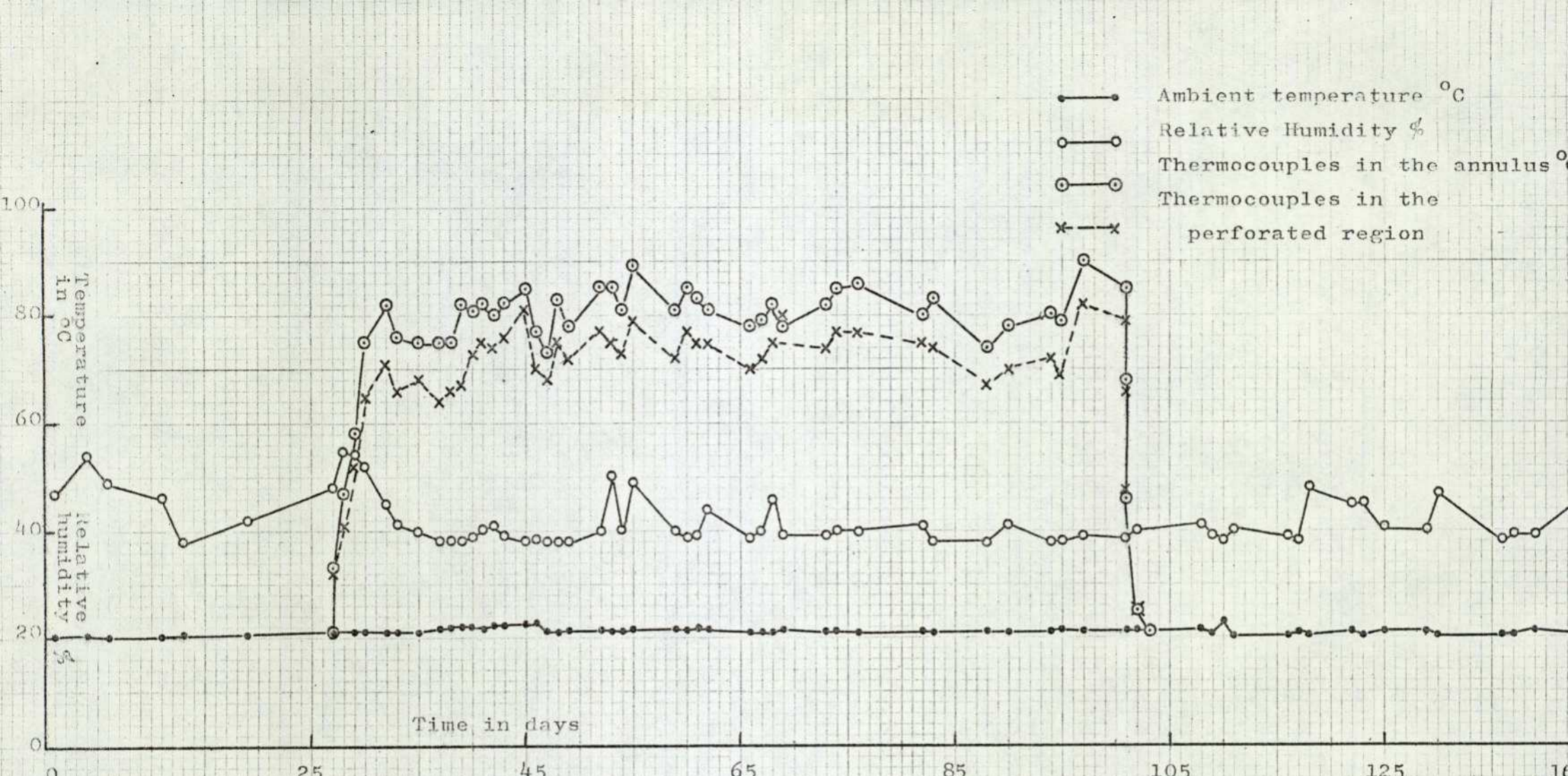


FIG. 93 SERIES 1
MODEL 9/10 COMPOSITE CREEP SPECIMEN

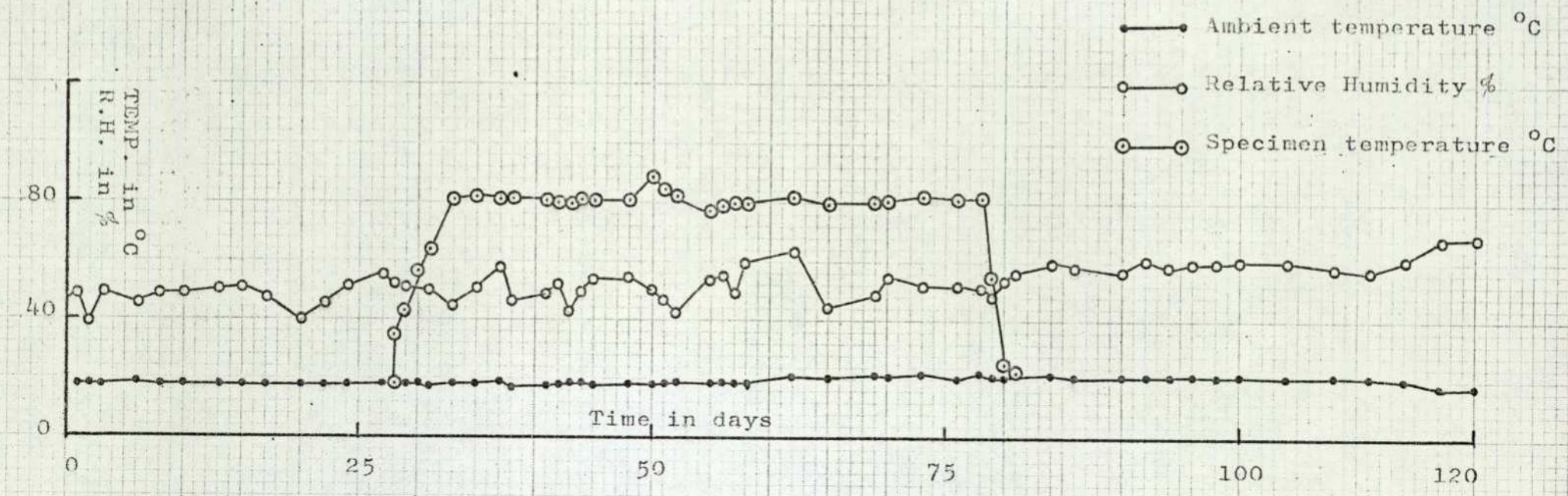


FIG. 94 SERIES 2
MODEL 1/2, TEMPERATURE AND RELATIVE HUMIDITY

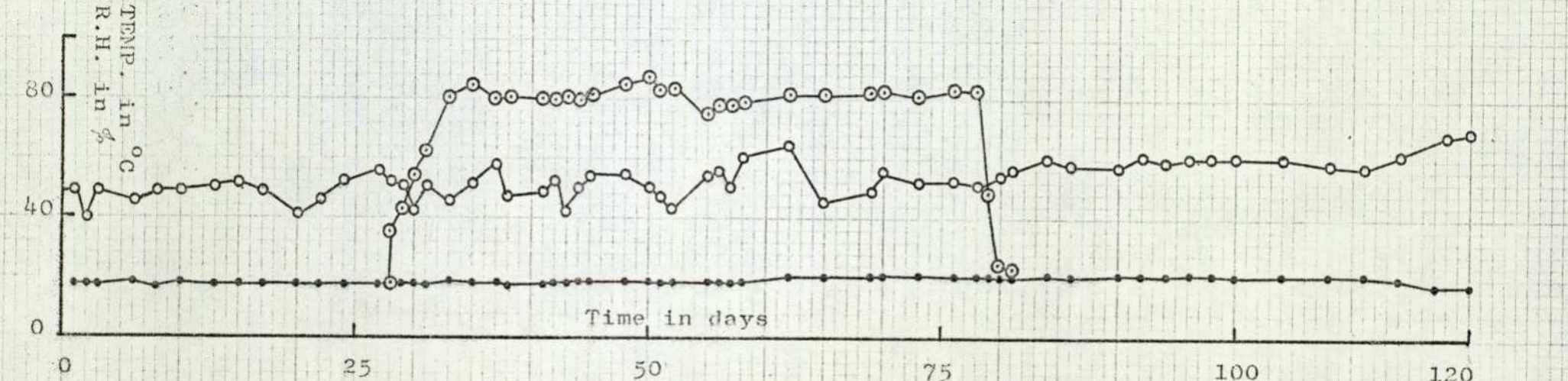


FIG. 95 SERIES 2
MODEL 3/4, TEMPERATURE AND RELATIVE HUMIDITY

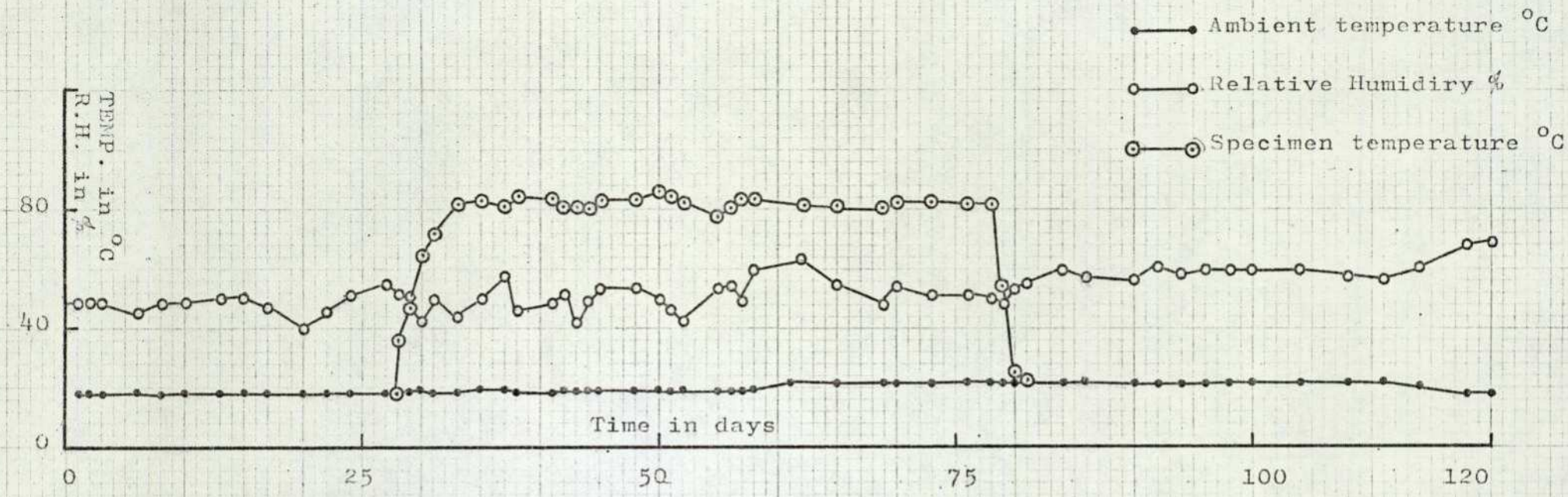


FIG. 96 SERIES 2
MODEL 5/6, TEMPERATURE AND RELATIVE HUMIDITY

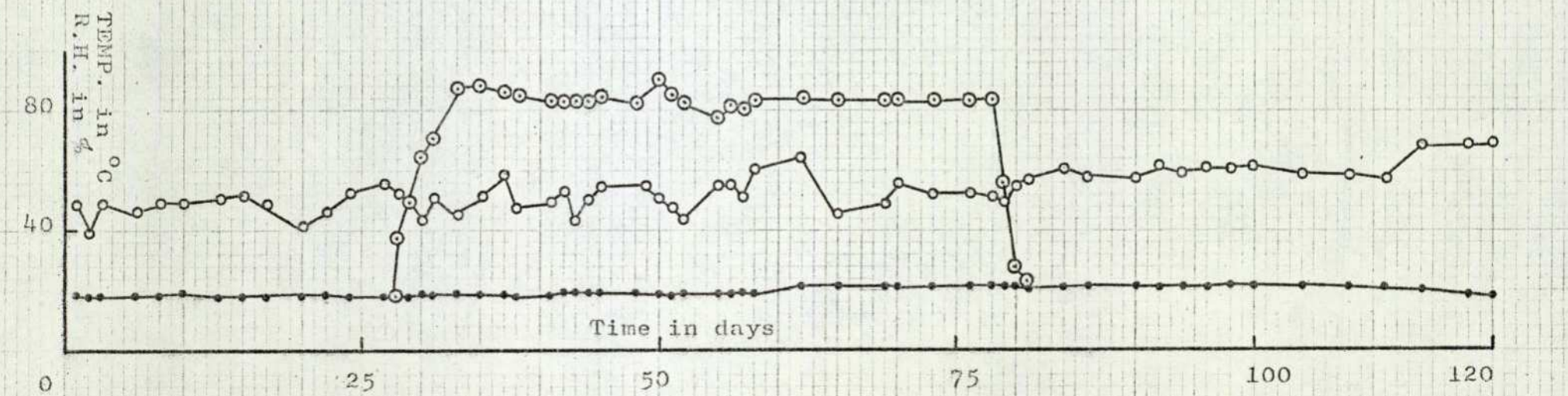


FIG. 97 SERIES 2
MODEL 7/8, TEMPERATURE AND RELATIVE HUMIDITY

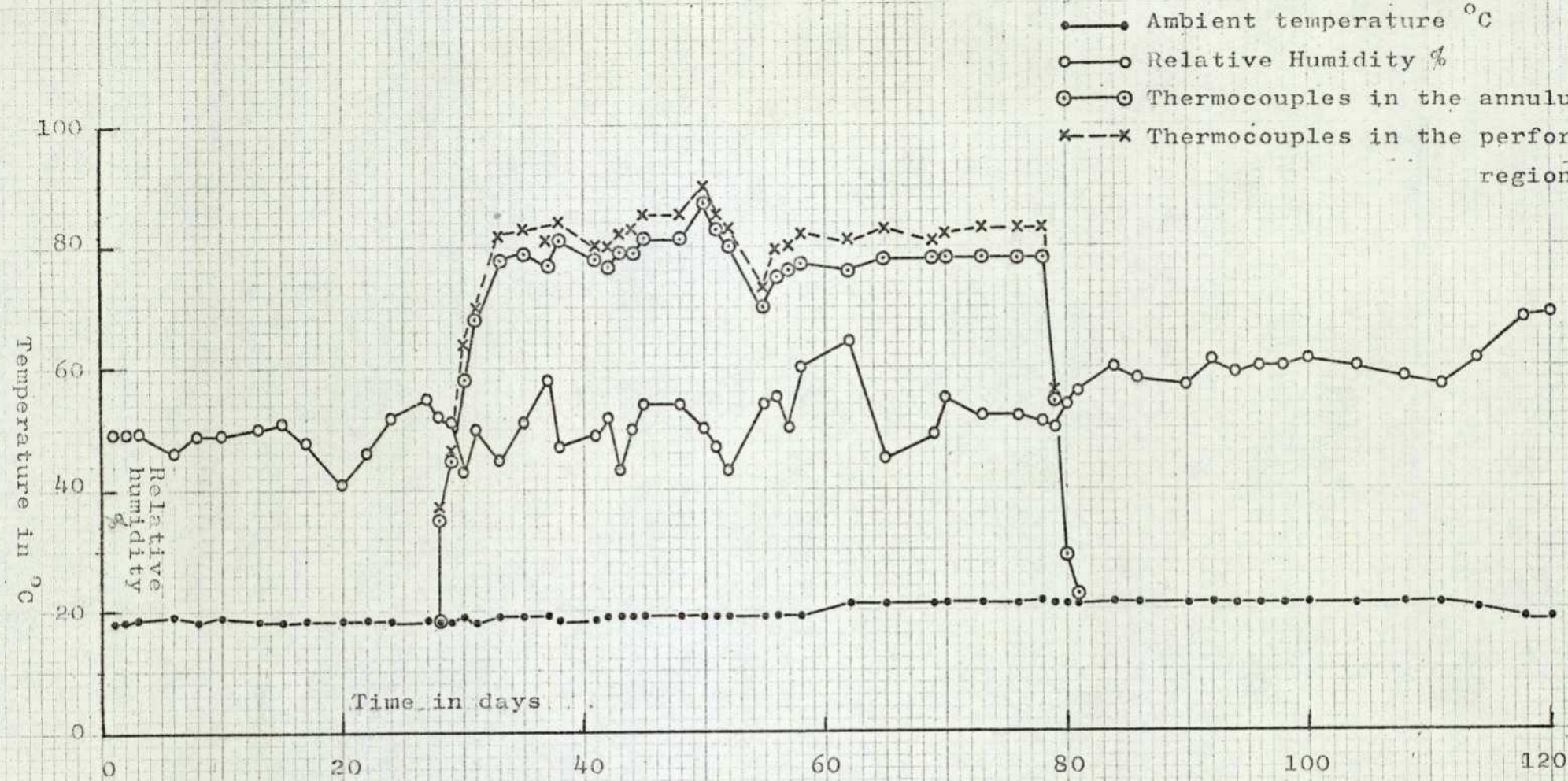


FIG. 98 SERIES 2 —
MODEL 9/10 COMPOSITE CREEP SPECIMEN

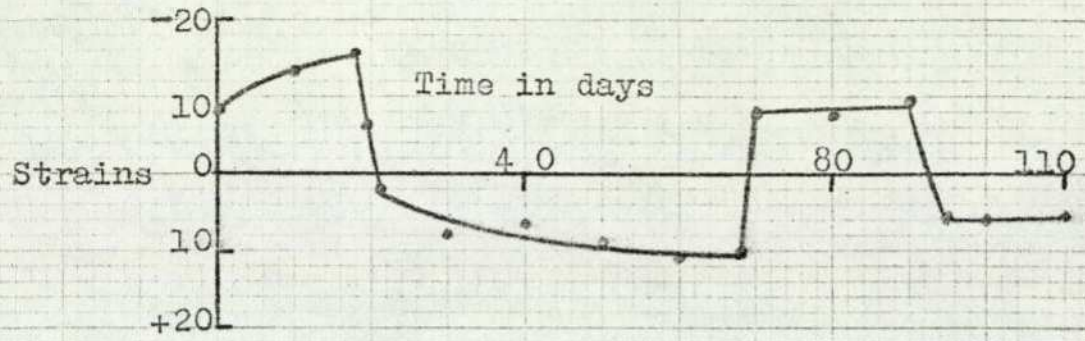


FIG. 99 . Series 2:
Standpipe strains at positions
1/2, 3/4, 9/10, 11/12: (Fig. 29).
Model 3/4:

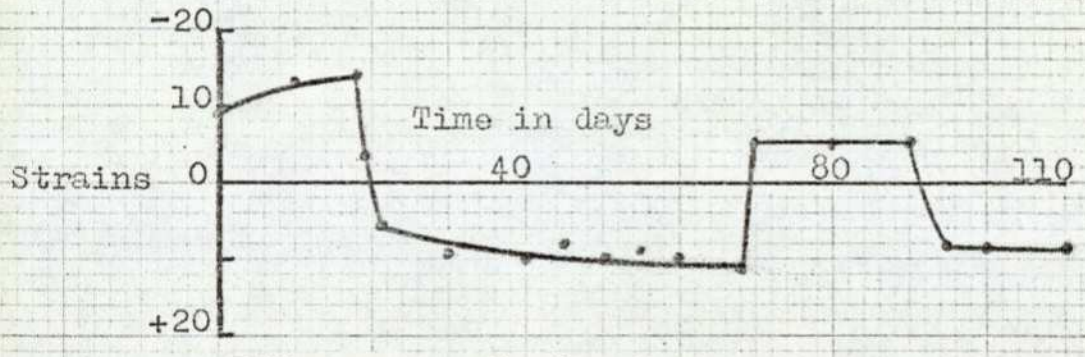


FIG. 100 . Series 2:
Standpipe strains at positions
5/6, 13/14: (Fig. 29).
Model 3/4:

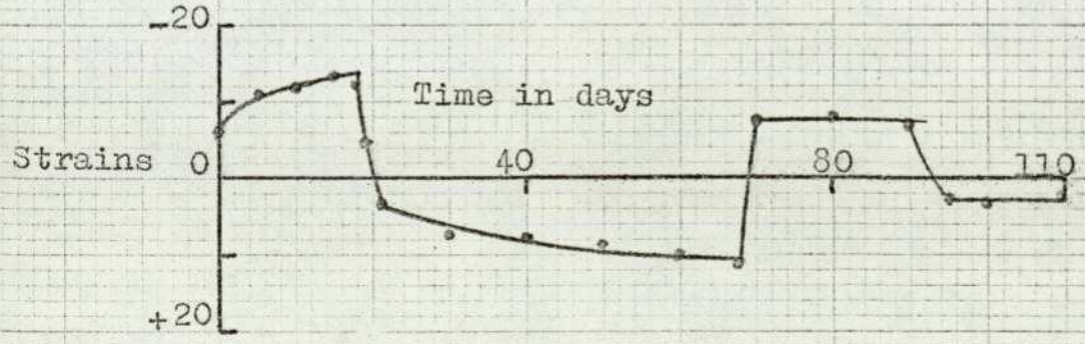


FIG. 101 . Series 2:
Standpipe strains at positions
7/8, 15/16: (Fig. 29).
Model 3/4:

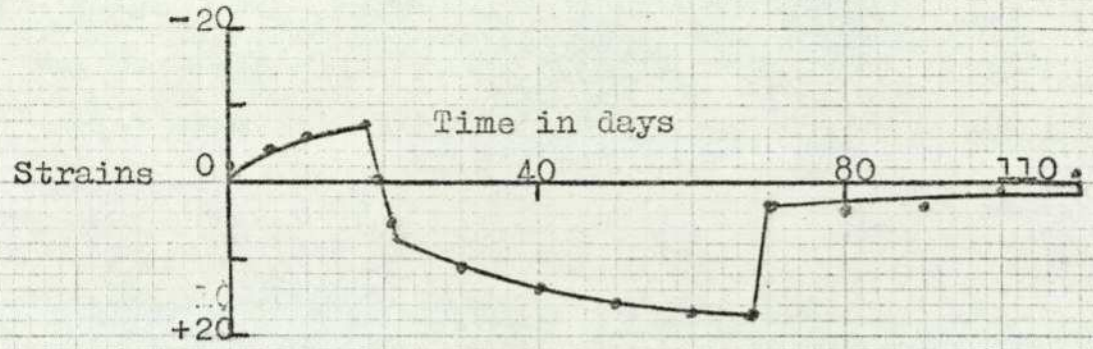


FIG. 102 . Series 2:
Standpipe strains at positions
33/34, 35/36, 41/42, 43/44: (Fig. 30)
Model 5/6:

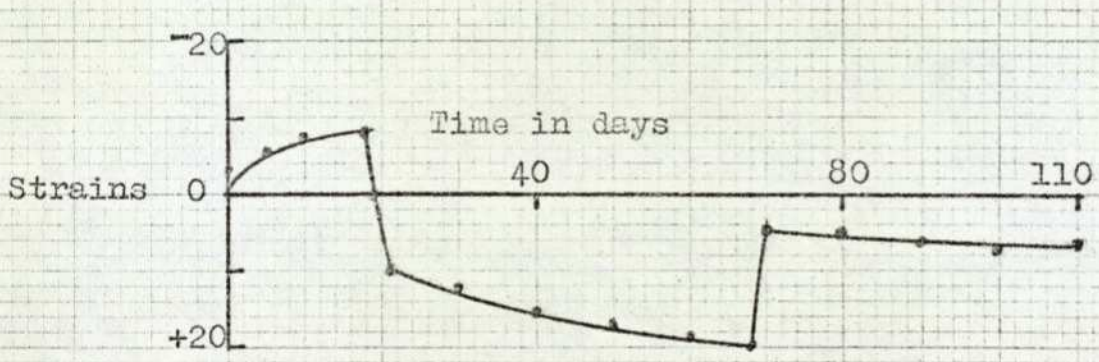


FIG. 103 . Series 2:
Standpipe strains at positions
37/38, 45/46: (Fig. 30).
Model 5/6:

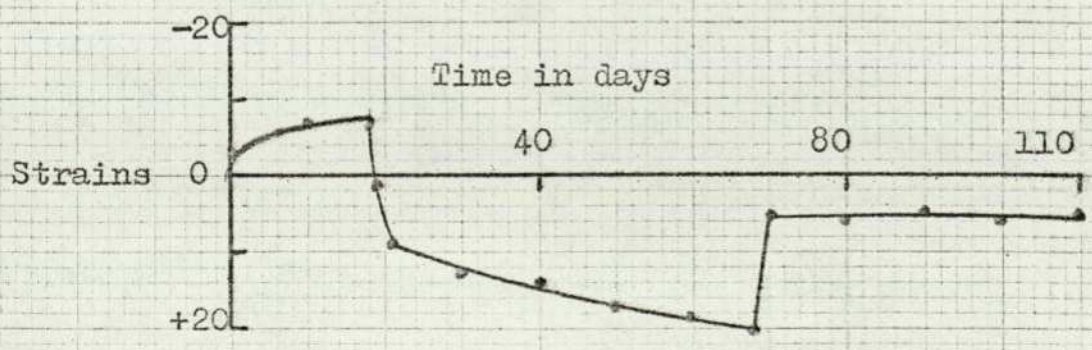


FIG. 104 . Series 2:
Standpipe strains at positions
39/40, 47/48: (Fig. 30).
Model 5/6:

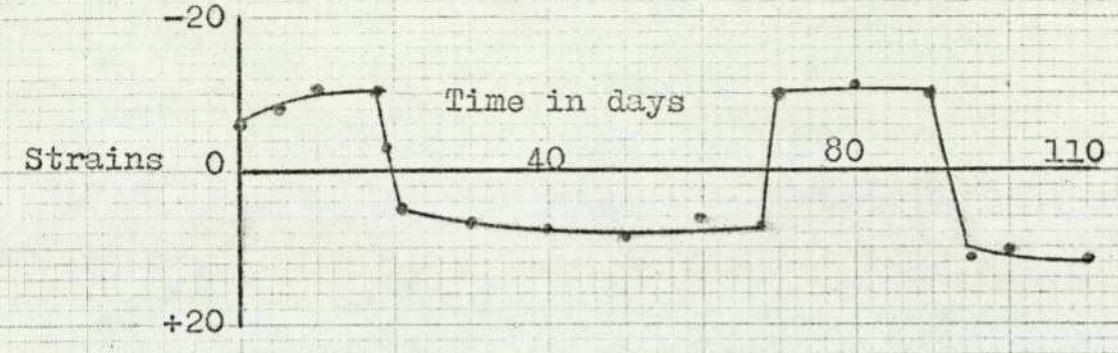


FIG. 105 Series 2:
Standpipe strains at positions
65/66, 67/68, 73/74, 75/76: (Fig. 33)
Model 9/10:

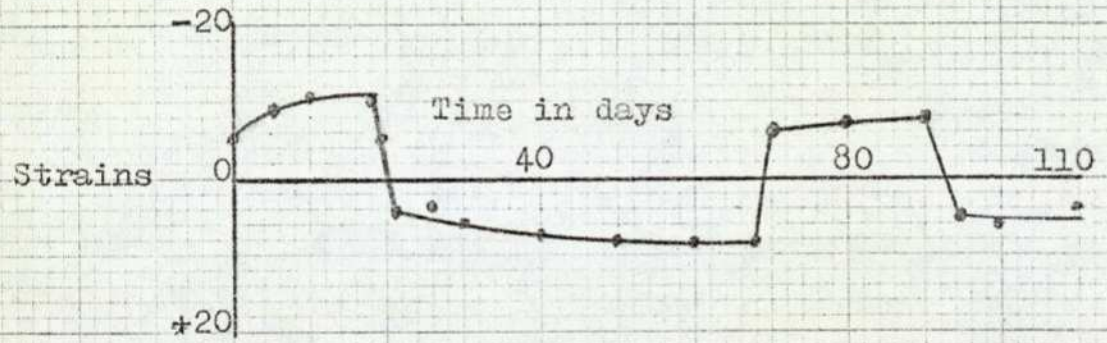


FIG. 106 Series 2:
Standpipe strains at positions
69/70, 77/78: (Fig. 33).
Model 9/10:

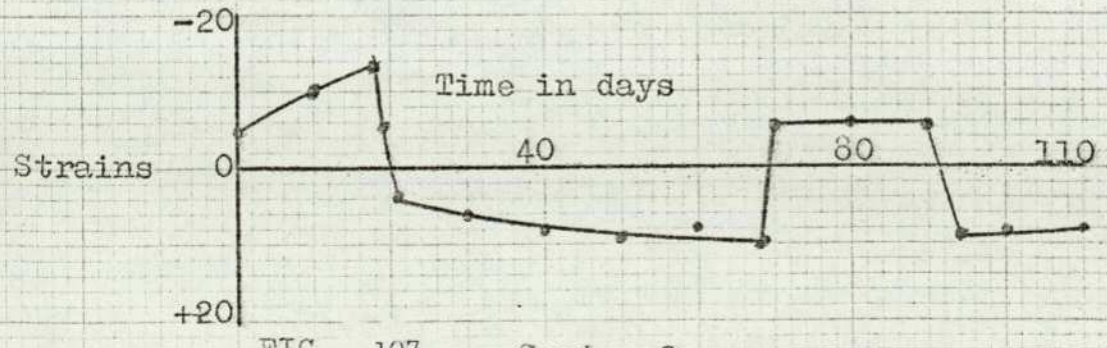


FIG. 107 . Series 2:
Standpipe strains at positions
71/72, 79/80: (Fig. 33).
Model 9/10:

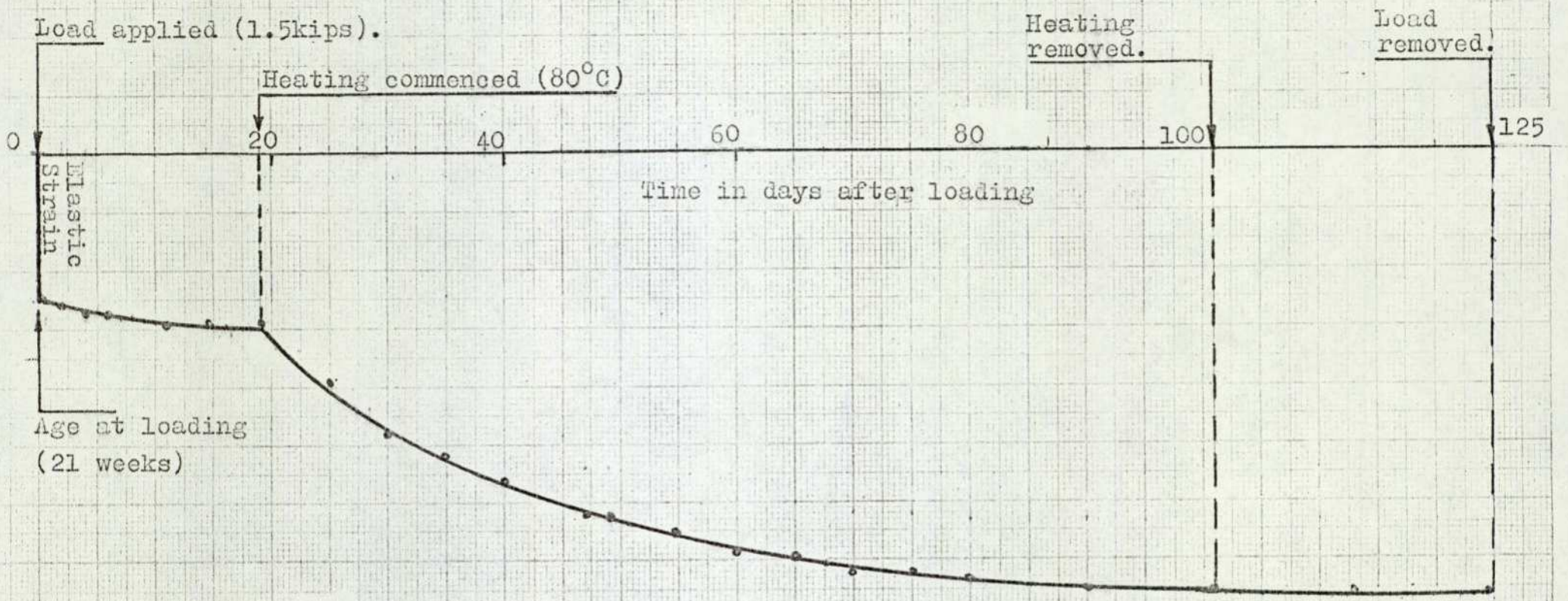


Fig. 108 . Series 1:
Specific creep curve.

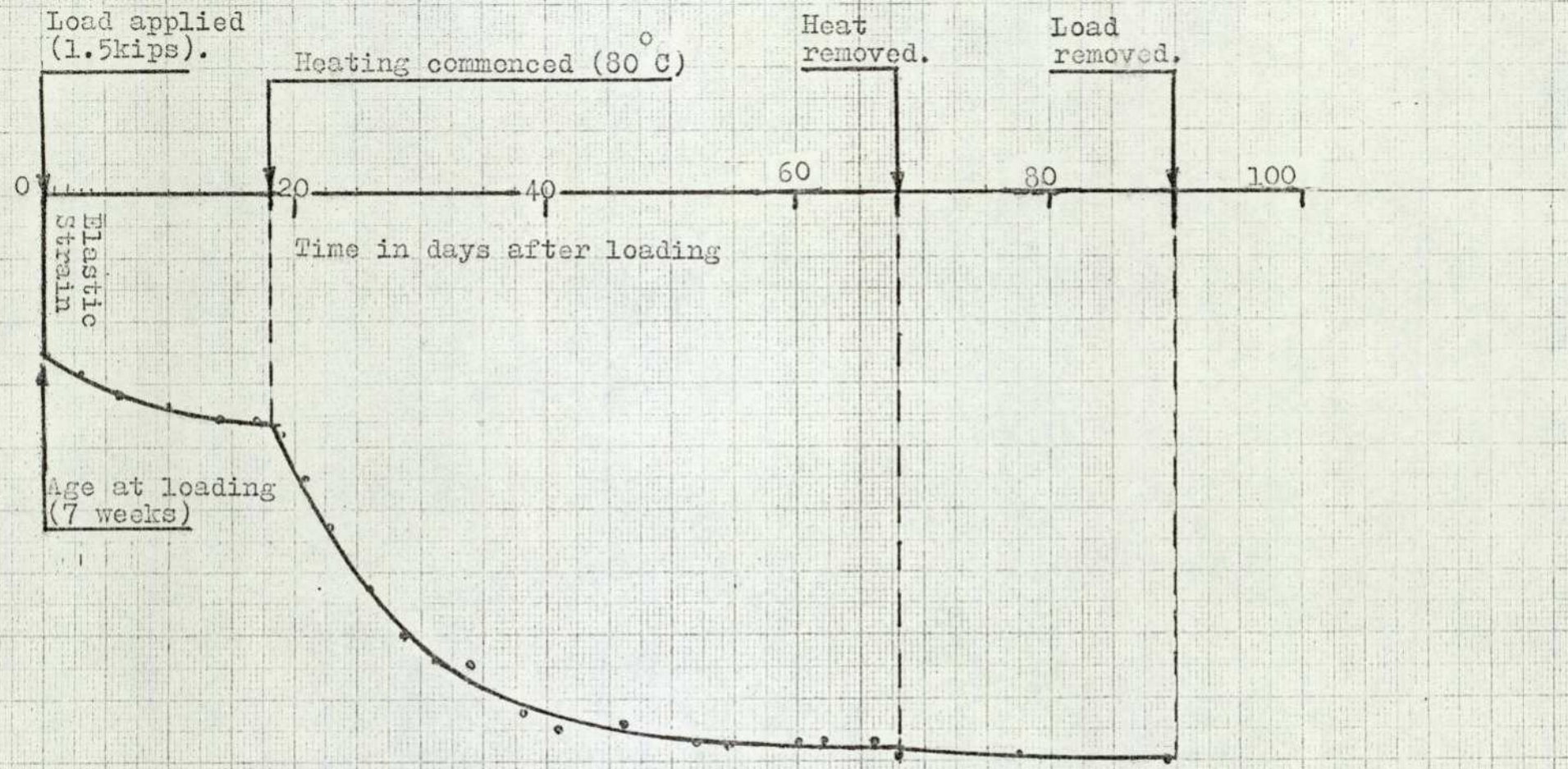


Fig. 109 . Series 2:
Specific creep curve.

SECTION XII

INTERPRETATION OF EXPERIMENTAL RESULTS

The results obtained in both series have been presented in graphical form in Section XI. They include the total strains obtained from 2" gauge length Demec readings, in the tangential and radial directions, the three-pitch Demec readings, and the standpipe diametral observations.

Separate graphs for the two series are drawn for the specific creep calculated from the total strain readings by appropriate subtraction. The net creep strains were divided by the applied stress to obtain the specific creep curves which were plotted against time.

Shrinkage Specimens

The small unloaded solid and perforated specimens (7/8 & 5/6 respectively), were subjected only to the influence of drying shrinkage, and the differences in strain observed between the two, give a direct indication of the way in which the tubes lining the holes in the perforated specimen 5/6 affected the shrinkage strains.

During the period of shrinkage under ambient temperature, the Demec readings indicated the appropriate shrinkage strains increasing at a decreasing rate in the ligaments.

During the subsequent heating period at 80°C for specimens 5/6 and 7/8, the thermal expansions caused a general increase in dimensions, followed by an accelerated shrinkage rate reducing with time.

Some secondary thermal creep strains may have occurred in the ligaments of the unloaded perforated specimen under the influence of the standpipe tubes. This is unlikely to have seriously affected the validity of the method of isolating the creep strains in the loaded specimens because the creep occurring in the ligaments due to

the changes in diameter of the standpipes was common to all perforated specimens.

On cooling to ambient temperatures, the contraction of the concrete was recorded followed by a reduced rate of shrinkage reducing further with time.

Creep and Shrinkage in the small loaded specimens.

These specimens were 1/2 (solid) and 3/4 (perforated). The differences in strain between them in corresponding positions, indicated the influence, for each series, of the standpipe penetrations.

For specimen 1/2, the early shrinkage which occurred in the days before loading, was indicated by an appropriate reduction in readings. When the load was applied, there occurred the expected elastic compressive strain, supplemented immediately thereafter by continuing creep and shrinkage strains the rate of which reduced over the period before the heat was applied. The slope of the combined creep and shrinkage curve plotted for this stage is steep at first gradually reducing with time in the expected manner.

The application of the temperature of 80°C caused the expected thermal expansion during the transient stage which gave place thereafter to thermal creep rates and hygrothermal shrinkage at rates higher than those observed at ambient temperatures. For virtually all specimens in both series the thermal expansion on first heating as expected, took the total strain curve above the original datum.

The thermal creep and shrinkage strains for the loaded specimens were so great, however, during the 6-8 weeks of the test at 80°C, that by the end of this period the strains were at a point below the datum lower than that achieved before heating.

On cooling specimens 1/2 and 3/4 to laboratory temperatures, a contraction strain recovery occurred after which the ambient creep

and shrinkage rates showed themselves to be lower than those at the start of the experiment when loading was first applied. At this cooling stage the concrete was of the order of 120 days old. The creep rate could be expected to be relatively lower due to the fact that the moisture content must have been much reduced after the heating phase.

On unloading after a further three weeks both small specimens showed an elastic strain recovery and a subsequent ill-defined creep recovery.

The elastic unloading strain was in some cases of the same order and in others greater than the corresponding initial elastic compression on first loading. The heating phase may have removed so much moisture from the specimens that the elastic constants were affected, the concrete being unable to gain strength with age.

The Large Composite Specimen 9/10.

The data obtained from the loaded and unloaded small specimens were intended to be used in interpreting the strain readings from specimen 9/10.

At the start of the tests, specimen 9/10 was allowed to shrink for the same short period as the small specimens.

Thereafter it was loaded radially for about three weeks, and the elastic, creep and shrinkage strains were measured in the central perforated zone as well as in the satellite gauge lengths, and subsequently plotted.

Since the externally-applied rim loading on specimen 3/4 was arranged to be the same as the internal compressive field stress around the interface between the solid annulus and the perforated zone of the large composite specimen, the strains observed in specimen 3/4 could be used in calculations to isolate the separate strain components in the large specimen.

During the heating phase on the large specimen, difficulty was constantly encountered in maintaining a uniform temperature between the perforated zone and the outer annulus. The annulus temperatures were higher (Series 1) than those in the perforated region and this had an influence on the stresses in both zones. The thermal expansions of the central zone were affected to some extent by the solid concrete ring around it. For Series 2 the perforated zone was hotter.

As was expected, the thermal creep and shrinkage strain rates for the central zone of specimen 9/10 were higher than those at ambient temperature and in a relatively short time brought the total strain curve below the original datum line of strain, to a point below the level reached before heating.

Removal of heat caused a further sudden increase in strain due to the contraction of the concrete and the subsequent period of creep and shrinkage strain under ambient loading, as expected, revealed a rate lower than the rate under the initial ambient loading at the start of the experiment.

Unloading produced, as before described, an elastic unloading strain followed by a short somewhat ill-defined period of creep recovery.

Without question, the effect of the relative creep strains within the concrete annulus and within the perforated zone , particularly at the elevated temperature, was to redistribute the stresses resulting from the external loading; these stresses would presumably tend to be frozen in as the creep effect levelled off. Removal of the loading subsequently would consequently develop tensile stresses sufficiently large to crack the annulus radially, a response accentuated by the differences in temperature between the annulus and the perforated zone. Cracking was, in fact, observed in both the annulus and in the ligaments on unloading, but only at very low levels of stress.

Standpipe Strains

Difficulties were encountered in both taking and interpreting the diametral liner readings. The basis of the measuring difficulty lay in the insensitivity of the Mercer bore gauge.

Interpretation proved difficult because although the diameters were measured, there was no fixed frame of reference against which the changing shape of the bore could be assessed. It is likely that the bores of the standpipes became irregularly non-circular under the succession of stress variations and reversals to which they were subjected throughout the period of the testing programme.

The unexpected behaviour of the tubes may partly be explained if the concrete had in places shrunk away from the tube wall, after the latter had been originally compressed by the setting of the concrete.

Elevated Temperatures

The figures showing the temperatures in the models indicate that reasonably uniform distribution was achieved in most of the specimens in both series.

However, for Series 1 in the perforated zone of the composite specimen, lower temperatures were recorded than in the surrounding annulus despite considerable efforts, in the form of differential heating and cooling, to equilibrate the distribution. For Series 2 in contrast, the annulus was cooler than the central zone. The greater loss of heat towards the rim of the specimen and the associated imponderables of convection and insulation are likely to have been responsible. Temperatures across the thickness of the specimens, however, were reasonably uniform.

On the application of heat, a considerable time was required, for the large specimen to establish thermal equilibrium. On the graphs of thermal strain, the transient regime is recorded together with ex-

trapolated strain curves which represented what the strain curves should have been, had the temperature rise been more immediate and the temperature control more precise. Some fluctuations may also have occurred due to variations in the input wattage.

The graphs showing changes in ambient relative humidity show fluctuations which must have affected the creep and shrinkage readings temporarily. Although strain fluctuations due to occasional changes in ambient humidity indicated temporary reversals in the expected directions of strain, the general trends were unaffected overall. Temporary increases in humidity occasionally caused a temporary swelling of the concrete.

The rates of creep strain during the initial ambient loading, the subsequent 80°C period, and the final ambient loading period, were of expected magnitudes, the thermal creep rates being greater than during the two ambient periods.

Towards the end of the transient heating period, rapidly increasing creep and shrinkage rates tended to offset the thermal straining effects.

Strain Fluctuations

Smooth strain curves were obtained in very few cases and this needs explanation in view of the constant applied stress and temperature conditions which were aimed at.

The reasons for these fluctuations are likely to have been:

1) Variations in the specimen temperatures due to difficulties in heating and insulation control,
2) Variations in ambient temperatures and humidities,
3) Malfunctions in control of the pressure circuit.

The trends of the plotted points were reasonably clear, however, and it was felt to be justifiable to draw smooth curves through the

clusters of plotted readings.

Effect of the Liners

For the first series, the effects of the 1/16" tube liners to the penetrations can be seen by comparing the graphs obtained from the solid and perforated specimens. These strain differences were much smaller for the second series with the thicker liners. This was due to the fact that the effective modulus of the inner zone was very close to that of the outer concrete, and despite the irregular geometry of the penetrations affecting the strain distributions.

Similarly, particularly for Series 1, strain differences are apparent when comparing the perforated zone of the composite specimen with the annular region.

Young's Moduli

The results for the actual and effective Young's moduli for the solid and perforated specimens, reveal differences in magnitude in Series 1 which partly explain the differences in strain between the perforated concrete and the solid.

For the second series, with $\frac{1}{4}$" thick liners, the effective modulus of the perforated zone was found to be very close to the modulus for the concrete itself.

The relatively small changes in magnitude of strain rate observed during the second ambient period may be explained by realizing that, particularly for Series 1, the concrete was mature and probably did not have much residual creep potential. The concrete was much dryer at this stage, and moisture migrations may have reduced or have been offsetting the effects due to creep.

Removal of Load

There occurred the expected unloading strain when the load

was removed. However, the magnitude of the elastic recovery was in some cases rather greater than the strain on first loading, although a clear pattern did not always emerge. Certainly the elastic properties had changed during the testing, the influences of heating and ageing probably offsetting each other.

Comparison of Test Results between Series 1 and 2

Two important differences between Series 1 and 2 explain the significant differences in response between the comparable experimental regimes at corresponding times.

First there was the difference in standpipe liner thickness. Secondly, for the first series, the age of the concrete at loading was twenty one weeks, whereas for the second series it was only eight weeks. The two concretes exhibited quite different elastic and creep properties due to this large difference in loading age.

The long period before loading the series 1 specimens elapsed because of various experimental problems and especially because of difficulties with the projecting brass hexagonal studs.

The first set of hexagonals screwed into the ends of the steel members cast across the thickness of the concrete, projected for too great a distance from the concrete face and problems were encountered in obtaining meaningful Demec readings because the brass hexagonals were flexing. Shorter studs were eventually used.

Having solved the problem for the first series, it did not affect the second series which was loaded much earlier. As expected, therefore, the elastic, creep and shrinkage strains were smaller under the same load for the much older Series 1 concrete.

There were problems encountered in the first series particularly, in stabilizing the 80°C temperature on first heating the specimens. A shorter period for stabilization was required for the second series.

For the first series there are no records of strain changes during the extended transient heating period, and the results as shown in the graphs for this length of time had to be extrapolated. The extrapolations are shown dotted in the graphs, and are utilized in drawing the specific thermal creep curve for this series during this period.

Crack Formation

A detailed description has previously been given of the unloading phase of the tests. The load decrements were each of 50 psi and cracking was revealed in the composite specimen at the ultimate loading stage at an externally-applied pressure of 50 psi.

Various techniques were employed for crack-detection including the use of an electrical resistance strain gauge circuit. These have been fully described. The cracking indicated that elastic and creep recovery had created residual stresses within the ligament zone. Tensile stresses within the central zone and also tensile hoop stresses in the annulus, had been generated, large enough to cause cracking.

Cracks were also observed in the perforated specimen 5/6 on removal of heating. These were probably due to a combination of tensile shrinkage and contraction stresses.

SECTION XIII

CORRELATION OF OBSERVED AND PREDICTED RESULTS

The graphs which compare observed and predicted total strains are presented in this section and have been numbered to correspond with the total strain graphs presented in Section XI. For example, the graph SOLID 1 tangential, representing observed strains in Section XI and numbered Fig. 51 corresponds to the comparison graph Fig. 51a herein. The suffix a applies to all such corresponding graphs whatever the number.

Any comparison of total strain curves predicted by the viscoelastic theory, with those obtained from the experimental observations, must take into account those factors which have affected the theory and the observations.

Some of the difficulties encountered during the Series 1 observations have already been described in Sections V and VI. The magnitude of these difficulties was reduced by the time Series 2 was undertaken. In a few cases the problems had been eliminated. This accounts for the fact that the correlation between observed and predicted total strains is better for Series 2 than for Series 1.

In particular, the following practical difficulties occurred ;

a) The control of temperature in the concrete was never precise ; there was a variation with time above and below 80°C.

b) The maintenance of a uniform temperature of 80°C in all parts of each specimen could not be achieved ; this was due to variations in heat input, to convection and to differential cooling from the concrete surface ; for Series 1 the annulus in specimen 9/10 was about 10°C hotter than the central perforated zone, whilst for Series 2 the perforated zone was about 5°C hotter than the annulus.

c) The insulation conditions were somewhat dissimilar between the shrinkage specimens and the loaded specimens.

d) A period varying between three and five days for the different specimens in the two series was required to establish steady state conditions at approximately 80°C on the onset of heating.

e) The magnitude of loading was subject to variation particularly for specimen 3/4.

f) At several stages in both Series 1 and 2, variations in ambient humidity occurred due to breakdown of the control apparatus.

The following factors affecting the theoretical analysis may have caused discrepancies when the theoretical results were compared with the observations ;

a) The boundary conditions were assumed to be free for the theoretical analysis, whereas the support arrangements in practice for the loaded models in the rigs, including as they did the partial restraint of the cement mortar bedding, must have imposed some degree of fixity.

b) The assumption was made that the unloaded shrinkage was identical to the loaded shrinkage ; this may not be justifiable, and differences were even, in fact, observed in the early days before loading between the shrinkage rates in the shrinkage specimens and those in the comparable specimens in the rigs.

Fig 51a shows the relationship between observed and predicted total strains on 2" tangential gauge lengths for the loaded solid specimen in Series 1, known as SOLID 1. Here the total strains when the load was first imposed at ambient temperature, show a close fit. Also during the 80°C regime the two curves are close. The predicted curve, showing lower tensile strains on first introducing the higher temperature, crosses the observed curve almost half way along it and finishes the hot run at a lower compressive strain than the observed

curve. During the second ambient period the fit is not so close, but the two curves are roughly parallel.

The other two SOLID 1 graphs, Figs 52a and 53a reveal a fit not nearly so close. One aspect of the observed graphs for Series 1 which makes a true comparison difficult in almost all cases, is that the extrapolation which was necessary for approximately two weeks after the onset of heating was naturally somewhat inexact.

Again for the three correlation graphs for the small perforated specimen PERFO 1, the observed and predicted curves during the elevated temperature run , neither exhibit the same gradients nor start from the same origin, although only in the 2" tangential gauge length case do the two curves fail to cross.

In the case of the composite specimen COMPO 1, (Figs 63a, 64a, and 65a) the two curves for the 2" radial gauge length give a reasonably close fit. The scatter of observed results is very wide. The tangential and three pitch curves do not give a very close correlation during the hot run, although in both cases the fit during the first ambient period is very close.

For the outer and inner satellites again the fit is poor and the outer radial satellite correlation is particularly disappointing. The projecting studs on which the readings were taken were particularly vulnerable to movements of the heating shield and experimental difficulties due to this and to the other control problems previously discussed may account partly for the deviations between the two curves.

There is a consistency about the predicted curves which is not paralleled in the observed curves, leading to a supposition that the theory represents the real situation in these cases more reliably.

Certainly in situations where the geometry is symmetrical and the stress fields uniform the observed strain curves should be more comparable than those revealed for example in SOLID 1 in the tangential, radial and three pitch directions. However, consistency in theoretical results may merely indicate a consistent defect in the argument.

When the predicted and observed curves are compared in Series 2 a much closer similarity is revealed. In only four cases (Figs 74a, 75a, 83a and 88a), do the curves fail to cross and for Fig 75a the fit is otherwise quite acceptable. There is justification for making the origins coincide for the start of the first ambient period and for the start of the hot run, since the objectives were primarily to forecast the time-dependent behaviour of the model concrete. If this is done, some comparisons reveal a very close fit viz Figs 74a, 75a, 83a and 88a. See fig 74b.

Correlation between the two curves during the hot run, is particularly close for Figs 82a, 84a, 85a and 86a.

In the case of every total strain graph for Series 1, the curve representing the theoretical prediction runs above the experimental curve for the elevated temperature regime. This indicates a lower strain. In almost all these cases the strains are compressive and far below the ultimate compressive strain of the concrete.

For the elevated temperature regime in Series 2, the predicted curve for strain also runs above the observed values for SOLID 2. For PERFO 2, however, the theoretical radial and three pitch strain curves for the hot run are below the corresponding measured curves. This is also true for the theoretical COMPO 2 radial and three pitch strain curves.

A full range of displacements, stresses and strains in specimen 9/10 at nodal points and at the centre of gravity of elements is given for Series 1 and for Series 2 in the two computer printouts for COMPO 1 and COMPO 2. A similar set of results is also available for SOLID 1, SOLID 2, PERFO 1 and PERFO 2.

Section II, " The Objectives of the Investigations ", lists the ligament zone, the annulus and the notional periphery between the two as positions at which the stress and strain distributions are required. The computer output gives all this information and its variation with time until the models were unloaded. The stresses and strains are also plotted in the figures hereafter presented.

The theory forecasts displacements, stresses and strains at many more locations in the geometry than were covered by the observations. Also the results are calculated at each of thirty one time intervals, although the strains were only plotted at every third interval.

The stresses and the cracks in the composite specimens in Series 1 and Series 2 were predicted by the analysis. The actual cracking is shown in Plate 10, and the predicted stresses are plotted in Fig 111 et seq.

Stress concentrations and stress relaxations in the ligament concrete are clearly shown in various positions in these figures and the tensile cracking is predicted on unloading. Positions 5 and 6 outside the ligament zone also indicate high tensile stress on unloading and the results forecast the observed cracking.

As hereafter suggested, it appears essential, in full-scale design, to stiffen the geometry of the perforated zone in relation to standpipe thickness and ligament width so that no harmful consequences are experienced due to differences in stiffness between the inner and

outer sections of the slab.

In addition, the stresses in the standpipe steel are plotted in Figs 123 and 124. Generally the steel stresses are increased as the concrete compressive creep strains developed. The results indicate that the yield point of the steel may have been exceeded in Series 1. Clearly steel liner thicknesses must also be determined in practical full-scale design to avoid this possibility.

Since the strains and stresses are given in the results at the centres of gravity of elements, the averaging procedures necessary in most cases to obtain theoretical values comparable with observed values measured between gauge points, were characterized by positional inaccuracies since the element locations tended generally to be only adjacent to the corresponding measured positions.

SERIES 1 CORRELATION GRAPHS

Fig 51a Tangential Strains. Model 1/2.

Fig 52a Radial Strains. Model 1/2.

Fig 53a Three Pitch Strains. Model 1/2.

Fig 54a Tangential Strains. Model 3/4.

Fig 55a Radial Strains. Model 3/4.

Fig 56a Three Pitch Strains. Model 3/4.

Fig 63a Tangential Strains. Model 9/10.

Fig 64a Radial Strains. Model 9/10.

Fig 65a Three Pitch Strains. Model 9/10.

Fig 66a Outer Satellite Tangential Strains. Model 9/10.

Fig 67a Outer Satellite Radial Strains. Model 9/10.

Fig 68a Inner Satellite Tangential Strains. Model 9/10.

Fig 69a Inner Satellite Radial Strains. Model 9/10.

SERIES 2

Fig 70a Tangential Strains. Model 1/2.

Fig 71a Radial Strains. Model 1/2.

Fig 72a Three Pitch Strains. Model 1/2.

Fig 73a Tangential Strains. Model 3/4.

Fig 74a Radial Strains. Model 3/4.

Fig 75a Three Pitch Strains. Model 3/4.

Fig 82a Tangential Strains. Model 9/10.

Fig 83a Radial Strains. Model 9/10.

Fig 84a Three Pitch Strains. Model 9/10.

Fig 85a Outer Satellite Tangential Strains. Model 9/10.

Fig 86a Outer Satellite Radial Strains. Model 9/10.

Fig 87a Inner Satellite Tangential Strains. Model 9/10.

Fig 88a Inner Satellite Radial Strains. Model 9/10.

Fig 74b Radial Strains. Model 3/4. Effect of coinciding the origins.

Fig 110 Series 1 and 2. Positions 1 to 6 at which stresses were predicted

Fig 111 Series 1. Position 1. Tangential and Radial Stresses.

Fig 112 Series 1. Position 2. Tangential and Radial Stresses.

Fig 113 Series 1. Position 3. Tangential and Radial Stresses.

Fig 114 Series 1. Position 4. Tangential and Radial Stresses.

Fig 115 Series 1. Position 5. Tangential and Radial Stresses.

Fig 116 Series 1. Position 6. Tangential and Radial Stresses.

Fig 117 Series 2. Position 1. Tangential and Radial Stresses.

Fig 118 Series 2. Position 2. Tangential and Radial Stresses.

Fig 119 Series 2. Position 3. Tangential and Radial Stresses.

Fig 120 Series 2. Position 4. Tangential and Radial Stresses.

Fig 121 Series 2. Position 5. Tangential and Radial Stresses.

Fig 122 Series 2. Position 6. Tangential and Radial Stresses.

Fig 123 Series 1. Steel Stresses in Standpipes.

Fig 124 Series 2. Steel Stresses in Standpipes.

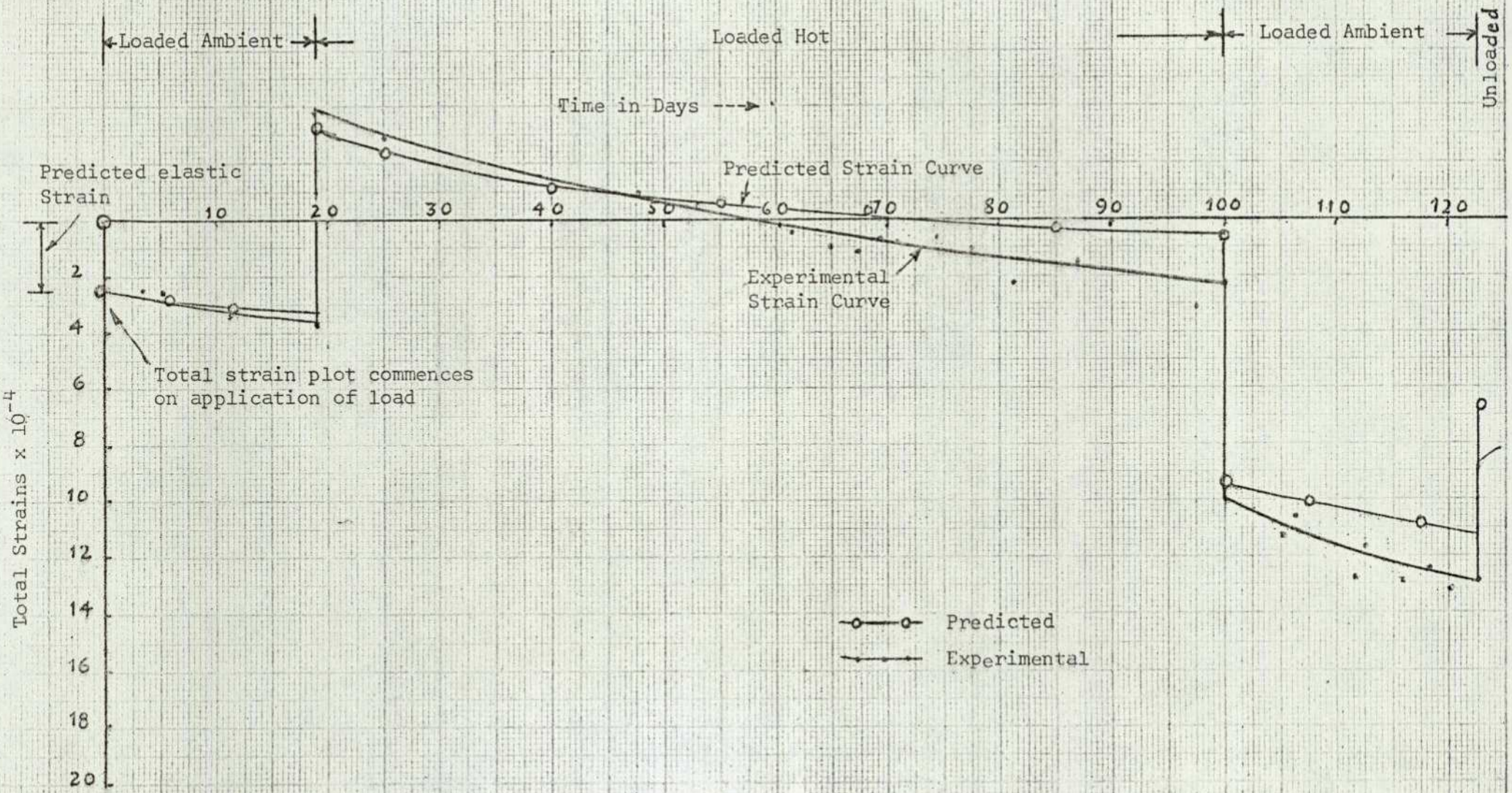


FIG 51a SERIES 1 SIDES 1/2 SOLID 1
TANGENTIAL TOTAL STRAINS 2"

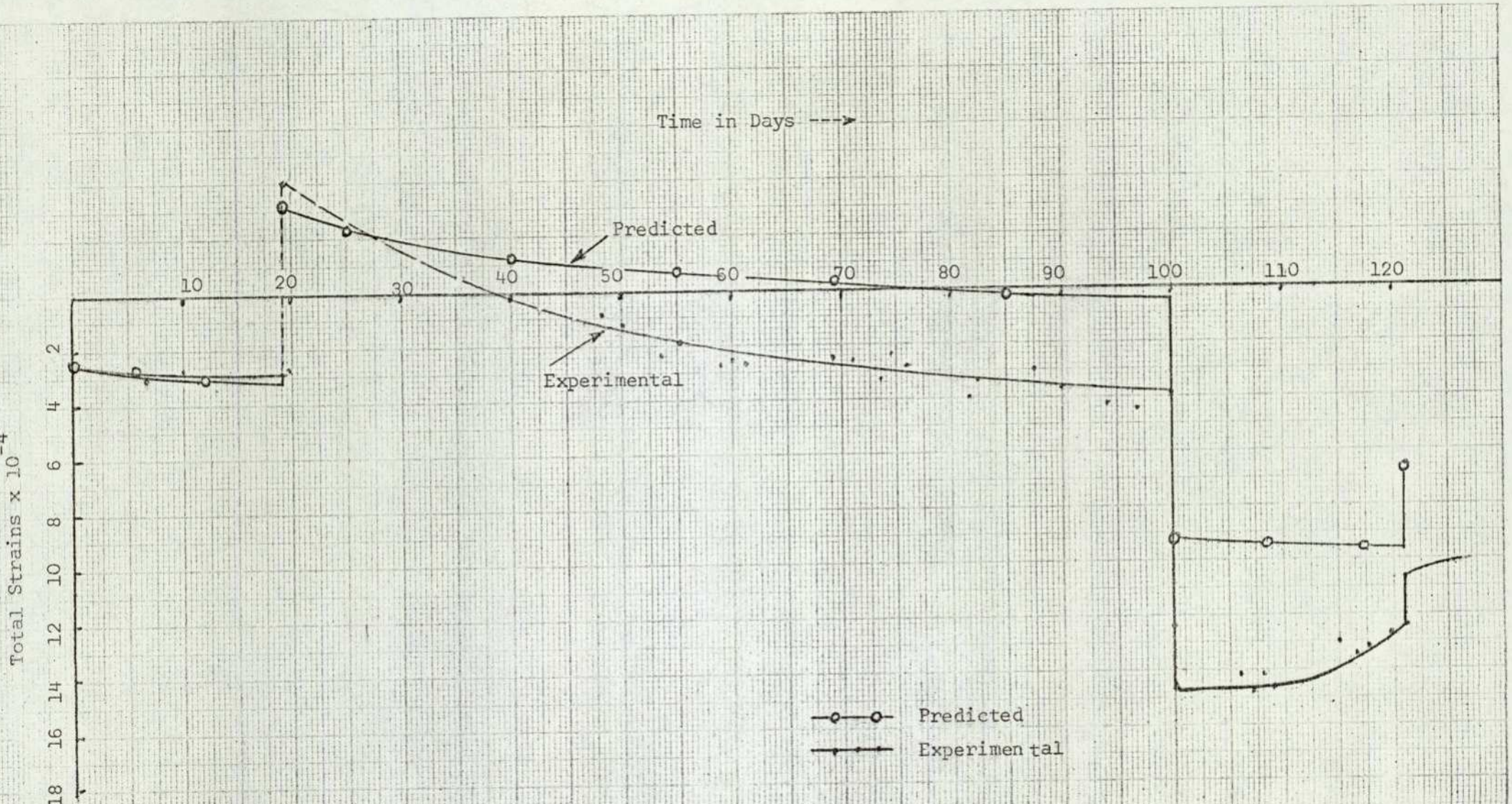


FIG 52a SERIES 1 SIDES 1/2 SOLID 1

RADIAL TOTAL STRAINS 2" G.L.

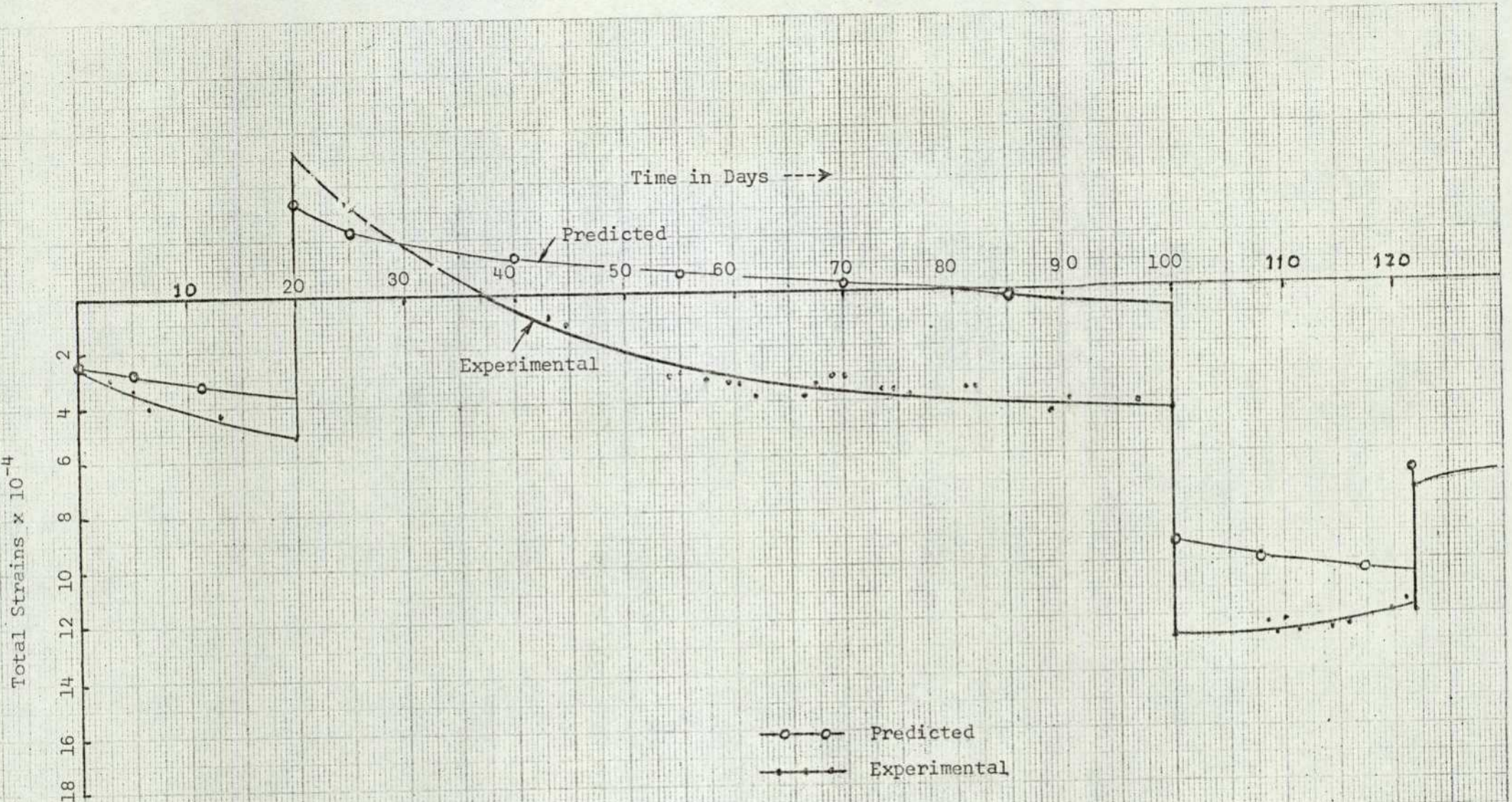


FIG 53a SERIES 1 SIDES 1/2 SOLID 1
THREE PITCH TOTAL STRAINS

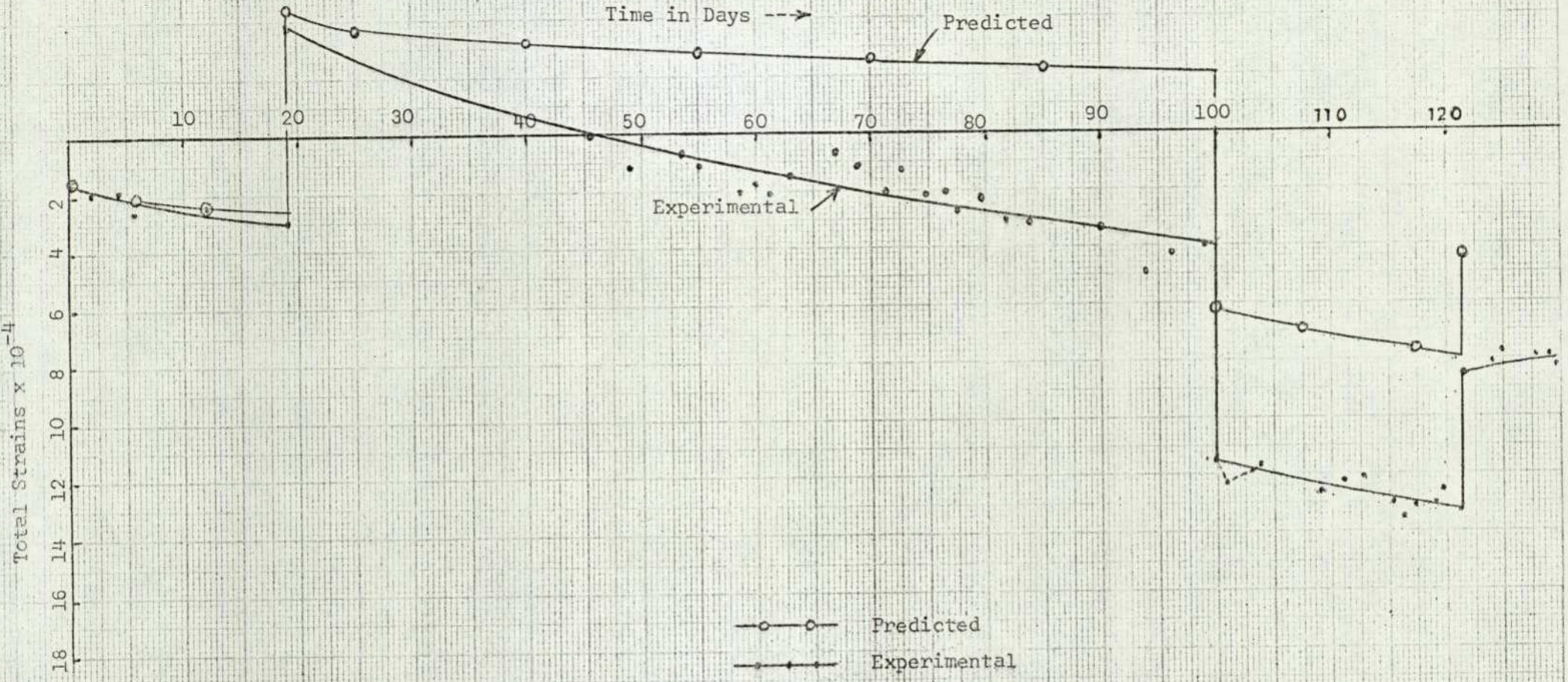


FIG 84a SERIES 1 SIDES 3/4 PERFO 1

TANGENTIAL TOTAL STRAINS 2" G.L.

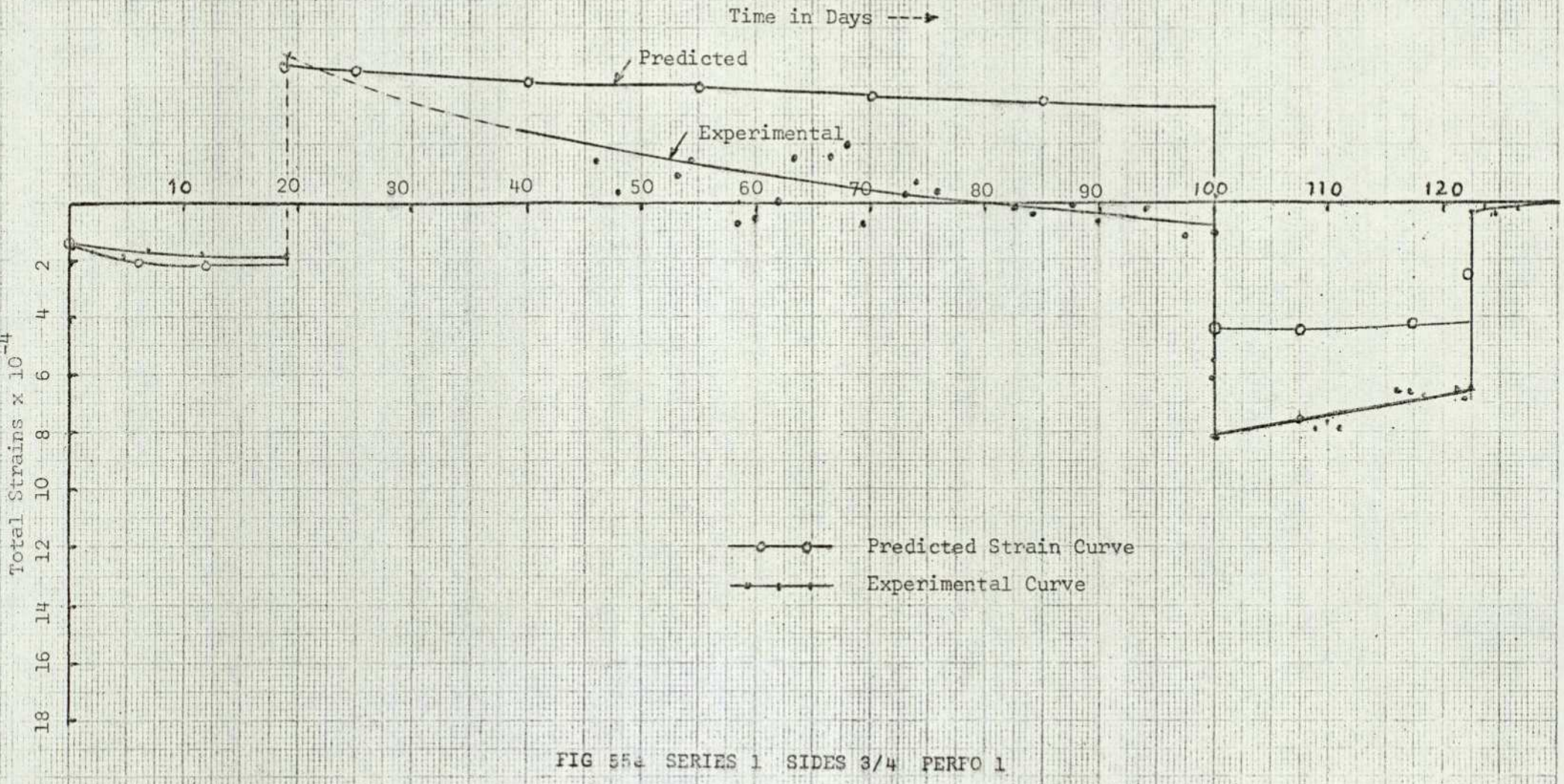


FIG 55a SERIES 1 SIDES 3/4 PERFO 1
RADIAL TOTAL STRAINS 2" G.L.

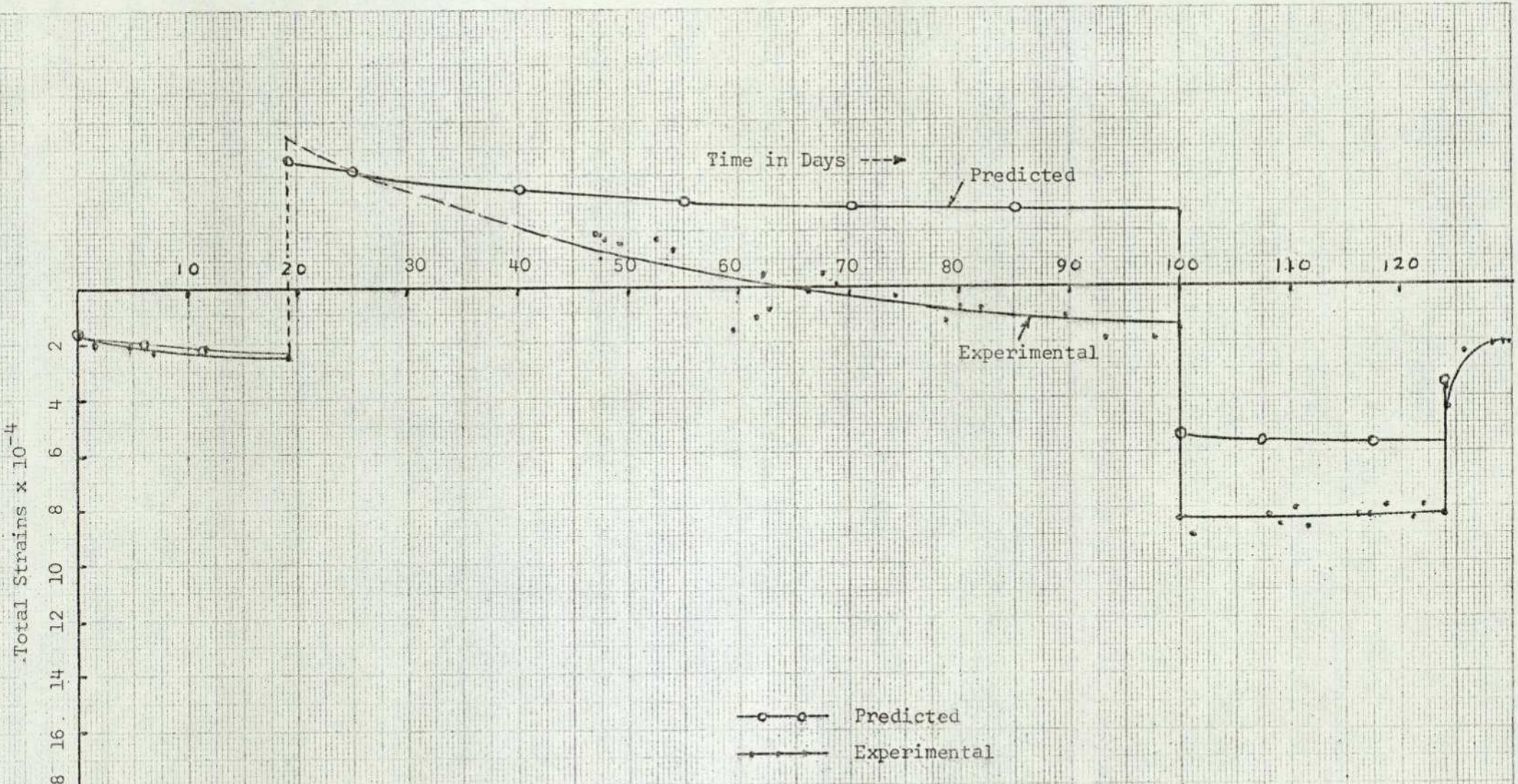


FIG 56a SERIES 1 SIDES 3/4 PERFO 1
THREE PITCH TOTAL STRAINS

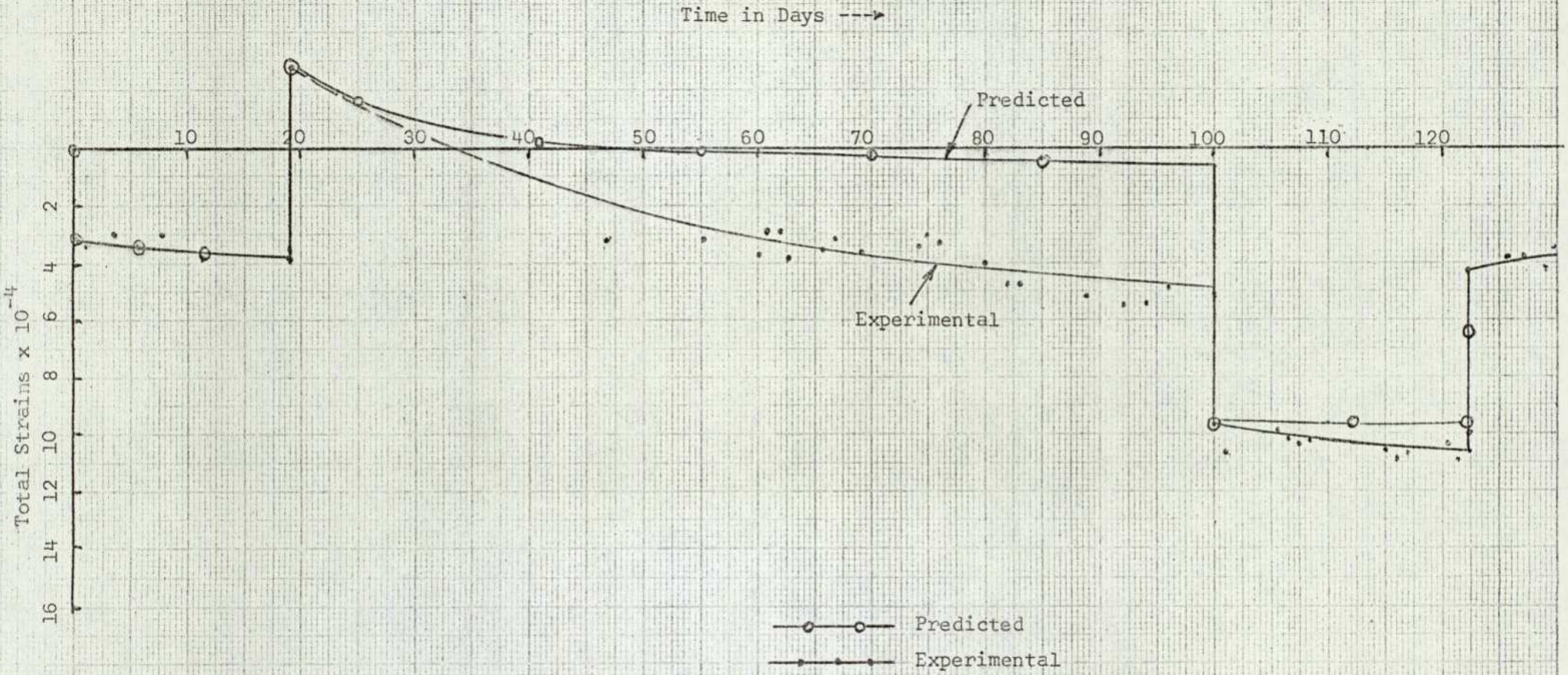


FIG 63a SERIES 1 SIDES 9/10 COMPO 1

TANGENTIAL TOTAL STRAINS 2" G.L.

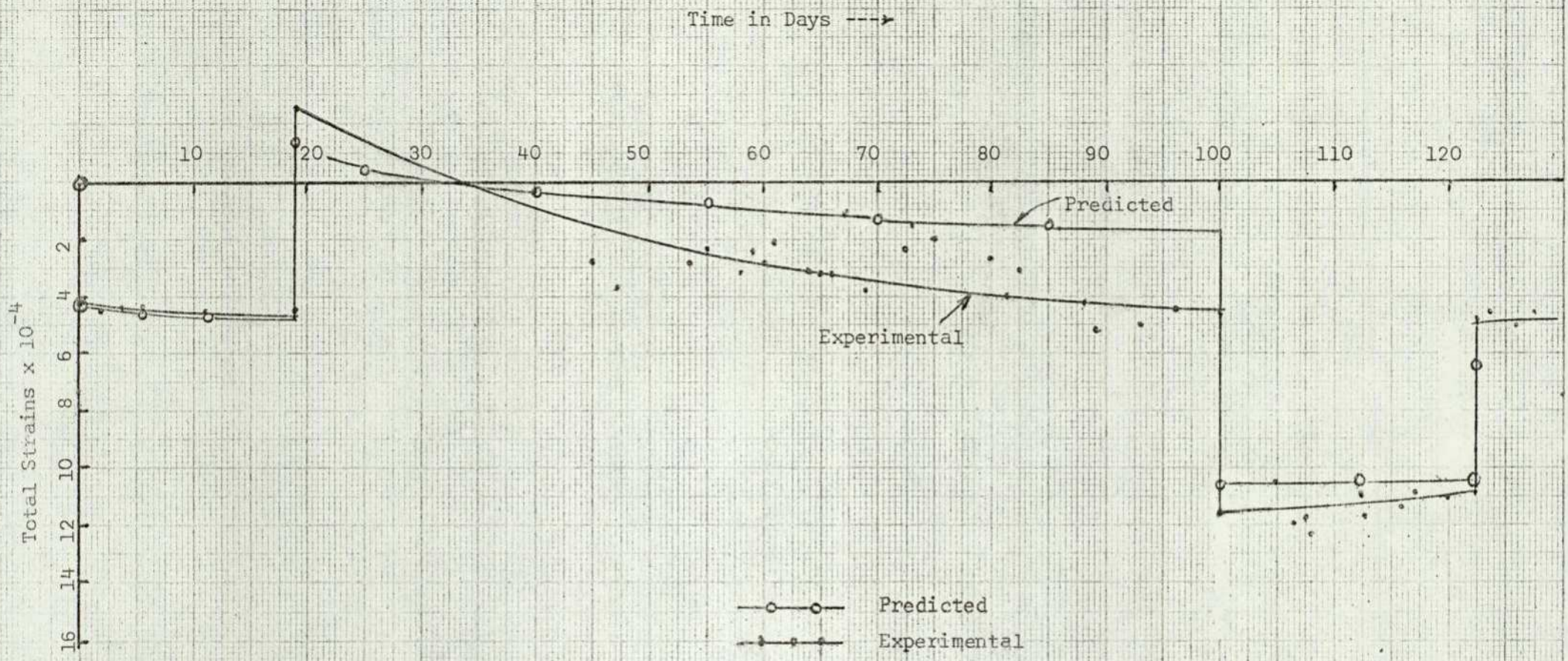


FIG 64a SERIES 1 SIDES 9/10 COMPO 1
RADIAL TOTAL STRAINS 2" G.L.

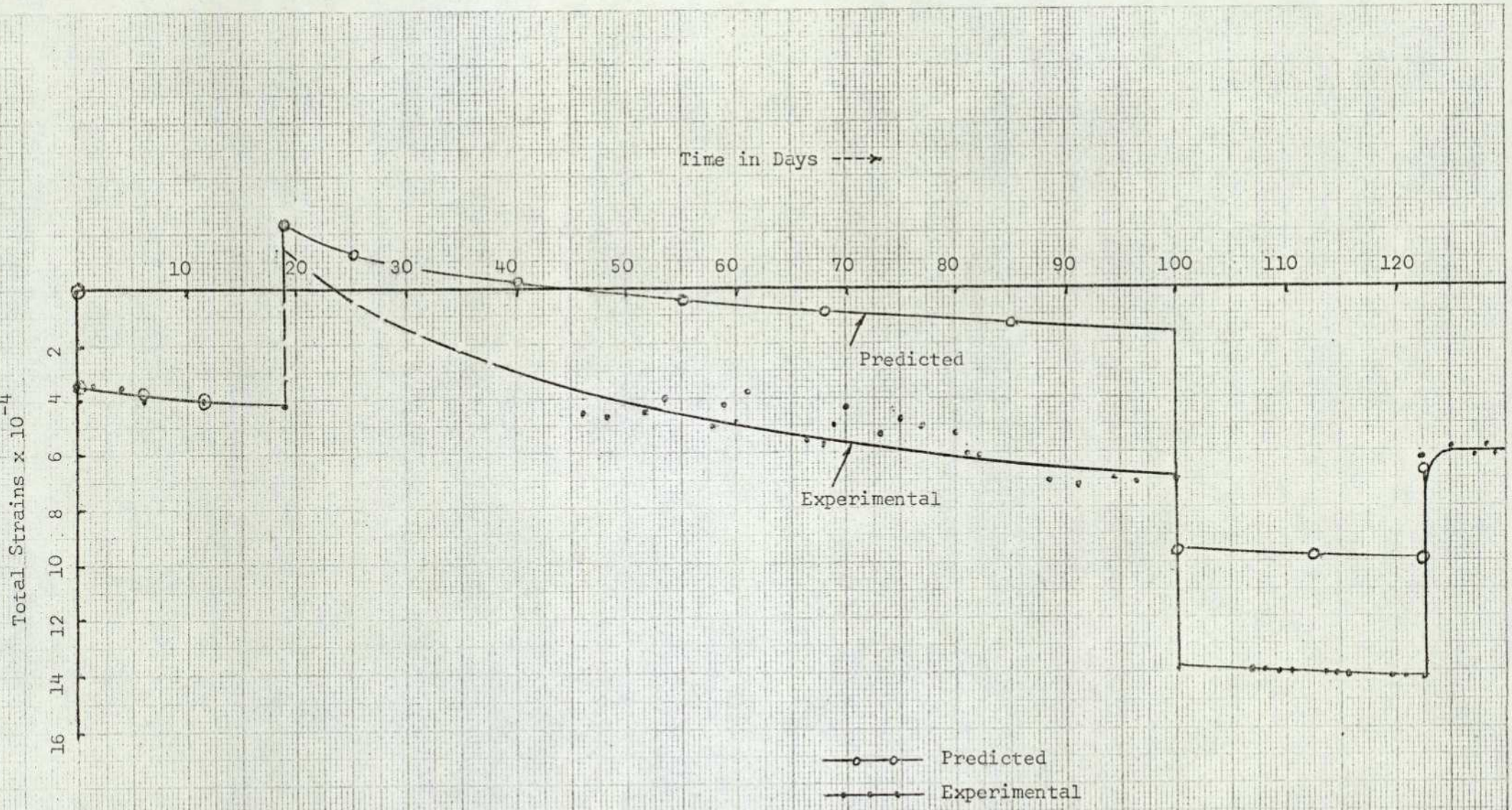


FIG 65a SERIES 1 SIDES 9/10 COMPO 1
THREE PITCH TOTAL STRAINS

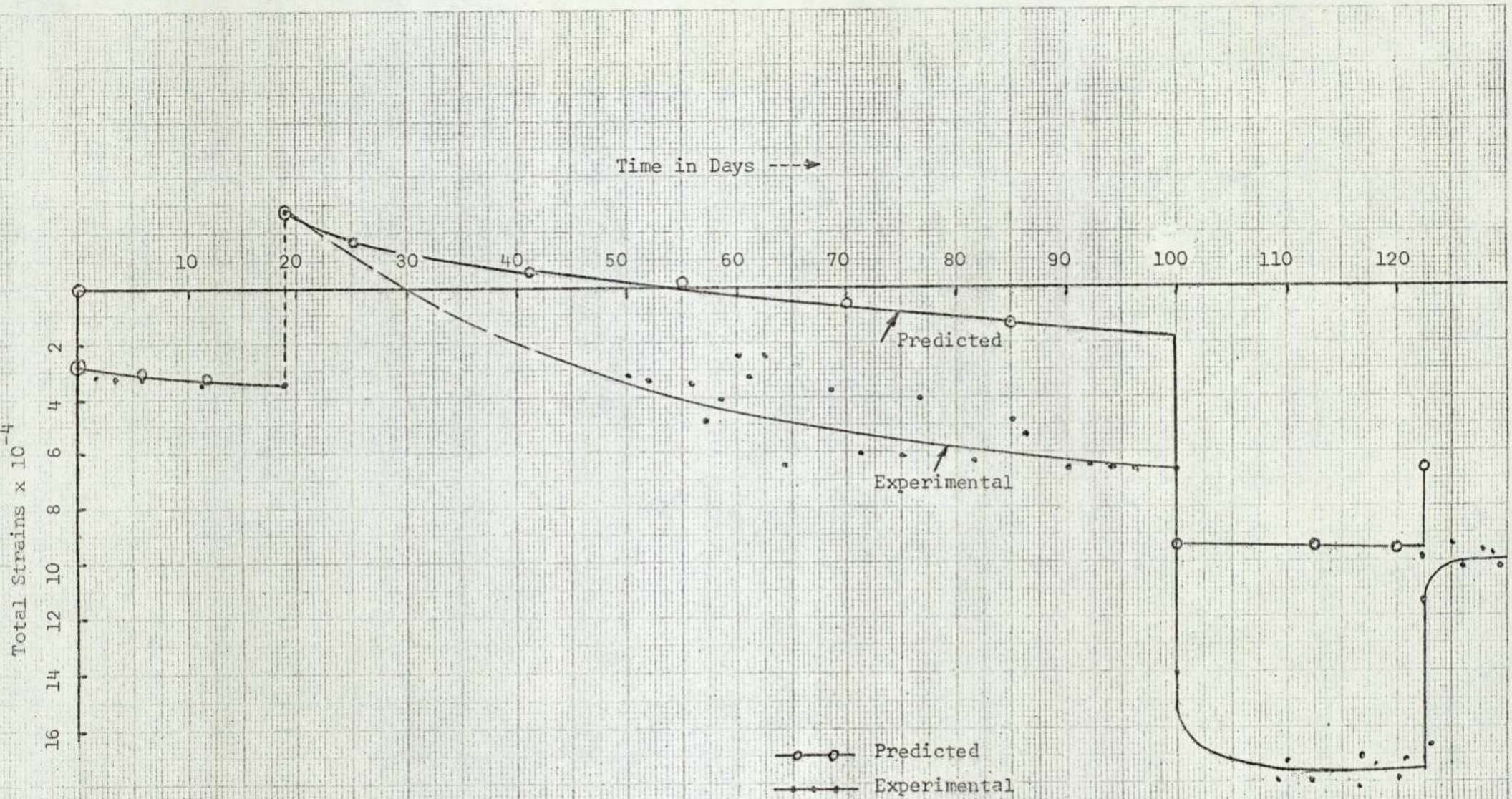


FIG 66a SERIES 1 SIDES 9/10 COMPO 1
OUTER SATELLITE TANGENTIAL STRAINS 2" G.L.

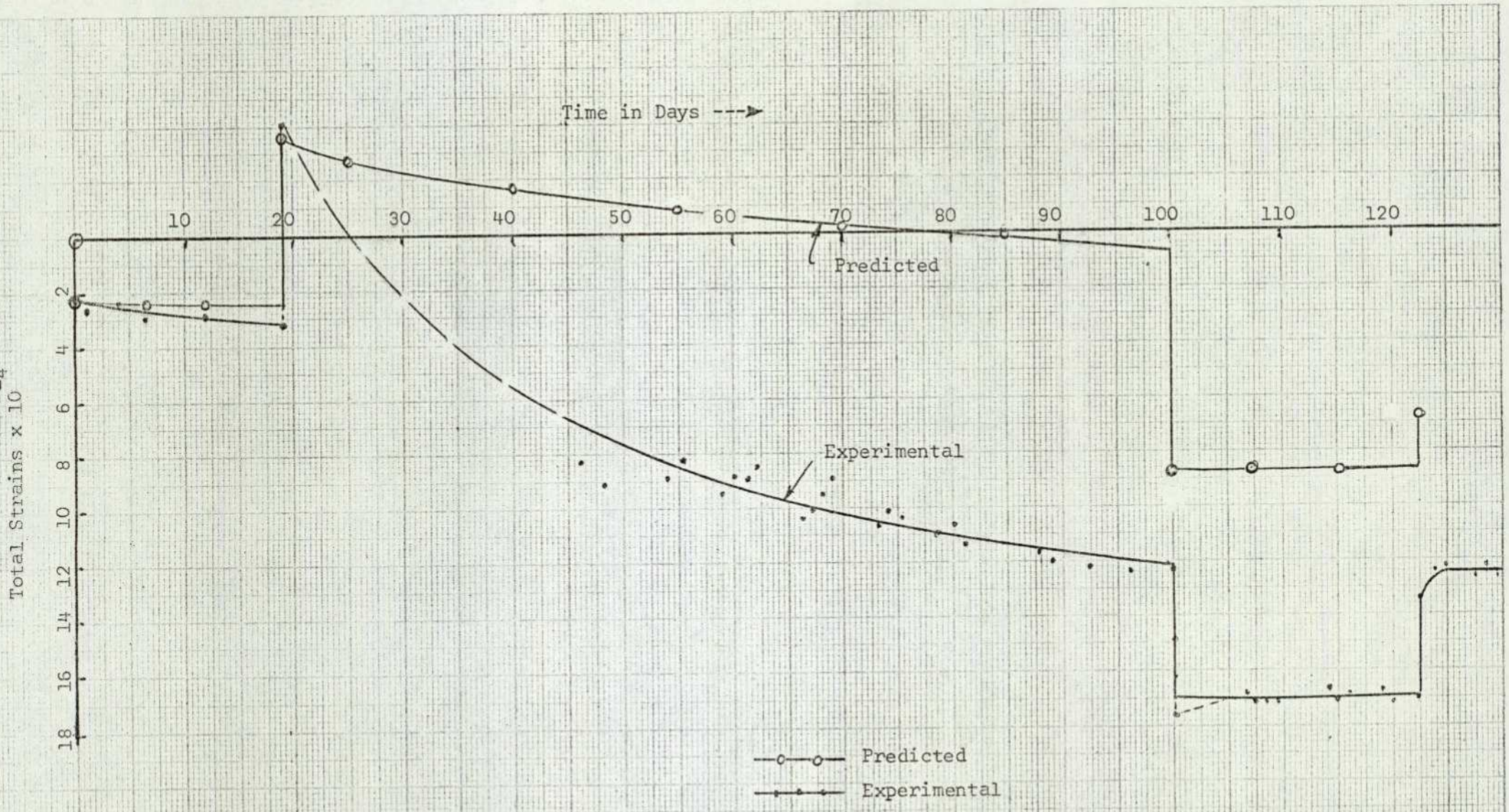


FIG 67a SERIES 1 SIDES 9/10 COMPO 1
OUTER SATELLITE RADIAL STRAINS 2" G.L.

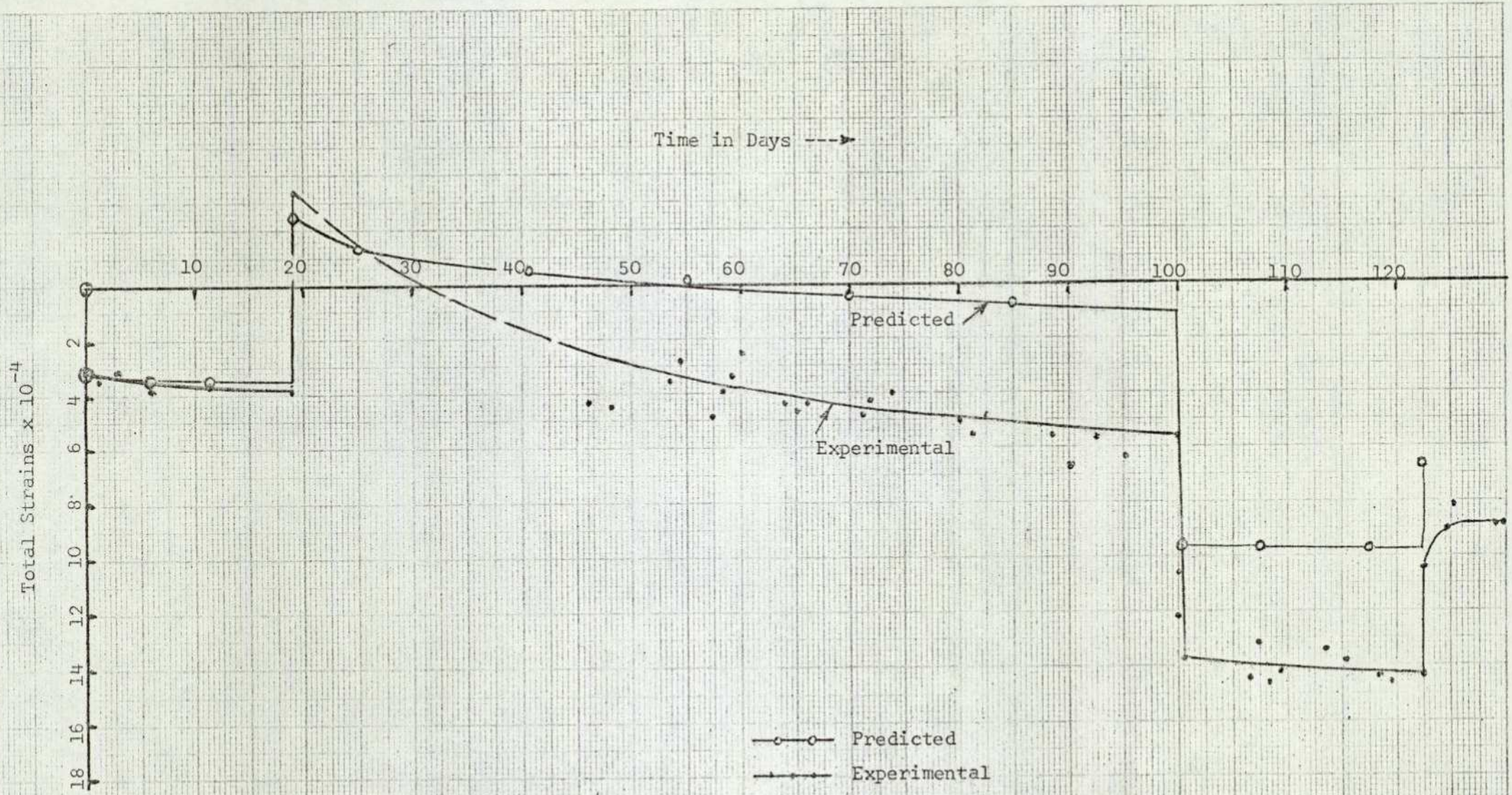


FIG 68a SERIES 1 SIDES 9/10 COMPO 1

INNER SATELLITE TANGENTIAL STRAINS 2" G.L.

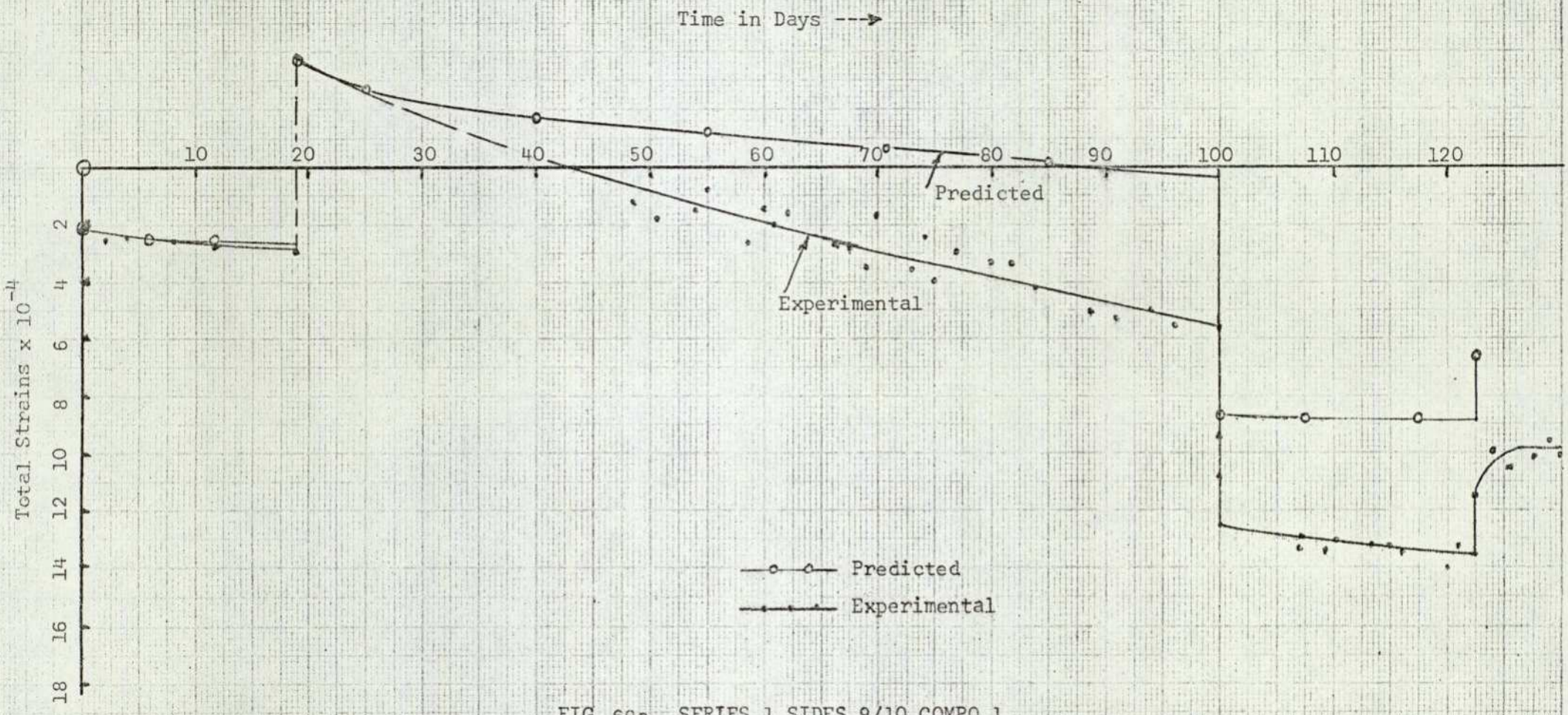


FIG 69a SERIES 1 SIDES 9/10 COMPO 1
INNER SATELLITE RADIAL STRAINS 2" G.L.

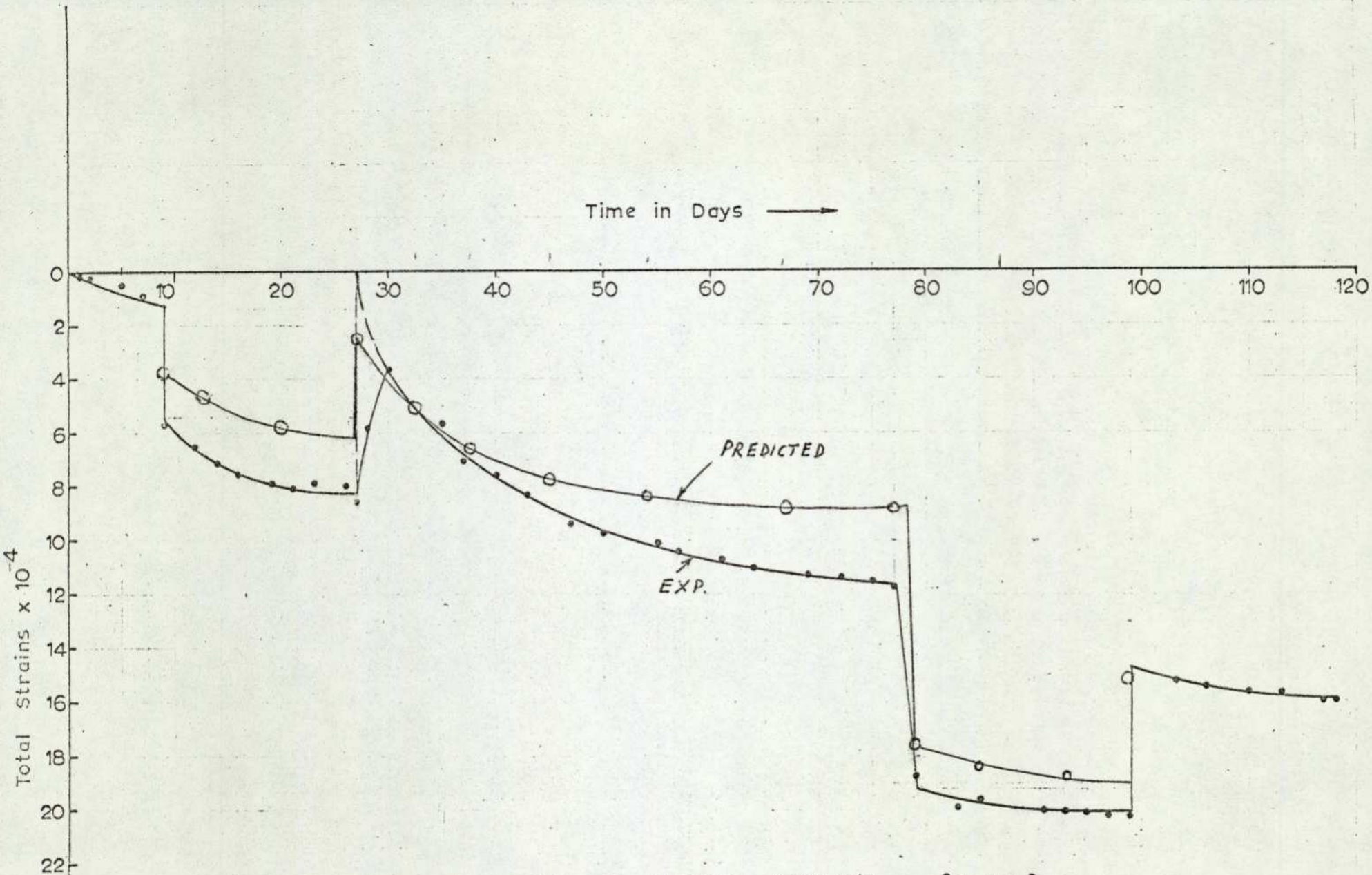


FIG 70a SERIES 2. SIDES I/2. SOLID 2

TANGENTIAL TOTAL STRAINS.

2" G.L.

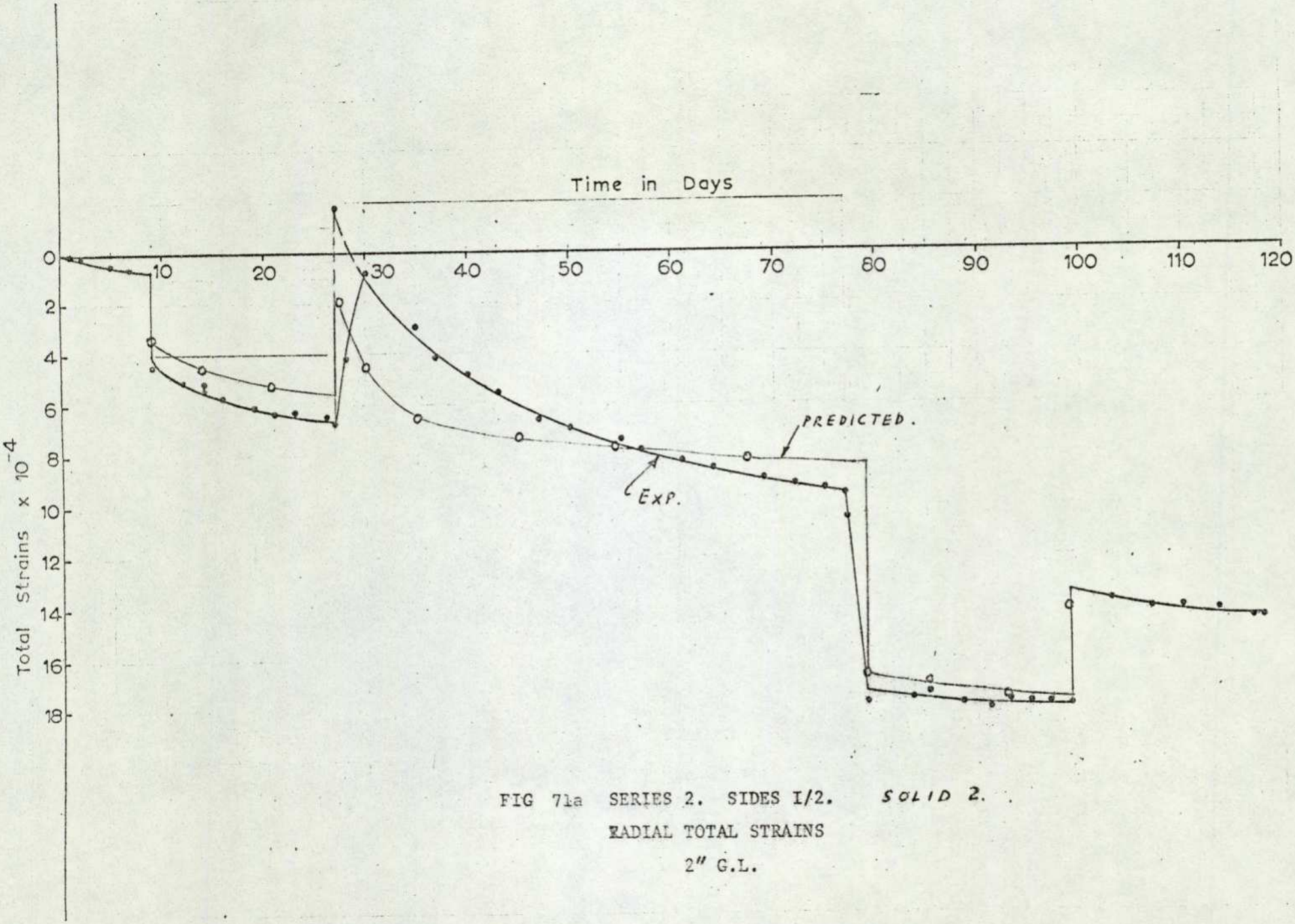


FIG 71a SERIES 2. SIDES I/2. SOLID 2.

RADIAL TOTAL STRAINS

2" G.L.

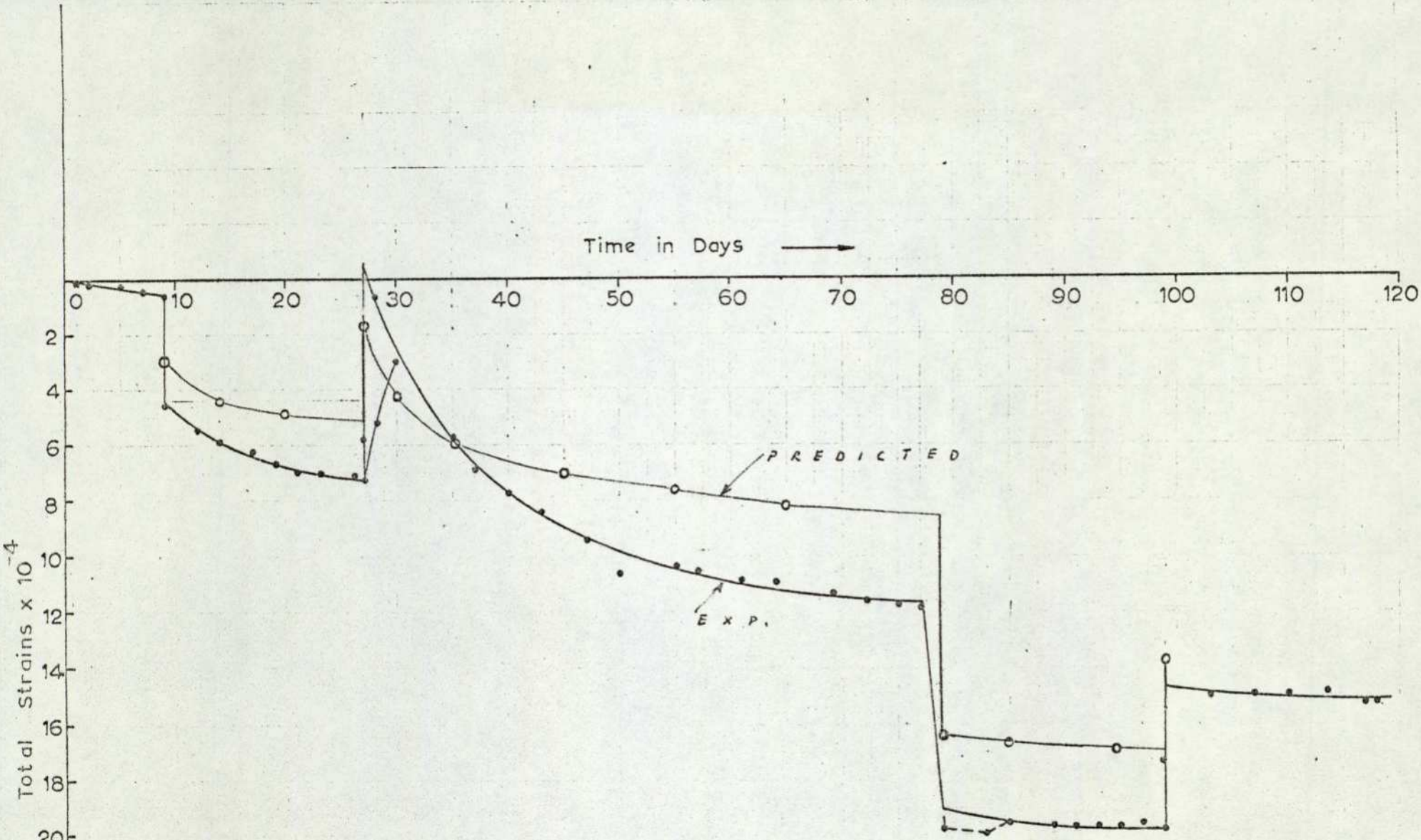


FIG 72a SERIES 2.
SIDES I/2. SOLID 2.
THREE PITCH TOTAL STRAINS.

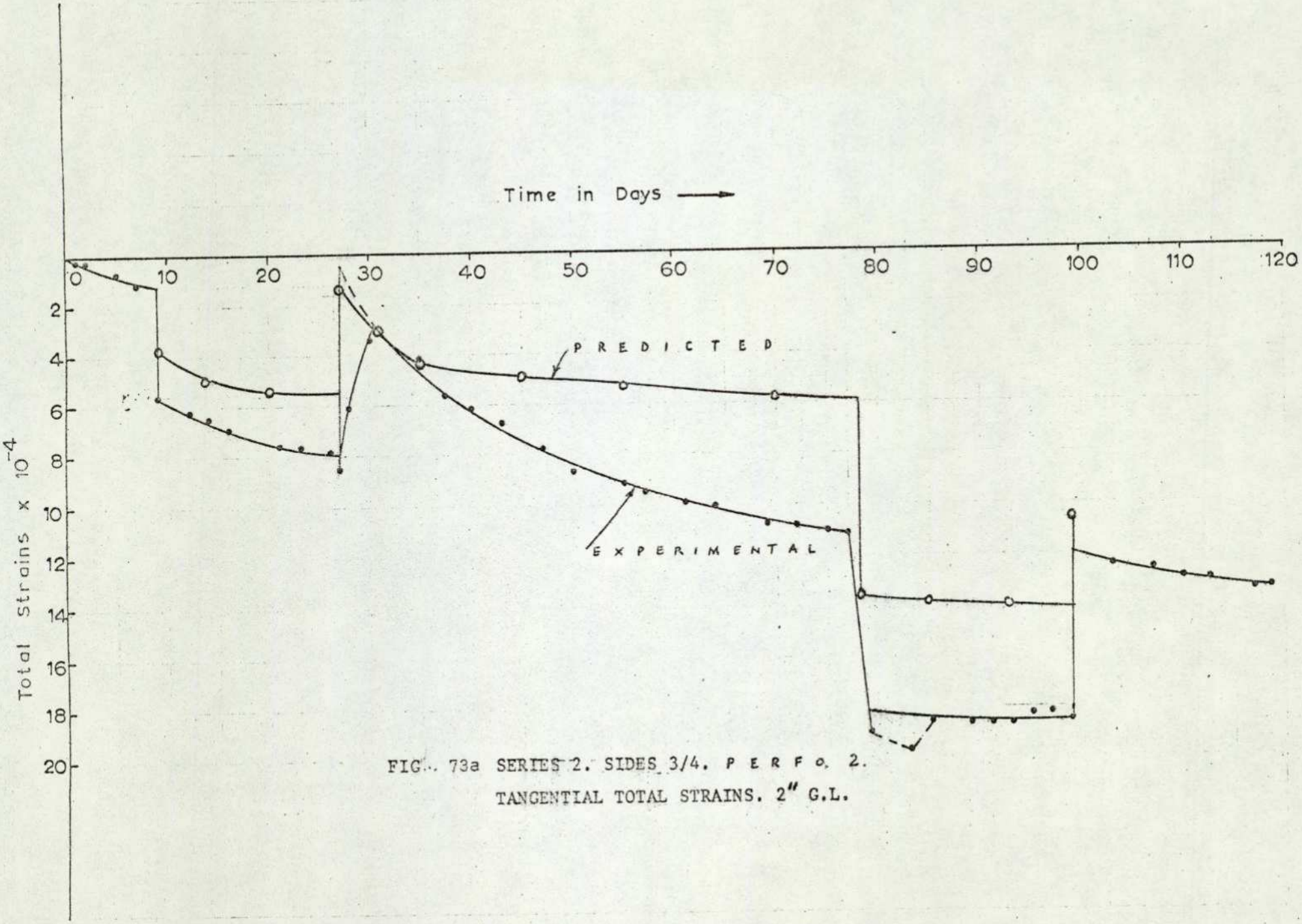


FIG. 73a SERIES 2. SIDES 3/4. P E R F o. 2.
TANGENTIAL TOTAL STRAINS. 2" G.L.

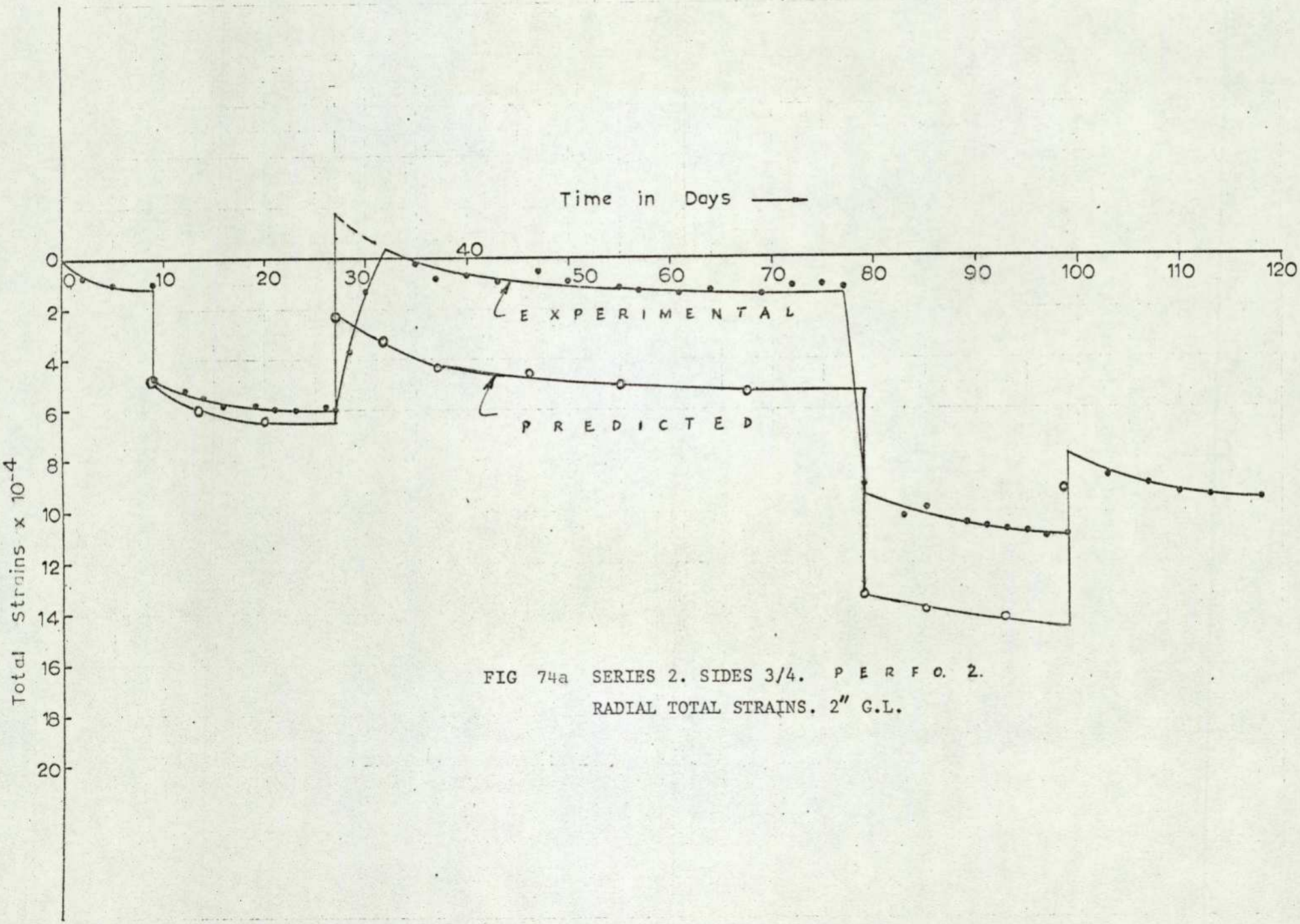


FIG 74a SERIES 2. SIDES 3/4. PERFO. 2.
RADIAL TOTAL STRAINS. 2" G.L.

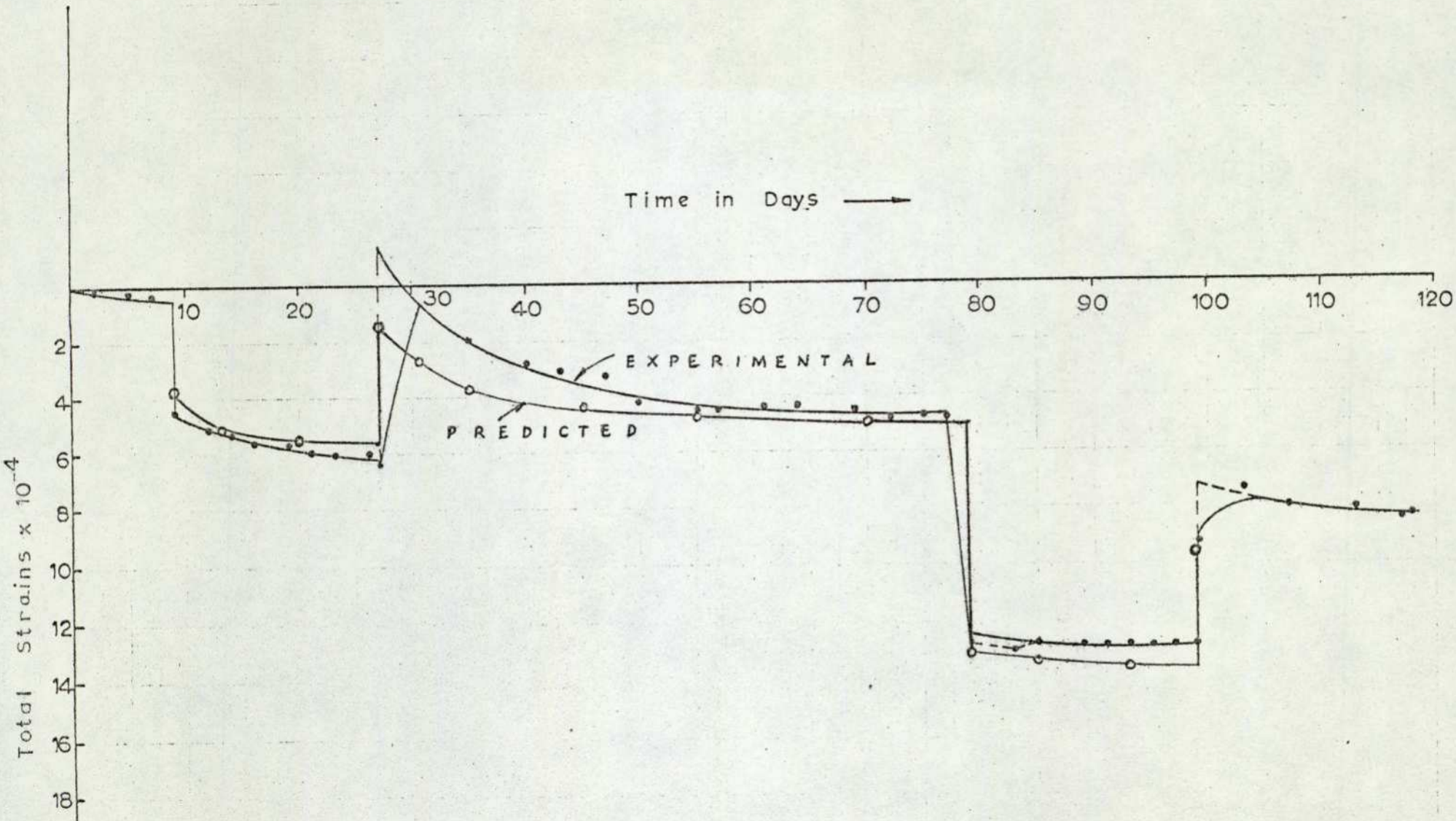


FIG 75a SERIES 2. SIDES 3/4. P E R F O. 2.
THREE PITCH TOTAL STRAINS.

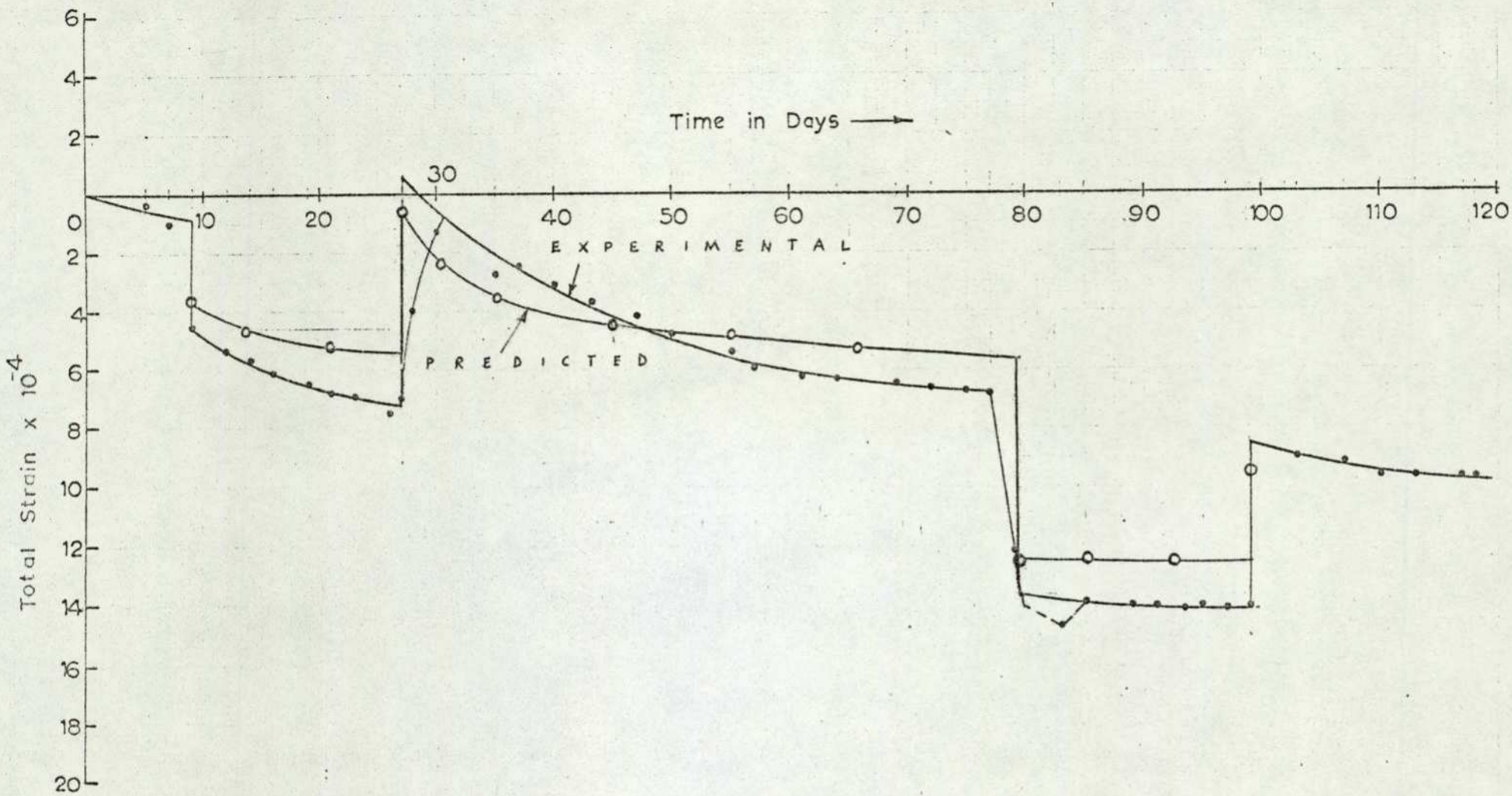


FIG 82a . SERIES 2. SIDES 9/10 COMPO. 2.

TANGENTIAL TOTAL STRAINS 2" G.L.

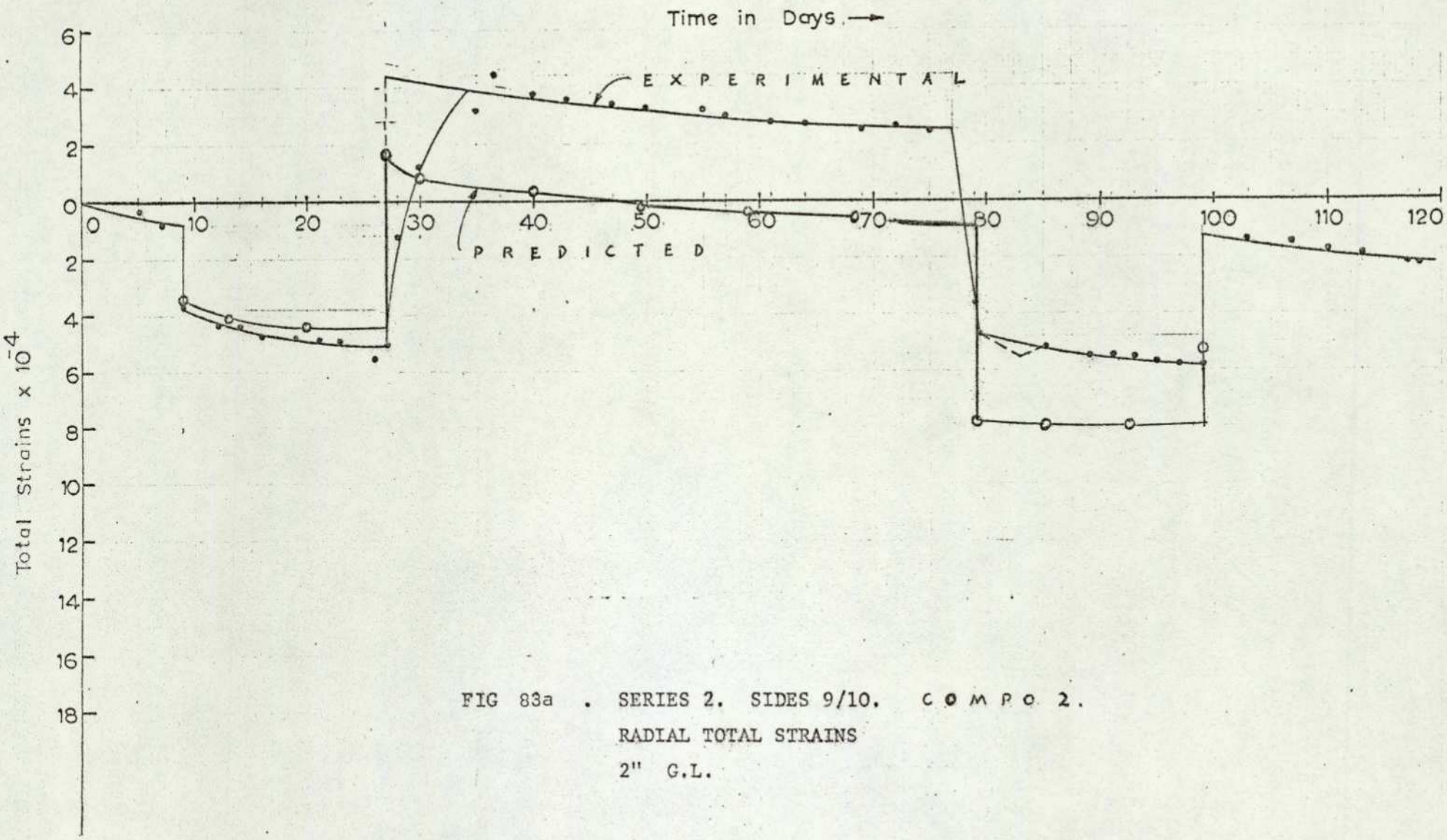


FIG 83a . SERIES 2. SIDES 9/10. COMPO 2.
RADIAL TOTAL STRAINS
2" G.L.

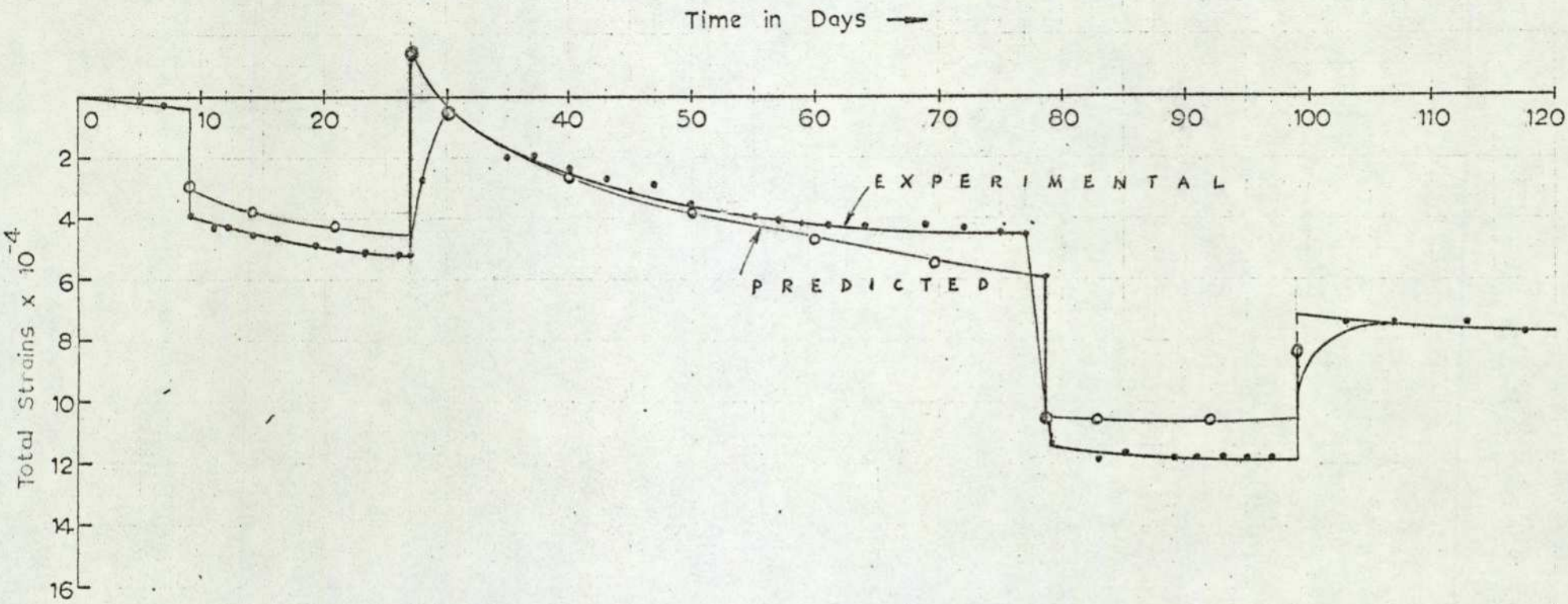


FIG 84a . SERIES 2. SIDES 9/10. THREE PITCH TOTAL STRAINS. COMPO. 2

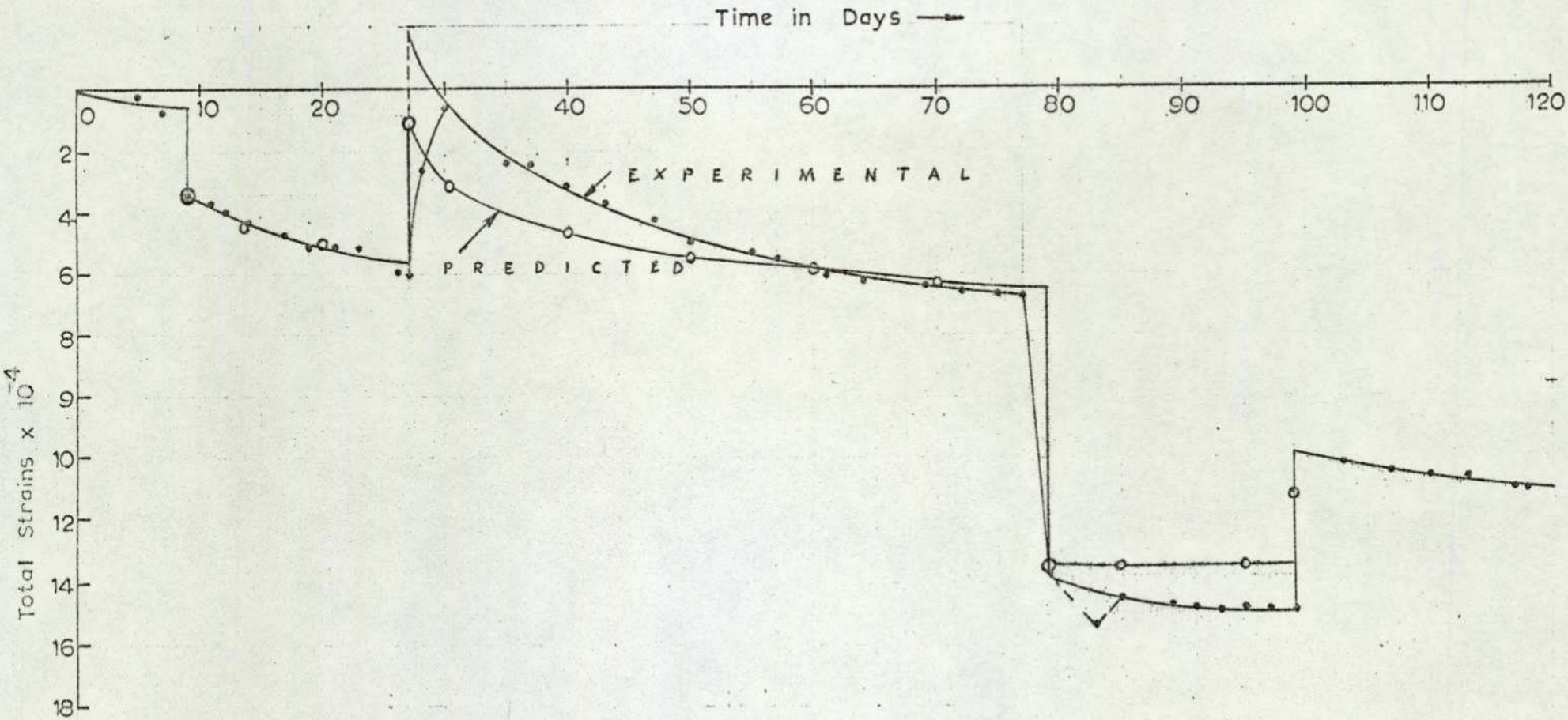


FIG. 85a. SERIES 2. SIDES 9/10. TANGENTIAL TOTAL STRAINS
OUTER SATELLITES 2". G.L. COMPO.-2.

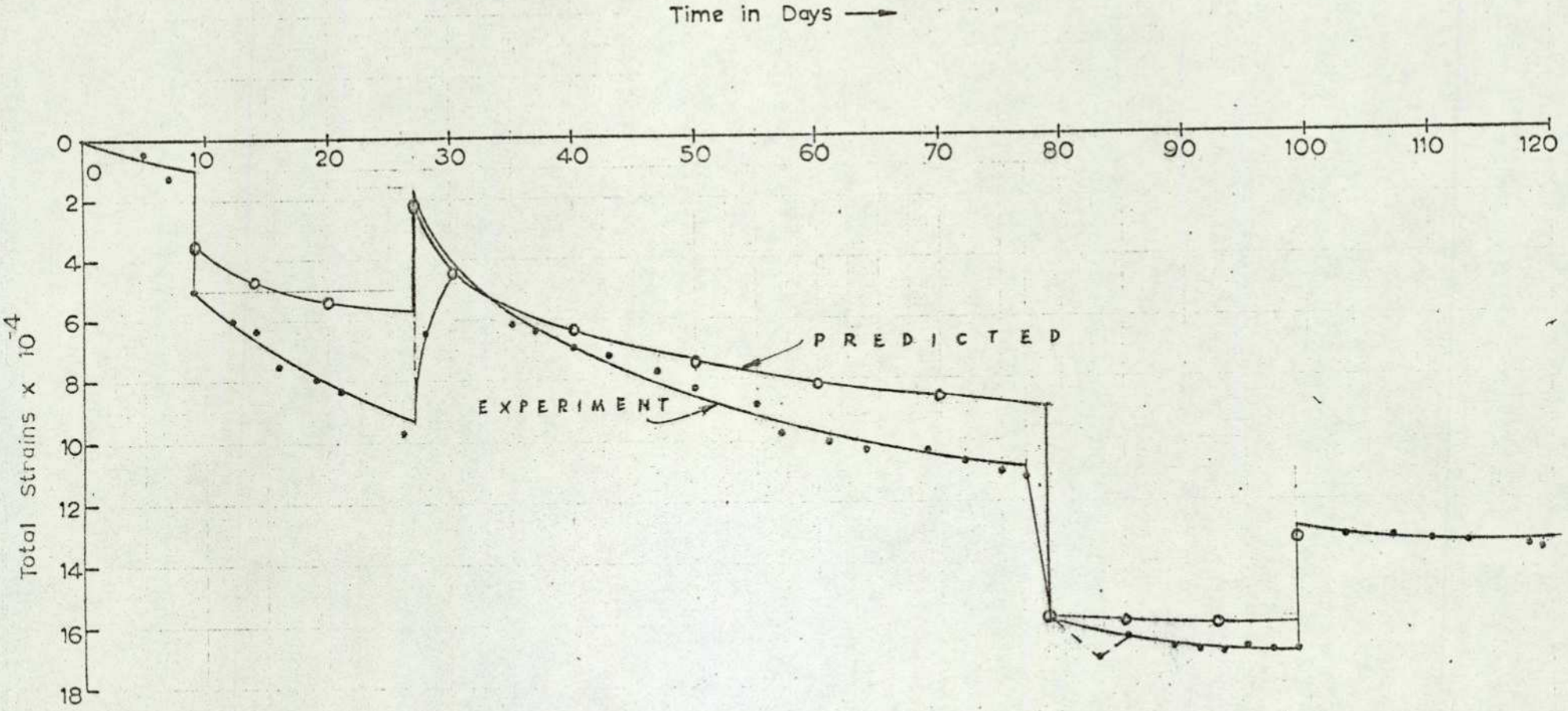


FIG 86a . SERIES 2. SIDES 9/10. RADIAL TOTAL STRAIN
OUTER SATELLITES. 2" G.L. COMPO. 2.

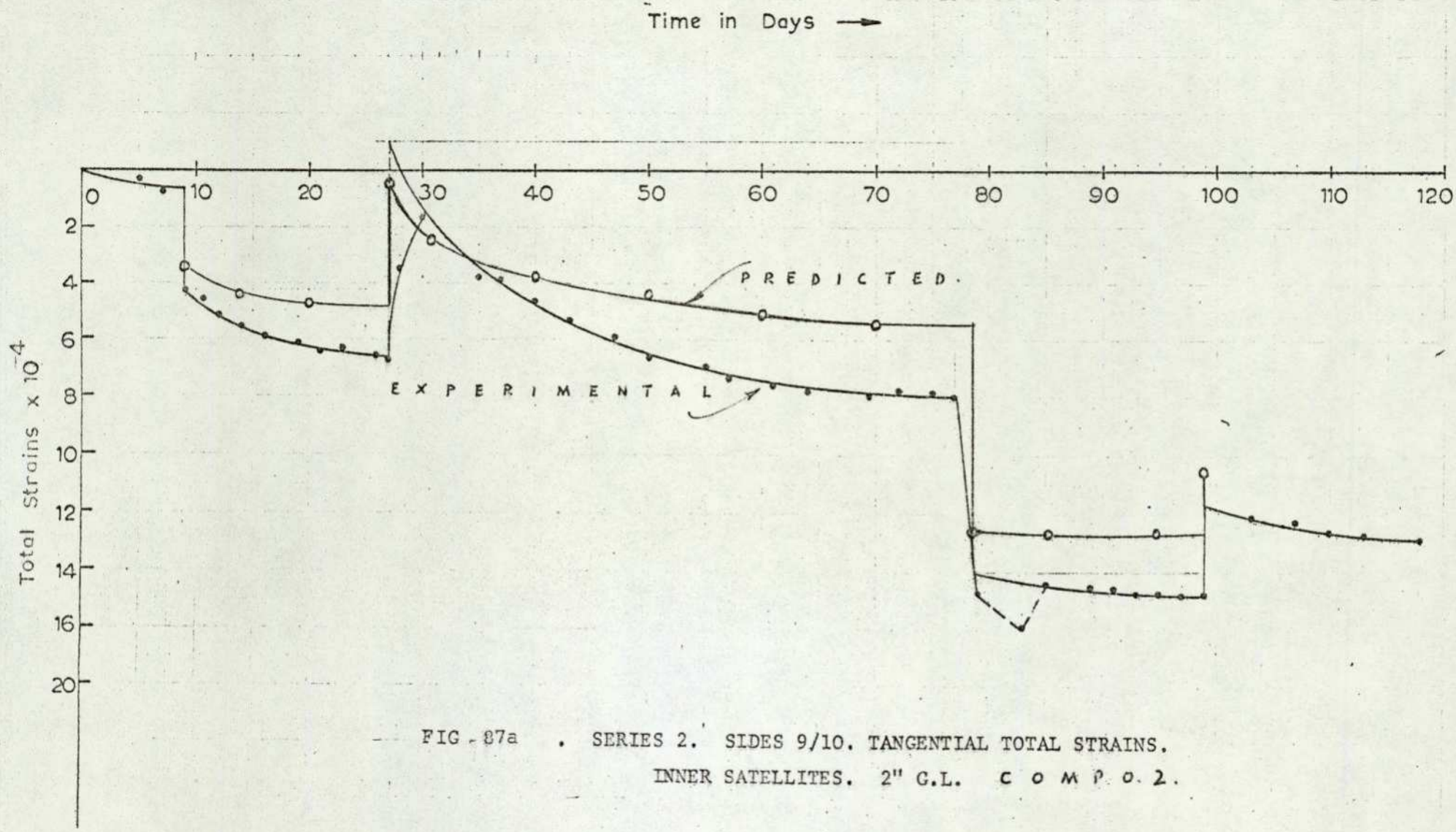


FIG - 87a . SERIES 2. SIDES 9/10. TANGENTIAL TOTAL STRAINS.
INNER SATELLITES. 2" G.L. C O M P O. 2.

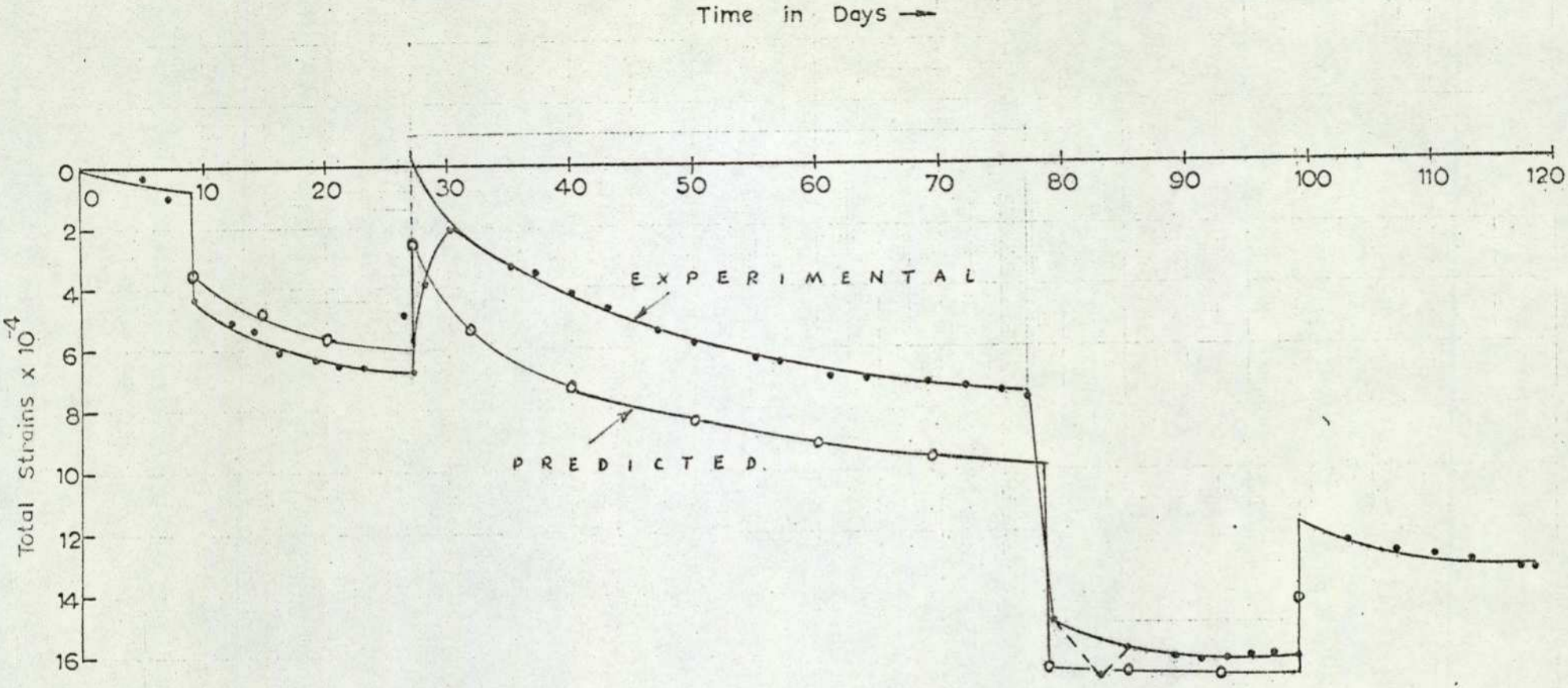


FIG 88a . SERIES 2. SIDES 9/10. RADIAL TOTAL STRAINS.
INNER SATELLITES. 2". G.L. COMPO. 2.

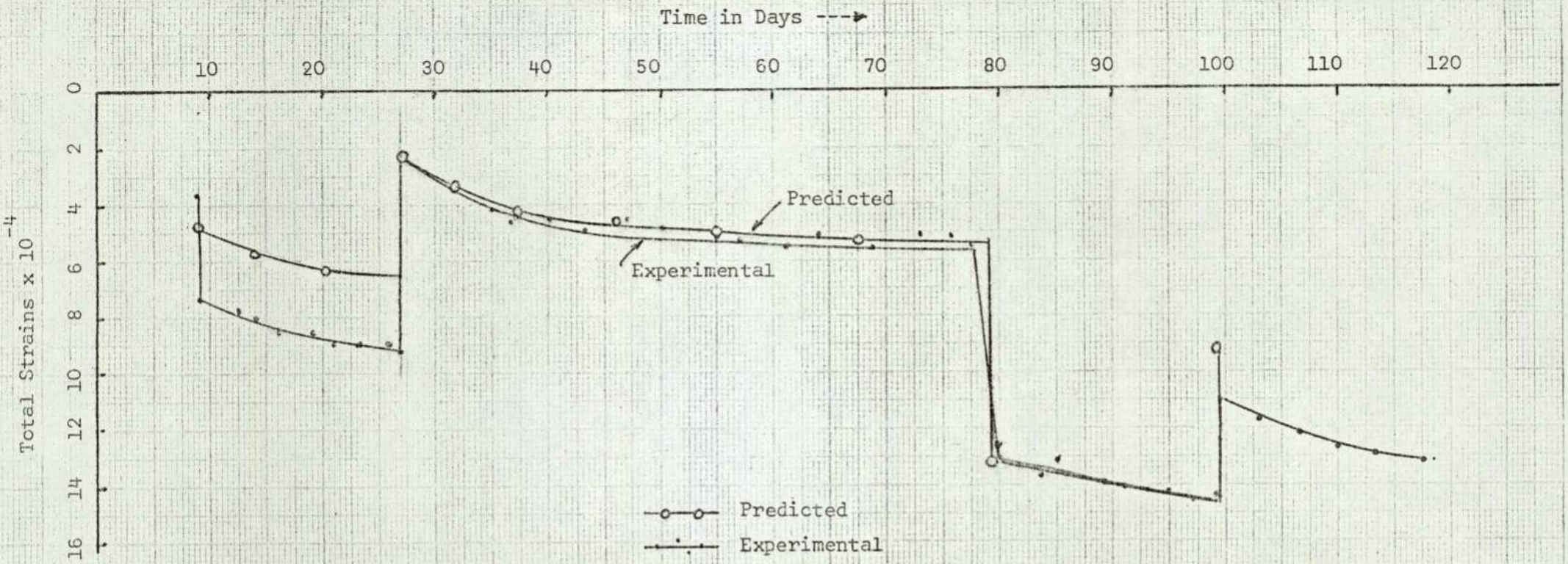


FIG 74b SERIES 2. SIDES 3/4. 2" RADIAL STRAINS
THE EFFECT OF MAKING THE ORIGIN FOR THE
ELEVATED TEMPERATURE REGIME COINCIDE
FOR THE PREDICTED AND OBSERVED STRAINS.

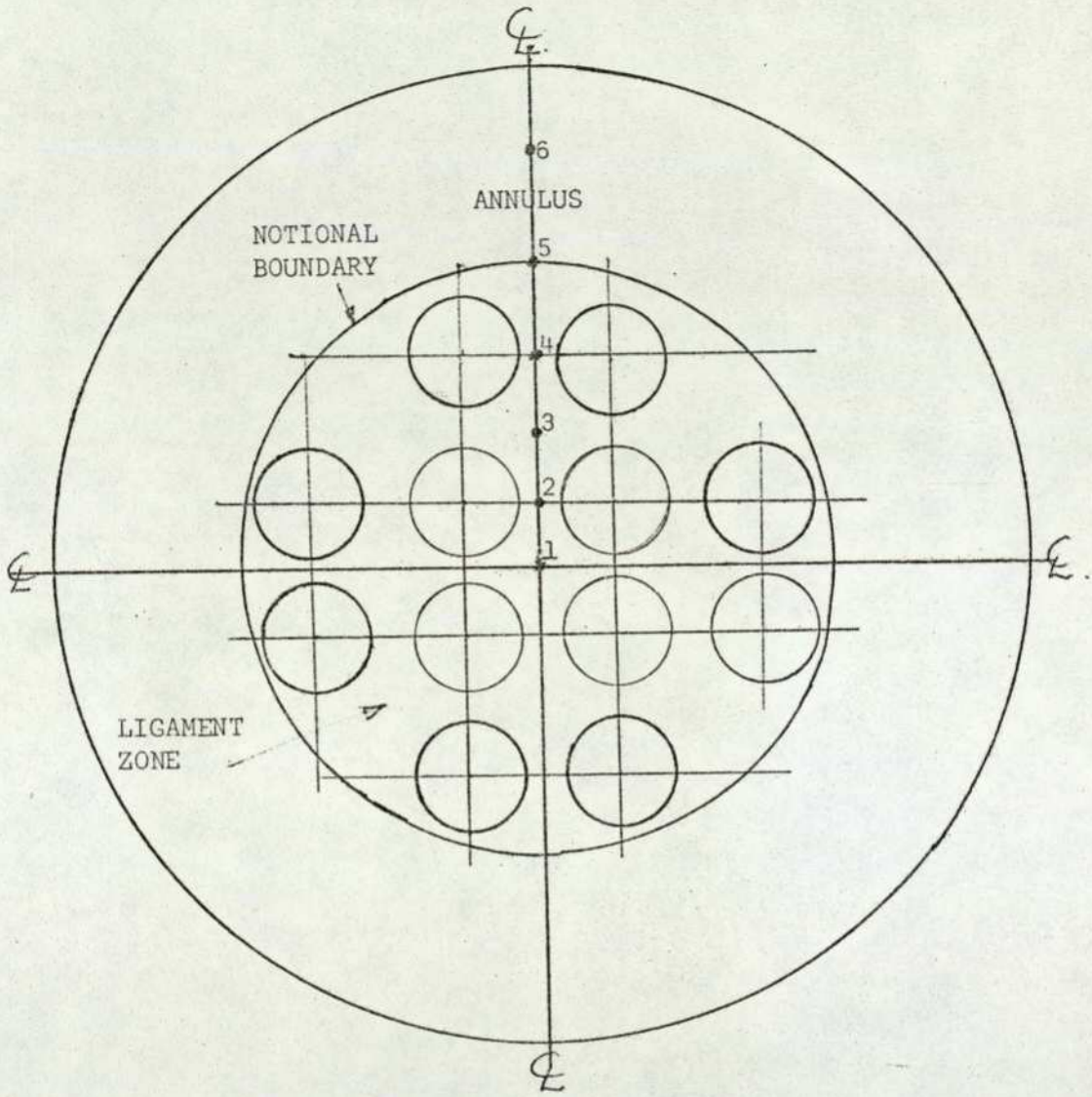


Fig 110. Series 1 & 2.Sides 9/10. COMPO 1 and 2.
Positions 1 to 6 at which stresses
were theoretically predicted by
the viscoelastic method.
See figs 111 et seq.

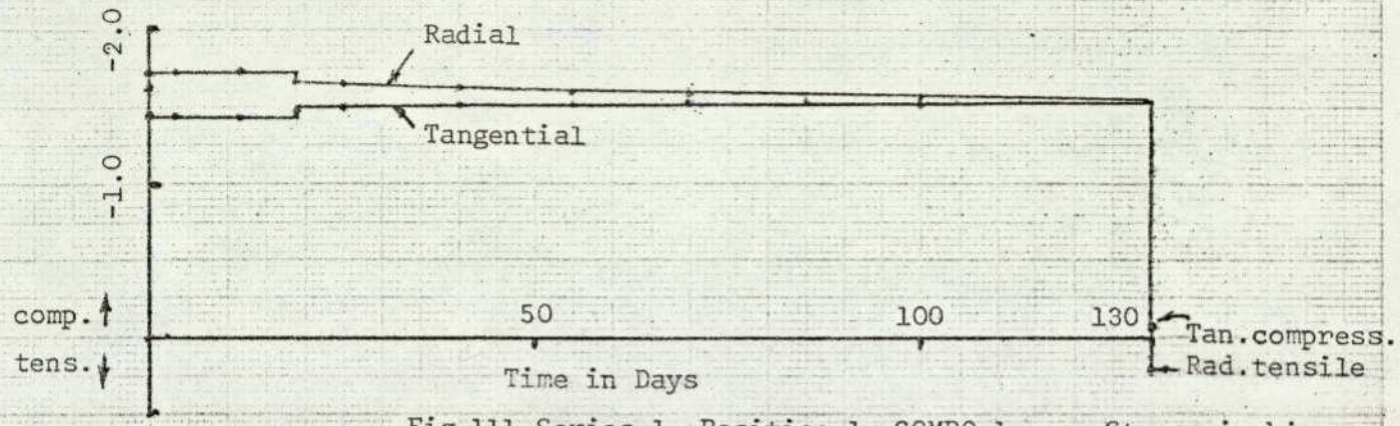


Fig 111 Series 1. Position 1. COMPO 1. Stress in kips.
Tangential and Radial Stresses.

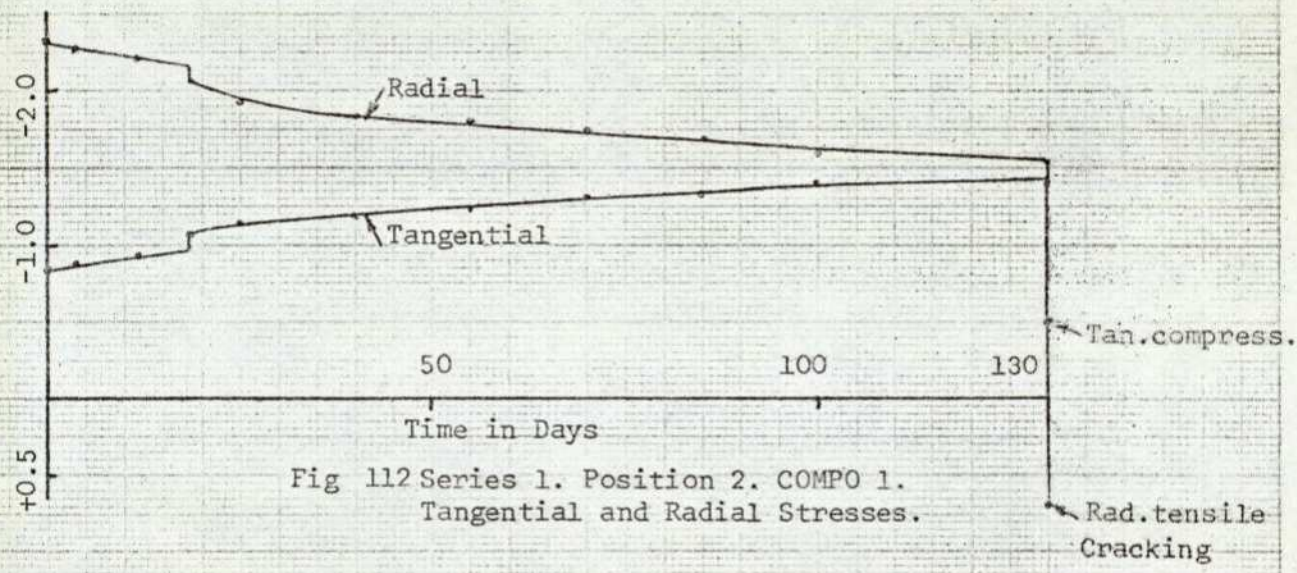


Fig 112 Series 1. Position 2. COMPO 1.
Tangential and Radial Stresses.

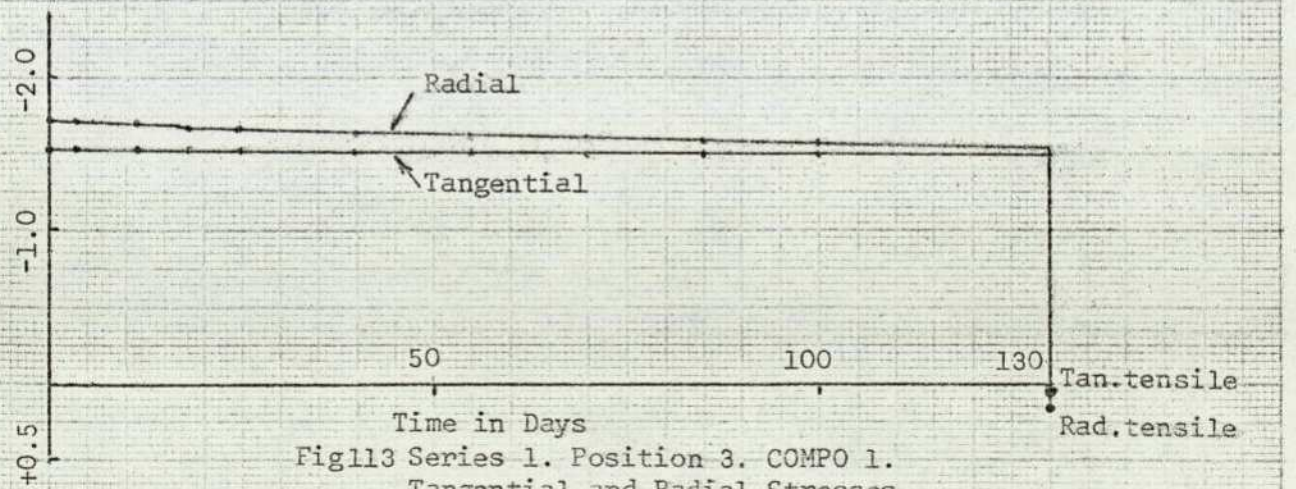


Fig113 Series 1. Position 3. COMPO 1.
Tangential and Radial Stresses.

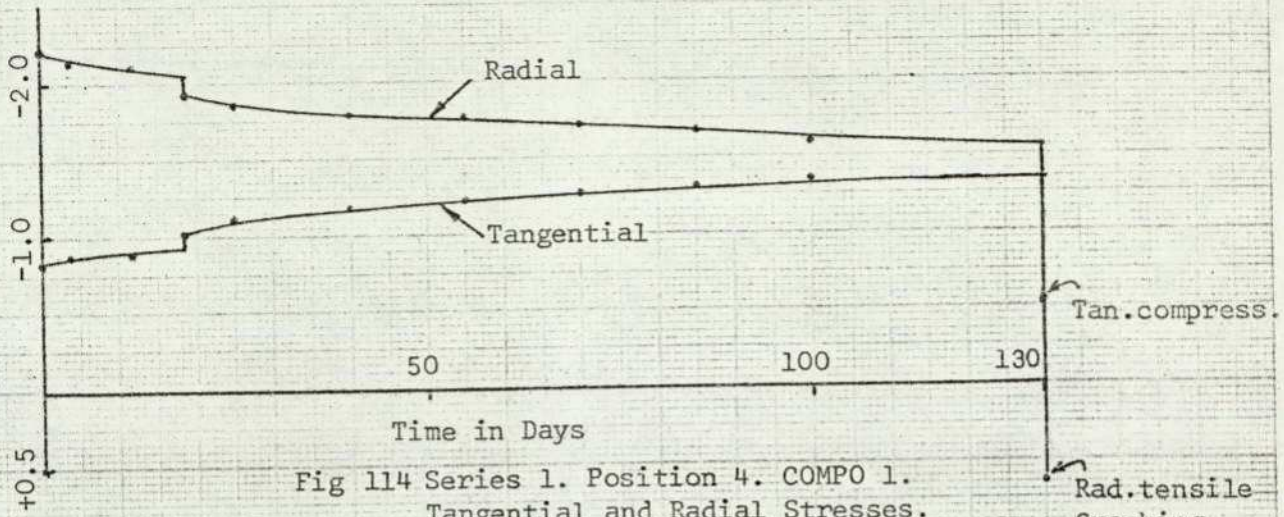


Fig 114 Series 1. Position 4. COMPO 1.
Tangential and Radial Stresses.

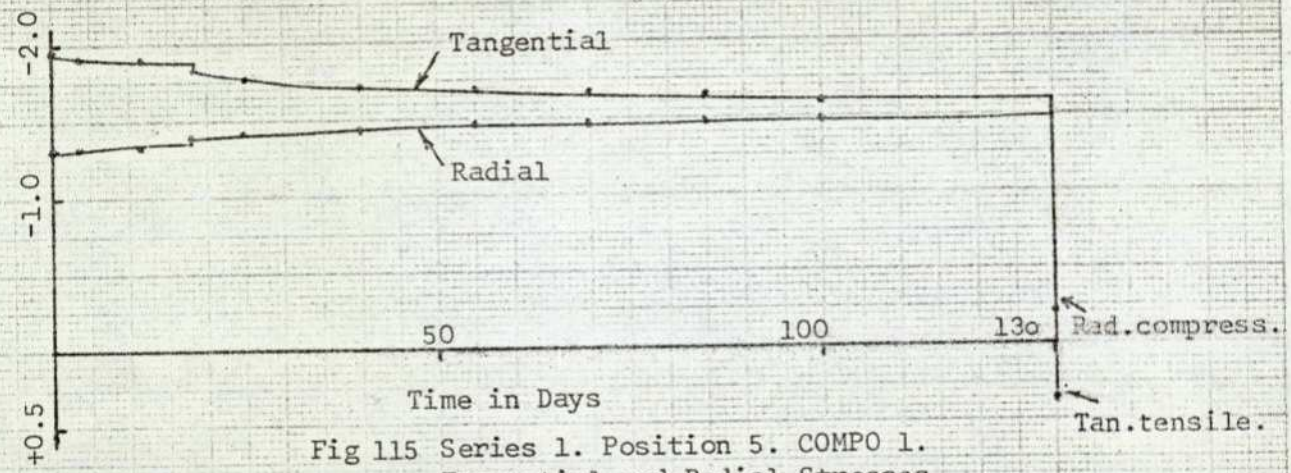


Fig 115 Series 1. Position 5. COMPO 1.
Tangential and Radial Stresses.

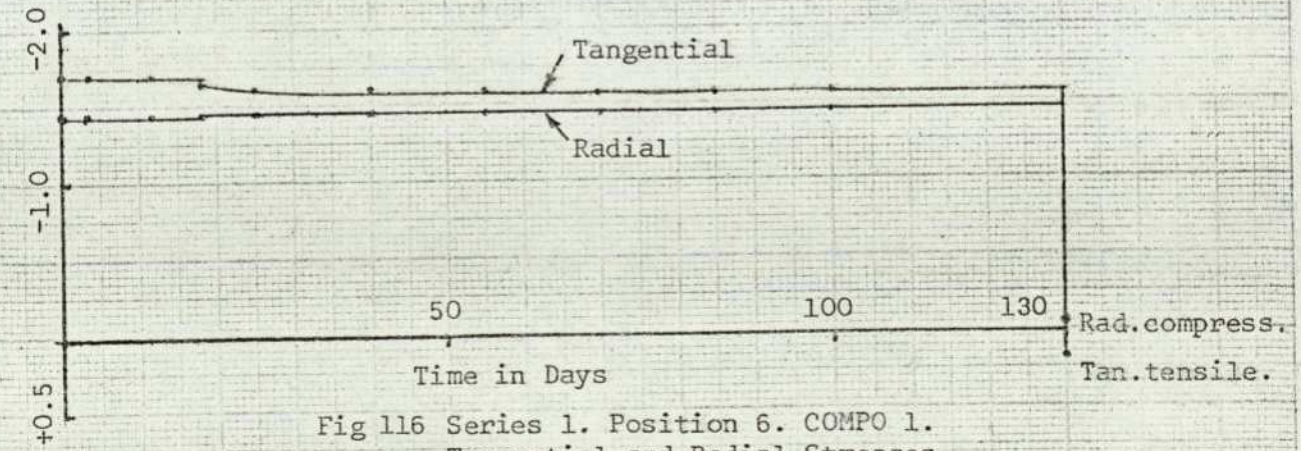


Fig 116 Series 1. Position 6. COMPO 1.
Tangential and Radial Stresses.

Theoretically Predicted Stresses.

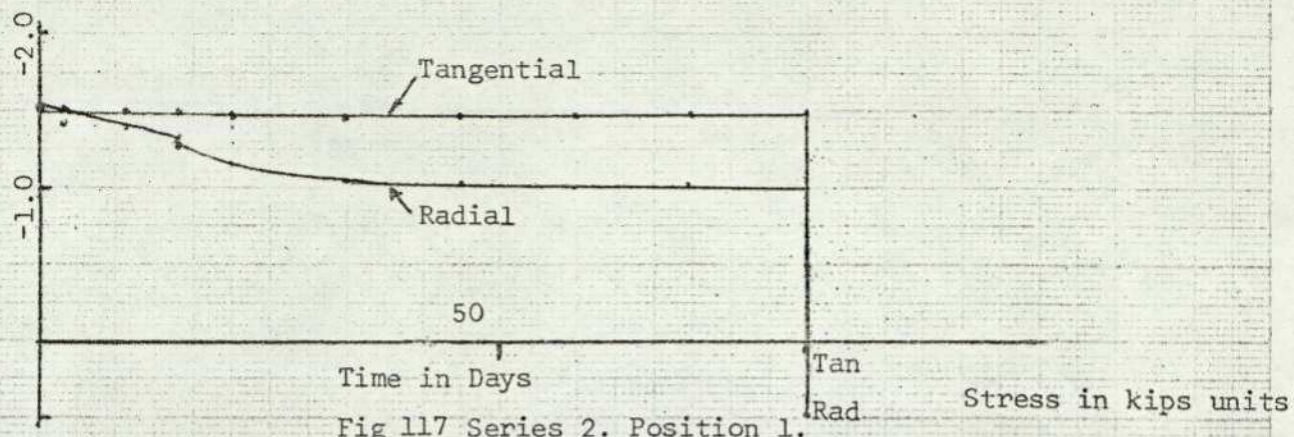


Fig 117 Series 2. Position 1.
COMPO 2
Tangential and Radial Stresses.

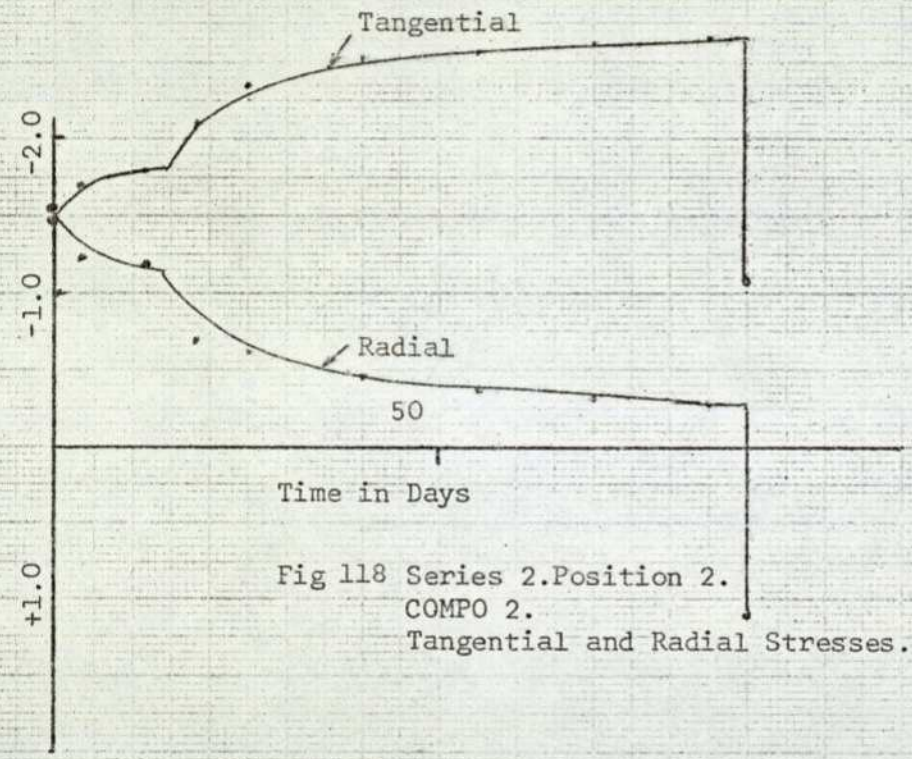


Fig 118 Series 2.Position 2.
COMPO 2.
Tangential and Radial Stresses.

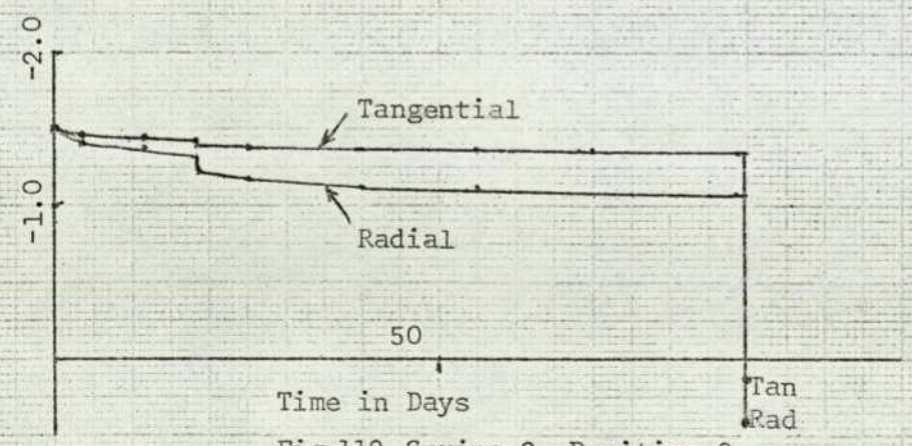


Fig 119 Series 2. Position 3.
Compo 2.
Tangential and Radial Stresses.

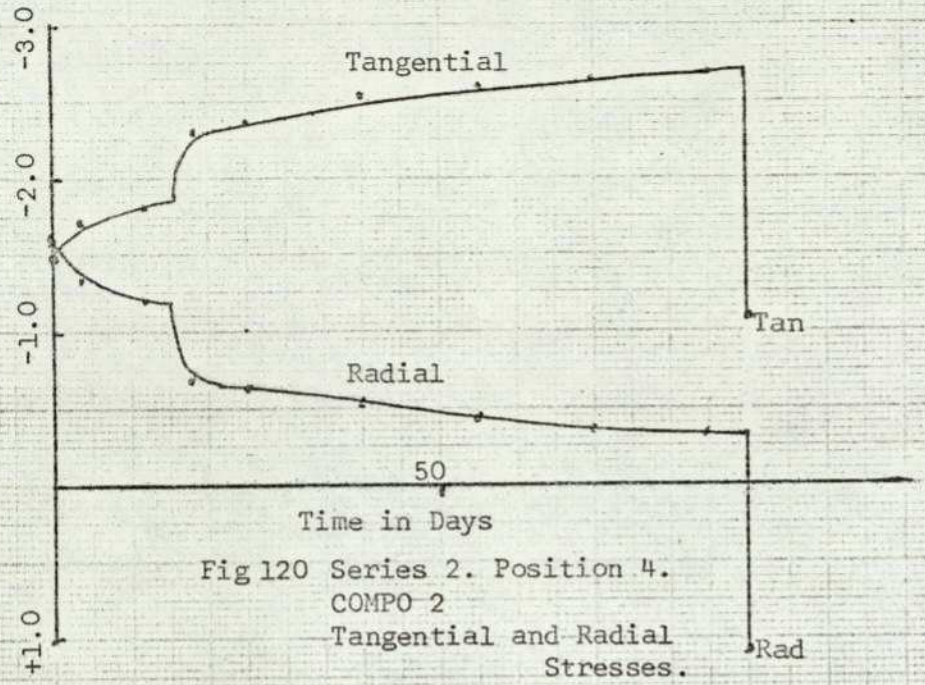


Fig 120 Series 2. Position 4.
COMPO 2
Tangential and Radial Stresses.

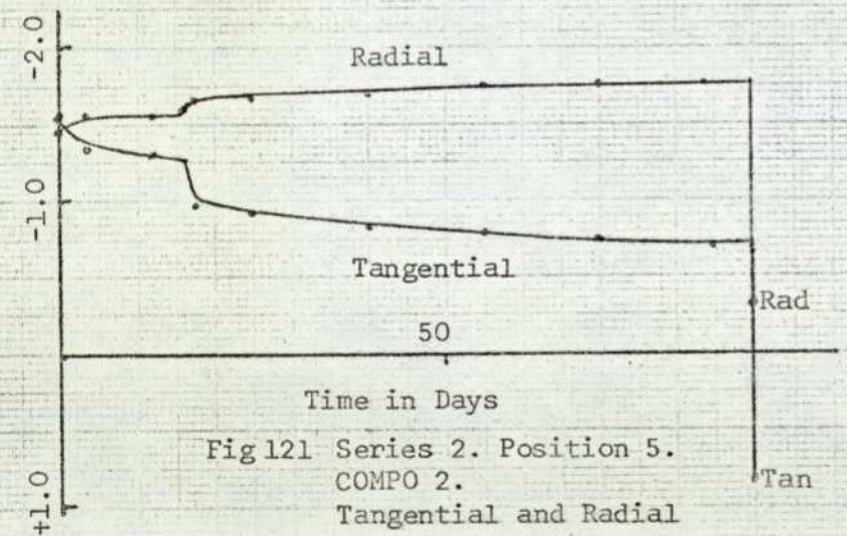


Fig 121 Series 2. Position 5.
COMPO 2.
Tangential and Radial Stresses.

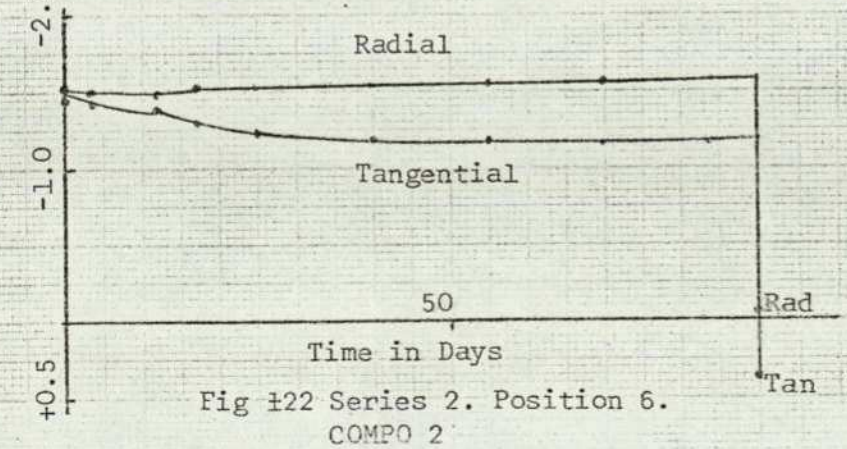
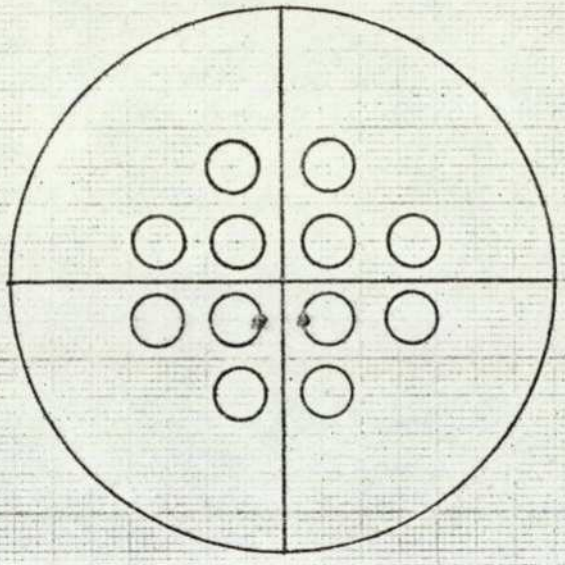


Fig 122 Series 2. Position 6.
COMPO 2
Tangential and Radial Stresses.

Stress in kips units.

Theoretical Prediction of Standpipe Stresses.



Positions in standpipes at which stresses are given below.

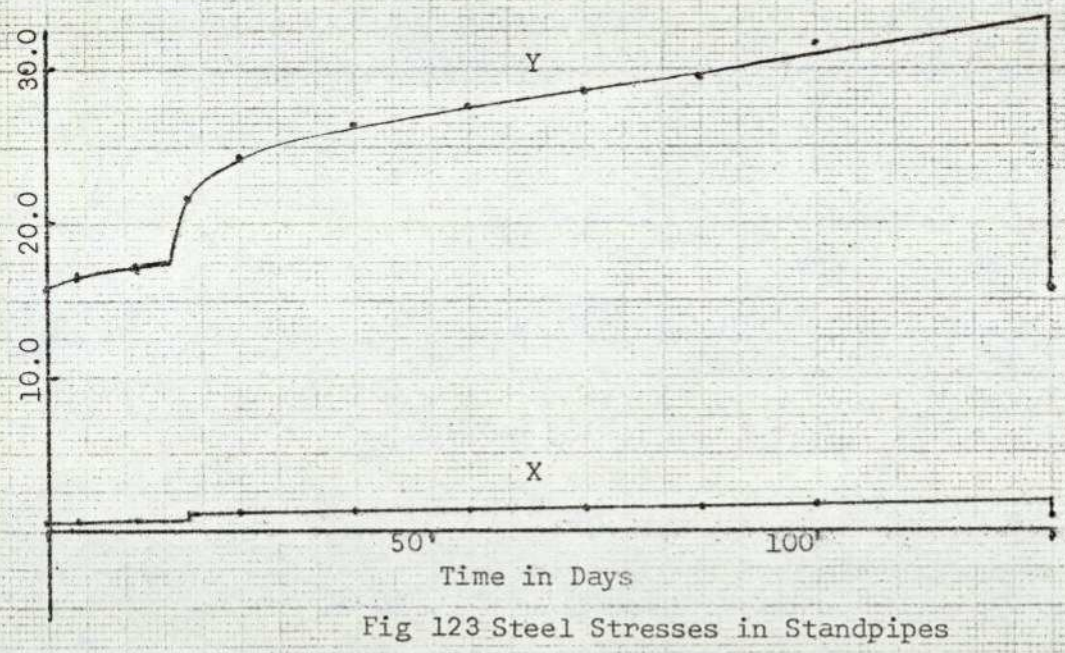


Fig 123 Steel Stresses in Standpipes

Series 1. COMPO 1. X & Y directions

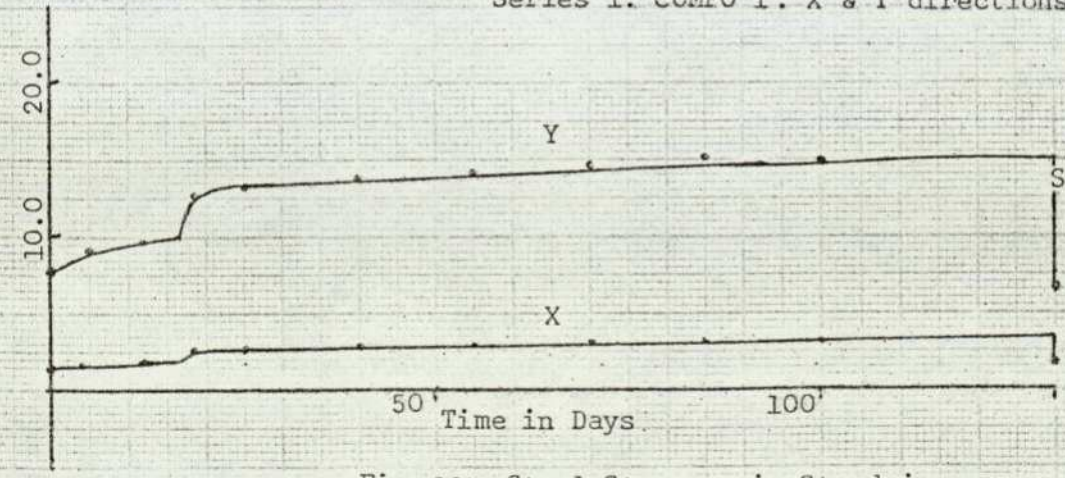


Fig 124 Steel Stresses in Standpipes

Series 2. COMPO 2. X & Y directions.

SECTION XIV

CONCLUSIONS AND RECOMMENDATIONS

CONCLUSIONS

In Section II of this thesis, the seven objectives of the investigations were first stated. Accordingly, it is in relation to these listed objectives that the following statements are made and conclusions drawn.

1. The strains occurring with time have been measured and plotted for all five specimens for both Series 1 and 2.

These strains were

a) the total strains which comprised

b) the separate components of elastic, thermal, creep and shrinkage strain,

when the specimens were subjected to thermal, and where appropriate, external mechanical loading. T he total strains have also been calculated.

2. As a result of the viscoelastic analysis undertaken, the field stresses at the interface between the perforated zone and the outer annulus have been evaluated. Thus the distribution of load at this boundary, referred to in Section II, has been assessed. Again this was done for both series of tests.

3. The internal stress distribution within the ligament zone, for the steel liners and in the adjacent concrete, for both test series, has also been assessed from the analysis.

4. The elastic strains and the equivalent Young's modulus for the perforated zone have been evaluated by measurement. See the Appendices.

In addition the creep and shrinkage behaviour of the perforated zone has been established under the loading and heating programme imposed.

Thus the elastic responses and the time-dependent behaviour,

under the test regimes, of a notional, homogeneous material structurally equivalent to the perforated zone, have been determined. These data were obtained for both series.

5. For both series of tests, those elastic constants affecting the response of the concrete to stress and temperature, have been evaluated e.g compressive strength, tensile strength, Young's modulus, the coefficient of thermal expansion. These parameters have been obtained at different points in time, and at the different temperatures in the testing programme.

The actual concrete of the models and various control specimens were used to determine these constants. See the Appendices.

In addition, the required time-dependent data, such as the specific creep and shrinkage strains, have been plotted against time for both series.

6. Series 1 models had standpipe liners $\frac{1}{16}$" thick whilst the liners for Series 2 were $\frac{1}{4}$" thick.

Initial calculations, using Sheffield's theory, and given in the Appendices, indicated that the ratio of equivalent Young's modulus for the perforated zone to the Young's modulus for the surrounding concrete should be approximately 0.5 for Series 1 and approximately 1.0 for Series 2.

The corresponding experimental values of these ratios for Young's modulus proved in no case to be greater than about 7% different from the calculated values. This was true at all stages of test and even under the elevated temperature conditions.

Significant differences in strains and in the consequential stresses, due to the differences in liner wall thickness for the two series, were observed.

Diminution of stress undoubtedly occurred in the ligament

zones, leading to some cracking ; comments are made elsewhere in these conclusions concerning the change in magnitude of the effective prestress within the perforated zone.

7. A time-dependent solution, based upon a viscoelastic analogue, has been presented herein, for forecasting the behaviour of the models investigated in these experiments. The predictions show an acceptable correlation with observed data.

The tested specimens were not, however, even scale models of a full-size end slab structure. They weremerely generally representative. Moreover, the testing conditions in the laboratory could not simulate actual operating conditions in a real reactor, and the support restraints were markedly dissimilar.

These significant differences, therefore, demand extreme caution in the utilization of the results and conclusions from these experiments, for the assessment of the behaviour of a real, full-size reactor charging face end slab.

Loss of Prestress

One of the main reasons for the commissioning of these experiments by the U.K.A.E.A was to ascertain if a loss of prestress occurred in the end slabs of P.C.P.Vs due to time-dependent effects.

The dissimilarity in detail, loading, restraint and scale between reactor end slabs and the models tested, has already been emphasized. Nevertheless, the results show that losses of stress did occur in the models, and a conservative interpretation in relation to full-size structures would indicate that the fears of the U.K.A.E.A were well-founded. Losses were revealed in the calculated redistribution of stresses both in the ligament zone and in the outer annulus of the composite specimen.

The losses in the ligament zone were particularly marked in the first series of tests employing the thinner standpipe wall thickness.

Cracking on unloading

The possibility of cracks appearing on unloading of the models had always been anticipated. The analysis predicted and the tests revealed such cracking.

During the final stages of the unloading programme, radial cracking occurred in the annulus, and cracks also appeared within the ligaments at the final decrement of loading.

Redistribution of Stress

The redistribution of stresses which occurred as steady state conditions were approached was predicted by the analysis.

Moreover, the geometrical discontinuities in the ligament zone, due to the penetrations and also to the effect of the standpipe liners, gave rise to stress concentrations, which were confirmed by the analysis.

Standpipe Liner Stresses

The creep and shrinkage of the concrete around the standpipe liners created strains which increased the stresses in the steel of the liners. This again was forecast by the analysis.

Summary

It is considered that the objectives of Section II of this thesis have been achieved, that the information listed under the seven headings therein has been obtained, and that the particular viscoelastic method of analysis presented is practicable for the geometrical configuration, the thermal conditions and the mechanical loading of the tested slabs.

RECOMMENDATIONS

A. Concerning Design Proposals on Future Reactors

These investigations have given some cause for concern about the structural integrity of the charging face end slabs in cylindrical prestressed concrete pressure vessels used to house reactor cores. These fears relate particularly to the interface between the perforated inner zones and the annuli, and also within the annuli themselves. The ligament concrete also needs consideration.

Several practical proposals may be put forward in order to alleviate the problem. This is true in view of the fact that the results of these tests have in no way indicated that the present concept of design of the prestressed vessel and its closing slabs is fundamentally unsound.

In the detailed design of the slab geometry, in the location of prestressing cables, in the magnitude of prestress provided, and particularly in the procedures for operation and maintenance of the reactor, much may be achieved to improve the safety and reliability of the structure.

1. The width of the concrete ligaments between penetrations should be increased, and the zone stiffened. This may be achieved by

   a) the development of charging probes capable of servicing more fuel channels in the core from a single penetration through the slab ; this would reduce the overall number of penetrations.

   b) increasing the thickness of the wall of the steel tubes lining the penetrations ; attempts should be made to equate, as far as practicable, the stiffness of the perforated zone and the annulus.

   c) improving the cooling efficiency in the region of the

penetrations through the slab ; more efficient insulation, better heat transfer, more efficient coolants could lead to a minimization of the dimension required for the annular cooling lobes around the penetrations.

2. The use of a higher grade of concrete, particularly within the ligament zone, would increase the strength and the elastic modulus and would reduce the creep and shrinkage effects.

3. The provision of increased amounts of high grade reinforcement steel within the ligaments would improve the structural stiffness and limit the time-dependent movements. Anti-crack reinforcement should also be provided in the annulus.

4. The employment of better grade prestressing steel and the imposition of a greater magnitude of initial prestress would offset the loss of prestress at the critical sections. Checking of prestress and restressing of the cables, (which would remain ungrouted), should become a routine maintenance operation.

5. If the ligament thickness can be increased, it may become possible to relocate the prestressing elements within the ligaments.

6. The combined effects of cooling and pressure blow-down could give cause for concern, particularly at positions of geometrical restraint and in positions where even but indeterminate temperature gradients occur, and sharp temperature differences develop.

Sophisticated techniques have been employed for many years in identifying dangerous operating conditions, and in assessing the consequences of malfunction. However, it seems only prudent to ensure that the structure is called upon to suffer thermal expansion and contraction stresses at as slow a rate as may be practicable.

Similarly, pressurization and blow-down should be very slow

procedures. Moreover, simultaneous shut-down and blow-down will cause a further indeterminate transient state of stress, and should be avoided.

Finally, it appears necessary always to maintain a temperature somewhat above the ambient, so that the full severity of cooling may be avoided. Similarly, depressurization should not lead, most particularly in the early months of operation, to the internal gas pressure being reduced to zero.

B. Concerning Further Research and Analysis

A number of viable analytical methods are available for the investigation of the stress distributions in vessels and sections of vessels of the P.C.P.V type.

The viscoelastic method, inter alia, requires for its utilization, data concerning the concrete used in the construction. These data are the elastic constants and the deformational parameters characterizing the creep and shrinkage behaviour.

From such experimental results, creep and shrinkage laws could be established, which could be fed into the analytical programme as input data. For the present series of tests only two types of concrete were investigated, and to that extent, the applicability of the method proposed herein, is limited. Whilst the principles put forward are general, the appropriateness of the data obtained relates only to the concrete material actually employed.

Thus there is a need for a range of practical concrete mixes to be tested, and a range of values and a corresponding spectrum of creep and shrinkage expressions evaluated, with their coefficients and indices numerically determined, in order that the viscoelastic method may be more widely and appropriately applied. Similarly, the viscoelastic model may need extension or refinement to cover wider ranges of variables.

The results of tests of this kind would be applicable not only in the analysis of nuclear reactor P.C.P.Vs, but also for a whole class of structural problems and geometries, for which time-dependent deformation laws govern the redistribution of stresses.

One important experimental verification in particular is needed. Is the magnitude of shrinkage occurring in unloaded concrete, of the same order as that taking place in loaded concrete?

Finally, the work carried out in the present experiments could be readily extended to include an investigation of the effects of peripheral moments resulting from rim fixity, of transverse uniformly distributed loading of the slabs, and of realistic temperature gradients across the slabs. This would simulate more closely real conditions in an operating reactor vessel.

SECTION XV

APPENDICES

APPENDIX A. CONTROL TESTS.

APPENDIX B. SHEFFIELD'S THEORY.

APPENDIX C. EFFECTIVE MODULUS METHOD.

APPENDIX D. EXPRESSIONS PROPOSED FOR CREEP.

APPENDIX E. COMPUTER OUTPUT.

APPENDIX F. CURVE-FITTING PROGRAM AND OUTPUT.

APPENDIX A.

CONTROL TESTS

Series 1

Control specimens were cast at the same time, and from the same mix as that used for the actual specimens, as follows:

Batch 1. 4/4" X 4" X 4" cubes for compression testing

2/4" X 4" X 12" prisms for elastic modulus tests one prism containing two thermocouples.

2/4" X 4" X 12" prisms for coefficient of thermal expansion tests, each prism containing two thermocouples.

2/6" X 9" cylinders for the cylinder-splitting tests (Brazilian tests).

Batch 2. As for Batch 1.

Batch 3. Also as for Batch 1, except for the cylinders.

Curing was carried out under wet hessian, until the specimens were required for testing.

The requirements of B.S. 1881. Methods of Testing Concrete were satisfied during the tests. One 4" X 4" X 4" cube from each batch was crushed after 14 days and one from each batch thereafter after 28 days, 8 weeks and 3 months respectively.

The results and averages of the tests at each age are given in the following table.

CONCRETE COMPRESSION TESTS ON 4" CONTROL CUBES

	AGE	FAILURE LOAD	CRUSHING STRENGTH	AVERAGE STRENGTH
BATCH 1	14 days	39 tons	5470 psi	
2	14 days	39 tons	5470 psi	
3	14 days	37 tons	5180 psi	5370 psi
BATCH 1	28 days	47.8 tons	6680 psi	
2	28 days	47.75 tons	6680 psi	
3	28 days	41.8 tons	5860 psi	6410 psi
BATCH 1	8 weeks	54 tons	7560 psi	
2	8 weeks	57 tons	7960 psi	7760 psi
BATCH 2	3 months	65 tons	9100 psi	
3	3 months	62 tons	8690 psi	8895 psi.

CYLINDER SPLITTING TESTS.

This test was applied to the cylindrical specimens on their sides. The splitting tensile strength is given approximately by:

$$\sigma = \frac{2p}{\pi d.l}$$

where p = the failure load in lbs.

d = the diameter of the cylinder in inches.

l = the length in inches.

The stress so obtained is considered to be approximately 15% higher than the direct tensile strength.

The 6" X 9" cylinders were loaded in compression on their sides, in contact with $\frac{1}{8}$" X 1" hardboard strips at the top and bottom.

The load was applied without impact and was increased continuously at approximately 200 psi per minute until the specimens split into two parts.

Two cylinders were crushed from Batch 1 after 28 days, and the remaining two from Batch 2 after 3 months. The results and averages of these tests at each age are given in the following table.

TENSILE TEST RESULTS

	AGE	FAILURE LOAD	AVERAGE FAILURE LOAD	SPLITTING TENSILE STRENGTH	DIRECT TENSILE STRENGTH
BATCH 1	28 days	15.7 tons 16.5 tons	16.1 tons	425 psi	370 psi
BATCH 2	3 months	18.74tons 18.30tons	18.52 tons	487 psi	424 psi

Splitting tensile strength $= \frac{2p}{\pi dl} = \sigma$ psi.

Direct tensile strength $= \frac{100\,\sigma}{115}$ psi

MODULUS OF ELASTICITY TESTS

Batch 1 and batch 3 specimens were used for these tests. They were 4" X 4" X 12" long and were tested at ages of 11 weeks and 3 months. In addition, E values for the concrete were obtained at each stage in the testing regime by load-cycling the actual models. This was done at every significant change in the loading and heating programme.

The concrete prisms were loaded axially in an Amsler compression machine. 8" Demec gauge lengths were employed on opposite 12" X 4" faces of the control specimens. The gauge lengths were set out using Demec studs affixed to the prism faces by adhesive.

The platen faces of the machine were bedded on to the ends of the specimens by means of 4" X 4" X $\frac{1}{2}$" steel plates and $\frac{1}{2}$" asbestos board. Extreme care was taken to ensure verticality of the specimens in the machine, concentricity of the load positioning, and accuracy in the setting-out of the gauge lengths.

Loading increments of 2 tons were employed upto 20 tons. Similar decrements were employed on unloading. Demec strain readings were taken on each of the opposite faces during four load cyclings.

Averaged readings of the two corresponding opposite-face strains were utilized for plotting stress-strain graphs. This was done for the fourth cycle only. The linear gradient of the graph gave the required value of E. The strain was calculated by multiplying the differences in readings by the 8" Demec gauge factor which was 1.005×10^{-5}.

The room temperature tests gave a value of the modulus of elasticity for the control specimens of 4.97×10^6 psi, and 4.94×10^6 psi for 11 weeks and 3 months respectively.

Similar tests were also carried out at 80°C on batch 1 and batch 3 specimens at 15 weeks.

Two thermocouples were symmetrically introduced into each of these heated specimens, being coated with PS adhesive and allowed to dry before casting into the concrete.

Flexible compensating cables were joined to the thermocouples by twisting together the two appropriate pairs of bared ends, by soldering, and then by wrapping in insulation tape. The lengths and resistances of the cable leads and the dummy lead were identical. The leads were connected to a switch-box in series with a Scalamp galvanometer. The scale of the galvanometer was calibrated against the boiling point of pure water.

Isopad heating tapes, wrapped around the control specimens leaving only the Demec studs accessible, were used to raise the temperature of the concrete. Heat input was controlled by a variac which achieved the required temperature of 80°C in three hours. The variac was sensitive enough to maintain the temperature constant during the tests. The heating, the temperature and strain measurement all were in operation whilst the specimens were under compression in the Amsler machine.

The 80°C tests gave E values for the batch 1 specimen at 15 weeks of 4.80×10^6 psi and for the batch 3 specimen at the same age of 5.0×10^6 psi.

MODULI OF ELASTICITY FROM THE ACTUAL MODELS.

Additionally, the elastic moduli of the concrete weredetermined

from the changes in strain whichoccurred when the solid specimen (1/2) was load-cycled at three different stages of the test programme.

Stage 1. At ambient temperature, at the commencement of test.

Stage 2. Before heat was switched off.

Stage 3. Before load was removed.

These results are given in the following tables.

Similarly, the effective elastic modulus of the perforated zone was determined from the perforated specimen, and for the same stages.

MODULI OF ELASTICITY FROM ACTUAL MODELS.

Series 1.

Stage	Temperature	Modulus of elasticity of concrete
Commencement of test	Ambient	4.95×10^6 psi
		5.25×10^6 psi
		5.30×10^6 psi
Before removal of heat	$80^{\circ}C$	4.90×10^6 psi
		4.75×10^6 psi
		5.00×10^6 psi
Before unloading	Ambient	4.87×10^6 psi
		4.75×10^6 psi
		4.90×10^6 psi

A comparison of the elastic moduli results obtained from the control specimens and from the actual models, reveals acceptably small differences. In general, the moduli values for the models reduced with time to a small degree. Changes in the properties of the concrete due to temperature and time-dependent straining effects were only to be expected. A representative value of the modulus of

elasticity could be taken to be about 5.0 X 10^6 psi. As will be seen later, this value could also be acceptable for the second series.

ELASTIC MODULI OF PERFORATED ZONE

Series 1.

Stage	Temperature	Equivalent Modulus of Perforated Zone
Commencement of test	Ambient	3.06 X 10^6 psi 3.16 X 10^6 psi 2.84 X 10^6 psi
Before removal of heat	80°C	3.00 X 10^6 psi 2.85 X 10^6 psi 2.95 X 10^6 psi
Before unloading	Ambient	2.85 X 10^6 psi 2.90 X 10^6 psi 2.78 X 10^6 psi

As expected, the equivalent notional modulus of the perforated zone was considerably lower than the modulus of the real concrete as given earlier. Again there were reductions with time in the values of the equivalent modulus due mainly to thermal effects.

COEFFICIENT OF LINEAR THERMAL EXPANSION OF CONCRETE

The concrete prisms, 4" X 4" X 12" previously described,were used for these tests. Each prism contained two symmetrically-disposed thermocouples, and for the expansion tests were wrapped with a $\frac{7}{8}$" thick layer of cellular asbestos/aluminium insulation. Demec studs on a 4" gauge length were glued on opposite faces of the prisms. Average readings could thus be calculated from paired observations.

The 4" Demec gauge factor was 2.03×10^{-5}, and by multiplying this value by the differences between averaged readings, the actual strain could be calculated. The tests were carried out on prisms cast from batch 1 at ages of 3 months and 30 weeks.

Thermostatically-controlled ovens were used to generate the required temperature rises and falls. The prisms were supported on rollers made of $\frac{3}{4}$" steel bars and were heated slowly from the ambient temperature of 20°C upto 80°C over a period of two days, and then allowed to cool again at a similar rate.

Hourly strain readings were taken. It took less than one minute to take the observations on each occasion and re-establish thermal equilibrium. Losses were negligbly small. The reading cycle during heating and cooling took five days. Shrinkage was allowed for by subtracting such strains from those due to thermal expansion and contraction. Shrinkage strains were calculated from the initial and final readings.

The specimens used in these tests were initially cured for 28 days, and thus the results presented are those of concrete prisms under drying conditions.

Arthanari (46) states that the linear coefficient of thermal expansion of concrete varies little with the age at test but tends to reduce as the drying-out process continues. Certainly in the present tests, results for the coefficient after removal of heat in the actual models 1-2 and 7-8 were higher than the results obtained for the same models at the commencement of heating. It is not possible to say, however, from the evidence available, whether these facts confirm Arthanari's findings.

The above paragraph indicates that values of thermal coeffic-

ient were also measured on the actual models during the main tests, and these results are tabulated later.

It is of interest to note that the dry conditions of the control specimens during the expansion tests probably reflected quite closely the conditions obtaining for the actual models during the main testing, and also the real drying conditions for an operating reactor shield slab.

The control tests gave an average value for the coefficient of linear thermal expansion for concrete of 13.78 X 10^{-6}.

COEFFICIENT OF THERMAL EXPANSION FOR THE MODELS (1-2,7-8)

Series 1.

Commencement of heat	Model 1-2	13.50 X 10^{-6} per ^{o}C
	Model 7-8	12.85 X 10^{-6} per ^{o}C
		12.65 X 10^{-6} per ^{o}C
		13.00 X 10^{-6} per ^{o}C
Removal of heat	Model 1-2	13.70 X 10^{-6} per ^{o}C
	Model 7-8	14.00 X 10^{-6} per ^{o}C
		12.90 X 10^{-6} per ^{o}C
		13.50 X 10^{-6} per ^{o}C

SERIES 2.

Apart from the compression strength tests on cubes, there were no special control tests undertaken for Series 2 concrete.

However, the tests on elastic properties which have been described for Series 1 on the actual models, were also carried out during the Series 2 main testing programme, and the values obtained are listed in the following tables.

MODULI OF ELASTICITY FROM ACTUAL MODELS

Series 2

Stage	Temperature	Modulus of elasticity of concrete
Commencement of test	Ambient	4.80×10^6 psi 5.10×10^6 psi
Before removal of heat	80°C	4.78×10^6 psi 4.95×10^6 psi
Before unloading	Ambient	4.84×10^6 psi 4.70×10^6 psi

ELASTIC MODULI OF PERFORATED ZONE

Series 2

Stage	Temperature	Equivalent Modulus of Perforated Zone
Commencement of test	Ambient	4.90×10^6 psi
Before removal of heat	80°C	4.84×10^6 psi
Before unloading	Ambient	4.75×10^6 psi

The coefficient linear thermal expansion of concrete obtained from mean strain readings on models 1-2 and 7-8 for Series 2 was 13.2×10^{-6} per °C.

APPENDIX B.

SHEFFIELD'S THEORY APPLIED TO THE ELASTIC STIFFNESS OF A PERFORATED ZONE IN ORDER TO EVALUATE p_2 (References 88 & 89)

p_2 is the udl (radial compression) applied to the periphery of the small specimen i.e. the perforated zone.

For standpipe tubes 3" (76 mm) O.D., $\frac{1}{16}$" (1.6 mm) thick (series 1), $3\frac{13}{16}$" (96.8 mm) pitch, $\frac{Ec}{Es} = \frac{1}{6}$, $\nu c = 0.15$ and $\nu s = 0.3$

the expressions $$\frac{Ee}{Ec} = \frac{1 - \nu_c}{\frac{1 + \Omega (1-2G)}{1-\Omega} - \nu_c}$$

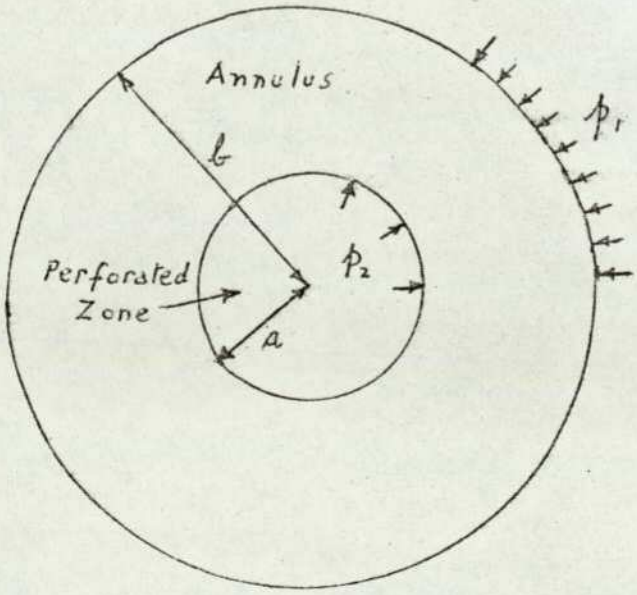
and $$G = \frac{\frac{2}{1-\Omega}}{\frac{1+\Omega}{1-\Omega} + \nu c + \left[\frac{2Ah - As}{As} - \nu s\right]\frac{Ec}{Es}}$$

give $$\frac{Ee}{Ec} \triangleq 0.5$$

and for pipes $\frac{1}{4}$" (6.35 mm) thick (series 2),

$$\frac{Ee}{Ec} \triangleq 1$$

Consider the geometrical compatibility of a disc and a surrounding ring.



According to Roark (92), for the ring

$$\Delta_{aR} = p_1 \frac{a}{Ec} \frac{2b^2}{b^2-a^2} - p_2 \frac{a}{Ec} \left(\frac{b^2 + a^2}{b^2 - a^2} + \nu_c \right)$$

and for the disc

$$\Delta_{aD} = p_2 \frac{a}{Ee} (1 - \nu_c)$$

where a = radius of the perforated zone and b = radius of the full composite slab.

For geometrical compatibility

$$\Delta_{aR} = \Delta_{aD}.$$

Thus

$$p_2 = p_1 \cdot \frac{2b^2}{a^2 \left(1 - \frac{Ec}{Ee}\right)(1 - \nu_c) + b^2 \left[1 + \frac{Ec}{Ee} + \nu_c \left(1 - \frac{Ec}{Ee}\right)\right]}$$

and for a = $8\frac{3}{8}$" (213 mm), b = 18" (457 mm),

$\nu_c = 0.15$, $\frac{Ec}{Ee} \simeq 2$ i.e. series 1.

then $p_2 \simeq 0.75\, p_1$

and for $\frac{Ec}{Ee} \simeq 1$ i.e. series 2.

then $p_2 \simeq p_1$.

Thus if p_1 = 1500 p.s.i. (10342 kN/m^2)

then p_2 = 0.75 x 1500 = 1125 p.s.i. (7756 kN/m^2) for series 1 with $\frac{1}{16}$" (1.6 mm) liners

and $p_1 = p_2 \simeq$ 1500 p.s.i. (10342 kN/m^2) for series 2 with $\frac{1}{4}$" (6.35 mm) liners.

This calculation illustrates the way in which the value of p_2 = 1125 p.s.i. (7756 kN/m^2) was arrived at for the first series.

Comparison of the experimental and calculated values of the ratios $\frac{Ee}{Ec}$ for Series 1 and Series 2.

Series 1 At ambient temperature

$$G = \frac{\frac{2}{1-\Omega}}{\frac{1+\Omega}{1-\Omega} + \nu_c + \left[\frac{2.Ah - As}{As} - \nu_s\right]\frac{Ec}{Es}}$$

$$\Omega = \frac{n.Ah}{Ap} = \frac{12 \times \frac{\pi 3^2}{4}}{\frac{\pi}{4} \times 16^2} = \frac{27}{64} = 0.422$$

$\frac{2}{1-\Omega} = \frac{2}{0.58} = 3.45$ n = number of perforations

$1+\Omega = 1.42$ A_p = area of perforated zone

$1-\Omega = 0.58$

$\nu_c = 0.15$

$2xAh = 2 \times 7.07 = 14.14$ A_h = overall area of a perforation

$As = 0.573$ A_s = area of steel liner

$\nu_s = 0.3$

$\frac{Ec}{Es} = \frac{5.16 \times 10^6}{30 \times 10^6} = 0.17$

$\therefore G = 0.526$

$$\frac{Ee}{Ec} = \frac{1-\nu_c}{\frac{1+\Omega(1-2G)}{1-\Omega} - \nu_c}$$

$$= \frac{0.85}{\frac{1 + 0.42\ (1 - 2 \times 0.526)}{1 - 0.42} - 0.15}$$

$$= \underline{0.556}$$

For Series 1, at ambient temperatures,

mean measured value of Ee = 3.02×10^6 p.s.i. (20.8×10^3 N/mm^2)

mean measured value of Ec = 5.16×10^6 p.s.i. (35.5×10^3 N/mm^2)

$\therefore$ Experimental ratio $\frac{Ee}{Ec} = \frac{3.02}{5.16}$

$$= \underline{0.585}$$

Series 2 At ambient temperature

Ω = 0.42 & $1+\Omega$ = 1.42

$\frac{2}{1-\Omega}$ = 3.45 & $1-\Omega$ = 0.58

ν_c = 0.15 $2xAh$ = 14.14

As = 2.16 ν_s = 0.3

$\frac{Ec}{Es} = \frac{4.95 \times 10^6}{30 \times 10^6}$

= 0.165

$\therefore$ G = 0.994

$\therefore \frac{Ee}{Ec} = \frac{0.85}{\frac{1 + 0.42\ (1 - 1.988)}{1 - 0.42} - 0.15} = \underline{0.957}$

For Series 2, at ambient temperature,

measured value of Ee = 4.90×10^6 p.s.i. (33.7×10^3 N/mm^2)

mean measured value of Ec = 4.95×10^6 p.s.i. (34.1×10^3 N/mm^2).

$\therefore$ Experimental ratio $\frac{Ee}{Ec} = \frac{4.90}{4.95} = \underline{0.985}$

Series 1 At 80° C

$$G = \frac{3.45}{\frac{1.42}{0.58} + 0.15 + \left[\frac{14.14 - 0.573}{0.573} - 0.3\right] \frac{Ec}{Es}}$$

$$\frac{Ec}{Es} = \frac{4.88 \times 10^6}{30 \times 10^6} = 0.163$$

$$\therefore G = \frac{3.45}{2.6 + 23.3 \times 0.163} = 0.541$$

$$\frac{Ee}{Ec} = \frac{0.85}{\frac{1 + 0.42\ (1 - 2 \times 0.541)}{1 - 0.42} - 0.15}$$

$$= \frac{0.85}{1.52} = \underline{0.56}$$

For Series 1, at 80°C

mean measured value of Ee = 2.93×10^6 p.s.i. (20.2×10^3 N/mm^2)

mean measured value of Ec = 4.88×10^6 p.s.i. (33.5×10^3 N/mm^2)

$\therefore$ Experimental ratio, $\frac{Ee}{Ec} = \frac{2.93}{4.88} = \underline{0.6}$

Series 2 At 80°C

$$G = \frac{3.45}{\frac{1.42}{0.58} + 0.15 + \left[\frac{14.14 - 2.16}{2.16} - 0.3\right] \frac{Ec}{Es}}$$

$$\frac{Ec}{Es} = \frac{4.88 \times 10^6}{30 \times 10^6} = 0.162$$

$$\therefore G = \frac{3.45}{2.6 + 5.22 \times 0.162} = 1.001$$

$$\frac{Ee}{Ec} = \frac{0.85}{\frac{1 + 0.42\ (1 - 2 \times 1.001)}{1 - 0.42} - 0.15}$$

$$\therefore \frac{Ee}{Ec} = \frac{0.85}{0.85} = \underline{\underline{1.00}}$$

For Series 2, at 80°C

measured value of Ee = 4.84×10^6 p.s.i. (33.3×10^3 N/mm^2)

mean measured value of Ec = 4.86×10^6 p.s.i. (33.5×10^3 N/mm^2)

$\therefore$ Experimental ratio, $\frac{Ee}{Ec} = \frac{4.84}{4.86} = \underline{0.996}$.

Series 1 At ambient temperature for the second time

$$G = \frac{3.45}{\frac{1.42}{0.58} + 0.15 + \left[\frac{2 \times 7.07 - 0.573}{0.573} - 0.3\right] \frac{Ec}{Es}}$$

$$\frac{Ec}{Es} = \frac{4.84 \times 10^6}{30 \times 10^6} = 0.1614$$

$$\therefore \quad G = \frac{3.45}{2.6 + 23.3 \times 0.16} = \underline{0.546}$$

$$\frac{Ee}{Ec} = \frac{0.85}{\frac{1 + 0.42\ (1 - 2 \times 0.546)}{1 - 0.42} - 0.15}$$

$$= \frac{0.85}{1.509} = \underline{0.565}$$

For Series 1, at ambient temperature for the second time,

mean measured value of Ee = 2.84×10^6 p.s.i. (19.5×10^3 N/mm^2)

mean measured value of Ec = 4.84×10^6 p.s.i. (33.3×10^3 N/mm^2)

$$\therefore \text{ Experimental ratio, } \frac{Ee}{Ec} = \frac{2.84}{4.84} = \underline{0.587}$$

Series 2 At ambient temperature for the second time

$$G = \frac{3.45}{\frac{1.42}{0.58} + 0.15 + \left[\frac{14.14 - 2.16}{2.16} - 0.3\right] \frac{Ec}{Es}}$$

$$\frac{Ec}{Es} = \frac{4.77 \times 10^6}{30 \times 10^6} = 0.159$$

$$\therefore \quad G = \frac{3.45}{2.6 + 5.23 \times 0.159}$$

$$= \frac{3.45}{3.431} = 1.005$$

$$\frac{Ee}{Ec} = \frac{0.85}{\frac{1 + 0.42\ (1 - 2.01)}{1 - 0.42} - 0.15}$$

$$= \frac{0.85}{0.844} = \underline{1.005}$$

For Series 2, at ambient temperature for the second time,

measured value of Ee = 4.75×10^6 p.s.i. (32.5×10^3 N/mm^2)

mean measured value of Ec = 4.77×10^6 p.s.i. (32.6×10^3 N/mm^2)

$\therefore$ Experimental ratio, $\frac{Ee}{Ec} = \frac{4.75}{4.77}$

$= \underline{0.998}$

Condition	Series	Experimental ratio $\frac{Ee}{Ec}$	Sheffield's Value of ratio $\frac{Ee}{Ec}$	Percentage Difference Sheffield's Value above Experimental Value
At ambient temperature	1	0.585	0.556	- 4.96
	2	0.985	0.957	- 2.84
At 80°C	1	0.6	0.56	- 6.67
	2	0.996	1.000	+ 0.4
At ambient temperature again	1	0.587	0.565	- 3.75
	2	0.998	1.005	+ 0.7

APPENDIX C.

ESTIMATION OF PERIPHERAL FIELD STRESSES p_2 AROUND THE PERIMETER OF THE PERFORATED ZONE USING THE EFFECTIVE MODULUS METHOD.

Series 1

Significance of time interval symbols.

T_1 : Load applied
T_2 : Heat applied
T_3 : Heat removed
T_4 : Load removed
T_5 : End of test; creep recovery

1. Immediately after time T_1.

External rim compression 1500 psi (10342 kN/m^2)

Ambient temperature 22.5°C.

The effective modulus at this time is identical with the equivalent modulus of the perforated zone as measured in the specimen 3/4.

E_e the equivalent modulus for the first series at ambient temperature was 3.02×10^6 psi.

The elastic strain immediately after loading was assessed as 3.75×10^{-4}.

$$\therefore \text{stress } p_2 = E \times 3.75 \times 10^{-4}$$
$$= 3.02 \times 10^6 \times 3.75 \times 10^{-4}$$
$$= 1125 \text{ psi } (7756 \text{ kN/m}^2).$$

2. Immediately before heating at time T_2

$$\text{Effective modulus } E' = \frac{1}{\frac{1}{3.02.10^6} + c}$$

$$c, \text{the specific creep} = \frac{\text{creep strain between } T_1 \text{ and } T_2}{1125}.$$

creep and shrinkage strains on specimen 9/10 between T_1 and T_2 = 0.7×10^{-4}

shrinkage strains on specimen 5/6 between T_1 and T_2 } were negligible

$\therefore$ net creep strain between T_1 and T_2 = 0.7×10^{-4}.

$$\therefore c = \frac{0.7 \times 10^{-4}}{1125}$$

$$\therefore c = 6.21 \times 10^{-8}$$

$$\therefore E' = \frac{1}{\frac{1}{3.02.\ 10^6} + 6.21.\ 10^{-8}}$$

$$= \frac{3.02 \times 10^6}{1 + 3.02.\ 6.21.\ 10^{-2}}$$

$$= \frac{3.02.\ 10^6}{1.188}$$

$$= 2.14 \times 10^6.$$

$\therefore$ stress p_2 = E' X strain

= 2.14×10^6 X (elastic strain + creep strain)

= 2.14×10^6 X (3.75 + 0.7). 10^{-4}

= 951 psi (6520 kN/m^2)

Subsequent shrinkage strain values will be assessed from the shrinkage curve from specimen 5/6 which was unloaded and exhibited shrinkage only; the value of shrinkage strain for the period T_1 to T_2 was considered negligible. Shrinkage strains are not taken into account in computing stresses.

3. Immediately after heating at time T_2

Temperature rise in perforated zone = $(75 - 22.5) = 52.5^{\circ}C$

Temperature rise in annulus = $(68 - 22.5) = 45.5^{\circ}C$

Coefficient of thermal expansion = 12.8×10^{-6} per $^{\circ}C$

E_e , the equivalent modulus for the perforated zone at this temperature = 2.94×10^6 psi

$\therefore$ Effective modulus $$E' = \frac{1}{\frac{1}{2.94.\ 10^6} + c}$$

The specific creep, c at this point in time is identical with the previous value

$$\therefore E' = \frac{1}{\frac{1}{2.94.10^6} + 6.21.\ 10^{-8}}$$

$$\therefore E' = \frac{2.94.\ 10^6}{1 + 2.94.\ 6.21.10^{-2}}$$

$$= \frac{2.94.\ 10^6}{1.18}$$

$$= 2.49.\ 10^6$$

Thermal strain in the perforated zone = $52.5.\ 12.8.\ 10^{-6} = 6.71.10^{-4}$

Thermal strain in the annulus = $45.5.\ 12.8.\ 10^{-6} = 5.81.10^{-4}$

$\therefore$ Net thermal strain = $(6.71 - 5.81).10^{-4}$

= $0.90.\ 10^{-4}$

$\therefore$ stress p_2 = $2.49.\ 10^6.\ (\ 3.75 + 0.7 + 0.90\ ).\ 10^{-4}$

= 1330 psi (9100 kN/m^2)

4. Immediately before cooling at time T_3

Temperature difference between perforated zone and annulus

= (85-79) = 6^oC

$\therefore$ Thermal strain = $6 \times 12.8.\ 10^{-6} = 0.77.\ 10^{-4}$

E_e , the equivalent modulus = $2.94.\ 10^6$ psi

From the strain curve for specimen 9/10, the creep and shrinkage strain from T_2 to T_3 = $7.8.\ 10^{-4}$

From the shrinkage strain curve for specimen 5/6 from T_2 to T_3, the shrinkage strain = $+ 0.7.\ 10^{-4}$

This figure, however, shows itself as an increase in dimension not as a true shrinkage and it is possible that the temperature variations were such as to indicate an apparent continuing expansion.

The value of 0.7×10^{-4} is not a very high proportion of the total creep and shrinkage strain, however, and it has been decided to utilize the 7.8×10^{-4} strain as representing the net thermal creep.

$\therefore$ the specific creep, $c = \frac{\text{total creep strain}}{1125}$

$$= \frac{0.7.\ 10^{-4} + 7.8.\ 10^{-4}}{1125}$$

$$= 75.6.\ 10^{-8}$$

$$\therefore \text{ Effective modulus, } E' = \frac{1}{\frac{1}{2.94.\ 10^6} + 75.6.\ 10^{-8}}$$

$$= \frac{2.94.\ 10^6}{3.22}$$

$$= 0.93.\ 10^6$$

$$\therefore \text{ Stress, } p_2 = 0.93.\ 10^6.\ (\ 3.75 + 0.7 + 7.8 + 0.77\ )\ X\ 10^{-4}$$

$$= 0.93.\ 13.02.\ 10^2$$

$$= 1230 \text{ psi } (\ 8440\ kN/m^2\ )$$

5. Immediately after cooling at time T_3

Temperature = 22.5^oC

The contraction strains recorded on cooling were negligibly different from the previous expansion strains and no net thermal strain will be considered.

E_e after cooling $= 2.85.\ 10^6$

$$\therefore \text{ E' the effective modulus } = \frac{1}{\frac{1}{2.85.10^6} + c}$$

where c, the specific creep has the same value as the previous case,

$$\therefore E' = \frac{1}{\frac{1}{2.85.\ 10^6} + 75.6.\ 10^{-8}}$$

$$= \frac{2.85.\ 10^6}{3.15}$$

$$= 0.91.\ 10^6$$

$$\therefore \text{ stress } p_2 = 0.91.\ 10^6.\ (\ 3.75 + 0.7 + 7.8\ ).10^{-4}$$

$$= 0.91.\ 12.25.\ 10^2$$

$$= 1110 \text{ psi } (\ 7610\ kN/m^2\ )$$

6. Immediately before unloading at time T_4

$E_e = 2.85.\ 10^6$

Creep and shrinkage strains for specimen 9/10 between T_3 and T_4

are equal to 0.3 X 10^{-4}. The shrinkage strains for specimen 5/6 for this period appear negligible.

Thus the total creep upto point T_4

$$= (0.7 + 7.8 + 0.3). 10^{-4}$$

$$= 8.8. 10^{-4}$$

$$\therefore c \text{ the specific creep} = \frac{8.8. 10^{-4}}{1125}$$

$$= 78.2. 10^{-8}$$

$$\therefore E' = \frac{1}{\frac{1}{2.85.10^6} + c}$$

$$= \frac{2.85. 10^6}{3.23}$$

$$= 0.88. 10^6$$

$$\therefore \text{stress } p_2 = 0.88. 10^6. (3.75 + 0.7 + 7.8 + 0.3) \times 10^{-4}$$

$$= 0.88.12.55. 10^2$$

$$= 1110 \text{ psi } (7610 \text{ kN/m}^2)$$

7. Immediately after unloading at time T_4

$E_e = 2.85. 10^6$

E' is also unchanged from the previous case at $0.88. 10^6$.

The elastic unloading strain observed = $6.8. 10^{-4}$.

This will reduce the stress.

$$\therefore \text{stress } p_2 = 0.88. 10^6. (3.75 + 0.7 + 7.8 + 0.3 - 6.8) \times 10^{-4}$$

$$= 0.88. 5.75. 10^2$$

$$= 505 \text{ psi } (3470 \text{ kN/m}^2)$$

8. After creep recovery at time T_5

$E_e = 2.85. 10^6$

Specimen 3/4, without an annulus, recorded a creep recovery strain of approximately $0.7. 10^{-4}$.

Specimen 9/10, with an annulus, recorded negligible creep recovery strain.

The net difference in creep recovery strain is tensile and

equal to $0.7.\ 10^{-4}$.

$$E' = \frac{2.85.\ 10^6}{3.05} = 0.935.\ 10^6$$

The tension caused by the net outward creep recovery strain

$$= 0.935.\ 10^6.\ 0.7.\ 10^{-4}$$

$$= 0.65.\ 10^2 = 65 \text{ psi tension}$$

$\therefore$ The net strain = 505 - 65 = 440 psi compression

$\therefore$ The residual stress on the perforated zone = 440 psi.

At this stage there is zero applied stress and yet this calculation indicates a stress of 440 psi at the periphery of the zone.

The hoop stress in the annulus as a result of this is

$$440 \times \frac{18^2 + 8^2}{18^2 - 8^2}$$

$$= 440.\ \frac{388}{260}$$

= 658 psi tension (4520 kN/m^2)

This tensile hoop stress is great enough to cause the cracking which was observed.

Series 2.

1. Immediately after time T_1

External rim compression 1500 psi (10342 kN/m^2)

Ambient temperature = 22.5°C.

The effective modulus at this time is identical with the equivalent modulus of the perforated zone, as measured in the specimen 3/4.

E_e the equivalent modulus for the second series at ambient temperature was 4.90×10^6 psi.

The elastic strain measured was $3.40.\ 10^{-4}$

Thus $E_e = \frac{\text{stress}}{3.40.\ 10^{-4}} = 4.90.\ 10^6$

$\therefore$ stress $p_2 = 4.90.\ 3.40.\ 10^2$

= 1660 psi (11400kN/m^2)

2. Immediately before heating at time T_2

$$\text{Effective modulus } E' = \frac{1}{\frac{1}{E_e} + c}$$

$$\text{The specific creep } c = \frac{0.7.\ 10^{-4}}{1500} = 4.67.\ 10^{-8}$$

$$\therefore E' = \frac{1}{\frac{1}{4.9.\ 10^{6}} + 4.67.\ 10^{-8}}$$

$$= 3.95.\ 10^{6}.$$

$$\therefore \text{stress } p_2 = E' \text{ X strain}$$

$$= 3.95.\ 10^{6} \text{ X (elastic strain + creep strain)}$$

$$= 3.95.\ 10^{6}.(3.4 + 0.7).10^{-4}$$

$$= 1620 \text{ psi} \quad (11140 \text{ kN/m}^2).$$

3. Immediately after heating at time T_2

Temperature rise in perforated zone = $(81.7 - 22.5) = 59.2^{\circ}C$

Temperature rise in annulus = $(71.9 - 22.5) = 49.9^{\circ}C$

Coefficient of thermal expansion = $12.8.\ 10^{-6}$ per $^{\circ}C$.

The equivalent modulus E_e for the perforated zone at this temperature

$$= 4.84.\ 10^{6} \text{ psi}$$

$$\text{The Effective modulus } E' = \frac{1}{\frac{1}{4.84.\ 10^{6}} + c}$$

The specific creep c at this point is identical with the previous value

$$\therefore E' = \frac{1}{\frac{1}{4.84.\ 10^{6}} + 4.67.10^{-8}}$$

$$= \frac{4.84.\ 10^{6}}{1.226}$$

$$= 3.94.\ 10^{6}$$

Thermal strain in the perforated zone = $59.2.\ 12.8.\ 10^{-6} = 7.59.10^{-4}$

Thermal strain in the annulus = $49.4.\ 12.8.\ 10^{-6} = 6.3.\ 10^{-4}$

$\therefore$ Net thermal strain = $(7.59 - 6.3).\ 10^{-4}$

= $1.29.10^{-4}$.

$\therefore$ Stress p_2 = $3.94.\ 10^{6}.\ (3.4 + 0.7 + 1.29).\ 10^{-4}$

= $3.94.\ 5.39.\ 10^{2}$

= 2120 psi (14520 kN/m^2)

4. Immediately before cooling at time T_3

Temperature difference between perforated zone and annulus

= $(86.4 - 79.8) = 6.6^{o}C$

$\therefore$ Thermal strain = $6.6.\ 12.8.\ 10^{-6}$

= $0.84.\ 10^{-4}$

The equivalent modulus E_e = $4.84.\ 10^{6}$

From the strain curves for specimen 9/10, creep and shrinkage strain, from T_2 to T_3 = $6.5.\ 10^{-4}$

From the shrinkage strain curve for specimen 5/6 from T_2 to T_3, the shrinkage strain = $1.2.\ 10^{-4}$

$\therefore$ thermal creep = $5.3.\ 10^{-4}$

The specific creep c = $\dfrac{\text{Total creep upto this point}}{1500}$

= $\dfrac{0.7.\ 10^{-4} + 5.3.\ 10^{-4}}{1500}$

= $40.0.\ 10^{-8}$.

$\therefore$ Effective modulus E' = $\dfrac{1}{\dfrac{1}{4.84.\ 10^{6}} + 40.0.\ 10^{-8}}$

= $1.65.\ 10^{6}$.

$\therefore$ stress p_2 = E' X strain

= $1.65.\ 10^{6}.\ (3.4 + 0.7 + 5.3 + 0.84).10^{-4}$

= 1690 psi (11600 kN/m^2)

5. Immediately after cooling at time T_3

Temperature = $22.5^{\circ}C$

The contraction strains recorded on cooling were negligibly different from the previous expansion strains and no net thermal strains will be considered.

E_e after cooling = $4.75. 10^6$ psi i.e at ambient for the second time.

$$\therefore E' = \frac{1}{\frac{1}{4.75. 10^6} + c}$$

where c the specific creep has the same value as for the previous case

$$\therefore E' = \frac{1}{\frac{1}{4.75. 10^6} + 40.0. 10^{-8}}$$

$$= \frac{4.75. 10^6}{2.90}$$

$$= 1.64. 10^6$$

$$\therefore \text{stress } p_2 = E' \text{ X strain}$$

$$= 1.64. 10^6. (3.4 + 6.0). 10^{-4}$$

$$= 1540 \text{ psi } (10600 \text{ kN/m}^2)$$

6. Immediately before unloading at time T_4

The equivalent modulus of the perforated zone E_e when at ambient temperature for the second time, was measured as $4.75. 10^6$ psi.

Creep and shrinkage strains for specimen 9/10 between T_3 and T_4 = $0.40. 10^{-4}$

Shrinkage strains from T_3 to T_4

= $0.28. 10^{-4}$

$\therefore$ Creep strain = $0.12. 10^{-4}$

$\therefore$ Total creep = $(6.0 + 0.12). 10^{-4}$

= $6.12. 10^{-4}$

$\therefore$ The specific creep $c = \frac{6.12.\ 10^{-4}}{1500}$

$= 40.8.\ 10^{-8}$

$\therefore E' = \frac{1}{\frac{1}{4.75.\ 10^{6}} + 40.8.\ 10^{-8}}$

$= \frac{4.75.\ 10^{6}}{2.94}$

$= 1.62.\ 10^{6}$

$\therefore$ stress p_2 = E' X strain

$= 1.62.\ 10^{6}.\ (3.4 + 6.12).\ 10^{-4}$

$= 1540$ psi $(10600\ kN/m^2)$

7. Immediately after unloading at time T_4

$E_e = 4.75.\ 10^{6}$ psi

$E' = \frac{1}{\frac{1}{4.75.\ 10^{6}} + 40.8.\ 10^{-8}}$

$= 1.62.\ 10^{6}$

The elastic strain observed from the curve for specimen 9/10 equals $4.6.\ 10^{-4}$. This will reduce the stress.

$\therefore$ stress p_2 = E' x strain

$= 1.62.\ 10^{6}.\ (3.4 + 6.12 - 4.6).\ 10^{-4}$

$= 795$ psi $(5460\ kN/m^2)$

8. After creep recovery at time T_5

$E_e = 4.75 \times 10^{6}$

$E' = \frac{1}{\frac{1}{4.75.\ 10^{6}} + c}$

The creep recovery strain observed $= 1.6.\ 10^{-4}$

This was associated with a negligible amount of shrinkage strain.

$\therefore c = \frac{(6.12 - 1.6).\ 10^{-4}}{1500}$

$= 30.0.\ 10^{-8}$

$$\therefore E' = \frac{1}{\frac{1}{4.75.\ 10^6} + 30.0.\ 10^{-8}}$$

$$= \frac{4.75.\ 10^6}{2.42}$$

$$= 1.96.\ 10^6$$

$$\therefore \text{stress } p_2 = 1.96.\ 10^6.\ (3.4 + 4.52 - 4.6).\ 10^{-4}$$

$$= 1.96 \times 3.32 \times 10^2$$

$$= 650 \text{ psi}$$

Therefore, the residual stress on the perforated zone

$$= 650 \text{ psi}$$

At this stage, there is no externally-applied stress on the rim, and yet there is a stress of 650 psi at the periphery of the zone.

The hoop stress in the annulus as a result of this is

$$650 \times \frac{18^2 + 8^2}{18^2 - 8^2}$$

$$= 650.\ \frac{388}{260}$$

$$= 975 \text{ psi} \quad \text{tension} \quad (6700 \text{ kN/m}^2)$$

This tensile hoop stress is great enough to cause the cracking which was observed.

.....

Establishment of expression used above for E', the Effective Modulus

The elastic Young's Modulus E

$$= \frac{\sigma}{\varepsilon_{el}}$$

The Effective Modulus E'

$$= \frac{\sigma}{\varepsilon_{el} + \varepsilon_c}$$

σ is the applied stress

ε_{el} is the elastic strain

ε_c is the creep strain

$$\therefore E' = \frac{1}{\frac{\varepsilon_{el}}{\sigma} + \frac{\varepsilon_c}{\sigma}}$$

$$\therefore E' = \frac{1}{\frac{1}{E} + c}$$

where c is the specific creep

APPENDIX D.

MATHEMATICAL EXPRESSIONS PROPOSED FOR CREEP

Expressions that have been proposed in the past to represent the creep behaviour of concrete with time, can be classified into the following groups : logarithmic, power, exponential, and hyperbolic.

Of these, the logarithmic and power groups indicate no finite limit to the total creep, whereas the exponential and hyperbolic expressions do record a limiting value.

Measurable rates of creep have been observed in concrete loaded for more than thirty years, but for structures operating under normal service conditions, it is reasonable to suppose that for design purposes, a practical ultimate value of creep has been reached after about five years.

Rational consideration of design requirements would indicate that since the designer can only be interested in structural behaviour and the magnitude of creep during the lifetime of the structure, the assumption of a limiting value for creep is justified.

The more important mathematical expressions proposed to represent the creep laws of concrete will now be reviewed.

Power Expressions.

1. The creep law proposed by Chang and Kesler expresses creep strain as a power function of time :

$$\varepsilon_c = \varepsilon_{c1}\, t^{n_{\varepsilon c}}$$

where ε_{c1} and $n_{\varepsilon c}$ are coefficients derived from the dynamic properties and creep curves for concrete.

2. Saliger suggested an expression of the form :

$$\varepsilon_c = \alpha_t \sigma$$

where ε_c is the creep strain, σ is the applied stress, and α_t is a creep coefficient given by,

$$\alpha_t = A\phi(t) \qquad \text{where}$$

$$\phi(t) = t^{\frac{1}{3}}$$

$$A = 0.422 \times 10^{-6} \text{ in imperial units.}$$

t is the time.

3. Straub presented a power function as follows :

$$\varepsilon_c = k\,\sigma^p\,t^q$$

where ε_c is the creep strain after time t.

σ is the applied stress

k is an empirical constant,

and p and q are further empirical constants for stress and time respectively.

Stress/creep proportionality is not assumed by this expression.

4. Shank modified Straub's expression in assuming stress/creep proportionality in the form :

$$c = C^a\sqrt{t}$$

where c is the specific creep and C and a are empirical constants. The expression was found to fit experimental data between the ages of one day and one year only.

5. Friedrich assumed that creep was proportional to the fourth root of time in the following expression :

$$c = A\left(\frac{t}{1400}\right)^{\frac{1}{4}}$$

where t is the time in days and A is an empirical constant.

Thus after 1400 days $c = c_\infty = A$ and this is taken to be the limiting creep.

Exponential Expressions

6. Thomas proposed the exponential equation :

$$\varepsilon_c = c_\infty \sigma\left[1 - e^{-A(t+B)^C - B^C}\right]$$

where ε_c = creep strain

c_∞ = ultimate specific creep

σ = applied stress

A, B, and C are constants

and t is the time after loading.

7. Mc Henry used the following exponential expression :

$$\varepsilon_c = \alpha (1 - e^{-rt}) + \beta e^{-pk} (1 - e^{-mt})$$

where k = the age at loading, and

α, β, r,p,m = experimental constants

McHenry suggested that application of the load mobilizes the creep potential of the concrete and the rate of creep is proportional to the creep yet to come. The equation is claimed valid only for periods between five days and one year. The first term in the expression represents the behaviour of a Kelvin model.

8. Arutyunyan proposed an expression of the type :

$$\varepsilon_c(t,\tau) = \phi (t) \left[1 - e^{-\gamma(t-\tau)} \right]$$

where t = the age of concrete at the time considered

ϕ (t) = empirical time function

τ = the age at loading

γ = an empirical constant.

9. Lyse presented an expression in the form :

$$\varepsilon_c = s_\infty (1 - e^{-mt}) V_{cp} \frac{\sigma}{\sigma_s}$$

where s_∞ = the ultimate shrinkage strain

σ = the applied stress

σ_s = magnitude of stress which would give creep of the same magnitude as the shrinkage at the relative humidity of storage

m = the rate of shrinkage corresponding to the relative humidity of storage and is determined experimentally.

V_{cp} = the fractional volume of cement paste i.e the absolute volume of cement paste as a fraction

of the volume of concrete.

10. L'Hermite gives the expression :

$$c = c_{\infty}\left[1 - e^{\left(-A.\log\left(\frac{k+t}{k}\right) + Bt\right)}\right]$$

where c = the specific creep

c_{∞} = the ultimate specific creep

k = the age at loading

A and B = empirical constants.

11. Glanville and Thomas have suggested a creep expression which is a particular case of L'Hermite's expression :

$$c = c_{\infty}\left(1 - e^{-F(t)}\right)$$

where F(t) is a function of the time after loading.

12. Erzen put forward an expression of the form :

$$c = A.\ e^{B\left[1-\left(\frac{k}{t}\right)^{D}\right]}$$

where A, B and D are empirical constants

k = the age at loading

and t = the age at the time considered.

13. Freudenthal and Roll suggested a creep expression on the basis of a multi-parameter rheological model :

$$\varepsilon_c(\sigma,t) = C.\ e^{-b}.\ T_m\left(1 - e^{\frac{-t}{T_m}}\right) + \sum_{i=1,2,k} \sigma \alpha_i \left(1 - e^{-t/\tau_i}\right)$$

where C = a constant of magnitude unity, with units representing the reciprocal of time

σ = the applied stress

b = an empirical constant

$T_m, \tau_1, \tau_2, \tau_k$ = relaxation or retardation times of various elements of the model

$\alpha_m, \alpha_1, \alpha_2, \alpha_k$ = the spring compliances of the various elements.

14. Vaishnav devised an expression for specific creep, (based upon a modified Burgers model), of the following form :

$$c = c_{k\infty}\left(1 - e^{-p_k\, t^{0.5}}\right) + c_{m\infty}\left(1 - e^{-\beta t}\right)$$

where c = the specific creep

$c_{k\infty}$ = ultimate specific creep for the Kelvin element

$c_{m\infty}$ = ultimate specific creep for the Maxwell element

p_k = a coefficient controlling change in retardation time in the Kelvin element

$$= \frac{t^{0.5}}{\tau_{ret}}$$

τ_{ret} = the retardation time

β = a constant controlling the rate of decrease of fluidity (the reciprocal of viscosity).

15. Zienkiewicz, Watson and King produced an equation for multi-axial conditions, based upon two Kelvin elements in series :

$$\left\{\varepsilon_c^r\right\}_{t+\Delta t} = e^{-b_r \Delta t}\left\{\varepsilon_c^r\right\}_t + a_r \frac{[A]\{\sigma\}}{b_r}(1 - e^{-b_r \Delta t})$$

where a_r = the fluidity of the rth element $= \frac{1}{\eta}$

b_r = the value of $\frac{E}{\eta}$ for the rth element

t = the time after loading

σ = the applied stress

$[A]$ = a matrix dependent only on the Poisson's ratio.

Hyperbolic Expressions

16. An early and very important expression by Ross gives the limiting creep directly, as follows :

$$c = \frac{t}{a + bt}$$

where c = the specific creep

and a and b are constants.

At $t = \infty$, $c = c_\infty = \frac{1}{b}$. A plot of $\frac{t}{c}$ against t gives a straight line of slope b, and a is the intercept on the $\frac{t}{c}$ axis. The expression fits creep data well after a period of time has elapsed under loading, and it readily gives an estimation of ultimate creep.

17. Lorman's expression is very similar to Ross's, and is as follows :

$$c = \frac{mt}{n + t}$$

where m = creep coefficient representing ultimate specific creep.

n = creep time constant representing the half life.

When $t = \infty$, $c_{\infty} = m$ and when $t = n$, $c = \frac{1}{2}m$.

Logarithmic Expression

18. The U.S Bureau of Reclamation's logarithmic expression is of the type :

$$c = F(\alpha) \log_e (t + 1)$$

where α = the age at loading

and t = the time since loading.

$F(\alpha)$ represents the rate of specific creep with the logarithm of time and needs to be determined for each age and set of variables.

The expression requires only the evaluation of $F(\alpha)$ to specify the complete creep behaviour. At low values of time, the equation does not fit creep data well. The fit at greater ages is good. Although the creep rate reduces with time in this expression, it fails to predict an ultimate limiting creep value.

APPENDIX E.

Typical Computer Output. COMPO 2.

Approximately fifteen lines of each time interval output are given for displacements, stresses and strains. This page gives the elastic solution.

D I S P L A C E M E N T S

NODAL POINT NO.	DIS. IN-X (IN.)	DIS. IN-Y (IN.)
1	0.	0.
2	-.11070781E-03	-.11066476E-03
3	0.	-.22341174E-03
4	-.20596203E-03	-.20588508E-03
5	-.22349959E-03	0.
6	0.	-.47419744E-03
7	-.12735396E-03	-.61815006E-03
8	-.88138566E-04	-.47402702E-03
9	-.97031256E-04	-.47413061E-03
10	-.12681008E-03	-.33002831E-03
11	-.19952449E-03	-.19946388E-03
12	-.33015314E-03	-.12679063E-03
13	-.47427496E-03	-.97833236E-04
14	-.47417297E-03	-.88139896E-04
15	-.61831413E-03	-.12732829E-03

NORMAL AND SHEARING STRESSES AT C.G. OF ELEMENT

ELEMENT NO.	NORMAL STRESS IN-X (KIP/SQ IN)		NOI
1	-.15021688E+01	-.15115667E+01	.49016553E-02
2	-.15119821E+01	-.15017652E+01	.49057346E-02
3	-.14934217E+01	-.15227444E+01	.49758890E-02
4	-.15003599E+01	-.15273505E+01	.92826094E-02
5	-.14967590E+01	-.15061754E+01	.86546165E-02
6	-.15065722E+01	-.14963739E+01	.86586958E-02
7	-.15277530E+01	-.14999958E+01	.91681039E-02
8	-.15229923E+01	-.14932793E+01	.49210198E-02
9	-.26999873E+01	-.74620890E+01	-.38598889E+01
10	-.13721865E+01	-.90133186E+01	-.23907852E+01
11	-.13270920E+01	-.79807158E+01	-.69544584E+00
12	-.14885505E+01	-.15314435E+01	-.41558529E-02
13	-.14886203E+01	-.15318310E+01	.28422735E-02
14	-.13268040E+01	-.79797558E+01	.69399772E+00
15	-.13704175E+01	-.90112652E+01	.23881413E+01

ELEMENT STRAINS AT C.G. OF ELEMENT

	STRAINS IN X-AXIS	STRAINS IN Y-AXIS	STRAINS IN XY-AXIS
1	-.24601737E-03	-.24823527E-03	.23135813E-05
2	-.24833287E-03	-.24592169E-03	.23155067E-05
3	-.24386554E-03	-.25078570E-03	.23486196E-05
4	-.24508736E-03	-.25145714E-03	.43813916E-05
5	-.24512948E-03	-.24735176E-03	.40849790E-05
6	-.24744498E-03	-.24503818E-03	.40869044E-05
7	-.25155075E-03	-.24500006E-03	.43273450E-05
8	-.25084040E-03	-.24382813E-03	.23227213E-05
9	-.15378686E-04	-.22173643E-03	-.33452370E-03
10	.44393636E-04	-.26672209E-03	-.20720138E-03
11	.35570759E-04	-.25275294E-03	-.60271973E-04
12	-.24257814E-03	-.25270089E-03	-.19615626E-05
13	-.24257814E-03	-.25277587E-03	.13415531E-05
14	.35570759E-04	-.25272382E-03	.60146469E-04
15	.44432069E-04	-.28667133E-03	.20697225E-03

3rd Time Interval. COMPO 2.

D I S P L A C E M E N T S

NODAL POINT NO.	DIS. IN-X (IN.)	DIS. IN-Y (IN.)
1	0.	0.
2	-.17276540E-03	-.17237501E-03
3	0.	-.32587578E-03
4	-.32874523E-03	-.32803315E-03
5	-.32666498E-03	0.
6	0.	-.64650324E-03
7	-.22717280E-03	-.81565022E-03
8	-.17600935E-03	-.64694883E-03
9	-.18567372E-03	-.64670847E-03
10	-.22839828E-03	-.47796289E-03
11	-.32048676E-03	-.31992168E-03
12	-.47909240E-03	-.22819399E-03

NORMAL AND SHEARING STRESSES AT C.G. OF ELEMENT

ELEMENT NO.	NORMAL STRESS IN-X (KIP/SQ IN)		NOR
1	-.15030470E+01	-.14167825E+01	-.41499832E-01
2	-.14280883E+01	-.14997895E+01	-.41483015E-01
3	-.17302947E+01	-.12661936E+01	-.53762385E-01
4	-.15229966E+01	-.12375421E+01	-.15430751E+00
5	-.15487046E+01	-.14625166E+01	-.73254601E-01
6	-.14697459E+01	-.15455237E+01	-.73237785E-01
7	-.12406798E+01	-.15199530E+01	-.15519934E+00
8	-.12682761E+01	-.17289160E+01	-.54178508E-01
9	-.33372771E+01	-.90585925E+01	-.47389928E+01
10	-.16686369E+01	-.10594741E+02	-.29524424E+01
11	-.16548962E+01	-.93820681E+01	-.94506078E+00
12	-.18233823E+01	-.11710586E+01	.48044725E-01
13	-.18282578E+01	-.11703670E+01	-.45599670E-01
14	-.16554960E+01	-.93840674E+01	.94768084E+00
15	-.16723425E+01	-.10598519E+02	.29567160E+01

ELEMENT STRAINS AT C.G. OF ELEMENT

	STRAINS IN X-AXIS	STRAINS IN Y-AXIS	STRAINS IN XY-AXIS
1	-.38392311E-03	-.36208420E-03	-.20971385E-04
2	-.36296109E-03	-.38305558E-03	-.20962014E-04
3	-.43922746E-03	-.32062747E-03	-.27340961E-04
4	-.39516908E-03	-.32270983E-03	-.78898902E-04
5	-.39193570E-03	-.37011812E-03	-.37017899E-04
6	-.37097368E-03	-.39108950E-03	-.37008527E-04
7	-.32354053E-03	-.39435753E-03	-.79372744E-04
8	-.32115199E-03	-.43883459E-03	-.27561654E-04
9	-.20656643E-04	-.26858031E-03	-.41071271E-03
10	.50326183E-04	-.33647167E-03	-.25587834E-03
11	.38657474E-04	-.29618664E-03	-.81905268E-04
12	-.46418429E-03	-.29628104E-03	.24404544E-04

6th Time Interval. COMPO 2.

D I S P L A C E M E N T S

NODAL POINT NO.	DIS. IN-X (IN.)	DIS. IN-Y (IN.)
1	0.	0.
2	-.19679018E-03	-.19625224E-03
3	0.	-.36460304E-03
4	-.37658760E-03	-.37559618E-03
5	-.36568538E-03	0.
6	0.	-.70946889E-03
7	-.26734269E-03	-.88642568E-03
8	-.21216042E-03	-.71018153E-03
9	-.22022246E-03	-.70978902E-03
10	-.26933482E-03	-.89384293E-03
11	-.36773838E-03	-.36092220E-03
12	-.53504016E-03	-.26904415E-03
13	-.71156680E-03	-.22201892E-03
14	-.71194616E-03	-.21214416E-03
15	-.88842504E-03	-.26709777E-03

NORMAL AND SHEARING STRESSES AT C.G. OF ELEMENT

ELEMENT NO.	NORMAL STRESS IN-X (KIP/SQ IN)		NORM
1	-.15020679E+01	-.13863871E+01	-.55780631E-01
2	-.13905307E+01	-.14979527E+01	-.55770763E-01
3	-.18047656E+01	-.11873886E+01	-.70753202E-01
4	-.15285779E+01	-.11450704E+01	-.20578182E+00
5	-.15634731E+01	-.14478372E+01	-.98467631E-01
6	-.14519359E+01	-.15594028E+01	-.98457763E-01
7	-.11489825E+01	-.15246704E+01	-.20693071E+00
8	-.11899575E+01	-.18029346E+01	-.71315917E-01
9	-.35401132E+01	-.95625542E+01	-.50181746E+01
10	-.17623014E+01	-.11080683E+02	-.31318494E+01
11	-.17610781E+01	-.98150739E+01	-.10313547E+01
12	-.19390369E+01	-.10635560E+01	.65658613E-01
13	-.19388284E+01	-.10623976E+01	-.62010223E-01
14	-.17618804E+01	-.98177481E+01	.10354499E+01
15	-.17679776E+01	-.11086555E+02	.31392146E+01

ELEMENT STRAINS AT C.G. OF ELEMENT

	STRAINS IN X-AXIS	STRAINS IN Y-AXIS	STRAINS IN XY-AXIS
1	-.43731152E-03	-.40511449E-03	-.31001610E-04
2	-.40631709E-03	-.43611610E-03	-.30994433E-04
3	-.51795158E-03	-.34486585E-03	-.39591481E-04
4	-.45385514E-03	-.34694870E-03	-.11538110E-03
5	-.44916526E-03	-.41698457E-03	-.54725428E-04
6	-.41817083E-03	-.44798618E-03	-.54718252E-04
7	-.34808579E-03	-.45272428E-03	-.11604565E-03
8	-.34557996E-03	-.51739260E-03	-.39914227E-04
9	-.22378231E-04	-.28335067E-03	-.43490847E-03
10	.52063453E-04	-.35173310E-03	-.27142694E-03
11	.39448134E-04	-.30955835E-03	-.89384071E-04
12	-.55505614E-03	-.30972039E-03	.36544435E-04
13	-.55505614E-03	-.30947742E-03	-.34650093E-04

9th Time Interval. COMPO 2.

D I S P L A C E M E N T S

NODAL POINT NO.	DIS. IN-X (IN.)	DIS. IN-Y (IN.)
1	0.	0.
2	-.51859994E-04	-.49960775E-04
3	0.	.13478538E-04
4	-.13447819E-03	-.13082279E-03
5	.97359575E-05	0.
6	0.	.26547430E-03
7	-.22019780E-03	.48321227E-03
8	-.34169996E-04	.26224374E-03
9	-.24075506E-03	.26409687E-03
10	-.22941586E-03	.43261821E-04
11	.19419433E-04	.22316483E-04
12	.37749257E-04	-.22824557E-03
13	.25804928E-03	-.24068734E-03
14	.25625783E-03	-.34077020E-04
15	.47663597E-03	-.21926637E-03

NORMAL AND SHEARING STRESSES AT C.G. OF ELEMENT

ELEMENT NO.	NORMAL STRESS IN-X (KIP/SQ IN)		NOR
1	-.14855940E+01	-.11791800E+01	-.14850998E+00
2	-.11882876E+01	-.14761484E+01	-.14862741E+00
3	-.23024982E+01	-.67446735E+00	-.17346380E+00
4	-.15538396E+01	-.51872608E+00	-.55007601E+00
5	-.16494849E+01	-.13425363E+01	-.26221456E+00
6	-.13521786E+01	-.16395047E+01	-.26233199E+00
7	-.52708666E+00	-.15441018E+01	-.55295988E+00
8	-.67961346E+00	-.22971372E+01	-.17521881E+00
9	-.49189234E+01	-.12950606E+02	-.69093357E+01
10	-.23927426E+01	-.14246055E+02	-.43533718E+01
11	-.24978361E+01	-.12660146E+02	-.16766942E+01
12	-.27115492E+01	-.38851493E+00	.19372589E+00

ELEMENT STRAINS AT C.G. OF ELEMENT

	STRAINS IN X-AXIS	STRAINS IN Y-AXIS	STRAINS IN XY-AXIS
1	-.11524443E-03	.14976153E-04	-.12660010E-03
2	.10817731E-04	-.11102394E-03	-.12606216E-03
3	-.44118434E-03	.25199576E-03	-.15110557E-03
4	-.18244285E-03	.25498126E-03	-.46647103E-03
5	-.16354298E-03	-.33181119E-04	-.22245592E-03
6	-.37480822E-04	-.15918122E-03	-.22251798E-03
7	.25107678E-03	-.17825824E-03	-.46898501E-03
8	.24960717E-03	-.43893379E-03	-.15253426E-03
9	.74854195E-03	.40050236E-03	-.59880910E-03
10	.84570246E-03	.33205894E-03	-.37729222E-03
11	.82634025E-03	.38597351E-03	-.14531350E-03
12	-.60188765E-03	.38513795E-03	.15933498E-03
13	-.60188765E-03	.38670494E-03	-.15005011E-03
14	.82634025E-03	.38586938E-03	.14666053E-03
15	.84521682E-03	.33153956E-03	.38057070E-03

D I S P L A C E M E N T S

NODAL POINT NO.	DIS. IN-X (IN.)	DIS. IN-Y (IN.)
1	0.	0.
2	-.16610198E-03	-.16338788E-03
3	0.	-.15720134E-03
4	-.36647501E-03	-.36110123E-03
5	-.16247369E-03	0.
6	0.	.20343703E-04
7	-.43564202E-03	.22857156E-03
8	-.24151155E-03	.15541469E-04
9	-.44789037E-03	.18339503E-04
10	-.44936543E-03	-.19464773E-03
11	-.21159774E-03	-.20732897E-03
12	-.20254349E-03	-.44753046E-03
13	.98820525E-05	-.44769925E-03
14	.71827910E-05	-.24130159E-03
15	.21957491E-03	-.43420706E-03

NORMAL AND SHEARING STRESSES AT C.G. OF ELEMENT

ELEMENT NO.	NORMAL STRESS IN-X (KIP/SQ IN)		NORM
1	-.14714955E+01	-.11366958E+01	-.16253575E+00
2	-.11458651E+01	-.14616667E+01	-.16276488E+00
3	-.23959494E+01	-.59293013E+00	-.18148879E+00
4	-.15453328E+01	-.39488193E+00	-.61483718E+00
5	-.16511493E+01	-.13153064E+01	-.26701745E+00
6	-.13255189E+01	-.16402773E+01	-.28724659E+00
7	-.40313580E+00	-.15346040E+01	-.61794726E+00
8	-.59780517E+00	-.23893339E+01	-.18362282E+00
9	-.52101353E+01	-.13616509E+02	-.72987422E+01
10	-.25176169E+01	-.14757211E+02	-.46091349E+01
11	-.26712985E+01	-.13155857E+02	-.18864980E+01
12	-.28988219E+01	-.30830407E+00	.23991419E+00
13	-.28976141E+01	-.30159434E+00	-.21842450E+00
14	-.26701003E+01	-.13151863E+02	.19060198E+01

ELEMENT STRAINS AT C.G. OF ELEMENT

	STRAINS IN X-AXIS	STRAINS IN Y-AXIS	STRAINS IN XY-AXIS
1	-.36911551E-03	-.17466816E-03	-.18841602E-03
2	-.18052633E-03	-.36308418E-03	-.18858918E-03
3	-.86416429E-03	.17754504E-03	-.21882838E-03
4	-.47030117E-03	.19004327E-03	-.70546304E-03
5	-.44144626E-03	-.24660473E-03	-.33268335E-03
6	-.25285708E-03	-.43502075E-03	-.33282655E-03
7	.18456182E-03	-.46413190E-03	-.70916845E-03
8	.17422906E-03	-.86863550E-03	-.22113133E-03
9	.74549391E-03	.38121772E-03	-.63255766E-03
10	.84665155E-03	.31626912E-03	-.39945836E-03
11	.82551529E-03	.37118441E-03	-.16349649E-03
12	-.11197259E-02	.36988302E-03	.25220961E-03
13	-.11197259E-02	.37260697E-03	-.23815445E-03
14	.82551529E-03	.37134557E-03	.16518838E-03
15	.84601383E-03	.31563492E-03	.40466765E-03

15th Time Interval. COMPO 2.

DISPLACEMENTS

NODAL POINT NO.	DIS. IN-X (IN.)	DIS. IN-Y (IN.)
1	0.	0.
2	-.24466669E-03	-.24145731E-03
3		-.27880752E-03
4	0.	-.51824585E-03
5	-.52463449E-03	
6	-.28502465E-03	0.
7	0.	-.16502768E-03
8	-.57677460E-03	.28018895E-04
9	-.37424954E-03	-.17079064E-03
10	-.58091472E-03	-.16742362E-03
11	-.59325904E-03	-.36621319E-03
12	-.36822759E-03	-.36347504E-03
13	-.37555508E-03	-.59104046E-03
14	-.17739901E-03	-.58064804E-03
15	-.18064583E-03	-.37396305E-03
	.17441048E-04	-.57504563E-03

NORMAL AND SHEARING STRESSES AT C.G. OF ELEMENT

ELEMENT NO.	NORMAL STRESS IN-X (KIP/SQ IN)		NORM
1	-.14667456E+01	-.10782827E+01	-.18867576E+00
2	-.10887623E+01	-.14555205E+01	-.18893480E+00
3	-.25387590E+01	-.44540702E+00	-.21170792E+00
4	-.15526227E+01	-.21854637E+00	-.71338965E+00
5	-.16752728E+01	-.12856306E+01	-.33317473E+00
6	-.12972895E+01	-.16628684E+01	-.33343377E+00
7	-.22799510E+00	-.15403782E+01	-.71688947E+00
8	-.45105293E+00	-.25311360E+01	-.21411282E+00
9	-.56105158E+01	-.14591116E+02	-.78447473E+01
10	-.26991144E+01	-.15671399E+02	-.49986041E+01
11	-.28854126E+01	-.13984114E+02	-.20796757E+01
12	-.31236493E+01	-.11280331E+00	.26849173E+00
13	-.31222683E+01	-.10513134E+00	-.25411289E+00
14	-.28834223E+01	-.13977479E+02	.21025667E+01
15	-.27314630E+01	-.15703251E+02	.50310256E+01

ELEMENT STRAINS AT C.G. OF ELEMENT

	STRAINS IN X-AXIS	STRAINS IN Y-AXIS	STRAINS IN XY-AXIS
1	-.54370377E-03	-.30978613E-03	-.22678566E-03
2	-.31669405E-03	-.53657181E-03	-.22700971E-03
3	-.11408828E-02	.11377983E-03	-.26217500E-03
4	-.66561766E-03	.13019156E-03	-.85048544E-03
5	-.63078495E-03	-.39635732E-03	-.40043805E-03
6	-.40377523E-03	-.62314300E-03	-.40866208E-03
7	.12372975E-03	-.65827763E-03	-.85486799E-03
8	.10986304E-03	-.11366163E-02	-.26494527E-03
9	.74189396E-03	.35273464E-03	-.67987810E-03
10	.84974351E-03	.28761119E-03	-.42974569E-03
11	.82666072E-03	.34571699E-03	-.18023856E-03
12	-.14522868E-02	.34414263E-03	.30701811E-03
13	-.14522868E-02	.34749261E-03	-.29007773E-03
14	.82666072E-03	.34591824E-03	.18222245E-03
15	.84898375E-03	.28687293E-03	.43602222E-03

18th Time Interval. COMPO 2.

D I S P L A C E M E N T S

NODAL POINT NO.	DIS. IN-X (IN.)	DIS. IN-Y (IN.)
1	0.	0.
2	-.28731731E-03	-.28382986E-03
3	0.	-.34366393E-03
4	-.61088245E-03	-.60391051E-03
5	-.35040463E-03	0.
6	0.	-.26092805E-03
7	-.65555320E-03	-.73678817E-04
8	-.44942910E-03	-.26723181E-03
9	-.65614546E-03	-.26354134E-03
10	-.67359033E-03	-.45710064E-03
11	-.45431373E-03	-.44876238E-03
12	-.46725621E-03	-.67114107E-03
13	-.27435389E-03	-.65582652E-03
14	-.27791860E-03	-.44909134E-03
15	-.85109737E-04	-.65364826E-03

NORMAL AND SHEARING STRESSES AT C.G. OF ELEMENT

ELEMENT NO.	NORMAL STRESS IN-X (KIP/SQ IN)		NORMA
1	-.14632986E+01	-.10553737E+01	-.19819289E+00
2	-.10662202E+01	-.14516348E+01	-.19847689E+00
3	-.25935602E+01	-.39116993E+00	-.22155644E+00
4	-.15534473E+01	-.14996230E+00	-.75119612E+00
5	-.16823780E+01	-.12731600E+01	-.34998520E+00
6	-.12852995E+01	-.16694211E+01	-.35026920E+00
7	-.15972311E+00	-.15406393E+01	-.75483037E+00
8	-.39699243E+00	-.25854619E+01	-.22409113E+00
9	-.57690165E+01	-.14969228E+02	-.80593140E+01
10	-.27696790E+01	-.16009400E+02	-.50964991E+01
11	-.29727886E+01	-.14295839E+02	-.21669202E+01
12	-.32161788E+01	-.45015389E-01	.28483897E+00
13	-.32147136E+01	-.36875275E-01	-.26982988E+00
14	-.29701179E+01	-.14286937E+02	.21913657E+01
15	-.28044907E+01	-.16043380E+02	.51764780E+01

ELEMENT STRAINS AT C.G. OF ELEMENT

	STRAINS IN X-AXIS	STRAINS IN Y-AXIS	STRAINS IN XY-AXIS
1	-.63848290E-03	-.38184882E-03	-.24888421E-03
2	-.38933848E-03	-.63073302E-03	-.24914442E-03
3	-.12953660E-02	.82735883E-04	-.28656372E-03
4	-.77241303E-03	.10204227E-03	-.93493687E-03
5	-.73406856E-03	-.47684211E-03	-.43946816E-03
6	-.48492414E-03	-.72572631E-03	-.43972338E-03
7	.95038594E-04	-.76439853E-03	-.93970846E-03
8	.78489972E-04	-.12906559E-02	-.28961974E-03
9	.74039173E-03	.34171591E-03	-.69847388E-03
10	.85077137E-03	.27705013E-03	-.44169659E-03
11	.82686544E-03	.33619991E-03	-.18779975E-03
12	-.16483637E-02	.33446757E-03	.33984555E-03
13	-.16483637E-02	.33820229E-03	-.32126792E-03
14	.82686544E-03	.33646995E-03	.18992309E-03
15	.84995078E-03	.27626556E-03	.44862809E-03

21st Time Interval. COMPO 2.

D I S P L A C E M E N T S

NODAL POINT NO.	DIS. IN-X (IN.)	DIS. IN-Y (IN.)
1	0.	0.
2	-.31578813E-03	-.31212801E-03
3	0.	-.38819714E-03
4	-.66804418E-03	-.66072332E-03
5	-.39526970E-03	0.
6	0.	-.32996166E-03
7	-.70587121E-03	-.14915780E-03
8	-.49635275E-03	-.33660336E-03
9	-.70321394E-03	-.33271393E-03
10	-.72488119E-03	-.52016838E-03
11	-.51097928E-03	-.50514790E-03
12	-.53082764E-03	-.72230240E-03

NORMAL AND SHEARING STRESSES AT C.G. OF ELEMENT

ELEMENT NO.	NORMAL STRESS IN-X (KIP/SQ IN)		NORMA
1	-.14619175E+01	-.10307624E+01	-.20949224E+00
2	-.10422224E+01	-.14496190E+01	-.20978360E+00
3	-.26542273E+01	-.32768534E+00	-.23502221E+00
4	-.15573051E+01	-.75391521E-01	-.79305082E+00
5	-.16934620E+01	-.12609804E+01	-.36993513E+00
6	-.12737669E+01	-.16798370E+01	-.37022649E+00
7	-.85720619E-01	-.15438434E+01	-.79685972E+00
8	-.33388113E+00	-.26457387E+01	-.23766347E+00
9	-.59369926E+01	-.15380980E+02	-.62889524E+01
10	-.28463019E+01	-.16402223E+02	-.52432032E+01
11	-.30614558E+01	-.14649329E+02	-.22432906E+01
12	-.33089613E+01	.40677264E-01	.29994755E+00
13	-.33074294E+01	.49188037E-01	-.28408883E+00
14	-.30586021E+01	-.14639816E+02	.22690830E+01
15	-.28830617E+01	-.16438046E+02	.53276902E+01

ELEMENT STRAINS AT C.G. OF ELEMENT

	STRAINS IN X-AXIS	STRAINS IN Y-AXIS	STRAINS IN XY-AXIS
1	-.70175140E-03	-.43133015E-03	-.26228764E-03
2	-.43918856E-03	-.69361780E-03	-.26256284E-03
3	-.13940023E-02	.58235474E-04	-.30194710E-03
4	-.84289467E-03	.78638559E-04	-.98527460E-03
5	-.80248602E-03	-.53143831E-03	-.46313043E-03
6	-.53992318E-03	-.79372596E-03	-.46340563E-03
7	.71289649E-04	-.83447801E-03	-.99027623E-03
8	.53775206E-04	-.13890431E-02	-.30515531E-03
9	.73891005E-03	.32967059E-03	-.71837587E-03
10	.85214550E-03	.26472225E-03	-.45441095E-03
11	.82744470E-03	.32530360E-03	-.19441851E-03
12	-.17580349E-02	.32347684E-03	.35857008E-03

D I S P L A C E M E N T S

NODAL POINT NO.	DIS. IN-X (IN.)	DIS. IN-Y (IN.)
1	0.	0.
2	-.33949395E-03	-.33570158E-03
3	0.	-.42651745E-03
4	-.71522550E-03	-.70765250E-03
5	-.43385182E-03	0.
6	0.	-.39248513E-03
7	-.74545200E-03	-.21963845E-03
8	-.53208184E-03	-.39338790E-03
9	-.73917188E-03	-.39534817E-03
10	-.76521630E-03	-.57509319E-03
11	-.55757660E-03	-.55154373E-03
12	-.58613632E-03	-.76255462E-03
13	-.40712644E-03	-.73881831E-03
14	-.41102118E-03	-.53170583E-03
15	-.23211147E-03	-.74338250E-03

NORMAL AND SHEARING STRESSES AT C.G. OF ELEMENT

ELEMENT NO.	NORMAL STRESS IN-X (KIP/SQ IN)		NORMA
1	-.14615919E+01	-.10007943E+01	-.22387673E+00
2	-.10131338E+01	-.14484209E+01	-.22416565E+00
3	-.27290728E+01	-.24739640E+00	-.25308362E+00
4	-.15637328E+01	.15914991E-01	-.84463825E+00
5	-.17089716E+01	-.12466586E+01	-.39532761E+00
6	-.12605135E+01	-.16944852E+01	-.39561654E+00
7	.47543931E-02	-.15494430E+01	-.84874312E+00
8	-.25414866E+00	-.27201805E+01	-.25583665E+00
9	-.61398270E+01	-.15884993E+02	-.85676634E+01
10	-.29399622E+01	-.16897324E+02	-.54208222E+01
11	-.31661762E+01	-.15089915E+02	-.23257877E+01
12	-.34178395E+01	.15245377E+00	.31666213E+00
13	-.34162390E+01	.16134543E+00	-.29985764E+00
14	-.31634432E+01	-.15080825E+02	.23529771E+01
15	-.29786603E+01	-.16935127E+02	.55085336E+01

ELEMENT STRAINS AT C.G. OF ELEMENT

	STRAINS IN X-AXIS	STRAINS IN Y-AXIS	STRAINS IN XY-AXIS
1	-.75443099E-03	-.47390827E-03	-.27209525E-03
2	-.48205758E-03	-.74600352E-03	-.27237342E-03
3	-.14715698E-02	.34032314E-04	-.31386470E-03
4	-.90076438E-03	.54502040E-04	-.10210679E-02
5	-.85892261E-03	-.57776666E-03	-.48044525E-03
6	-.53654919E-03	-.84986191E-03	-.48072342E-03
7	.46879026E-04	-.89205875E-03	-.10262343E-02
8	.29397716E-04	-.14664512E-02	-.31716446E-03
9	.73718903E-03	.31489850E-03	-.74253083E-03
10	.85397450E-03	.24915548E-03	-.46980459E-03
11	.82836014E-03	.31166454E-03	-.20156827E-03
12	-.18479297E-02	.30976953E-03	.37086247E-03
13	-.18479297E-02	.31383528E-03	-.35090347E-03

27th Time Intreval. COMPO 2.

D I S P L A C E M E N T S

NODAL POINT NO.	DIS. IN-X (IN.)	DIS. IN-Y (IN.)
1	0.	0.
2	-.70609707E-03	-.70232195E-03
3	0.	-.11607240E-02
4	-.13992345E-02	-.13916877E-02
5	-.11680208E-02	0.
6	0.	-.19445355E-02
7	-.11680065E-02	-.22386581E-02
8	-.10627618E-02	-.19514037E-02
9	-.10638919E-02	-.19473823E-02
10	-.11876699E-02	-.16601321E-02
11	-.13899849E-02	-.13839725E-02
12	-.16711260E-02	-.11850119E-02
13	-.19590962E-02	-.10635354E-02
14	-.19629729E-02	-.10023840E-02
15	-.22510510E-02	-.11659404E-02

NORMAL AND SHEARING STRESSES AT C.G. OF ELEMENT

ELEMENT NO.	NORMAL STRESS IN-X (KIP/SQ IN)		NORMA
1	-.14612642E+01	-.10097699E+01	-.21937123E+00
2	-.10218066E+01	-.14483836E+01	-.21966444E+00
3	-.27063257E+01	-.27246997E+00	-.24713767E+00
4	-.15612616E+01	-.11589266E-01	-.82899993E+00
5	-.17036939E+01	-.12508647E+01	-.38737555E+00
6	-.12642363E+01	-.16894785E+01	-.38766876E+00
7	-.22458855E-01	-.15472281E+01	-.83296710E+00
8	-.27896610E+00	-.26975327E+01	-.24986355E+00
9	-.60794570E+01	-.15732921E+02	-.84842902E+01
10	-.29117421E+01	-.16743509E+02	-.53678494E+01
11	-.31357193E+01	-.14954424E+02	-.23041677E+01

ELEMENT STRAINS AT C.G. OF ELEMENT

	STRAINS IN X-AXIS	STRAINS IN Y-AXIS	STRAINS IN XY-AXIS
1	-.15691046E-02	-.12896933E-02	-.27102219E-03
2	-.12978009E-02	-.15087154E-02	-.27130371E-03
3	-.22839806E-02	-.78381154E-03	-.31224847E-03
4	-.17149109E-02	-.76300129E-03	-.10176343E-02
5	-.16731901E-02	-.13931378E-02	-.47855218E-03
6	-.14018864E-02	-.16641600E-02	-.47883374E-03
7	-.77058424E-03	-.17062345E-02	-.10227844E-02
8	-.78841879E-03	-.22788690E-02	-.31554839E-03
9	-.85819359E-04	-.50413612E-03	-.73530515E-03
10	.29877022E-04	-.56949955E-03	-.46521362E-03
11	.45202653E-05	-.50762361E-03	-.19969453E-03
12	-.26597297E-02	-.50951172E-03	.37016873E-03
13	-.26597297E-02	-.50544606E-03	-.34998568E-03
14	.45202653E-05	-.50733417E-03	.26202052E-03
15	.28975117E-04	-.57036018E-03	.47276794E-03

30th Time Interval. COMPO 2.

DISPLACEMENTS

NODAL POINT NO.	DIS. IN-X (IN.)	DIS. IN-Y (IN.)
1	0.	0.
2	-.59577241E-03	-.59203194E-03
3	0.	-.93725607E-03
4	-.11942595E-02	-.11867649E-02
5	-.94447930E-03	0.
6	0.	-.14686120E-02
7	-.10425402E-02	-.16175031E-02
8	-.97699858E-03	-.14756665E-02
9	-.96917988E-03	-.14715304E-02
10	-.10627918E-02	-.13236852E-02
11	-.11915301E-02	-.11[illegible]E-02
12	-.13405798E-02	-.10601386E-02
13	-.14831164E-02	-.96881528E-03
14	-.14871055E-02	-.97661420E-03
15	-.16297387E-02	-.10404890E-02

NORMAL AND SHEARING STRESSES AT C.G. OF ELEMENT

ELEMENT NO.	NORMAL STRESS IN-X (KIP/SQ IN)	NORMAL
1	.41392429E-01	.49717554E+00	-.22180537E+00
2	.48574016E+00	.53697460E-01	-.22210754E+00
3	-.12009509E+01	.12367314E+01	-.24865279E+00
4	-.59220629E-01	.15014822E+01	-.83003160E+00
5	-.20374347E+00	.25341536E+00	-.39167604E+00
6	.24060420E+00	-.19006272E+00	-.39197821E+00
7	.14911969E+01	-.45689618E-01	-.83384179E+00
8	.12305525E+01	-.11923352E+01	-.25131442E+00
9	-.33487098E+01	-.81917639E+01	-.45815956E+01
10	-.15249128E+01	-.76469116E+01	-.29499803E+01
11	-.17936582E+01	-.69013797E+01	-.15999530E+01
12	-.18825613E+01	.16277967E+01	.31433394E+00
13	-.18809122E+01	.16369587E+01	-.29660398E+00
14	-.17909374E+01	-.68923104E+01	.16281097E+01

ELEMENT STRAINS AT C.G. OF ELEMENT

	STRAINS IN X-AXIS	STRAINS IN Y-AXIS	STRAINS IN XY-AXIS
1	-.13239387E-02	-.10413979E-02	-.27422868E-03
2	-.10494214E-02	-.13156265E-02	-.27451725E-03
3	-.20438304E-02	-.53135396E-03	-.31527869E-03
4	-.14712006E-02	-.50941695E-03	-.10259915E-02
5	-.14292609E-02	-.11460628E-02	-.48421546E-03
6	-.11547433E-02	-.14202915E-02	-.48450403E-03
7	-.51691809E-03	-.14625822E-02	-.10310148E-02
8	-.53591164E-03	-.20387281E-02	-.31857395E-03
9	-.70206022E-04	-.28007170E-03	-.39707162E-03
10	-.14861312E-04	-.28014792E-03	-.25566496E-03
11	-.31274809E-04	-.25260941E-03	-.13866259E-03
12	-.24229497E-02	-.25455647E-03	.37409644E-03
13	-.24229497E-02	-.25038725E-03	-.35315914E-03
14	-.31274809E-04	-.25233431E-03	.14110284E-03
15	-.15799142E-04	-.28105397E-03	.26349798E-03

APPENDIX F

CURVE-FITTING PROGRAM AND TYPICAL OUTPUT.

```
      LIST GILL
     MASTER GILL
     DOUBLE PRECISION Y(20),X(20),C(5),CT(5),A(5,11),
    1  V(5)
     READ(1,10) N
10   FORMAT(I0)
     READ(1,20) ((X(I),Y(I)),I=1,N)
20   FORMAT(2D0.0)
     READ(1,20) C
     DO 999 JJJ=1,10
     CALL FIT(N,X,Y,5,C,CT,11,A,1,V,1)
999  CONTINUE
     STOP
     END
     DOUBLE PRECISION FUNCTION F(NC,C,X)
     DOUBLE PRECISION C(NC),X
     LOGICAL YES
     COMMON YES
     IF(-C(2)*X**C(5).GT.75D0.OR.-C(4)*X.GT.75D0) GOTO 1
     YES=.TRUE.
     F=C(1)*(1D0-DEXP(-C(2)*X**C(5)))
    1  +C(3)*(1D0-DEXP(-C(4)*X))
     RETURN
1    YES=.FALSE.
     F=0D0
     RETURN
     END
     SUBROUTINE DERIV(NC,C,X,V)
     DOUBLE PRECISION V(NC),C(NC),X,P,Q,R,T
     P=X**C(5)
     Q=DEXP(-C(2)*P)
     R=DEXP(-C(4)*X)
     V(1)=1D0-Q
     V(2)=C(1)*P*Q
     V(3)=1D0-R
     V(4)=C(3)*X*R
     V(5)=C(1)*C(2)*Q*P*DLOG(X)
     RETURN
     END
     SUBROUTINE FIT(N,X,Y,NC,C,CT,NC2,A,NITS,V,IND)
     DOUBLE PRECISION X(N),Y(N),C(NC),CT(NC),A(NC,NC2),TSUMSQ,
    1  W,SUMSQ,V(NC),ELMAX,F,DF
     LOGICAL YES
     COMMON YES
     TSUMSQ=0D0
     IF(IND.EQ.0)GOTO 2
     WRITE(2,15)
15   FORMAT(12H INITIAL FIT)
     WRITE(2,52) ((J,C(J)),J=1,NC)
52   FORMAT(2H C,I2,1H=,D15.6)
     WRITE(2,1)
1    FORMAT(1H ,3X,8HABSCISSA,7X,7HREADING,8X,12HFITTED VALUE)
2    DO 16 I=1,N
     W=F(NC,C,X(I))
     IF(IND.EQ.0) GOTO 16
     WRITE(2,53) X(I),Y(I),W
16   TSUMSQ=TSUMSQ+(Y(I)-W)**2
53   FORMAT(1H ,3D15.6)
     DO 25 NUMB=1,NITS
     SUMSQ=TSUMSQ
     IF(IND.EQ.0) GOTO 3
     WRITE(2,40) SUMSQ
40   FORMAT(7H SUMSQ=,D20.10)
3    DO 170 I=1,NC
     DO 171 J=1,NC2
171  A(I,J)=0D0
```

```
170   A(I,I+NC)=1D0
      DO 18 K=1,N
      CALL DERIV(NC,C,X(K),V)
      W=F(NC,C,X(K))-Y(K)
      DO 18 I=1,NC
      DO 4 J=1,NC
4     A(I,J)=A(I,J)+V(I)*V(J)
18    A(I,NC2)=A(I,NC2)+W*V(I)
      N1=NC-1
      DO 123 I=1,N1
      ELMAX=0D0
      DO 119 J=I,NC
      IF(ELMAX.GE.DABS(A(J,I))) GOTO 119
      ELMAX=DABS(A(J,I))
      IL=J
119   CONTINUE
      DO 120 J=I,NC2
      W=A(IL,J)
      A(IL,J)=A(I,J)
120   A(I,J)=W
      IP1=I+1
      DO 123 J=IP1,NC
      W=A(J,I)/A(I,I)
      DO 123 IJ=I,NC2
123   A(J,IJ)=A(J,IJ)-W*A(I,IJ)
      DO 234 I=1,NC
      W=A(I,I)
      DO 234 J=I,NC2
234   A(I,J)=A(I,J)/W
      DO 238 K=1,N1
      KK=NC-K
      K1=KK+1
      DO 238 I=1,KK
      W=A(I,K1)
      DO 238 J=K1,NC2
238   A(I,J)=A(I,J)-W*A(K1,J)
      W=1D0
22    DO 211 I=1,NC
211   CT(I)=C(I)-W*A(I,NC2)
      TSUMSQ=0D0
      DO 23 I=1,N
      DF=F(NC,CT,X(I))-Y(I)
      IF(.NOT.YES) GOTO 26
23    TSUMSQ=TSUMSQ+DF*DF
      IF(TSUMSQ-SUMSQ) 24,26,26
24    DO 25 I=1,NC
25    C(I)=CT(I)
      GOTO 27
26    W=W/2D0
      IF(W.GT.1D-10) GOTO 22
      IF(IND.EQ.0) GOTO 5
28    WRITE(2,29)
29    FORMAT(12H F TOO SMALL)
27    WRITE(2,31)
31    FORMAT(10H FINAL FIT)
      WRITE(2,1)
      DO 30 I=1,N
      W=F(NC,C,X(I))
30    WRITE(2,53) X(I),Y(I),W
      WRITE(2,33)
33    FORMAT(13H COEFFICIENTS)
      WRITE(2,35) (I,C(I)),I=1,NC)
35    FORMAT(2H C,I2,1H=,D15.6)
      W=TSUMSQ/(N-NC)
      DO 34 I=1,NC
      P=SQRT(W*A(I,I+NC))
34    WRITE(2,36) I,P
36    FORMAT(21H STANDARD ERROR OF C(,I2,2H)=,E15.6)
5     RETURN
      END
```

```
INITIAL FIT
C 1=    0.4088130-02
C 2=    0.2554940-05
C 3=    0.1284920-03
C 4=    0.1076150 00
C 5=    0.6666660 00
    ABSCISSA          READING          FITTED VALUE
    0.2000000 01    0.1600000-04    0.2486510-04
    0.5000000 01    0.3300000-04    0.5343870-04
    0.7000000 01    0.7300000-04    0.6795870-04
    0.1200000 02    0.9300000-04    0.9311590-04
    0.1400000 02    0.1150000-03    0.9994980-04
    0.1500000 02    0.1170000-03    0.1028530-03
    0.1900000 02    0.1010000-03    0.1117880-03
    0.2000000 02    0.1150000-03    0.1134820-03
    0.2500000 02    0.1200000-03    0.1196840-03
    0.2700000 02    0.1210000-03    0.1213670-03
    0.3000000 02    0.1220000-03    0.1233000-03
    0.3300000 02    0.1200000-03    0.1246980-03
    0.3500000 02    0.1230000-03    0.1254080-03
    0.3600000 02    0.1240000-03    0.1257090-03
    0.4100000 02    0.1300000-03    0.1268090-03
    0.4300000 02    0.1250000-03    0.1271070-03
    0.4700000 02    0.1260000-03    0.1275390-03
    0.5000000 02    0.1310000-03    0.1277590-03
SUMSQ=    0.1127312750D-08
F TOO SMALL
FINAL FIT
    ABSCISSA          READING          FITTED VALUE
    0.2000000 01    0.1600000-04    0.2486510-04
    0.5000000 01    0.3300000-04    0.5343870-04
    0.7000000 01    0.7300000-04    0.6795870-04
    0.1200000 02    0.9300000-04    0.9311590-04
    0.1400000 02    0.1150000-03    0.9994980-04
    0.1500000 02    0.1170000-03    0.1028530-03
    0.1900000 02    0.1010000-03    0.1117880-03
    0.2000000 02    0.1150000-03    0.1134820-03
    0.2500000 02    0.1200000-03    0.1196840-03
    0.2700000 02    0.1210000-03    0.1213670-03
    0.3000000 02    0.1220000-03    0.1233000-03
    0.3300000 02    0.1200000-03    0.1246980-03
    0.3500000 02    0.1230000-03    0.1254080-03
    0.3600000 02    0.1240000-03    0.1257090-03
    0.4100000 02    0.1300000-03    0.1268090-03
    0.4300000 02    0.1250000-03    0.1271070-03
    0.4700000 02    0.1260000-03    0.1275390-03
    0.5000000 02    0.1310000-03    0.1277590-03
COEFFICIENTS
C 1=    0.4088130-02
C 2=    0.2554940-05
C 3=    0.1284920-03
C 4=    0.1076150 00
C 5=    0.6666660 00
```

Series 1. 80°C.

Specific Creep Curve-fitting.

Final Iteration.

SECTION XVI

BIBLIOGRAPHY

I. Bellier J, Tourasse M. "Prestressed concrete pressure vessels at Marcoule nuclear centre". Annales de l'Institut Technique du Bâtiment et des Travaux Publics. July-August 1959.

2. Yu C.W., Gill S. "A review of the safety aspects of the design of prestressed concrete pressure vessels with reference to limit state design." Meeting of specialists on the reliability of systems for nuclear reactor safety. Risø, Denmark, September 1969.

3. Baker A.L.L, Moncrieff M.L.A, Hannah I.W, Gill S. "The design, construction and testing of a prestressed concrete reactor pressure vessel model". December 1961. Proc. Institution of Civil Engineers. Vol. 20, pp 555-586.

4. Ross A.D. "Concrete creep data". Institution of Structural Engineers. 1937. 15.8 pp 314-325.

5. Ross A.D. "Creep and shrinkage in plain, reinforced and prestressed concrete." 1943. Proceedings Institution of Civil Engineers, Vol. 21, No. 1.

6. Lea F. M., Lee C. R. "Shrinkage and creep in concrete". Symposium on the Shrinkage and Cracking of Cementitious Materials. 1947 Proc. Soc. of Chemical Industry.

7. Sherbourne A. N. "Shrinkage and creep in reinforced concrete construction". November, 1961. Civil Engineering and Public Works Review No. 56, 664.

8. Neville A. M. "Creep and shrinkage of concrete" R.C.A. November, 1961.

9. Neville A. M. "Theories of Creep in Concrete" Proc. A.C.I.V. 52. 1955. pp 47-60.

10. Davis R. E, Davis H. E. "Flow of concrete under sustained compressive stress" ASTM. Proc. V. 30 Part II. 1930 p707.

11. Ross A. D. "Creep of concrete under variable stress". A.C.I. Proc. V. 54 1958 pp 739-758.

12. Whitney C. S. "Plain and reinforced concrete arches" A.C.I. Proc. V. 28 1932 pp 479-519.

13. Evans R. H. "Some new facts concerning creep in concrete". V. 37 No. 12 1942 pp 429-432.

14. Neville A. M. "Role of cement in the creep of mortars". A.C.I. Proc. V. 54, 1958-59 p 963.

15. Shank F. R. "The flow of concrete at high overload". A.C.I. Proc. V. 45 1949 pp 493-500.

16. Davis R. E., Davis H. E., Hamilton J. S. "Plastic flow of concrete under sustained stress". A.S.T.M. Proc. V. 34 Part II 1934, pp 354 -386.

17. Illston J. M. "The creep of concrete under uni-axial tension". M.C.R. Vol.17 No.51 June 1965 pp 77-84.

18. Hansen T. C., Mattock A. H. "Influence of size and shape of members on the shrinkage and creep of concrete". P.C.A. Research and Development Labs. Bulletin D.103.

19. Ross A. D. "Experiments on creep of concrete under two-dimensional stresses". M.C.R. Vol. 6 No.16 June 1954 pp 3-10.

20. Lee C. R. "Creep and shrinkage in restrained concrete". Fourth Congress on Large Dams, 1951. Vol.3 Question 15. R 46.

21. Barrett N. T., Murray J. T. "Creep in pressure vessels at elevated temperatures". I.C.E. Conference on Prestressed Concrete Pressure Vessels. March 1967. Paper 14. Group C. pp 33 et seq.

22. Troxell G. E., Raphael J. M., Davis R. E. "Long-term creep and shrinkage tests of plain and reinforced concrete". A.S.T.M. 1958 p.91.

23. Ross A. D. "Shape, size and shrinkage". C.C.E. Vol.39 No.8. August 1944 pp193-199.

24. Weil G. "Influence of dimensions and stress on the shrinkage and creep of concrete". R.I.L.E.M. Bulletin No.3 July 1959. pp 4-14.

25. Davis R. E., Davis H. E., Brown F. H. "Plastic flow and volume changes of concrete". Proc. A.S.T.M., Vol 38 Part II. 1938. pp 410-417.

26. Neville A. M "Tests on the influence of the properties of cement on the creep of mortars".
R.I.L.E.M. colloquium Munich 1948.

27. Neville A. M. "Creep as a function of cement paste content".
M.C.R. Vol. 16. No.46. March 1964
pp 21-30.

28. Neville A. M. "Properties of concrete".
Sir Isaac Pitman, London 1963.

29. Neville A. M. "The relationship between creep of concrete and the stress-strength ratio".
Applied Scientific Research Vol. 9 A.
1960. pp 285-292.

30. Nasser K. W., Neville A. M.
"Creep of concrete at elevated temperatures".
A.C.I. December 1965. Proc V 62
pp 1567-1597.

31. England G. L., Ross A. D.
"Reinforced concrete under thermal gradients".
M.C.R. Vol.14 No.40. March 1962 pp 5-12.

32. Arthanari S, Yu C. W. "Creep of concrete under uniaxial and biaxial stresses at elevated temperatures".
M.C.R. Vol.19 No.60. September 1967.

33. Carlson R. W. "Drying shrinkage of concrete as affected by many factors".
Proc A.S.T.M. V 38. Part II 1938
pp 419-437.

34. Davis R. E., Carlson R. W., Troxell G. E., Kelley J. W.
"Cement investigation for the Hoover Dam".
A.C.I. Proc V 29. 1933 pp 275-284.

35. Davis R. E. "Summary of results of investigations into volumetric changes in cement mortars and concretes due to causes other than stress". A.C.I. Proc V 26. 1930 pp 407-443.

36. Hannah I. W. "Thermal stress in concrete". Nuclear Engineering Vol.6. February 1961 pp 60-74.

37. Hansen T. C. "Creep and stress relaxation of concrete; a theoretical and experimental investigation". Swedish Cement and Concrete Research Institute, Stockholm. Proc No.31. 1960.

38. Roll F. "Long-term creep recovery of highly-stressed concrete cylinders". Symposium on Creep of Concrete. A.C.I. Special Publication SP 9. 1964.

39. Browne R. D. "Properties of concrete in reactor vessels". Proc. of Conference on P.C.P.V's. Group C. Paper 13. March 1967. I.C.E.

40. Klein A., Pirtz D., Adams R. F. "Thermal properties of mass concrete during adiabatic curing". A.C.I. Symposium on Mass Concrete S.P.-6 1963.

41. Pickett G. "The effect of change in moisture content on the creep of concrete under a sustained load". Proc. A.C.I. Vol.38 p. 333.

42. Saemann, J. C., Washa G. W. "Variation of mortar and concrete properties with temperature". Proc. A.C.I. Vol.54. November, 1957. pp 385-395.

43. Saemann J. C., Warren C., Washa G. W.,
"Effect of curing on the properties affecting shrinkage cracking of concrete blocks".
A.C.I. Vol. 51. 1955 pp 833-852.

44. Fulton F. S.
"Concrete Technology".
A South African Handbook : Portland Cement Institute, Johannesburg 1964.

45. England G. L.
"A study of the time-dependent strains in concrete maintained at elevated temperatures and their effects on reinforced concrete".
Ph.D. thesis. University of London 1961.

46. Arthanari S.
"Influence of temperature and biaxial stresses on creep in concrete".
Ph.D. thesis. University of London 1966.

47. Glucklich J.
"Long-term compressive strength of concrete".
Proceedings of the Conference on P.C.P.V's. Group C. Paper No.18.
I.C.E. 1968.

48. Kordina K.
"Experiments on the influence of the mineralogical character of aggregates on the creep of concrete".
R.I.L.E.M. Bulletin No.6 March 1960 pp 7-22.

49. Murdock L. J.
"Concrete Materials and Practice".
Edward Arnold (Publishers) Ltd. 1955.

50. Mironov S. A., Buzhevich G. A.
"Experience in concreting in regions with dry and torrid climate in the U.S.S.R.".
R.I.L.E.M. Symposium on concrete and reinforced concrete in hot countries.
Haifa. July 1960. Part I.

51. Davis R. E., Troxell G. E.
"Variation of mortar and concrete properties with temperature".
Proc. A.C.I. Vol.54. November 1957 pp 385-395.

52. L'Hermite R.
"Volume changes of concrete".
Proc. 4th International Symposium on Chemistry of Cement. Washington 1960. Monograph No.43. Nat.Bureau of Standards. 1962. Vol.2 pp 659-694.

53. Duke C. M., Davis R. E.
"Some properties of concrete under sustained combined stress".
A.S.T.M. Proc. Vol.44 1944. pp 888-896.

54. Hannant D. J.
"Strain behaviour of concrete up to 95°C under compressive stresses".
Proc. of Conference on P.C.P.V's. Group C. Paper 17. I.C.E. 1968.

55. European Committee for Concrete.
"Recommendations for an international code of practice for reinforced concrete".
C. & C. A., London 1963. p 156.

56. Philleo R.
"Some physical properties of concrete at high temperatures".
Proc. A.C.I. Vol.54. 1957. pp 857-864.

57. Bonnell D. G. R., Harper F. C.
"The thermal expansion of concrete".
Nat. Bldg Study. Tech. Paper No.7
London H.M.S.O.

58. Ross A. D., Bray J. W.
"The prediction of temperatures in mass concrete by numerical computation".
M.C.R. Vol.I. No.1. January, 1949.
pp 9-12.

59. L'Hermite R, Mamillan M. "Further results of shrinkage and creep tests".
Int. Conference on the Structure of Concrete. London 1965. Paper H2.

60. Lyse, Ing. "The shrinkage and creep of concrete".
Mag. Con. Research November 1959.
Vol.II. No.33 pp143-150.

61. Czernin W. "The shrinkage of concrete".
Revue des Materiaux de Construction et de Travaux Publics. February 1961.
No.545 pp 73-78.

62. U.S. Bureau of Reclamation
"10-year study of creep properties of concrete".
Report S P-38. Denver, Colorado. 1953.

63. Serafim J. L., Guerriro M. Q.
"Influence of temperature on the creep of mass concrete".
R.I.L.E.M. Bulletin No.6. March 1960.
pp 23-32.

64. Otter J. R. H. "Computations for prestressed concrete reactor pressure vessels, using dynamic relaxation".
Nuclear Struct. Eng. 1965, 1, pp 61-75.

65. Otter J. R. H., Cassell A. C., Hobbs R. E.
"Dynamic Relaxation".
Proc. I.C.E. 1966, 35. pp 633-656.

66 Cassell A. C., Kinsey P. J., Sefton D. J.
"Cylindrical Shell analysis by dynamic relaxation".
Proc. I.C.E. January 1968, 39 pp 75-84.

67. Otter J. R. H. "Dynamic Relaxation compared with other Iterative Finite Difference Methods". Nuclear Eng. and Design 3. 1966 pp 183-185.

68. Przemienieki J. S. "Theory of matrix structural analysis". McGraw-Hill. New York. 1968.

69. Morice P. B. Report on Discussion on Group F Papers - "Design and Analysis of Vessel Structures". Conference on P.C.P.V. I.C.E. London March 1967.

70. Baker A. L. L. "Safety of Pressure Vessels". Conference on P.C.P.V. London 1967.

71. Barrett N. T., Davidson I. "Design Philosophy and Safety". Conference on P.C.P.V. London 1967.

72. Gill S. "Structures for Nuclear Power". C. R. Books Limited. 1964. Chapters 13 and 14.

73. Penny R. K. "Symmetric Bending of the General Shell of revolution by Finite-Difference Methods." Journal of Mech. Eng. Sciences. Vol.3 No.4 1961. pp 369-377.

74. Forsythe G. E., Wasow W. R. "Finite-difference methods for partial differential equations". Wiley. 1960. pp 381-382.

75. The British Standard Specification for P.C.P.V. for Nuclear Reactors.
British Standards Institute
1973 B.S 4975

76. Zienkiewicz O. C., Cheung Y. K.
"The Finite Element method in structural and continuum mechanics".
McGraw-Hill. London-New York, 1967.

77. Clough R. W.
"The finite element method in plane stress analysis".
Proc. A.S.C.E. 2nd Conference on Electronic Computation. Pittsburgh September, 1960.

78. Clough R. W.
"The finite element method in structural mechanics".
Ch.7. Stress Analysis. Eds.Zienkiewicz and Hollister. Wiley, New York 1965.

79. Zienkiewicz O. C., Watson M., Cheung Y. K.
"Stress Analysis by the finite element method - thermal effects".
Int. Conference on P.C.P.V. I.C.E. and B.N.E.S. London March 1967.

80. Slot T.
"Note on stresses and displacements in square plates and cylinders with pressurized central circular holes".
Nuclear Eng. and Design 5. 1967. p 142.

81. Kinkead A. N.
"Round holes in reactor vessels".
I.C.E. p 6896. Abstract - "The Dragon Project". Report 353.

82. Horvay G.
"Plane Stress Problems of perforated plates".
J. Applied Mechanics. 1952. Vol.19
p 355.

83. Duncan J. P. "Structural efficiency of tube-plates for heat exchangers". 1955. Proc. Instit. Mechanical Engs. London. Vol.169. p 789.

84. Bailey R. W., Hicks R. "Behaviour of perforated plates under plane stress". 1960. Journal Mech. Eng. Sciences. Vol.2.

85. Bailey R. W., Fidler R. "Stress analysis of plates and shells containing patterns of reinforced holes". Nuclear Eng. and Design 3. 1966 pp 41-53.

86. Harrop J., Abdul-Wahab H. M. S. "An experimental study of the rigidity of perforated plates". Nuclear Eng. and Design 4. 1966 pp 480-489.

87. Abdul-Wahab H. M. S, Harrop J. "The rigidity of perforated plates with reinforced holes". Nuclear Eng. and Design 5. 1967 pp 134-141.

88. Sheffield C. "The Stress Analysis of a plane uniform circular plate containing a number of circular holes, with special reference to concrete pressure vessel calculations". English Electric Co. Report No.W/AT854 CS/JT. March 1962.

89. Forbes E. "Amendment to report W/AT854." English Electric Co. October 1962.

90. Sokolnikoff I. S. "Mathematical Theory of Elasticity". 2nd Edition. McGraw-Hill. Ch.5. 1956.

91 Muskhelishvili N. I. "Some basic problems of the Mathematical Theory of Elasticity". P. Noordoff. Groningen-Holland 1953.

92. Roark R. J. "Formulas for Stress and Strain". McGraw-Hill 1954.

93. Timoshenko S. P., Woinowsky-Krieger S.
"Theory of Plates and Shells".
McGraw-Hill 1959.

94. McHenry D.
"Towards a generalized treatment of delayed elasticity in concrete."
Int. Ass. for Br.& Str. Eng.26.1966 .

95. Davis H. S.
"Thermal considerations in the design of concrete shields".
Proc. A.S.C.E. Vol.84. No.ST5.
September 1958. Part I. p 1755.

96. McHenry D.
"A new aspect of creep in concrete and its applications to design".
Proc. A.S.T.M. Vol.43. 1943.

97. Gill S.
"The Design of Concrete Biological Shields for Nuclear Reactors".
Parts I and II. 1960. Concrete and Constructional Engineering. Vol.55, 8 & 9.

98. England G. L., Illston J. M.
"Methods of computing stress in concrete from a history of measured strain".
Civil Eng. and Public Works Review.
April 1965. pp 513-517.

99. England G. L.
"Numerical creep analysis applied to concrete structures".
Proc. A.C.I. Vol.64. June 1967. pp 301-311.

100. Ross A. D., England G. L., and Suan R. H.
"Prestressed concrete beams under a sustained temperature crossfall".
Magazine of Concrete Research, 1965. No.17.

101. England G. L.
"Long-term thermal stresses in prestressed concrete structures".
Conference on P.C.P.V. London 1967.

102. England G. L "Steady State Stresses in concrete structures subjected to sustained temperatures and loads". Parts I and II. Nuclear Engineering and Design. 1966. pp 54 to 65 and pp 246-255.

103. England G. L. "Time-dependent stresses in creep-elastic materials: a general method of Calculation". Joint British Committee for Stress Analysis: Conference on Recent Advances in Stress Analysis. March 1968.

104. Lewis D. J., Irving J. "Operational Stresses in nuclear prestressed concrete pressure vessels". June and July 1968. Parts I and II Civil Engineering and Public Works Review.

105. Irving J., Lewis D. J. "A comparison of three direct methods of estimating long term stresses in concrete structures". B.S.I. 1967.

106. Irving J., Goodall I. W. "Creep behaviour of prestressed concrete slabs". C.E.G.B. Paper No.11. 2nd E.E.C. Conference on P.C.P.V. Brussels 1969.

107. Zienkiewicz O. C. "Analysis of viscoelastic behaviour of concrete structures with particular reference to thermal stress". Proc. A.C.I. Vol.58. pp 383-394.

108. Zienkiewicz O. C., Watson M., King I. P. "A numerical method of viscoelastic stress analysis". Int. J. of Mech. Sciences 1968. Vol.10. pp 807-827.

109. Lee E. H. "Viscoelasticity". Handbook of Eng. Mechanics (Ed. Flugge) Chapter 53. McGraw-Hill. New York 1962.

110. Hall I. H. "Deformation of Solids". Nelson. Ch. 7. pp 176-202.

111. Stefanou G. D., Yu C. W., Gill S. "An experimental investigation into the behaviour of perforated end slabs for concrete pressure vessels under temperature and external load". Int. Conference on Model Techniques for P.S.C.P.V. B.N.E.S. London. July 1969.

112. Ali I., Kesler C. E. "Mechanism of creep in concrete". Symposium on Creep of Concrete. Paper No.2 A.C.I. SP-9. 1964.

113. Taylor R. S., Burrow R. E. D. "The Basis of Design of Prestressed Concrete Pressure Vessels". Prestressed Concrete Development Group R.C. Association. London. March 1966.

114. Gill S., Hannah I. W. "The Prestressed Concrete Pressure Vessel". Nuclear Power. March 1962.

115. Davidson I. "Some contributions from Nuclear Power to Engineering Practice". Proc. I.C.E. Vol.17. 1960. pp 121-136.

116. Gill S., Hannah I. W., Russell J., Severn B., Wilson J. H. "The Prestressed Concrete Pressure Vessel : Feasibility Study, Design and Costs". G.E.C. -Simon-Carvis Atomic Energy Group Report. 1958-60.

117. Erntroy H.C., Shacklock B.W.
"Design of high strength concrete mixes"
C & C.A. Reprint No. 32. 1954.

118. Johnson R.P. "Structural Concrete." McGraw-Hill 1967.

119. Smolira M. "Analysis of shrinkage stresses and deformations in concrete beams." Unpublished communication.1970.

120. Evans R.H., Bennett E.W.
"Prestressed Concrete: theory and design."
Chapman and Hall. pp 180-183. 1958.

121. Evans R.H., Kong F.K.
"Estimation of shrinkage of concrete in reinforced and prestressed concrete design." Civil Engineering & Public Works Review. May 1967. pp 559-561.

122. Mears A.R. "The effects of aggregate size and grading on initial air-drying shrinkage."
C & C.A. Technical Report TRA 449.
September 1970.

123. Mamillan M. "Investigation of the shrinkage of concrete." Third Int. Congress of the Precast concrete industry. Stockholm 1960.

124. Neville A.M. "Creep of concrete: plain, reinforced, and prestressed." North-Holland. 1970.

125. Vaishnav R.N., Kesler C.E.
"Correlation of creep of concrete with its dynamic properties."
University of Illinois. T & AM Report No 603. 1961.

126. Stefanou G.D., Yu C.W., England G.L.
"Two-dimensional time-dependent analysis of perforated end caps by the finite element method."
Proc. Int. Conf. S.M.I.R.T. Vol 3H.
September 1971.

127. Langan D., Garas F.K.
"Behaviour of end slabs of P.C.P.V."
Proc. S.M.I.R.T. Sept. 1971. Vol.3H.

128. England G.L., Allen S.J.
"Calculation of time-dependent stresses in P.C.P.Vs by an approximate method." Proc. Int. Conf. S.M.I.R.T. Vol. 3H. September 1971.

129. Kruml F.
"Influence of mix proportions on final value of shrinkage in concrete." RILEM. Colloq. Madrid 1968.

130. Flügge W.
"Viscoelasticity" Blaisdell Publ. Co. 1967.

131 Bennett E.W., Loat D.R.
"Shrinkage and creep of concrete as affected by the fineness of Portland cement" Mag. of Concrete Research. 22. 1970.